Doctoral Theses at NTNU 2005:189

Hedda Vikan

Rheology and reactivity of cementitious binders with plasticizers

NTNU
Norwegian University
of Science and Technology
Doctoral thesis
for the degree of Philosophiae Doctor
Faculty of Natural Sciences and Technology
Department of Materials Science and Engineering

Hedda Vikan

Doctoral thesis 2005:189

NTNU

ISBN 82-471-7271-2 (printed vers.)
ISBN 82-471-7270-4 (electronic vers.)
ISSN 1503-8181

Hedda Vikan

Rheology and reactivity of cementitious binders with plasticizers

Doctoral thesis
for the degree of Philosophiae Doctor

Trondheim, 2005

Norwegian University of Science and Technology
Faculty of Natural Sciences and Technology
Department of Materials Science and Engineering

IMT-Report 2005:75
IUK-Thesis 116

NTNU
Innovation and Creativity

NTNU
Norwegian University of Science and Technology
Doctoral thesis
for the degree of Philosophiae Doctor
Faculty of Natural Sciences and Technology
Department of Materials Science and Engineering

ISBN 82-471-7271-2 (printed ver.)
ISBN 82-471-7270-4 (electronic ver.)
ISSN 1503-8181

Doctoral theses at NTNU, 2005:189

Printed by NTNU-trykk

This thesis has been submitted to the Department of Materials Science and Engineering

NTNU-Norwegian University of Science and Technology

in partial fulfilment of the requirements for the academic degree

PHILOSOPHIAE DOCTOR (PhD)

September 2005

Acknowledgements

First of all I would like to thank my supervisor Prof. Dr. Harald Justnes for helping and guiding me through the work with this thesis. His enthusiasm and extensive knowledge of chemistry, cement and concrete has been inspiring and helpful.

Many thanks also to Dr. Frank Winnefeld for guiding me through the excellent laboratories of EMPA, Switzerland for five months. Thank you for all ideas, advice and inspiration which have helped me immensely. I would also like to express my gratitude to Barbra Lothenbach, Boris Ingold, Luigi Brunetti, and Renato Figi for all their help with the laboratory work at EMPA.

Many thanks also to Tor Arne Hammer who has been the manager of the SINTEF project which initiated this thesis. I would also like to express gratitude to Borregaard Lignotech, Elkem Materials, NorBetong, Norcem FoU, Optiroc, Rescon Mapei and Veidekke who has supported the work financially.

Many thanks also to all colleagues at SINTEF Concrete who have made my working experience most pleasant due to their personal warmth and joy of life.

Finally, I would like to thank my mother for looking after me and my wardrobe throughout my years of study and Martin for his love, support and patience.

Abstract

The rheological behaviour of cementitious pastes has been studied by various means. Six different cements have been studied in main parts of the work and all of them have been characterized according to the Rietveld method in order to determine the exact content of minerals. Easily soluble alkalis were measured by plasma-emission-spectroscopy of the fluid filtered from paste.
Three types of plasticizers namely naphthalene sulfonate formaldehyde condensate (SNF), lignosulphonate and polyacrylate grafted with polyether (PA) have been used throughout the work. The influence of the plasticizer type on the rheological properties of the cementitious pastes, their adsorption characteristics and their effects on heat of hydration of the pastes has been studied.
Limestone has been used as a nonreactive model material for cement in some parts of the work.

All rheological measurements were performed with a parallel plate rheometer. Rather than describing the shear stress-shear rate flow curve with the usual Bingham model resulting in plastic viscosity and yield stress, the area under the curve (Pa/s) was used as a measure of "flow resistance".

The effect of silica fume and limestone on the rheology of cementitious pastes
The rheological behaviour of cementitious pastes, with the cement being increasingly replaced by densified and untreated silica fume (SF) or limestone was studied. Three plasticizers were investigated namely two types of polyacrylate (PA1 and PA2) and SNF. PA2 proved to be the most efficient plasticizer of the three while PA1 and SNF provided comparable results.

The flow resistance was found to increase with increasing silica fume replacement when SNF and polyacryalte (PA1) were added as plasticizers which was explained by ionization of the silica fume surface and possible bridging with polyvalent cations like calcium.
The flow resistance decreased, however, with increasing silica fume replacement when the second and more efficient type of polyacrylate (PA2) was utilized which was believed to occur since the cement pastes were better dispersed by PA2 than SNF and PA1. The silica fume particles could thus pack between the cement grains and displace water. An alternative explanation for reduced flow resistance with increasing silica fume replacement could be a ball-bearing effect of silica spheres.

There was found a trend of *increasing* gel strength with increasing silica fume replacement of cement even though the pastes seemed to be dispersed by PA2. Cement pastes with densified SF developed lower gel strengths than pastes with untreated SF. This phenomenon was

attributed to more grain shaped agglomerates with lower outer surface in densified SF compared to dendritic agglomerated in untreated SF.
Decreasing gel strength was found for pastes with increasing limestone filler replacement. Thus silica fume may be advantageous as stabilizing agent for self-compacting concrete preventing segregation upon standing due to a more rapid gel formation.

Effect of cement characteristics on flow resistance

Rheological experiments were performed on pastes prepared from 4 cements originating from the same clinker, but ground to different finenesses (Blaine). The results showed that the flow resistance increased exponentially with increasing Blaine number. No correlations between single cement characteristics such as Blaine, content of C_3A, cubic C_3A (cC_3A) and C_3S with the flow resistance were however found when cements from different clinkers were used. This finding indicates that cement should not be treated as a univariable material. However, the combined cement characteristic (Blaine$\cdot\{d\cdot cC_3A+[1-d]\cdot C_3S\}$) was found to correlate with flow resistance, where the factor d represents relative reactivity of C_3A and C_3S. The flow resistance was found to be either a linear or exponential function of the combined cement characteristic depending on plasticizer type and dosage. Correlations were found for a mix of pure cement and cement with fly ash, limestone filler (4%), as well as pastes with constant silica fume dosage when the minerals were determined by XRD.

Influence of cement and plasticizer type on the heat of hydration

The initial heat of hydration peak was measured for the 6 main cements with 0.32% SNF, lignosulphonate and PA2 by cement weight. Correlations were attempted between the maximum heat of hydration rates of the initial peaks with various cement characteristics. The maximum heat of hydration rate seemed to correlate with the product of the cement fineness and C_3A content regardless of plasticizer type. The fly ash cement had to be left out of the correlation plots due to its low initial heat of hydration.

The second, third and fourth hydration peaks were measured on the cement pastes with 0-0.8% SNF, lignosulphonate and PA2 by weight of cement. Lignosulphonate was found to be the strongest retarder while SNF had the least effect on the setting time of the three plasticizers.
No correlations could be found between the setting times and cement characteristics such as cement fineness, aluminate and alkali contents for un-plasticized pastes probably because the setting times might have been too close to each other to be able to obtain accurate values.
Correlations between setting time and cement characteristics were however found for pastes with plasticizers. The setting times did not correlate with the cement fineness (Blaine) as a single parameter. The product of cement Blaine and C_3A content, however, resulted in a correlation. Furthermore the setting time correlated with the cubic modification of C_3A. It may seem that the setting times depend more on the cubic modification of C_3A than the sum of orthorhombic and cubic aluminate. This finding indicates that the cubic aluminate modification is more reactive than the orthorhombic.
The setting time decreased with increasing content of easily soluble K-ions in the cements probably due to the formation of syngenite, $K_2SO_4\cdot CaSO_4\cdot H_2O$, which removes some sulphate from solution that would otherwise retard C_3A hydration. A similar correlation was not found between the setting time and the sodium equivalent.

Cement interactions with plasticizers

Three plasticizers were studied namely SNF, lignosulphonate and polyacrylate (PA2). PA2 was the most efficient plasticizer of the three tested even thought it was found to adsorb to a lesser extent on cement than SNF and lignosulphonate. SNF and lignosulphonate brought about comparable results.

PA2 was observed to induce flow gain within the 2 hours of rheological measurements which might be caused by the polymer expanding in the water phase and thus improve the dispersion of the paste. Furthermore the grafted side chains of the polymer are considered to be long enough to provide steric dispersion even thought the backbone might be embedded in the hydration products. Cement pastes with SNF and lignosulphonate exhibited flow loss as a function of time which indicates that the plasticizer molecules were consumed by the hydration products.

The concentrations of superplasticizer in the pore water were not found to change markedly in the time range 20-95 min after water addition, indicating that most of the plasticizer molecules were consumed (i.e. adsorbed or intercalated in surface hydration products) within the first 20 minutes after water addition.

The adsorption characteristics were found to depend on the plasticizer type. The adsorption curves of SNF and lignosulphonate reached a plateau at saturation characterizing high-affinity adsorption or increased continuously as a sign of low affinity adsorption. The adsorbed amounts of polyacrylate decreased, however, after saturation had been reached which might indicate that surplus molecules in the water phase compress the ionic double layer or that adsorbed molecules expand and hinder molecules in the water phase to attach at the surface (i.e. osmosis).

The plasticizer saturation dosages were found to depend on cement surface area (Blaine), amount of cubic C_3A and easily soluble sulphates. The saturation dosage of lignosulphonate seemed to have a dependency on the amount of soluble alkali that was somewhat stronger than observed for pastes with SNF. This difference might be caused by lignosulphonate forming complexes with solvated ions in a higher degree than SNF. Moreover alkali sulphates are furthermore often added to commercial SNF based products as the one used in this work.
The best correlation, overall, was found for the product of cubic C_3A and Blaine which is logical since high surface and cubic aluminate contents accounts for high cement reactivity and since the plasticizers are known to coordinate with calcium sites. Correlations were also found between saturation dosage with the product of Na_{eqv} and Blaine as well as the product of Na_{eqv} and cubic C_3A.
The investigations seemed to indicate that the plasticizer saturation concentration increase with increasing alkali content. These findings, however, are rather unclear. According to literature an increased concentration of alkali sulphate in solution results in both an increased hydration rate (which would lead to a higher plasticizer intercalation) and a reduced plasticizer adsorption (due to SO_4^{2-} - superplasticizer competition). The easily soluble sulphates might, of course, entail the opposing effects of Blaine and C_3A in a way that smoothen the correlation plots of the plasticizer saturation dosage with the cement characteristics.

Effect of temperature on rheology and plasticizer adsorption

Flow resistance and adsorbed amounts of SNF, lignosulphonate and PA2 were measured at temperatures ranging from 11 to 40°C. Limestone was used as a nonreactive model material for cement. The adsorbed amounts of SNF and lignosulphonate on limestone were found to decrease after reaching a maximum which occurred at approximately 25°C. Decreased amounts of adsorbed plasticizer with increasing temperature might be explained by increased kinetic energy to the molecules or by an entropy effect.

The adsorption of PA2 on limestone seemed to be independent of paste temperature in the range of 16-34°C which might be caused by low reduction of entropy at adsorption due to its short backbone and long, grafted side chains.

The flow resistance of the limestone pastes generally increased with increasing temperature which may be caused by reduced amounts of adsorbed plasticizer and/or dehydration of the paste during the rheological measurements.

Two types of cements were used to study adsorption and flow resistance with increasing temperature namely CEM I 42.5 RR and CEM I 52.5 R-LA. Amounts of plasticizer adsorbed and intercalated (consumed) by cement reached a plateau or even decreased with increasing temperature in the case of SNF and lignosulphonate. This finding might be caused by two opposing effects namely: increased number of adsorption sites due to increased hydration rate with increasing temperature and reduced adsorption due to increased kinetic energy and/or reduced entropy of the plasticizer.

Amounts of PA2 consumed by cement increased linearly with increasing temperature as might be explained by the experiments with limestone where the adsorbed amounts of PA2 seemed to be independent of temperature. Increased consumption of plasticizer by the cements with rising temperature is thus probably governed by the increased number of adsorption cites due to increased hydration rate.

The flow resistance of CEM I 52.5 R-LA cement increased exponentially with increasing temperature as a function of temperature most likely because of the increased hydration rate. The pastes of CEM I 42.5 RR cement were generally highly viscous and probably agglomerated. The flow resistance reached a plateau value with increasing temperature in this case.

Table of Contents

List of symbols

Notation

A	Area under the flow curve (= Flow Resistance)
A	Al_2O_3
a	Radii of spherical particle
AF_m	Monosulphate phase: $[Ca_2(Al,Fe)(OH)_6]\cdot X\cdot xH_2O$ where X denotes one formula unit of a doubly charged anion or half a formula unit of a doubly charged anion (generally written in short hand notation as $C_4A\overline{S}H_{12}$)
AF_t	Trisulphate phase (ettringite): $[Ca_3(Al,Fe)(OH)_6\cdot 12H_2O]_2\cdot X_3\cdot xH_2O$ where $x \leq 2$ and X represents one formula unit of a doubly charged or two formula units of a singly charged anion (generally written in short hand notation as $C_6A\overline{S}_3H_{32}$)
BNS or β-NS	β-naphtalene sulfonat-formaldehyde condensate
C	CaO
C_{el}	electrolyte concentration
CSH	Calcium silicate hydrate (= $CaO\cdot SiO_2\cdot H_2O$)
cC_3A	Cubic tricalcium aluminate
CLS	Calcium Lignosulfonate
D	Delayed (addition of plasticizer)
d	Densified (silica fume) or relative reactivity
e	ion charge
F	Fe_2O_3 or Force
FR	Flow Resistance
FA	Fly Ash
G	Rigidity modulus (Hooke's law)
G'	Storage modulus
G''	Loss modulus
G*	Complex shear modulus
H	H_2O or distance between two spherical particles
HA	High Alumina Portland (cement)
K	K_2O
k	Boltzmann's constant
ls	Limestone
LS	Lignosulfonate
M	MgO
N	Na_2O
Na	Avogadro's number
NLS	Sodium lignosulfonate
OPC	Ordinary Portland cement

PA	Polycarboxylic acid
S	SiO_2
$\overline{S}$	SO_3
SF	Silica Fume
SR	Sulfate Resistant (cement)
SMF	Sulfonated melamine formaldehyde condensate
SNF	Naphthalene sulfonate formaldehyde condensate
V_A	Attracting potential energy
V_R	Repulsive potential energy
V_{SR}	Steric repulsive energy
V_T	Total interaction energy
w/c	Water to cement ratio by mass
w/(c+s)	Water to cement and silica ratio by mass
w/ls	Water to limestone ratio by mass
Z	Ionic charge

Greek

γ	parameter for surface potential
$\dot{\gamma}$	Shear rate
δ	distance from the particle surface
ε	Liquid permittivity
ξ	Zeta potential
η	Apparent viscosity
η_c	Viscosity of continuous phase (i.e. liquid in suspension)
$[\eta]$	Intrinsic viscosity of suspension
κ^{-1}	thickness of the ionic double layer
φ	Volume concentration of solids
φ_m	Maximum volume concentration of solids
μ	Plastic viscosity
τ	Shear stress
τ_y	Yield stress
ψ_0	Electric potential at the particle surface
ψ_δ	Stern potential where δ is the distance from the particle surface

Chapter 1

Introduction

1.1 Background

Many people believe that cement is a grey and sometimes lumpy powder which is simply mixed with water, vibrated into place or poured into a mold to harden. Similarly it is believed that concrete is simply cement mixed with gravel and water. Those are gross simplifications. Cement is in fact a material consisting of a number of constituents which interact with each other and the surroundings in various ways. There are an enormous number of different cements on the market with fairly different properties. Today's concrete can furthermore contain a number of constituents such as various mineral fillers (e.g. limestone) and supplementary materials such as slag, fly ash and silica fume and admixtures such as air entrainers, stabilizers, plasticizers, accelerators, retarders etc.

Rheology is a tool to describe the flow characteristics of a material. The development of self compacting concrete (SCC) has enforced the need for more knowledge about paste rheology (i.e. the binder in concrete) and the influence of interactions between cement, fillers, admixtures etc. A self-compacting concrete mix should flow easily and completely fill spaces between reinforcement and forms by virtue of its own weight - thus reducing dependence on vibration techniques.
Self-compacting concrete is achieved by adjusting the aggregate content and using a combination of chemical and mineral admixtures. These admixtures typically consist of high-range water-reducing and viscosity-modifying admixtures. Various filler materials are often used for replacing some of the aggregates and modifying the viscosity. High doses of plasticizers produce a mix with high fluidity and allow for a reduced water-powder ratio. Without a viscosity-modifying admixture, the mixture would tend to segregate and/or bleed.

This thesis was initiated by a SCC project at SINTEF. The project has been studying ways to control and alter the rheological properties of concrete and cementitious materials This includes the viscosity, yield stress, stability against separation and their dependencies on time and temperature up until setting.

1.2 Aim of the work

The aim of the work has been to give a contribution to the fundamental understanding of the rheological properties of cementitious materials. This thesis reports on how the cement constituents interact with different types and dosages of plasticizers and fillers both chemically and physically as a function of time and temperature.

Chapter 2

Theory

2.1 Cement chemistry

2.1.1 Dry cement

Cement chemists use in general a short hand notation; C = CaO, S = SiO_2, A = Al_2O_3, F = Fe_2O_3 and $\overline{S}$ = SO_3, for the main elements in the chemical analyses of cement in addition to H = H_2O to describe hydration processes. The elements are either determined by X-ray fluorescence (process control) or analytical chemistry (according to codes for specification) and given as the corresponding oxides. The main minerals in the cement are alite, C_3S (i.e. Ca_3SiO_5), belite, C_2S (i.e. Ca_2SiO_4), aluminate phase, C_3A (i.e. $Ca_3Al_2O_6$), ferrite phase, C_4AF (i.e. $Ca_4Al_2Fe_2O_{10}$) and anhydrite, $C\overline{S}$ (i.e. $CaSO_4$). The first four minerals are formed during equilibrium conditions in the burning of the cement clinker, while the latter mineral (or gypsum, $C\overline{S}H_2$, or hemihydrate, $C\overline{S}H_{0.5}$) is added to the mill when clinker is ground to cement. The content of these minerals may be calculated through mass balances (i.e. Bogue calculations) assuming that only the preceeding main minerals are present or more directly by Rietveld analysis of X-ray diffractograms.

The results of the Bogue calculation are often called potential phase compositions, because when the procedure was devised, it was generally considered that the principal source of error was failure to reach equilibrium during cooling of the clinker during production. The results do indeed differ, probably often markedly, from the true phase compositions, notably in underestimating alite and overestimating belite. It severely underestimates the C_4AF content and overestimates C_3A (De La Torre et al. 2002). It is furthermore unlikely that equilibrium is maintained during cooling, but the direct source of error is that the compositions of the clinker phases differ considerably from those of the pure compounds by contaminants, solid solution etc. (Taylor 1990).
The importance of knowing the clinker mineralogy has been stressed by the fact that many cement plants use secondary fuels which influence the final quality of the clinker (Klaska et al. 2003). Chemical analysis might in some cases still indicate that

the clinker has the correct chemistry although the actual clinker mineralogy deviates from optimum values. This lack of knowledge about the clinker mineralogy can be solved by the application of the Rietveld method (Paul et al. 2004) on X-ray diffractograms with structural information of crystalline phases.

Optical microscopy, either by visual linear analysis or by point counting, is the most widely adopted experimental method for the quantitative determination of the mineralogical composition of clinker. This method has however some disadvantages. It is time-consuming (at least a thousand points need to be considered) and operator dependent, and some difficulties may arise when determining the aluminate phases (C_3A, C_4AF). Actually, since their micro-crystallinity may sometimes make them insufficiently resolved, the aluminate phases are usually quantified as a group and reported as "interstitial phase" (Costa and Marchi 2003).

In the cement specification sheets the content of other oxides such as N (i.e. Na_2O), K (i.e. K_2O) and M (i.e. MgO) are also given. Note that the alkalis often are found as the mineral aphtitalite, $K_3N\overline{S}_4$, or in solid solution in the main minerals. "Free lime" is the content of free CaO due to insufficient burning or the decomposition of C_3S into C_2S and "free lime" if the cooling rate is too low.

The specific surface area (m^2/kg) of cement is commonly determined directly by an air permeability method called the Blaine method. In addition to the specific surface, the particle size distribution is of importance for the hydration rate of cement, since the hydration takes place at the interface between the cement grain and the water phase. However, it is important to realise that the surface of a cement grain is inhomogeneous as sketched in Fig. 2.1. The distribution of C_3S/C_2S- and C_3A/C_4AF-domains are determined by the milling process and the difference in resistance against fracture.

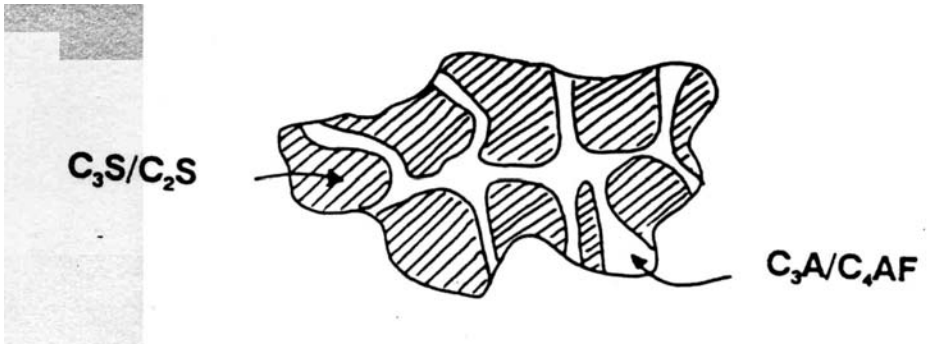

Fig. 2.1: The inhomogeneous nature of a cement grain showing domains of C_3S/C_2S and C_3A/C_4AF (about 100μm, while d_{median} typically is 10-20μm).

2.1.2 Early cement hydration

In the discussion of rheology of cement paste and the interaction with plasticizing admixtures, it is of importance to know something about the hydration until setting. Many believe that no hydration takes place in the so called "dormant" period between water addition and initial setting, while actually a substantial growth of hydration products takes place on the surface of the cement grains.

The interstitial phases C_3A/C_4AF

Among the cement minerals tricalcium aluminate is distinguished by high activity to water at the early stages of hydration. Pure C_3A is cubic and does not exhibit polymorphism. The crystal structure of C_3A has however the ability to change under the influence of impurities. Ca^{2+} and Al^{3+} ions may be isomorphously substituted by a number of ions such as Na, K, Mg, Fe, Si as well as of Mn, Ti, and Cr. C_3A can for instance incorporate Na^+ by substitution of Ca^{2+} with inclusion of a second Na^+ ion in an otherwise vacant site, thus giving solid solutions of general formula $Na_{2x}Ca_{3-x}Al_2O_6$. The substitution occurs without a change in structure up to a limit of about 1% Na_2O. Higher degrees of substitution lead to a series of variants of the structure (Taylor, 1990).

Four crystal forms of solid solutions of Na_2O in C_3A may be obtained: cubic, orthorhombic, tetragonal and monoclinic (Regourd et al. (1973), Maki (1974, a and b)). Boikova et al (1980) found from their investigations that the phase containing more than 3 wt% $Na_2O + K_2O$ appeared to be orthorhombic. Aluminates with less content of alkalis were cubic.
Incorporation of foreign ions in the crystal structure does not only influence the morphology, but also the hydration rate: Boikova et al (1977) found that the degree of hydration of pure C_3A was approximately 60 % at 10 minutes while the degree of hydration of the cubic and orthorhombic solid solution was approximately 43 % and 37 % respectively. Bilanda et al (1980) found similarly that the hydration rate without gypsum decreased with increasing Na_2O concentration while a reverse behaviour was found in hydration with gypsum.

In the absence of calcium sulphates the first hydration product of C_3A is gel-like with no detectable XRD lines, which appear to grow at the C_3A surface. Later this material transforms into hexagonal crystals corresponding to the phases C_2AH_8 and C_4AH_{19}, with additional amounts precipitating from the liquid phase. The formation of these hexagonal phases slows down further hydration of C_3A as they function as a hydration barrier. Finally the hexagonal phases convert to the thermodynamically stable cubic phase C_3AH_6, the diffusion barrier is disrupted and the hydration proceeds again with a fairly high speed. The overall hydration process may thus be written;

$$2\ C_3A + 27\ H \rightarrow \underbrace{C_2AH_8 + C_4AH_{19}}_{\text{(hexagonal phases)}} \rightarrow \underbrace{2\ C_3AH_6}_{\text{(cubic phase)}} + 15\ H \qquad (2.1)$$

In the presence of calcium sulphate (as in a Portland cement) the amount of hydration of C_3A in the initial state of hydration is distinctly reduced when compared to that consumed in the absence of $C\overline{S}$. Needle formed crystals of ettringite (trisulphate, also called AFt) is formed as the main product of hydration;

$$C_3A + 3\,C\overline{S}\,H_2 + 26\,H = C_6A\overline{S}_3H_{32} \qquad (2.2)$$

Minor amounts of the monosulphate $C_4A\overline{S}\,H_{12}$ or even C_4AH_{19} may also be formed if an imbalance exists between the reactivity of C_3A and the dissolution rate of calcium sulphate, resulting in an insufficient supply of SO_4^{2-} ions.

The ettringite formation is accompanied by a significant liberation of heat. After a rapid initial reaction, the hydration rate is slowed down significantly. The length of this dormant period may vary and increases with increasing amounts of calcium sulphate in the original paste.

A faster hydration, associated with a second heat release maximum, gets under way after all the available amount of calcium sulphate has been consumed. Under these conditions the ettringite, formed initially, reacts with additional amounts of tricalcium aluminate, yielding calcium aluminate monosulphate hydrate (monosulphate, also called AFm) as the product of reaction;

$$C_6A\overline{S}_3H_{32} + 2\,C_3A + 4\,H = 3\,C_4A\overline{S}\,H_{12} \qquad (2.3)$$

As ettringite is gradually consumed, hexagonal calcium aluminate hydrate (C_4AH_{19}) also starts to form. It may be present in the form of a solid solution with $C_4A\overline{S}\,H_{12}$ or as separate crystals.

The origin of the dormant period, characterised by a distinctly reduced hydration rate, is not obvious and several theories have been forwarded to explain it. The theory most widely accepted assumes the build-up of a layer of ettringite at the surface of C_3A that acts as a barrier responsible for slowing down the hydration. Ettringite is formed in a through-solution reaction and precipitates at the surface of C_3A due to its limited solubility in the presence of sulphates. The validity of this theory has been questioned arguing that the deposited ettringite crystals are not dense enough to account for the retardation of hydration. The four proceeding alternative theories have been proposed;

i) The impervious layer consists of water-deficient hexagonal hydrate stabilised by incorporation of SO_4^{2-}. It is formed on the surface of C_3A and becomes covered by ettringite.
ii) C_3A dissolves incongruently in the liquid phase, leaving an aluminate rich layer on the surface. Ca^{2+} ions are adsorbed on it, thus reducing the number of active dissolution sites and thereby rate of C_3A dissolution. A subsequent adsorption of sulphate ions results in a further reduction of the dissolution rate.
iii) SO_4^{2-} ions are adsorbed on the surface of C_3A forming a barrier. Contrary to this theory it has been found that C_3A is not slowed down if calcium sulphate is replaced by sodium sulphate (which indicate that Ca^{2+}-ions are necessary to form layers of ettringite).

iv) Formation of an amorphous layer at the C_3A surface that acts as an osmotic membrane and slows down the hydration of C_3A

The termination of the dormant period appears to be due to a break down of the protective layer, as the added calcium sulphate becomes consumed and ettringite is converted to monosulphate. In this through-solution reaction both C_3A and ettringite dissolve and monosulphate is precipitated from the liquid phase in the matrix.

The composition of the calcium aluminoferrite phase (ferrite phase), usually written as C_4AF, may vary between about $C_4A_{1.4}F_{0.6}$ and $C_4A_{0.6}F_{1.4}$. Under comparable conditions the hydration products formed in the hydration of the ferrite phase are similar in many respects to those formed by C_3A although the rates differ and the aluminium in the products are partially substituted by ferric ions. The reactivity of the ferrite may vary over a wide range, but seems to increase with increasing A/F ratio.

The main mineral alite, C_3S

The hydration of alite can be divided into 4 periods:

a) Pre-induction period. Immediately after contact with water, an intense, but short-lived hydration of C_3S gets under way. An intense liberation of heat may be observed in this stage of hydration. The duration of this period is typically no more than a few minutes.

b) Induction (dormant) period. The pre-induction period is followed by a period in which the rate of reaction slows down significantly. At the same time the liberation of heat is significantly reduced. This period lasts typically a few hours.

c) Acceleration (post-induction) period. After several hours the rate of hydration accelerates suddenly and reaches a maximum within about 5-10 h. The beginning of the acceleration period coincides roughly with the beginning of the second, main heat evolution peak. The $Ca(OH)_2$ concentration in the liquid phase attains a maximum at this time and begins to decline; crystalline calcium hydroxide starts to precipitate. The initial set as determined by Vicat-needle is often just after the start of this period and the final setting time just before the ending of it.

d) Deceleration period. After reaching a maximum the rate of hydration starts to slow down gradually; however, a measurable reaction may still persist even after months of curing. The reason is that the hydration reaction becomes diffusion controlled due to hydration products growing around the unhydrated cement core in increasing thickness.

The overall alite hydration reaction may ideally be written as

$$2\ C_3S + 7\ H = C_3S_2H_4 + 3\ CH \qquad (2.4)$$

The calcium hydroxide, CH, is crystalline, while the calcium silicate hydrate is amorphous with a variable composition and therefore often simply denoted CSH-gel.

The mechanism of hydration and setting of C_3S is not yet fully known and different existing theories are summarised in Table 2.1.

Table 2.1: Theories on the mechanism of C_3S hydration (Odler 1998)

Theory on Mechanism	**Impermeable hydrate layer**		**Electrical double layer**	**CH nucleation**	**CSH nucleation**
Pre-induction period	First stage CSH formed				
Beginning of Induction period	First stage CSH acts as diffusion barrier		Impedes passage of ions	Supersaturation of liquid phase with respect to CH stops further rapid dissolution of C_3S	
Changes during Induction period	Ageing of CSH	Osmotic pressure increases	Gradually weakening of double layer	Slow nucleation of CH	Slow nucleation of second stage CSH
End of Induction period	Increased permeabil-ity of CSH	Bursting of CSH layer	Breakdown of double layer	CH nuclei reach critical size	Nuclei of second stage CSH reach critical size
Acceleration period	Accelerated dissolution of C_3S and growth of second stage CSH and CH				

Hydration and setting of ordinary Portland cement

The hydration of Portland cement is associated with the liberation of heat. The heat evolution curve for a typical Portland cement paste is shown in Fig. 2.3. In cements that contain at least a fraction of the K^+ in the form of potassium sulfate, the hydration process may be marked by a distinct initial endothermic peak immediately after mixing (marked 1) which is due to the dissolution of this cement constituent in the mixing water (Odler 1998). The initial peak (marked 2) is attributable to a combination of exothermic wetting and the early stage reactions, which with cement give a gelatinous coating of rods of AFt phase (Eq. 2.3). Rehydration of hemihydrate to give gypsum may contribute. During the first minute after water addition to the cement, the pH of the aqueous solution increases from 7 to >12; the additional OH^- ions thus generated, the solvation of Ca^{2+} and, to a lesser extent Al, all contribute to the enthalpy changes. Not only does the structure of the solids begin to change, albeit slowly in the first minute, but a large and a very rapid relaxation occurs in the structure of liquid water. This is believed, makes an important contribution to the first peak (Yilmaz and Glasser, 1991).

A distinct minimum (marked 3) occurs in the heat of hydration curve due to the existence of a dormant period in which the overall rate of hydration is slowed down. Even though very little seems to happen in the induction or "dormant" period according to isothermal calorimetry there is a continuing hydration of alite (C_3S). Trettin (1997) showed by Atomic Force Microscopy (AFM) that alite crystals in water build up a 50 nm thick hydration layer during the first 15 minutes as reproduced in Fig. 2.4.

It is believed that the main peak of the curve (marked 4) which is reached after a few hours depicts the hydration of the aluminate phases since they produce more heat during the initial reaction with water than the silicates. The gradually decreasing rate of heat evolution after 24 hours corresponds to the continuing slow reactions of the late stage, which mainly give CSH and CH (Taylor 1990). In most, but not all cements, a shoulder or small peak (marked 5) may be observed at the descending branch of the main peak, which is probably due to renewed AFt formation. There may even be a second shoulder (marked 6) which is attributed to AFt-AFm conversion (Scrivener, 1989) or hydration of the ferrite phase (Pratt. and Ghose, 1983). In all these reactions involving the aluminate or ferrite phase, the principal exothermic reaction is probably the reaction of the anhydrous compound with water and not the precipitation or subsequent reactions of hydrated compounds (Taylor, 1990).

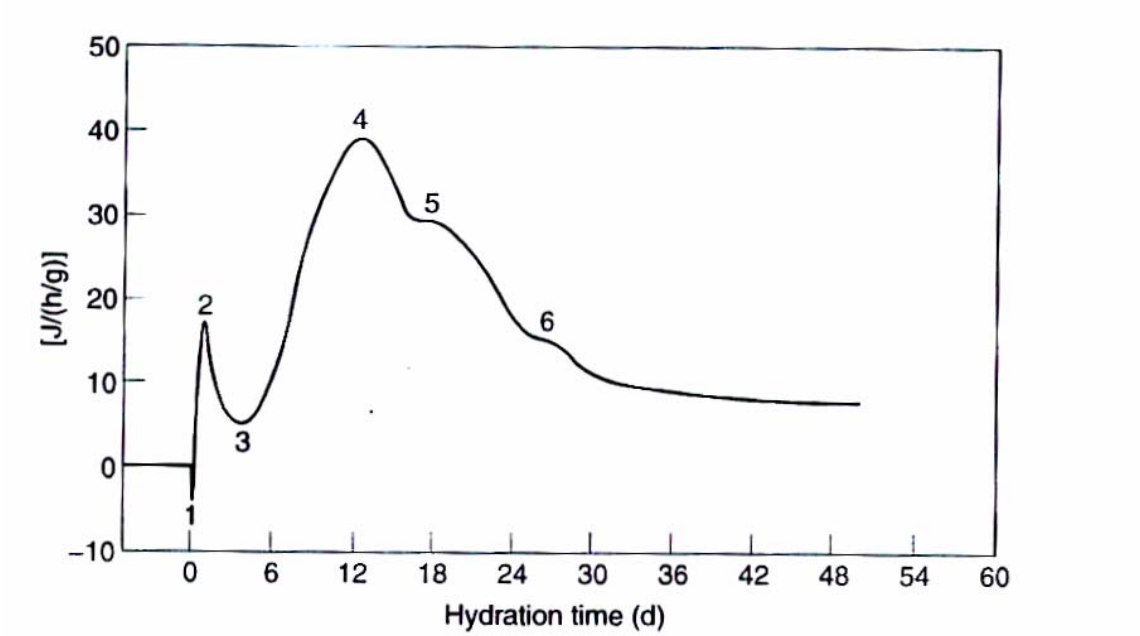

Fig. 2.3: Hydration heat evolution of an ordinary Portland cement. 1: K_2SO_4 dissolution; 2: early stage reaction; 3: dormant period; 4: middle-stage reaction (CSH formation); 5:AFt formation; 6: AFt-AFm conversion (Odler 1998).

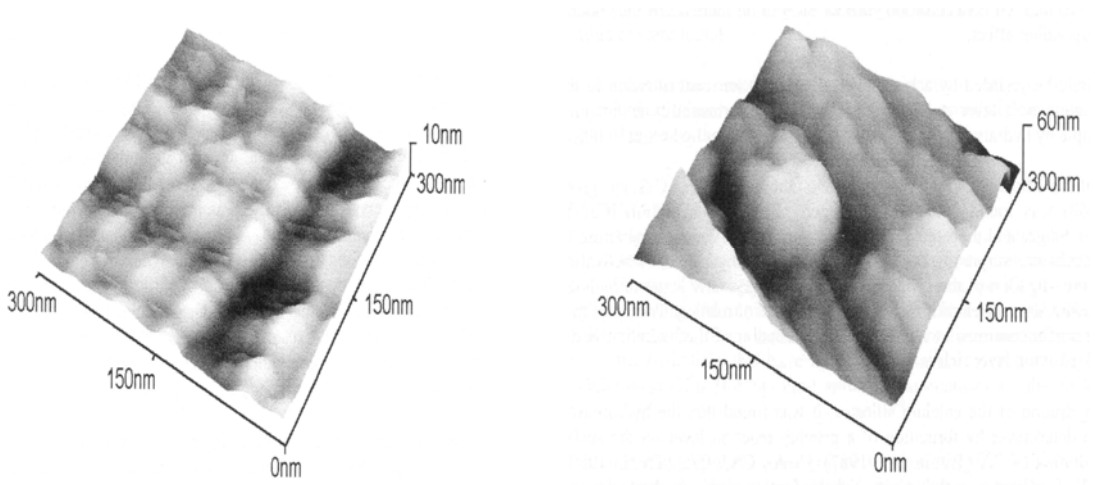

Fig. 2.4: AFM images of a C_3S single crystal surface after 15 second (left image) and 15 minutes (right image) hydration according to Trettin (1997).

2.2 Stability of dispersions (DLVO-theory)

In the discussion of stability of plasticized cement paste, the DLVO-theory is often referred to and thus an introduction is given here. The DLVO-theory is the classic, quantitative theory for the connection between surface potential and stability of *lyophobic* systems (particles suspended in a liquid to which they have low affinity). Oil droplets dispersed in water is generically a *lyophobic* system and specifically *hydrophobic* since the liquid is water. This theory was simultaneously developed in the years 1940-45 by Deryagin & Landau (1941) in Soviet Union and Verwey & Overbeek (1948) in the Netherlands and named DLVO after them. Note that cement paste contrary to their system is a hydrophilic system (i.e. cement particles have great affinity to water). Cement pastes have furthermore, very high solid contents; at w/c = 0.50, the cement and water occupy comparable volumes (equal volumes at w/c ~ 0.32). The colloidal chemistry concepts invoked in discussing the behaviour of these systems, such as electrostatic and steric stabilization were derived for dilute colloidal systems; hence, they should be applied to cement pastes with due caution. Finally, most of the cement particles in a paste are much larger than particles normally considered in the colloidal domain since colloidal size is defined as at least one dimension of the particle in the area of 1 nm to 1 μm (Mørk 2001, Lewis et al. 2000), and the average size of a cement grain is typically 10-15 μm.

The DLVO-theory considers the energy change that takes place when two particles with surface charges approach each other. The total energy change, or interaction energy (V_T) is given by

$$V_T = V_A + V_R + V_{SR} \qquad (2.5)$$

where V_A is the attracting potential energy caused by London-van der Waal forces, V_R is the repulsive potential energy arising by overlapping electrical double layers and V_{SR} is the steric

repulsive force generated by organic admixtures adsorbed on the solid surface of the particles. Both quantitative and qualitative evaluation of stability starts with $V_T = f(H)$, where H is the distance between the surfaces of the particles. An example of a V_T versus H curve is depicted in Fig. 2.5, showing that V_T at first passes through a weak secondary minimum as H decreases, followed by a maximum (V_{Max}) before the deep, primary minimum is reached (i.e. the coagulated state). V_{Max} represents thus an energy barrier against coagulation. If two approaching particles can overcome this barrier, the attracting forces will dominate and the potential energy will rapidly fall to the primary minimum. The two particles will then behave as one kinetic unit. They have coagulated.

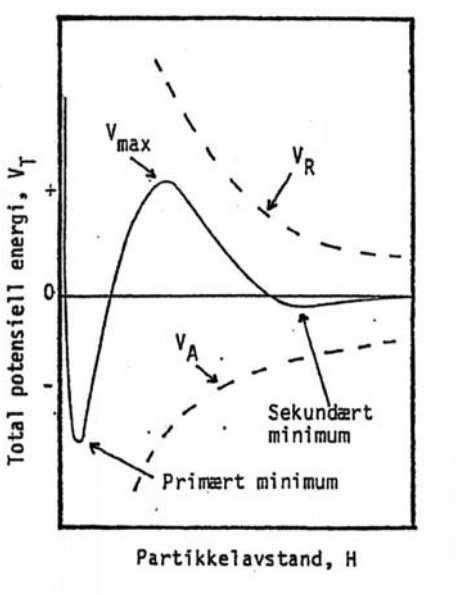

Fig. 2.5: Schematic illustration of the total interaction energy, V_T, as a function of distance, H, between two particles.

The particles in a dispersion have a mean thermal energy of the order kT (k = Boltzman constant = $1.38 \cdot 10^{-23}$ J/K·molecule and T = absolute temperature in Kelvin). The dispersion will be relatively stable (i.e. metastable) if $V_{Max} >> kT$. However, this applies only for thermal movements, not if the dispersion is stirred. Stirring will lead to increased number of particle collision and increases their kinetic energy.

Calculations based on the DLVO-theory have shown that the total energy can pass through the secondary minimum if the particles are relatively large (radius a > 0.1 μm, which applies both for cement and silica fume). If the secondary minimum is somewhat deeper than kT, the particles can be trapped and *flocculate*. However, since the minimum is small, flocculates are completely reversible and may be easily redispersed by stirring.

A charged surface will influence the distribution of the near-by ions in a polar medium as water by attracting ion of opposite charge (i.e. counter-ions) towards the surface and repelling ions of same charge (i.e. co-ions). Together with a blending effect due to the thermal movements of ions, this will lead to the formation of an electrical double-layer.

O. Stern proposed in 1924 a model for the electrical double layer that not only took into account that ions have a given size, but also that ions could be adsorbed to the surface with an adsorption energy specific to different ions. As illustrated in Fig. 2.6, Stern divided the diffuse part of the electrical double layer by a plane called the Stern plane (also known as the inner

Helmholtz plane) localised at a distance δ from the charged surface. The distance δ corresponds roughly to the size of a solvated ion. The potential at the distance δ is called the Stern potential, ψ_δ.

The diffuse double layer consists of two parts according to the Stern model:

1. The Stern layer (or inner part) consisting of specifically adsorbed ions on the charged surface (electrostatic and/or van der Waals bonds)
2. The Gouy-Chapman layer (or the diffuse layer) stretching from x = δ to infinity. The ions in the diffuse part of the layer follow the distribution law of Boltzman and can be regarded as point charges.

Fig. 2.6 depicts how ions are distributed close to a positively charged surface. In the Stern layer the potential drops quickly from ψ_0 to ψ_δ since specifically adsorbed ions neutralises a part of the surface charge. Thereafter the potential flattens out somewhat and follows the Gouy-Chapman expression in the diffuse double layer. It is difficult to calculate the Stern potential, ψ_δ, mainly since it requires knowledge to a number of parameters which are difficult to obtain. It is therefore common to assume that ψ_δ is approximately equal to the potential at the shear plane between the liquid and the charged surface, the so called zeta-potential, ζ. The zeta-potential can be determined experimentally.

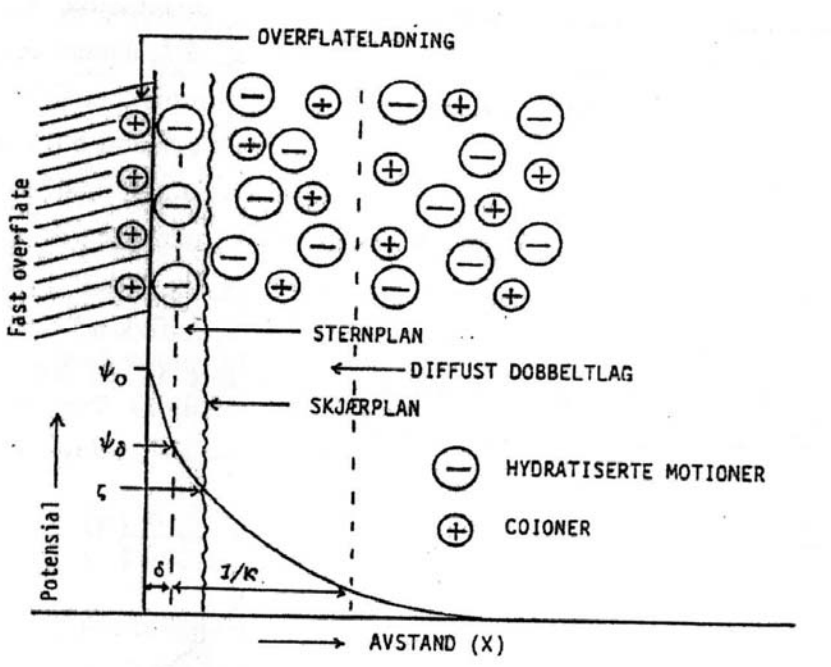

Fig. 2.6: Schematic illustration of the Stern model (Mørk, 2001).

Mørk (2001) shows calculations of how the potential,ψ, varies with the distance, x , from the surface for different electrolyte concentrations, C_{el}, and charges of the counter-ion, z. An important parameter is κ which expresses the effect of the ions' charge and concentration. κ^{-1} is furthermore a measure of the thickness of the electrical double layer.

$$\kappa = \left(\frac{2e^2 N_A C_{el} z^2}{\varepsilon \cdot k \cdot T} \right)^{1/2} \qquad [m^{-1}] \qquad (2.6)$$

Were

C_{el} is the concentration of the electrolyte
N_A is Avogardro's number
Z is the ionic charge
ε is the permittivity of the liquid
k is Boltzmann's constant
T is the Temperature

Some graphs of ψ versus x are plotted in Fig. 2.7. The graphs show that increased electrolyte concentration results in a compressed double layer which again reduce the electric potential.

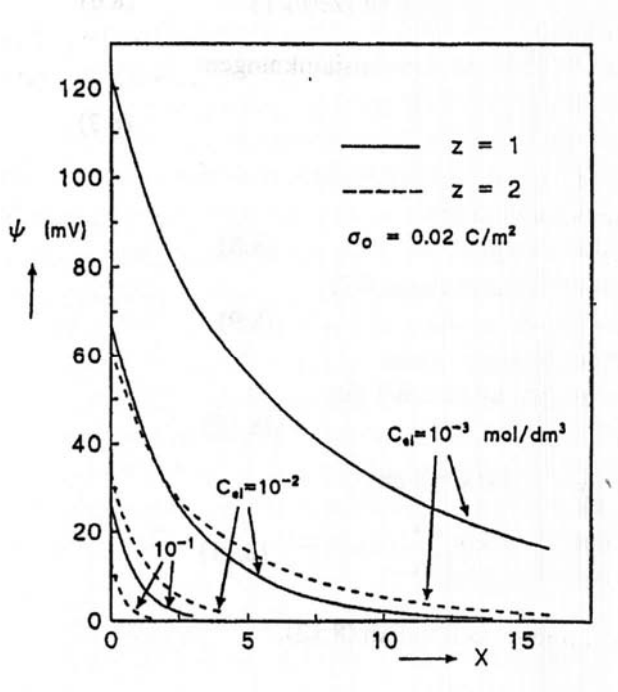

Fig. 2.7: The effect of electrolyte concentration, C_{el}, on the potential,ψ, drop as a function of the distance, x, from a surface with charge $\sigma_0 = 0.02$ C/m^2 when the valence of the counter-ion is either z = 1 or z = 2 (Mørk, 2001).

Note that for a cement paste, C_{el} may be ≥ 0.2 M and z = 1. The electrolyte concentration of cement paste is more than double of the highest values in Fig. 2.7. This is why some scientists claim that electrostatic repulsion as dispersion mechanism for plasticized cement paste plays a lesser role than steric hindrance (see chapter 2.3.3).

2.3 Superplasticizers

The incorporation of superplasticizers in fresh Portland cement concrete yields a variety of immediate benefits related to concrete workability. As fresh concrete can be made highly fluid, even at low water contents, superplasticizers thus open a range of new possibilities for concrete handling and placing practices. Pumpable concrete, self-leveling and self-compacting concretes are direct results of superplasticizer technologies. These have radically changed construction practices, for example, placing concrete in heavily reinforced formwork, enhancing concrete placing rate and associated time and cost savings.

A less visual, but equally important benefit of superplasticizers is their direct impact on properties of hardened concrete. Because superplasticizers allow a 20-30% reduction of the required amount of water in the fresh cement paste, they provide a concomitant reduction of the total capillary pore volume of the hardened paste. The influence of this on the strength and permeability of concrete is spectacular: strength may be enhanced three-fold or more, while permeability will be reduced considerably. An important consequence of the reduction in the permeability of concrete is a major enhancement of its durability. The permeability of concrete to gases (oxygen, CO_2), and water (carrying chlorides, sulfates, acids and carbonates) is paramount to its durability. Low concrete permeability translates directly into lower degradation rate, by reducing the ingress of deleterious chemicals; this in turns, leads to extended service life and lower maintenance and repair costs through the life of the structure. The durability of superplasticized concrete now allows the design of exposed concrete structures for a 100-year service life (Spiratos et al., 2003).

2.3.1 Common plasticizer types

There are four generations of plasticizers/water reducers in terms of time of discovery/use:

1. Salts of carboxylic acids (e.g. sodium gluconate) with strong retarding effects
2. Calcium or sodium lingosulphonate (denoted CLS or NLS) as by-products from pulping industry with medium retarding properties.
3. Synthetic compounds like naphthalene-sulphonate-formaldehyde condensates (SNF) and sulphonated melamine-formaldehyde condensates (SMF) with small retarding properties.
4. Synthetic polyacrylates with grafted polyether side chains (PA) with small retarding properties.

The first generation plasticizers will not be treated here, since they are mostly used for their dominating retarding behaviour. The second generation will dominate the number of references since it has been around for the longest time. Less fundamental investigations are performed for the third generation, but a number of publications in the later years have been focusing on the fourth generation due to its special properties and its usefulness in producing self-consolidating concrete. Admixtures from third and fourth generation are often referred to as superplasticizers. Note that the second generation lignosulphonate may be further developed (e.g. fractionation of large sizes by ultrafiltration or chemical modification of functional groups or grafting on new groups) to achieve similar performance as newer generation plasticizers.

2.3.2 Structure of plasticizing admixtures

Lignosulphonates are sulphonated macromolecules from partial decomposition of lignin by calcium hydrogen sulphite. Under sulphite pulping, lignin is sulphonated and rendered water soluble. The spent sulphite liquor contains sulphonated lignin fragments of different molecular sizes and sugar monomers after removing the pulp. It can be further purified by fermentation to remove hexoses and by ultra filtration to enrich larger molecular fractions. In addition to chemical modification of functional groups for special applications, simple treatment by sodium sulphate will ion exchange calcium through formation of gypsum that is removed. A part of the lignin macromolecule is illustrated in Fig. 2.8.

Fractionations to enrich larger molecules tend to increase the effectiveness of lignosulphonate as a dispersant for cement in water and to reduce the retarding effect. Sodium lignosulphonate retards in general less than calcium lignosulphonates. Due to the size of the molecule, it cannot be ruled out that lignosulphonate disperse cement both through electrostatic repulsion and steric hindrance. The average molecular weight of common lignosulphonates used as plasticizers for cement may be about 5,000-10,000.

The general view for lignosulphonates in solution is that the sulphonic groups are positioned at the surface of a mainly hydrophobic hydrocarbon core (Rezanowich and Goring 1960) as illustrated in Fig. 2.9. The bulk of the model is assumed to be made up of cross linked, poly-aromatic chains which are randomly coiled. The negatively charged groups are positioned mainly on the surface or near the surface of the particle, and a double layer of counter ions is present in the solvent.
The lignosulphonate molecules behave as expanding polyelectrolytes. Thus they expand at low and contracts at high salt concentrations (Rezanowich and Goring 1960, Gupta and McCarthy 1968).

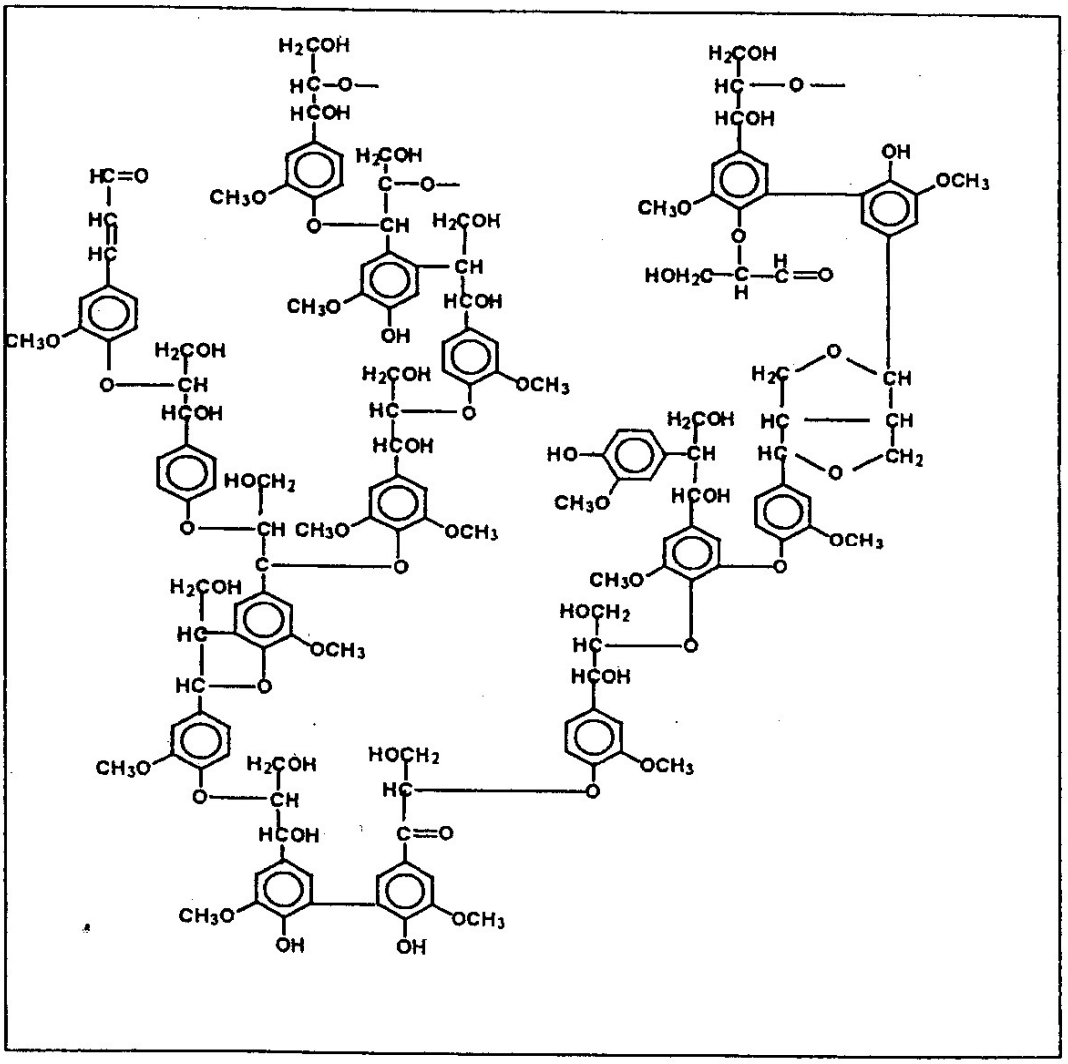

Fig. 2.8: Structure of the lignin polymer showing the different functional groups. Note that in particular the phenol group will interact strongly with aluminates.

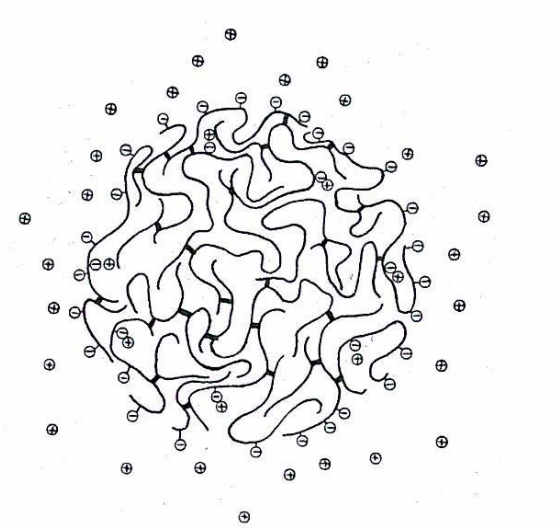

Fig. 2.9: Lignosulphonate macromolecule (Rezanowich and Goring 1960).

The third generation plasticizers are synthesised polymers with sulphonated groups. SNF is made by polycondensation of naphthalene sulphonate with formaldehyde. Its basic structure is shown in Fig. 2.10a. SMF is made by polycondensation of melamine with formaldehyde and a subsequent sulphonation step. Note the difference in synthesis sequences. The basic structure of SMF is shown in Fig. 2.10b. SNF seems to be more used than SMF in the later years. In condensation polymerisation, the molar ratio of formaldehyde to sulphonated naphthalene or melamine determines the molecule size, with a 1:1 ratio in theory giving an infinite polymer chain. However, a realistic number of structural units for SNF will be from 10 to 20, and it is expected to be of the same order for SMF. Thus these molecules are somewhat smaller than lignosulphonates, with relative molecular weights ranging from 2,350 (n = 10) to 4,700 (n = 20) for SNF and 2,800 (n = 10) to 5,700 (n = 20) for SMF.

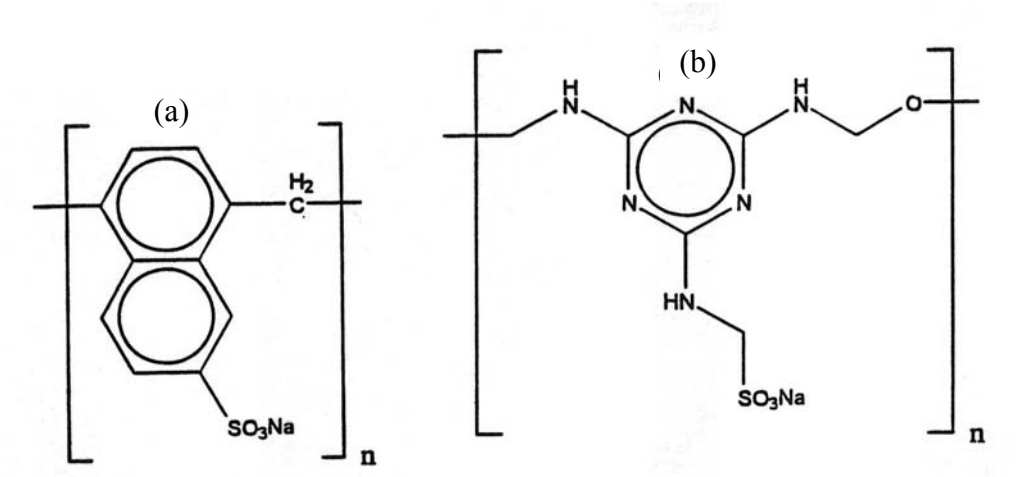

Fig. 2.10: The structural units of (a) naphthalene sulphonate – formaldehyde condensate (SNF) and (b) sulphonated melamine –formaldehyde condensate (SMF). Degree of polymerisation, n, may be in the order of 20 (Ramachandran et al. 1998).

The fourth generation of plasticizers is based on a polyacrylate (PA) backbone that is obtained by free radical polymerisation of different vinyl monomers. This backbone may vary widely in composition depending on the choice of monomers as shown in Fig. 2.11. The second step is to graft on side chains of polyether (polyethylene oxide). Variations in the nature and relative proportions of the different monomers in the copolymer yield a group of products having broad ranges of physico-chemical and functional properties: Yamada et al. (2000) studied the dispersing properties of polycarboxylate-type plasticizers with polyether side chains. Polymers were synthesized with polycarboxylate chain length of 66 to 313 groups, degree of polymerization of the polyeteher side chains were between 9 and 40 and the number of sulphonic groups per molecule were between 3 and 31. Polymers with longer polyether side chains, lower degrees of backbone polymerization and higher contents of sulphonic groups were found to have highest dispersing power. Geffroy et al. (2000) studied the adsorption of un-grafted polyacrylates on calcite. The average molecular weight of the polymers ranged from 2,100-170,000. They found that a narrow fraction with intermediate molar mass of approximately 5000 g/mol was preferably adsorbed. This selection results from a kinetic process where these macromolecules are the first to bind to the surface. Smaller molecules did not bind at all and larger ones could bind, but were repelled by the macromolecules that arrived first at the surface.

The steric size of the polyether chains is found to be almost independent of ionic strength of the solution. The backbone expands in aqueous solutions by the dissociation of the carboxylic

groups. The dissociated state of the backbone is however expected to change depending on the ionic strength. In higher ionic solutions the repulsive forces between the carboxylic groups are weaker due to less dissociation and charge compensation. Thus the size of a polymer with a long backbone will decrease more with increased ionic strength than a polymer with a shorter backbone (Yamada et al. 2001).
Since some of the PA seems to enhance the segregation tendencies to in particular concrete, they are often combined with viscosifiers to counteract this effect (Yamamura et al. 2001). These stabilisers may be cellulose derivatives or similar molecules with many hydroxyl groups (e.g. Welan gum).

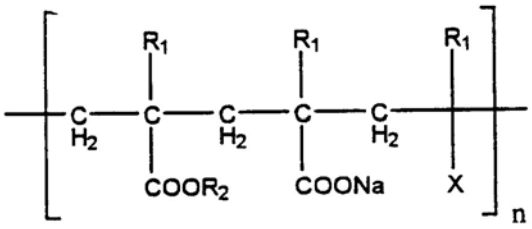

Fig. 2.11: Illustration of a generic group of polyacrylate copolymers where R_1 equals H or CH_3, R_2 is a poly-ether side chain (e.g., polyethylene oxide) and X is a polar (e.g., CN) or ionic (e.g., SO_3^-) group (Ramachandran et al. 1998).

2.3.3 Mode of adsorption

There are generally two main mechanisms of how plasticizers disperse particles in a suspension; electrostatic repulsion and steric hindrance sketched in Figs. 2.12 and 2.13 respectively. Any fractured mineral particle will have domains of positive and negative charged sites since the ionic lattice or covalent bonds are broken. Negatively charged polymers (common feature of most plasticizers) will adsorb to the positive charged sites and render the total particle surface negatively charged. As negatively charged particles approach each other there will be an *electrostatic repulsion* preventing them from attaching to form agglomerates. The latest generation of grafted polymers may also have some negative charges on their backbone that can co-ordinate on positive sites, but note that the ester group of acrylates may co-ordinate strongly to calcium anyway without any charge. Thus, the grafted polyether chains perpendicular to the backbone may stretch out and hinder the particles to get close enough to form agglomerates. This so called *steric hindrance* is based on *size* of adsorbed molecules perpendicular to the particle surface.

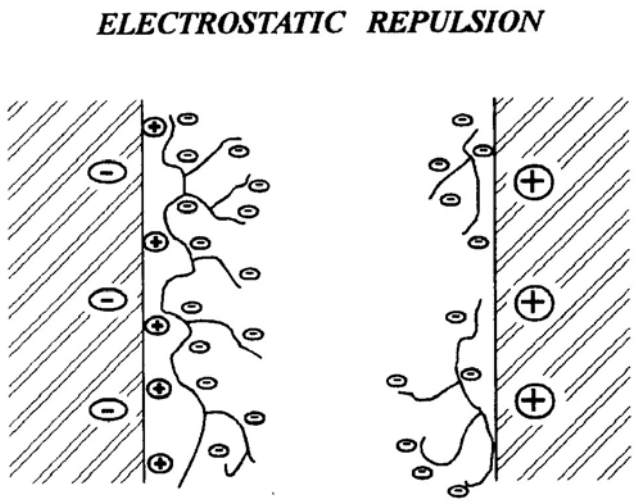

Fig. 2.12: Schematic representation of electrostatic repulsion: Increasing with polymer charge (Ramachandran et al. 1998).

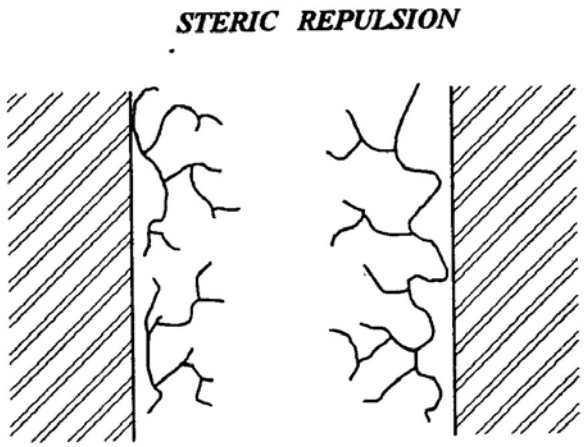

Fig. 2.13: Idealised model of how a grafted polymer will lead to steric hindrance by adsorbing the polymer backbone to the surface and stretching the grafted side chains into the water phase (Ramachandran et al. 1998).

It is not clear how the molecules adsorb on the cement surface: The model of the grafted polymer dispersing according to steric hindrance may be a simplification. It would then be necessary for all the intramolecular bonds (van der Waal type, hydrogen bonds) to break and unwind the polyether chains to let them stretch out into the water phase (even though the hydrophilic nature of polyethers may aid in stabilising such a configuration). Alternatively, the molecules may stay unwound as polymeric balls or "miscelles" that equally well will lead to steric hindrance.

Andersen et al. (1988) found furthermore that the most effectively adsorbed polymer was not necessarily the one which gave the largest negative zeta potential. Thus, the zeta potential depends probably both on the amount of polymer adsorbed and on the fraction of electronegative charges that can be introduced into the Stern layer without actually being adsorbed on the surface. They explained these findings by the "loop" and "train" adsorption mechanisms which are illustrated in Fig. 2.14.

Polymer size has also so found to be of importance for the adsorption capacity. Bonen and Sarkar (1995) found for instance for SNF that monomer, dimer, and probably other low molecular weight polymers were more likely to remain differentially in the pore solution, while higher molecular weight polymers were absorbed on the cement particles. Basile et al.

(1989) found similarly for sodium salts of polynaphtalene sulphonate superplasticizer (PNS) that the fluidity increased with decreasing monomer content.

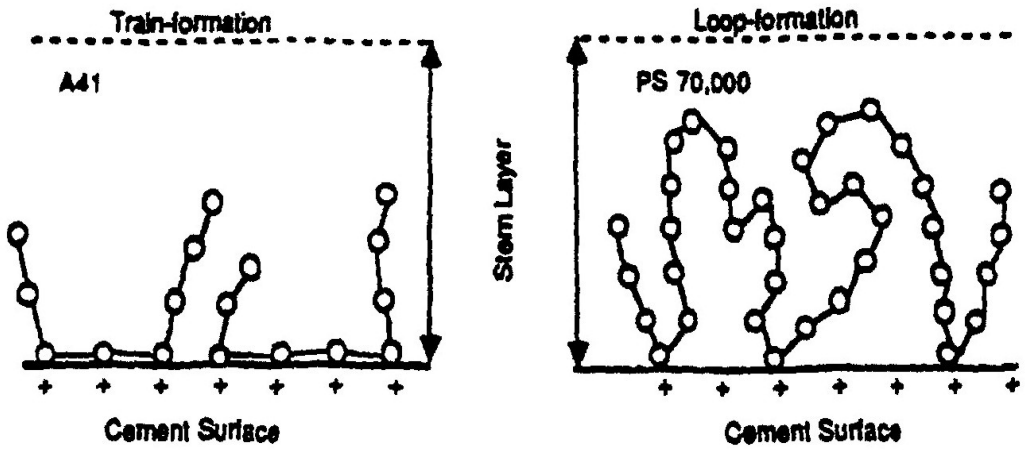

Fig. 2.14: Models of polymer adsorption (Andersen et al. 1987)

While the first three generations of plasticizers are said to rely on electrostatic repulsion as mechanism for their dispersion of cement agglomerates, the fourth generation is the first to be *designed* to function through steric hindrance. Many scientists (e.g. Neubauer et al., 1998) believe that the contribution from electrostatic repulsion is limited in highly ionic systems like cement paste (i.e. see Fig. 2.7 and corresponding text). Uchikawa et al. (1997) claimed furthermore that the contribution of steric hindrance to dispersion of cement particles is considerable even for lignosulphonate and sulphonated melamine-formaldehyde condensate which are generally thought to disperse by electrostatic repulsion. Flatt et al. (2000) discussed the dispersing mechanisms of super-plasticizers and suggested that both mechanisms should be taken into account in a so-called "electrosteric repulsion", but that steric hindrance was dominating.

Another effect that will prevent agglomerate formation is called *depletion* as sketched in Fig. 2.15. Depletion is caused by surplus polymer molecules which stay in the water phase between the particles and prevent them from getting close enough to form agglomerates. As the hydration reaction proceeds, the amount of free water decreases, and so does the distance between the hydration surfaces of the neighboring cement (hydrate) particles. As the interparticle volume becomes smaller, the polymer concentration becomes higher. The concentration of polymers confined in this volume may create a substantial osmotic pressure effect. The latter would either tend to expel the polymers from the confined interparticle volume or create a water flow to dilute the polymer molecules in that region. The first effect would induce a particle-particle attraction, while the latter would induce particle-particle repulsion (Chandra and Björnström 2002, a).

Rheology may also be improved by a *tribology effect* as sketched in Fig. 2.16. Tribology is the science of friction, abrasion and lubrication. Low molecular weight compounds may reduce the friction between particles and also reduce the surface tension of the water phase.

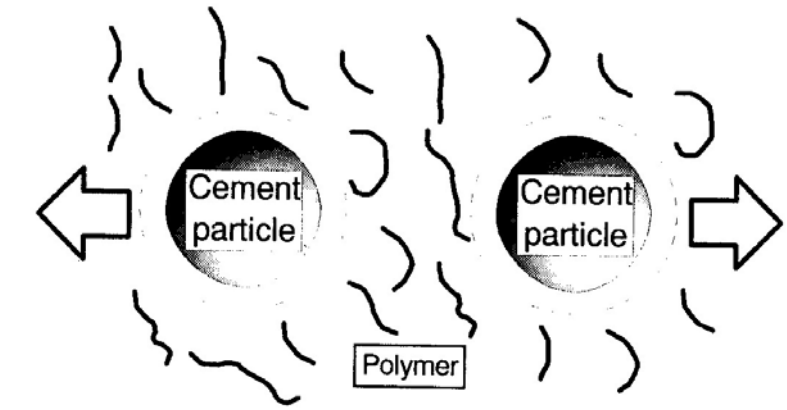

Fig. 1—Outline of the depletion effect

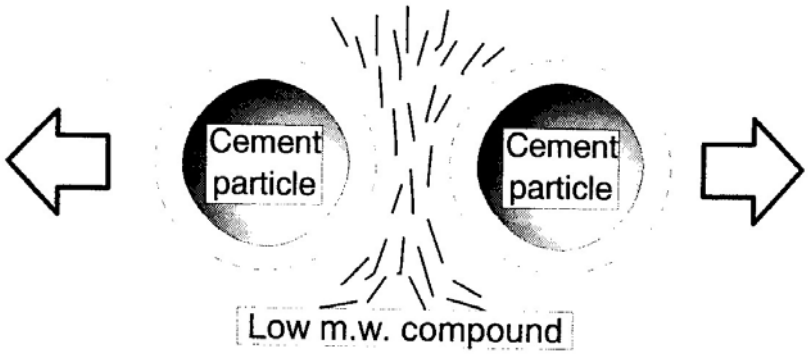

Fig. 2.15/2.16: Upper picture: Surplus polymer in the water phase (not adsorbed) may prevent the cement particles to get close enough to form agglomerates. The depletion effect will not disperse by itself, but rather help stabilize dispersions by preventing flocculation.
Lower picture: Low molecular compounds in the water phase may improve rheology of particle suspensions by lubrication and by lowering the surface tension of the water phase, which may be denoted a tribology effect (Otha et al., 1997)

Initial rheology of cement pastes is also governed by early hydration, unlike inert particle (e.g. limestone) suspensions. Thus, interactions between plasticizers and cement may influence the rheology in cement pastes. The plasticizer molecules might for instance adsorb on active sites and retard the formation of hydration products (see Fig. 2.17). Plasticizers might furthermore alter the morphology of the hydration products by reducing growth (Fig. 2.18) or by intercalation (Fig. 2.19). The long ettringite needles may for instance be short and ”stubby” if a retarding molecule is selectively adsorbed on the tip of the needles.

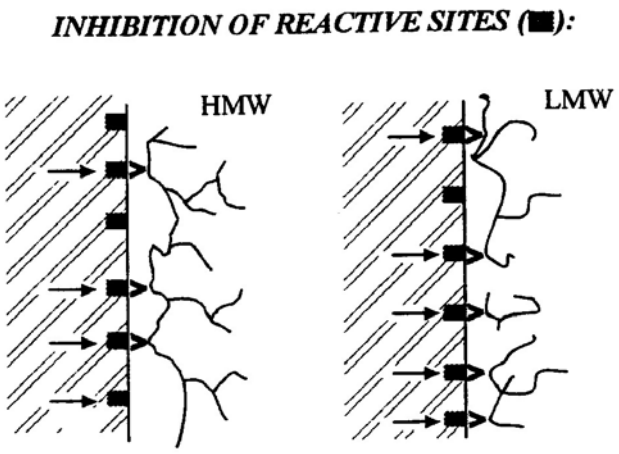

Fig. 2.17: Schematic presentation of inhibition of reactive sites: Increasing with decreasing molecular weight of polymer. (Ramachandran et al. 1998)

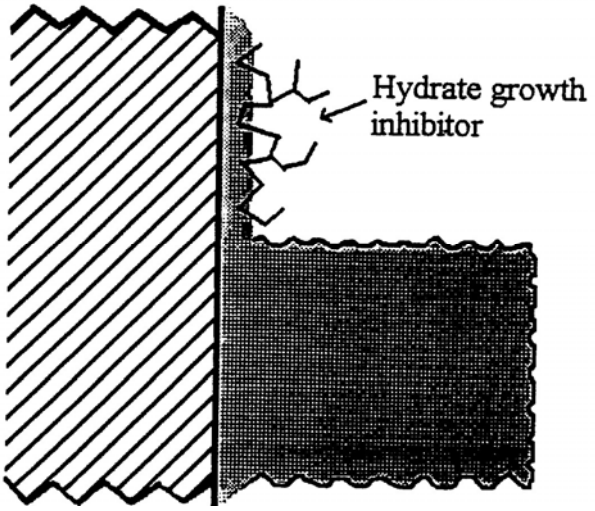

Fig. 2.18: Schematic illustration of hydrate nucleation and growth inhibition by adsorbed superplasticizer molecules (Ramachandran et al. 1998).

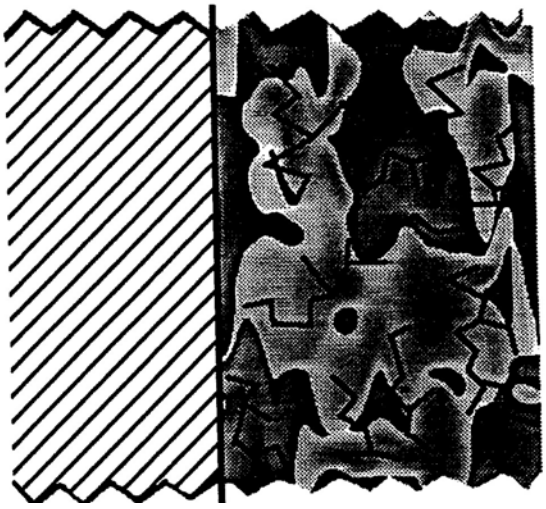

Fig. 2.19: Intercalation of the admixture in the cement hydrates with structural alterations (Ramachandran et al. 1998).

2.3.4 Preferential adsorption of plasticizer molecules on clinker minerals

The adsorption of admixtures on cement particles or cement hydrate depends upon the kind of admixture, clinker mineral and hydrate. Uchikawa et al. (1992) found for instance that cement paste adsorbed more β-NS than LS. Both plasticizers were furthermore found to adsorb more on the interstitial phase and free lime than on the calcium silicate phase. The required amount of admixture in order to prepare the same fluidity of fresh paste was larger for an easily adsorbed admixture than that of a hard adsorbed one. This finding indicates that admixture in solution affects the fluidity (e.g. steric effect/depletion).
Blank et al. (1963) and Rossington and Runk (1968) studied the adsorption of calcium lignosulphonates on ordinary Portland cement and Portland cement hydration products. They found that more than 30 mg/g lignosulphonate adsorbs onto clinker minerals which represents several molecular layers on the surface. The amount of lignosulphonate adsorbed from aqueous solution onto cement compounds was found to be in the following order both in the presence and absence of gypsum:
$C_3A > C_4AF > OPC > C_3S = \beta\text{-}C_2S$.
Bonen and Sarkar (1995) found similarly a correlation between SNF adsorption and C_3A content. An even better correlation was found between adsorption against the product of the C_3A fraction and cement fineness.
Young (1969) found further that the adsorption of lignosulphonate on C_3A decreased if the C_3A was prehydrated. Ramachandran (1972) found that lignosulphonate at low concentrations was much more adsorbed on hydrated C_3S than on anhydrous C_3S. The different behaviour of C_3A vs. C_3S is understood by the different hydration mechanisms.

2.3.5 Retardation

It is well known that addition of superplasticizers affects the setting behaviour of cementitious pastes. The mechanisms of retardation have been discussed by numerous authors.

Lignosufonates may contain a small amount of sugars left from the production which can cause retardation. The magnitude of the role of sugars in the retarding effect of lignosulphonate has however been found to be questionable: Milestone (1979) reported that an addition rate of 0.1% high sugar lignosulphonates caused a delay in hydration of C_3S with subsequent acceleration, while low sugar lignosulphonates at the same addition rate had little influence on the hydration. At a higher dosage rate, however, the hydration of C_3S was completely inhibited regardless of the sugar content. Milestone (1979) concluded that sugars cannot be solely responsible for the retardation, since sugar-free lignosulphonates caused as much delay in hydration as the corresponding sugar-containing lignosulphonates. The results were supported by Ramachandran (1978) who tested three lignosulphonates, namely commercial calcium lignosulphonate, sugar-free sodium lignosulphonate and sugar-free calcium lignosulphonate in mixtures with C_3A, C_3S and Portland cement. At low concentration, all three admixtures retarded both the initial and final set of mortar, but higher concentrations of commercial lignosulphonate promoted quick setting.

Young (1962) and Ciach and Swenson (1971, a) found that lignosulphonate retards the transformation of the hexagonal phase of the calcium aluminate hydrate to the cubic phase. Young (1962) found further that lignosulphonate did not alter the sequence of reactions but modified the morphology of the hexagonal hydrates after gypsum was consumed. These findings were contradicted by Monosi et al. (1983) who found that sugar free sodium

lignosulphonate did not cause any substantial changes in C_3A hydration. Khalil and Ward (1973) found that the presence of lignosulphonate appeared to alter the rate of reaction rather than affect fundamental changes in the products of hydration. The effectiveness of the admixture in delaying the occurrence of peak hydration rate and in reducing the one-day heat of hydration was greatest for the cement low in C_3A content.

Ciach and Swenson (1971, a) found that the addition of calcium lignosulphonates resulted in the retardation of silicates hydration whether gypsum was present or not. The addition of C_3A did however reduce the retarding action of lignosulphonates. The ultimate microstructure of the silicate-aluminate system was not found to be significantly influenced by lignosulphonate. This finding was contradicted by Odler Becker (1980) who studied the effect of a naphthalene sulphonate resin (SNF) and a sulphonated lignin (LS) on the rheological properties and the hydration of Portland cement and tricalcium silicate pastes. They found that both substances retarded the hydration of C_3S and altered the stoichiometric composition of the CSH phase formed.
Young (1972) stressed that alite is the major cement component responsible for the early strength development. Thus retardation (as well as acceleration) of cement hydration happens predominantly through the effect of the admixture on the kinetics of C_3S hydration. C_3A in cement remove most of the admixture from solution and thus prevent its strong effect on C_3S hydration.

Polymer size has been found to be of importance for the adsorption capacity. Bonen and Sarkar (1995) found for instance that the degree of SNF that monomer, dimer, and probably other low molecular weight polymers were more likely to remain differentially in the pore solution, while higher molecular weight polymers were absorbed on the cement particles. Basile et al. (1989) found as a result that the dormant period increased with the molecular weight of the admixture.

Yilmaz and Glasser (1991) stated that although the SMF molecule is too large to be included in crystalline phases, it can bind into gels. They claimed that this gel, the so-called ettringite precursor, is in fact stabilized by incorporation of organic molecules. SMF incorporation tends to increase the volume of the amorphous material and delay the nucleation and inhibit crystal growth of ettringite. The ettringite crystals had a very fibrous morphology when they eventually crystallized. Thus, soluble organic materials are not just passengers in the cement system; they affect the morphology and order of formation of the hydration products. The mechanism by which this is achieved appears to be two-fold; direct incorporation of the organic constituents into the bulk of amorphous gels, and by surface sorption onto the more crystalline phases.
Prince et al. (2002) found similarly that superplasticizer molecules are adsorbed not only on the unreacted constituents but also on ettringite germs just after their formation. Ettringite growth is stopped as soon as these germs are formed so that the usual needle like ettringite crystals cannot develop. Prince et al. (2002) found it probable that the crystallites that are formed during this phase include superplasticizer molecules so that the natural periodicity of ettringite crystal structure is broken. The ettringite crystals start to grow again in their usual shape when there are no more superplasticizer molecules left to block the development of ettringite crystals.

Gu et al. (1994) believed that the influence of SNF superplasticizers on the hydration of cement particles originated as a result of three main effects:

1. Adsorbed superplasticizer molecules which hinder the diffusion of water and calcium ions at the cement/solution interphase
2. The Ca^{2+}complexing action of superplasticizers polymers which inhibits nucleation and precipitation of Ca-containing products
3. The dispersing action of the polymers alters the growth kinetics and morphology of the hydration products.

A similar model was proposed by Mollah et al. (1995) who investigated the effects of sodium lignosulphonate on the hydration of Portland cement. Reduced formation of $Ca(OH)_2$ as well as lower degree of polymerization of the silicate anions indicated that the superplasticizer inhibited the hydration reaction. The hydration reaction seemed to be controlled by dispersions of various ionic charges present in the alkaline pore solution. A "Charge Dispersed Tri-layer Model" (Fig. 2.20) was proposed to explain the observed effects on the hydration reactions. According to this model, the Ca^{2+} ions from initial hydration reactions form a tightly-bound bi-layer of counter ions with the negatively charged calcium-silica-hydrate surface. Consequent to this intrinsic process, a tri-layer consisting of superplasticizer anions is immediately formed which inhibits further reactions. Since the negative surface is charge compensated by Ca^{2+} ions that form an electrical bilayer, the Ca^{2+} ions released from the system will not be available for reactions to form $Ca(OH)_2$, which in effect will reduce the pH of the medium. Removal of Ca^{2+} ions from solution will prevent them from entering into setting and curing reactions in hydrating cement systems, thus inhibiting or retarding the hydration.

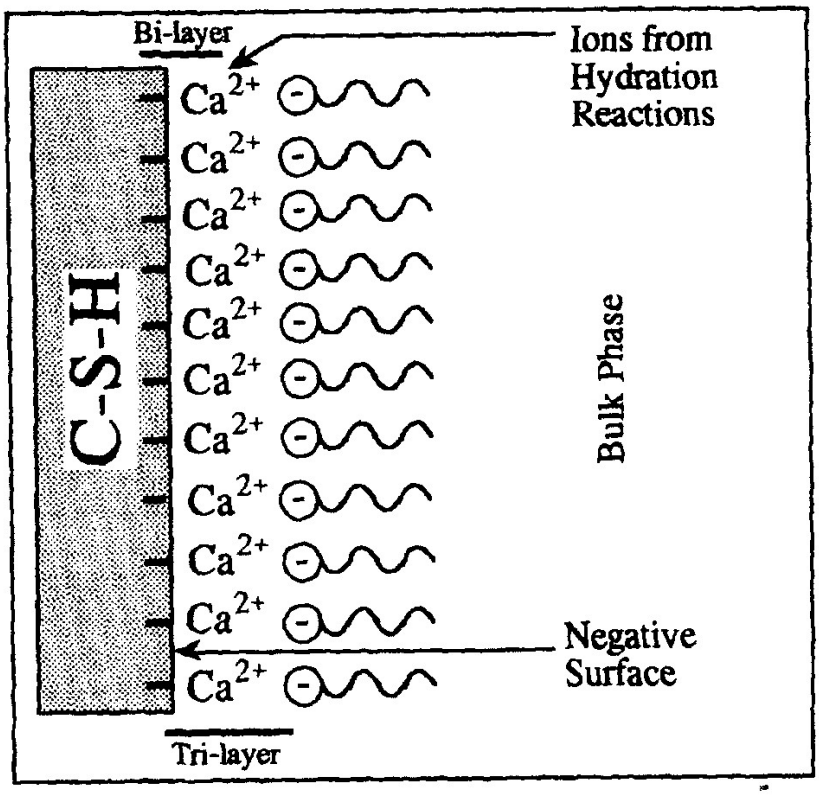

Fig.2.20: Illustration of the Charge Dispersed Tri-layer Model (**Mollah et al. (2000)**).

2.3.6 Plasticizer-cement compatibility

Phenomena such as production of stiffness, variation of initial slump, and large slump loss using some types of cement with constant plasticizer dosage are said to be interaction problems between cement and admixture (Hanehara and Yamada 1999). Slump loss involves chemical and physical processes such as hydration and/or coagulation. The phenomenon of cement-superplasticizer compatibility is however characterized by loss of consistency in the cement paste during the dormant stage mainly attributed to coagulation of cement particles (Chandra and Björnström 2002, b).

The phenomenon of cement-superplasticizer incompatibility has been related to the concentration of SO_4^{2-} ions in solution. The presence of SO_4^{2-} ions has been found to cause decreased consumption of superplasticizer, leaving more of the latter available in the solution phase for paste fluidification. In other words, there seems to be a competition between $-SO_3^-$ groups from sulphonated superplasticizers and SO_4^{2-} ions for available adsorption sites.
Khalil and Ward (1978) studied the reaction rates of Portland cement in the presence of calcium lignosulphonate. They found that the influence of lignosulphonate depended on the sulphate and aluminate content in the cement. A decrease in SO_3 content of the cement caused excessive retardation, while an increase in SO_3 content reduced the retarding effect.
Kim et al (1999) found that the addition of a SNF superplasticizer to high-alkali cement retarded hydration for a few hours then accelerated it slightly. They explained this phenomenon with the hypothesis that the alkali sulphate present in high-alkali-cements hinders the adsorption of a SNF on the aluminate phase, permitting larger adsorption on the silicate phase such as C_3S and C_2S, which delay the early hydration.

Bonen and Sarkar (1995) observed that the flow loss appeared to be strongly governed by the ionic strength of the pore solution and marginally to C_3A content and ettringite formation. The negatively charged surfaces of the cement particles were found to be more affected by a strong electrolyte in the pore solution rather than a weak one. High ionic strength pore solutions induced greater polarization of the double surface layer formed around the particles and this in turn would probably generate more electrostatic bonds that reduce the fluidity (compression of the electric double layer).

Thus, adequate soluble alkali content in the solution during the first few minutes after mixing has been found to be of primary importance to ensure cement/superplasticizer compatibility. Andersen et al. (1986) found that the addition of alkali sulfates (Na_2SO_4/K_2SO_4) can improve the rheological properties of plasticized cement pastes. Cements with less than the optimum soluble alkali content showed significant increases in fluidity when Na_2SO_4 was added while cements with more than the optimum soluble alkali content showed slightly decreased fluidity with the addition of Na_2SO_4. Several researchers have found that when the alkali content is above the optimum value it can cause a flow loss by synergetic effect resulting in the precipitation of syngenite (Odler and Wonnemann 1983, Rechenberg. and Sprung 1983), increase in the reactivity of mineral phases (particularly C_3A) (Chandra and Björnström 2002, a) or compression of the electric double layer. These results were supported by Jiang et al (1999) who found that there exists an optimum soluble alkali content with respect to the fluidity and fluidity loss for the cement-SNF system. This optimum value was found to be 0.4-0.5% Na_2O equivalent. The optimum soluble alkali content was found to be independent of the superplasticizer dosage and cement composition. These results were not corroborated

by Li et al. (2003) who found that the optimal amount of soluble alkalis varied as a function of the superplasticizer dosage.

2.3.7 Delayed addition of superplasticizer

In addition to the quality of the superplasticizer and cement, the addition method of the superplasticizers is usually specified as one of the important factors determining workability.

Admixtures are generally more adsorbed to the interstitial phase than to alite and the hydration reaction of C_3A-gypsum mixtures is found to be markedly influenced by the presence of organic compounds. Mannonen (1996) found that the adsorption appeared to depend on the specific surface area of C_3A. Therefore, the advantage of the delayed addition was greater with the cements having a high C_3A content compared to those having low C_3A content.

The optimum time of the addition of plasticizer is considered to be at the beginning of the dormant period. Chiocchio and Paolini (1985) found that the adsorption of SNF and SMF was terminated only 1-2 minutes after mixing. Bonen and Sarkar (1995) report similar results. Aiad et al. (2002) found on the other hand for SMF and SNF that the optimum delaying time of admixture was 10-15 minutes. The optimal time of addition was not found to depend on cement and superplasticizer type. Chiocchio and Paolini (1985) found similarly that the changes in workability with time was unaffected by the nature of the polymer when the additions of the SNF and SMF based polymers were delayed. Conversely, the changes in fluidity with time were greatly affected by the nature of the admixture when the addition was immediate. This result might have been a result of retardation of the cement hydration.

The effect of delayed addition has been explained as follows: Since the delayed addition of the polymer is not followed by a further considerable hydration of the cement, the renewal of the surfaces active in adsorption does not occur and the amount of polymer adsorbed is therefore much lower than that observed in the case of immediate addition. However, the lower adsorption of polymer could also be due, at least in part, to changes in electrokinetic characteristics of the cement surfaces caused by changes in the composition of the aqueous phase during hydration of the cement. Morphology changes might also influence the flow characteristics of the pastes. Mannonen (1996) found for instance that cement pastes without SNF superplasticizer and with the delayed addition of superplasticizer contained large fibrious ettringite crystals. The paste with the simultaneous addition of superplasticizer had on the other hand much smaller ettringite crystals without any visible fibrous character.

Time of plasticizer addition has been found to affect the setting time: Uchikawa et al. (1995) found that the retardation for cement paste prepared by later addition of SNF and SMF type admixture was larger than for pastes with simultaneous addition. It was believed that the setting of cement paste begins at the time when the concentration of Ca^{2+} reaches a constant value. The delay of the setting of cement paste was therefore attributed to admixture still remaining in solution forming complexes with dissolved calcium. Supersaturation of calcium in the mixing water is thereby inhibited; the active hydration of alite is prevented and the high fluidity of cement paste is kept.
The effect of delayed addition depends however, upon the type of the admixture: Uchikawa et al. (1995) found that the amounts of aminosulphonic acid-based and naphtalenesulphonic acid-based admixture adsorbed to C_3A were significantly reduced by later addition, while

those of polycarboxylic acid-based and lignin sulphonic acid-based admixture were hardly changed. These results were confirmed by Hanehara and Yamada (1999) and are illustrated in Fig. 2.21 for cement pastes with SNF and PA made in the present study.

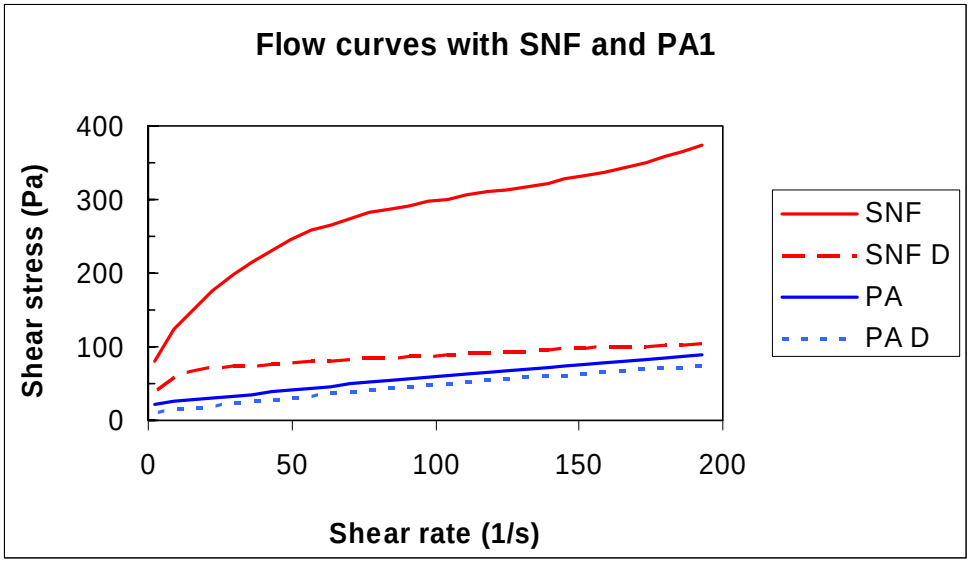

Fig. 2.21: Flow curves for cement pastes with SNF or PA added to the mix with the water or delayed (D).

2.4 Rheology

2.4.1 General viscosity

Rheology means the study of deformation and flow of matter. Much of the introductory rheology is taken from Barnes et al. (2001).

Isaac Newton published the "Principa" in 1687 where there appears a hypothesis associated with steady simple shearing flow as shown in Fig. 2.22: "The resistance which arises from the lack of slipperiness of the parts of the liquid, other things being equal, is proportional to the velocity with which the parts of the liquid are separated from each other".

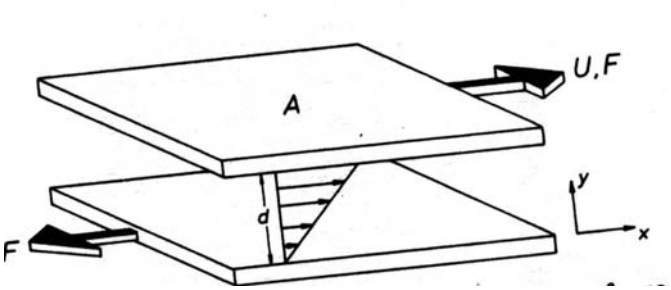

Fig. 2.22: Showing parallel planes, each of area A, at y = 0 and y = d, the intervening space being filled with sheared liquid. The upper plane moves with relative velocity U and the lengths of the arrow between the planes are proportional to the local velocity v_x in the liquid (Barnes et al. 1989).

This lack of slipperiness is what we now call "viscosity". It is synonymous with "internal friction" and is a measure of "resistance to flow". The force per unit area required to produce the motion F/A is denoted shear stress (τ) and is proportional to the "velocity gradient" U/d (or "shear rate", $\dot{\gamma}$), i.e. if you double the force you double the velocity gradient. The constant of proportionality, η, is called the shear viscosity (also called "apparent" viscosity);

$$\eta = \tau / \dot{\gamma} \tag{2.7}$$

The simplest rheological behaviour for liquids is the Newtonian viscous flow and Hook's law for solid materials. Ideal viscous (or Newtonian) flow behaviour is described formally using Newton's law;

$$\tau = \eta \cdot \dot{\gamma} \tag{2.8}$$

Hook's law states similarly that the shear force acting on a solid is equal to the resulting deformation:

$$\tau = G \cdot \gamma \tag{2.9}$$

where G is referred to as the "rigidity modulus".

Examples of ideal viscous materials are low molecular liquids such as water, solvents, mineral oils etc and they are often called Newtonian liquids:

Many materials – especially those of colloidal nature – show a mechanic behaviour in-between these border lines (Hook's and Newton's laws), i.e. they have both viscous and elastic properties and are called viscoelastic.
Samples with yield point (also called yield stress or yield value) only begin to flow when the external forces acting on the material are larger than the internal structural forces. Below the yield point, the material shows elastic behaviour, i.e. it behaves like a rigid solid that under load displays only a very small degree of deformation that does not remain after removing the load.

A common example of non-linearity is known as "shear thinning". This is a reduction of the viscosity with increasing shear rate in steady flow. Examples of Newtonian, shear thinning and shear thickening flow are illustrated in Fig. 2.23. Samples with shear thinning behaviour can be macromolecule (e.g. polymer) solutions or melts where the individual molecules are entangled. Under high shear load the macromolecules will stretch out and may be disentangled, and the viscosity will be reduced. Furthermore, in dispersions or suspensions shearing can cause particles to orient in the flow direction, agglomerates to disintegrate or particles to change their form (see Fig. 2.24). During this process the interaction forces between the particles usually decrease and this also lowers the flow resistance.

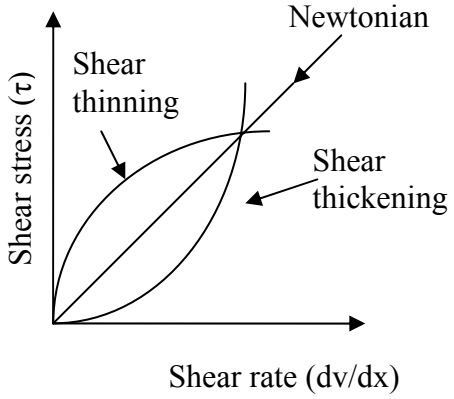

Fig. 2.23: Different types of flow behaviour.

Shear thickening is increase of viscosity with increasing shear rate. Shear thickening flow behaviour occurs in concentrated chemically unlinked polymers due to mechanical entanglements between the mostly branched molecule chains. The higher the shear load the more the molecule chains prevent each other from moving. Similar consequences might occur for highly concentrated suspensions if particles touch each other more and more (they may even become wedged together) during the shearing process: The resistance to flow increases. The particle shape plays an important role here. Due to the shear gradient during shearing, the particles are rotating as they move in the shear direction. Cubic particles take up more volume when rotating than at rest and as a consequence there is less free volume left between the particles for the dispersing liquid. On the other hand, spherical particles take up the same amount of volume when rotating as when at rest.

The flow behaviour of cementitious pastes is known to be dependent on the properties of the admixtures. Lewis et al. (2000) showed that SNF and carboxylated acrylic ester (CAE) grafted copolymers, dramatically affected the rheological properties of dense cement suspensions by promoting a transition from strongly shear thinning to a Newtonian flow response (flocculated → stable) at their respective critical concentrations (ϕ^*).

Papo and Piani (2004) compared the effects of three different superplasticizers based on melamine resin, modified lignosulphonate and modified polyacrylate. They found that the polyacrylate based superplasticizer presented different rheological behaviour than the other superplasticizers studied, since it showed marked shear thickening properties above a critical deflocculant concentration as well as slight elastic effects. The shear thickening behaviour was explained by the presence of linear polyacrylate chains, which at high deflocculant concentrations caused disperse phase aggregation instead of particle repulsion.

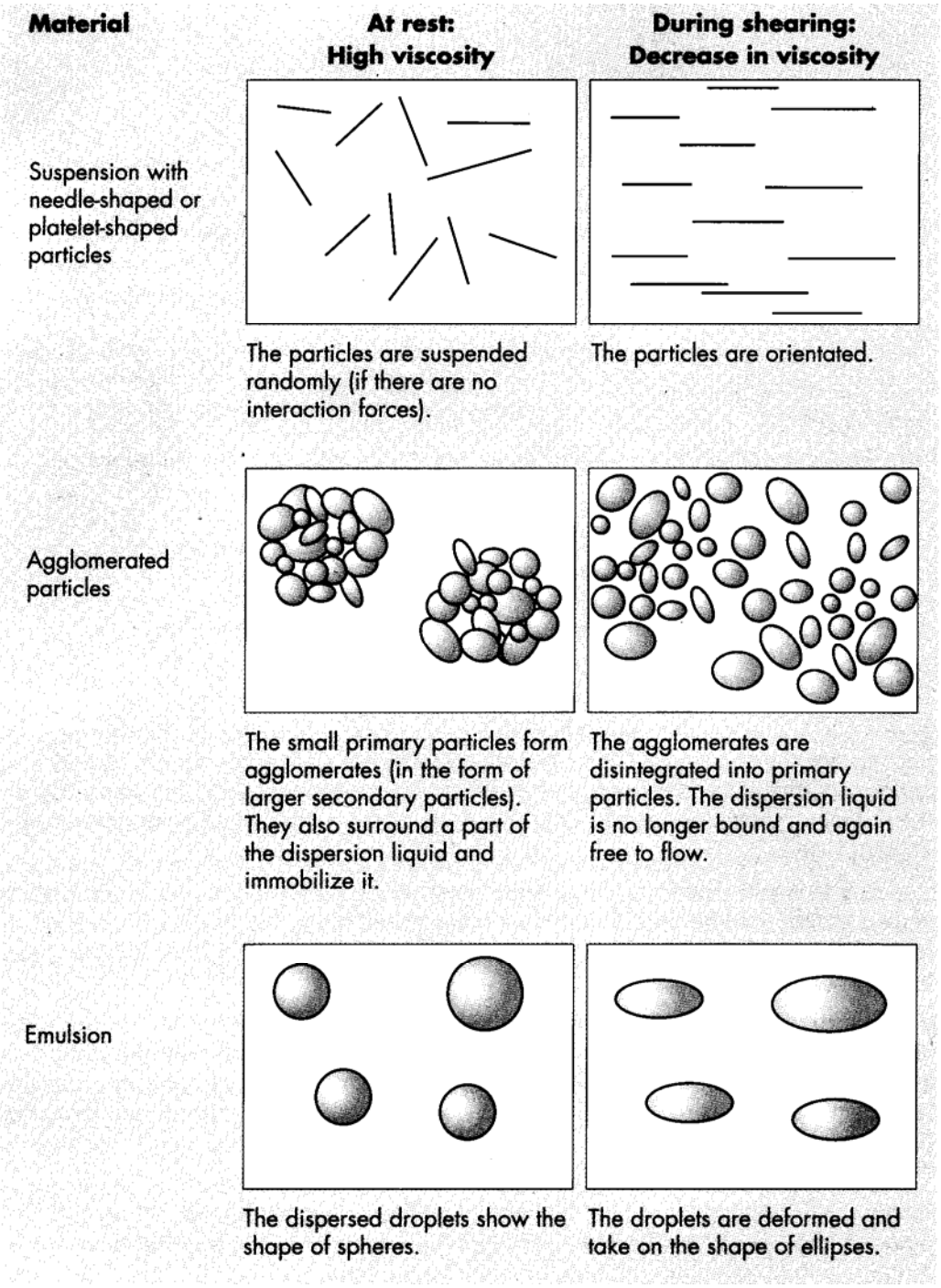

Fig. 2.24: Three examples of situations that will lead to shear thinning behaviour in a material. Note that an extreme case of the last example (emulsion) will be entrained air. Air bubbles will deform easily under shear load and even sub-divide. The sketch is reproduced from Mezger (2002).

2.4.2 Rheological models

Many researchers have tried to find a rheological model which describes the rheological behaviour of cementitious pastes. Among the numerous models proposed are:

Power-law model: $\tau = K \cdot \dot{\gamma}^n$ (2.10)

Bingham plastic $\tau = \tau_y + \mu_p \cdot \dot{\gamma}$ (2.11)

Herschel-Bulkley $\tau = \tau_y + K \cdot \dot{\gamma}^n$ (2.12)

Robertson Stiff $\tau = A \cdot (\dot{\gamma} + B)^n$ (2.13)

Casson $\tau^{1/2} = \tau_y^{1/2} + (\mu_p \cdot \dot{\gamma})^{1/2}$ (2.14)

Sisko $\tau = \mu_\infty \cdot \dot{\gamma} + K \cdot \dot{\gamma}^n$ (2.15)

Eyring $\tau = A \cdot \sinh^{-1} \cdot (B \cdot \dot{\gamma})$ (2.16)

De Kee $\tau = \tau_y + \mu_p \cdot \dot{\gamma} \cdot \overline{e}^{\alpha\dot{\gamma}}$ (2.17)

Vom Berg $\tau = \tau_y + B \cdot \sinh^{-1}\left(\frac{\dot{\gamma}}{C}\right)$ (2.18)

where A, B and C are constants, τ_y is a yield stress parameter, μ_p is the plastic viscosity, μ_∞ is the viscosity at infinite shear rate, α is a time dependent parameter, K is the "consistency" [Pa·s^n] and n is the power law index.
The Robertson-Stiff model becomes equal to the Bingham model n is equal to 1, giving τ_y equal to AB and the plastic viscosity as A. The model becomes equivalent to the Newton model when B is equal to 0 and n is equal to 1. Herschel-Bulkley also becomes equal to Bingham when n = 1.

Shear thinning and shear thickening behaviour can be evaluated with rheological models which do not have a term for the power law index, n. The Bingham model can for instance describe such behaviour if the plastic viscosity is calculated at both low (μ_{pl}) and medium (μ_{pm}) shear rate ranges. The viscosity dependence of shear rate can then simply be evaluated by the ratio μ_{pm}/μ_{pl} where

$\mu_{pm}/\mu_{pl} < 1$ means shear thinning behaviour (thinking from low towards high rate).
$\mu_{pm}/\mu_{pl} = 1$ means no dependence of shear rate.
$\mu_{pm}/\mu_{pl} > 1$ means shear thickening behaviour.

Turian et al. (1997) investigated the rheology of concentrated aqueous slurries of titanium dioxide, laterite, gypsum and silica flour. The two-parameter power law, Bingham plastic and Casson models and the three-parameter Herschel-Bulkley and Sisko models were tested.

The Sisko model which combines low- and intermediate shear power law with high shear Newtonian limiting behaviour, was found to provide the best overall description of the flow curves for all slurries, at all solid loadings and over the entire range of shear rates.

Yahia and Khayat (2001) evaluated the effectiveness of various rheological models to estimate yield stress of high-performance cement grouts containing supplementary cementitious materials and rheology-modifying admixtures. The rheological models considered in the investigation included Bingham, Casson, Herschel-Bulkley and De Kee as well as a model proposed by the authors. Different estimates of the yield value were obtained when using the different models. The Bingham model resulted in higher yield stress estimates than the other models, while the Herschel-Bulkley model resulted in the lowest values for all tested mixtures.

Atzeni et al. (1985) found from their investigations that the best results for fitting the rheological data of Portland cement pastes were obtained with Eyring's, Herschel-Bulkley and the parabolic equation, while Vom Berg's model only held for low shears. The authors proposed another equation derived from Eyring's, but explicitly containing the yield stress term.

Yahia and Khayat (2003) investigated the Bingham, Herschel-Bulkley, Casson, Eyring, Robertson-Stiff, De Kee and Vom Berg model on high-performance grouts containing supplementary cementitious materials and viscosity enhancing admixture. They found that none of the evaluated models could enable accurate fitting of shear stress-shear rate data of all investigated mixtures. Difficulties were mostly encountered modeling the non-linear portion of the flow curve observed at the low shear rate range.

Thus, researchers have not agreed upon a rheological model which satisfactorily describes the flow of cementitious paste. Many researchers are in effect using the Bingham and Herschel-Bulkley model due to their simplicity.

2.4.3 Time effects

A gradual decrease of the viscosity under shear stress followed by a gradual recovery of structure when the stress is removed is called "thixotropy". The opposite type of behaviour, involving a gradual increase in viscosity under stress followed by recovery, is called "rheopexe", "negative thixotropy" or "anti-thixotropy". Thixotropy usually occurs in circumstances where the liquid is shear-thinning. In the same way, anti-thixotropy is usually associated with shear-thickening behaviour. Thixotropy is given various meanings in industry, but the following definition is taken from Mezger (2002): *Thixotropic behaviour means the reduction in structural strength during the shear load phase and the more or less rapid, but complete, structural regeneration during the subsequent rest phase.* This decomposition/regeneration cycle is a completely reversible process. Fig. 2.25 illustrates thixotropic behaviour.

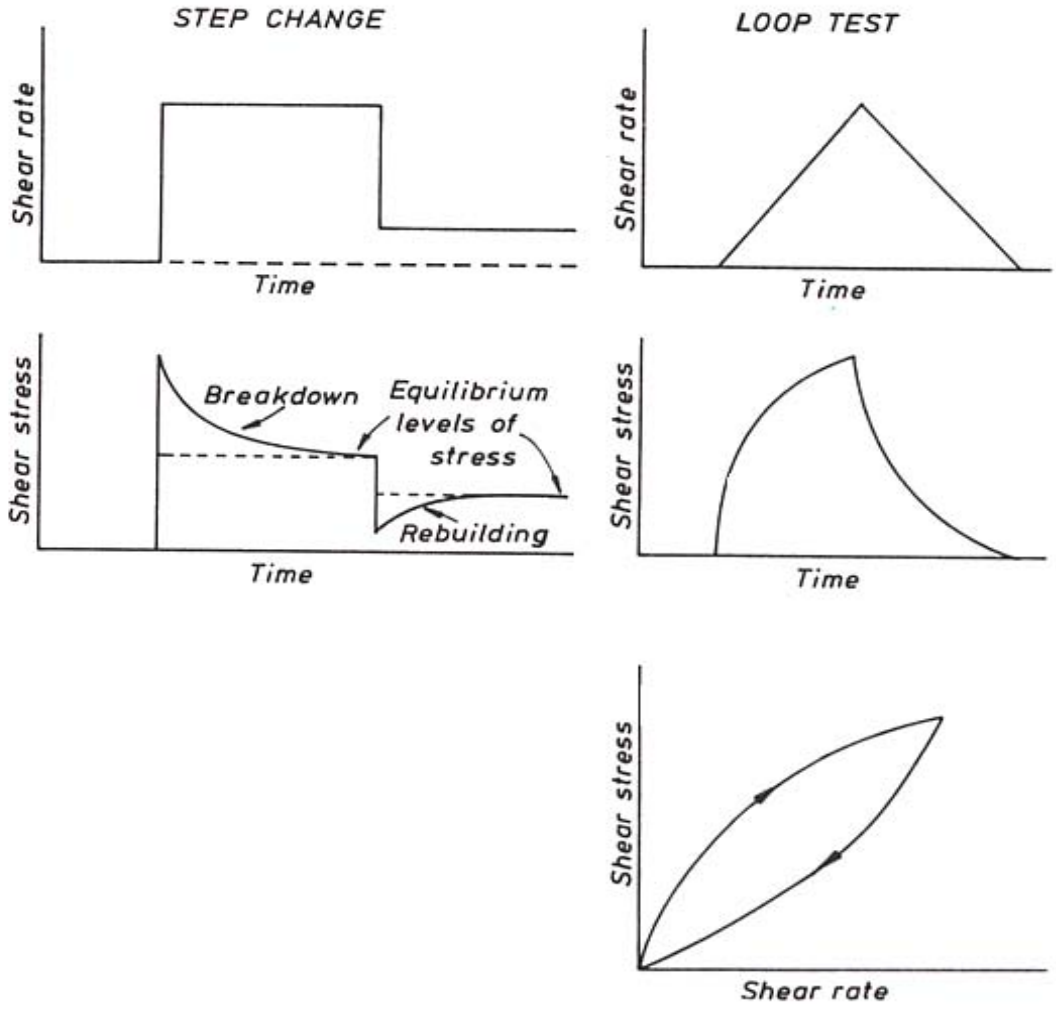

Fig. 2.25: Schematic representation of the response of an inelastic thixotropic material to two shear rate histories (Barnes 1989)

Cement pastes are known to show thixotropic behaviour (Banfil 1994, Wallevik 2000, Collepardi 1971). Thixotropic behaviour is present whenever the paste is allowed to hydrate without agitation while an anti-thixotropic one is obtained if the paste is mechanically agitated during the hydration process. Thus, during hydration at rest a structure is formed in the paste that can be at least partially broken down even by a mild agitation.

Banfil (1994) stressed that the rheological data measured at any instant depend upon the previous shear history of the sample. The area in the hysteresis loop has the dimensions of "energy" related to the volume of the sample sheared which indicates that energy is required to break down the thixotropic structure. A hysteresis loop gives evidence only that the structural breakdown has occurred during the test and an infinite number of different loops are possible depending on the experimental details. Therefore hysteresis loops cannot unambiguously characterize structural breakdown.

Banfil and Saunders (1981) found hysteresis loops of three main types, depending on the length of time taken to complete a shear cycle. At short cycle times the downcurve was at lower stress levels than the upcurve (structural breakdown), while at long cycle times they are reversed (structural build up). At intermediate cycle times the lines crossed, and double or

triple loops may be obtained. The variations of loop shape with cycle time depend on cement type. Banfill and Saunders recommended that hysteresis loops should not be used in viscometric study of cement pastes other than at short cycle times (<2 minutes) where the shape of the loop is reproducible between cements.

2.4.4 Rheology of suspensions

Some important factors affecting cement paste rheology are summarized as follows (Nehdi and Rahman 2004**,** Collepardi et al. 1971, Sheinn et al. 2002, Greszczyk and Kucharska 1990):

- Water-solid ratio
- Chemical composition of cement
- Chemical reactivity of filler
- Particle size distribution, specific gravity, surface texture and geometrical shape of powders (cement and fillers)
- Properties of chemical admixtures
- Hydration time
- Temperature and humidity of the place where the paste is prepared and placed
- Initial mixing conditions, such as mixing procedure, mixer speed, duration and capacity
- Testing procedure such as test duration, measuring elements, extent of agitation during the period of hydration, geometry of the test accessory, the gap and friction capacity of its shearing surfaces

It has been shown that the most important of the factors listed above are the w/c ratio and specific surface. Studies performed on cement pastes of different chemical composition indicated this factor bears a less effect on the rheology than w/c ratio and/or fineness of cement (Banfill 1981, Collepardi 1971).

The flow behaviour of Portland cement as a function of its concentration was studied by Struble and Sun (1995). They found the relationship between viscosity and concentration to be well described by the Krieger-Dougherty (1959) equation;

$$\frac{\eta}{\eta_c} = \left(1 - \frac{\varphi}{\varphi_m}\right)^{-[\eta]\varphi_m} \tag{2.19}$$

where η_c is the viscosity of the continuous phase (1 cP for water at 20°C), φ_m is the maximum volume concentration of solids (about 0.65) and $[\eta]$ is the intrinsic viscosity of the suspension given by

$$[\eta] = \lim_{\varphi \to 0} \frac{\frac{\eta}{\eta_c} - 1}{\varphi} \tag{2.20}$$

where η is the apparent viscosity of the suspension, η_c is the viscosity of the continuous phase (i.e. liquid), φ is the concentration of solids by volume and φ_M is the maximum solids concentration by volume.

The maximum solid volume fraction, φ_M, depends on the particle size distribution and particle shape, and falls typically between 0.6 to 0.7 for monosized spherical particles.

The intrinsic viscosity, $[\eta]$, also depend on particle shape, being 2.5 for a spherical particle.

Thus, all independent variables in the Krieger-Dougherty equation; concentration, particle size distribution and particle shape, relate to the density at which particles are packed in suspension. However, there is no theoretical basis for calculating φ_M for polydisperse particles; it can only be determined empirically from viscosity values measured at various volume fractions.

Both parameters in the Krieger-Dougherty equation, φ_M and $[\eta]$, depend on shear (whether strain rate or stress). Barnes et al. (1989) summarized data for spherical index particles in which φ_M was shown to be 0.63 at $\tau \rightarrow 0$ and 0.71 at $\tau \rightarrow \infty$. They noted that the maximum volume fraction of monodisperse spheres depends on the particular geometric arrangement; ranging from 0.52 for simple cubic to 0.74 for face-centered cubic. Thus, it is reasonable that randomly packed spheres will pack more densely when subjected to a higher shear stress.

Hinch and Leal (1972) showed how $[\eta]$ varied with the aspect ratio of the particle. For an aspect ratio of unity (i.e. spheres), $[\eta]$ does not vary with shear level. However, for low aspect ratios (i.e. disc shaped) and high aspect ratios (i.e. rod shape), $[\eta]$ decreases with increasing shear, reflecting the tendency of anisotropic particles to be aligned by the shear and thereby offer an average volume lower than that provided by the same particles randomly oriented.

The Krieger-Dougherty equation was derived for dispersed particles, in which particle interactions are limited to random effects produced by Brownian movements. However, the equation is valid for flocculated suspensions, but the constants do not have the same physical significance (Ball and Richmond, 1980).

The dispersed cement slurries investigated by Struble and Sun (1995) gave values for φ_M ranging from 0.64 to 0.80 (average 0.7), and values for $[\eta]$ ranging from 4.5 to 6.0 (average 5). Pastes that were not dispersed (i.e. without naphthalene sulphonate-formaldehyde condensate) were found to be considerably higher in viscosity.
Justnes and Vikan (2005) found similarly that the Krieger-Dougherty equation is able to describe the influence of solids concentration on apparent viscosity of cement slurries well as illustrated in Fig. 2.26. Measurements shortly after mixing, using high shear mixer and plasticizers to ensure good dispersion gave reasonable values for the variables, in particular if the shear rates were not too low ($> 90\ s^{-1}$). The estimated maximum volume fractions of solids, φ_M, ranged from 0.5 to 0.6 and intrinsic viscosity, $[\eta]$, at about 5. The liquid viscosity seemed to be estimated too high when compared with measurements on the pore water. This can be due to the formation of hydration products which occurs immediately after contact with water consuming water and forming solids and thereby in a twofold manner increasing the concentration of solids. For instance as elucidated by Justnes et al. (2003), 3% hydration will increase apparent viscosity from 42.4 to 52.3 mPa·s (23 % increase) when average

density of hydration products is assumed to be 2.67 kg/m^3 and 40 % water is bound per anhydrous cement reacted (probably higher since ettringite dominates the early reactions).

Hunter (1989) proposed that the lower maximum volume fraction of a flocculated suspension is an indication of the openness of the agglomerated structure, even for viscosity measured at high strain rate, and that shear thinning behaviour of flocculated suspensions at low strain rates is due to breaking of bonds between individual agglomerates.

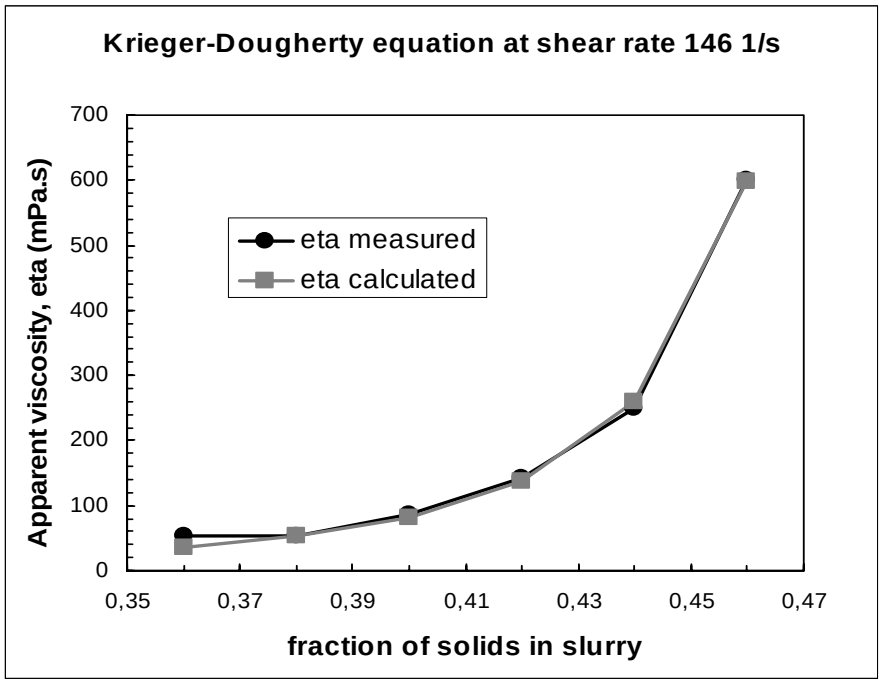

Fig. 2.26: Measured and calculated apparent viscosity (η, eta) for cement slurries as a function of volume fraction of solids (φ) at a shear rate ($\dot{\gamma}$) of 146 s^{-1}.

2.4.5 Influence of mixing methods

Yang and Jennings (1995) investigated the relationship between mixing methods, rheological properties and microstructure of cement paste. When they mixed a cement paste with w/c = 0.37 at a constant shear rate of 2 s^{-1}, a peak stress (i.e. gel strength) was observed before the equilibrium stress was obtained after 30 s as shown in Fig. 2.27. They also found that the peak stress was higher for less effective mixing methods (e.g. hand versus high-energy blender) and that it increased with time. As seen from Fig. 2.27, pastes made by hand mixing sieved cement had nearly the same peak stress as that made by the high-energy blender. This suggests that agglomerates could be responsible for the higher values and the faster increase in the peak stresses.

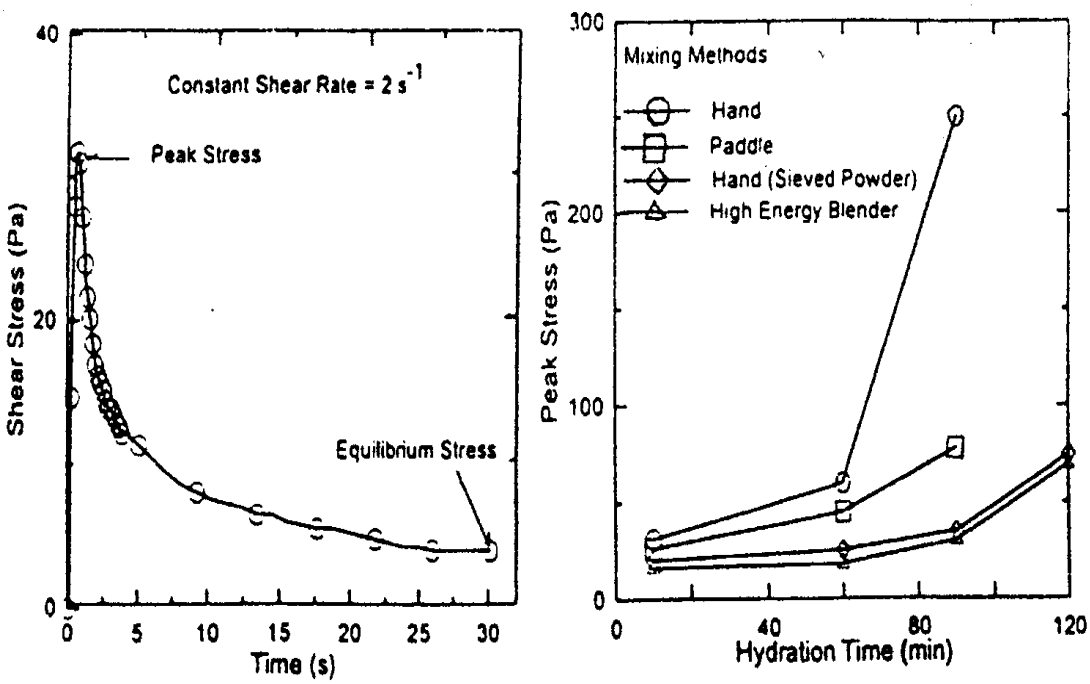

Fig. 2.27: Shear stress versus time of cement paste under a constant shear rate (left) and influence of mixing methods on the peak stress of cement paste (right) (Yang and Jennings, 1995).

Tadmore and Gogos (1979) pointed out that forces to break the structure of agglomerates are transmitted through the fluid during mixing. In the case of two particles forming a dumbbell, the maximum dispersive force, F_{max}, for a steady shear flow of a Bingham plastic slurry is;

$$F_{max} = 3\pi R_1 R_2(\tau_y + \mu_p \cdot \dot{\gamma}) \qquad (2.21)$$

where R_1 and R_2 are the two radii of the particles, μ_p is the plastic viscosity, τ_y is the yield shear stress and $\dot{\gamma}$ is the shear rate.

Roy and Asaga (1979) investigated the effects of mixing procedures on viscometric properties of cement slurries with and without SNF as dispersant. They found that in the absence of a dispersant, yield stress and plastic viscosity decreased substantially with increased intensity of mixing which caused a break down of particulate agglomerates. However, with the dispersant present, the rheological properties of already well-dispersed mixes did not change much with increasingly intense mixing.

The increasing viscosity of paste with increasing cement fineness (see Fig. 2.28) and increasing viscosity with decreasing w/c-ratio (see Fig. 2.29) as reported by Justnes et al (1992) confirms the preceding theory.

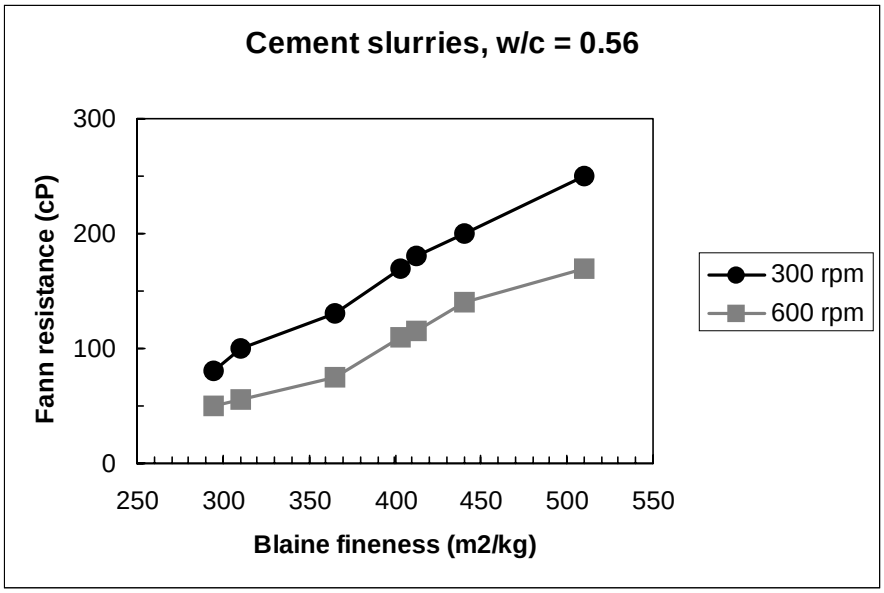

Fig. 2.28: Rheology of cement paste (w/c = 0.56) as a function of the fineness (m^2/kg) of the cement according to Justnes et al. (1992).

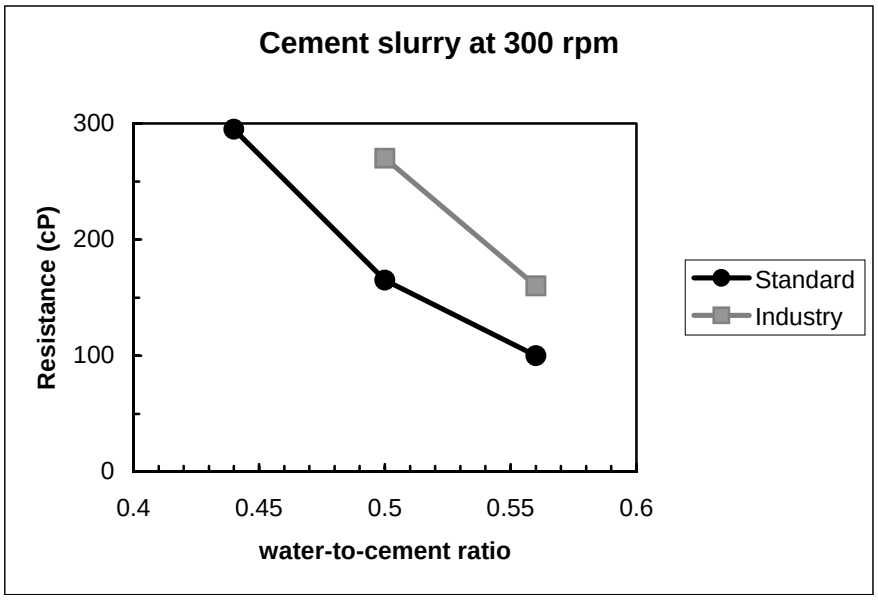

Fig. 2.29: Rheology of cement paste (Fann-viscometer at 300 rpm) as a function of w/c for two different cements after Justnes et al. (1992).

Chapter 3

Materials, apparatus and experimental program

3.1 Main cements

Six cements have been studied in the main parts of the thesis. Their physical characteristics are given in Table 3.1, chemical analysis according to producer and minerals by Bogue estimation is given in Table 3.2 and the mineralogy of the cements determined by multicomponent Rietveld analyses of XRD profiles, specific surface determined by the Blaine method and content of easily soluble alkalis determined by plasmaemissionspectrometry are given in Table 3.3.

Table 3.1: Physical characteristics of Portland Cements according to EN 196

Cement no.	1	2	3	4	5	6
Cement type	CEM I 42.5 RR	CEM I 42.5 R	CEM II A-V 42.5 R	CEM I 52.5 R-LA	CEM I 42.5 R-LA	CEM I 42.5 N
Fineness:						
Grains +90µm	0.1%	2.9%	0.0%	1.7%	0.0%	0.0%
Grains +64µm	0.5%	6.6%	0.2%	4.1%	0.6%	3.8%
Grains -24µm	89.2%	63.1%	83.0%	66.3%	86.6%	-
Grains -30µm	94.8%	71.2%	90.3%	75.6%	93.3%	-
Blaine (m^2/kg)	546	360	467	359	450	315
Water demand	32.0%	26.8%	29.4%	26.7%	28.2%	27.2%
Le Chatelier	0 mm	0 mm	0.3 mm	0.5 mm	0.0 mm	1.0 mm
Initial set time	115 min	140 min	125 min	145 min	100 min	171 min
σ_c (MPa) at						
1 day	32.7	19.7	22.5	17.1	21.7	-
2 days	39.9	32.7	32.1	27.5	32.5	26.8
7 days	49.3	43.5	43.8	42.5	46.1	-
28 days	58.9	51.2	57.1	58.6	62.0	59.2

Table 3.2: Chemical analysis (%) of the Portland cements according to producer and minerals (%) by Bogue estimation.

Cement no.	1	2	3	4	5	6
Cement Type	CEM I 42.5 RR	CEM I 42.5 R	CEM II A-V 42.5 R	CEM I 52.5 R-LA	CEM I 42.5 R-LA	CEM I 42.5 N
Chemical Analyses						
CaO	61.98	62.25	-	63.71	63.15	63.3
SiO_2	20.15	19.69	-	20.92	21.98	19.7
Al_2O_3	4.99	4.55	-	4.21	3.47	5.3
Fe_2O_3	3.36	3.41	-	3.49	5.13	2.7
SO_3	3.55	3.43	2.68	2.67	2.26	2.7
MgO	2.36	2.32	-	1.87	1.56	1.9
Free CaO	1.23	0.87	0.78	0.84	0.94	-
K_2O	1.08	1.15	-	0.46	0.54	0.87
Na_2O	0.42	0.41	-	0.19	0.21	0.33
Equiv. Na_2O	1.13	1.17	-	0.49	0.57	0.90
Cr^{6+} (ppm)	0.00	5.30	5.00	0.30	-	-
Carbon	0.04	0.55	-	0.17	-	-
Chloride	0.03	-	-	0.02	-	0.03
LOI	1.34	2.93	1.82	1.72	0.90	-
Fly Ash	-	-	16.3	-	-	-
Minerals by Bogue[1]						
C_3S	50.7	48.1	-	50.4	53.0	51.0
C_2S	19.5	20.2	-	22.0	23.0	18.0
C_3A	7.5	6.3	-	5.3	0.5	9.5
C_4AF	10.2	10.4	-	10.6	15.6	8.2
$C\overline{S}$	7.7	7.4	-	5.8	4.9	5.8

[1]Taking into account SO_3 and $CaCO_3$ from QXRD (Table 3.3)

Table 3.3: Mineral composition (%) and alkali content of Portland cements obtained by QXRD and Plasmaemissionsspectrometry

CEMENT NO.	1	2	3	4	5	6
Cement Type	CEM I 42.5 RR	CEM I 42.5 R	CEM II A-V 42.5 R	CEM I 52.5 R-LA	CEM I 42.5 R-LA	CEM I 42.5 N
Alite	64.7	66.0	60.3	65.0	61.9	51.6
Belite	14.8	9.4	7.1	12.9	19.7	17.3
Ferrite	7.5	8.7	7.1	9.6	12.0	5.4
Cubic Aluminate	5.9	3.4	3.1	0.5	0.4	3.6
Orthorhombic Aluminate	1.1	1.7	3.4	3.0	1.7	8.7
Lime	1.0	1.2	0.2	0.6	0.7	0.4
Periclase	1.6	1.2	1.7	0.3	0.4	0.9
Gypsum	0.0	0.2	0.0	1.4	1.3	3.2
Hemihydrate	1.8	2.0	2.1	1.5	0.4	1.2
Anhydrite	0.6	0.5	0.4	0.4	0.4	0.8
Calcite	0.5	4.6	0.6	4.0	0.7	4.3
Portlandite	0.3	0.4	0.5	0.3	0.2	0.4
Quartz	0.0	0.4	1.5	0.4	0.2	0.4
Arcanite	0.3	0.4	0.1	0.0	0.0	1.8
Mullite	-	-	2.6	-	-	-
Amorphous	-	-	9.3	-	-	-
Blaine	546	360	467	364	447	308
K (%)	0.92	0.88	0.58	0.32	0.36	0.42
Na (%)	0.22	0.17	0.12	0.74	0.84	0.04
Na_{eqv} (%)	0.76	0.69	0.46	0.26	0.30	0.29

Experiments were performed to investigate the influence of the surface area on the rheological properties. Table 3.4 gives the characteristics of 4 cements made of the same clinker, but ground to different fineness.

Table 3.4: Characteristics of the 4 cements made of the same clinker, but ground to different fineness (Blaine).

Blaine	Sulfur	Free lime	Loss of ignition	SiO_2	Al_2O_3	Fe_2O_3	CaO	K_2O	MgO	Na_2O	Alkali
496	2.97	0.90	1.11	20.47	4.83	3.34	62.48	1.06	2.29	0.45	1.15
444	2.92	0.90	1.06	20.50	4.87	3.33	62.47	1.07	2.30	0.44	1.14
392	2.94	0.81	1.15	20.47	4.77	3.34	62.44	1.06	2.26	0.45	1.15
356	3.00	0.69	1.17	20.10	4.60	3.28	62.48	1.05	2.21	0.41	1.10

3.2 Main plasticizers

Three different categories of plasticizers have been studied namely

- Sodium lignosulphonate sugar reduced and molecular size enriched by ultra filtration. Molecular weight of the polymer was 51,000.
- Sodium naphthalene sulphonate – formaldehyde condensate (SNF) in water solution with 42 % solids. The number of structural units (n) in the SNF molecule was presumably between 10 and 20. The molecular weight is 2,350 for n = 10 (number of structural units) and 4,700 for n = 20.
- -Polyether grafted polyacrylate (PA1) containing 25% solids. No stabilizer was added and the molecular weight was 250,000.
  -Polyether grafted polyacrylate (PA2) water solution containing 18 % solids and a viscosifying agent. The molecular weight of the polyacrylate was 220,000.

3.3 Rheometer

All rheological measurements have been performed with a MCR 300 rheometer produced by Physica as illustrated by Fig. 3.1. A parallel plate measuring system was chosen as illustrated in Fig. 3.2. The surfaces of both the bob and the motionless plate were flat, but the upper plate had a serrated surface of 150 μm depth to avoid slippage.

The geometry of the plate is determined by the plate radius, R. The radius of the upper plate was 3 cm. The distance, H, between the plates must be H<<R and have been recommended to be at least 10 times larger than the largest of the particles in the sample (Mezger 2002). The average particle size of unhydrated cement is approximately 10 μm (Taylor (1990). The gap between the plates was therefore set to 1 mm for all measurements. The bottom plate was temperature controlled.

The parallel plate measuring system was chosen since it is able to measure dispersions containing relatively large particles as well as samples with three-dimensional structures. The disadvantage of the measuring system is however that there is no constant shear gradient in the gap because the shear rate (or shear deformation) increases in value from zero at the center of the plate to the maximum at the edge. Another disadvantage is that several unwanted phenomena can occur at the edge of the plate such as: inhomogeneities, emptying of the gap, flowing-off and spreading of the sample, evaporation of solvents, or skin formation. The upper and lower plates were thus covered with a plastic ring and a metallic lid in order to reduce evaporation from the paste while a water trap attached to the upper plate was filled with water to ensure saturated water pressure.

Fig. 3.1: MCR 300 rheometer.

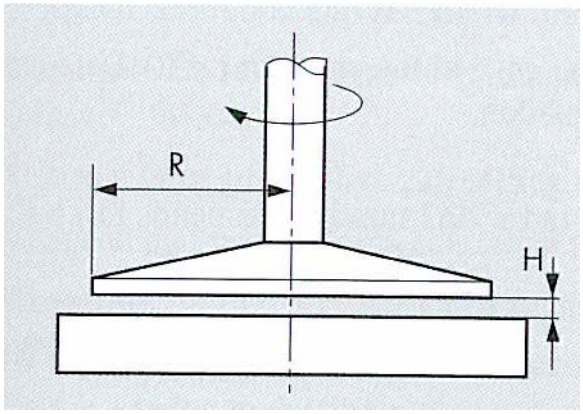

Fig. 3.2: The parallel plate measuring system (Mezger 2002).

3.3.1 Mixing and measurement sequence

The cements were blended in high shear mixers by Tefal (Rondo 500) and Braun (MR5550CA) as illustrated in Fig. 3.3. The mixers had a rotational speed of approximately 800 rpm. The same blender was used within each measurement series to ensure reproducible mixing. The following chapters will notify which of the blenders which has been used.
The blending was performed by adding solids to the water and mix for ½ minute, resting for 5 minutes and blending again for 1 minute. Total paste volume was approximately 200 ml.

Fig. 3.3: High shear blenders from Tefal (left) and Braun (right)

The following measurement sequence lasted 25 minutes and was performed on most of the pastes. The measurement sequence was often repeated 4 times in order to measure time dependencies:

1. 1 minute with constant shear rate ($\dot{\gamma}$) of 100 s^{-1} to stir up the paste
2. Stress (τ) – shear rate ($\dot{\gamma}$) curve with linear sweep of $\dot{\gamma}$ from 200 down to 2 s^{-1} in 30 points lasting 6 s each (down curve).
3. Stress (τ) – shear rate ($\dot{\gamma}$) curve with linear sweep of $\dot{\gamma}$ from 2 up to 200 s^{-1} in 30 points lasting 6 s each (up curve).
4. 10 s resting as 5 points lasting 2 s each had no recording.
5. Shear rate ($\dot{\gamma}$) – stress (τ) curve with logarithmic sweep of τ from 0.2 to 50 Pa in 46 points lasting 5 s each to measure gel strength after 10 s rest.
6. Oscillatory time sweep with 30 points lasting 20 s each with amplitude γ = 0.1 % and angular frequency ω = 6 s^{-1} measuring storage (G') and loss (G") moduli (not discussed in the thesis since amplitude sweeps were not performed to determine the limit of the linear viscoelastic range. Unstable measurements may be the result if the amplitude is too high.).

7. Shear rate ($\dot{\gamma}$) – stress (τ) curve with logarithmic sweep of τ from 0.5 to 200 Pa (range may vary) in 60 points lasting 5 s each to measure gel strength after 10 minutes rest (i.e. oscillation).

The mixing and measurement sequence is illustrated in Fig. 3.4. Some measurement sequences done early in the work are somewhat shorter than the one given here. This will be notified in the given chapters.

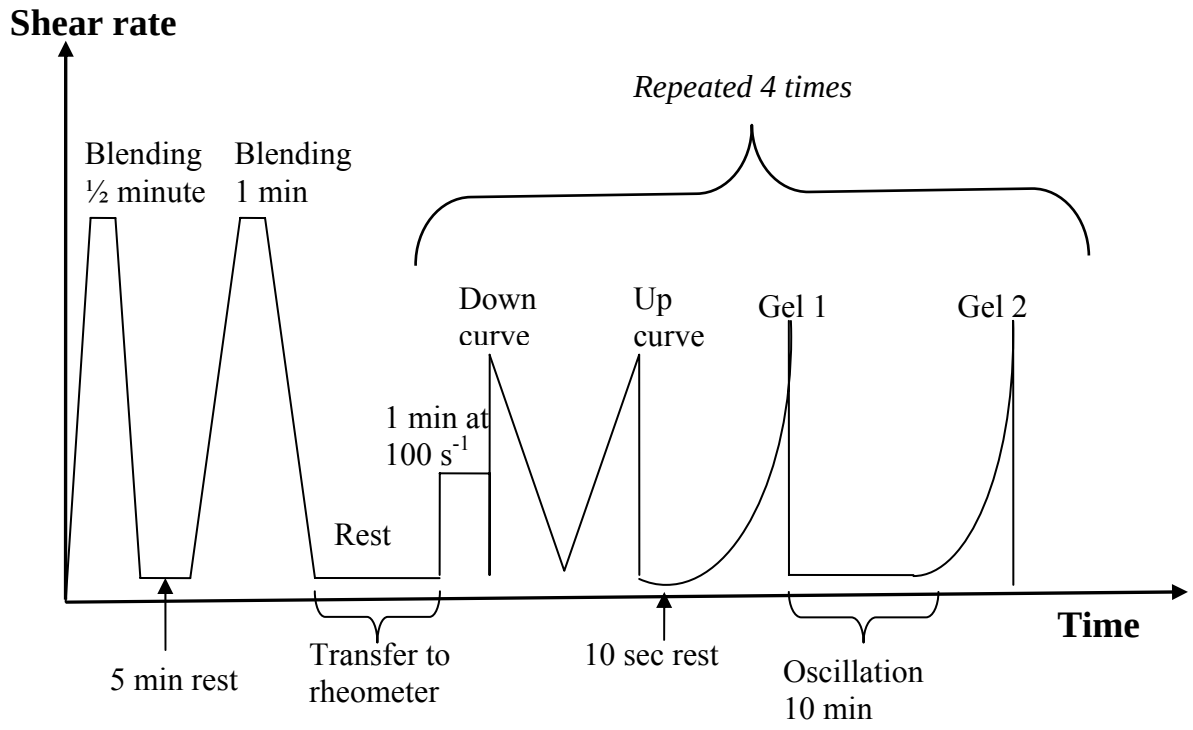

Fig. 3.4: Flow chart of the measurement sequence

3.4 Viscometer

The viscosity of the pore water was not measured by the Rheometer due to the risk of the sample to flow off from the gap during the measurement. The kinematic viscosity (m^2/s) of the pore water was therefore measured with an Ostwald viscometer with inner diameter of 0.3 mm (Fig. 3.3) produced by Schott-Geräte. 3 ml of the sample was filled in the wider one of the tubes. The viscometer was thereafter suspended into a temperature bath for 10 minutes to ensure equalization of the temperature. The liquid was then siphoned above the upper measuring mark on the thinner tubes. The flow time between the two timing marks was then measured. The kinematic viscosity was calculated by

$$\nu = K \cdot (t - \upsilon) \tag{3.1}$$

were K is a constant equal to 0.004 for the given capillary and υ is the Hagenback correction given by

$$\upsilon = \frac{0.12}{K \cdot t} \tag{3.2}$$

were t is the time in seconds.

The apparent viscosity (Pa·s) was derived by multiplying the measured density of the liquid with the kinematic viscosity. The density of the liquid was determined with a pycnometer (Fig. 3.3): The dry pycnometer was weighed on an analytical balance and thereafter filled with the liquid. The pycnometer containing the fluid was weighed again and the difference between this mass and the mass of the empty pycnometer was taken. Knowing the mass of the unknown fluid and the volume of the pycnometer, the density of the unknown fluid can be calculated using the equation

$$\rho = \frac{M}{V} \tag{3.3}$$

were ρ is the density, M is the mass and V is the volume of the liquid sample.

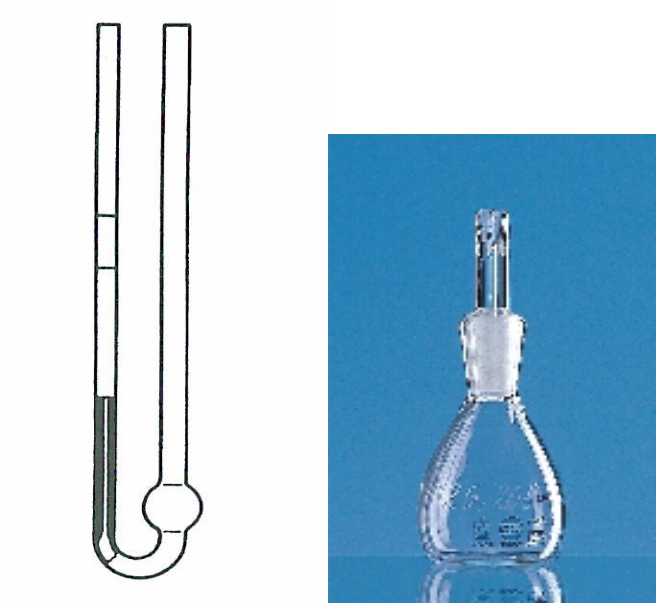

Fig. 3.3: Ostwald viscometer (left) and Pycnometer (right)

3.5 Calorimeter

An 8 channel TAM Air Isothermal Calorimeter from Thermometric AB, Sweden was used for the heat of hydration measurements. A cross section of the aperture is shown in Fig. 3.4.

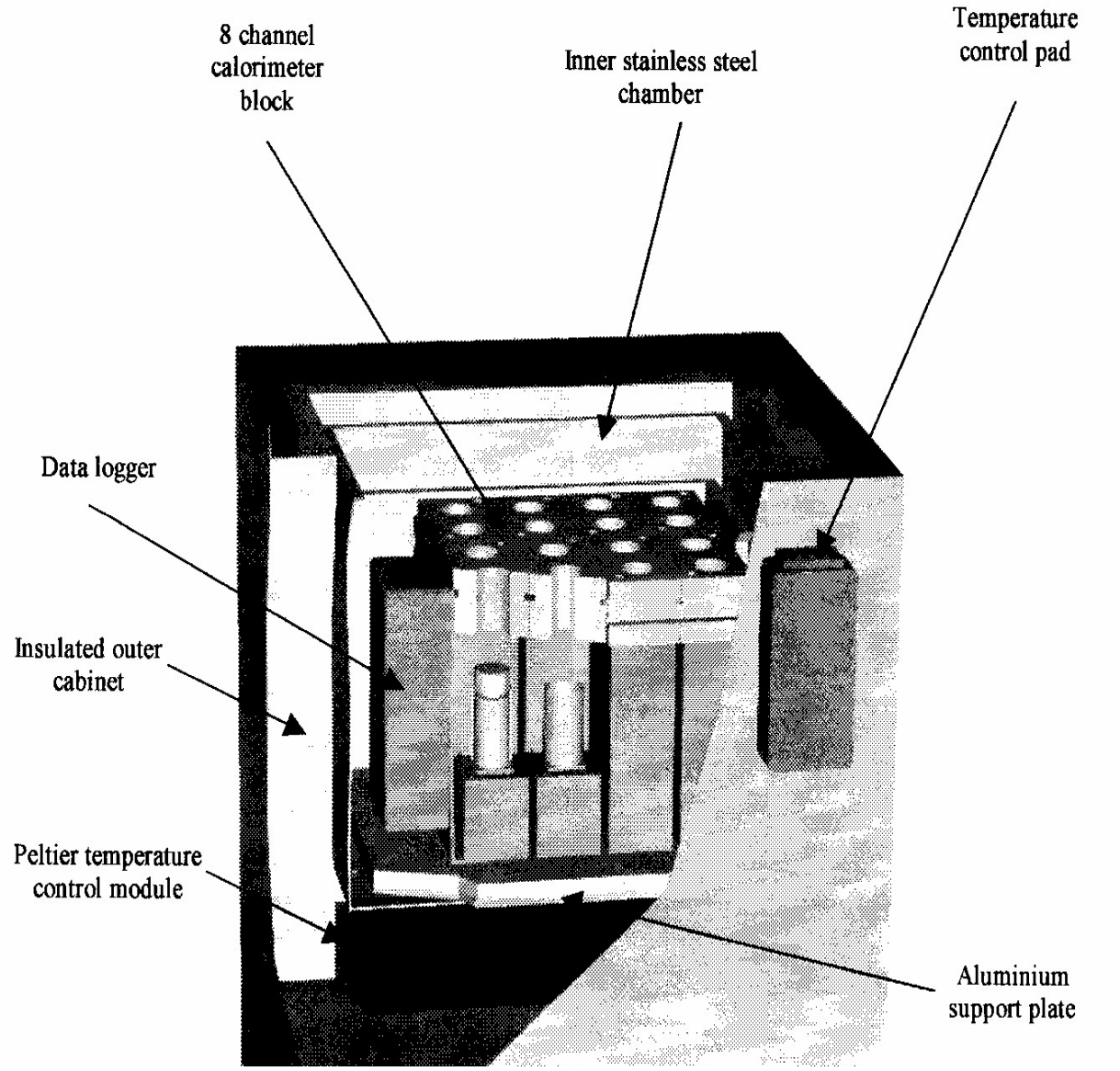

Fig. 3.4: Cross section of the Tam Air calorimeter

The calorimeter was calibrated at 20ºC whereby the baselines of the calorimeter were determined. The initial heat of hydration peak was measured separately from the following.

3.5.1 Measurement of the initial heat of hydration peak

5 grams of each of the cements 1-6 described by Table 3.1 and 3.2 and was weighed into glass ampoules which were loaded into the calorimeter. The ampoules were wiped with a paper napkin to make sure that they were perfectly clean and dry when they were inserted into the calorimeter. The three plasticizers SNF, lignosulfonate and polyacrylate were added to the cements in a dosage of 0.32% by cement weight. 2 ml of the water/plasticizer solution was added to the cements corresponding to a w/c = 0.4. The samples were then mixed internally in the calorimeter for to minutes with a stirrer produced by Thermometric AB. The heat of hydration was logged until the start of the dormant period which appeared approximately 1 hour after water addition.

3.5.2 Measurement of the main heat of hydration peaks

The cements 1-4 and 6 described by Table 3.1 and 3.2 were used for the measurements. Cement number 5 was not studied since it was not available at the time of measurement. 6 grams of each cement was weighed into glass ampoules. 2.40 grams of liquid was added to each sample (corresponding to w/c = 0.4) and the time noted when this was done. The dosage of superplasticizer was 0.0, 0.32% and 0.80% of cement weight for the three plasticizers lignosulfonate, polyacrylate and SNF. The samples were mixed in a motorized stirrer (IKA-WERK, RM 18 (60 Watt)) from Janke & Kunkel KG, for two minutes and the exact weight of the cements were noted. The ampoule was sealed with an aluminium cap and wiped with a paper napkin to make sure that it was perfectly clean and dry when it was inserted into the calorimeter. The heat of hydration measurement was logged until 72 hours after water addition.

3.6 Adsorption of plasticizers

The ultraviolet absorption spectrum of dilute aqueous solutions provides a method for the detection of aromatic and other UV-active (conjugated bonds) groups in superplasticizers. The UV spectra of different superplasticizers (SNF, SMF and lignosulfonate) are quite different and can be used for chemical identification purposes (Yilmaz et al. 1992, Bonen and Sarkar 1995). Polyacrylate-type products generally do not contain aromatic groups and do not show UV-adsorption in a readily accessible spectral region, i.e.>200 nm (Spiratos et al. 2003). The effect of pH on absorbance at 292 nm and 328 nm has been found to be negligible. Yilmaz et al. (1992) found, however, an increasing interference from OH^- ions at 227 nm especially at pH 14.

Various wave lengths have been used to study the adsorption of plasticizers on cement: Mannonen (1996), Chiocchio and Paolini (1985) and Nagataki et al. (1984) determined the total amount of bound and adsorbed SNF superplasticizer by measuring adsorption at 228 nm while Uchicawa et al. (1992) chose 293 nm for their investigations on β-SNF. Uchikawa et al (1992) and Reknes and Myrvold (2003) both chose 284 nm to investigate the adsorption of lignosulfonates. The adsorption studies in this present work utilized the wavelengths 292 nm for SNF and 283 nm for LS

A UV Spectrophotometer from Thermo Spectronic (illustrated in Fig. 3.5) was used to measure the adsorbed amounts of SNF and lignosulfonate on the cement.
The pore solutions were extracted from the cementitious pastes by filtering the pastes through 0.45 μm-filters 20 minutes after water addition. They were then diluted 100-200 times with a solution of "artificial pore water" (NaOH and KOH with a K/Na molar ratio equal to 2 and pH=13.2). The amount of superplasticizer in the water phase was read from the standard curve which had been made with a dilution series of SNF (290 nm) and lignosulfonate (283 nm). The difference between the added and measured content of superplasticizer gave the bound portion. The calibration curves for SNF and lignosulfonate can be found in Appendix A.4.

The adsorption of polyacrylate on cement was done by measuring Total Organic Carbon (TOC) left in the pore water with a Shimadzu TOC Analyzer 5000A. Preparation of pastes and measurement of rheology was done as described above. The pore water was filtrated from the pastes as described above, but diluted 1:10 with 0.1M HCl. The amount of plasticizer bound to the cement was calculated by difference between the added and the measured content of organic carbon.

Fig. 3.5: UV Spectrophotometer from Thermo Spectronic.

Chapter 4

Flow Resistance

Numerous rheological models have been proposed to describe cementitious materials as discussed in Chapter 2.4.5. The Bingham model has become very popular due to its simplicity and ability to describe cementitious flow. The model describes the shear stress (τ) as a function of yield stress (τ_y), plastic viscosity (μ_p) and shear rate ($\dot{\gamma}$) as follows:

$$\tau = \tau_y + \mu_p \cdot \dot{\gamma} \tag{4.1}$$

The concept of yield stress is sometimes a very good approximation for practical purposes. It is however clear that the Bingham model often only applies for limited parts of the flow curve if the tested material have shear thinning or shear thickening flow behaviour. Figure 4.1 illustrates how the Bingham model is dependent on the shear rate range for shear thickening materials. The shear thickening flow behaviour results furthermore in a negative yield stress values at the high shear rate which has no physical meaning. Fig. 4.2 shows similarly the strong effect of the shear rate range on the flow parameters of a shear thinning paste.
There has been raised a question whether or not a yield stress exists or whether all non-Newtonian materials will exhibit a finite zero-shear viscosity. Barnes and Walters (1985) states that the yield stress concept is an idealization and that given accurate measurements, no yield stress exists. They claim that even concentrated systems flow in the limit of very low stresses and that these materials appear not to flow merely because the zero shear viscosity is so high. Yahia and Khayat (2001) support this statement by finding that the yield stress correlated well to the apparent viscosity at low shear rate (5 s^{-1}).

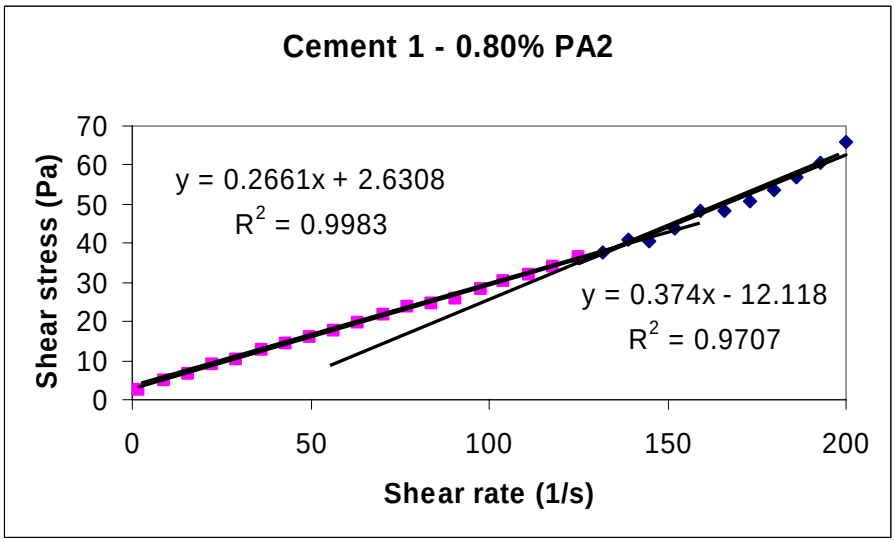

Fig. 4.1: Flow curve of CEM I 42.5 RR (Cement 1 described in Table 3.1-3-3) paste with w/c = 0.40 and 0.80% polyacrylate (PA) per weight of cement. The curve illustrates shear thickening flow and negative yield stress at high shear rates.

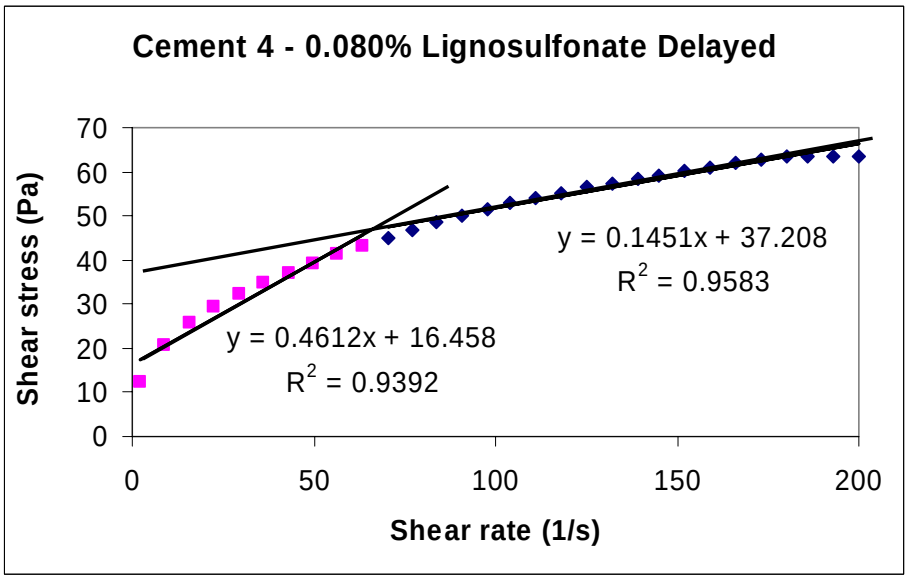

Fig. 4.2: Shear thinning flow curve of CEM I 52.5 R-LA (Cement 4 described in Table 3.1-3.3) paste with w/c = 0.40 and 0.08% lignosulfonate per weight of cement.

Thus, rather than describing the flow curve with the usual Bingham model, it was decided to use the area under the curve (Pa/s) as a measure of "flow resistance" in this thesis. The Bingham model has been applied to all rheological measurements performed and can be found in Appendix for comparative reasons. The question is whether area under the flow curve represents something more "physical" than an "apparent" yield stress from Bingham modeling.

In a parallel plate set-up with shear area, A [m^2], and gap h [m] between the plates;

$\tau = F/A$ [N/m^2 or Pa] (average shear stress over a shear rate interval) (4.2)

$\Delta\dot{\gamma} = v/h$ [$m/s \cdot m$ or s^{-1}] (shear rate difference over an interval) (4.3)

where F [N] is the force used to rotate the upper plate and v [m/s] is the velocity.

$$\text{Area under the curve} = \tau \cdot \Delta\dot{\gamma} = (F/A)\cdot(\Delta v/h) = F\cdot\Delta v/A\cdot h = F\cdot\Delta v/V \qquad (4.4)$$

where V [m^3] is the volume of the sample. The unit of the area under the curve is then [$N\cdot m/m^3\cdot s$ or $J/m^3\cdot s$ or W/m^3]. It is in other words the power required to make a unit volume of the paste flow with the prescribed rate in the selected range. The power, P [W], required to mix concrete for a certain time interval is actually sometimes measured by simply monitoring voltage (U [V]) and current (I [A]) driving the electrical motor of the mixer, since $P = U\cdot I$. The flow resistance could of course have been obtained at constant shear rate, but a shear rate range was used in order to compare with parameters from the Bingham model. An alternative is also to use the torque of the rheometer directly.
Table 4.1 and Fig. 4.3 show values of flow resistance, yield stress and plastic viscosity measured on cementitious pastes. The data show that there are linear correlations between the Bingham parameters yield stress and plastic viscosity with the flow resistance.

Table 4.1: Comparison of Flow Resistance versus the Bingham values for plastic viscosity and yield stress

Flow Resistance [Pa/s]	Viscosity [Pa·s]	Yield Stress [Pa]
6913	4.13	94.82
5409	3.02	79.34
2740	1.37	44.67
2002	0.78	38.01
904	0.37	16.89
783	0.27	16.00
492	0.26	7.70
352	0.24	1.94
156	0.17	0.16

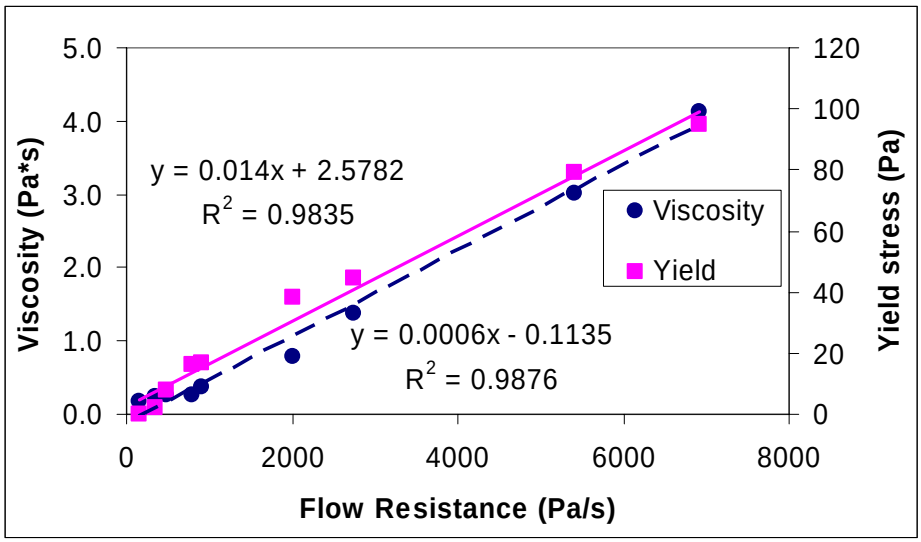

Fig. 4.3: Correlations of the plastic viscosity and yield stress derived from the Bingham equation at low hear rate range (6 measuring points from 43-8.8 s^{-1}) with the flow resistance.

Chapter 5

Reproducibility

5.1 Rheological measurements

Table 5.1-5.4 shows reproducibility data of four repeated rheological measurements on cement pastes. The rheological data has been transformed into Flow Resistance (area under the flow curve), plastic viscosity and yield stress from the Bingham model and gel strength measured after 10 minutes of rest (oscillation). The rheological data are measured in four intervals each lasting 25 minutes. The data show that the reproducibility of the Flow Resistance is reasonable. It can further be detected that the deviation is mainly dictated by the yield stress which have a much higher deviation than the viscosity. Measurements of the gel strength show high deviations. It can be noted that the parameters from the Flow Resistance and Bingham curves undergo a noticeable increase with time (interval 1-4) while the gel strength is not affected to the same extent.

Table 5.1: Reproducibility of Interval 1 at high and low shear rate range (152-118 s^{-1} and 43-8.8 s^{-1} respectively)

INTERVAL 1 **20 minutes after water addition**	**FLOW RESISTANCE**		**BINGHAM**				
	FR (high) (Pa/s)	**FR (low) (Pa/s)**	μ_p **(high) (Pa·s)**	μ_p **(low) (Pa·s)**	τ_y **(high) (Pa)**	τ_y **(low) (Pa)**	**Gel (Pa)**
	2417	1385	0.303	0.244	30.25	34.26	44.75
	2294	1269	0.301	0.232	26.92	31.19	47.10
	2332	1325	0.303	0.234	27.75	32.73	42.50
	2273	1275	0.299	0.233	26.47	31.31	38.40
average	**2329**	**1314**	**0.301**	**0.236**	**27.84**	**32.37**	**43.19**
Standard deviation	63	54	0.002	0.005	1.69	1.44	3.70
% std dev	**2.7**	**4.1**	**0.5**	**2.3**	**6.1**	**4.4**	**8.6**

Table 5.2: Reproducibility of Interval 2 at high and low shear rate range (152-118 s^{-1} and 43-8.8 s^{-1} respectively)

INTERVAL 2	**FLOW RESISTANCE**		**BINGHAM**				
45 minutes after water addition	**FR (high) (Pa/s)**	**FR (low) (Pa/s)**	μ_p **(high) (Pa·s)**	μ_p **(low) (Pa·s)**	τ_y **(high) (Pa)**	τ_y **(low) (Pa)**	**Gel (Pa)**
	2202	1258	0.246	0.253	31.62	30.31	34.70
	2007	1104	0.234	0.235	27.45	26.26	34.70
	2068	1172	0.233	0.242	29.39	28.06	34.70
	2023	1138	0.230	0.244	28.41	26.99	31.35
average	**2075**	**1168**	**0.236**	**0.243**	**29.22**	**27.90**	**33.86**
Standard deviation	88	66	0.007	0.007	1.79	1.77	1.67
% std dev	**4.3**	**5.7**	**2.9**	**3.1**	**6.1**	**6.3**	**4.9**

Table 5.3: Reproducibility of Interval 3 at high and low shear rate range (152-118 s^{-1} and 43-8.8 s^{-1} respectively)

INTERVAL 3	**FLOW RESISTANCE**		**BINGHAM**				
70 minutes after water addition	**FR (high) (Pa/s)**	**FR (low) (Pa/s)**	μ_p **(high) (Pa·s)**	μ_p **(low) (Pa·s)**	τ_y **(high) (Pa)**	τ_y **(low) (Pa)**	**Gel (Pa)**
	2336	1308	0.262	0.282	33.35	30.99	40.40
	2018	1096	0.236	0.247	27.48	25.67	29.80
	2125	1188	0.238	0.258	30.45	28.09	34.70
	2078	1155	0.232	0.262	29.74	27.01	32.95
average	**2139**	**1187**	**0.242**	**0.263**	**30.26**	**27.94**	**34.46**
Standard deviation	138	90	0.013	0.015	2.42	2.26	4.45
% std dev	**6.5**	**7.5**	**5.6**	**5.5**	**8.0**	**8.1**	**12.9**

Table 5.4: Reproducibility of Interval 4 at high and low shear rate range (152-118 s^{-1} and 43-8.8 s^{-1} respectively)

INTERVAL 4 **95 minutes after water addition**	**FLOW RESISTANCE**		**BINGHAM**				
	FR (high) (Pa/s)	**FR (low) (Pa/s)**	μ_p **(high) (Pa·s)**	μ_p **(low) (Pa·s)**	τ_y **(high) (Pa)**	τ_y **(low) (Pa)**	**Gel (Pa)**
	2610	1437	0.303	0.324	35.82	33.67	44.75
	2071	1124	0.242	0.258	28.28	26.25	32.95
	2275	1267	0.254	0.280	32.58	29.86	47.10
	2223	1234	0.230	0.244	28.41	26.99	44.75
average	**2295**	**1265**	**0.257**	**0.276**	**31.27**	**29.19**	**42.39**
Standard deviation	227	130	0.032	0.035	3.63	3.37	6.39
% std dev	**9.9**	**10.2**	**12.5**	**12.7**	**11.6**	**11.5**	**15.1**

5.2 Viscometric measurements

The flow time through the viscometer was measured 4 times for cement pore water at 40^{o}C. The flow times were 174, 170, 172 and 173 seconds giving a standard deviation of 1.71 (corresponding to 0.99%).

Table 5.5 shows that there is a deviation of 13% between measured viscosities of distilled water in the temperature range of 15-43^{o}C and tabulated data given by Weast (1978). Thus, measured viscosities on pore water are most likely 13% lower than the actual values.

Table 5.5: Measured viscosities of distilled water at different temperatures compared by viscosities given by Weast (1978)

Temperature (^{o}C)	**Measured viscosity (mPa·s)**	**Tabulated viscosity (mPa·s)**	**Deviation (%)**
15	0.979	1.139	14
25	0.778	0.8904	13
33	0.648	0.7491	13
43	0.543	0.6178	12

5.3 Adsorption measurements by UV Spectrophotometry

Adsorption measurements were performed on four individual CEM I 42.5 RR pastes (cement 1 in Table 3.1-3.3) with 0.80% SNF by cement weight. The results are given in Table 5.6:

Table 5.6: Reproducibility of adsorption measurements

Paste no.	Adsorbance	Adsorbed SNF (% of added)	Standard deviation	% St.dev
1	2040	54.1	0.65	1.20
2	2018	54.7		
3	2083	53.1		
4	2059	53.7		

Chapter 6

Effect of silica fume on the rheology of cementitious paste

6.1 Introduction

The objective of this part of the present study was in relation to self-compacting concrete (SCC) technology to investigate the effect of silica fume (SF) on the rheology of cement pastes. The pastes were plasticized by polyether grafted polyacrylate (PA) recommended for SCC and compared with a common superplasticizers like naphthalene sulphonate – formaldehyde condensate (SNF).

SF is focused on since the Norwegian SCC technology utilises silica fume for stabilisation, while other countries rather use high amounts of fillers like limestone. Thus, the effect of limestone filler replacing cement was investigated as well. The approach was fundamental by keeping the volume fraction of solids constant within each series and replacing cement with limestone and SF in volume increments. In this way it should be easier to see effects of fineness, particle packing and surface chemistry. Pure limestone slurries were prepared as inert slurries to study effects not disturbed by surface hydration. The effect of pH on the limestone pastes was studied by modifying the mix water.

Reported research on the effect of SF on paste rheology seems limited, while some have been done on concrete (Wallevik 1990, and Nehdi et al. 1998). Zhang and Han (2000) investigated the effect of a number of fine mineral admixtures on cement paste rheology using the Casson equation (Eq. 2.14). They used w/(c+s) = 0.25, 10 % SF and 5 % high performance superplasticizer and found that both viscosity and yield point *decreased* relative to pure cement paste. Park et al. (2005) found on the other hand for cementitious pastes with constant water to binder ratio of 0.35 and 2 % polynaphtalene sulphonate based plasticizer that the yield stress and plastic viscosity *increased* steeply with increasing SF replacement. Cyr et al (2000) focused on the shear thickening effect of superplasticizers on the rheological behaviour of cement pastes with and without mineral additives using the Herschel-Bulkley equation (Eq. 2.12). They replaced cement with 10 and 25 % silica fume, varied w/b while keeping the superplasticizer dosage constant (3 %), and found that SF lead to a small shear thinning effect. Salem (2002) investigated the rheology of OPC-SF system with high replacement rates of 10, 20, 30 and 50 % and w/(c+s) of 0.6 and 0.8. He found increasing hysteresis in up/down flow curves with increasing SF dosages as a sign of thixotropy.

6.2 Experimental

Please note that cement used in Series 1 and measuring procedures in this chapter differ from the ones described in Chapter 3:

6.2.1 Materials for series 1

A rapid Portland cement (CEM I 42.5 RR) was used with composition 62.44% CaO (C), 19.35% SiO_2 (S), 4.66% Al_2O_3 (A), 3.17% Fe_2O_3 (F), 3.50% SO_3 ($\overline{S}$), 2.61% MgO, 1.14% K_2O and 0.38% Na_2O. This corresponds to the potential minerals 56.4% C_3S, 12.9% C_2S, 7.0% C_3A, 9.6% C_4AF and 7.6% $C\overline{S}$ according to Bogue calculations and using cement chemists' short hand notation. The loss of ignition (LOI) was 2.71 %, the specific density 3,120 kg/m^3 and the specific surface 543 m^2/kg according to the Blaine method. The clinker was interground with 4% limestone filler.

The silica fume was obtained from a ferro-silicon manufacturer and consisted of 94.7% SiO_2 with a specific surface of 22,000 m^2/kg as measured by nitrogen adsorption (i.e. BET).

The superplasticizers sodium naphthalene sulphonate-formaldehyde condensate (SNF) and polyacrylate grafted with polyether (denoted PA1) are described in Chapter 3.2. The dosage of admixtures was kept constant to 1.32 % admixture as received of dry powder mass for all mixes.

6.2.2 Materials for series 2

A rapid Portland cement (CEM I 42.5 RR) as described by Table 3.1-3.3 was used.

The silica fume (SF) was obtained from a ferro-silicon manufacturer as described above. Untreated and densified versions of the same SF were used.

High purity limestone powder (98-99 % $CaCO_3$) was used.

The polyacrylate grafted with polyether superplasticizer (denoted PA2) is described in Chapter 3.2. The dosage was kept constant to 0.79 % admixture as received of dry powder mass for all mixes.

6.2.3 Slurry composition and mixing

Cement pastes were made with a constant total particle volume of 0.442 corresponding to w/c about 0.40 as basis, while the amount of silica fume (SF) was replacing cement in volume increments of 0.01 from 0.00 to 0.06 (corresponding to mass SF of total powder from 0.0 to 9.9% or from 0.0 to 13.6 vol%). The blending was performed in a high shear mixer (Rondo 500, Tefal see Chapter 3.3.1) by adding solids to the water and mix for ½ minute, resting for 5 minutes and blending again for 1 minute. The admixtures were either added in the water first or added to the paste after the 5 minutes resting period (delayed addition).

Pure limestone (ls) slurries (150 ml) were made in the same way as the cement pastes, but with a constant total particle volume fraction of 0.60, corresponding to w/ls = 0.25 as basis, and with SF

replacing limestone in volume increments of 0.01 from 0.00 to 0.06 (corresponding to mass SF of total powder from 0.0 to 8.4 %, or from 0.0 to 10.0 vol%).

6.2.4 Rheological measurements

The rheological parameters were recorded by a parallel plate (1 mm gap, upper plate serrated to 150 μm depth) rheometer MCR 300 produced by Physica (see Chapter 3.3). The temperature was set to 20^{o}C.

The following sequence for series 1 lasted 20 minutes. It started when the paste was 20 minutes old from the first contact with water and was repeated 4 times to monitor time dependencies:

1. Stress (τ) – shear rate ($\dot{\gamma}$) curve with linear sweep of $\dot{\gamma}$ from 200 down to 2 s^{-1} in 30 points lasting 6 s each (intervals 1, 5, 9 and 13 lasting 3 minutes each).
2. Stress (τ) – shear rate ($\dot{\gamma}$) curve with logarithmic sweep of $\dot{\gamma}$ from 1 down to 0.01 s^{-1} in 30 points lasting 6 s each (intervals 2, 6, 10 and 14 lasting 3 minutes each).
3. Oscillatory time sweep with 30 points lasting 20 s each with amplitude γ = 0.1 % and angular frequency ω = 6 s^{-1} (intervals 3, 7, 11 and 15 lasting 10 minutes each) measuring storage and loss modules G' and G" (not discussed).
4. Shear rate ($\dot{\gamma}$) – stress (τ) curve with logarithmic sweep of τ from 30 to 300 Pa in 48 points lasting 5 s each (intervals 4, 8, 12 and 16 lasting 4 minutes each) to measure gel strength after 10 minutes rest (i.e. oscillation).

The following sequence for series 2 lasted 25 minutes. It started when the paste was 20 minutes old from the first contact with water and was repeated 4 times to monitor time dependencies.

1. Stress (τ) – shear rate ($\dot{\gamma}$) curve with linear sweep of $\dot{\gamma}$ from 200 down to 2 s^{-1} in 30 points lasting 6 s each (intervals 1, 7, 13 and 19 lasting 3 minutes each).
2. Stress (τ) – shear rate ($\dot{\gamma}$) curve with linear sweep of $\dot{\gamma}$ from 2 up to 200 s^{-1} in 30 points lasting 6 s each (intervals 2, 8, 14 and 20 lasting 3 minutes each).
3. 10 s resting as 5 points lasting 2 s each had no recording (intervals 3, 9, 15 and 21)
4. Shear rate ($\dot{\gamma}$) – stress (τ) curve with logarithmic sweep of τ from 0.2 to 50 Pa in 46 points lasting 5 s each (intervals 4, 10, 16 and 22 lasting 3 minutes and 50 s each) to measure gel strength after 10 s rest).
5. Oscillatory time sweep with 30 points lasting 20 s each with amplitude γ = 0.1 % and angular frequency ω = 6 s^{-1} (intervals 5, 11, 17 and 23 lasting 10 minutes each) measuring storage and loss modules (G') and (G") (not discussed).
6. Shear rate ($\dot{\gamma}$) – stress (τ) curve with logarithmic sweep of τ from 0.5 to 200 Pa (range may vary) in 60 points lasting 5 s each (intervals 6, 12, 18 and 24 lasting 5 minutes each) to measure gel strength after 10 minutes rest (i.e. oscillation).

The change in the measurement sequence for Series 2 was made to measure possible hysteresis and to get an idea of how fast the gel strength will form (i.e. difference between 10 seconds and 10 minutes).

6.3 Results and discussion

6.3.1 Results and discussion of series 1

The volume concentration of solids was kept constant throughout both test series since the apparent viscosity,η, of slurries can be expressed as a function of the volume concentration of solids, φ, as proposed by Krieger-Dougherty (1959) (see Eqs. 2.19 and 2.20 in Chapter 2.4.4).

Examples of flow curves are presented in Fig. 6.1 for Portland cement pastes (φ = 0.412) with SF (φ = 0.030) corresponding to mass ratios w/(c+s) = 0.409 and s/(c+s) = 0.048. Fig. 2.21 show similar flow curves for cement pastes (φ = 0.442) without silica fume corresponding to mass ratio w/c = 0.401. The pastes were added 1.32 % of the super-plasticizers PA1 and SNF by mass of powder either with the mix water or delayed (D). The curves were recorded from high shear rate towards low rate in order to simulate what is happening when concrete is mixed and poured. The flow curves were selected from the 2nd cycle (40 minutes after water addition, test interval 5).

It can be seen from the flow curves that pastes with SNF have much higher shear stresses and higher shear thinning tendencies than pastes with PA1. These findings indicate that SNF was not able to disperse the pastes as well as PA1 at the given dosage. The shear thinning originates thus probably from broken silica fume and cement agglomerates which align in the flow direction at high shear rates.

The flow curves illustrate further that delayed addition of plasticizers resulted in reduced shear stress compared to pastes were the plasticizers were added with the water. The reduction in shear stress is high both with and without silica fume for pastes with SNF, while the corresponding effect for PA1 is marginal in comparison. The reason is simply that SNF is absorbed into the C_3A hydration products when added together with the mixing water and only a fraction is left to act as dispersion agent: When the plasticizer is added 5 minutes after water addition, ettringite can form first and SNF will not incorporate into the C_3A hydration products to the same extent. PA1 is probably not incorporated into the hydration products as SNF and the effect of delayed addition is therefore minor. These results are confirmed by Uchikawa et al. (1995) and Hanehara and Yamada (1999) who found that the amounts of aminosulphonic acid-based and naphtalenesulphonic acid-based admixture adsorbed to C_3A were significantly reduced by later addition, while those of polycarboxylic acid-based and lignin sulphonic acid-based admixture were hardly changed. A similar effect of delayed addition of SNF and SMF on flow curves was reported by Aiad et al (2002). The reduction of shear stress as a result of delayed addition of plasticizer was furthermore found to be much larger for pastes with SF than for pure pastes.

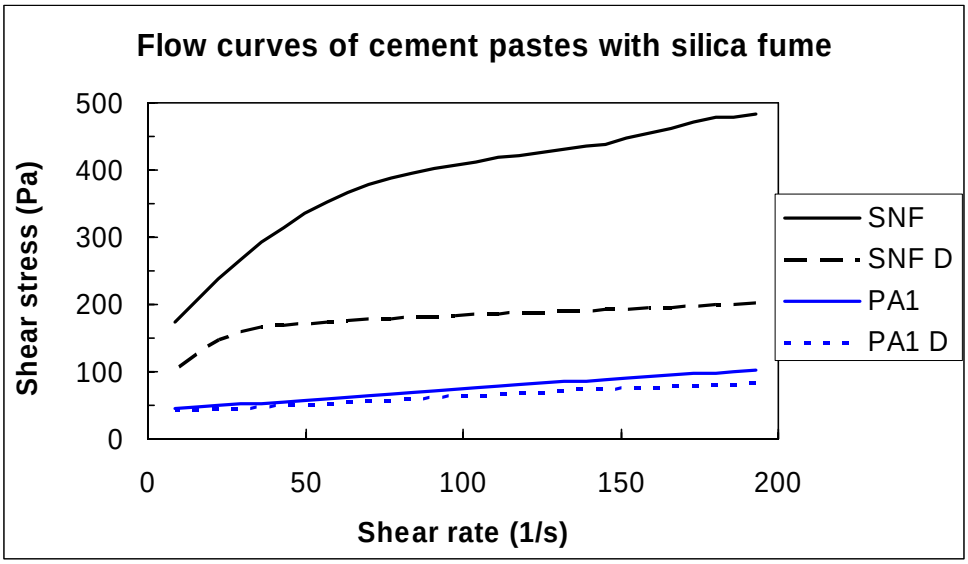

Fig. 6.1: Examples of flow curves of Portland cement (φ = 0.412) with silica fume (φ = 0.030) corresponding to 6.79 % by volume or 4.84 % by mass. The pastes were added 1.32 % of the super-plasticizers PA1 and SNF by mass of powder either with the mix water or delayed (D)

Flow resistance (FR) has been derived by integrating the area under the flow curves at medium and low shear rate range (6 points from 152 to 118 s^{-1} and 43 to 8 s^{-1} respectively). The Bingham model is employed by many researchers. All calculations made in this chapter can therefore be found recalculated into the Bingham parameters in Appendix A.1 for comparison.

Flow resistances at medium and low shear rate ranges for cement pastes with 1.32 % PA1 are depicted in Figs. 6.2 and 6.3 as a function of silica fume replacement. The figures illustrate that the flow resistance increases with increasing SF dosage independently of the shear rate range. Delayed PA1 addition does not affect this trend, but the flow resistance values are somewhat lower for pastes with immediate plasticizer addition. These findings are in accordance with the results of Park et al (2005), but opposed to the ones of Zhang and Han (2000) who found *decreasing* yield value with increasing silica fume content. The contradicting results might originate from the different types and dosages of plasticizers used in the studies: The results of Zhang and Han indicate that the pastes were well dispersed (low yield stress values) while the gel strength measurements given in Table 6.2 and 6.3 bear witness of un-dispersed pastes. The importance of superplasticizer type is further illustrated by the experiments performed with PA2 as plasticizer which show *decreasing* flow resistance with increasing SF replacement (see results and discussion of Series 2).

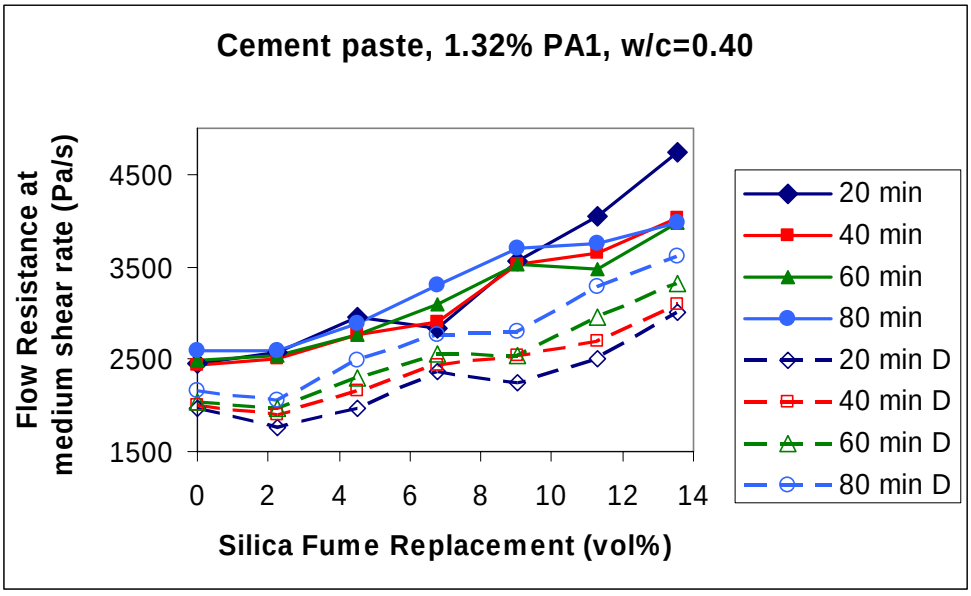

Fig. 6.2: Flow resistance as a function of silica fume replacing cement and time (20 minutes between each interval) derived from medium shear rate range. 1.32 % PA1 superplasticizer was added by mass of powder (D = delayed plasticizer addition)

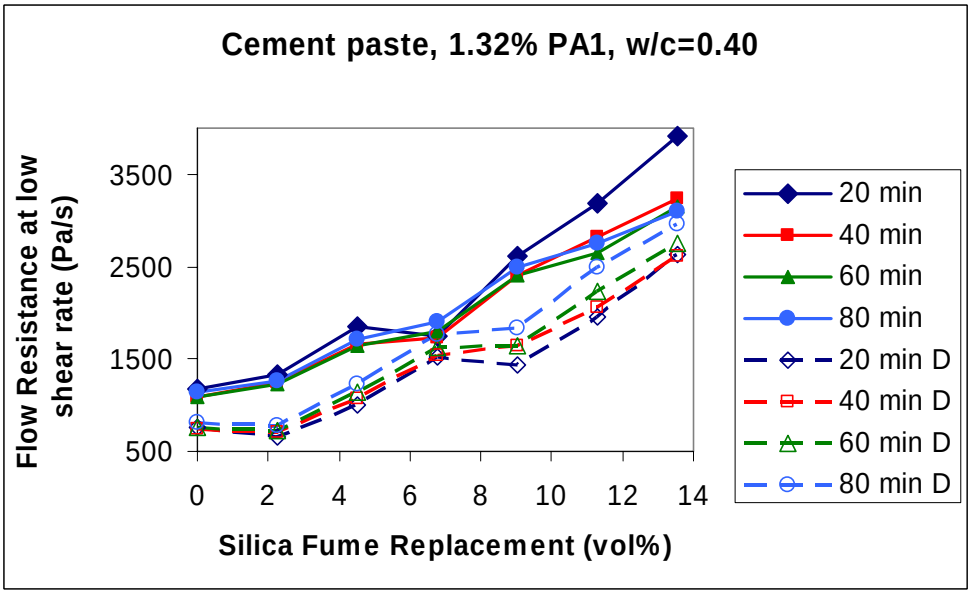

Fig. 6.3: Flow resistance as a function of silica fume replacing cement and time (20 minutes between each interval) derived from low shear rate range. 1.32 % PA1 superplasticizer was added by mass of powder (D = delayed plasticizer addition)

Flow resistances at medium and low shear rate range for cement pastes with 1.32% delayed SNF additions are depicted as functions of SF replacement in Fig. 6.4 and 6.5. The flow resistances for cement pastes with immediate addition of SNF are not included in the figures since the values were much higher than for the pastes with delayed addition of SNF. The measurements became furthermore increasingly inaccurate with increasing SF replacement as the mixes became less workable (only up to 6.79% SF could be tested). The obtained results for pastes with immediate addition of SNF are listed in Table 6.1. The general trend is increasing flow resistance with

increasing SF replacement independently of shear rate range as found for pastes with PA1. There is furthermore a high shear thinning effect of cementitious pastes with SNF as $\mu_{pm}/\mu_{pl} << 1$ (from 0.50 to 0.15). As a comparison, pastes with PA1 start out with a small shear thinning effect $\mu_{pm}/\mu_{pl} \approx 0.85$, which transfers into shear thickening as the SF replacement dosage increases (ends up with $\mu_{pm}/\mu_{pl} \approx 5$). Papo and Piani (2004) found similar results when they compared the effects of three different superplasticizers based on melamine resin, modified lignosulphonate and modified polyacrylate. They found that the polyacrylate based superplasticizer presented different rheological behaviour than the other superplasticizers studied, since it showed marked shear thickening properties above a critical deflocculant concentration as well as slight elastic effects. The shear thickening behaviour was explained by the presence of linear polyacrylate chains, which at high concentrations causes disperse phase aggregation instead of particle repulsion.

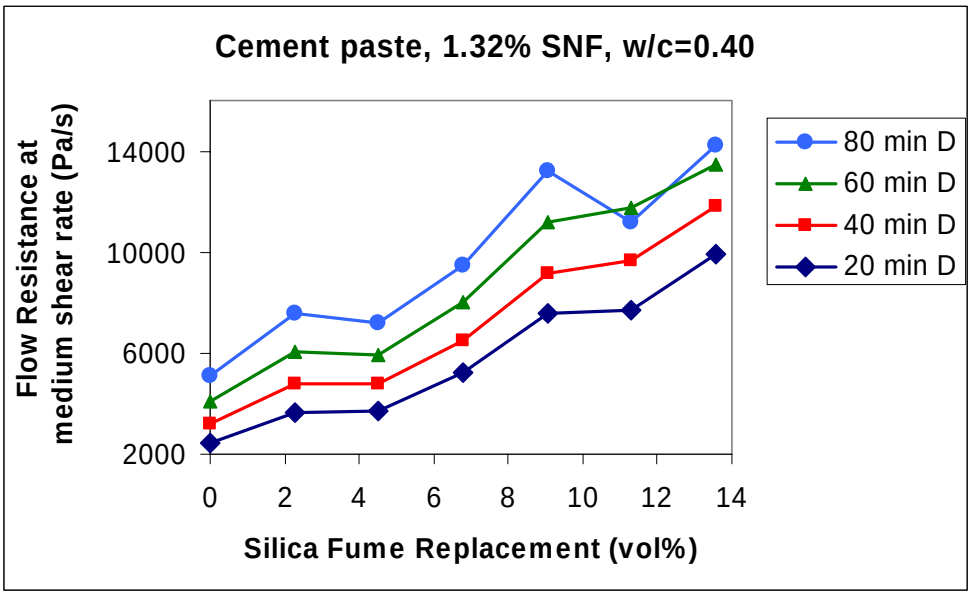

Fig. 6.4: Flow resistance as a function of silica fume replacing cement and time (20 minutes between each interval) derived from medium shear rate range. 1.32 % SNF superplasticizer was added by mass of powder (D = delayed plasticizer addition).

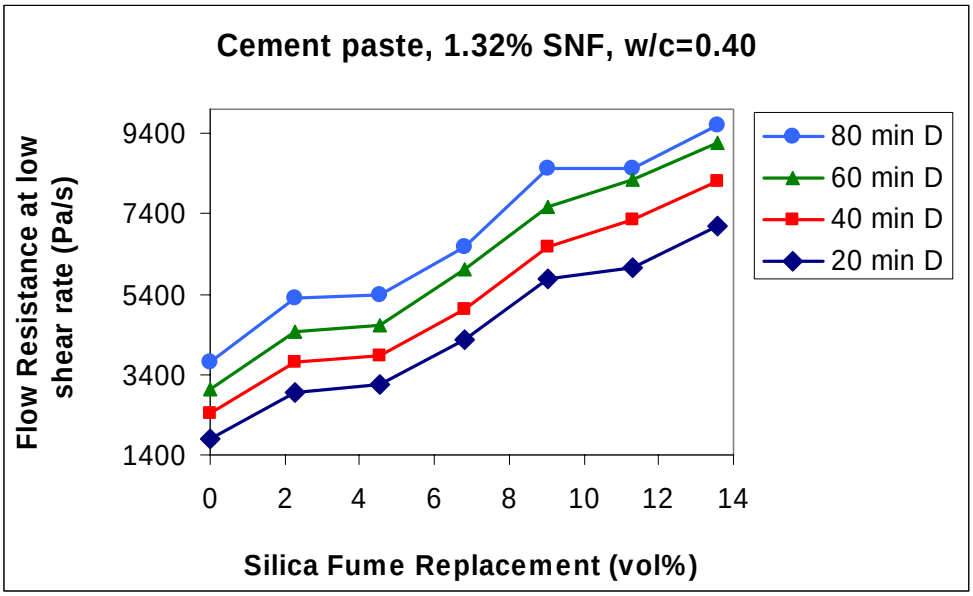

Fig. 6.5: Flow resistance as a function of silica fume replacing cement and time (20 minutes between each interval) derived from low shear rate range. 1.32 % SNF superplasticizer was added by mass of powder (D = delayed plasticizer addition).

Table 6.1: Flow curve evaluation of cementitious paste with 1.32% SNF (added with mix water)

		Medium shear rate range		Low shear rate range		Shear thinning/ Shear thickening
SF (vol%)	Interval / Time (min)	Flow Resistance	μ_{pm} (mPa·s)	Flow Resistance	μ_{pl} (mPa·s)	μ_{pm}/μ_{pl}
0.00	1/20	9948	616	5851	3086	0.20
2.26	1/20	8552	421	5652	2805	0.15
4.52	1/20	11182	704	6507	3337	0.21
6.79	1/20	14083	1163	7546	3810	0.31
0.00	2/40	10900	678	6264	3157	0.21
2.26	2/40	9585	481	6209	3069	0.16
4.52	2/40	12049	666	7105	3613	0.18
6.79	2/40	14729	747	8527	4145	0.18
0.00	3/60	12148	602	7050	3521	0.17
2.26	3/60	11182	590	6809	3337	0.18
4.52	3/60	13073	1105	7416	3228	0.34
6.79	3/60	13403	1434	8075	2847	0.50
0.00	4/80	13004	689	7648	3847	0.18
2.26	4/80	12457	725	7399	3730	0.25
4.52	4/80	13784	906	8226	3559	0.25
6.79	4/80	11266	696	7333	2311	0.30

The gel strengths measured 10 minutes after resting (weak oscillation) reported in Tables 6.2 and 6.3 are of the same magnitude for pastes with SNF and PA1. The data show that delayed addition of superplasticizer generally causes reduced gel strength.

Delayed addition of superplasticizer within the dormant period is known to reduce the amount of molecules incorporated into the hydration products (Chiocchio and Paolini 1985, Uchikawa et al. 1995, Hanehara and Yamada 1999). Thus more plasticizer is left for dispersion of the paste and the gelling tendencies reduced. Reduced gel strength might also be an indication of increased retardation of the cement hydration due to superplasticizer molecules adsorbing onto active hydration sites.

Table 6.2: Gel strength (Pa) measured after 10 minutes oscillation for cementitious pastes with 1.32 % SNF as a function of SF replacement and time (D = delayed SNF addition)

SF (vol%)	Int 1/Int 1D	Int 2/Int 2D	Int 3/Int 3D	Int 4/Int 4D
0.00	>120/110	>120/130	>120/130	>120/170
2.26	220/120	130/140	160/160	220/220
4.52	140/180	180/220	230/270	230/270
6.79	190/150	290/210	>300/160	280/180
9.05	-/190	-/130	-/150	-/210
11.31	-/140	-/260	-/>300	-/>300
13.57	-/190	-/180	-/>300	-/>300

Table 6.3: Gel strength (Pa) measured after 10 minutes oscillation for cementitious pastes with 1.32 % PA1 as a function of SF replacement and time (D = delayed PA1 addition)

SF (vol%)	Int1/Int1D	Int 2/Int2D	Int 3/Int3D	Int 4/Int4D
0.00	190/120	190/125	190/130	230/155
2.26	160/130	170/120	170/125	180/135
4.52	170/155	155/150	160/210	200/180
6.79	210/215	210/215	220/210	230/240
9.05	280/210	265/180	250/190	250/230
11.31	190/260	275/250	>300/260	280/280
13.57	210/275	>300/>300	250/>300	>300/>300

The substantial increased flow resistance and gel strength with increasing SF replacement can be explained by the ionisation of SF surface and possible bridging with polyvalent cations like calcium;

$$2 \equiv Si\text{-}OH + Ca^{2+} + 2\ OH^- = \equiv Si\text{-}O^-\ {}^+Ca^+\ {}^-O\text{-}Si\equiv + 2H_2O \qquad (6.1)$$

Alternatively, Ca^{2+} can adsorb to the surface of SF and then the anionic polymers (PA1 and SNF) can adsorb on the positive charged sites thus created. Jolicoeur and Simard (1998) pointed out this effect after the observation of SNF being adsorbed to minor extent by SF slurry, but being equally adsorbed by cement paste and cementitious paste with SF replacing cement.

The influence of time

The influence of time (20 minutes between each interval) on the flow resistance is minor when PA1 is added with the mixing water. It is generally decreasing to a small extent with time indicating that the hydration is within the dormant period and that the internal structure of the paste is broken due to the shearing of the paste during the rheological measurements. It is also possible that the performance of the polymer might improve within the dormant period (e.g. the grafted chains might expand in the water phase).

The flow resistance is on the other hand increasing to a stronger extent with time when the superplasticizer is added delayed. An explanation for this result might be that PA1 molecules form complexes with Ca^{2+} ions dissolved in the liquid phase. Thus, adsorption of molecules on "active hydration cites" and formation of complexes with Ca^{2+} will inhibit Ca^{2+}-supersaturation and thereby retard the cement hydration (Uchikawa 1984). At delayed addition Ca^{2+} ions get the chance to dissolve in the liquid phase before the plasticizer is added and the retardation of early hydration will not be as strong as for pastes with immediate addition.

Table 6.4 illustrates that flow loss rates are higher for pastes with SNF than for pastes with PA1. Pastes with SNF obtain the highest flow loss rates due to consumption of SNF molecules by the hydration products (Matsukawa and Diamond 1991, Carazeanu et al. 2002). The performance of PA type molecules are not affected by the hydration to the same extent since the grafted chains might be long enough to ensure steric stabilization even though the backbone is buried in the cement hydrates (Nawa et al. 2000). These findings are illustrated well by the flow curves in Fig.2.21 and 6.1. PA is also found to retard cement hydration to a greater extent than SNF (see calorimetric measurements in Chapter 8) and thus the flow loss rate will be low.

Table 6.4: Measured flow loss for Portland cement paste as a function of time, silica fume and superplasticizer. All pastes are prepared with delayed addition of superplasticizer.

		PA1		SNF	
SF (vol %)	**Time (min)**	**FR(low)**	**Flow Loss (%)**	**FR(low)**	**Flow Loss (%)**
0.00	20	760	-	1811	-
	40	747	-2	2418	34
	60	763	0	3040	68
	80	810	7	3729	106
2.26	20	660	-	2947	-
	40	709	-7	3718	26
	60	732	-4	4458	51
	80	771	1	5303	80
4.52	20	1008	-	3142	-
	40	1076	7	3864	23
	60	1137	13	4644	48
	80	1229	22	5399	72
6.79	20	1528	-	4266	-
	40	1547	1	5043	18
	60	1624	6	6007	41
	80	1759	15	6575	54
9.05	20	1435	-	5771	-
	40	1575	10	6588	14
	60	1647	15	7553	31
	80	1829	27	8523	48
11.31	20	1960	-	6044	-
	40	2056	5	7258	20
	60	2241	14	8232	36
	80	2486	27	8519	41
13.57	20	2633	-	7101	-
	40	2622	0	8195	15
	60	2761	5	9152	29
	80	2955	12	9600	35

6.3.2 Results and discussion of series 2

As for series 1 the volume concentration of solids was kept constant throughout the test series since the apparent viscosity,η, of slurries is proposed to be a function of the volume concentration of solids, φ, in accordance with the Krieger-Dougherty equation (2.19). Examples of flow curves for material series 2 are presented in Fig. 6.6 for Portland cement pastes (φ = 0.442) without silica fume (SF) corresponding to mass ratio w/c = 0.401 and for cement paste (φ = 0.382) with untreated and densified SF (φ = 0.060) corresponding to mass ratios w/(c+s) = 0.418 and s/(c+s) = 0.099. The pastes were added 0.79% PA2 by mass of powder either immediately with the mix water (I) or delayed (D). The flow curves were recorded from high shear rate towards low rate in order to simulate what is happening when concrete is mixed and poured and selected from the 2nd cycle (45 minutes after water addition). The reduction in shear stress caused by delayed versus momentary PA2 addition (Fig. 6.6) is small (0-10 Pa at 100 s^{-1}), and there is little to gain in rheology by such action for PA2. As comparison, the reduction in shear stress as function of shear rate simply due to delayed addition of 1.32% naphthalene sulphonate – formaldehyde condensate (SNF) was very high (≈200 Pa at 100 s^{-1}) both without and with silica fume as shown in Figs. 2.21 and 6.1.

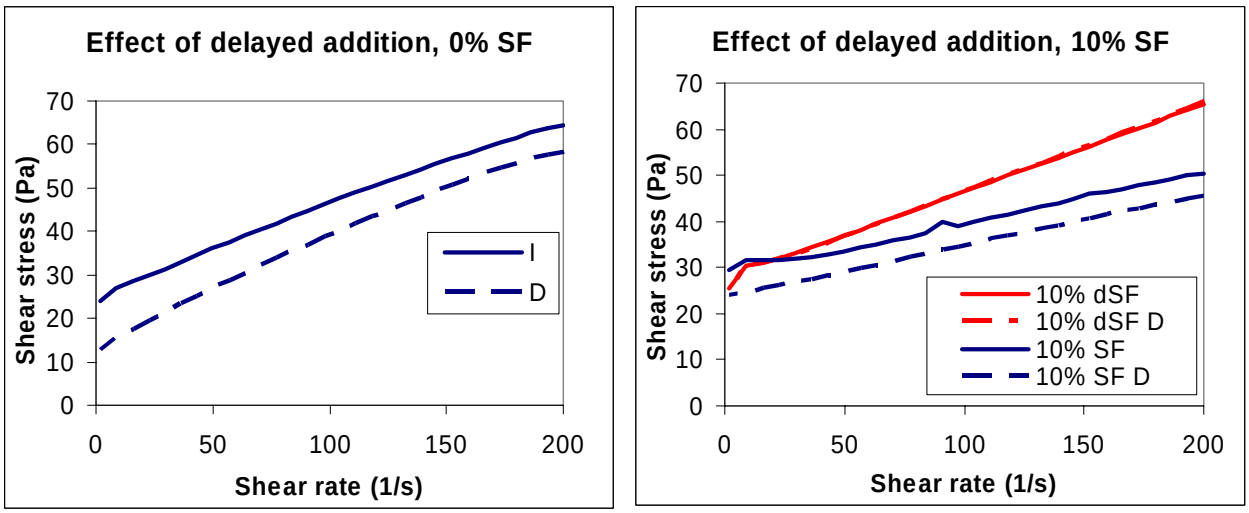

Fig. 6.6: Examples of flow curves of Portland cement (φ = 0.442, w/c = 0.401) paste without (left) and with 10 wt% (13.6 vol%) silica fume replacement (right). The pastes were added 0.79 % PA2 immediately with the mixing water (I) or delayed (D). Silica fume was either untreated or densified (d)

The up and down flow curves (interval 2) are shown in Fig. 6.7 for the same mixes as in Fig. 6.6, but only with momentary addition of PA2 rather than delayed. Higher shear stress in the lower shear rate range for the up curve than for the down curve (as for 10 % untreated SF) indicates hysteresis. The hysteresis might be caused by rapid formation of agglomerates which are ruptured or aligned in the flow direction at higher shear rates. This hysteresis effect is negligible for 10 % densified silica fume (dSF) and for paste without SF.

Fig. 6.7 illustrates that the hysteresis effect is stronger at high shear rate range than at lower when no silica fume is added. This effect might be caused by the measurement sequence where the

down-curve is measured before the up-curve. Hydration of the paste and formation of gel structure will therefore probably result in higher shear stresses with time.

Another interesting observation from Figs. 6.6 and 6.7 is that the flow curve for cementitious paste with densified SF is similar to cement paste without SF (≈same slope), while the flow curve for cement paste with 10 % untreated silica fume has much smaller slope. This finding indicates that densified SF may consist of agglomerates with lesser outer surface which do not disperse the cement as effectively as untreated silica fume.

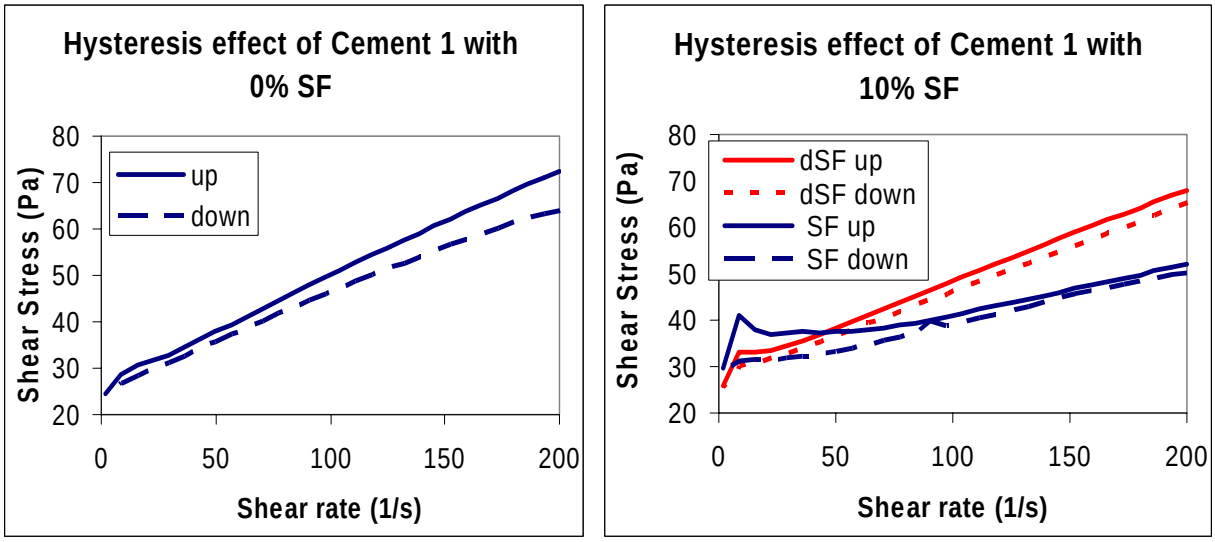

Fig. 6.7: Examples of up and down flow curves as a measure of hysteresis for Portland cement (φ = 0.442, w/c = 0.401) paste without (left) and with 10 wt% (13.6 vol%) silica fume replacement (right). Silica fume was either untreated or densified (d)

It can be seen from the flow curves in Figs. 6.6 and 6.7 that there is no large apparent shear thinning/thickening behaviour. A break point occurs at low shear rates for pastes with SF. This is probably caused by gel rupture. Cement pastes without silica fume and pastes with delayed addition of PA2 (μ_{pm}/μ_{pl} = 0.77 for interval 7) were found to obtain the largest shear thinning, while there was a shear thickening effect for cement paste with 10 % SF (μ_{pm}/μ_{pl} = 3.3 for interval 7) and immediate PA2 addition.

Flow resistances as a function of silica fume replacement with immediate addition of 0.79 % PA2 at medium and low shear rate ranges are plotted in Figs. 6.8 and 6.9. The corresponding Bingham parameters can be found in Appendix A.1.3. Fig. 6.8 depicts reduced flow resistance with increasing SF replacement (untreated unless else is specified) in the medium shear rate range. Fig. 6.9 illustrates on the other hand that the flow resistance do not vary much with increased SF replacement in the low shear rate range up to 70 minutes after water addition. The flow resistance obtained 95 minutes after water addition show a decreasing trend and reach a minimum at 9% SF. Decreasing flow resistance with increasing SF can be understood with packing of SF particles (average 0.15 μm) in the gaps between cement grains (average 10 μm) and thereby squeezing water out between the cement grains. Another possible explanation is the ball-bearing effect of rather spherical small particles on the irregular cement grains. Wallevik (1990) reported for

concrete plasticized with lignosulphonate that replacing cement with SF until a certain amount (2, 4 and 6 % SF for 200, 300 and 400 kg cement/m^3, respectively) significantly reduced (20, 30 and 50 %, respectively) the h-value (analogous to plastic viscosity), while the g-value (analogous to yield stress) was roughly constant. Further replacement of cement with SF up to 20 % gave a substantial increase (80, 140 and 180 % for 200, 300 and 400 kg cement/m^3, respectively) of the g-value, while the h-value increased more gradually. However, one should bear in mind that results for concrete can not be directly transferred to paste even though the rheology of matrix dominates the rheology of concrete. For instance, since matrix of concrete contains a lot of filler and air that is not stable in paste.

The flow resistance for pastes with PA2 is not changing with SF replacement to the same extent as pastes with SNF and PA1: The flow resistance for the paste with PA2 is almost independent of SF content in the low shear rate range while the flow resistances for pastes with SNF and PA1 change by approximately 300% when the SF replacement increases from 0% to 13.6 vol%. The flow resistance curves for pastes with SNF, PA1 and PA2 show that PA2 is by far the most efficient plasticizer of the three. Thus, agglomerates of cement and silica fume are better dispersed or prevented from reforming when PA2 is utilized.

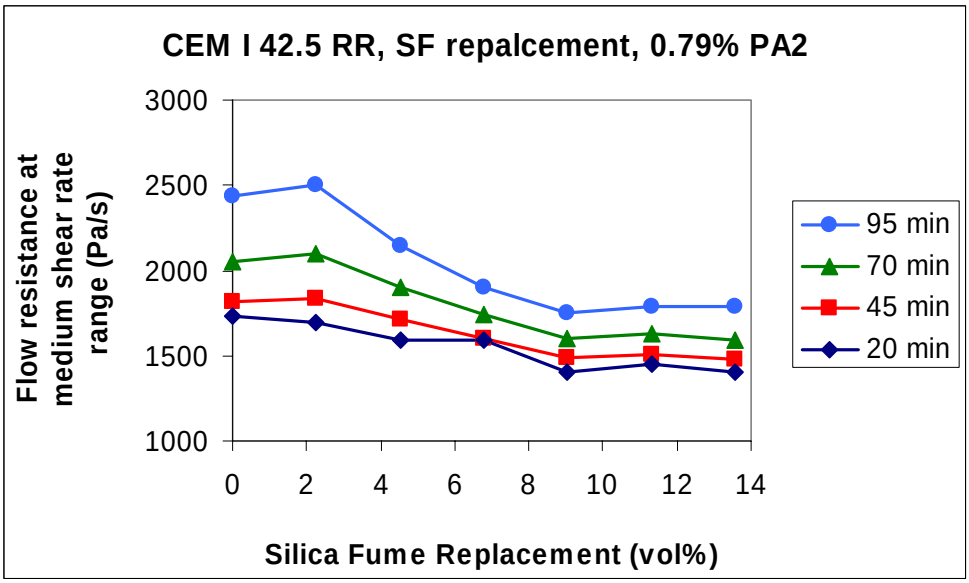

Fig. 6.8: Flow resistance as a function of silica fume replacing cement and time (25 minutes between each interval) derived from medium shear rate range. 0.79 % PA2 was added by mass of powder.

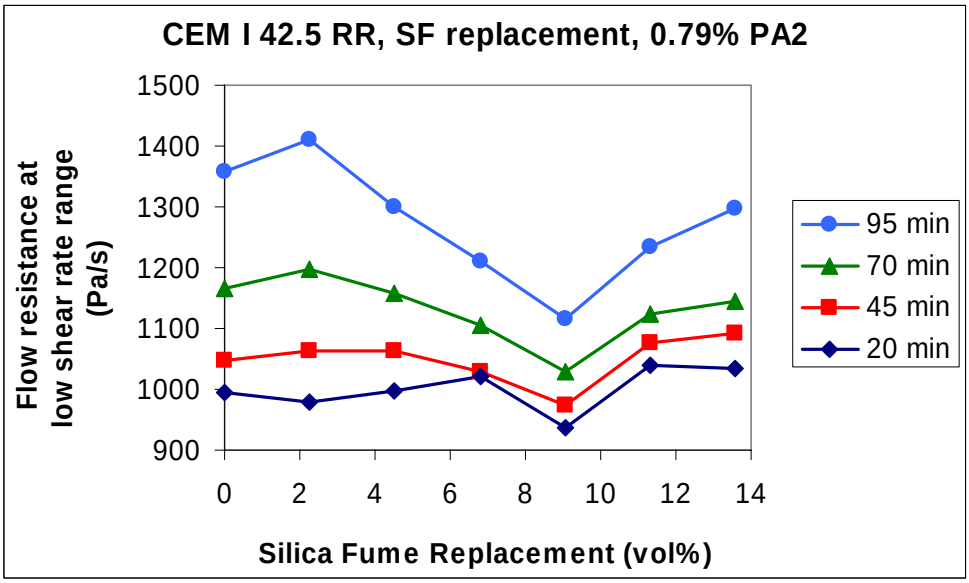

Fig. 6.9: Flow resistance as a function of silica fume replacing cement and time (25 minutes between each interval) derived from low shear rate range. 0.79 % PA2 was added by mass of powder.

Fig. 6.10 shows flow resistance curves from the low shear rate range for cement pastes with 0.79% PA2 as a function of limestone replacement and time. Plots from the medium shear rate range were omitted since the trends were independent of rate ranges. The figure shows decreasing flow resistance with increasing limestone replacement which indicate that the limestone particles disperse the cement particles more efficiently than SF or that less gel is formed for limestone replaced cement pastes than for SF replaced pastes.

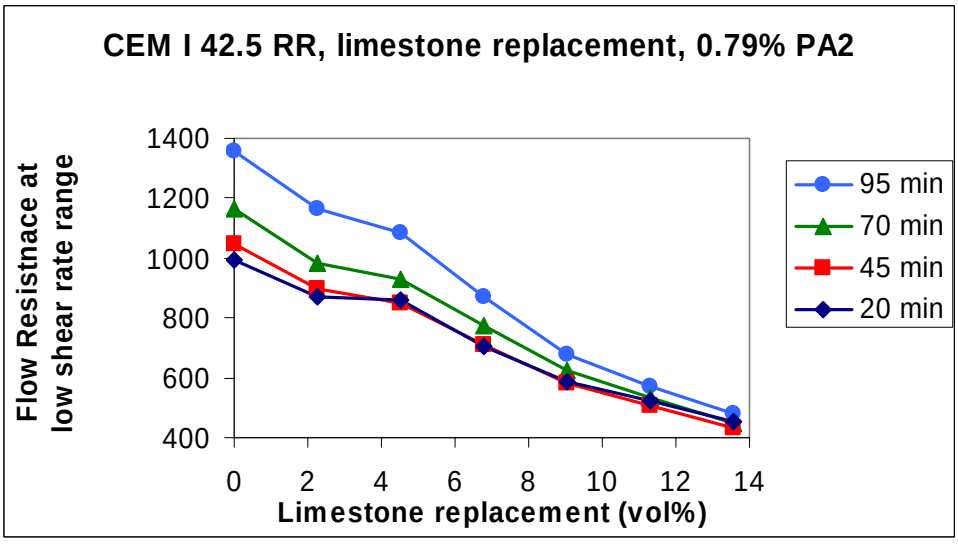

Fig. 6.10: Flow resistance at low shear rate range as a function of limestone replacement and time.

The gel strengths (τ) measured after 10 seconds rest and 10 minutes oscillation are plotted as a function of SF and limestone replacement and time (25 min between the 4 intervals) in Figs. 6.11 and 6.12. Fig.6.11 illustrates that the gel strength is nearly independent of limestone replacement up until 8 vol% before they decrease at the highest limestone replacement ratios (11.3 vol% and

13.5 vol%). The same trend is found for the 10-minute gel strengths illustrated in Fig. 6.12. The gel strength values do not increase much during the 10 minutes rest (i.e. oscillation) until the 4th interval (114 minutes after water addition) where the gel strength initially has an increasing tendency. The increased gel strength can be caused by the onset of early set. The results might indicate that limestone filler disperses the cement paste and that it may act as nucleation sites when the hydration sets in as proposed by Gjørv and Løland (1982).

A marked increase of gel strength is found for pastes with increasing SF replacement both after 10 seconds and 10 minutes rest. The gel strengths have furthermore increased after the 10 minutes rest (i.e. oscillation) compared to the values found after 10 seconds rest. The substantial increased gel strength with increasing SF replacement seen in the figures can be explained by the ionisation of SF surface due to the high pH and possible bridging with polyvalent cations like calcium (i.e. precursor to pozzolanic reaction) as indicated by Eq. 6.1.

The differing trends for the flow resistance as a function of SF and limestone replacement may thus be caused by the different gelling tendencies of the two materials. Silica fume may as a consequence be advantageous as a stabilizing agent for self-compacting concrete preventing segregation upon standing and reduced formwork pressure due to the formation stronger gel compared to pastes with limestone.

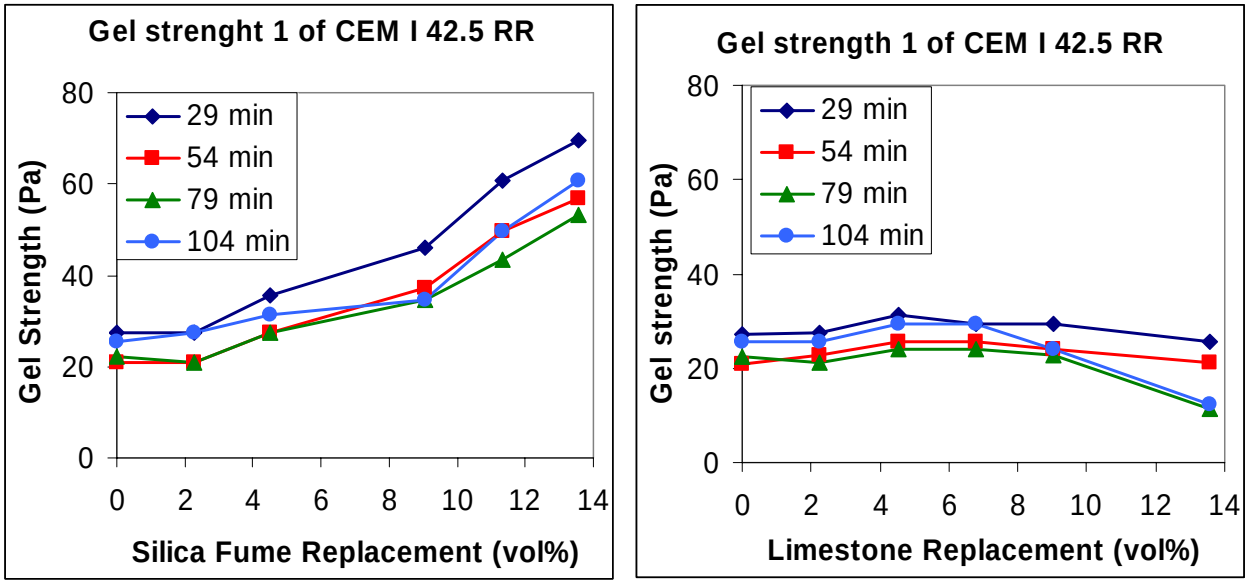

Fig. 6.11: Gel strength built up after 10 seconds rest as a function of SF and limestone dosage and time (25 min intervals).

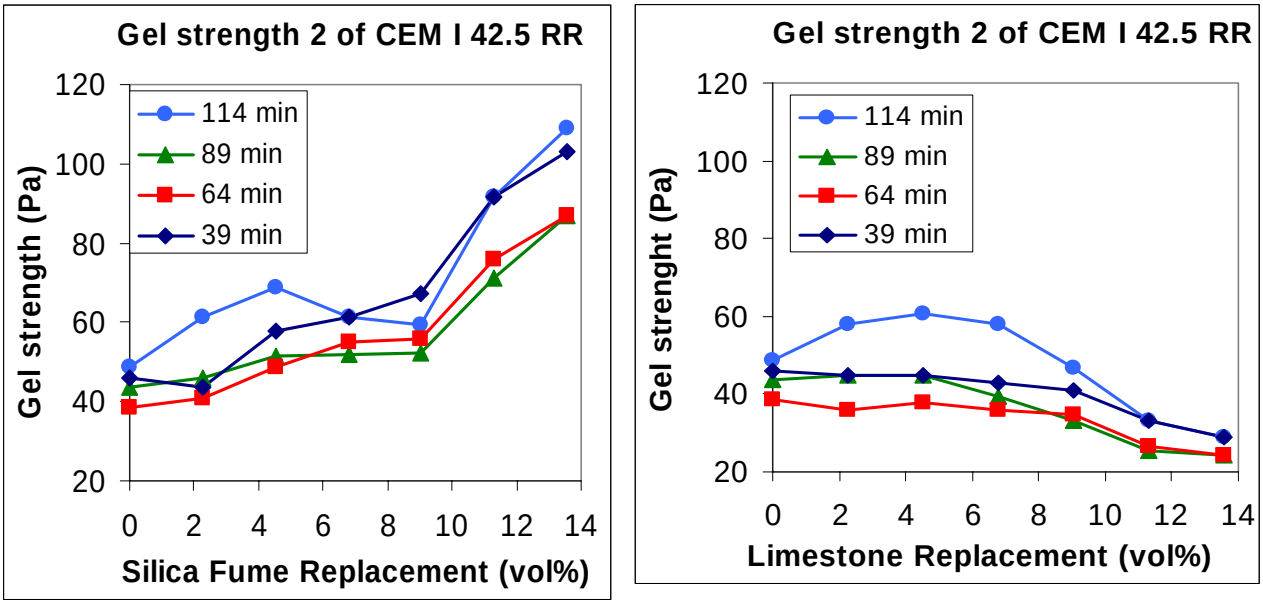

Fig. 6.12: Gel strength built up after 10 min rest (i.e. weak oscillation) as a function of SF and limestone dosage and time (25 min intervals).

The influence of delayed PA2 addition (D), and densified SF (d) versus untreated SF, on the measured gel strength may be found from listed values in Table 6.6. The reduction in gel strength due to densification of SF (see $\tau_{10\ min}$ in Table 6.6) may be due to increased agglomeration of SF with lesser outer surface ("grains" of SF), even though the total surface measured by N_2-adsorption (BET) may be the same. Thus, fewer outer sites may be bridged by Ca^{2+}.

Delayed addition of PA2 results in a reduction of the gel strength of approximately 50 % for pastes without SF and with 13.6 vol% untreated SF. This might be caused by increased adsorption of PA2 on SF: When PA addition is delayed 5 minutes, Ca^{2+} can adsorb on the SF surface and subsequently PA may adsorb to these Ca-sites by co-ordination with the carboxylic groups attached to the "backbone" polymer chain. Jolicoeur and Simard (1998) pointed out this effect after the observation of SNF being adsorbed to minor extent by SF slurry, but being equally adsorbed by cement paste and cementitious paste with SF replacement. Delayed addition of superplasticizer within the dormant period is also known to reduce the amount of molecules incorporated into the hydration products (Chiocchio and Paolini 1985, Uchikawa et al. 1995, Hanehara and Yamada 1999). Thus more plasticizer is left for dispersion of the paste and the gelling tendencies reduced. Reduced gel strength might also be an indication of increased retardation of the cement hydration due to superplasticizer molecules adsorbing onto active hydration sites.

There was nearly no change in gel strength by delayed plasticizer addition for pastes with densified SF. The small effect of delayed plasticizer addition may be caused by low outer surface of the densified SF resulting in a relatively low number of adsorption sites compared to untreated SF. The lower outer surface of the densified SF may furthermore counteract the ball-bearing and dispersing effect of the silica fume as illustrated in Fig. 6.7 which again may reduce the potential number of available adsorption sites on the cement surface.

Table 6.6: Gel strength after 10 minutes rest (i.e. oscillation) and flow curve evaluation of cementitious paste (w/c = 0.40) with 0.79% PA2. Untreated and densified (d) silica fume, and momentary and delayed (D) addition of PA2 are compared for 0 and 13.6 vol% SF as a function of time.

SF (vol%)	densified/ Delayed	Time for FR (min)	FR (medium) (Pa/s)	FR (low) (Pa/s)	Time for τ_{10} (min)	τ_{10} (Pa)
0.00		20	1736	995	39	46
0.00	D	20	1426	604	39	21
13.6		20	1405	1035	39	103
13.6	D	20	1186	787	39	46
13.6	d	20	1697	1034	39	65
13.6	d/D	20	1720	1055	39	74
0.00		45	1919	1048	64	39
0.00	D	45	1606	705	64	21
13.6		45	1481	1091	64	87
13.6	D	45	1327	915	64	44
13.6	d	45	1803	1116	64	61
13.6	d/D	45	1819	1123	64	69
0.00		70	2053	1166	89	44
0.00	D	70	1886	820	89	26
13.6		70	1593	1145	89	87
13.6	D	70	1501	1042	89	46
13.6	d	70	2113	1318	89	69
13.6	d/D	70	2112	1305	89	74
0.00		95	2436	1357	114	49
0.00	D	95	2280	968	114	37
13.6		95	1791	1298	114	109
13.6	D	95	1696	1193	114	55
13.6	d	95	2564	1653	114	130
13.6	d/D	95	2533	1612	114	123

Gelling tendencies for inert limestone paste with silica fume

Limestone was used as a nonreactive model system for cement in this part of the work to study the influence of silica fume on the gelformation. Gel strengths, $\tau_{10\ min}$, for neutral limestone slurries are listed in Table 6.7 as a function of silica fume replacement and time (25 min intervals). There is a steady increase in gel strength with increasing silica fume replacement above 5 vol% SF. Hardly any time effects were observed. Furthermore, 10 vol% densified SF resulted in 1/10 gel strength as compared to 10 vol% untreated SF, while less differences was found for cementitious pastes (Table 6.5). The reduced gel strength might be caused by lower active surface area for densified SF than for the untreated powder. Agglomerates of spherical SiO_2 particles (average diameter 0.15 μm) in untreated SF may furthermore be dendritic in nature with larger possibility of mechanical or adhesive interaction than perhaps more grain shaped agglomerates in densified silica fume.

Table 6.7: Gel strength (Pa) measured after 10 minutes oscillation for limestone pastes with 1.32 % SNF as a function of SF replacement and time (d = densified silica fume)

SF (vol%)	Int1	Int 2	Int 3	Int 4
0.0	0	0	0.23	0.21
1.67	0	0	0.21	0.21
3.33	0.26	0.21	0.29	0.32
5.00	<5	<5	<5	<5
6.67	7.6	7.6	7.6	6.8
8.33	14.3	12.9	11.6	11.6
10.0	69.3	69.3	69.3	69.3
10.0d	7.6	6.1	5.5	5.0

The flow curves in Fig. 6.13 for pure limestone slurry with 10 vol% silica fume replacement reveal a dramatic higher shear stress at shear rates below 100 s^{-1} for untreated silica fume than for densified silica fume. These results coincide with the ones found for cement pastes (Fig. 6.7) and might be caused by agglomerates formed at low shear rates. Formation of agglomerates at low shear rates could explain the low sensitivity of silica fume replacement found for cement pastes at low shear rate ranges in Fig. 6.8 compared to the medium shear rate range in Fig. 6.9.

The flow resistances at low and medium shear rate ranges are listed in Table 6.8 for all limestone slurries with silica fume. The rheological parameters from Bingham fits as a function of silica fume replacement are given in Appendix A.1.3.

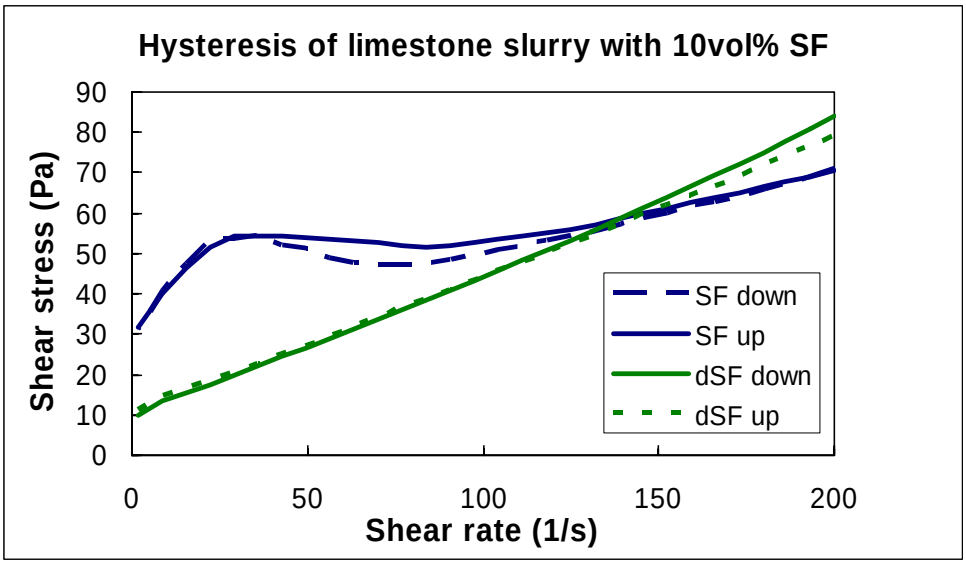

Fig. 6.13: Effect of densified silica fume (dSF) versus untreated silica fume (SF) on up/down flow curves (interval 7) of limestone slurry (w/ls = 0.30) with 10 vol% SF replacement of limestone

Table 6.8: Flow curve evaluation of limestone slurry (w/ls = 0.30) with 0.79% PA2. Untreated and densified (d) silica fume are compared for 0 to 10 vol% (8.4 mass%) replacement of limestone with silica fume as a function of time (25 min between each interval). Note that the mixes with 0.00 and 1.67 vol% silica fume had segregation tendencies (not stable).

SF (vol%)	Time (min)	Flow Resistance (medium shear rate range)	Flow Resistance (low shear rate range)
0.00	20	1400	108
1.67	20	903	109
3.33	20	974	143
5.00	20	1013	184
6.67	20	1164	375
8.33	20	1507	890
10.00	20	2038	1818
10.0 0d	20	2165	1082
0.00	45	891	92
1.67	45	937	114
3.33	45	839	138
5.00	45	940	175
6.67	45	1190	368
8.33	45	1465	736
10.00	45	1931	1751
10.0 0d	45	1944	642
0.00	70	1038	100
1.67	70	1056	127
3.33	70	898	144
5.00	70	968	177
6.67	70	1254	373
8.33	70	1480	681
10.00	70	1923	1659
10.0 0d	70	1830	509
0.00	95	1162	110
1.67	95	1217	144
3.33	95	1030	159
5.00	95	1034	185
6.67	95	1347	386
8.33	95	1517	657
10.00	95	1924	1588
10.0 0d	95	1831	469

Finally, the effect of pH was checked by dissolving KOH and NaOH in the mix water with ratio 2:1 until pH 13.2 in order to simulate the water composition in Portland cement paste. This water was then used for limestone slurry mixes. The flow curves (decreasing followed by increasing shear rates) for limestone slurry with 10 vol% SF replacement with pH 8 and 13.2 are reproduced in Fig. 6.14. It can be seen that the shear stress is much higher for the mix with high pH, which can be explained by agglomerate formation caused by ionised silica which attach at the limestone

surface as outlined in Eq. 6.1. There was no sign of hysteresis in the low shear rate range, but rather at the medium shear rate range for the mix with high pH which might indicate that the agglomerates are broken due to the high shear energy.

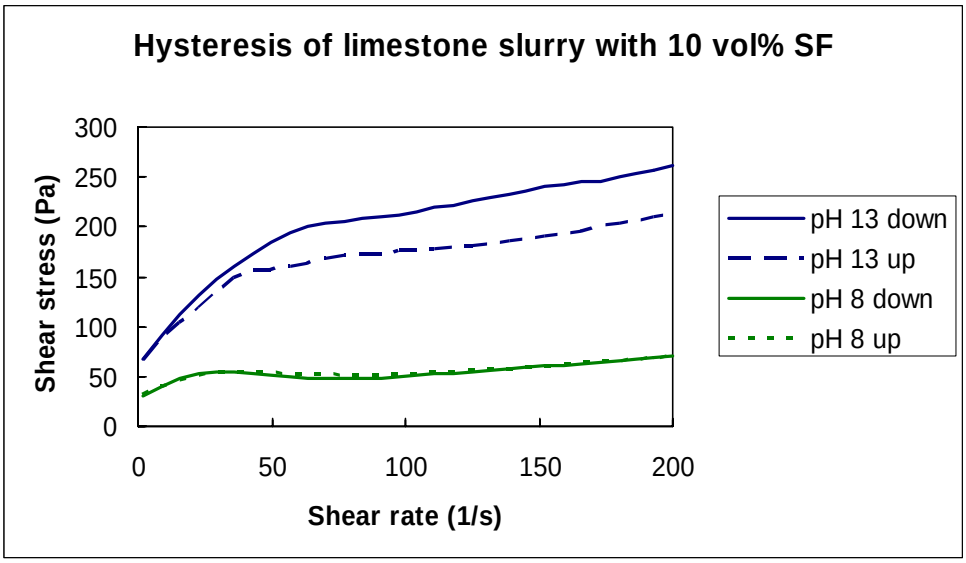

Fig. 6.14: Effect of pH on the up/down flow curves of limestone slurry with 10 vol% silica fume replacement of limestone. pH is assumed to be 8 in pure water in equilibrium with limestone, while pH 13 of the water is achieved by adding KOH/NaOH = 2/1

6.1.3 Conclusions

The following conclusions can be drawn from studying the rheology of cementitious pastes where cement is increasingly replaced by silica fume (SF) and two superplasticizers have been used as dispersants added delayed or with mix water (series 1):

1. The polyacrylate with grafted polyether chains (PA1) seems better suited for self-compacting concrete (SCC) production than naphthalene sulphonate-formaldehyde condensate (SNF) since the shear stress is kept lower over a wide shear rate range (200 to 2 s^{-1}).
2. Delayed addition of superplasticizer lowers the shear stress substantially for cementitious pastes with SNF but only marginally for pastes with PA1, which removes the necessity for delayed addition of PA1 in SCC production.
3. Analysing the flow curves with the flow resistance approach for a medium and low shear rate range, shows increasing flow resistance with increasing SF replacement for pastes with SNF and PA1.
4. SNF leads to a shear thinning behaviour of the paste. PA1 leads only to marginal shear thinning without SF and for the lowest SF dosage, which transfers into a substantial shear thickening behaviour at the highest SF replacement (13.6 vol%).
5. The change in rheological properties as a function of time (flow loss measured every 20 minutes for 80 minutes) was much smaller for pastes plasticized with PA1 compared with SNF.

The following conclusions can be drawn from studying the rheology of cementitious paste where cement is increasingly replaced by silica fume (SF) dispersed with a polyether grafted polyacrylate combined with a viscosifier (PA2) added delayed or with mix water (series 2):

1. Flow curves of cementitious paste with 13.6 vol% SF show a tendency of hysteresis probably due to rapid agglomerate formation at low shear rates for untreated silica fume, while this effect is absent for densified silica fume.
2. There are no large shear thinning/thickening effects in general for the cementitious pastes. The largest shear thinning occurred for cement pastes without silica fume and delayed addition of PA2 while the largest shear thickening occurred for cementitious pastes with 13.6 vol % SF.
3. The flow resistance had a decreasing tendency with increasing SF replacement at medium shear rate, while it was rather constant at low shear rate range. This can be due to particle packing between cement grains displacing water or by a ball-bearing effect of silica spheres.
4. A tendency of increasing flow resistance with time (measured in 25 min intervals) was explained by surface hydration increasing the fraction of solids in the slurry both by removing liquid and by creating solid hydrates.
5. A substantial increase in gel strength after 10 min rest with increasing SF replacement might be due to ionisation of SF surface by high pH and possible bridging with polyvalent cations like calcium. The lower gel strength for mixes with densified SF versus untreated SF could be attributed to more grain shaped agglomerates with lower outer surface in densified SF compared to dendritic agglomerates in untreated SF.
6. Delayed PA2 addition reduced the gel strength for cementitious pastes with 13.6 % SF, which can be attributed to more adsorption of PA2 on the SF grains since calcium cations is allowed to adsorb first in the case of delayed addition.
7. There was a trend of *increasing* gel strength with increasing silica fume replacement of cement and *decreasing* gel strength with increasing limestone filler replacement. Thus silica fume may be advantageous as a stabilising agent for self-compacting concrete preventing segregation upon standing due to a more rapid and strong gel formation.
8. Neutral limestone pastes with increasing SF replacement obtained increased gel strength after 6 vol% replacement. Densified silica fume gave 10 times less gel strength than untreated SF, supporting the difference in agglomerate shape (grains versus dendrites). Furthermore, flow curves of limestone pastes with 10 vol% SF had much higher shear stress at shear rates below 100 s^{-1} than for slurry with densified SF, explainable by the same agglomerate shape difference.
9. Increasing pH from 8 to 13.2 in limestone slurries with 10 vol% SF increased the shear stresses substantially, supporting bridge formation between SF agglomerates after ionization by OH^- with active calcium sites on limestone grains.

Chapter 7

Effect of cement characteristics on flow resistance

7.1 Introduction

Numerous factors have been found to affect the rheological behaviour of cementitious paste (see Chapter 2.4). The objective of the following investigations has been to find some correlations between cement characteristics such as cement fineness and clinker composition with the "flow resistance" (area under the flow curve). The influence of three different types of plasticizers namely naphthalene sulphonate – formaldehyde condensate (SNF), polyether grafted polyacrylate (PA2), and lignosulphonate (LS) on the correlations have been investigated. The rheological properties have furthermore been monitored as a function of time.

7.2 Experimental

The rheological properties of 6 different Portland cement pastes (see properties in Table 3.1-3.3) with 3 different categories of plasticizers (lignosulphonate, naphthalene sulphonate – formaldehyde condensate and polyether grafted polyacrylate) have been measured by a Physica MCR 300 Rheometer (as described in Chapter 3.3).
Cement pastes were made with distilled water and with varying water-cement ratio and plasticizer dosages as listed in Table 7.1. The admixtures were added with the water (immediate addition). Silica fume replaced cement by volume fractions of 0.00 or 0.03 (corresponding to mass SF of total powder of 0.0 or 4.8%, alternatively 0.0 or 6.8 vol%).

Table 7.1: Experiments performed with various w/c, plasticizer type and dosage.

w/c	Plasticizer type	Plasticizer dosage (% by cement weight)
0.40	SNF, LS, PA2	0.53
0.37	LS	1.00
0.32	SNF, PA2	0.61

Blending of the pastes was performed in a high shear mixer from Braun (MR5550CA as described in Chapter 3.3.1) by adding solids to the water and mix for ½ minute, resting for 5 minutes and blending again for 1 minute.

Shear stress (τ) – shear rate ($\dot{\gamma}$) curves with linear sweep of $\dot{\gamma}$ from 200 down to 2 s^{-1} in 30 points lasting 6 s each were recorded by a parallel plate rheometer. The temperature was set to 20°C for all experiments. The rheological measurements were started 20 minutes after water addition. A full measurement sequence lasted 25 minutes due to included hysteresis, gel strength and oscillation sequences as discussed in Chapter 3. The measurements were repeated four times to monitor time dependencies.

Rheological properties were also measured on four cements which originated from the same clinker, but ground to different finenesses in order to investigate the plain effect of the cement surface. The mineral composition of the cements can be found in Table 3.4. Pastes were prepared with w/c = 0.40 and with 0.35% SNF by cement weight to achieve dispersed pastes.

7.3 Results and discussion

7.3.1 Effect of cement composition and plasticizer type

Figure 7.1 shows the flow resistance as a function of cement fineness for the four cements originating from the same clinker described in Table 3.4. The figure illustrates that the flow resistance is an exponential function of the cement fineness (Blaine). Fig. 7.2 illustrates, however, that cement fineness correlates poorly with flow resistance when the cements originate from different clinkers. This finding illustrates that cement cannot be treated as a univariable material. The flow resistance depends on several factors such as fineness, content of C_3A, alkali etc. and all these factors might increase or decrease from cement to cement pulling the flow resistance values in different directions. Thus, correlations cannot be made between flow and single cement characteristics unless there is only one variable differentiating the cements from each other. This finding is further emphasized by Figs. 7.3, 7.4 and 7.5 which show attempts of linear correlations with content of C_3S, total C_3A and cubic C_3A respectively. A more promising correlation was however found between flow resistance and Blaine multiplied with cubic C_3A as illustrated in Fig. 7.6. It is focused on the cubic crystal modification of C_3A since it is known to be more reactive than the orthorhombic crystal modification (Boikova et al. 1977, Bilanda et al. 1980). Thus, the idea behind multiplying cubic C_3A with Blaine is that this parameter represents the amount of active mineral on the surface (excluding the fraction inside the cement grain). However, C_3S is also quite reactive (although less than cubic C_3A) and it is much more of it (e.g. 60% versus 3%). It was therefore decided to include a weighed sum of the two minerals multiplied with Blaine giving the equation

$$\text{Blaine}\cdot[d\cdot\{\text{cubic } C_3A\} + (1\text{-}d)\cdot\{C_3S\}] \qquad (7.1)$$

where the factor d represent relative reactivity.

Attempts to make a linear correlation of the cement characteristics from eq. (7.1) with measured flow resistance for pastes with 0.53% by cement weight of SNF or polyacrylate as plasticizers gave surprisingly good fits (R^2 = 0.9908 and 0.9996 respectively) as depicted in Figs. 7.7 and 7.8. The results are surprisingly good since the series contain cements with and without 4% limestone interground as well as one with ≈17% Class F fly ash interground. However, using QXRD for determination of minerals of interest gives the correct value independently of other mineral additions.
The correlation has thus 3 variables (factors a, b and d) and 6 observations (number of cements):

$$\text{Flow Resistance} = a \cdot \text{Blaine} \cdot [d \cdot \{\text{cubic } C_3A\} + (1-d) \cdot \{C_3S\}] + b \qquad (7.2)$$

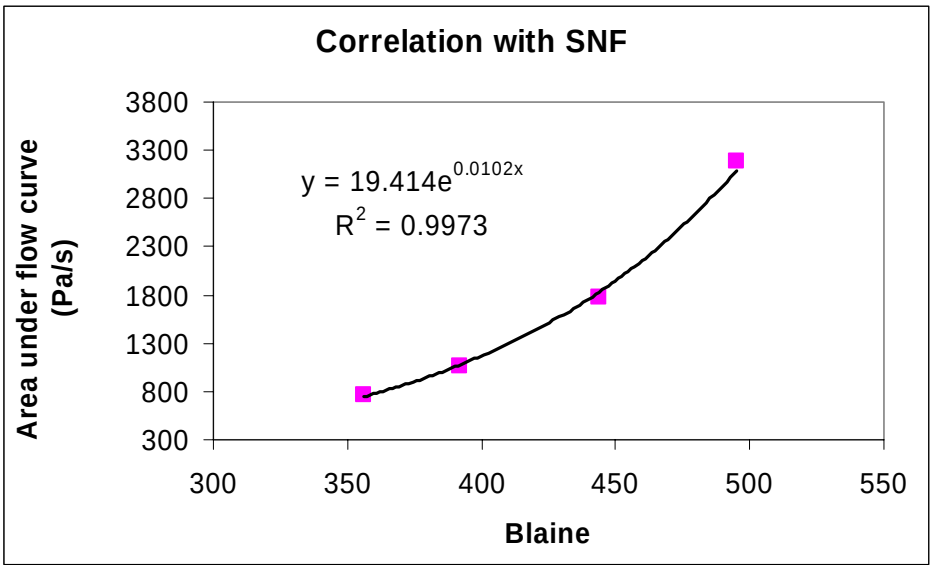

Fig. 7.1: Correlation of flow resistance in the medium shear rate range with Blaine (fineness) for 4 cements made of the same clinker, but ground to different fineness (see Table 3.4). The data are taken 20 minutes after water addition.

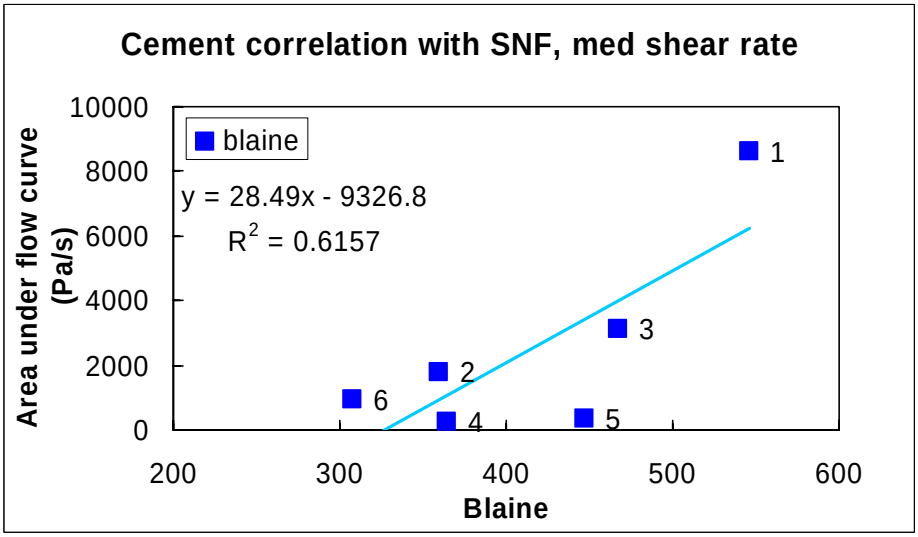

Fig. 7.2: Correlating the Blaine value of Cement 1-6 (described by Table 3.1-3.3) with area under the medium shear rate range of the flow curve for respective pastes with w/c ≈ 0.40 and 0.53% SNF. The data are taken from the first measurement sequence (20 minutes after water addition).

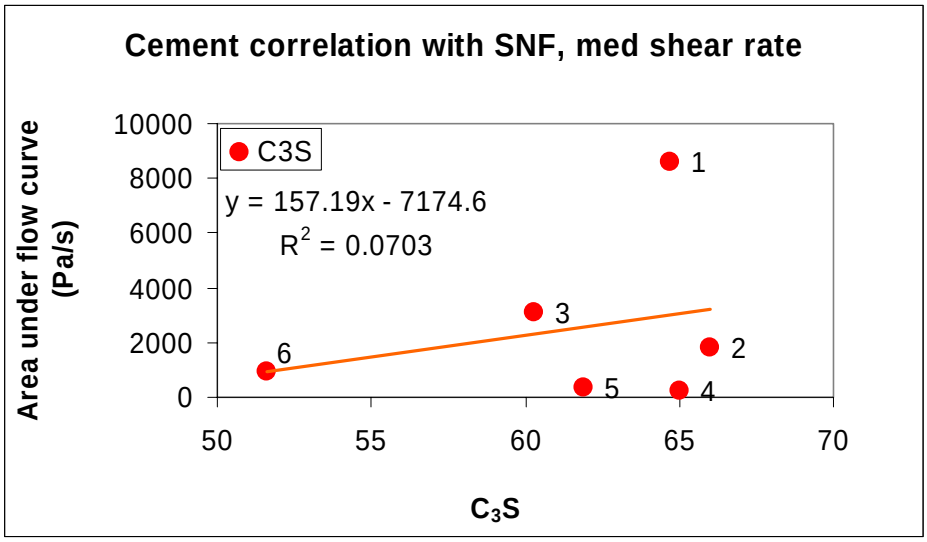

Fig. 7.3: Correlating the C_3S content in Cement 1-6 (described by Table 3.1-3.3) with area under the medium shear rate range of the flow curve for respective pastes with w/c ≈ 0.40 and 0.53% SNF. The data are taken from the first measurement sequence (20 minutes after water addition).

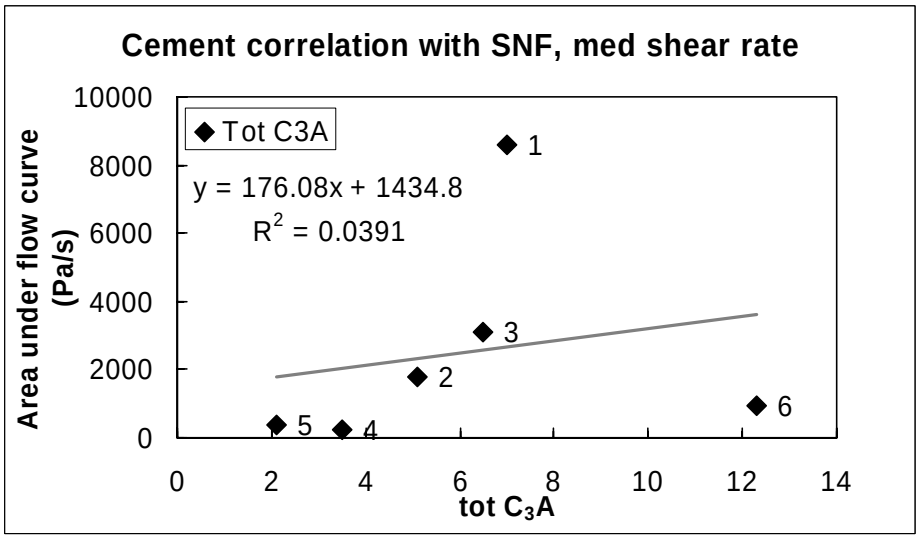

Fig. 7.4: Correlating the total amount of C_3A in Cement 1-6 (described by Table 3.1-3.3) with area under the medium shear rate range of the flow curve for respective pastes with w/c ≈ 0.40 and 0.53% SNF. The data are taken from the first measurement sequence (20 minutes after water addition).

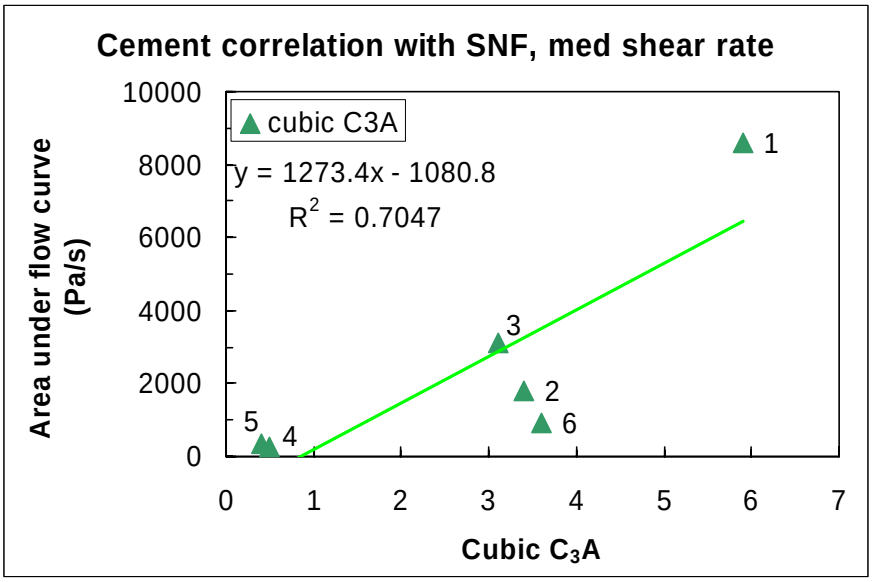

Fig. 7.5: Correlating the amount of cubic C_3A in Cements 1-6 (described by Table 3.1-3.3) with area under the medium shear rate range of the flow curve for respective pastes with w/c ≈ 0.40 and 0.53% SNF. The data are taken from the first measurement sequence (20 minutes after water addition).

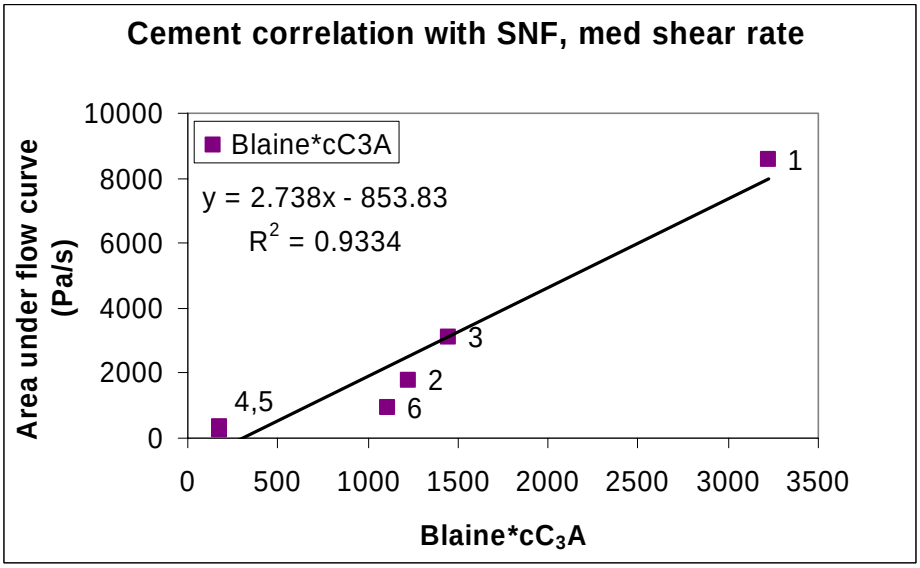

Fig. 7.6: Correlating the Blaine value multiplied with cubic C_3A for Cement 1-6 (described by Table 3.1-3.3) with area under the medium shear rate range of the flow curve for respective pastes with w/c ≈ 0.40 and 0.53% SNF. The data are taken from the first measurement sequence (20 minutes after water addition).

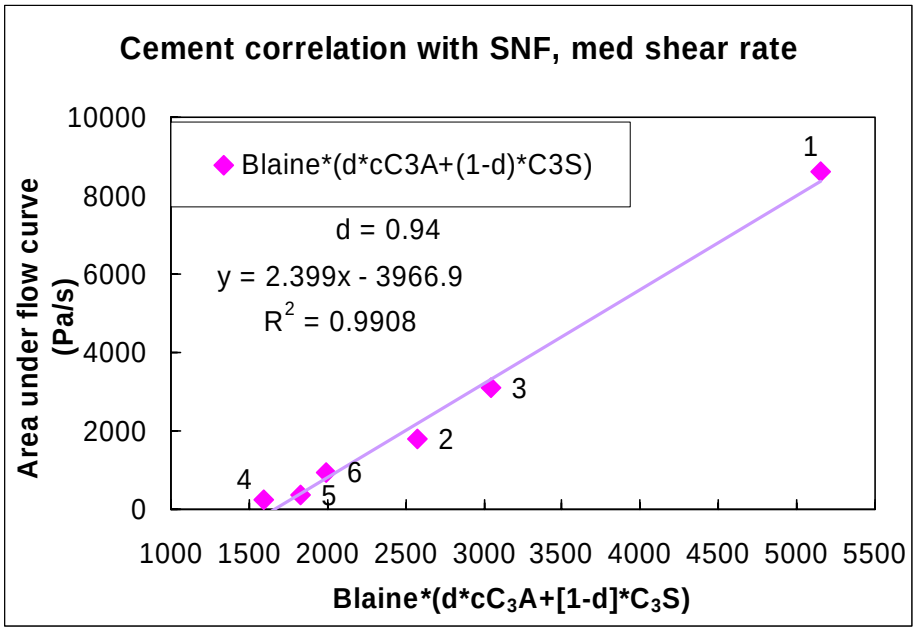

Fig. 7.7: Correlating the Blaine value multiplied with a weighed sum of cubic C_3A and C_3S for Cement 1-6 (described by Table 3.1-3.3) with area under the medium shear rate range of the flow curve for respective pastes with w/c ≈ 0.40 and 0.53% SNF. The data are taken from the first measurement sequence (20 minutes after water addition).

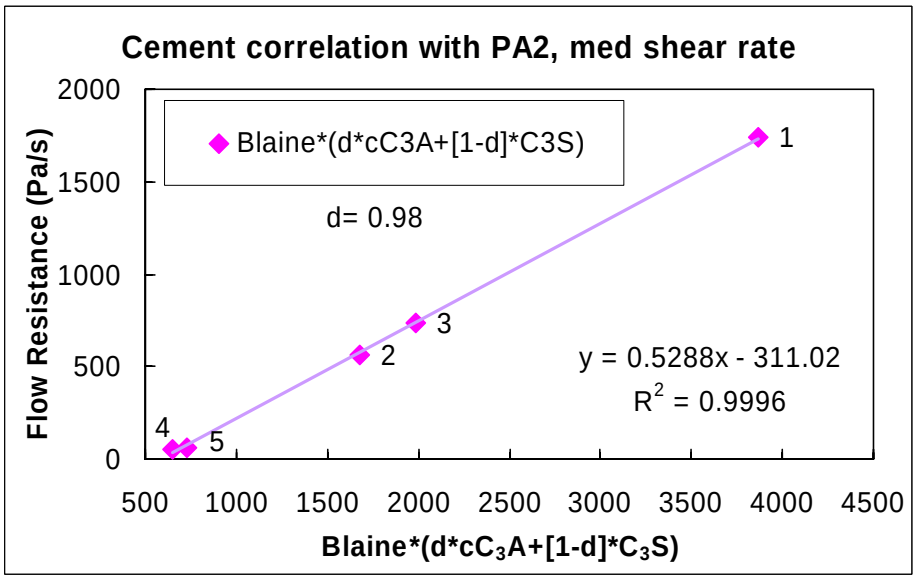

Fig. 7.8: Correlating the Blaine value multiplied with a weighed sum of cubic C_3A and C_3S for cements 1-5 (described by Table 3.1-3.3) with area under the medium shear rate range of the flow curve for respective pastes with w/c ≈ 0.40 and 0.53% PA. The data are taken from the first measurement sequence (20 minutes after water addition).

A linear relationship between cement characteristics and flow resistance was however not found to be a universal rule as illustrated by pastes with 0.53% lignosulphonate in Fig. 7.9. Table 7.3 classifies the type of correlation (linear or exponential) found for the different plasticizer types and dosages. Plots of all correlations made for pastes with SNF, lignosulphonate and polyacrylate can be found in Appendix A.2.1-A.2.7 while Bingham rheological data can be found in Appendix A.2.8.

Fig.7.9 illustrates that the paste of CEM I 42.5 RR has a much higher flow resistance than the others, resulting in an exponential correlation between flow resistance and cement characteristics similar to the correlation found for cement fineness and flow resistance in Fig. 7.1. The relationship between flow resistance and cement characteristics will in this case follow eq. (7.3).

$$\text{Flow Resistance} = a \cdot \exp(b \cdot \text{Blaine} \cdot [d \cdot \{\text{cubic C3A}\} + (1-d) \cdot \{\text{C3S}\}]) \qquad (7.3)$$

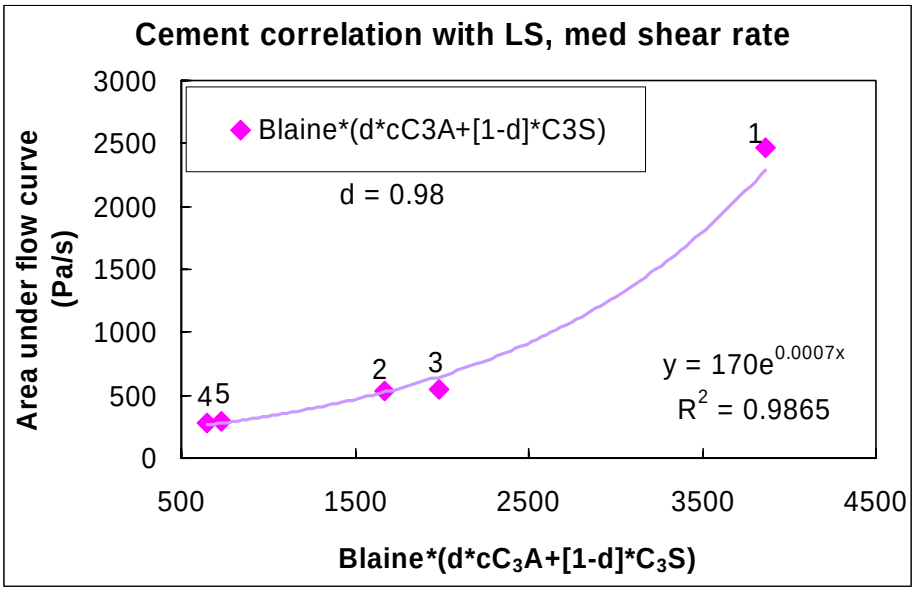

Fig. 7.9: Correlating the Blaine value multiplied with a weighed sum of cubic C_3A and C_3S for cements 1-5 (described by Table 3.1-3.3) with area under the medium rate range of the flow curve for respective pastes with w/c ≈ 0.40 and 0.53% lignosulphonate. The data are taken from the first measurement sequence (20 minutes after water addition).

The reason for the exponential growth of flow resistance might be influenced by the various finenesses and also possibly the C_3A content of the different cements.
Another possible explanation might be the different cement-plasticizer interactions. All cements have different saturation dosages of plasticizers as depicted for lignosuphonate and SNF in Table 7.2. The data illustrate that the saturation dosage depends on the cement type: A CEM I 42.5 RR paste has for example a plasticizer saturation dosage which is more than 3 times the saturation dosage for CEM I 52.5 R-LA cement. The particularly high flow resistance of CEM I 42.5 RR cement compared to the others might thus be caused by that this cement is under-plasticized at a plasticizer dosage of 0.53% SNF and lignosulphonate while some of the other cements are supersaturated.
The saturation dosages of polyacrylate are found to be significantly lower than for pastes with SNF and lignosulphonate. CEM I 42.5 RR requires for example 1.20% SNF by weight of cement or 0.32% PA2 to obtain a flow resistance of approximately 600 Pa/s (discussed in Chapter 9).

Another consequence of plasticizer addition is retardation of the cement hydration. The extent of retardation depends on cement type, plasticizer type and dosage. Lignosulphonate has been found to be the strongest retarder while SNF is the weakest of the three plasticizers studied (see Chapter 8). Pastes with plasticizer dosages below saturation will generally hydrate faster than supersaturated pastes.
CEM I 42.5 RR has relatively high surface area and C_3A content which cause a relatively high plasticizer saturation dosage and hydration rate compared to the other cements. The comparatively high hydration rate will in turn lead to relatively high flow resistance due to consumption of water

and precipitation of hydrate phases. The hydration of CEM I 42.5 RR will thus not be as retarded by the plasticizers as the others.

Table 7.2: Saturation dosage of SNF and LS for cements 1-5 (described by Table 3.1-3.3)

Cement number and type	Saturation dosage (% by cement weight)	
	SNF	**LS**
1 CEM I 42.5 RR	1.20	1.20
2 CEM I 42.5 R	0.56	0.80
3 CEM II A-V 42.5 R	0.72	0.64
4 52.5 R-LA	0.32	0.48
5 CEM I 42.5 R-LA	0.56	0.56

CEM I 42.5 RR and CEM I 52.5 R-LA are two cements at the opposite ends of the Blaine and C_3A content scale. CEM I 42.5 RR and CEM I 52.5 R-LA cement have thus the highest and the lowest plasticizer saturation dosage respectively. Figs. 7.10 and 7.11 depict the heat of hydration curves for CEM I 42.5 RR and CEM I 52.5 R-LA cements with 0.32% of the three plasticizers SNF, LS and PA2. The method of the calorimetric measurements together with full measurement series can be found in Chapter 8. The figures illustrate that CEM I 42.5 RR cement has much higher heat of hydration development than CEM I 52.5 R-LA. The initial hydration of CEM I 52.5 R-LA cement pastes is furthermore noticeably retarded by lignosulphonate compared to pastes with polyacrylate and SNF, while the initial hydration of CEM I 42.5 RR cement is not much affected by plasticizer type at the given dosage.

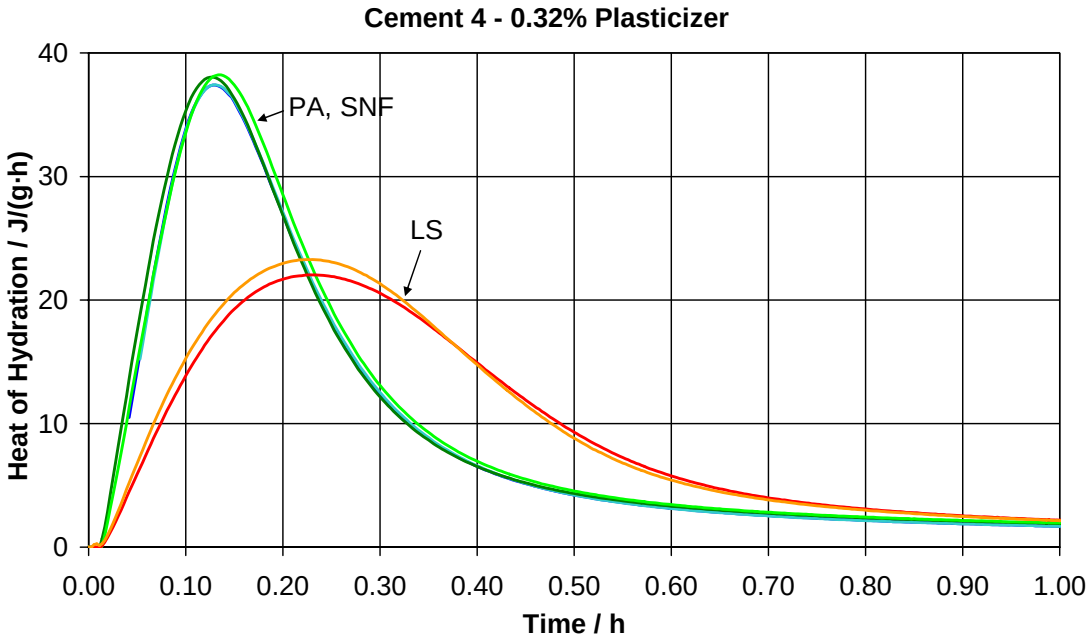

Fig. 7.10: Initial heat of hydration peak for CEM I 52.5 R-LA pastes with 0.32% polyacrylate, SNF and lignosulphonate. The heat of hydration curves for pastes with SNF and polyacrylate lay on top of each other. Each measurement has a parallel to monitor reproducibility.

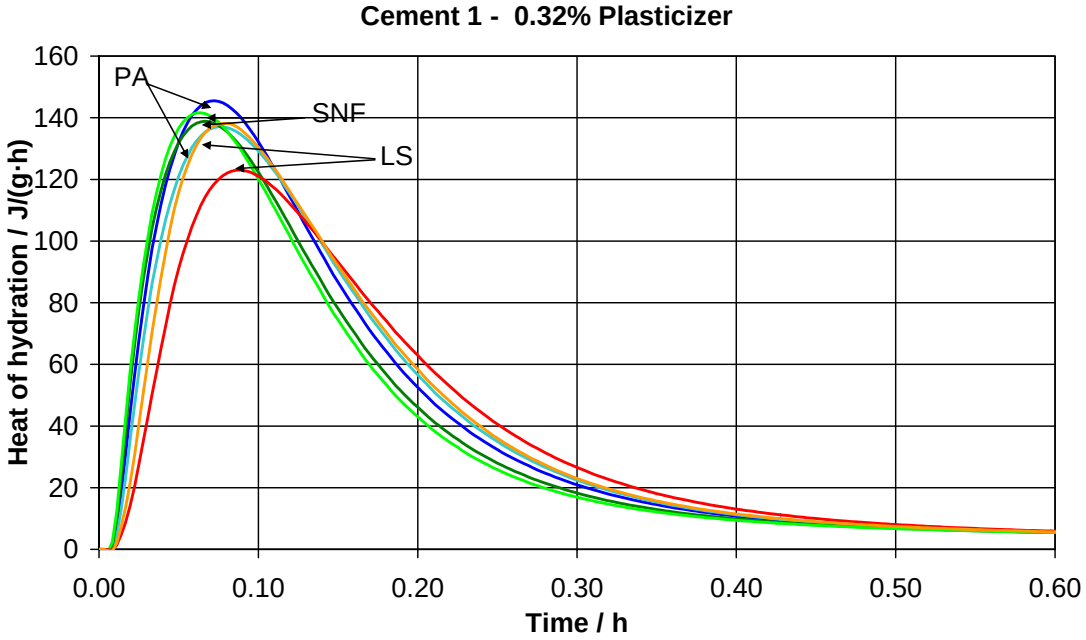

Fig. 7.11: Initial heat of hydration peak for CEM I 42.5 RR pastes with 0.32% polyacrylate, SNF and lignosulphonate. Pastes with polyacrylate develop most heat, while SNF and lignosulphonate pastes follow closely. Each measurement has a parallel to monitor reproducibility.

The relative reactivity parameter, d, given in equation (7.1) was determined by iteration. It can be seen from Table 7.3 that the values of d were found to be within the range of 0.9. This result is not surprising considering that the C_3A phase is the most active mineral during the initial couple of hours of hydration. Heat of hydration experiments (Chapter 8) have shown in the case of the fast

hydrating CEM I 42.5 RR cement that the dormant period ends and the main alite hydration starts approximately 2 hours after water addition which is within the time frame of the rheological measurements.
The value of d is furthermore found to vary with the plasticizer type, dosage and within the shear rate ranges, but no clear trends were found. A certain scatter of the d values should be expected since d is a measure of relative inhibition of hydration as well as a relative reactivity fraction for the cements investigated. The fact that d often varies within the shear rate range for the same paste might be caused by alteration of flow such as shear thinning and shear thickening.

Table 7.3: Values of the relative reactivity fraction, d, as a function of plasticizer type, dosage and shear rate range. All data are taken from the first measuring cycle (20 minutes after water addition.

Plasticizer	Plasticizer Dosage (%)	w/c	Shear rate range	Relative reactivity fraction, d	Flow resistance-cement characteristics correlation
SNF	0.53	0.40	Medium Low	0.940 0.945	linear
	0.61	0.32	Medium Low	0.990 0.990	exponential
LS	0.53	0.40	Medium Low	0.980 0.830	exponential
	1.00	0.37	Medium Low	0.960 0.990	exponential
PA2	0.53	0.40	Medium Low	0.980 0.935	linear
	0.61	0.32	Medium Low	1.000 1.000	linear

7.3.2 Influence of time

The flow resistance can increase or decrease with time during the initial hydration (dormant period): It will increase relative more with time for the cements with higher value of the cement characteristic Blaine·[d·{cubic C_3A} + (1-d)·{C_3S}] than for those with lower value, since higher specific surface and higher content of cubic C_3A lead to more surface hydration and thereby higher viscosity due to removal of water to form surface hydrates (see chapter 2.4.4). Some combinations of cements and plasticizers will however give increased flow within the dormant period as discussed in Chapter 9.3.2.
Table 7.4 recites the flow resistance data for cement pastes with 0.53% SNF, LS and PA2 as a function of cement type and time. It can be seen from the data that pastes with SNF markedly increase their flow resistance values as a function of time while pastes with LS and PA2 have minor increases of flow resistance values from the 2nd to the 4th measurement cycle (45 and 95 minutes after water addition respectively).

Table 7.4: Flow resistance as a function of time, cement and plasticizer type. All cement pastes are prepared with w/c = 0.40 and 0.53% plasticizer by cement weight and the flow resistance data are taken from the medium shear rate range (152 – 118 s^{-1}). The cements 1-6 are described by Table 3.1 - 3.3.

		Flow Resistance (Pa/s)			
Plasticizer	**Cement number**	**1st cycle**	**2nd cycle**	**3rd cycle**	**4th cycle**
SNF	1	8593	9875	11720	16500
	2	1797	2084	2490	2922
	3	3096	3817	4548	5370
	4	250	249	260	282
	5	364	376	432	495
	6	936	1131	1373	1616
PA2	1	1736	1819	2053	2436
	2	561	519	530	552
	3	738	595	581	576
	4	55	152	152	159
	5	61	122	132	139
LS	1	2460	2099	2092	2155
	2	529	361	382	382
	3	541	546	568	587
	4	278	205	208	237
	5	293	259	270	273

Tables 7.5 and 7.6 cite the measured effect of time (i.e. correlation at 25 min cycles) on the *linear* correlation variables a, b and d. Table 7.5 represent pastes with 0.53% by cement weight SNF which obtain flow loss (increased flow resistance) within the two hours of rheological measurements. It can be seen from the data and Fig 7.12 that the values of b decrease while the values of a increase given that d is constant.
The pastes in Table 7.6 represent pastes with 0.53% PA2 by cement weight which obtain both slight flow gain and flow loss. The data illustrate that the values of a increases slightly with time while the value of b decrease markedly. The relative reactivity fraction d is found to decrease with time which has a strong influence on the flow resistance values since the influence of C_3S content increase.
Table 7.6 shows furthermore that the linear regression parameter, R^2, decreases with time. This might be caused by the different hydration rates of the various cements. CEM I 42.5 RR cement hydrates particularly fast compared to the other cements due to its high surface and C_3A content. The decline in the regression parameter might also be caused by reduced reproducibility with time as discussed in Chapter 5.

Table 7.7 depicts the measured effect of time on the *exponential* correlation variables a, b and d. The pastes represented in Table 7.7 were added 0.53% lignosulphonate and obtained slight flow loss following initial flow gain as seen from Table 7.4. It can bee seen that the values of b are close to constant with time. The values of a and d decrease initially before they increase slightly from the 2nd to the 4th cycle.

It can be seen from Table 7.6 and 7.7 that the values of the relative reactivity factor, d, have been found to be lower at the low shear rate (43-8.8 s^{-1}) range the medium shear rate range (152 -

$118s^{-1}$). This might imply that the influence of the hydration products (initial CSH and ettringite) is stronger on the flow resistance at low shear rates.

Table 7.5: Linear correlation parameters for cement characteristics of Cement 1-6 versus area under flow curve for medium shear rate range (upper value) and low shear rate range (lower value) when 0.53% naphthalene sulphonate – formaldehyde condensate (SNF) is used as plasticizer.

Shear rate range	Parameter	1st cycle	2nd cycle	3rd cycle	4th cycle
Medium	R^2	0.9908	0.9928	0.9932	0.9842
Low		0.9973	0.9939	0.9905	0.9957
Medium	a	2.40	2.77	3.29	4.65
Low		1.69	1.84	2.05	2.57
Medium	b	-3967	-4547	-5417	-8019
Low		-2428	-2554	-2529	-3254
Medium	d	0.940	0.940	0.940	0.940
Low		0.945	0.950	0.955	0.955

Table 7.6: Linear correlation parameters for cement characteristics of Cement 1-6 versus area under flow curve for medium shear rate range (upper value) and low shear rate range (lower value) when 0.53% polyether grafted polyacrylate (PA2) is used as plasticizer.

Shear rate range	Parameter	1st cycle	2nd cycle	3rd cycle	4th cycle
Medium	R^2	0.9996	0.9793	0.9675	0.9521
Low		0.9794	0.9579	0.9454	0.9333
Medium	a	0.53	0.49	0.54	0.62
Low		0.23	0.29	0.30	0.34
Medium	b	-311	-629	-978	-1410
Low		-621	-673	-989	-1222
Medium	d	0.980	0.950	0.930	0.915
Low		0.935	0.900	0.880	0.870

Table 7.7: Exponential correlation parameters for cement characteristics of Cement 1-5 versus area under flow curve for medium shear rate range (upper value) and low shear rate range (lower value) when 0.53% lignosulphonate is used as plasticizer.

Shear rate range	Parameter	1st cycle	2nd cycle	3rd cycle	4th cycle
Medium	R^2	0.9871	0.9997	0.9991	0.9979
Low		0.9912	0.9846	0.9641	0.9805
Medium	a	170.53	45.45	54.2	66.06
Low		0.4644	0.5035	0.4375	0.1527
Medium	b	$672 \cdot 10^{-6}$	$597 \cdot 10^{-6}$	$600 \cdot 10^{-6}$	$601 \cdot 10^{-6}$
Low		$919 \cdot 10^{-6}$	$962 \cdot 10^{-6}$	$974 \cdot 10^{-6}$	$865 \cdot 10^{-6}$
Medium	d	0.98	0.900	0.910	0.920
Low		0.83	0.850	0.850	0.780

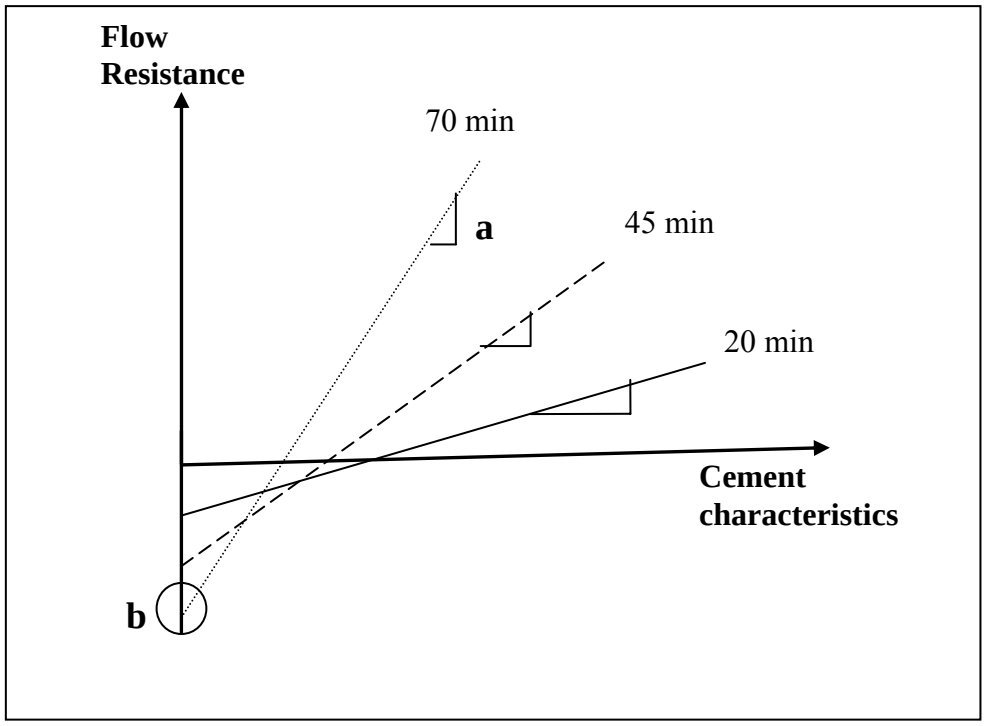

Fig. 7.12: Illustration of how the linear regression parameters a and b from eq. (7.2), Flow Resistance = a·Blaine·[d·{cubic C_3A} + (1-d)·{C_3S}] + b, change with time provided that the relative reactivity factor, d, is constant.

7.4 Conclusions

There is a correlation between the cement characteristic; Blaine·[d·{cubic C_3A} + (1-d)·{C_3S}] and the "flow resistance" measured as the area below the flow curve for selected shear rate ranges. The flow resistance is either a linear or exponential function of the cement characteristics depending on plasticizer type and dosage.
The minerals must be determined by XRD and holds then for a mix of pure cement and cement with fly ash, limestone filler (4%), as well as paste with constant silica fume dosage.

Chapter 8

Influence of cement and plasticizer type on the heat of hydration

8.1 Introduction

Six cements with different mineralogical composition and fineness have been studied in this thesis. Rheological studies have investigated their different flow behaviour while adsorption studies have shown that their adsorption of plasticizers depend on cement type as well as plasticizer type and dosage. This chapter investigates the heat of hydration curves for Cement 1-6 (as described by table 3.1-3.3) and how the hydration is altered by the addition of the three plasticizers SNF, lignosulphonate and polyacrylate (PA2).
Potential correlations between cement characteristics and initial setting time as determined from calorimetric curves will be discussed. The influence of superplasticizer type, content of alkali and cubic C_3A on setting time has been of special interest.

8.2 Results and discussion

Examples of the measured initial heat of hydration peaks are depicted in Figs. 8.1 and 8.2. Others can be found in Appendix A.3.1. The figures show that the rate of heat development depends on the superplasticizer and cement type. Pastes with polyacrylate and SNF tend to have a higher heat production rate than pastes with lignosulphonate. The addition of lignosulphonate tends to reduce the maximum heat rate and broaden the curves compared to pastes with polyacrylate and SNF. Thus, pastes with lignosulphonate have a lower hydration rate than pastes with polyacrylate and SNF, but they hydrate over a longer time span. The shapes of the initial heat peak were similar for all cement types tested.

Table 8.1 recites the time of occurrence of the maximum heat rate for the different cement and plasticizer combinations. The data illustrate that the time of the maximum initial hydration occurs within the first few minutes for all plasticizer and cement combinations. Cement 4 with lignosulphonate is however fairly retarded compared with the other cements. Cement 3 sticks out as well as having comparatively strongly retarded hydration with all plasticizer types. Some of the retardation of the initial hydration might be caused by the 16.3% inter-ground fly ash (Plowmann and Caberera 1981). Fly ash might also have different adsorption capacity of plasticizer as discussed in Chapter 9. The low adsorption capacity of fly ash leaves more plasticizer for the cement compared to the unblended cements. This might in turn lead to a more retarded cement hydration.

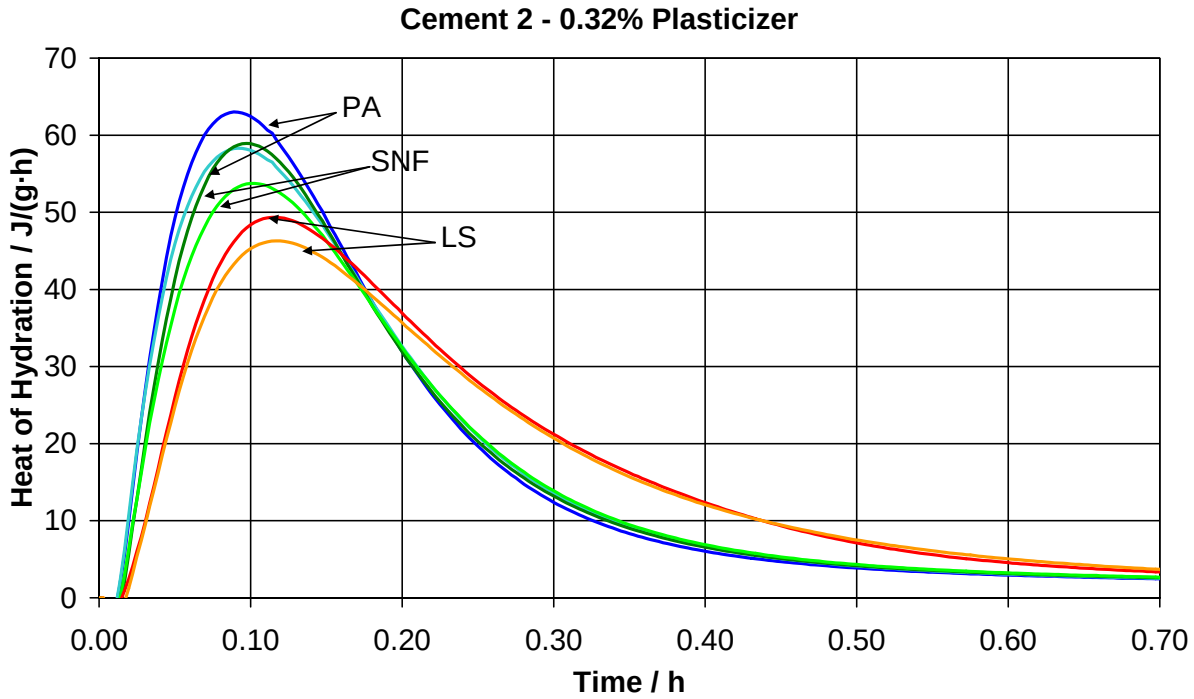

Fig. 8.1: Initial heat of hydration peak for Cement 2 with 0.32% PA2, LS and SNF. Two parallels are performed of each measurement to test the reproducibility.

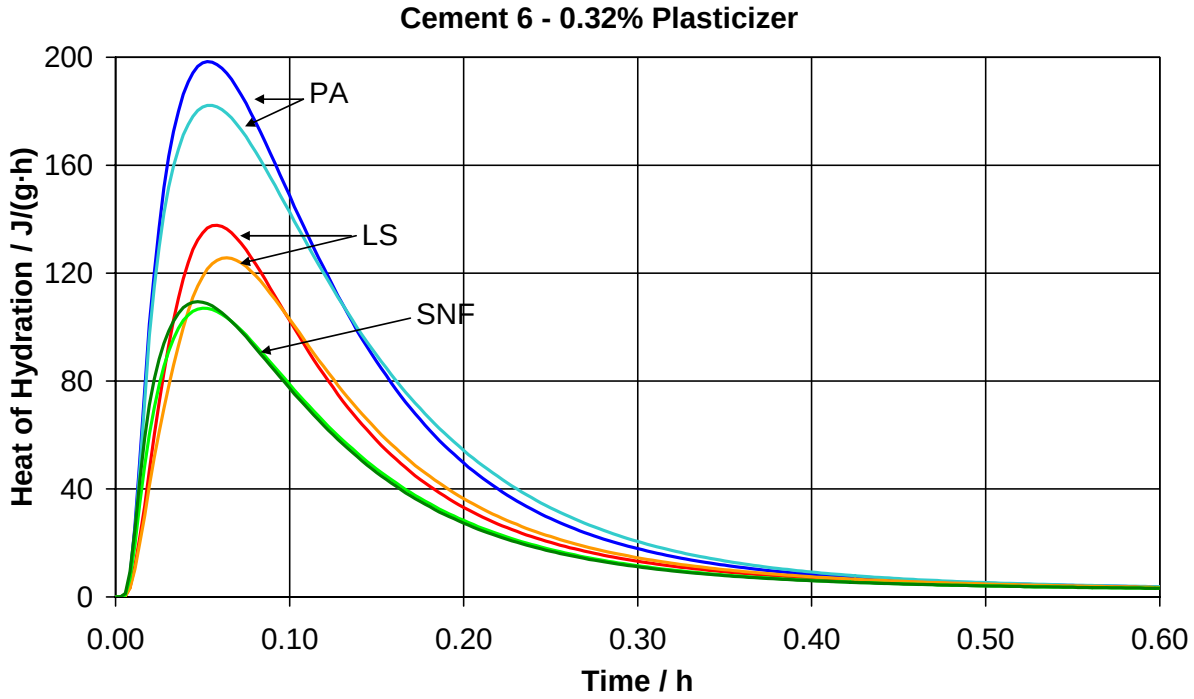

Fig. 8.2: Initial heat of hydration peak for Cement 6 with 0.32% PA2, LS and SNF. Two parallels are performed of each measurement to test the reproducibility.

Table 8.1: Time of maximum heat rate development for all cement and plasticizer combinations.

Cement number and type	Time of peak (min)		
	PA	**SNF**	**LS**
1 CEM I 42.5 RR	4.3	4.0	5.3
2 CEM I 42.5 R	5.5	6.2	7.1
3 CEM II A-V 42.5 R	*12.7*	*11.8*	*15.7*
4 52.5 R-LA	7.7	7.7	13.7
5 CEM I 42.5 R-LA	6.0	6.0	7.1
6 CEM I 42.5N	3.4	3.4	3.8

8.2.1 Correlation of initial heat of hydration peak with C_3A content

The initial heat of hydration peak is attributable to a combination of exothermal wetting and early stage reactions which with C_3A give a gelatinous coating of rods of AFt phase. It is believed that the main peak of the curve depicts the hydration of the aluminate phases since they produce more heat during the initial reaction with water than the silicates as seen from the enthalpy data in Table 8.2 (Taylor 1990). The main hydration of the silicate phases giving CSH and CH is believed to set in when the heat rate gradually decrease after approximately 24 hours.

Table 8.2: Enthalpy of hydration of pure clinker minerals (Odler 1998)

Starting phase	Reaction product	Enthalpy (kJ/kg)	Enthalpy (kJ/mol)
C_3S (+H)	CSH + CH	520	118
β-C_2S (+H)	CSH + CH	260	45
C_3A (+CH + H)	C_4AH_{19}	1160	314
C_3A (+H)	C_3AH_6	910	245
C_3A (+CSH_2 + H)	C_4ASH_{12} (AFm)	1140	309
C_3A (+CSH_2 + H)	$C_6AS_3H_{32}$ (AFt)	1670	452
C_4AF (+CH + H)	$C_3(A,F)H_6$	420	203

The heat of hydration curves were used to investigate if any correlations could be found between heat of hydration being produced the first hour after water addition and cement characteristics. Initial attempts were made to correlate the area under the heat of hydration curve (accumulated heat) against various cement characteristics. Integration of the heat evolution curves proved, however, to be difficult since it was hard to define an end point of the initial hydration peak due to the "tail" which appeared when the slopes flattened off. The maximal rate of heat evolution (top point of the curve) was therefore chosen as a correlation variable.

No correlations were found between the initial peak of the heat of hydration curve and the silicate phases alite and belite as expected. Correlations between maximal heat rate and the single cement variables C_4AF and total amount of C_3A were also found to be poor. There was however a correlation between the product of the cement fineness and C_3A content as illustrated for pastes with lignosulphonate in Fig. 8.3. This finding illustrate that cement cannot be treated as a univariable material as discussed in Chapter 7. Similar correlations were found for pastes with polyacrylate and SNF, but the correlation coefficients were somewhat poorer (0.8703 and 0.8054 respectively). The somewhat unfavorable regression coefficients (R^2<0.9) may be caused by the mixing procedure: The problem with mixing internally in the calorimeter is that one cannot control if the paste is evenly mixed and dispersed. Figs. 8.1 and 8.2 illustrate scattered reproducibility which is probably caused by agglomerates left after the internal mixing procedure.

It can be seen from Fig 8.3 that the fly ash cement (cement number 3) has to be left out of the plot in order to achieve a correlation. Cement number 3 stand out from the other cements since the clinker (a blend of 3 parts Cement 2 clinker with 1 part Cement 4 clinker) has been interground with 16.3% fly ash by weight. The fly ash might result in a retarding effect for C_3A as indicated by literature (Collepardi et al. 1978, Uchikawa and Uchida 1980). It has however been debated how the hydration of C_3S will be affected: Ogawa et al. (1980) found that fly ashes lengthen the dormant period and increase the height of the second peak while others have found a slight decrease of the second peak's intensity (Jawed and Skalny 1981, Collepardi et al. 1978, Uchikawa and Uchida 1980). These discrepancies may be caused by the origin of the fly ashes used since fly ashes may have even more variable chemistry than cements.

Another reason for the particularly low initial heat of hydration for cement 3 might be caused by altered adsorption of plasticizer as discussed above.

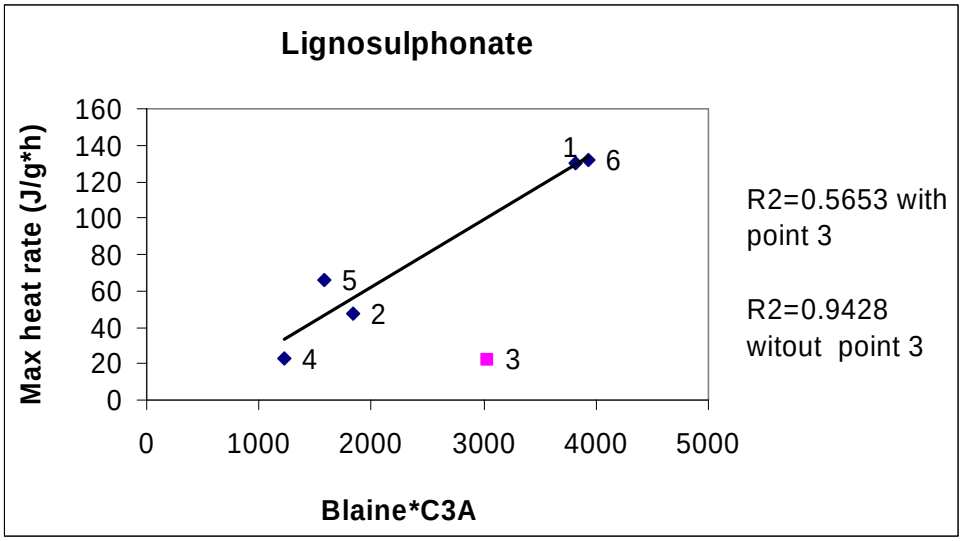

Fig. 6.29: Correlation between maximum heat rates at the initial peak of hydration against the product of the cement fineness (Blaine) with the total amount of C_3A for the cements 1-6. Lignosulphonate has been added as plasticizer. The best correlation is obtained when the fly ash cement is left out.

8.2.2 Heat of hydration curves for the second third and fourth hydration peaks

Heat of hydration curves for Cement 6 pastes with the three plasticizers SNF, lignosulphonate and polyacrylate are depicted in Figs. 8.4-8.6. Hydration curves for the remaining cements can be found in Appendix A.3.2. All plasticizers were found to prolong the dormant period. The retardation was found to depend on plasticizer type and dosage. It was furthermore found that the admixtures not only delayed the hydration, but also changed the hydration process. Figs.8.4-8.6 illustrate for example that the heat of hydration curve for Cement 6 have three main peaks when no superplasticizer is added. These peaks may be interpreted as CSH formation, AFt formation and AFt to AFm transformation (sulphate depletion peak). AFt formation and AFt-AFm transformation peaks are generally not as easily detected for the other cements as for Cement 6 as illustrated by Cement 2 in Fig. 8.7. A small AFt-AFm shoulder can however be distinguished. The difference can be explained by the high content of C_3A (12.3%) in Cement 6 versus Cement 2 (5.1%). The other cements had total C_3A contents ranging from 2.1 to 7.0%.
Increasing amounts of superplasticizer seem to increase the peak of AFt while the AFt-AFm transformation peak has broadened considerably or disappeared. Thus, the overall heat evolution might be increased even thought the second heat peak is delayed.
Sandberg and Roberts (2003) found similarly that *the aluminate reactivity increased while the main strength given by silicate hydration was retarded* as lignosulphonate was added to Portland cement pastes at increasing dosages. As a consequence, the sulphate depletion peak appeared closer and closer to the maximum of the main silicate hydration peak. Eventually, the sulphate depletion peak appeared before the now strongly retarded silicate hydration peak. Bensted (1987) noted similarly that the first heat peak of a retarded cement paste was increased in comparison with that of the corresponding neat cement slurry.
Much research has been done on the mechanisms causing the retarded hydration of plasticized cement pastes (Uchikawa et al. 1992, Odler and Becker 1980). Wilding et al. (1984) found that the precipitation of CSH gel appeared to be altered by preferential complexation of calcium and/or silicon either in solution or by incorporation into the precipitated gel. This resulted in the formation of less permeable, more adhesive gel coatings around the cement grains which again gave a retarding effect. Carazeanu et al. (2002) found similarly that plasticizers such as SMF and lignosulphonate react strongly with calcium aluminate hydrate and related substances delaying nucleation and inhibiting crystal growth of ettringite. Thus, the setting times' dependence on the plasticizer type might be caused by the differences adsorption and complexation with the hydration products.

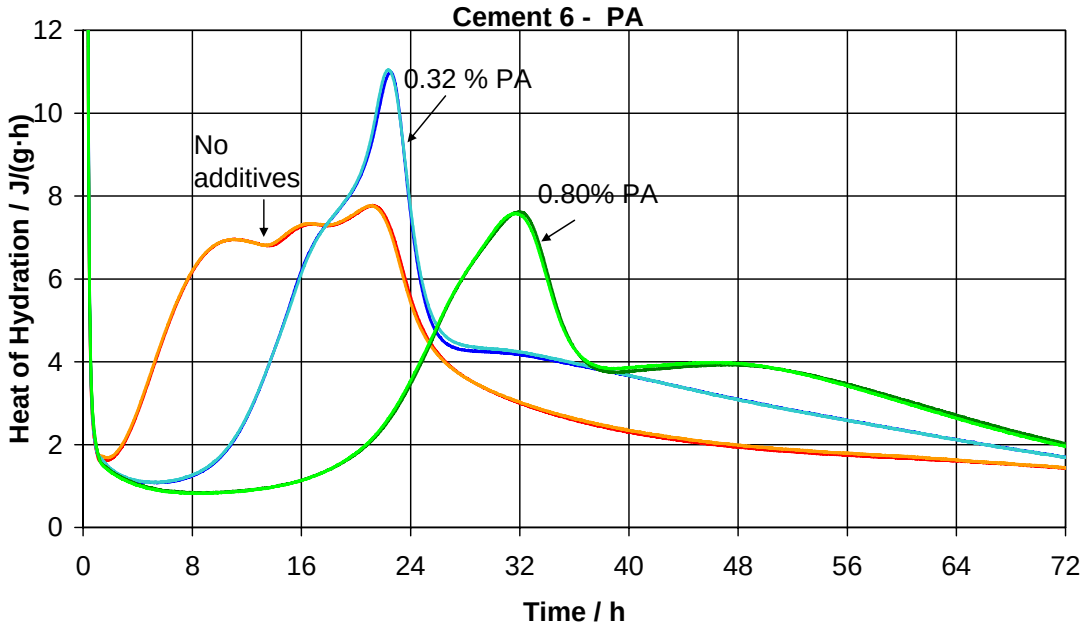

Fig. 8.4: Heat of hydration curves for Cement 6 with 0%, 0.32% and 0.80% polyacrylate (PA2) added as plasticizer.

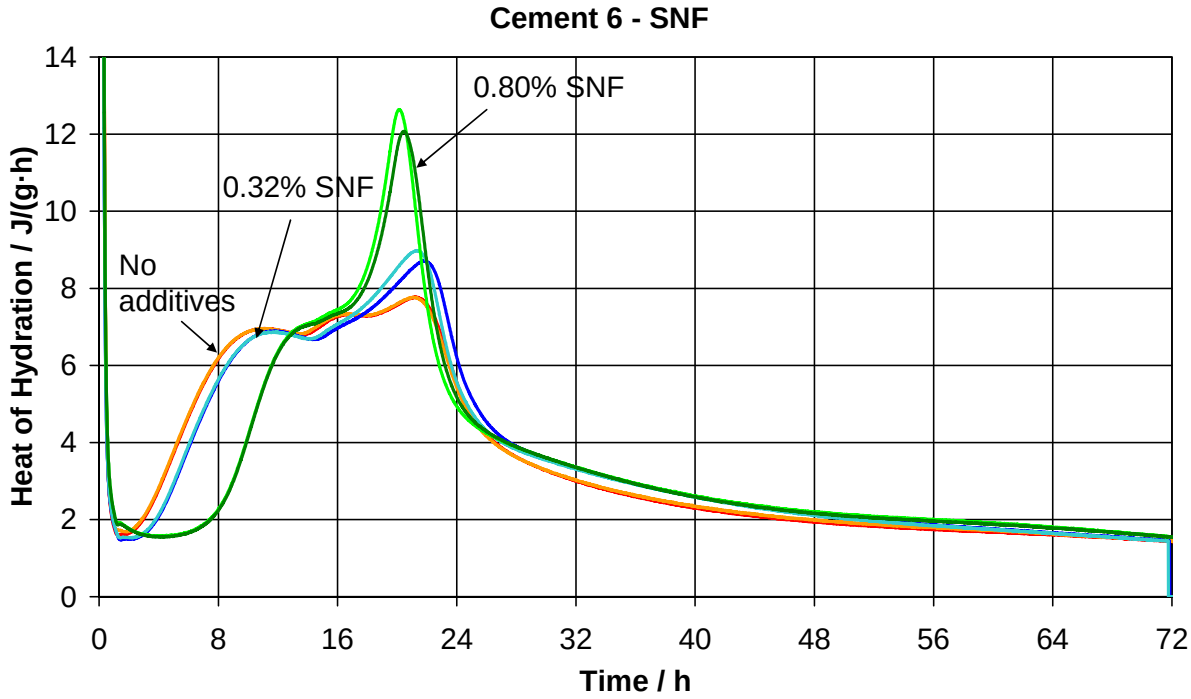

Fig. 8.5: Heat of hydration curves for Cement 6 with 0%, 0.32% and 0.80% SNF added as plasticizer.

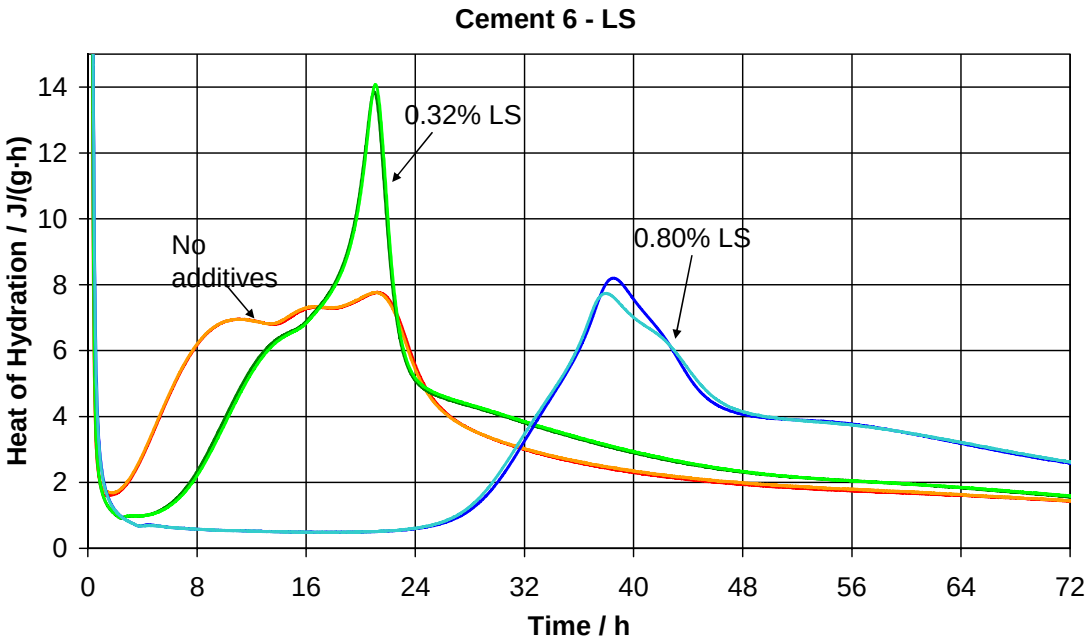

Fig. 8.6: Heat of hydration curves for Cement 6 with 0%, 0.32% and 0.80% lignosulphonate added as plasticizer.

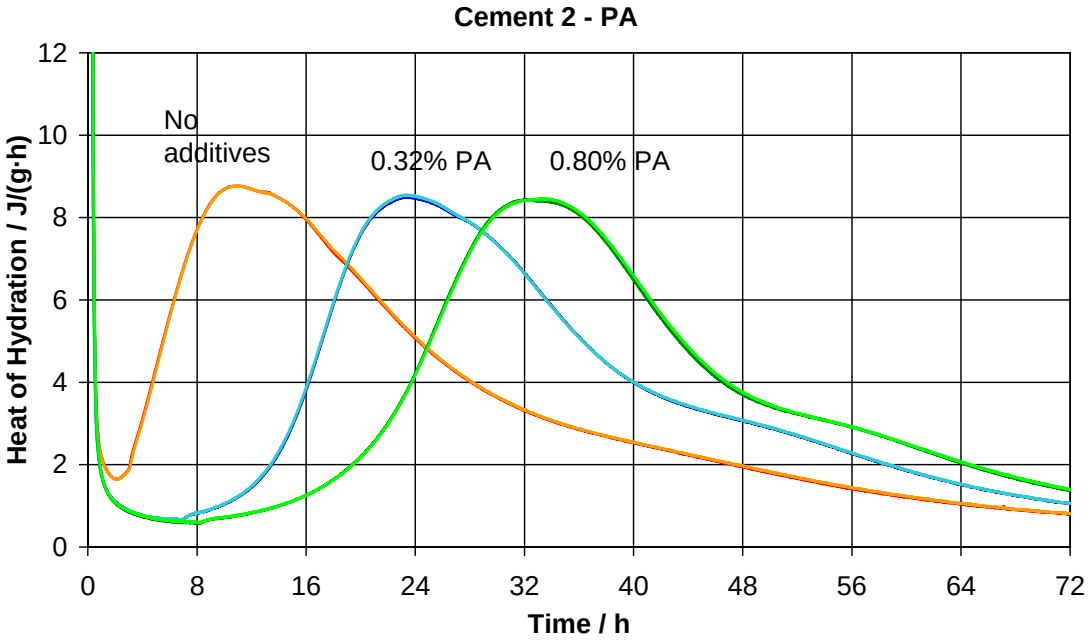

Fig. 8.7: Heat of hydration curves for Cement 2 with 0%, 0.32% and 0.80% polyacrylate (PA2) added as plasticizer.

8.2.3 Setting time as a function of cement characteristics

The initial setting times for the different cement-plasticizer combinations were determined from the calorimetric curves at the end of the dormant period as illustrated in Fig. 8.8. The setting of cement paste is caused by the combination of the hydration of the interstitial phase, including C_3A and C_4AF, and the hydration of alite. The hydration of the interstitial phase occurs mainly in the hours just after mixing with water. This hydration is affected by the concentration of Ca^{2+}, OH^- and SO_4^{2-} in the mixing water. The concentration of those ions depends upon the amounts of alkali sulphate, gypsum and free lime in the cement just after mixing with water; after that it depends upon the hydration reaction of alite (Uchikawa et al. 1984).

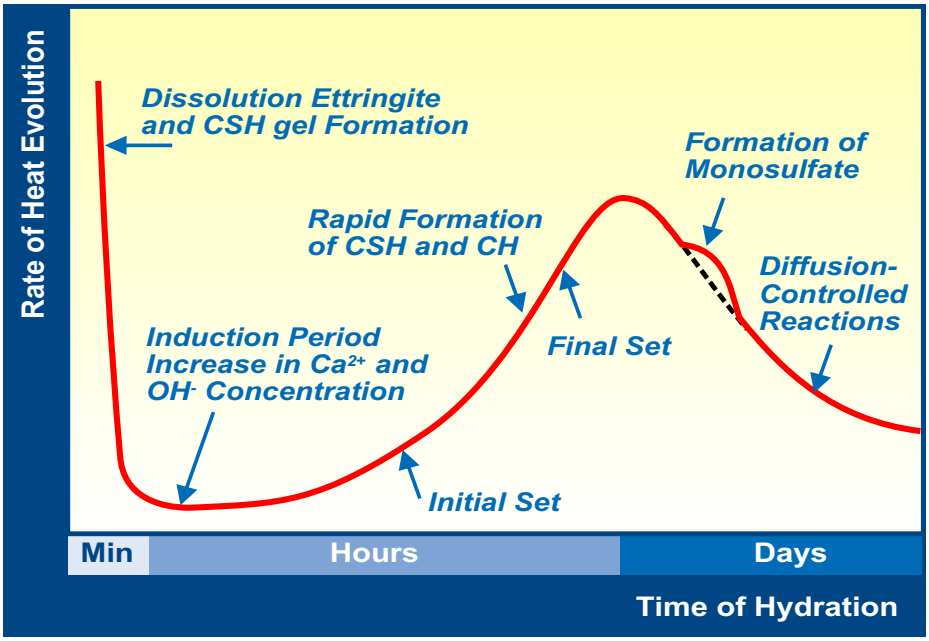

Fig. 8.8: Principal sketch of Portland cement hydration development and setting. Initial setting time is determined at the end of the dormant period.

Figs. 8.9-8.11 illustrate setting times as a function of plasticizer dosage. Lignosulphonate is found to be the strongest retarder of the three plasticizers under study while SNF has the least effect on the setting time. Uchikawa et al. (1992) found similar results while studying the effects of lignosulphonate and β-SNF on the cement hydration. They found that although the initial and final set were delayed by both lignosulphonate and β-SNF, the delay and the time between the initial and final set were more increased by lignosulphonate than β-SNF. A possible reason for the difference in setting times is that lignosulphonate produces a complex salt with Ca^{2+} in the liquid phase in a higher degree than β-SNF. The Ca-complexation reduces the concentration of Ca^{2+} in the liquid phase which delays the saturation of Ca^{2+} which again influences the morphology of hydrate produced, causes fluidity loss with time and delays the setting time of cement.

The shape of the setting time curves for pastes with polyacrylate differ from the curves for pastes with lignosulphonate and SNF. This difference might be caused by the finding that the polyacrylate based admixture has a much lower saturation point and different adsorption characteristics compared to SNF and lignosulphonate (see Chapter 9). This finding might partly be caused by the difference in molecular size: The polyacrylate used in these

experiments had a molecular weight of 220,000 while the lignosulphonate had a weight of 51,000. SNF contains much smaller molecule than the before mentioned with a molecular weight of 2,350 for n=10 and 4,700 for n=20. Thus, polyacrylate might be able to block a higher amount of active nucleation sites (simply by surface coverage) than SNF and lignosulphonate even if the saturation dosage is lower.
Lignosulphonate was found to be a stronger retarder than polyacrylate despite its lower molecular weight. This might be caused by the adsorption behaviour of polyacrylate: The adsorption study in Chapter 9 illustrates that adsorbed amount of polyacrylate decreases after the saturation dosage has been reached (see Fig. 9.6 of adsorption of polyacrylate on Cement 2). This adsorption behaviour is contrasted by SNF and lignosulphonate which reach a plateau value for adsorbed amount of plasticizer or follow low affinity adsorption behaviour. Thus, higher amounts of lignosulphonate and SNF can adsorb on the cement surface and intercalate in the hydration products.

An interesting feature of Fig. 8.10 is that SNF at low dosages increase the reaction rate and thereby reduce the setting times as seen for Cements 1 and 4. This effect has also been observed by Simard et al. (1993) who studied SNF. They believed that the increase of reaction rate was caused by physical effects, namely an improved dispersion of the cement particles in the presence of superplasticizer. The retardation effect of SNF became evident, however, as the concentration increased.

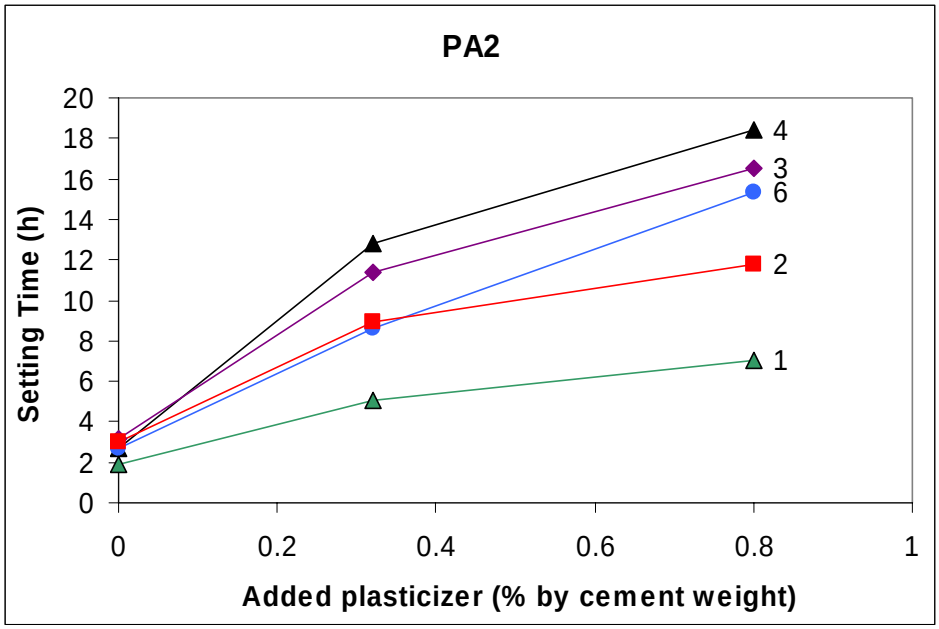

Fig. 8.9: Setting times for Cements 1-6 (described by Table 3.1-3.3) with added polyacrylate.

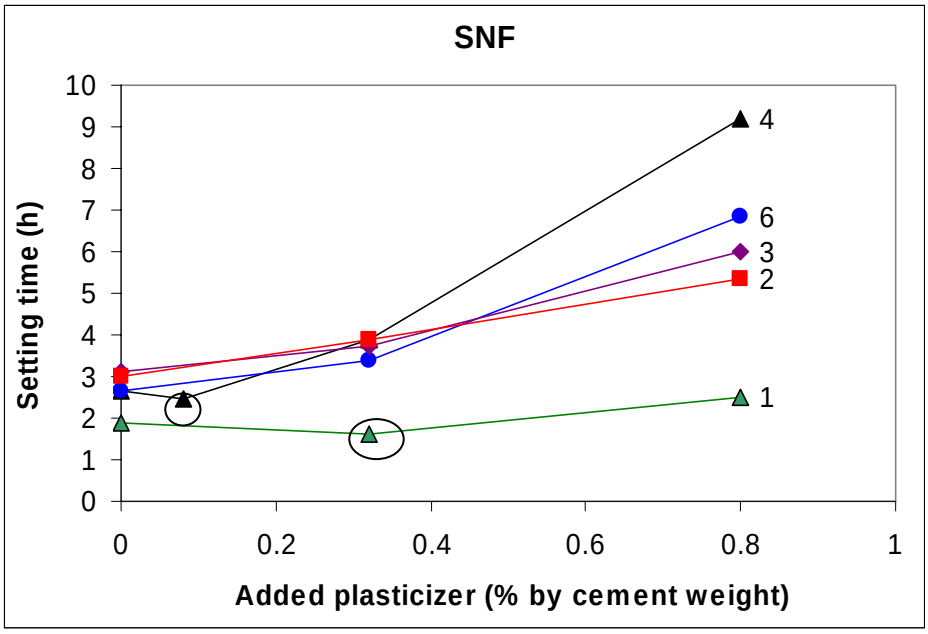

Fig. 8.10: Setting times for Cements 1-6 (described by Table 3.1-3.3) with added SNF. The circled measuring points are pastes with accelerated setting time.

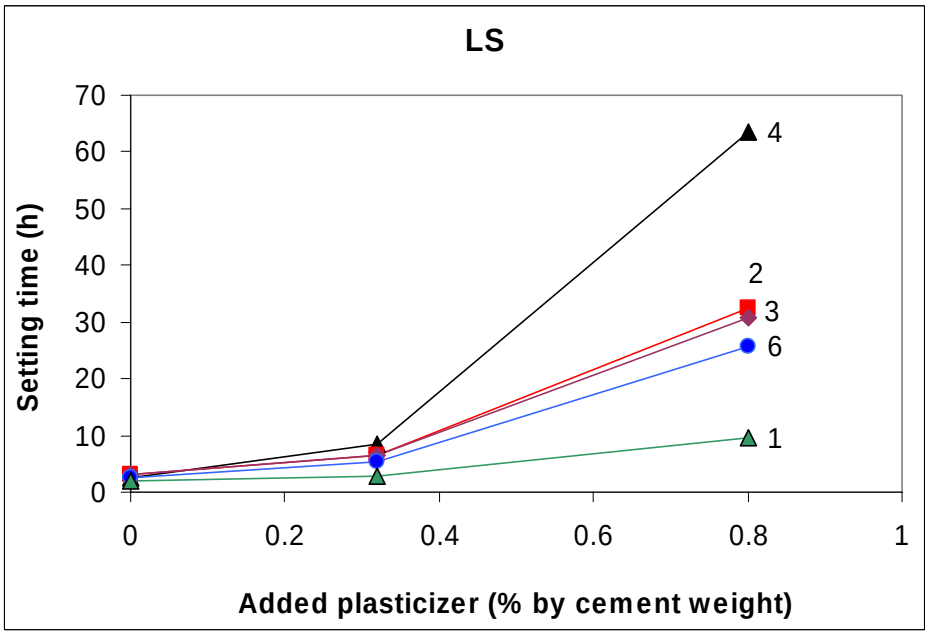

Fig. 8.11: Setting times for Cements 1-6 (described by Table 3.1-3.3) with added lignosulphonate.

No correlations between the setting times and cement characteristics such as cement fineness, aluminate and alkali contents could be found for pastes without plasticizer as illustrated in Table 8.3 and Figs. 8.12-8.15. Some correlations were however found for plasticized pastes as illustrated by Table 8.3 and Figs. 8.15-8.19. The correlations seem even to include the fly ash cement which might indicate that the fly ash does not have as strong influence on the main heat of hydration as on the initial.
It is unclear how the plasticizers influence the correlations. It can be seen from Figs. 8.6 and 8.7 that the reproducibility of the heat of hydration curves for pastes without plasticizer is as good as for the plasticized ones. Thus, the causes of the poor correlations for un-plasticized

pastes are probably not caused by the mixing procedure and reproducibility of the heat of hydration measurements.
The setting times vary however within a narrow range when no plasticizer is added. Small uncertainties in the determination of setting time could therefore have a strong effect on the correlations. The range of setting times for pastes with 0.32% SNF is also quite narrow as illustrated by Fig. 8.10. The setting times of these pastes correlate however with the cement characteristics similarly as pastes with a broader range of setting times (0.80% plasticizer). Thus the poor correlations for pastes without plasticizer are probably not merely caused by uncertain readings of the setting times.
The correlations' dependence on whether plasticizer is added or not might be caused by the influence of the plasticizers on the hydration processes. Plasticizers disperse agglomerates and adsorb on active hydration sites. Such adsorption can cause retardation and altered morphology of the hydration products formed by reducing growth or by intercalation in the hydration products. Dissolved ions might also form complexes with the superplasticizer molecules. Such plasticizer-cement interactions have been studied by Dodson and Hayden (1980) who found that the solubility rate of anhydrite decreased noticeably in the presence of lignosulphonate. The dissolution rate was not only controlled by the nature and the specific surface area of the minerals but also by the diffusion rate of the ions at the solid-liquid interface. This last parameter can become a limiting factor if a diffusional barrier is created at the interface of the reacting powders. Prince et al. (2003) found similarly formation of some monosulphate beside ettringite at the early beginning of hydration when superplasticizer (sodium salt of polynaphtalene sulfonate) was added. Usually, monosulphate aluminate is formed when there is a deficiency in SO_4^{2-} with respect to $Al(OH)_4^-$ (molar ratio < 3). Thus they found it possible that the superplasticizer reduced the dissolution rate of anhydrite. In the absence of the superplasticizer, ettringite was predominant even if some small amount of monosulphate aluminate was found.
Thus, the superplasticizer might decrease the dissolution rate of anhydrite and create a diffusional barrier at the surface of the reacting powders. This effect results in a modification of the sequence in which the various hydrated phases are appearing. Some monosulfoaluminate can for example be initially formed and then be transformed into ettringite, if later on the amount of sulphate ions reaches a sufficient level (Uchikawa et al. 1992).

Table 8.3: Regression coefficients for correlations between cement characteristics and setting time.

Characteristic	R^2			
	No plasticizer	**0.80% SNF**	**0.80% LS**	**0.80% PA**
Blaine	0.1278	0.5842	0.3334	0.3947
C_3A	0.1298	0.0291	0.3031	0.0086
Cubic C_3A	*0.4442*	*0.9175*	*0.9691*	*0.7959*
Na equivalent	0.2014	0.7953	0.4393	0.8066
K^+	0.1847	0.8046	0.4910	0.8090
Blaine·C_3A	0.3999	0.3991	0.7505	0.2309
Blaine·cC_3A	*0.5508*	*0.9345*	*0.8010*	*0.8093*
Na_{eqv}·cC_3A	0.5070	0.4528	0.1113	0.6154
K^+·cC_3A	*0.4967*	*0.9642*	*0.7222*	*0.9669*

Table 8.4: Regression coefficients for correlations between cement characteristics and setting time.

Characteristic	R^2		
	0.32% SNF	**0.32% LS**	**0.32% PA**
Blaine	0.5479	0.2529	0.4182
C_3A	0.0529	0.166	0.2413
Cubic C_3A	*0.6591*	*0.8926*	*0.9469*
Na equivalent	0.3215	0.5257	0.402
Blaine·C_3A	*0.8126*	*0.7887*	*0.8864*
Blaine·cC_3A	*0.8262*	*0.7846*	*0.8978*
Na_{eqv}·cC_3A	0.2118	0.2920	0.1452
K^+·cC_3A	*0.6972*	*0.8451*	*0.7857*

The setting times do not correlate with the cement fineness (Blaine) and content of C_3A when they are introduced as a single parameters as seen by Table 8.3 and 8.4. The product of cement Blaine and C_3A content results however in a good correlation. It may however seem from the tabulated data that the setting times depend stronger on the cubic modification of C_3A than the sum of orthorhombic and cubic aluminate. This finding indicates that the cubic aluminate modification is more reactive than the orthorhombic as found by Boikova et al. (1977) and Bilanda et al. (1980).
There is generally better correlations between the setting times and content of cubic C_3A for pastes with SNF and lignosulphonate than for pastes with polyacrylate. A reason for these differences might be that SNF and lignosulphonate has been found to intercalate in C_3A, while the same has not been found for polyacrylate (see Chapter 9).

The setting time seems to decrease with increasing content of easy soluble K-ions in the cements. A similar correlation was not found between the setting time and the sodium equivalent ($0.658\cdot(\%K_2O) + \%Na_2O$). Thus, easily soluble potassium sulphate has a stronger influence on the setting time than sodium sulphate. Similar results were reported by Odler and Wonnemann (1983, a) who found that the initial hydration rate of C_3A was slowed down appreciably by the presence of Na_2O in the crystal lattice and accelerated by the presence of K_2O. Additions of alkali sulphate to laboratory-prepared clinker did not cause changes to the degree of hydration of C_3A, but the setting times were significantly reduced, the potassium sulphate being more effective than the sodium sulphate.

Alkali sulphate is known to accelerate the hydration of Portland cement in the acceleration period and increase the rate of heat evolution towards its peak (Jawed and Skalny 1978, Li et al. 2003). The increased hydration rate has been linked to accelerated rate of ettringite formation (Odler and Becker 1980), but the alkali sulphates are not known to alter the progress of C_3S and C_3A hydration (Odler and Wonnemann 1983, b).
Acceleration of setting has been especially linked to potassium sulphate and has been linked to the formation of syngenite, $K_2SO_4 \cdot CaSO_4 \cdot H_2O$, which give rise to false setting. The formation of a rigid syngenite structure not only leads to quick setting, but also decreases the sulphate content in the liquid phase of the hydrating cement to the extent that it cannot adequately retard hydration of C_3A; this in turn leads to early stiffening (Jawed and Skalny 1977). There is no known sodium analogue of syngenite. This may explain the correlation with $K^+ \cdot cC_3A$.

Correlations of setting time versus the cement characteristics Blaine$\cdot(dC_3A_{cubic} + (1\text{-}d)C_3S)$ were attempted. The reactivity fraction, d, which indicates the relative amounts of C_3A and C_3S which have hydrated, was found to be equal to unity for all three plasticizers. This indicates that the C_3S phase is not one of the dominating components at the point of initial set. Thus, the cubic C_3A and amount of soluble alkali (particularly potassium) are driving factors for the set of the paste.

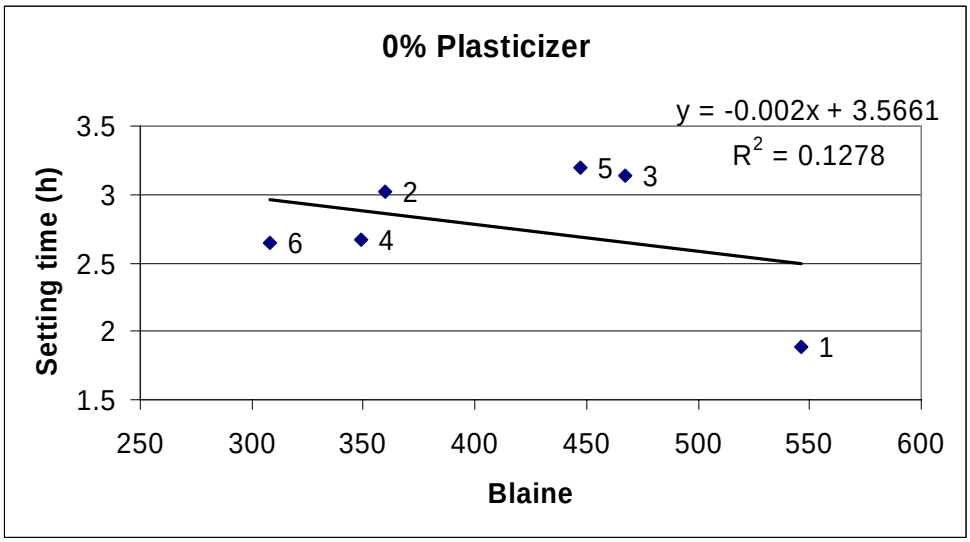

Fig. 8.12: Correlation between setting time and the cement fineness (Blaine) when no superplasticizer is added. The numbers at each measuring point refers to the cement number given in Table 3.1-3.3.

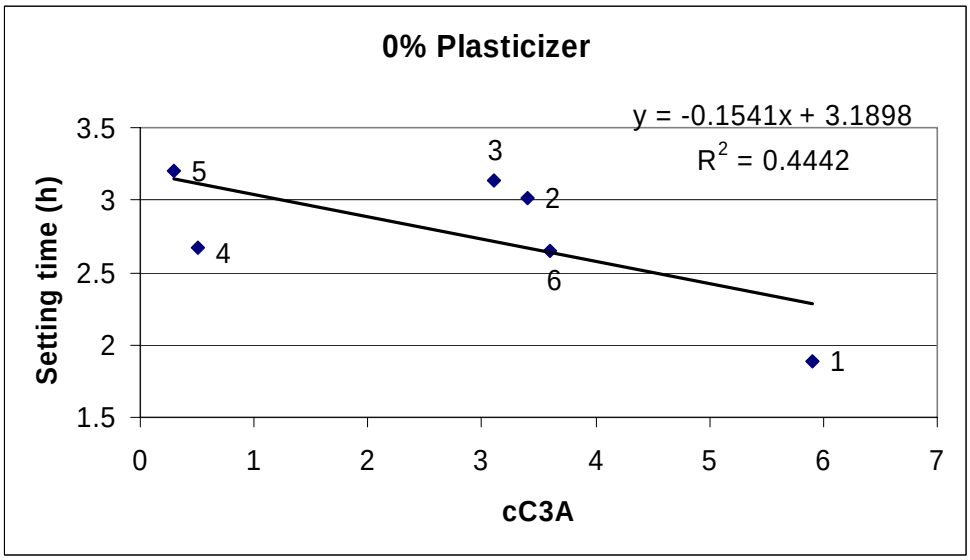

Fig. 8.13: Correlation between setting time and amount of cubic C_3A in the cements when no superplasticizer is added. The numbers at each measuring point refers to the cement number given in Table 3.1-3.3.

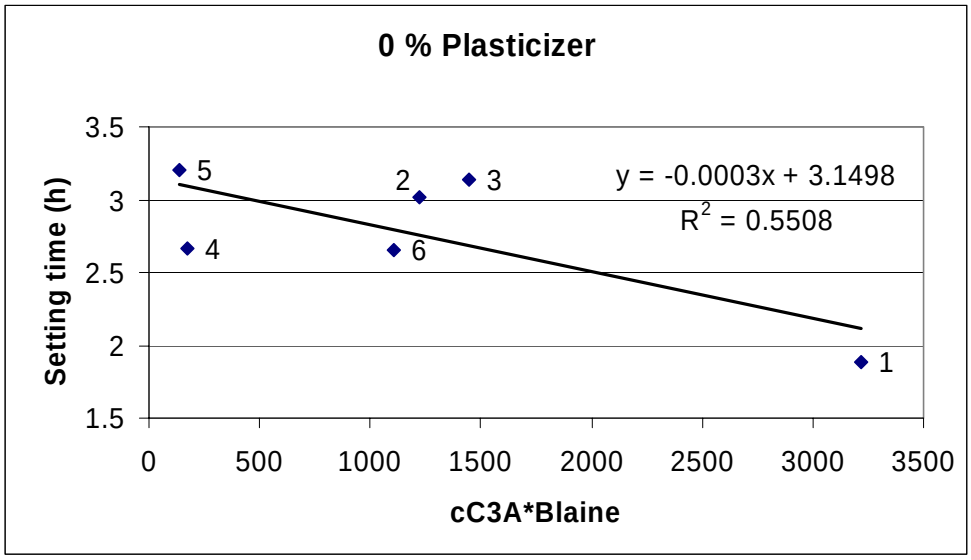

Fig. 8.14: Correlation between setting time and the product of cubic C_3A and Blaine when no superplasticizer is added. The numbers at each measuring point refers to the cement number given in Table 3.1-3.3.

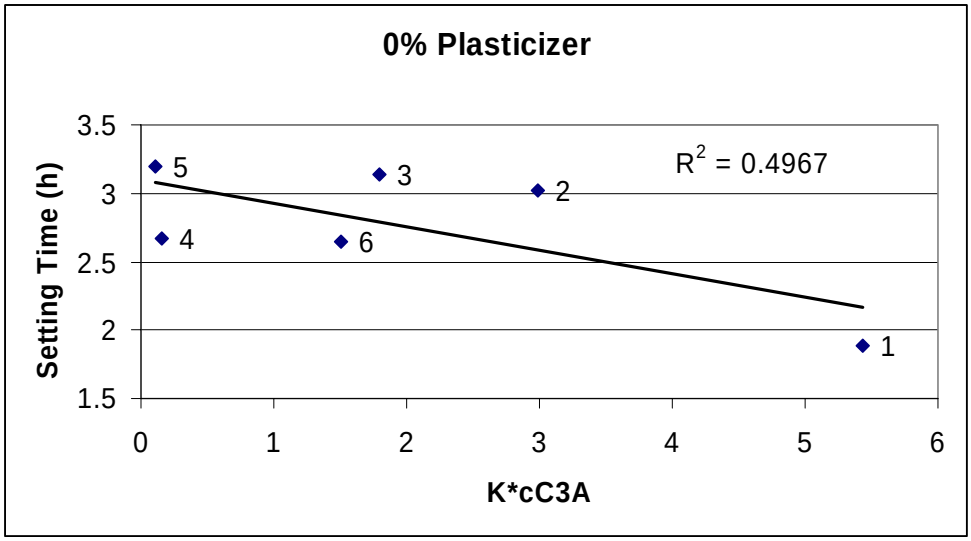

Fig. 8.15: Correlation between setting time and the product of soluble potassium with cubic C_3A when no superplasticizer is added. The numbers at each measuring point refers to the cement number given in Table 3.1-3.3.

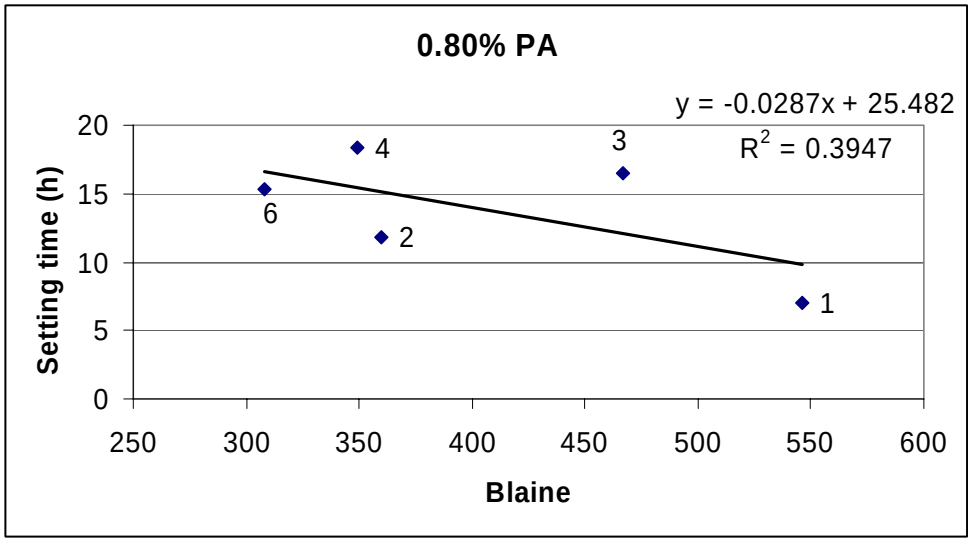

Fig. 8.16: Correlation between setting time and cement fineness (Blaine) when 0.80% polyacrylate is added. The numbers at each measuring point refers to the cement number given in Table 3.1-3.3. Setting time for cement number 5 has not been measured.

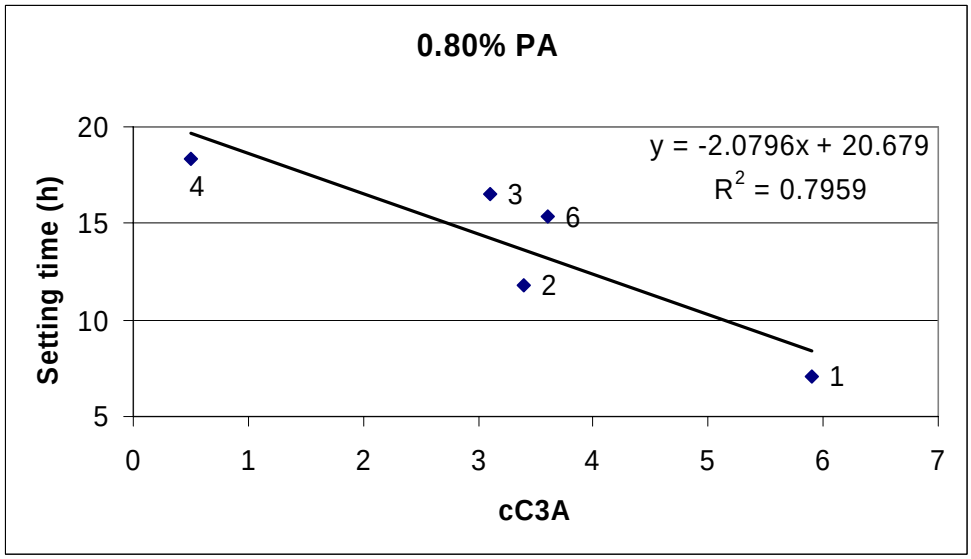

Fig. 8.17: Correlation between setting time and amount of cubic C_3A in the cements when 0.80% polyacrylate is added. The numbers at each measuring point refers to the cement number given in Table 3.1-3.3. Setting time for cement number 5 has not been measured.

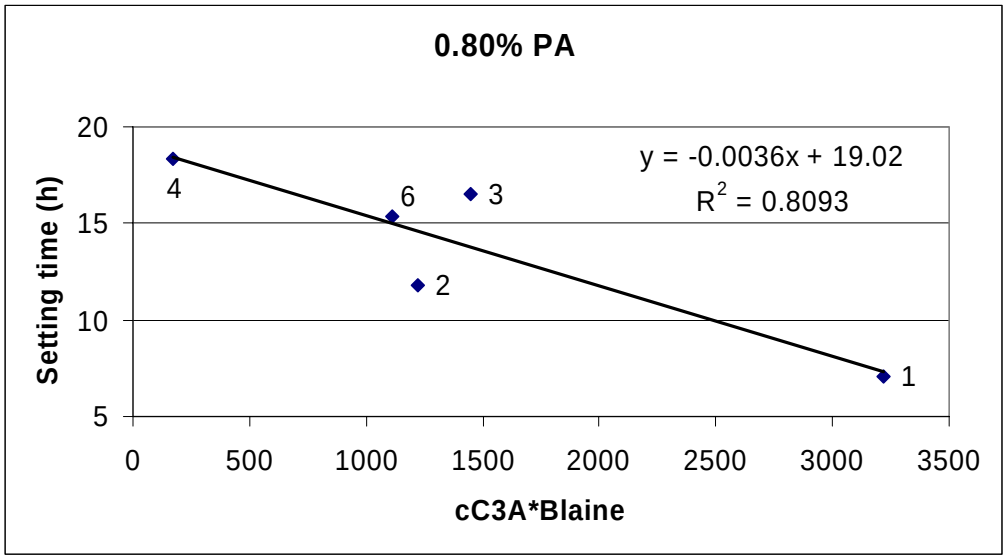

Fig. 8.18: Correlation between setting time and the product of cubic C_3A and Blaine when 0.80% polyacrylate is added. The numbers at each measuring point refers to the cement number given in Table 3.1-3.3. Setting time for cement number 5 has not been measured.

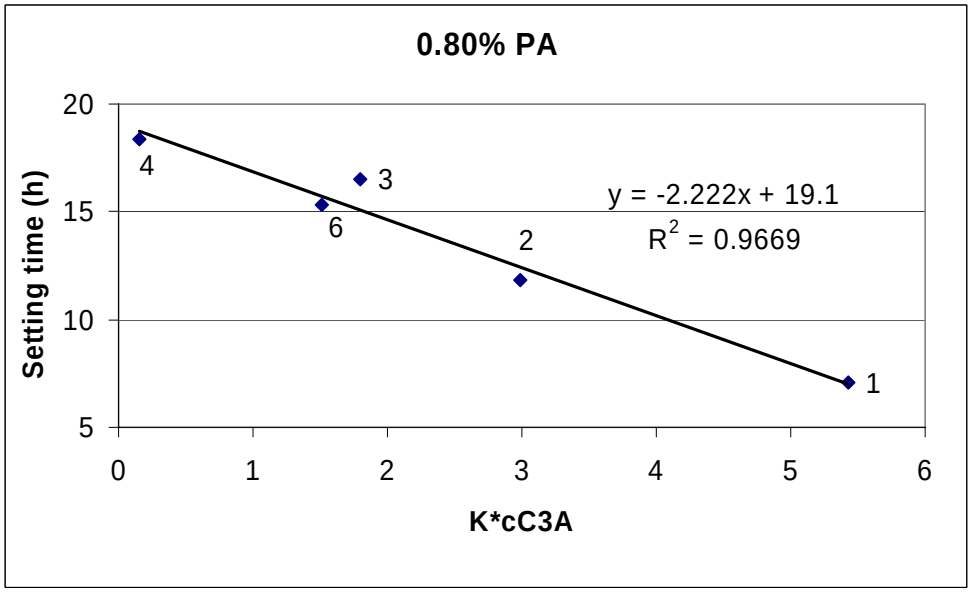

Fig. 8.19: Setting time as a function of easy soluble potassium times the cubic C_3A content for cements with 0.80% Polyacrylate. The numbers at each measuring point refers to the cement number given in Table 3.1-3.3. Setting time for cement number 5 has not been measured.

8.3 Conclusions

Attempts were made to find correlations between the maximum heat of hydration rate of the initial heat of hydration peak with various cement characteristics such as cement fineness, aluminate and alkali contents. A correlation between the product of the cement fineness and C_3A content with the maximum heat of hydration rate was found. The fly ash cement had to be left out of the plot due to its relative low initial heat of hydration.

Lignosulphonate was found to be the strongest retarder while SNF had the least effect on the setting time of the three plasticizers.

No good correlations ($R^2 \geq 0.80$) could be found between the setting times and various cement characteristics for un-plasticized pastes probably due to a narrow distribution of setting times and thus high uncertainty of the setting time readings. The setting times were however found to correlate with the content of cubic aluminate for plasticized pastes. It may seem that the setting times depend more on the cubic modification of C_3A than the sum of orthorhombic and cubic aluminate. This finding indicates that the cubic aluminate modification is more reactive than the orthorhombic.
The setting time correlated furthermore with the product of Blaine and C_3A content (cubic and total), but not with the Blaine number when it was introduced as a single parameter.

The setting times were found to decrease with increasing content of easily soluble K-ions in the cements probably due to the formation of syngenite, $K_2SO_4 \cdot CaSO_4 \cdot H_2O$, which removes some sulphate from solution that otherwise would retard C_3A hydration. A similar correlation was not found between the setting time and the sodium equivalent.

Chapter 9

Cement interactions with plasticizers

9.1 Introduction

The performance of superplasticizers in cementitious systems has been found to depend on cement fineness, cement composition, mode of introduction into the mixture, as well as the type and chemical composition of the superplasticizer itself (Bonen and Sarkar 1995, Aïtcin et al. 1994). This chapter investigates how the adsorption behaviour of the three superplasticizers SNF, lignosulphonate and Polyacrylate (PA2) depends upon various cement characteristics and how it affects rheological properties of cementitious pastes. The experimental work was done partly at EMPA in Switzerland and partly at SINTEF in Norway. The climatic conditions in the two labs varied. The results from the two labs will be compared.

9.2 Experimental

The UV absorption measurements were done in Norway. The cementitious pastes where prepared from cements 1-5 which are described by Table 3.1-3.3. Pastes with SNF and lignosulphonate were prepared with a w/c ratio of 0.40 which was kept constant throughout the measuring series. The cement pastes were prepared in a room where the temperature ranged between 20-25^{o}C and with a humidity of approximately 30%. The blending of the pastes was performed in a high shear mixer from Braun (MR5550CA, see chapter 3.3.1) by adding solids to the water and mix for ½ minute, resting for 5 minutes and blending again for 1 minute. The superplasticizers were either added with the water first (immediate addition) or 5 minutes after water addition (delayed addition).
Rheological parameters were recorded 20 minutes after water addition by a parallel plate rheometer MCR 300 produced by Physica. The measurements were done isothermally at 20^{o}C. The measurement sequence which is described in Chapter 3.3 lasted 25 minutes and was repeated 4 times to monitor time dependencies.
The flow resistances (area under the flow curve) were calculated in the low shear rate range of the shear stress - shear rate down curve (six measuring points within the shear rate range of 43-8.8s^{-1}). Water was filtrated of the paste 20 minutes after water addition for determination of plasticizer concentration in solution.

The adsorption of polyacrylate (PA2) on cement was done by measuring Total Organic Carbon (TOC) left in the pore water with a Shimadzu TOC Analyzer 5000A. Preparation of pastes and measurement of rheology were done as described above, but in a climatic room with constant temperature of 20^{o}C and high humidity (65%). Rheological and adsorption

measurements of pastes with polyacryates, lignosulphonates and SNF were performed for comparative reasons. Cement 1-6 described by Table 3.1-3.3 were subjected to the investigations. PA2 is a more efficient plasticizer than SNF and lignosulphonate and many cement pastes segregated even at low polyacrylate dosages when the w/c was set to 0.40. Cement pastes were therefore produced with w/c ratio in the region 0.30-0.40 in order to achieve stability. The pore water was filtrated from the pastes as described above, but this time filtrations were done every 25 minutes to study time effects.

9.3 Results and discussion

9.3.1 Consumed plasticizer and flow resistance

Table 9.1 and 9.2 compare some of the data from adsorption measurements done by UV and TOC measurements. Data for all measurements can be found in Appendix A5 and A.6. The w/c ratio was 0.40 for all rheological measurements done on samples subjected to the UV-method, while it ranged between 0.30-0.40 for the TOC samples. The different w/c explains most of the deviations in the rheological measurements made for UV-absorption and TOC analysis. Another contributor to the deviations might be that the rheological measurements done for TOC analysis in Switzerland and for UV-absorption analysis in Norway were made on two individual rheometers (albeit both of them a parallel plate rheometer MCR 300 produced by Physica with serrated upper plate).
The rheological data show that the values of flow resistance and consumed amount (adsorbed and intercalated) of plasticizer are generally lower for the TOC-pastes than pastes for UV measurements when the w/c ratio is 0.40 in both instances. These effects might be caused by the different conditions in the rooms were the samples were prepared: Samples prepared for TOC measurements were exposed to a constant temperature of 20^{o}C and a relative humidity of 65%. The samples prepared for UV-measurements on the other hand, were prepared at approximately 20-25^{o}C and a relative humidity of approximately 30%. Chapter 10 illustrates that a temperature difference of only 5^{o}C has a strong effect on the rheological behaviour of cement pastes since increased temperature results in increased hydration rate and increased adsorption of plasticizer due to the increased number of adsorption sites. If the discrepancies of the rheological measurements are put aside it seems, however, that the adsorption measurements from the TOC- and UV- methods are comparable, especially considering that both of the methods require separate sets of calibration.

Table 9.1: Comparison of results from TOC- and UV- measurements for pastes with SNF.

SNF		Adsorbed (% of cement weight)		Flow Resistance, Low shear rate range (Pa/s)		w/c (TOC)
Cement number and type	**Dosage SP (%)**	**UV**	**TOC**	**UV**	**TOC**	
1	0.32	0.28	0.25	6357	----	0.4
CEM I 42.5	0.80	0.44	0.46	3898	----	0.4
RR	1.20	0.47	0.51	1523	2209	0.4
2	0.32	0.22	0.24	1214	2130	0.37
CEM I 42.5 R	0.40	0.27	0.22	681	894	0.37
3	0.16	0.15	0.12	3436	4137	0.37
CEM II A-V	0.32	0.27	0.26	3200	2354	0.37
42.5 R	0.48	0.35	0.28	947	624	0.37
4	0.08	0.07	0.04	1686	1262	0.4
CEM I 52.5	0.16	0.15	0.12	1072	926	0.4
R-LA	0.32	0.26	0.25	143	98	0.4
5	0.32	0.30	0.28	2082	2846	0.37
CEM I 42.5	0.48	0.41	0.35	276	707	0.37
R-LA						

Table 9.2: Comparison of result from TOC- and UV- measurements for pastes with lignosulphonate.

LIGNOSULPHONATE		adsorbed (% of cement weight)		Flow Resistance, low shear rate range (Pa/s)		w/c (TOC)
Cement number and type	Dosage SP (%)	UV	TOC	UV	TOC	
1 CEM I 42.5 RR	0.32	0.27	0.23	7114	5225	0.4
	0.80	0.58	0.48	4833	2996	0.4
	1.20	0.67	0.56	904	464	0.4
2 CEM I 42.5 R	0.16	0.13	0.10	1779	2468	0.37
	0.32	0.25	0.24	1009	1604	0.37
	0.48	0.33	0.25	414	488	0.37
3 CEM II A-V 42.5 R	0.16	0.12	0.12	3681	2992	0.37
	0.48	0.27	0.30	1645	1174	0.37
4 CEM I 52.5 R-LA	0.08	0.08	0.05	1606	1189	0.4
	0.16	0.14	0.12	880	703	0.4
	0.32	0.26	0.24	320	213	0.4
5 CEM I 42.5 R-LA	0.16	0.15	0.11	2823	3248	0.37
	0.48	0.41	0.32	783	1719	0.37
	0.64	0.50	0.51	156	191	0.37

Flow resistances as a function of consumed superplasticizer measured by UV-spectroscopy are shown in Figs. 9.1 and 9.2. The figures show that the flow of the cement pastes is ranged in the same order for both lignosulphonate and SNF namely: 1 > 3 > 5 > 2 > 4. This trend seems to be mainly ruled by the surface of the cements since the Blaine numbers decrease in the exact same order. Chapter 7 shows however that the flow resistance depends upon the cement fineness as well as the content of cubic C_3A and C_3S:

$$\text{Blaine}\cdot(d\cdot C_3A_{cubic}+(1-d)\cdot C_3S)$$

where d is a relative reactivity parameter.

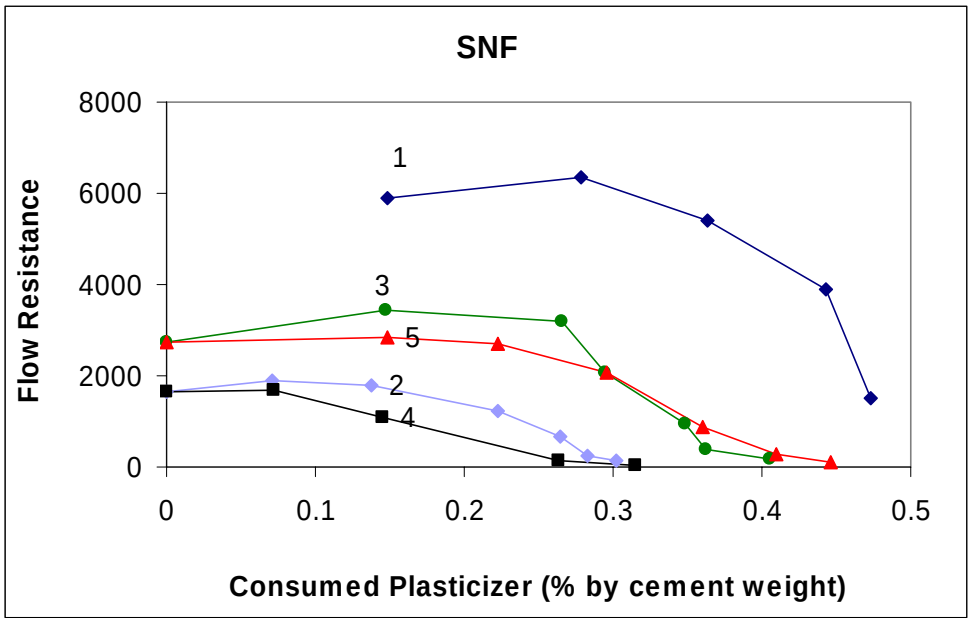

Fig. 9.1: Flow resistance as a function of consumed (adsorbed and intercalated) SNF and type of cement (numbered 1-5). Consumed amount of plasticizer is measured by UV-spectroscopy.

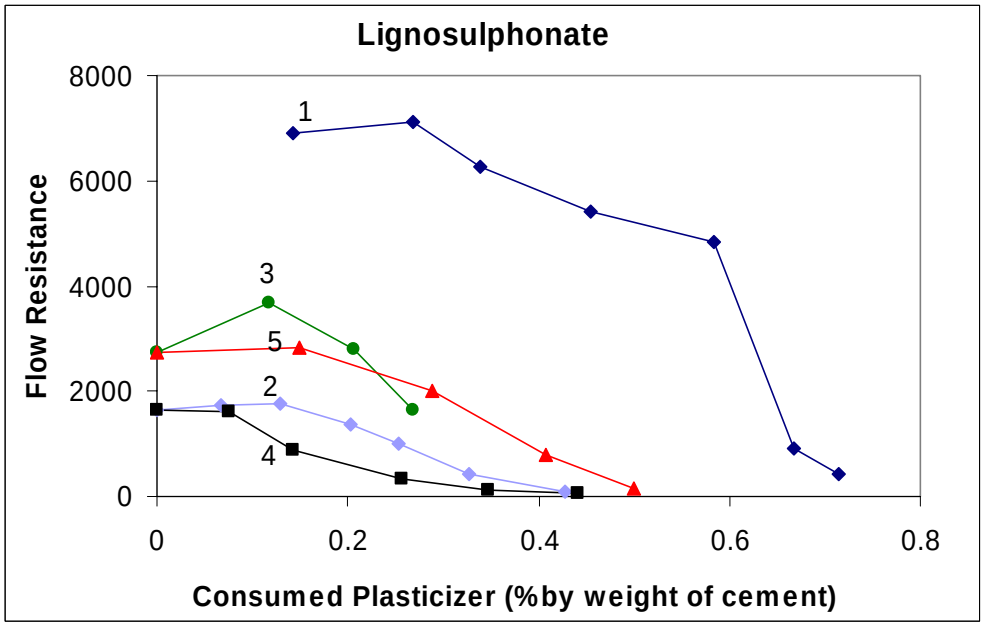

Fig. 9.2: Flow resistance as a function of consumed (adsorbed and intercalated) lignosulphonate and type of cement (numbered 1-5). Consumed amount of plasticizer is measured by UV-spectroscopy.

Graphs of consumed plasticizer and flow resistance as functions of added amount of superplasticizer are depicted in Figs. 9.3 and 9.4. Complimentary results can be found in Appendix A.5 and A.6. The figures illustrate that the concentration of superplasticizer reach a certain point were the effect of the superplasticizers are boosted and the flow resistance start to drop. This point will be referred to as “the activation point”. Another feature from the figures is that the dosage of superplasticizer can be increased until any further addition of

superplasticizers does not significantly reduce the flow resistance of the slurry. This point has been called “the saturation point” by Aïtcin et al. (1994).

The adsorption curve might reach a plateau value when the dosage of superplasticizer has reached saturation. Such adsorption behavior is characteristic for high-affinity adsorption in which virtually all the available polyelectrolyte binds to the adsorbent at specific surface sites until monolayer coverage is attained (i.e. Langmuir adsorption). It can be seen from Fig. 9.4 and Appendix A.5 and A.6 that a plateau is not always easily detectable which indicates lower affinity adsorption. Lower-affinity adsorption is characterized by curves in which the amount of polyelectrolyte adsorbed is always less than the polyelectrolyte dosage, with the isotherm gradually tapering off with increasing polyelectrolyte concentration rather than attaining a definite adsorption plateau (Ratinac et al. 2004).

In some cases as seen for the delayed addition and high concentration of SNF to Cement 1 (Fig. 9.3) the adsorbed amount of plasticizer is found to decrease after the saturation dosage has been reached. This might indicate that surplus molecules in the water phase are compressing the ionic double layer (which would explain the coagulation and segregation of cement particles in supersaturated solutions) or that adsorbed molecules expand and hinder molecules in the water phase to attach at the surface (osmosis). A similar phenomenon was discovered by Andersen et al. (1988) who measured zeta potential and adsorption curves as a function of sulphonated polystyrenes concentration. They found that the zeta potential increased until a monolayer was built up. After the maximum zeta potential and adsorbed amount of plasticizer had been reached the electrical double layer seemed to be compressed by an increasing negative charge concentration from the increased amount of polymer in the liquid causing a major drop in the amount of adsorbed polymer.

Figure 9.3 shows that delayed addition of SNF plasticizer to Cement 1 resulted in a strong reduction of the flow resistance and reduced amount of consumed plasticizer. The same effect of reduced flow resistance by delayed addition of lignosulphonate to Cement 4 can be found in Fig. 9.4 even if the amount of adsorbed plasticizer is not reduced to the same extent. This is a visual effect since the amount adsorbed lignosulphonate has in fact decreased by the delayed addition, but the polymer concentrations are so low that it makes changes difficult to detect on the scale of the graph: Consumed amount of 0.16% lignosulphonate by weight of cement was 88.7% at immediate addition while it was 85% at delayed addition. Similar results where found when the lignosulphonate dosage was 0.08% by cement weight; 95.6% of the plasticizer was consumed by Cement 4 at immediate addition while 85.5% was consumed when the plasticizer was added delayed.
The main reasons for reduced flow resistance and reduced amount of consumed superplasticizer by delayed addition have been considered to be reduced intercalation of the plasticizer in the newly formed hydration products: Since delayed addition of the polymer is not followed by further considerable hydration of the cement (dormant period), the renewal of the surfaces active in adsorption does not occur in this case and, therefore, the amount of polymer adsorbed is much lower than that observed in the case of immediate addition. Thus, the effective concentration of active polymer increases by delayed addition. Thus, it seems like “free” or available excess superplasticizers in the interstitial solution which do not intercalate or adsorb on the cement contribute to increased flow of the paste (Uchikawa et al. 1995, Kim et al. 2000).
The lower adsorption of polymer could also be due, at least in part, to changes in electrokinetic characteristics of the cement surfaces caused by changes in the composition of the aqueous phase during hydration of the cement.

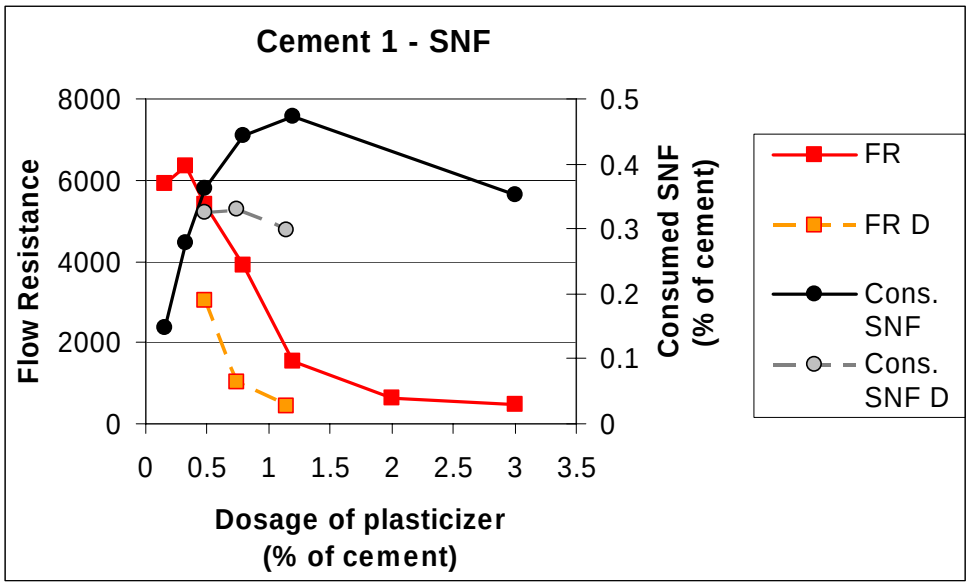

Fig. 9.3: Flow resistance (FR) and consumed (adsorbed and intercalated) superplasticizer as a function of plasticizer dosage for immediate and 5 min delayed addition (D).

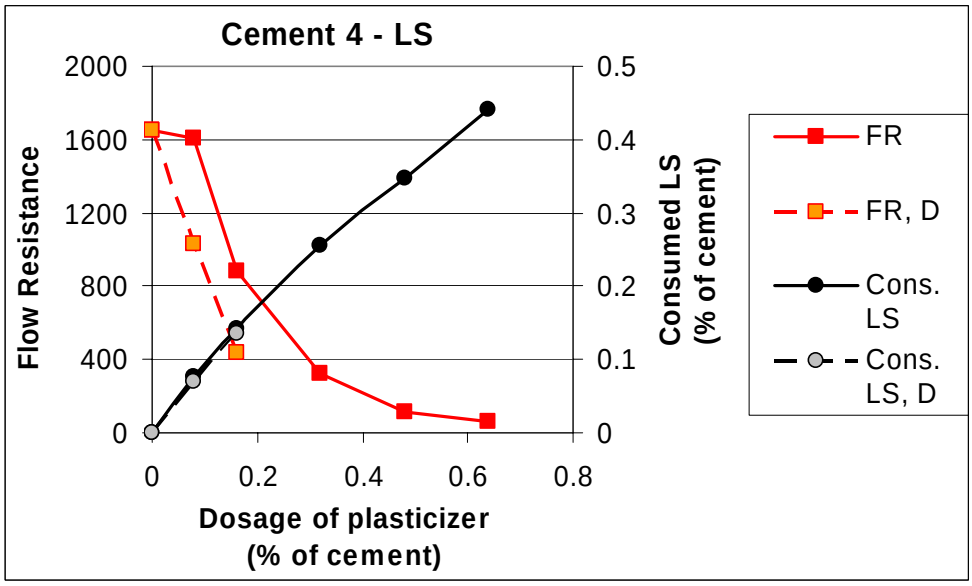

Fig. 9.4: Flow resistance (FR) and consumed (adsorbed and intercalated) superplasticizer as a function of plasticizer dosage for immediate and 5 min delayed addition.

Examples of adsorption isotherms for polyacrylate measured by TOC are shown in Fig. 9.5 and 9.6. Other results can be found in Appendix A.6.3. Experiments with delayed addition of polyacrylate have not been performed since Chapter 6 establishes that delayed addition of polyacrylate only causes marginal decrease of flow resistance.

The adsorption curves for polyacrylate show that the amount of adsorbed superplasticizer reaches a maximum before it decreases with increasing dosage. Similar results were found by Yoshioka et al. (2002) and might be caused by compression of the ionic double layer, macromolecules which are suppressing each other by osmosis or electrostatic repulsion as discussed for SNF and lignosulphonate.

TOC measurements of adsorbed amounts of the three superplasticizers on different cements are given in Table 9.3. The data show that the cements adsorb less polyacrylate than SNF and lignosulphonate. Polyacrylate was however found to be the most efficient dispersant of the

three plasticizers. Cement 1 required for example 1.20% SNF or 0.32% PA to obtain a flow resistance of approximately 600 Pa/s. This observation is supported by Golaszewski and Szwabowski (2004) who found that it was necessary to use approximately twice the dosage of SNF superplasticizer compared to a PA superplasticizer (especially for low w/c mortars) to obtain a specific value of yield stress by the Bingham model. On the other hand, viscosity values of mortars made with PA superplasticizer was up to three times higher than for that of mortars with SNF superplasticizer. Hanehara and Yamada (1999) found that the slump area ratio (paste spread) of a cement paste prepared by adding as little as 0.2% of polycarboxylic acid-based admixture increased enough to improve fluidity. Meanwhile, the fluidity of cement paste prepared using naphthalene sulphonic acid-based admixture was hardly changed by adding up to 0.8% of the admixture. By adding more than 0.8%, however, the fluidity increased more sharply than that of the cement paste prepared using polycarboxylic acid based admixture. Finally, both curves met each other at the addition level of 2% admixture.

The high dispersion ability of PA2 at relatively low dosages compared to SNF and lignosulphonate must mean that its dispersion mechanism is more effective (i.e. steric hindrance due to its long side chains) or that in-solution mechanisms play a larger role (i.e. depletion see Fig. 2.14). The long side chains of PA2 might also be able to disperse the paste even if the backbone is intercalated into the hydration products as opposed to lignosulphonate and SNF which loose dispersing power.

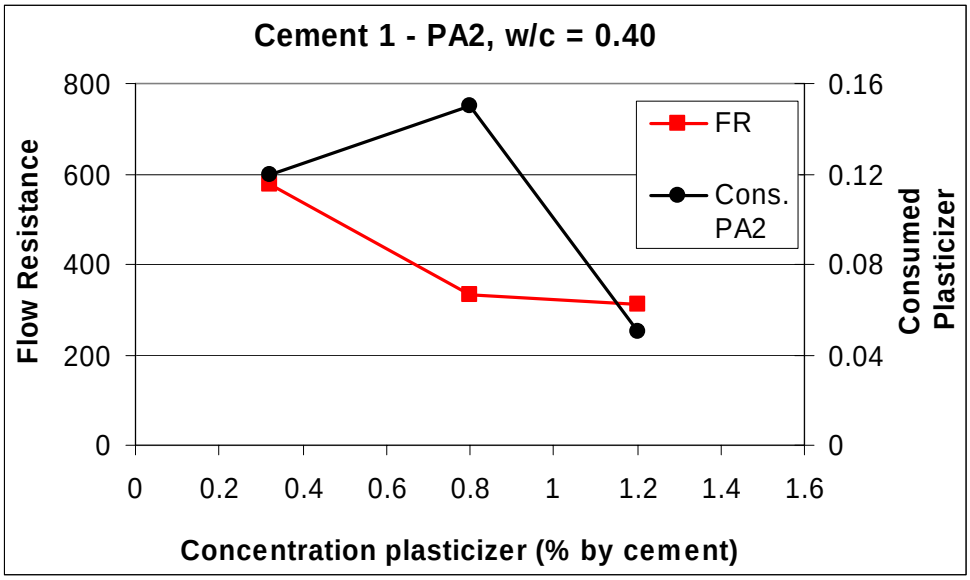

Fig. 9.5: Flow Resistance (FR) and amount of consumed (adsorbed and intercalated) PA2 as a function of added PA2 to Cement 1.

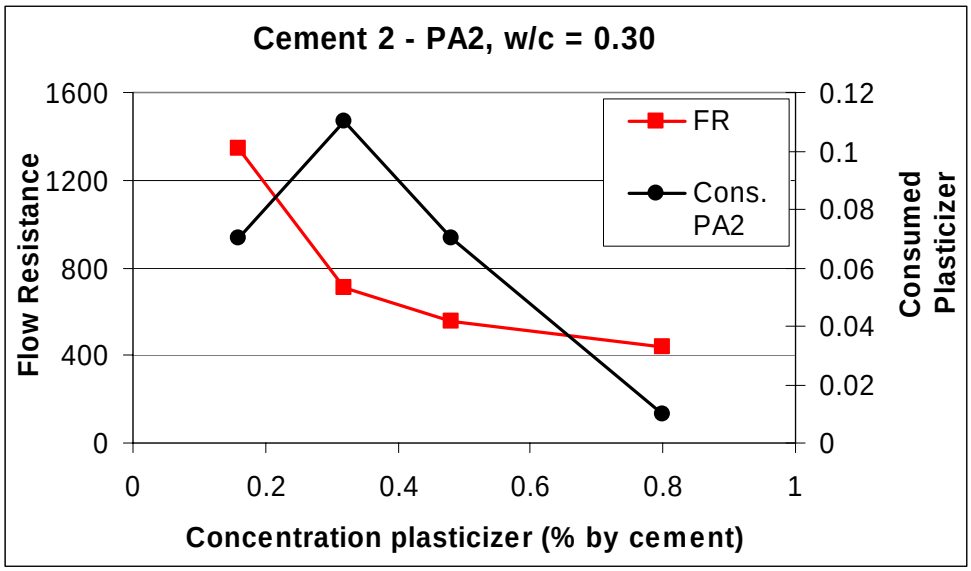

Fig. 9.6: Flow Resistance (FR) and amount of consumed (adsorbed and intercalated) PA2 as a function of added PA2 to Cement 2.

Table 9.3: Comparison of consumption of the three plasticizers PA2 SNF and LS by cement measured by TOC. The samples were taken 20 minutes after water addition.

Cement number and type	Plasticizer dosage (% of cement weight)	Consumed (mg/m^2)		
		PA2	SNF	LS
1	0.32	2.12	4.58	4.16
CEM I 42.5 RR	0.80	2.78	8.34	8.73
	1.20	0.96	9.33	10.21
2	0.16	1.81	2.70	2.79
CEM I 42.5 R	0.32	2.98	6.55	6.61
3	0.16	1.86	2.53	2.59
CEM II A-V 42.5	0.48	0.82	6.04	6.32
4	0.08	0.81	1.26	1.36
CEM I 52.5 R-LA	0.16	2.51	3.38	3.37
5				
CEM I 42.5 R-LA	0.08	0.84	0.62	------
6	0.16	3.05	3.65	3.55
CEM I 42.5 N	0.32	4.59	8.47	8.64

It is not straight forward to analyze the adsorption data as a function of time since the concentration of superplasticizer in the pore water might decrease due to encapsulation in the hydration products or increase as the pore water is consumed by the hydration. The concentration of polyacrylate, lignosulphonate and SNF in the pore water did, however, not seem to change with time as illustrated for polyacrylate in Table 9.4 (full measurement series for SNF, lignosulphonate and polyacrylate can be found in Appendix A.8). This finding is

backed by Chiocchio and Paolini (1985) who claimed that the adsorption of SNF and SMF is complete only 1-2 minutes after water addition.

Table 9.4: Consumption of PA2 as a function of time.

Polyacrylate (PA2)				
Cement number and type	**w/c**	**Dosage PA2 (% of cement weight)**	**Time (min)**	**Consumed (% pr cement weight)**
1 CEM I 42.5 RR	0.40	0.80	20	0.15
			45	0.15
			70	0.15
			95	0.13
2 CEM I 42.5 R	0.30	0.32	20	0.11
			45	0.09
			70	0.09
			95	0.09
3 CEM II A-V 42.5 R	0.30	0.32	20	0.05
			45	0.12
			70	0.12
			95	0.13
4 CEM I 52.5 R-LA	0.30	0.16	20	0.09
			45	0.08
			70	0.09
			95	0.09
5 CEM I 42.5 R-LA	0.30	0.16	20	0.09
			45	0.09
			70	0.09
			95	0.09
6 CEM I 42.5 N	0.37	0.32	20	0.14
			45	0.15
			70	0.15
			95	0.15

9.3.2 Flow loss

All cements except Cement 6 showed flow loss as a function of time when no superplasticizer was added (see Appendix A.9). Cement 6 has a high content of aluminate which causes a rapid formation of initial bonds and hydrates. Flow gain indicates that the forces applied to the paste during the rheological measurements are strong enough to break these initial bonds irreversibly.

Table 9.5 shows some data of flow measurements done for all studied cements and plasticizers. The full measurement series can be found in Appendix A.9. A general trend found in Table 9.5 is that the flow loss depends on the cement type and type and dosage of superplasticizer: Flow loss occurs for pastes with SNF. Pastes with lignosulphonate generally develop lower flow loss than pastes with SNF and flow gain is observed for several pastes. These results coincide with the heat of hydration measurements in Chapter 8 which show that lignosulphonate is the strongest retarder of the three plasticizers under study. Similar results

have been found by Uchikawa et al. (1992) who found that lignosulphonate forms complex salts with Ca^{2+}more easily than SNF. Thus, the concentration of Ca^{2+} in the liquid phase, delays the saturation of Ca^{2+}, which influences the morphology of hydrate produced (larger AFt crystals are produced with lignosulphonate than with SNF) and delays the setting time of cement.
Table 9.5 and Appendix A.9 show furthermore that flow gain is the general trend for most pastes with polyacrylate. These results are backed up by Golaszewski and Szwabowski (2004) who found that the rate of change of the yield stress with time was clearly lower for mortars with PA superplasticizer than for SNF superplasticizer. The values of viscosity of tested mortars generally decreased with time. Similar results have been found by Nawa et al. (2000).

The data in Appendix A.9 show that increasing SNF dosage results in increasing flow loss rate for all cements. The trends are somewhat weaker for Cement 1 pastes which might be caused by rapid hydration (due to high surface and content of aluminate) which consumes the plasticizer molecules. Another noticeable feature for SNF is that the flow loss has a turning point at the saturation dosage (determined by the adsorption curves) where the flow loss rates increase noticeably.
Pastes with lignosulphonate tend to transform flow loss to flow gain when the added dosages reach supersaturation. Nawa et al. (2000) found similarly that cement pastes with SNF and SMF superplasticizer had large flow loss rates, but the flow loss rate decreased with a higher superplasticizer dosage. Reduced flow loss rate or flow gain at supersaturation might indicate inhibited or reduced hydration rate due to the formation of complexes with Ca^{2+} as discussed above. Surplus plasticizer molecules in the water phase might also adsorb onto the newly formed hydration products enabling increased flow.
No flow loss - flow gain turning point was found with increasing polyacrylate dosage. Flow gain found for most pastes with PA2 might be caused by the grafted chains on the polyacrylate molecules which may seem to be long enough to provide steric stabilization even if the stem is adsorbed and covered by hydration products. The polymer might also expand in the water phase with time and thus improve the dispersion of the paste. Nawa et al. (2000) found similarly that cement pastes with grafted copolymers hardly showed flow loss except for low dosages and that almost all pastes with copolymer showed an increase of flow value with time until 60 minutes after mixing.

Table 9.5: Flow loss measurements in the low shear rate range (43-8.8 s^{-1}) for cement pastes with SNF, LS or PA2. Negative flow loss means flow gain.

			SNF		LS		PA2	
Cement number and type	**Dose (%)**	**Time (min)**	**FR (low)**	**Flow Loss (%)**	**FR (low)**	**Flow Loss (%)**	**FR (low)**	**Flow Loss (%)**
1 CEM I 42.5 RR	0.32	20	6357		7114		578	
		45	7613	20	7784	9	488	-16
		70	8817	39	3225	-55	461	-20
		95	7064	11	3657	-49	437	-24
	0.80	20	3898		4833		331	
		45	4198	8	4156	-14	328	-1
		70	4835	24	4337	-10	321	-3
		95	6448	65	4594	-5	319	-4
2 CEM I 42.5R	0.16	20	1787		1779		1737	
		45	2012	13	1910	7	1556	-10
		70	2165	21	2054	15	1502	-14
		95	2232	25	2124	19	1483	-15
	0.32	20	1214		1009		709	
		45	1619	33	1083	7	662	-7
		70	2003	65	1183	17	644	-9
		95	2316	91	1265	25	634	-11
3 CEM II A-V 42.5 R	0.32	20	3200		2801		516	
		45	3710	16	2873	3	520	1
		70	4054	27	2962	6	503	-3
		95	4259	33	3132	12	493	-4
	0.48	20	947		1645		383	
		45	1550	64	1442	-12	395	3
		70	2049	116	1480	-10	392	2
		95	2539	168	1534	-7	380	-1
4 CEM I 52.5 R-LA	0.16	20	1072		880		205	
		45	1412	32	1045	19	215	5
		70	1667	56	1227	39	222	8
		95	1832	71	1351	54	226	10
5 CEM I 42.5 R-LA	0.16	20	2835		2823		502	
		45	3387	19	3208	14	525	5
		70	3542	25	3377	20	527	5
		95	3599	27	3421	21	560	12
6 CEM I 42.5 N	0.16	20	1786		2223		2367	
		45	1903	7	2063	-7	1652	-30
		70	1897	6	1997	-10	1405	-41
		95	1884	5	1989	-11	1319	-44
	0.32	20	1839		2570		440	
		45	2080	13	2466	-4	360	-3
		70	2201	20	2410	-6	353	-4
		95	2415	31	2410	-6	373	-3

9.3.3 Correlation of adsorbed plasticizer with cement characteristics

The consumed amounts of superplasticizer at the point of activation and saturation are given in Table 9.6 and 9.7 respectively. The tables and the Flow Resistance- Plasticizer Consumption curves (Fig. 9.1 and 9.2) show that the activation- and saturation dosages of the superplasticizers mainly depend on the cement and to a lesser extent on the superplasticizer type when SNF and lignosulphonate are considered. PA2 has a lower saturation and activation dosage than SNF and lignosulphonate, but this plasticizer will not be discussed in the following part of the chapter due to scarce amount of data.

Ranking of the adsorption capacity of the cements seems to depend upon the superplasticizer dosage. SNF molecules adsorb somewhat more on cement than lignosulphonate at the activation point as shown by Table 9.6. The opposite trend is however found in Table 9.7 which depicts adsorbed amounts of plasticizers at saturation dosage. All in all, it can be concluded that SNF and lignosulphonate are adsorbed on the cements roughly to the same extent. Uchikawa et al. (1992) found on the other hand, that the amounts of adsorbed β-SNF on cement were higher than that of the lignosulphonate. They operated however with only one concentration per plasticizer where the SNF dosage was higher than that of lignosulphonate.

Table 9.6: Consumed (adsorbed and intercalated) superplasticizer at the activation point of the superplasticizer.

Point of superplasticizer activation					
Cement number	**Blaine (m^2/kg)**	**Cubic C_3A (%)**	**$Na_{eqv,soluble}$ (kg/m^3)**	**Consumed LS (mg/m^2)**	**Consumed SNF (mg/m^2)**
1	546	5.9	0.76	4.93	5.11
2	360	3.4	0.88	3.58	3.83
3	*467*	*3.1*	*0.59*	*2.51*	*4.84*
4	364	0.5	0.32	2.09	1.98
5	447	3.1	0.36	3.33	4.99

Table 9.7: Consumed (adsorbed) superplasticizer at the point of saturation for SNF and lignosulphonate.

Saturation point					
Cement number	**Blaine (m^2/kg)**	**Cubic C_3A (%)**	**$Na_{eqv,soluble}$ (kg/m^3)**	**Consumed LS (mg/m^2)**	**Consumed SNF (mg/m^2)**
1	546	5.9	0.76	12.23	8.66
2	360	3.4	0.88	11.86	8.39
3	*467*	*3.1*	*0.59*	*5.14*	*7.75*
4	364	0.5	0.36	13.19	7.23
5	447	3.1	0.32	11.19	10.74

Cement 3 adsorbs less superplasticizer than expected regarding its relatively high surface (Blaine) as shown in Table 9.6 and 9.7. The low adsorption is especially protruding at the point of saturation and might be caused by a lower adsorption capacity of the fly ash.

Experiments to study the influence of fly ash on the superplasticizer adsorption were therefore performed. Adsorbance of lignosulphonate and SNF were measured on pastes of pure Cement 1, pure FA, pure FA with 2% by weight $Ca(OH)_2$ and pastes of 50% FA and 50% Cement 1 measured by weight.

The results given in Table 9.8 show that pure fly ash adsorbs less superplasticizer than cement, while the amount of consumed plasticizer for the cement - FA mix was found to be close to the results found for pure cement. These findings seem to coincide with the work of Nagataki et al. (1984) who found that adsorbed amounts of naphthalene type superplasticizer on heat treated fly ashes (free of uncombusted carbon) were approximately one half the adsorption of cement. The *rate* of adsorption on untreated fly ash was however found to be higher than in the case of cement and the amount of adsorbed superplasticizer on fly ash-cement was roughly equal to that in the case of cement only.

Pure FA pastes with 2% $Ca(OH)_2$ adsorbed approximately the same or slightly higher amount of plasticizer as pure cement paste. This result indicates that Ca^{2+} can adsorb on the FA surface and that the anionic superplasticizer molecules can adsorb on the positive charged sites thus created. Jolicoeur and Simard (1998) pointed out a similar effect after the observation of SNF being adsorbed to a minor extent by silica fume slurry, but being equally adsorbed by cement paste and cementitious paste with silica fume replacement.

Table 9.8: Adsorbance of LS and SNF on FA and Cement 1.

Adsorbant	Plasticizer	Dosage (% of cement weight)	Consumed plasticizer (% of added)
Pure FA	SNF	1.00	36.73
50/50 Cement 1+FA			55.73
Cement 1			51.17
Pure FA + 2% $Ca(OH)_2$			58.90
Pure FA	LS	1.00	24.27
50/50 Cement 1+ FA			67.38
Cement 1			69.16
Pure FA + 2% $Ca(OH)_2$			69.30

Correlations of plasticizer dosage at the point of plasticizer activation with cement characteristics will not be discussed due to narrow range of the values and thus high uncertainty of the correlations.

Correlations of saturation dosages of SNF and lignosulphonate with the cement characteristics Blaine, contents of total C_3A, cubic C_3A, soluble potassium (K^+), soluble sodium equivalent (Na_{eqv}) and the products of some of the cement characteristics were attempted. The same procedures were not performed for pastes with polyacrylate due to the scarce amount of available data.

The regression coefficients, R^2, in Table 9.9 indicate that the saturation dosage of SNF depends on the single cement characteristics Blaine and content of cubic C_3A. The best correlation, overall, was found between the plasticizer saturation dosage and the product of cubic C_3A and Blaine. This is logical since high surface and cubic aluminate content implies

high cement reactivity. Plasticizers are furthermore found to adsorb more on the aluminate than on the silicate phases as discussed in Chapter 2.3.3.
Bonen and Sarkar (1995) found similarly a correlation between the adsorbed amount of plasticizer with the total C_3A content, while an even better correlation was found between the adsorption and the product of the C_3A fraction times the cement fineness. Lewis et al. (2000) attributed the adsorption of SNF to total C_3A content, while Aïtcin et al (1994) stated that the viscosity and superplasticizer dosage at the saturation point depend on the water-cement ratio of the grout, the fineness of the cement (Blaine), total amount of C_3A, reactivity of the C_3A phase, sulphate content, the rate of dissolution of the sulphates as well as the efficiency of the mixing system used to prepare the grout.

The critical role of sulphates on the rheology of Portland cement slurries is well known. Alkali sulphates, which form during cement production in the clinkerization phase, are the most soluble of the sulphates contained in the cement. Together with calcium sulphate added as set regulator, they provide the sulphate ions necessary for the reaction with C_3A in the early stages of cement hydration. According to Aïtkin et al. (1994) it is not the total amount of SO_3 in cement that is important, but rather the availability, or the rate of dissolution of SO_4^{2-} ions, that must be balanced with the chemical reactivity of the C_3A.

In the absence of superplasticizers, cements containing high levels of alkalis will usually exhibit poorer rheological behaviors than cements having low alkali contents, other conditions being the same. Effects which may be promoted by alkalis are flocculation of cement or other fine particles induced by the electrolytes or formation of new hydrates containing alkali ions (e.g., syngenite) (Ramachandran et al. 1998). Odler and Wonnemann (1983, b) found that early hydration and setting of cement is accelerated due to the presence of Na_2SO_4 and especially of K_2SO_4.

In the presence of superplasticizers the influence of sulphate content is known to depend on the superplasticizer type. It has been found in the presence of SNF type superplasticizers that addition of alkali sulphates (Na_2SO_4) can lead to improvements in the rheological properties of cement pastes since the presence of SO_4^{2-} ions leads to a decreased adsorption or intercalation of SNF superplasticizer in early C_3A hydrates leaving more of the latter available for paste fluidification (Nawa et al. 1989). Magarotto et al. (2003) found similarly, that increased amount of sodium sulphate leads to lower adsorption of polycarboxylate superplasticizer, but reduced performance in terms of water reduction. When it was employed in the presence of added sodium sulphate, the performances of a polycarboxylate superplasticizer became close to those of SNF (i.e. reduced performance). However, the performance of SNF type admixture was found to be almost independent from the alkali sulphate addition, at least up to 1% sodium sulphate of cement mass.
In some instances alkali content in cements can be linked to cement – superplasticizer incompatibility which is characterized by rapid flow loss attributed to the lack of SO_4^{2-} and the reaction of SO_3^- sites of polysulphonated plasticizers with C_3A (Li et al. 2003). Jiang et al. (1999) found for β-naphtalene sulphonate polymers (SNF) that the ideal amount of soluble alkali is 0.4-0.5% (expressed as equivalent sodium). The initial fluidity was maximum and fluidity loss minimum at this optimum alkali content. Too high soluble sulphate content brings about compression in the electrical double layer which increases the viscosity (see DLVO theory in Chapter 2.2)

Table 9.9 indicates that there are correlations between the plasticizer saturation dosages with the product of Na_{eqv} and Blaine as well as the product of Na_{eqv} and cubic C_3A. The regression

coefficients for correlations involving Na_{eqv} were somewhat better than similar correlations involving K^+. These findings indicate that the easily soluble sulphate ions are more active than the alkali ions in influencing the plasticizer saturation dosage.
The saturation dosage of lignosulphonate seems to have a stronger dependency on the amount of soluble alkali than observed for pastes with SNF. This result might be caused by lignosulphonate forming complexes with solvated ions in a higher degree than SNF as discussed above. Commercial SNF is furthermore sometimes added Na_2SO_4, which may explain less dependence on the soluble sulphate content of the cement.

Correlations were found between the plasticizer saturation dosages with the single cement characteristics soluble sodium equivalent and cubic C_3A. A correlation was also found for the product of cC_3A with Blaine, but the best fits were found for the products Na_{eqv}·Blaine and Na_{eqv}·C_3A_{cubic}. These results imply in accordance with Aïtcin et al. (1994) that easily soluble alkalis (easily soluble sulphates) as well as surface (Blaine) and cubic aluminate have strong influences on the rheology of cementitious pastes.

Table 9.9: Regression coefficients for correlations of superplasticizer saturation dosage with various cement characteristics.

Cement Characteristic	**R^2**	
	SNF	**LS**
Blaine	0.8187	0.4541
C_3A_{tot}	0.5954	0.5372
C_3A_{cubic}	*0.8846*	*0.8270*
Na_{eqv}	0.5561	0.8253
K^+	0.5046	0.7742
C_3A_{tot}·Blaine	0.7763	0.6565
C_3A_{cub}·Blaine	*0.9702*	*0.8395*
Na_{eqv}·Blaine	*0.8787*	*0.9741*
K^+·Blaine	0.8571	0.9617
Na_{eqv}·C_3A_{cub}	*0.8511*	*0.9914*
Na_{eqv}·C_3A_{cub}·Blaine	0.8805	0.9761
K^+·C_3A_{cub}	0.8363	0.9864

Figs. 9.7-9.12 show examples of some of the correlations of saturation dosages of lignosulphonate with the cement characteristics for the five cements. Similar correlations for cement pastes with SNF can be found in Appendix A.7.
Figure 9.7 and 9.8 show that high surface and aluminate content in the cement will enforce rapid hydration which in turn leads to a high superplasticizer saturation concentration. Figs. 9.10, 9.11 and 9.12 seem to indicate that increased alkali content will increase the saturation value of the superplasticizer indicating that more of the superplasticizer molecules are being consumed by the hydration products. These findings are however somewhat unclear since literature has reported that increased alkali sulphate in solution results in both increased hydration rate (which would lead to a higher plasticizer intercalation) and reduced plasticizer adsorption (due to SO_4^{2-} - superplasticizer competition). It is possible of course that Na_{eqv} govern opposite effects of Blaine and cubic C_3A in a way that will bring the measuring points into a linear function and increase the correlation coefficient (R^2). This possibility is indicated in the case of lignosulphonate where the correlations for the single cement characteristics Blaine and sodium equivalent give regression coefficients approximately equal to 0.8187 and

0.5561 respectively while the product of the two characteristics give a regression coefficient equal to 0.8797.

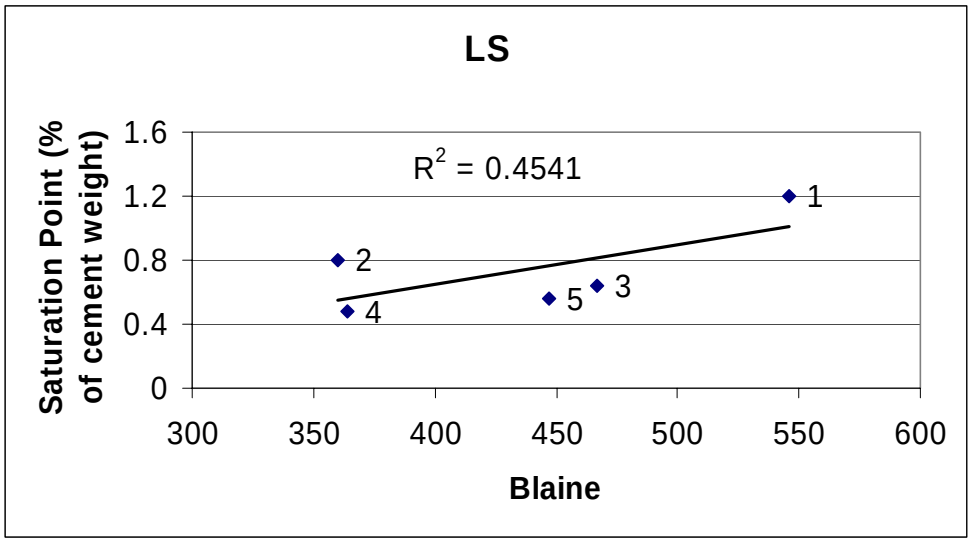

Fig. 9.7: Saturation point of adsorbed LS superplasticizer as a function of cement surface (Blaine). The cements are numbered according to Table 3.1-3.3.

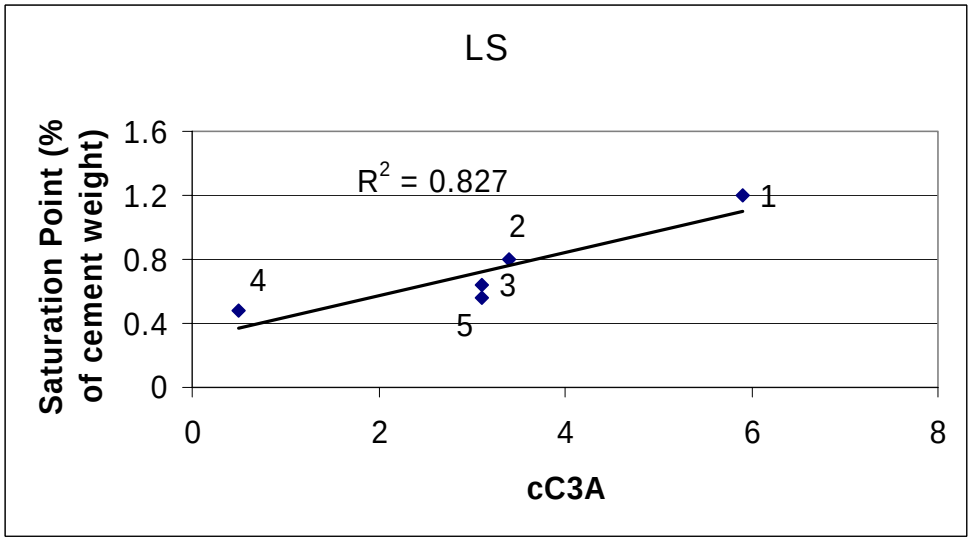

Fig. 9.8: Saturation point of adsorbed LS superplasticizer as a function of cubic C_3A content in the cements. The cements are numbered according to Table 3.1-3.3.

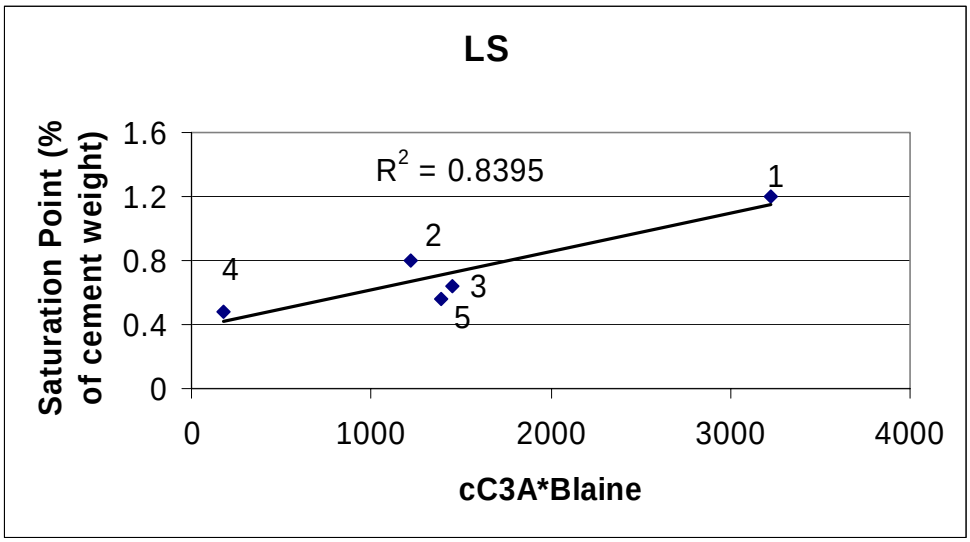

Fig. 9.9: Saturation point of adsorbed LS superplasticizer as a function of cubic C_3A and Blaine. The cements are numbered according to Table 3.1-3.3.

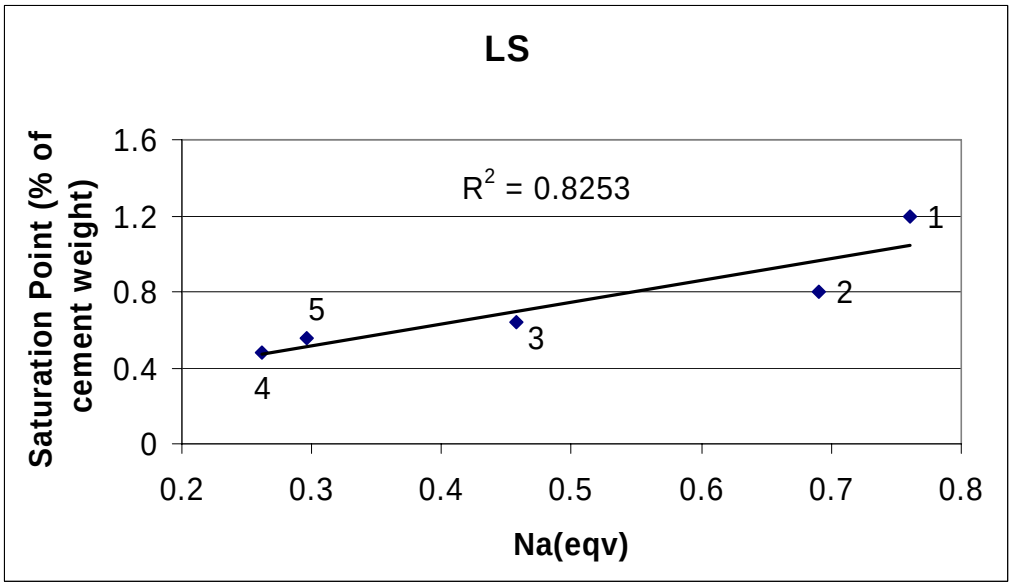

Fig. 9.10: Saturation point of adsorbed LS superplasticizer as a function of soluble alkalis (sodium equivalent). The cements are numbered according to Table 3.1-3.3.

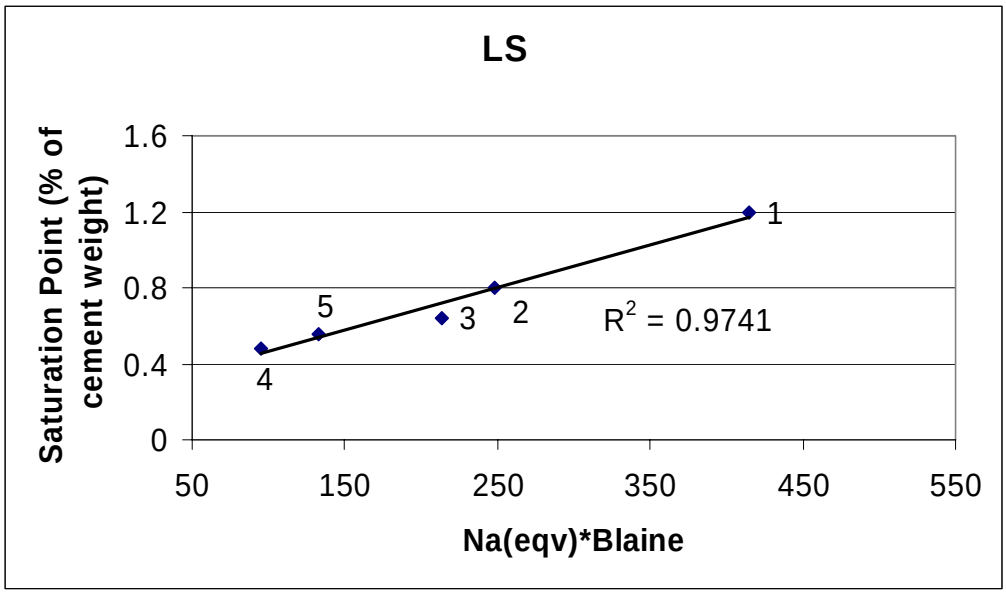

Fig. 9.11: Saturation point of adsorbed LS superplasticizer as a function of soluble alkalis (sodium equivalent) and Blaine. The cements are numbered according to Table 3.1-3.3.

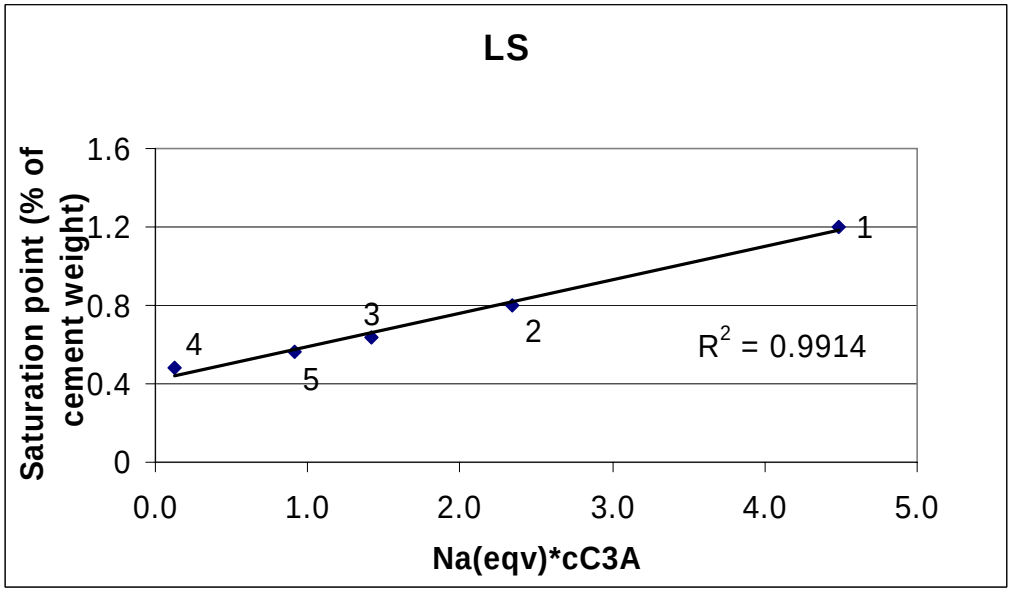

Fig. 9.12: Saturation point of adsorbed LS superplasticizer as a function of soluble alkalis (sodium equivalent) and cubic C_3A. The cements are numbered according to Table 3.1-3.3.

9.4 Conclusions

PA2 was found to be a more effective plasticizer than SNF and lignosulphonate even though it was consumed (i.e. adsorbed or intercalated in surface hydration products) to a lesser extent by the cements. SNF and lignosulphonate gave comparable results.

The concentrations of superplasticizer in the pore water was not found to change in the time range 20-95 min after water addition, indicating that most of the plasticizer molecules are consumed within the first 20 minutes after water addition.

Polyacrylate was found to result in flow gain as a function of time while SNF and lignosulphonate resulted in cement pastes with flow loss.

The adsorption characteristics were found to depend on the plasticizer type. The adsorption curves of SNF and lignosulphonate reached a plateau at saturation characterizing high-affinity adsorption or continued to increase characterizing low affinity adsorption. The adsorbed amounts of PA2 decreased however after saturation was reached which might indicate that surplus molecules in the water phase compress the ionic double layer or that adsorbed molecules expand and hinder molecules to attach at the surface (i.e. osmosis).

The plasticizer saturation dosages were found to depend on cement surface area (Blaine), amount of cubic C_3A and easily soluble sulphates. The saturation dosage of lignosulphonate seemed to have a dependency on the amount of soluble alkali which was somewhat stronger than observed for pastes with SNF. This difference might be caused by lignosuphate forming complexes with solvated ions in a higher degree than SNF. Alkali sulphates are furthermore often added to commercial SNF based products as the one used in this work.
The best correlation, overall, was found for the product of cubic C_3A and Blaine which is logical since high surface and cubic aluminate contents equals high cement reactivity and since the plasticizers are known to coordinate with calcium sites. Correlations were also found between saturation dosage with the product of Na_{eqv} and Blaine as well as the product of Na_{eqv} and cubic C_3A.
The investigations seemed to indicate that the plasticizer saturation concentration increase with increasing alkali content. These findings are however somewhat unclear since literature reports that the increased concentration of alkali sulphate in solution results in both increased hydration rate (which would lead to a higher plasticizer intercalation) and reduced plasticizer adsorption (due to SO_4^{2-} - superplasticizer competition). It is possible of course that the easily soluble sulphates govern opposite effects of Blaine and C_3A in a way that smoothen the correlation plots of the plasticizer saturation dosage with the cement characteristics.

Chapter 10

Effect of temperature on the rheology of limestone and cement pastes and the adsorption of plasticizers

10.1 Introduction

The effect of temperature on the rheology of Portland cement is important not only because of climatic variations prevailing throughout the world, but also because of the exothermic nature of early hydration reactions involved. There have been few studies made on the effect of temperature on the rheology of cement pastes and its effect on the adsorption of superplasticizers. This chapter investigates therefore the effect of temperature on the rheological behaviour of cement pastes with lignosulphonate (LS), naphthalene sulphonate formaldehyde condensate (SNF) and polyacrylate (PA2) as superplasticizers. Limestone was used as a nonreactive model system for cement. Adsorbed amounts of on cement and limestone as a function of temperature have been studied.

10.2 Experimental

Limestone pastes were prepared with a particle volume fraction of 0.60 (corresponding to a w/ls ratio of 0.25) and "artificial" pore water which was prepared of NaOH and KOH in distilled water with a K/Na molar ratio equal to 2 and pH = 13.2. The water was heated or cooled to obtain paste temperatures in the range of 15-43^{o}C. The plasticizers were added to the limestone with the "artificial pore water" (immediate addition) in the concentration 0.32% by weight for SNF and LS and 0.10% by weight of PA2.

Pastes of Cement 1 and Cement 4 were prepared with a particle volume fraction equal to 0.442 (w/c=0.40) with distilled water and SNF, LS and PA2 as plasticizers. The water was heated or cooled in order to produce pastes with varying temperatures. The plasticizers were added to the cements with the water (immediate addition). Table 10.1 lists the various combinations of temperatures, limestone and cements, plasticizers and plasticizer dosages. Cement 1 and 4 are described by Table 3.1-3.3.

Table 10.1: Measurements performed on limestone and cement pastes with SNF, LS and PA2 as superplasticizers at varying temperatures.

Adsorbents	Plasticizer	Plasticizer dosage (% of cement weight)	Paste temperature (^{o}C)
Limestone	SNF	0.32	16, 25, 30, 33, 40
	LS	0.32	15, 25, 33, 43
	PA2	0.10	16, 24, 34
Cement 4	SNF	0.25	12, 18, 27, 39
	LS	0.25	12, 26, 32, 40
	PA2	0.10	11, 18, 31
Cement 1	SNF	0.65	13, 22, 33, 38
	LS	0.65	14, 25, 35, 39
	PA2	0.20	11, 22, 36, 39

The cement and limestone pastes were mixed in a high shear blender from Braun (MR5550CA, see Chapter 3.3.1) for ½ minute and rested for 5 minutes before they were blended once more for 1 minute. The paste temperatures were measured after the last mixing sequence.
A sample of the paste was transferred to a parallel plate rheometer MCR 300 produced by Physica. The temperature of the rheometer was set equal to the temperature of the paste and the rheological properties were recorded 11 minutes after water addition.

The rheological measurement sequence is described in Chapter 3 and was performed once for all pastes. Flow resistance (area under the flow curve) was calculated for both medium and low shear rate range of the down curve (152-118 s^{-1} and 43-8.8 s^{-1} respectively).

The pore water of the remaining paste was filtrated from the pastes through 0.45μm filters 11 minutes after water addition. The concentration of plasticizer left in solution was measured by UV adsorption spectrum for pastes with added SNF and LS (292 and 283 nm were used respectively). Total Organic Carbon (TOC) measurements were performed on pastes with added PA2.

The densities of the extracted pore water were measured with pycnometers and the kinematic viscosities (m^2/s) were measured with an Ostwald viscometer produced by Schott-Geräte. The apparent viscosity (Pa·s) was derived by multiplying the measured density and the kinematic viscosity.

10.3 Results and discussion

10.3.1 Limestone paste rheology

Figs. 10.1-10.3 illustrate that the measured shear stresses in the limestone pastes increased slightly with temperature in the range of 15-34^{o}C and increased markedly when the temperature reached 40^{o}C. This trend was found both for pastes with SNF and LS. The rheological properties of pastes with PA2 were not measured at 40^{o}C.
Flow resistances in the low and medium shear rate range of limestone pastes are similarly found to increase with increasing temperature as shown in Fig. 10.4. The flow resistance does, however, reach a minimum at 30-33^{o}C for pastes with SNF and LS. The trends are found to be independent of shear rate range when SNF and LS are added to the pastes as opposed to the pastes with PA2. The discrepancy for PA2 pastes occurs since the flow curves of 24 and 34^{o}C cross at high shear rates as seen by Fig. 10.3.
Yield stresses and plastic viscosities calculated from the Bingham model are found to increase consistently with increasing temperature. Bingham rheological data can be found in Appendix A.12.5 while flow resistance data for medium shear rate range (152-118 s^{-1}) can be found in Appendix A.12.2.

The apparent viscosity of the pore water decreased as much as 42% when the temperature increased from 15 to 43^{o}C as shown by Table 10.2. These results are found to be consistent with measured viscosities of pure water. Thus, the viscosity of the pore water does not seem to depend upon the how the behaviour of polymers might alter with increasing temperature.
Decreasing apparent viscosity of the continuous phase should result in the same reduction in paste viscosity according to the Krieger- Dougherty equation (Equation 2.19) when all other factors are equal. The flow curves illustrate however that the effect of the reduced viscosity of the pore water is suppressed by other factors (i.e. dehydration of the paste or altered adsorption of plasticizer on the limestone surface) which result in increased flow resistance with increasing temperature. Reduced viscosity of the pore water with increasing temperature might however be the cause of the minimum of the flow resistance curves which occurred in the range of 30^{o}C.

Table 10.2: Viscosity of pore water extracted from limestone pastes as a function of temperature. Viscosities of pure water as a function of temperature are included for comparison.

Limestone -Lignosulphonate			**Pure water**	
Temperature (^{o}C)	**Measured viscosity (mPa·s)**	**Reduction of viscosity (%)**	**Measured viscosity (mPa·s)**	**Reduction of viscosity (%)**
15	1.040	----	0.979	----
25	0.834	20	0.778	21
33	0.713	31	0.648	34
43	0.600	42	0.543	45

Increased flow resistance with increasing temperature cannot be explained by increased solubility of limestone in water since the limestone solubility is known to decrease with increasing temperature (Macphee and Lachowski 1998).

Reduced repulsive potential, V_R, and thus increased degree of flocculation of the limestone particles with increasing temperature can also be ruled out since a temperature change from 15-38°C would increase the potential by a factor of only $(311/288)^2 = 1.17$ when equation (10.1) is used. The equation is a general expression for the repulsive potential between two spherical particles (radii a_1 and a_2) with distance H:

$$V_R = \left(\frac{64 \cdot \pi \cdot \varepsilon \cdot a_1 \cdot a_2 \cdot k^2 \cdot \gamma_1 \cdot \gamma_2 \cdot T^2}{(a_1 + a_2) \cdot e^2 \cdot z^2} \right) \cdot \exp(-\kappa \cdot H) \qquad (10.1)$$

were ε is the permittivity of the liquid, k is Boltzmann's constant, γ is a parameter of the surface potential, *e* is the ion charge, z is the ionic valence and κ expresses the effect of the ion charge and concentration (Mørk 2001).

Nawa et al. (2000) found similar results while studying the effect of temperature on the degree of flocculation of particles determined by the extent of the minimum value of the potential energy curve (V_{min}, see Fig. 2.5). They found that V_{min} hardly varies in the temperature range of 10°C to 30°C. Coagulation tendencies are therefore probably not influenced much by the temperature. Thus, the altered flow resistances may be caused by dehydration of the pastes and/or altered adsorption behaviour of the superplasticizers as will be discussed later.

Paste dehydration seemed to have occurred in spite of the measures taken to minimize paste dehydration: The parallel plate measuring system of the rheometer (see Fig.3.2) was covered with a plastic ring and a metallic lid during the measurements. The upper plate of the rheometer had furthermore a water trap filled with water to ensure saturated water pressure. Condensed water was however observed at the top surface of the upper plate at 40°C. This condensation might have occurred due to the temperature difference between upper and lower plate since only the lower plate was heated. Thus, water might have evaporated from the 1 mm gap between the plates. Oil or paraffin could be applied between the plates at the outer circumference of the sample to avoid this potential problem in future experiments.

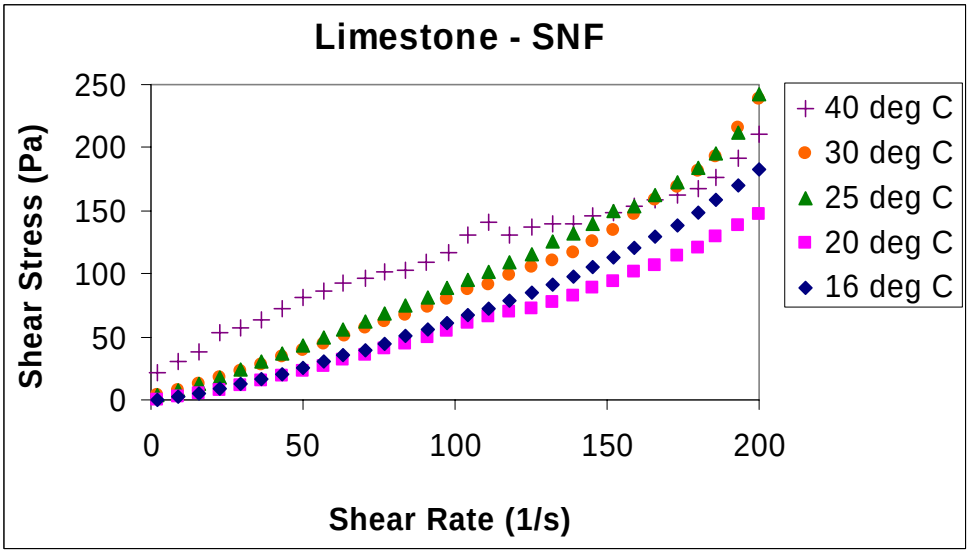

Fig. 10.1: Flow curve for limestone pastes (w/ls = 0.25) with 0.32% SNF by weight at varying temperatures.

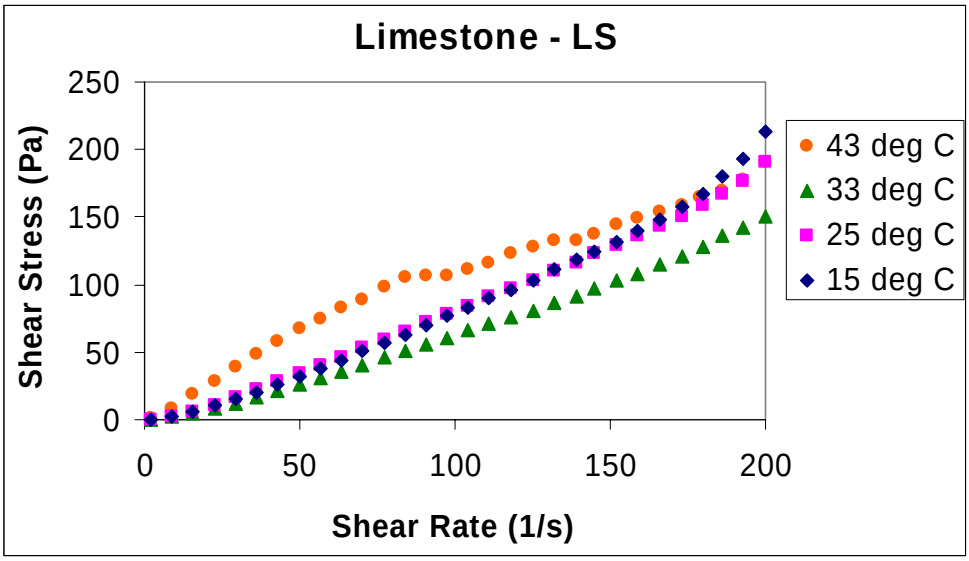

Fig. 10.2: Flow curve for limestone pastes (w/ls = 0.25) with 0.32% LS by weight at varying temperatures.

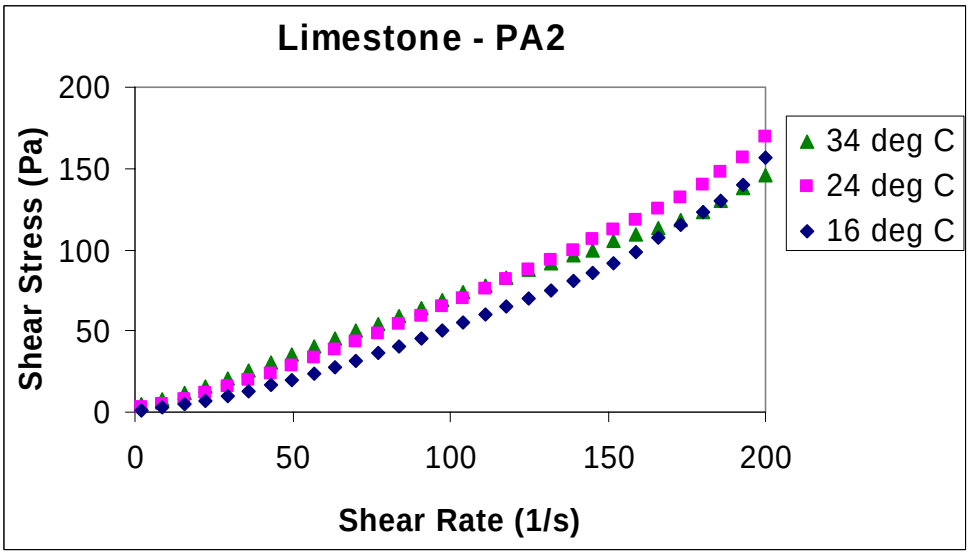

Fig. 10.3: Flow curve for limestone pastes (w/ls = 0.25) with 0.10% PA by weight at varying temperatures.

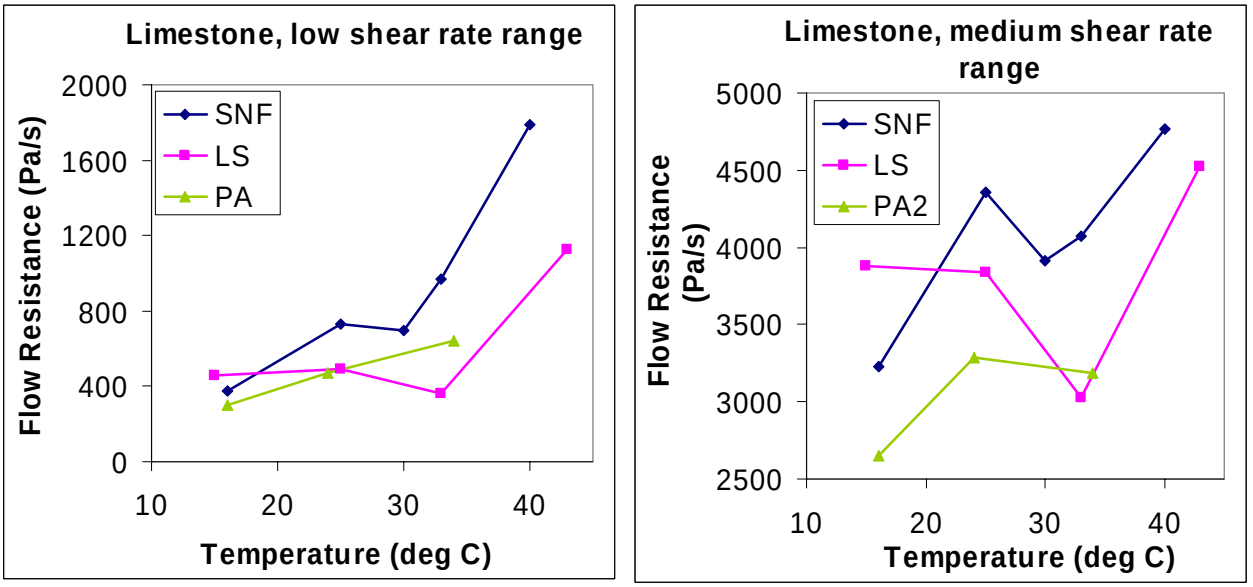

Fig. 10.4: Flow Resistance in the low shear rate (43-8.8 s^{-1}) and medium shear rate (152-118s^{-1}) for limestone pastes with SNF, LS and PA as superplasticizers at various temperatures.

10.3.2 Adsorption of plasticizer by limestone pastes

Increased flow resistance with increasing temperature might partially be caused by reduced amount of adsorbed plasticizer at elevated temperatures. Fig. 10.5 shows relative adsorbed amounts of SNF, LS and PA2 plasticizers on limestone as a function of temperature. The figure illustrates that the adsorbed amounts of SNF reach a maximum at approximately 25°C before it start to decrease. The adsorbed amounts of LS are generally found to decrease in the whole temperature range, while the adsorption of PA2 is found to be independent of temperature within the range of 16-34°C.

The shape of the adsorption curves for limestone pastes may partly be explained by the entropy of the polymers. The entropy of a polymer molecule decreases when it adsorbs onto a solid surface because the configuration of the polymer becomes restricted. Nawa et al. (2000) suggests that the adsorption of polymer onto a solid surface is an exothermic reaction which causes the adsorption to decrease with increasing temperature. Geffroy et al. (2000) states furthermore that loss of entropy by adsorption onto a solid surface is less for large macromolecules than for smaller ones. This might explain why the adsorption of PA2 is less temperature dependent than the smaller LS and SNF molecules.
An alternative explanation for the different adsorptive behaviour of SNF, LS and PA2 with increasing temperature might be that smaller SNF and LS molecules obtain a higher kinetic energy than the bigger PA2 molecules with increasing temperature and thus dislocate in a higher degree from the limestone surface.

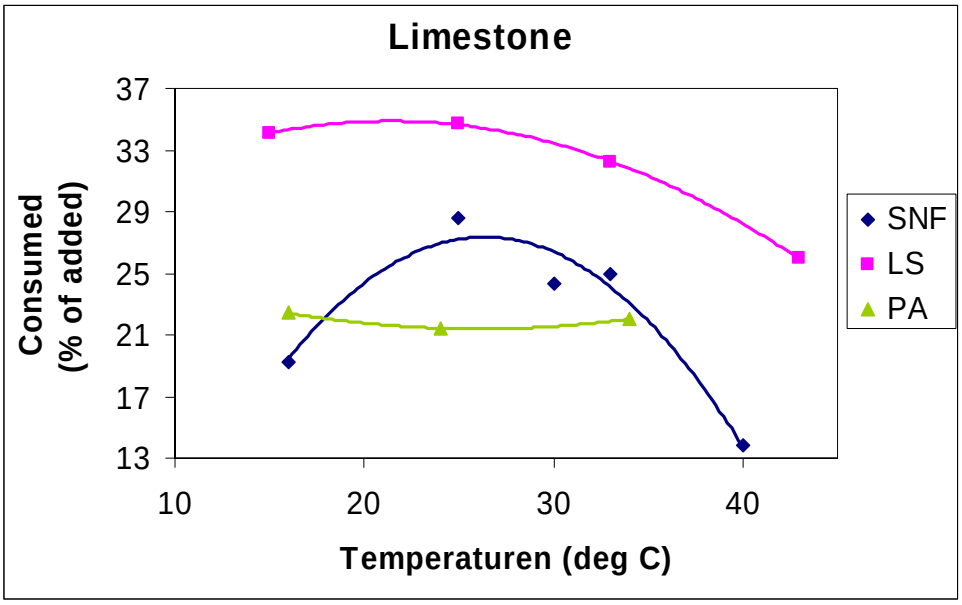

Fig. 10.5: Adsorbed amounts (% of added) SNF, LS and PA on limestone.

10.3.3 Cement paste rheology

The flow curves of Cement 4 and Cement 1 pastes with SNF as superplasticizer are depicted in Figs. 10.6 and 10.7 respectively. The figures show that the shear stresses increase with increasing temperature and that the shape of the flow curves depends on the cement type: Pastes of Cement 4 have shear thinning behaviour whereas the shear stresses of Cement 1 pastes reach a plateau. Pastes with lignosulphonate are found to have similar temperature dependencies as SNF while pastes with polyacrylate show tendencies of shear thickening (see Appendix A12.1).

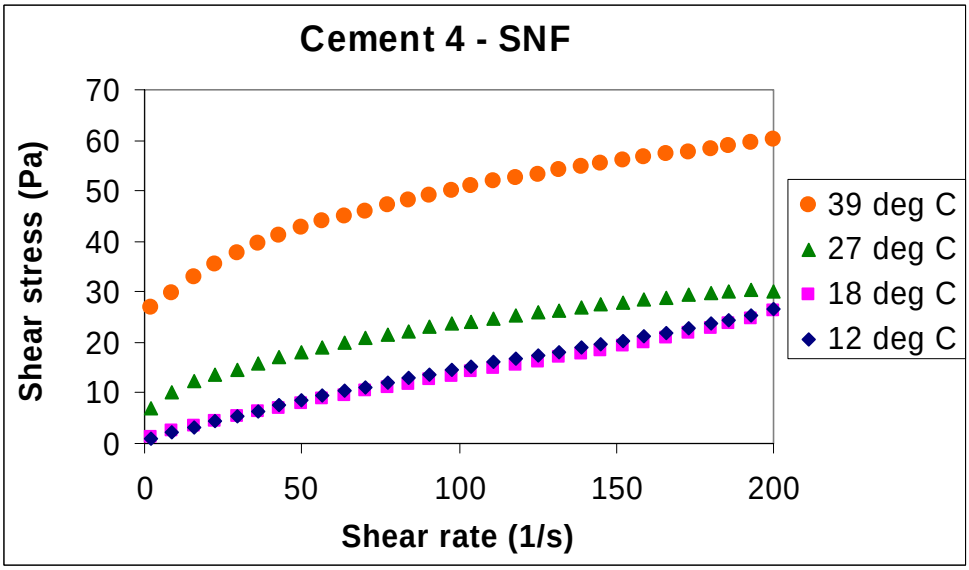

Fig. 10.6: Effect of temperature on shear stress measurements on Cement 4 pastes (w/c = 0.40) with 0.10% SNF by weight.

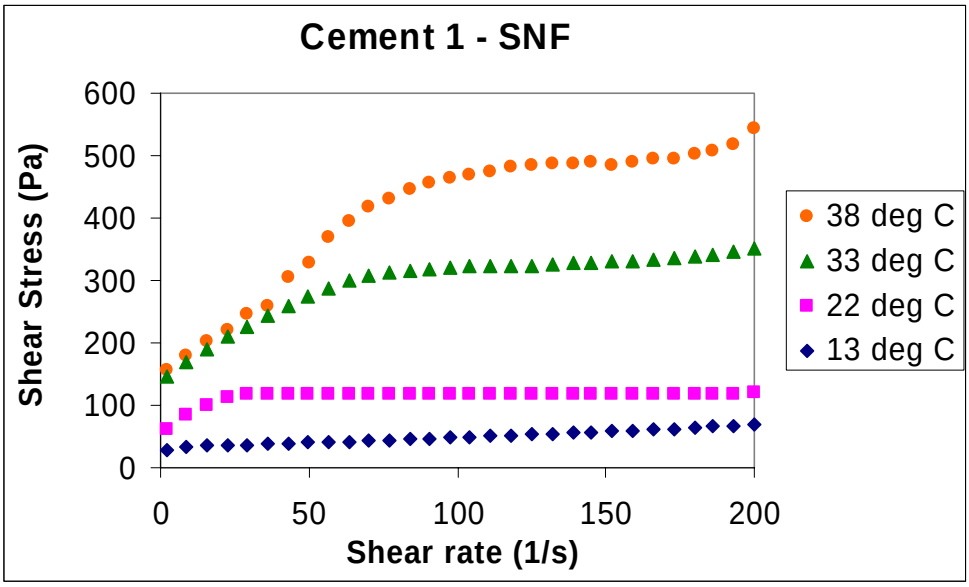

Fig. 10.7: Effect of temperature on shear stress measurements on Cement 1 pastes (w/c = 0.40) with 0.65% SNF by weight.

Cement hydration increase the volume concentration of solids in a twofold manner: formation of hydration products and consumption of water. The increased flow resistance with increasing temperature is thus probably originating from the increased hydration rate at elevated temperatures and possibly altered plasticizer adsorption as will be discussed later.
It is known that the cement hydration has a strong influence on the paste rheology. Justnes et al. (2003) found according to the Krieger-Dougherty equation (2.19) that a 3% degree of hydration of cement paste with w/c = 0.40 will increase the apparent viscosity by 22%. They assumed that the average density of hydration products was 2.67 kg/m^3 and that 40% water is bound per anhydrous cement reacted (probably higher since ettringite dominates the early reactions). The effect of increased volume fraction of solid becomes even more important at lower w/c ratios since equation (2.19) is a power function.

The flow resistances of Cement 4 pastes with SNF and LS as superplasticizers show in accordance to the Krieger-Dougherty equation exponential growth (since φ increases) as a function of temperature in both medium and low shear rate range as depicted in Fig. 10.8.
Cement 4 pastes with PA2 seem to exhibit the same trend, but the number of experiments is too scarce to make any conclusions.

Cement 1 pastes with SNF and LS do not seem to follow the Krieger-Dougherty equation as seen in Fig. 10.9. This result might be explained by the finding that Cement 1 hydrates much faster than Cement 4 as seen from the heat of hydration curves in Chapter 8 and needs higher superplasticizer dosages than Cement 4 to be dispersed. The measured gel strengths which are given in Table 10.3 show that Cement 1 pastes build very high gel strengths compared to pastes of Cement 4. The high gel strengths indicate that the pastes are strongly flocculated due to hydration. It is therefore dubious that Cement 1 pastes follow the the Kriger-Dougherty model which assume dispersed suspensions.
Cement 1 pastes with PA2 show similar gel strengths as Cement 4 when the temperature is up to 22°C. The gel strengths increase however rapidly at elevated temperatures leaving the pastes more solid-like than liquid-like.

Values of yield stress and plastic viscosity have been extracted from the same measurements as discussed above by using the Bingham model and can be found in Appendix A.12.5. Both yield stress and plastic viscosity increase with increasing temperature in both medium and low shear rate range (6 measuring points in the shear rate ranges 152-118 s^{-1} and 43-8.8 s^{-1} respectively).

Table 10.3: Measured gel strength as a function of temperature and plasticizer type

Temperature (^oC)	**Cement number**	**Plasticizer type**	**Gel Strength (Pa)**
11	Cement 4	PA2	11
18	Cement 4	PA2	18
31	Cement 4	PA2	31
12	Cement 4	LS	10
26	Cement 4	LS	16
32	Cement 4	LS	34
40	Cement 4	LS	194
14	Cement 1	LS	>180
25	Cement 1	LS	140
35	Cement 1	LS	>300
39	Cement 1	LS	>250
11	Cement 1	PA	39
22	Cement 1	PA	26
36	Cement 1	PA	>250
39	Cement 1	PA	>250

The viscosity of the pore water is found to decrease with increasing temperature in a similar manner as for limestone pastes as shown in Table 10.4. The flow resistances increase however with increasing temperature as discussed above. Thus, the increased volume fraction of solids and coagulation of the pastes seems to be the dominating factors for the increased flow resistances.

Table 10.4: Viscosity of pore water extracted from pastes of Cement 4 with SNF, LS and PA2 as a function of temperature

Cement 4			
Temperature (^{o}C)	**Plasticizer type**	**Viscosity (Pa·s)**	**Reduction of viscosity (%)**
12	SNF	1.040	- - -
18	SNF	0.914	12
27	SNF	0.780	25
39	SNF	0.610	41
12	LS	1.104	- - -
26	LS	0.815	26
32	LS	0.698	37
40	LS	0.611	45
11	PA2	1.027	- - -
18	PA2	0.933	9
31	PA2	0.714	30

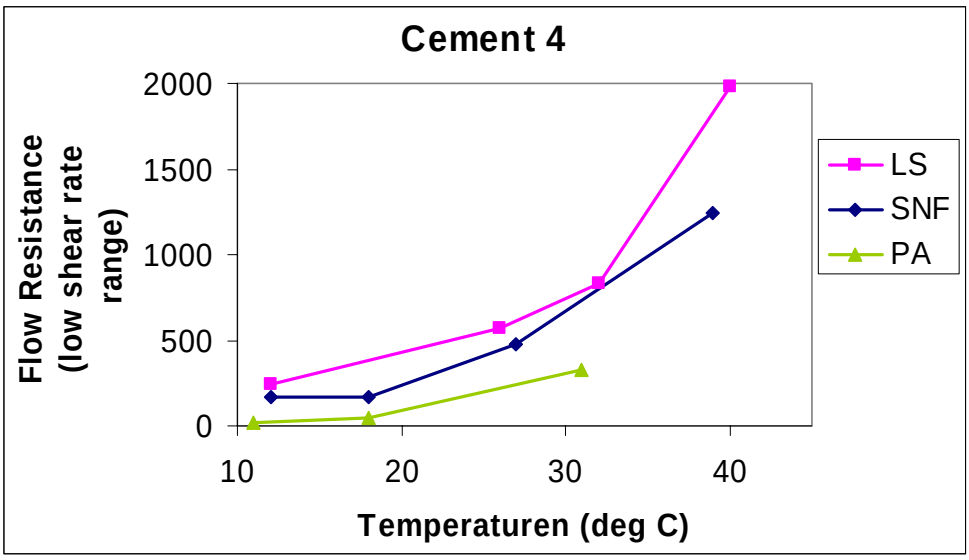

Fig. 10.8: Flow Resistances in the low shear rate range (43-8.3 s^{-1}) for Cement 4 pastes with SNF, LS and PA2 as superplasticizers at various temperatures.

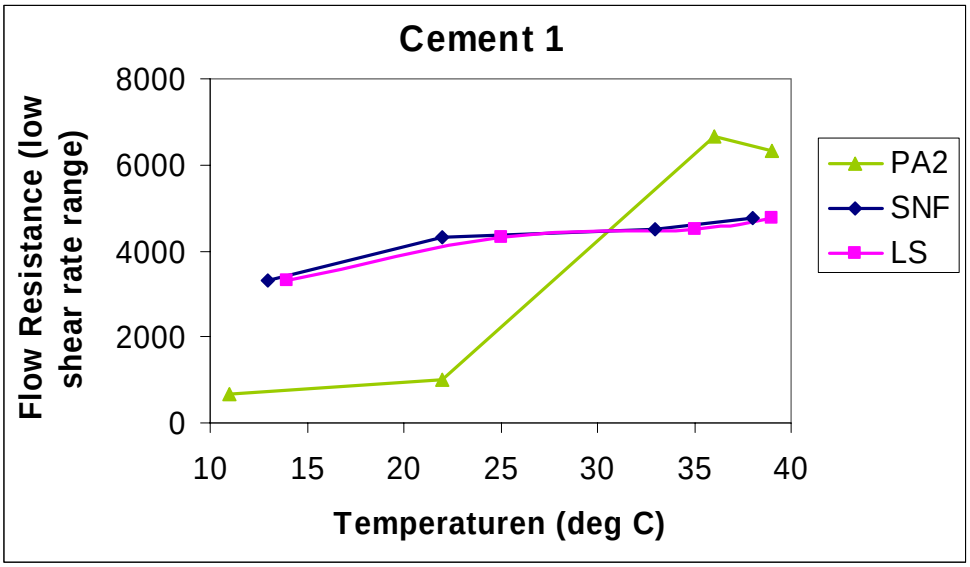

Fig. 10.9: Flow Resistances in the low shear rate range (43-8.3 s^{-1}) for Cement 1 pastes with SNF, LS and PA2 as superplasticizers at various temperatures.

Reports of the influence of temperature on the rheology of cementitious pastes found in literature is somewhat contradicting: Heikal et al. (2005) measured the rheology of cement pastes (w/c = 0.30) with the Rheotest cell with and without 1% by cement weight polycarboxylic acid (PC) in the temperature range of 20-55°C. They found that increased temperature resulted in a sharp *decrease* of the shear stresses of cement pastes. The decrease of the shear stress of the pastes with the addition of superplasticizer was higher than that of the specimens without superplasticizer. They believed that increased temperature might have changed the adsorption capacity of superplasticized cement which enhanced the paste fluidity.

Nawa et al. (2000) measured the fluidity (slump spreading area) of Portland cement pastes containing grafted co-polymers, SNF and SMF as a function of temperature ranging from 10 to 30°C. They found that the flow values for cement pastes with co-polymers clearly depended on the temperature and that it generally exhibited a minimum (i.e. maximum flow resistance) at 20°C. A similar trend was found for SMF. The mode of temperature dependence varied significantly however in the case of SNF according to the amount of superplasticizer added. The flow value of the paste decreased as the temperature rose until the addition of superplasticizer reached 1.35%. On the contrary, the flow value increased as the temperature rose when the amount of superplasticizer added was over 1.35%.

Jolicoeur et al. (1997) measured the rheological properties of normal Portland cement and blended silica fume pastes as a function of temperature (0-40°C). The rheological parameters measured included the mini-slump (spreading area) and the dynamic viscosity at various shear rates as a function of plasticizer concentration (SNF).

The normal cement exhibited only a weak overall trend to lower slump areas as the temperature increased while the slump values of SF cement pastes decreased sharply. The viscosity of the normal cement was found to decrease with increasing temperature, while the opposite was found for SF cement pastes.

Similar experiments were performed by Golaszwski and Szwabowski (2004) who investigated the influence of temperature (10, 20 and 30°C) on the rheological properties of mortars with different w/c ratios and with SNF and polycarboxylate ester as superplasticizers. They found that mortars containing both SNF and polycarboxylate ester type superplasticizer were strongly influenced by temperature. Generally, an increase of temperature increased the yield stress while the plastic viscosity decreased. An increase of *shear resistance* with increasing temperature was however

observed which indicates that the effect of the increased yield stress on the shear resistance must have dominated the effect of decreased viscosity. The rate of shear resistance increase was found to rise with increasing temperature.

10.3.3 Adsorption of plasticizer by cement

Consumed amounts (adsorbed and intercalated) of plasticizers on Cements 1 and 4 as a function of temperature are depicted in Figs. 10.10-10.11. The consumption curves show that the amounts of adsorbed and intercalated LS on Cements 1 and 4 reach a plateau. This might be caused by two opposing effects: increased number of adsorption sites and reduced adsorption with increased temperature (as seen for limestone pastes).
SNF behaves similarly as LS for Cement 4. The consumed amounts of SNF plasticizer for Cement 1 are, however, found to decrease somewhat with increasing temperature as shown in Fig. 10.10. The reasons for this behaviour might be that SNF adsorbs to a higher degree on clinker minerals than on the hydration products, decreased adsorption at elevated temperatures due to reduced entropy as discussed for limestone or that the molecules gain enough kinetic/thermal energy to dissociate from the surface.

Nawa et al. (2000) believed that the temperature dependency of the adsorption of polymer on the surface of cement is mainly governed by the increased number of adsorption sites. Jolicoeur et al. (1997) suggest on the other hand that part of the adsorbed plasticizer (SNF) might be released in the pore solution at high temperatures. This could occur if the hydrated phases do not incorporate the plasticizer initially adsorbed or if the ionic balance of the pore solution changes with time. They found an indication of this effect by the observation of negative SNF adsorption rate (desorption) with silica fume blended cement pastes in the temperature range of 30-40^{o}C.

Another possible explanation for reduced amount of consumed plasticizer with increasing temperature might be that the plasticizer molecules have different absorption behaviour on clinker minerals and hydration products. It is however unclear from literature if the hydration products adsorb more ore less plasticizer than the clinker minerals. Uchikawa et al. (1992) claimed that the adsorption of SNF and LS to the hydrates including CSH and ettringite is less than to the cement compounds while Prince et al. (2002) suggested that SNF type plasticizer might adsorb somewhat stronger on the initial ettringite germs than on the anhydrous constituents of the cement paste.

The temperature will also have an effect on the morphology of the hydration products. Verbeck and Helmuth (1968) believed that dense zones of hydration products would form around the hydrating grains at higher temperatures. Kjellsen et al. (1990, 1991) confirmed the existence of the "shells" by backscattered electron images of mature pastes. The shells were distinguishable in cement pastes hydrated at 20^{o}C and were denser at higher temperatures.
It is however unclear how the hydration products formed at elevated temperatures effect the adsorption and intercalation of plasticizers.

The adsorption of PA2 on Cement 1 and 4 (Fig. 10.12) increases linearly and do not show the same kind of plateau as seen for pastes with SNF and LS. This might be explained by the adsorption curves for limestone (Fig. 10.5) which show that PA2 is less dependent of temperature than SNF and LS. PA2 molecules are furthermore not found not to intercalate in the hydration products at the same degree as SNF and LS (Chapter 2.3.7 and 6.3.1).

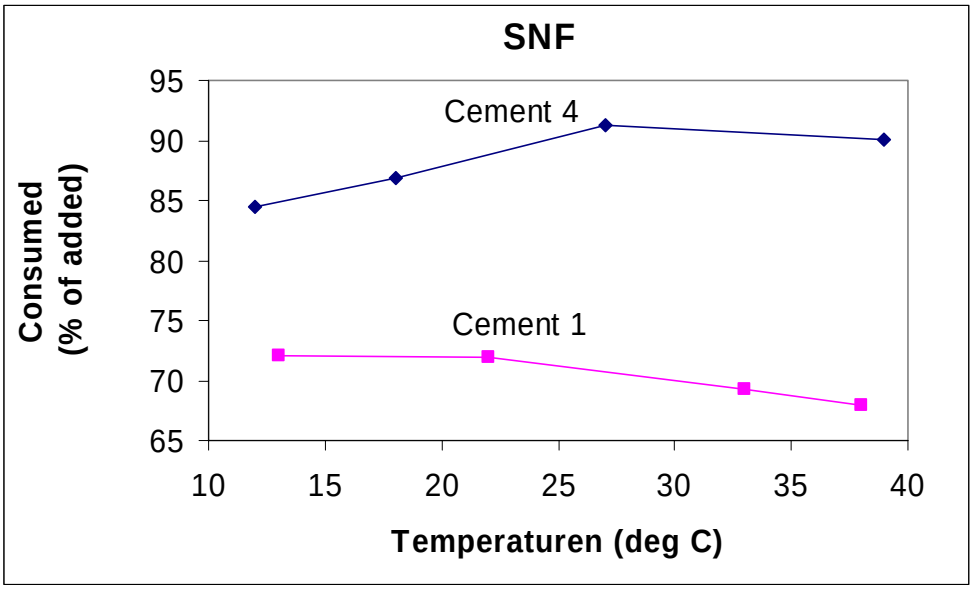

Fig. 6.67: Adsorbed and intercalated amounts (% of added) SNF on Cement 1 and 4.

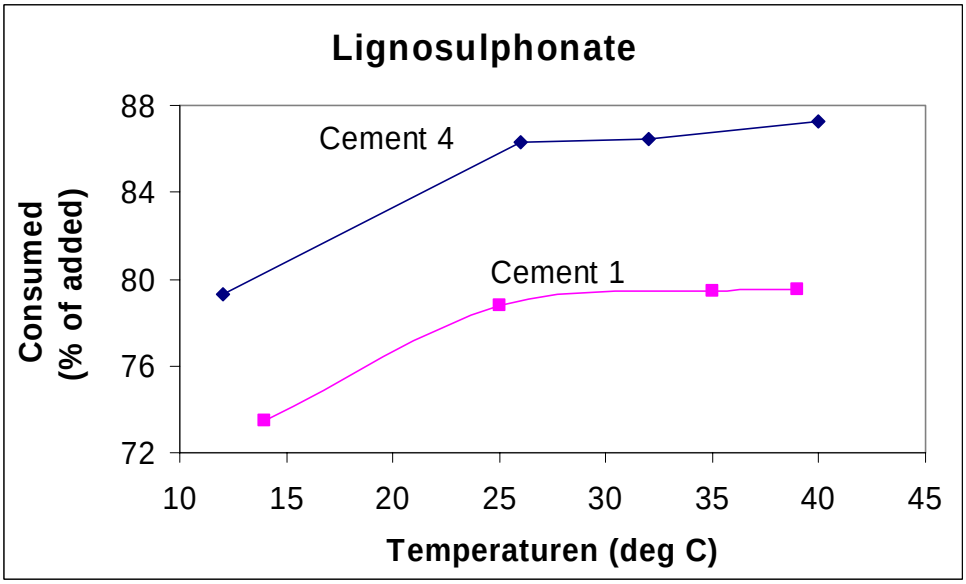

Fig. 6.68: Adsorbed and intercalated amounts (% of added) LS on Cement 1 and 4.

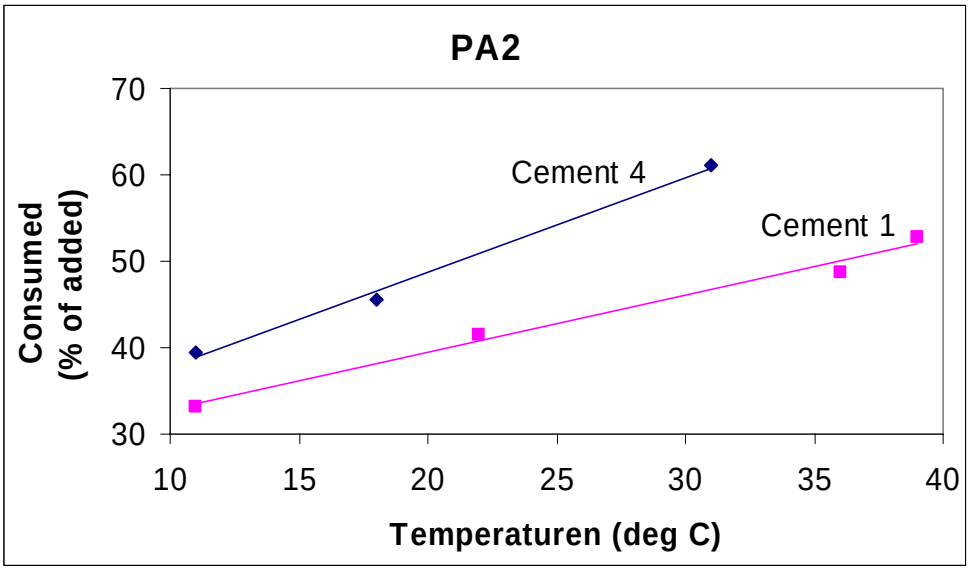

Fig. 6.69: Adsorbed (and intercalated) amounts (% of added) PA2 on Cement 1 and 4.

10.4 Conclusions

Limestone was used as a non-reactive model material for cement. The adsorbed amounts of SNF and lignosulphonate on limestone were found to decrease after reaching a maximum which occurred at approximately 25°C. SNF seemed to have a stronger dependency of the temperature than lignosulphonate. Decreased amounts of adsorbed plasticizer with increasing temperature might be explained by increased kinetic energy to the molecules or by an entropy effect.
Adsorbed amounts of polyacrylate on limestone seemed to be independent of paste temperature in the range of 16-34°C which might be caused by low reduction of entropy at adsorption due to its short backbone and long, grafted chains.
The flow resistance of the limestone pastes increased generally with increasing temperature. This result may be caused by reduced amounts of adsorbed plasticizer and/or dehydration of the paste during the rheological measurements.

Amounts of consumed (adsorbed and intercalated) plasticizer by cement reached a plateau or even decreased with increasing temperature in the case of SNF and lignosulphonate. This finding might be caused by two opposing effects namely: increased number of adsorption sites due to increased hydration rate with increasing temperature and reduced adsorption due to increased kinetic energy and/or reduced entropy of the plasticizer.
Amounts of polyacrylate consumed by cement increased linearly with increasing temperature as might be explained by the experiments with limestone where the adsorbed amounts of polyacrylate seemed to be independent of paste temperature. Increased consumption of plasticizer by the cements is thus probably governed by the increased number of adsorption cites due to increased hydration rate.
The flow resistance of Cement 4 increased exponentially with increasing temperature as a function of temperature. The pastes of Cement 1 were generally highly viscous and possibly agglomerated. The flow resistance reached a plateau value with increasing temperature in this case.

References

Aiad, I., "Influenece of time addition of superplasticizers on the rheological properties of fresh cement pastes", *Cem. Concr. Res*. **33** (2003) 1229-1234

Aiad, I., Abd El-Aleem, S., El-Didamony, H., “Effect of delaying addition of some concrete admixtures on the rheological properties of cement pastes”, *Cem Concr Res* **32** (2002) 1839-1843

Aïtcin, P.-C., Jolicoeur, C. and MacGregor, J. G., “Superplasticizers: How They Work and Why They occasionally Don’t”, *Concrete International* **16** (5) (1994) 45-52

Aïtcin, P. C., and Neville, A., High-performance concrete demystified, *Concrete International*, **15** (1) (1993) 21-26

Andersen, P. J., The effect of superplasticizers and air-entraining agents on the zeta potential of cement pastes, *Cem Concr Res* **16** (1986) 931-940

Andersen, P. J., Roy, D. M. and Gaidis, J. M., "The effect of superplasticizer molecular weight on its adsorption on, and dispersion of, cement"**,** *Cem. Concr. Res*., **18** (6) (1988), 980-986

Andersen, P. J., Roy, D.M. and Gaidis, J.M, “The effects of adsorption of superplasticizer on the surface of cement”. *Cem. Concr. Res*. **17** (5) (1987) 805-813

Andersen, P. J., Roy, D. M. and Gaidis, J. M, The effects of adsorption of superplasticizers on the surface of cement, *Cem Concr Res* **17** (1987) 805-813

Andersen, P.J., Kumar, A., Roy, D. M. and Wolfe-Confer, D., "The effect of calcium sulphate concentration on the adsorption of a superplasticizer on a cement: Methods, zeta potential and adsorption studies"**,** *Cem. Concr. Res.*, **16** (*2*) (1986) 255-259

Atzeni, C., Massida, C. and Sanna, U., "Comparison between rheological models for Portland cement pastes", *Cem. Concr. Res*. **15** (1985) 511-519

Banfil, P. F. G., “Rheological methods for assessing the Flow Properties of Mortar and Related Materials”, *Construction and Building Materials*, **8** (1) (1994) 43-50

Banfill, P.F.G., “A viscometric study of cement pastes containing superplasticizers with a note on experimental techniques”, *Mag. Concr. Res*., **33**, (1981) 37-47

Banfill, P.F.G., A discussion of the paper “Rheological properties of cement mixes.” *Cem Concr Res* **9** (1979) 795-796

Banfil, P. F.G. and Saunders, D.C., "On the Viscometric Examination of Cement Pastes”, *Cem. Concr. Res*. **11** (1981) 363-370

Barnes, H. A., Hutton, J. F. and Walters, K., “An Introduction to Rheology”, Rheology Series, 3, Elsevier, Amsterdam, 1989.

Barnes, H. A., and Walters, K., “The yield stress myth?”, *Rheol Acta* **24** (1985) 323-326

Basile, F., Biagini, S., Ferrari, G., Collepardi, M., in third CANMET/ACI International Conference, Superplasticizers and Other Chemical Admixtures in Concrete, Ed. V. M. Malhotra, Ottawa, 1989 pp.171-188

Bensted, J., “Some applications of conduction calorimetry to cement hydration”, *Advances in Cement Research.* **1 (1),** 1987

Bilanda N., Fierens, P., Tirlocq, J., Tenoutasse, N., "Hydration of tricalcium aluminate doped by sodium oxide", 7th International Congress on the Chemistry of Cement, vol. IV, Paris 1980

Birchall, J.D., Howard, A.J., Double, D.D., "Some general considerations of a membrane/osmosis model for Portland cement hydration", *Cem. Concr. Res*. **10** (1980) 145-155

Björnström, J. and Chandra, S., "Effect of superplasticizers on the rheological properties of cements", *Materials and Structures*, **36** (2003) 685-689

Blank, B., Rossington, D. R. and Weinland, L. A., “Adsorption of admixtures on Portland Cement”, *J Am Ceram Soc* **46** (8) (1963) 395-399

Boikova, A.I., Grischenko, L.V., Domansky, A.I., "Hydration of C_3A and solid solutions of various composition", From the Proceedings of The 7th International Congress on the Chemistry of Cement, vol.5, Paris 1980

Boikova, A.I., Domansky, A.I., Paramonova, V.A., Straviskaja, G.P., Nikuschenko, V.M., “The Influence of Na_2O on the Structure and Properties of $3CaO.Al_2O_3$”, *Cem Concr Res* **7** (1977).483-492

Bonen, D., Sarkar, S.L., “The superplasticizer adsorption capacity of cement pastes, pore solution composition, and parameters affecting flow loss”, *Cem. Concr. Res*. **25** (7) (1995) 1423-1434

Carazeanu, I., Chirila, E., Georgescu, M., “Investigation of the hydration process in $3CaO*Al_2O_3$-$CaSO_4*2H_2O$-plasticizer-H_2O systems by X-ray diffraction”, *Talanta* **57** (2002) 617-623

Chandra, S., Björnström, J., “Influence of cement and superplasticizers type and dosage on the fluidity of cement mortars-Part I”, *Cem. Concr. Res*. **32** (2002, a) 1605-1611

Chandra, S., Björnström, J., “Influence of cement and superplasticizers type and dosage on the slump loss of Portland cement mortars-Part II”, *Cem. Concr. Res* **32** (2002, b) 1613-1619

Chiocchio, G., Paolini, A.E., "Optimum time for adding superplasticizer to Portland cement paste", *Cem. Concr. Res*. **15** (5) (1985) 901-908.

Ciach, T. D. and Swenson, E. G., “Morphology and Microstructure of Hydrating Portland Cement and Its Constituents: I. Changes in Hydration of Tricalcium Aluminate Alone and in the Presence of Triethanolamine or Calcium Lignosulfonate”, *Cem Concr Res* **1** (2) (1971, a) 143-158

Ciach, T. D. and Swenson, E. G., “Morphology and Microstructure of Hydrating Portland Cement and Its constituents: III. Changes in the Hydration of a Mixture of C_3S, C_3A and Gypsum with and without Triethanolamine and Calcium Lignosulfonate Present”, *Cem Concr Res* **1** (3) (1971, b) 257-271

Ciach, T. D. and Swenson, E. G., “Morphology and Microstructure of Hydrating Portland Cement and Its constituents: IV. Changes in Hydration of a C_3S, C_2S, C_3A, C_4AF and Gypsum with and without the Admixtures Triethanolamine and Calcium Lignosulfonate”, *Cem Concr Res* **1** (4) (1971, c) 367-383

Collepardi, M., Monosi, S., Moriconi, G., Pauri, M., "Combined effect of lignosulfonate and carbonate on pure portland clinker compounds hydration. V. Hydration of dicalcium silicate alone and in the presence of tricalcium aluminate"**,** *Cem. Concr. Res.* **14** (**2)**, (1984) 275-284

Collepardi, M., Baldini, G., Pauri, M., Corradi, M., The effect of pozzolanas on the tricalcium aluminate hydration. *Cem. Concr. Res.* **8** (6) 1978, 741-752

Collepardi, M., "The rheological behaviour of cement pastes", *Il Cemento*, **68** (1971) 99-106

Costa, U. and Marchi, M., “Mineralogical composition of clincer by Bogue and Rietveld Method: the effect of minor element”, From the Congress Proceedings- volume 1: 11th International Congress on the Chemistry of Cement (ICC), Durban, South Africa 11-16 May 2003

Cyr, M., Legrand, C. and Mouret, M.: "Study of the shear thickening effect of superplasticizers on the rheological behaviour of cement pastes containing or not mineral additives", *Cem. Concr. Res*. **30** (2000) 1477-1483.

De La Torre, A.G., Bruque, S., Campo, J., Aranda, M.A.G.," The superstructure of C_3S from synchrotron and neutron powder diffraction and its role in quantitative phase analysis", *Cem Concr Res* **32** (2002) 1347-1356

Daimon, M. and Roy, D.M., "Rheological properties of cement mixes: II Zeta potential and preliminary viscous studies", *Cem. Concr. Res*. **9** (1979) 103-110

Daimon, M., Roy, D.M., "Rheological properties of cement mixes: I. Methods, preliminary experiments and adsorption studies", *Cem. Concr. Res* **8** (1978) 753-764

Dodson, V. H., Hayden, T., "Another look at the Portland cement/chemical admixture incompatibility problem", *Cement, Concrete and Aggregates*, **11 (1)** (1989) 52-56

Ferrari, G., Cerulli, T., Clemente, P. and Dragoni, M.: "Adsorption of Naphthalene Sulphonate Superplasticizers by Cement Particles through Gel Permeation Chromatography", SP 173-43, Proceedings of 5th CANMET/ACI International Conference on Superplasticizers and Other Chemical Admixtures in Concrete, Rome, Italy, October 7-10, 1997, pp. 869-892.

Flatt, R.J., "Towards a prediction of superplasticized concrete rheology", *Materials and Structures*, **37** (2004) 289-300

Flatt, R.J., Houst, Y.F., Bowen, P. And Hofmann, H.: "Electrosteric Repulsion Induced by Superplasticizers between Cement Particles – An Overlooked Mechanism?", Proc. 6th CANMET/ACI Int. Conf. Superplasticizers and Other Chemical Admixtures in Concrete, October 10-13, 2000, Nice, France, pp. 29-42

Fujii, K. and Kondo, W. (1983). *J. Am. Ceram. Soc.* **66**, C220

Gjørv, O.E and Løland, K.E, "Condensed Silica Fume in Concrete", Report BML 82.610, February 1982, NTNU, Norway

Golaszewski, J. and Szwabowski, J. „The Influence of superplasticizers on the rheological behaviour of fresh cement mortars“, *Cem Concr Res* **34** (2004) 235-248

Greszczyk, S. and Kucharska, L., "The Influence of Chemical Composition of Cement on the Rheological Properties", From the Proceedings of the International Conference organized by The British Society of Rheology; "Rheology of Fresh Cement and Concrete" Edited by P.F.G Banfill, The British Society of Rheology, E.& F.F.Spon, London 1990.

Gu, P., Xie, P., Beaudoin, J.J., Jolicoeur, C., "Investigation of the retarding effect of superplasticizers on cement hydration by impedance spectroscopy and other methods"**,** *Cem. Concr. Res.*, **24** (3) (1994) 433-442

Gupta, P.R. and McCarthy, J.L., “Lignin XIV. Gel Chromatography and the Distribution in the Molecular Size of Lignin Sulfonates at Several Electrolyte Concentrations”, *Macromolecules*, **1** (3) (1968) 236-244.

Hanehara, S. and Yamada, K., “Interaction between cement and chemical admixture from the point of cement hydration, absorption behaviour of admixture, and paste rheology”, *Cem Concr Res* **29** (1999) 1159-1165

Heikal, M., Morsy, M.S., Aiad, I., “Effect of treatment temperature on the early hydration characteristics of superplasticized silica fume blended cement pastes”, *Cem. Concr. Res.* **4** (4) (2005) 680-687

Hekal, E.E. and Kishar, E.A., “Effect of sodium salt of naphtalene-formaldehyde polycondensate on ettringite formation”, *Cem Concr Res* **29** (1999) 1535-1540

Jawed I. and Skalny J., “Hydration of tricalcium silicate in the presence of fly ash.” In: *Proceedings of Symposium N on Effects of Fly Ash Incorporation in Cement and Concrete*, Boston, 16-18 November, 1981. Materials Research Society: 60-70

Jawed, I. and Skalny, J., “Alkalies in Cement: A review II. Effects of Alkalies on Hydration and Performance of Portland Cement”, *Cem. Concr. Res.* **8** (1) (1978) 37-58

Jawed, I. and Skalny, J. **“**Alkalies in cement: A review I. Forms of Alkalies and their effect on clinker formation” *Cem. Concr. Res.*, **7** (6), (1977), 719-729

Jiang, S., Kim, B.-G., Aïtcin, P.-C., “Importance of adequate soluble alkali content to ensure cement/superplasticizer compatibility”, *Cem Concr Res* **29** (1999) 71-78

Jolicoeur, C. and Simard, M.-A., “Chemical Admixture-Cement Interactions: Phenomenology and Physico-chemical Concepts”, *Cement and Concrete Composites*, **20** (1998) 87-101.

Jolicoeur, C., Sharman, J., Otis, N., Lebel, A., Simard, M.-A., Pagé, M., “The Influence of Temperature on the Rheological propreties of Superplasticized Cement Pastes”, Proceedings the Fifth CANMET/ACI International Conference on Superplasticizers and other Chemical Admixtures in Concrete, Ed. V.M. Malhotra, Rome (1997) 379-415

Joubert, J. -M., “Contribution of the Rietveld method to non-stoichiometric phase modeling. Part I: generalities”, *Calphad*,**26** (3) (2002) 419-425

Justnes, H. (2003): “Rheology of Cement based Binders – State-of-the-Art”, SINTEF Report STF22 A0617, 2003-01-10, 60pp

Justnes, H. and Vikan, H., “Viscosity of Cement Slurries as a Function of Solids Content”, Annual Transactions of the Nordic Rheology Society **13** (2005)

Justnes, H., Van Dooren, M. and Van Gemert, D.: “Reasons for Workability Loss in Cementitious Binders”, 7th CANMET/ACI Intl. Conf. on Super-plasticizers and Other Chemical Admixtures in Concrete, Berlin, October 22-24, 2003, Supplementary paper.

Khalil, S. M., and Ward, M. A.,”Influence of SO_3 and C_3A on the Early Reaction Rates of Portland Cement in the Presence of Calcium Lignosulfonate”, *Am Ceram Soc Bull* **57** (12) (1978) 1116-1118, 1122

Khalil, S.M. and Ward, M.A., "Influence of a Lignin Based Admixture on the hydration of Portland Cements", *Cem. Concr. Res*. **3** (1973) 677-688.

Kim, B.-G. and Aïtcin, P.-C., “Dispersing mechanism of PNS superplasticizer in high-performance concrete”, From the Congress Proceedings- volume 1: 11th International Congress on the Chemistry of Cement (ICC), Durban, South Africa 11-16 May 2003

Kim, B.-G., Jiang, S., Jolicoeur, C., Aïtcin, P.-C., “The adsorption behaviour of PNS superplasticizer and its relation to fluidity of cement paste”, *Cem Concr Res* **30** (2000) 887-893

Kim, B.-G., Jiang, S., Aïtcin, P.-C., “Influence of molecular weight of PNS superplasticizers on the properties of cement pastes containing different alkali contents”, From the Proceedings of the RILEM Conference The Role of Admixtures in High Perfomance Concrete”, Edited by J. G. Cabrera and R. Rivera-Villarreal, RILEM Publications, 1999

Kirby, G.H., and Lewis, J.A., "Rheological Property Evolution in Concentrated Cement-Polyelectrolyte Suspensions", *J. Am. Ceram. Soc.* **85** (12) (2002) 2989-2994

Kjellsen, K.O., Detwiler, R.J., Gjörv, O.E., "Development of Microstructure in Plain Cement Pastes Hydrated at Different Temperatures", *Cem. Conr. Res.*, **21** (1) (1991) 179-189

Kjellsen, K.O., Detwiler, R.J., Gjörv, O.E., "Backscattered Electron Imaging of Cement Pastes Hydrated at Different temperatures", *Cem. Conr. Res.* **20** (2) (1990) 308-311

Klaska, R., Baetzner, S., Möller, H., Paul, M., Roppelt, T., “Effects of secondary fuels on clinker mineralogy”. *Cement International* **1** (4) (2003) 88-98

Krieger, I.M. and Dougherty, T.J. (1959): “A Mechanism for Non-Newtonian Flow in Suspensions of Rigid Spheres”, *Trans. Soc. Rheol*. **3**, (1959) 137-152.

Kucharska, L., "Effect of Products of the Hydration of C_3A on Rheology of Clinker and Cement Pastes", From the Proceedings of the International Conference organized by The British Society of Rheology; "Rheology of Fresh Cement and Concrete" Edited by P.F.G Banfill, The British Society of Rheology, E.& F.F. Spon, London 1990

Lerch, W. and Bogue, R.H. (1934). *J. Res. Natl Bur. Stand.* **12**, 645

Lewis, J.A., Matsuyama, H., Kirby, G., Morisette, S., and Young, J.F., "Polyelectrolyte Effects on the Rheological Properties of Concentrated Cement Suspensions", *J.Am.Ceram.Soc.*, **83** (8) (2000) 1905-1913

Li, G., Tagnit-Hamou, A., Aïtcin, P.-C., Improving cement-superplasticizer compatibility by using soluble alkalis as a chemical additive in concrete, From the Congress Proceedings-volume 1: 11th International Congress on the Chemistry of Cement (ICC), Durban, South Africa 11-16 May 2003

Luke, K., and Aitkin, P.-C., Advances in Cementitious Materials, ed. S. Mindess, Ceramic Transactions Vol. 16, Am. Ceram. Soc. Westerville (1991) 147-166

Macphee, D.E. and Lachowski, E.E., in Lea's Chemistry of Cement and Concrete, Fourth Edition, Edited by P.C. Hewlett, Arnold 1998, London

Magarotto, R., Torresan, I., Zeminian, N., "Effect of alkaline sulphates on the performance of superplasticizers", proceedings of the 11th International Congress on the Chemistry of Cement (ICCC) "*Cement's Contribution to the Development in the 21st Century*", Durban, South Africa, 2003.

Maki, I., "Morphology of the So-Called Prismatic Phase in Portland Cement Clinker", *Cem Concr Res*, **4** (1974, a) 87-97

Maki, I., "Nature of the Prismatic Dark Interstitial material in Portland Cement Clinker", *Cem Concr Res* **3** (1974, b) 295-313

Malhotra, V.M., (Ed.), Proceedings of Sixth CANMET/ACI International Conference on Superplasticizers and Other Chemical Admixtures in Concrete, Nice, France, 2000.

Mannonen, R., "Effects of addition time of sulfonated naphthalene-based superplasticizer on the properties of concrete", Doctoral thesis, Helsinki University of Technology, Faculty of Civil Engineering and Surveying, Concrete Technology, Espoo 1996

Matsukawa, K. and Diamond, S., Advances in Cementitious Materials, Ed. S. Mindess, Ceramic Transactions Vol. 16, Am. Ceram. Soc. Westerville, (1991) 41-55

Mezger, T.G., The Rheology Handbook: For users of rotational and oscillatory rheometers, Curt R. Vincentz Verlag, Hannover, 2002

Milestone, N. B., "Hydration of Tricalcium Silicate in the Presence of Lignosulfonates, Glucose, and Sodium Gluconate", *J Am Ceram Soc* **62** (7-8) (1979) 321-324

Mollah, M.Y.A., Yu, W., Schennach, R., Cocke, D.L., "A Fourier transform infrared spectroscopic investigation of the early hydration of Portland cement and the influence of sodium lignosulfonate", *Cem. Concr. Res*. **30** (2000) 267-273

Mollah, M.Y.A., Palta, P., Hess, T.R., Vempati, R.K., Cocke, D.L.," Chemical and Physical effects of sodium lignosulfonate superplasticizer on the hydration of Portland cement and solidification/stabilization consequences", *Cem Concr Res* **25** (3) (1995) 671-682,

Mondal, P. and Jeffrey, J.W., "The Crystal Structure of Tricalcium Aluminate, $Ca_3Al_2O_6$", *Acta Cryst*. B**31** (1975) 689-697

Monosi, S., Moriconi, G., Pauri, M. and Collepardi, M., "Influence of lignosulfonate, Glucose and Gluconate on the C_3A Hydration", *Cem Concr Res* **13** (4) (1983) 568-574

Myrvold, B.O. and Reknes, K., "Adsorption studies of Lignosulphonates on cement model compounds", From the Congress Proceedings- volume 1: 11^{th} International Congress on the Chemistry of Cement (ICC), Durban, South Africa 11-16 May 2003

Mørk, P.C., "Overflate og Kolloidkjemi. Grunnleggende Prinsipper og teorier", (in Norwegian) 7.utgave 2001, NTNU kompendium, Institutt for Kjemisk Prosessteknologi.

Nagataki, S., Sakai, E., Takeuchi, T., "The fluidity of fly ash-cement paste with superplasticizers", *Cem. Concr. Res.*, **14** (5) (1984) 631-638

Nawa, T., Ichiboji, H., Kinoshita, M., "Influence of Temperature on Fluidity of Cement Paste Containing Superplasticizer with Polyethylene Oxide Graft Chains", Proceedings the sixth CANMET/ACI International Conference on Superplasticizers and other Chemical Admixtures in Concrete, Ed. V.M. Malhotra, Nice, 2000, pp.195-210.

Nawa, T., Eguchi, H., Fukaya, Y., "Effect of Alkali Sulphate on the rheological Behaviour of Cement Paste Containing a Superplasticizer, Proceedings third CANMET/ACI International Conference, Superplasticizers and Other Chemical Admixtures in Concrete, Ed. V. M. Malhotra, Ottawa, 1989, pp.405-424.

Nehdi, M. and Rahman, M.-A. "Estimating rheological properties of cement pastes using various rheological models for different test geometry, gap and surface friction", *Cem. Concr. Res.* **34** (2004) 1993-2007

Nehdi, M., Mindness, S and Aïtcin, P.-C.: "Rheology of High-Performance Concrete: Effect of Ultrafine Particles", *Cem. Concr. Res*. **28 (5)** (1998) 687-697.

Neubauer, C. M., Yang, M. and Jennings, H.M.: „Interparticle Potential and Sedimentation Behaviour of Cement Suspensions: Effects of Admixtures", *Advanced Cement Based Materials*, **8** (1) (1998) 17-27

Noor, M.A. and Uomoto, T., "Rheology of high flowing mortar and concrete", *Materials and Structures* **37** (2004) 513-521

Odler, I., in Lea's Chemistry of Cement and Concrete, Fourth Edition, Edited by P.C. Hewlett, Arnold 1998, London

Odler, I. and Becker, T., "Effect of some liquefying agents on properties and hydration of Portland cement and tricalcium silicate pastes", *Cem. Concr. Res*. **10** (3) (1980) 321-331

Odler, I. and Wonnemann, R., "Effect of alkalies on portland cement hydration: I. Alkali oxides incorporated into the crystalline lattice of clinker minerals", *Cem. Concr. Res.*, **13** (6) (1983, a) 477-482

Odler, I. and Wonnemann, R., "Effect of alkalies on portland cement hydration: II. Alkalies present in form of sulfates", *Cem. Concr. Res.*, **13** (6) (1983, b) 771-777

Ogawa K., Uchikawa H., Takemoto K., Yasui I., The mechanism of the hydration in the system C_3S pozzolanas. *Cem. Concr. Res.* **10** (5) 1980, 683-696

Ohta, A., Sugiyama, T., Tanaka, Y.: "Fluidizing Mechanism and Application of Polycarboxylate-based Superplasticizers", SP 173-19, Proceedings of 5th CANMET/ACI International Conference on Superplasticizers and Other Chemical Admixtures in Concrete, Rome, Italy, October 7-10, 1997, pp. 359-378.

Papo, A. and Piani, L., "Effect of various superplasticizers on the rheological properties of Portland cement pastes", *Cem. Concr. Res.* **34** (2004) 2097-2101

Park, C.K., Noh, M.H. Park, T.H. “Rheological properties of cementitious materials containing mineral admixtures”, *Cem. Concr. Res*., **35** (2005) 842-849

Paul, M., Hornung, D., Enders, M., Schmidt, R., “Process monitoring in a cement plant: the combination of optimized preparation procedures for clinker and cement and Rietveld analysis”, *Cement International* **2** (1) (2004) 98-105

Plowman, C., Cabrera, J.G., The influence of pulverised fuel ash on the hydration reactions of calium aluminates. In: *Proceedings of Symposium N on Effects of Fly ash Incorporation in Cement and Concrete,* Boston, 16-18 November, 1981. Materials Research Society: 78-81.

Pratt, P.L. and Ghose, A. (1983). *Phil. Trans. R. Soc. Lond.* **A310**, 93

Prince, W., Espagne, M., Aïtcin, P.-C., “Ettringite formation: A crucial step in cement superplasticizer compatibility”, *Cem. Concr. Res.* **33** (2003) 635-641

Prince, W., Edwards-Lajnef, M., Aïtcin, P.-C., “Interaction between ettringite and a polynaphtalene sulfonate superplasticizer in a cementitious paste”, *Cem Concr Res* **32** (2002) 79-85

Ramachandran, V. S., “Effect of Sugar Free Lignosulfonates on Cement Hydration”, *Zem Kalk Gips* **31** (6) (1978) 144-146

Ramachandran, V. S., "Interaction of calcium lignosulphonate with tricalcium silicate, hydrated tricalcium silicate, and calcium hydroxide", *Cem. Concr. Res*. **2** (1972) 179-194.

Ramachandran, V.S., Malhotra, V.M., Jolicoeur, C., Spiratos, N., Superplasticizers: properties and applications in concrete, CANMET, Canada, 1998.

Ratinac, K.R., Standard, O.C., Bryant, P.J., “Lignosulfonate adsorption on and stabilization of lead zirconate titanate in aqueous suspension”, *Journal of Colloid and Interface Science* **273** (2004) 442-454

Rechenberg, W. and Sprung, S., „Composition of the solution in the hydration of cement“, *Cem. Concr. Res.,* **13** (1) (1983) 119-126

Regourd, M., Chromy, S., Hjorth, L., Mortureux, B., Guinier, A., "Polymorphisme des Solutions Solides du Sodium dans l'Aluminate Tricalcique" *J.Appl. Cryst*. **6** (1973) 355-364

Rezanowich, A, Goring, D.A.I., “Polyelectrolyte expansion of a lignin sulfonate gel” *J. Colloid Sci.,* **15** (5) (1960) 452-471

Rossington, D. R. and Runk, E. J., “Adsorption of Admixtures on Portland Cement Hydration Products”, *J Am Ceram Soc* **51** (1) (1968) 46-50

Roy, M. and Asaga, K., "Rheological properties of cement mixes: III. The effects of mixing procedures on viscometric properties of mixes containing superplasticizers", *Cem. Concr. Res.*,**9** (6), (1979),731-739

Saak, A.W., Jennings, H.M., Shah, S.P., "A generalized approach for the determination of yield stress by slump and slump flow", *Cem. Concr. Res*. **34** (2204) 363-371

Salem, Th.M.: “Electrical conductivity and rheological properties of ordinary Portland cement-silica fume and calcium hydroxide-silica fume pastes”, *Cem. Concr. Res*. **32** (2002) 1473-1481.

Sandberg, P. and Roberts, L.R., "Studies of Cement-Admixture Interactions Related to Aluminate Hydration Control by Isothermal Calorimetry", From the proceedings of the 7th CANMET/ACI International Conference on Superplasticizers and other chemical admixtures in Concrete, American Concrete Institute, Michigan, 2003

Schultz; M.A. and Struble, L.J., "Use of Oscillatroy Shear to Study Flow Behaviour of Fresh Cement Paste", *Cem. Conr. Res.* **23** (1993) 273-282

Sheinn, A.M.M., HO, D.W.S., Tam, C.T., “Rheological Model for Self-Compacting Concrete - Paste Rheology”, in the Proceedings of 27th Conference on Our World in Concrete and Structures, Singapore, 28-29 August 2002, Ed. CT Tam, CI-Premier Singapore, pp 517-523

Silverstein R. M, Bassler G. C.,Morrill T. C., Spectrometric identification of organic compounds - 5th ed. John Wiley & Sons,New York, USA, 1991

Simard, M.-A., Nkinamubanzi, P.-C., Jolicoeur, C., "Calorimetry, Rheology and Compressive Strength of Superplasticized Cement Pastes", *Cem.Conr.Res.***23** (1993) 939-950

Spiratos,N., Pagé, M., Mailvaganam, N.P., Malhotra, V.M., Jolicoeur, C., "Superplasticizers for Concrete: Fundamentals, Technology, and Practice", Supplementary Cementing Materials for Sustainable Development Inc., Ottawa, Canada, 2003

Stein, H.H., "Influence of some Organic Additives on the Hydration Reaction of Portland Cement" *J. Appl. Chem.* **11** (1961) 474-482

Tattersall, G.H. and Banfill, P.F.G., The Rheology of Fresh Concrete, Pitman Advanced Publishing Program, Boston, London, Melbourne 1983

Taylor, H.F.W., Cement Chemistry, Academic Press, London, 1990

Thomas, N.L. and Double, D.D., "Calcium and silicon concentrations in solution during the early hydration of Portland cement and tricalcium silicate", *Cem. Concr. Res.* **11** (1981) 675-687

Turian, R.M., Ma, T.W., Hsu, F.L.G., Sung, D.J., "Characterization, settling, and rheology of concentrated fine particulate mineral slurries", *Powder Technology* **93** (1997) 219-233

Uchikawa, H., Hanehara, S., Sawaki, D., "The role of steric repulsive force in the dispersion of cement particles in fresh paste prepared with organic admixture", *Cem. Concr. Res.* **27** (1) (1997) 37-50

Uchikawa, H., Sawaki, D., Hanehara, S., "Influenece of kind and added timing of organic admixture on the composition, structure and property of fresh cement paste", *Cem. Concr. Res.* **25** (2) (1995) 353-364

Uchikawa, H., Hanehara, S., Shirasaka, T., Sawaki, D., "Effect of admixture on hydration of cement, adsorptive behavior of admixture and fluidity and setting of fresh cement paste", *Cem. Concr. Res.* **22** (6) (1992), 1115-1129

Uchikawa, H., Uchida, S., Ogawa, K., Hanehara, S., " Influence of $CaSO_4*2H_2O$, $CaSO_4*1/2H_2O$ and $CaSO_4$ on the initial hydration of clinker having different burning degree**"** *Cem. Concr. Res*. **14** (1984), 645-656

Uchikawa, H. and Uchida, S., Influence of pozzolana on the hydration of C_3A. In:*Proceedings of the 7th International Congress on the Chemistry of Cement*, Paris, 1980; vol. III:IV-24-29

Verbeck, G.J., and Helmuth, R.H., "Structures and Physical Properties of Cement Pastes ", *Proceedings of the 5th International Congress on the Chemistry of Cement*, Toky, 1968

Vikan, H. and Justnes H.,: "Influence of Silica Fume on the Rheology of Cementitious Paste", Proceedings of the Eight CANMET/ACI International Conference on Fly Ash, Silica Fume, Slag and Natural Pozzolans in Concrete (Ed. V. Mohan Malhotra), Las Vegas, USA, May 23-29, 2004, CANMET/ACI SP-221-25, pp. 427-442.

Vikan, H. and Justnes, H.: "Influence of Silica Fume on Rheology of Cement Paste", Proc. Int. Symp. Self-Compacting Concrete, Reykjavik, Iceland, 17-20 August, 2003.

Wallevik, O.H., From the compendium written for Rheology the course;"Rheology of Coarse Particle Suspensions, such as Cement Paste, Mortar and Concrete", IBRI, Iceland 2000

Wallevik, O.H.: "The rheology of fresh concrete and application on concrete with and without silica fume" (in Norwegian). PhD thesis 1990:45, Inst. Building Materials, Norwegian University of Science and Technology, Trondheim, July 1990, 182 pp

Weast, R.C., *CRC Handbook of Chemistry and Physics*, 58th Ed., Florida, CRC Press, Inc., 1978

Wilding, C.R., Walter, A. and Double, D. D. A classification of inorganic and organic admixture by conduction calorimetry. *Cement and Concrete Research.* **14** (2), (1984), 185-94

Yahia, A. and Khayat, K.H., "Applicability of rheological models to high-performance grouts containing supplementary cementitious materials and viscosity enhancing admixture", *Materials and Structures*, **36** (2003) 402-412

Yahia, A. and Khayat, K.H., "Analytical models for estimating yield stress of high-performance pseudoplastic grout", *Cem. Concr. Res.* **31** (2001) 731-738

Yamada, K., Ogawa, S., Hanehara, S., "Controlling of the adsorption and dispersing force of polycarboxylate-type superplasticizer by sulfate ion concentration in aqueous phase", *Cem. Concr. Res*, **31** (2001, a) 375-383

Yamada, K., Ogawa, S. and Takahashi, T.: "Improvement of the Compatibility between Cement and Super-plasticizer by Optimising the Chemical Structure of the Polycarboxylate-type Super-Plasticizer", Proc. 2nd Int. Symp. Self-Compacting Concrete, Japan, (2001, b) pp. 159-168.

Yamada, K., Takahashi, T., Hanehara, S., Matsuhisa, M., "Effects of the chemical structure on the properties of polycarboxylate-type superplasticizer", *Cem. Concr. Res.*, **30** (2000) 197-207

Yilmaz, V.T., Kindness, A., Glasser, F.P., "Determination of sulphonated naphthalene formaldehyde superplasticizer in cement: A new spectrofluorimetric method and assessment of the UV method", *Cem. Concr. Res.* **22** (4) (1992), 663-670

Yilmaz, V.T. and Glasser, F.P., "Early hydration of tricalcium aluminate-gypsum mixtures in the presence of sulphonated melamine formaldehyde superplasticizers", *Cem. Concr. Res.* **21** (5) (1991) 765-776

Yoshioka, K., Tazawa, E., Kawai, K., Enohata, T., "Adsorption characteristics of superplasticizers on cement component minerals", *Cem. Concr. Res*. 32 (2002) 1507-1513

Yoshioka, Y., Sakai, E., Daimon, M., Kitahara, A., "Role of steric hindrance in the preformance of superplasticizers for concrete", *J. Am. Ceram. Soc*. 80 (10) (1997) 2667-2671

Young, J.F., "A review of the Mechanisms of Set-Retardation in Portland Cement Pastes Containing Organic Admixtures", *Cem Concr Res* **2** (4) (1972) 415-433

Young, J. F., "Influence of Tricalcium Aluminate on the Hydration of Calcium Silicates", *J Am Ceram Soc* **52** (1) (1969) 44-46

Young, J. F., “Hydration of Tricalcium Aluminate with Lignosulfonate Additives”, *Mag Concr Res* **14** (42) (1962) 137-142

Zhang, X. and Han, J., "The Effect of Ultra-Fine Admixture on the Rheological Property of Cement Paste", *Cem.Concr.Res.* **30** (2000) 827-830

Zhor, J., and Bremner, T.W., “Role of Lignosulfonates in high performance concrete”, From the Proceedings of the RILEM Conference The Role of Admixtures in High Performance Concrete”, Edited by J. G. Cabrera and R. Rivera-Villarreal, RILEM Publications, 1999

A.1 Bingham analysis for Chapter 6: "Effect of silica fume on rheology of cementitious paste"

A.1.1 Rheological measurements

The rheological parameters were recorded by a parallel plate (1 mm gap, upper plate serrated to 150 μm depth) rheometer MCR 300 produced by Physica.

The following sequence for series 1 lasted 20 minutes, was started when the paste was 20 minutes old from the first contact with water and repeated 4 times to monitor time dependencies:

1. Stress (τ) – shear rate ($\dot{\gamma}$) curve with linear sweep of $\dot{\gamma}$ from 200 down to 2 s^{-1} in 30 points lasting 6 s each (intervals 1, 5, 9 and 13 lasting 3 minutes each).
2. Stress (τ) – shear rate ($\dot{\gamma}$) curve with logarithmic sweep of $\dot{\gamma}$ from 1 down to 0.01 s^{-1} in 30 points lasting 6 s each (intervals 2, 6, 10 and 14 lasting 3 minutes each). Not discussed in the thesis.
3. Oscillatory time sweep with 30 points lasting 20 s each with amplitude γ = 0.1 % and angular frequency ω = 6 s^{-1} (intervals 3, 7, 11 and 15 lasting 10 minutes each) measuring storage and loss moduli G' and G" (not discussed in the thesis).
4. Shear rate ($\dot{\gamma}$) – stress (τ) curve with logarithmic sweep of τ from 30 to 300 Pa in 48 points lasting 5 s each (intervals 4, 8, 12 and 16 lasting 4 minutes each) to measure gel strength after 10 minutes rest (i.e. oscillation).

The following sequence for series 2 lasted 25 minutes, was started when the paste was 20 minutes old from the first contact with water and repeated 4 times to monitor time dependencies:

1. Stress (τ) – shear rate ($\dot{\gamma}$) curve with linear sweep of $\dot{\gamma}$ from 200 down to 2 s^{-1} in 30 points lasting 6 s each (intervals 1, 7, 13 and 19 lasting 3 minutes each).
2. Stress (τ) – shear rate ($\dot{\gamma}$) curve with linear sweep of $\dot{\gamma}$ from 2 up to 200 s^{-1} in 30 points lasting 6 s each (intervals 2, 8, 14 and 20 lasting 3 minutes each).
3. 10 s resting as 5 points lasting 2 s each had no recording (intervals 3, 9, 15 and 21)
4. Shear rate ($\dot{\gamma}$) – stress (τ) curve with logarithmic sweep of τ from 0.2 to 50 Pa in 46 points lasting 5 s each (intervals 4, 10, 16 and 22 lasting 3 minutes and 50 s each) to measure gel strength after 10 s rest).
5. Oscillatory time sweep with 30 points lasting 20 s each with amplitude γ = 0.1 % and angular frequency ω = 6 s^{-1} (intervals 5, 11, 17 and 23 lasting 10 minutes each) measuring storage (G') and loss (G") moduli (not discussed in the thesis).
6. Shear rate ($\dot{\gamma}$) – stress (τ) curve with logarithmic sweep of τ from 0.5 to 200 Pa (range may vary) in 60 points lasting 5 s each (intervals 6, 12, 18 and 24 lasting 5 minutes each) to measure gel strength after 10 minutes rest (i.e. oscillation).

A.1.2 Results and discussion of series 1

The plastic viscosity, μ_p, and yield stress, τ_y, were obtained from the linear Bingham relation between shear stress,τ, and shear rate, $\dot{\gamma}$, from flow curves for both a medium shear rate range (linear fit of 6 points from 152 to 118 s^{-1} to give μ_{pm} and τ_{ym}) and a low shear rate range (linear fit of 6 points from 43 to 8 s^{-1} to give μ_{pl} and τ_{yl}):

$$\tau = \tau_y + \mu_p \cdot \dot{\gamma} \qquad \text{(A.1.1)}$$

When Bingham relations are used for both low and medium shear rate ranges, the viscosity dependence of shear rate can simply be evaluated by the ratio μ_{pm}/μ_{pl}:

$\mu_{pm}/\mu_{pl} < 1$ means shear thinning behaviour (thinking from low towards high rate).
$\mu_{pm}/\mu_{pl} = 1$ means no dependence of shear rate.
$\mu_{pm}/\mu_{pl} > 1$ means shear thickening behaviour.

The plastic viscosities as a function of silica fume replacement with 1.32 % PA1 at medium and low shear rate ranges are plotted in Figs. A.1.1 and A.1.2, while the corresponding yield points are plotted in Figs. A.1.3 and 4, respectively. The regression factors (R^2) for the linear analyses were usually >0.99. However, sometimes the flow curves in the lower shear rate range resulted in lower R^2 when they were curved or when they were rather flat (even if they were linear, due to uncertain slope). Fitting of flow curves with very low slope (i.e. flat curve) sometimes resulted in negative plastic viscosity. In such cases, the viscosity should from a practical point of view just be regarded as very low.

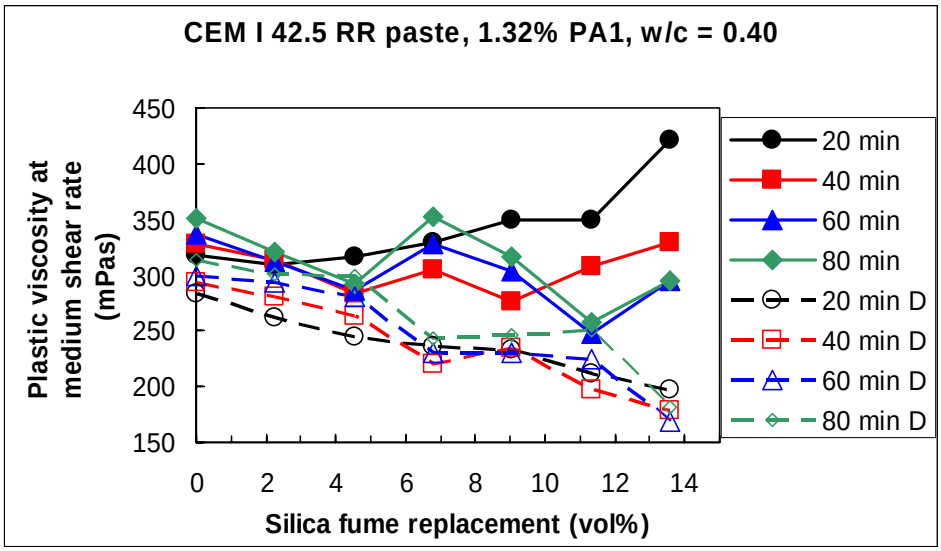

Fig. A.1.1: Plastic viscosity, μ_{pm}, as a function of silica fume replacing cement and time (20 minutes between each interval) derived from medium shear rate range. 1.32 % PA1 superplasticizer was added by mass of powder (D = delayed plasticizer addition)

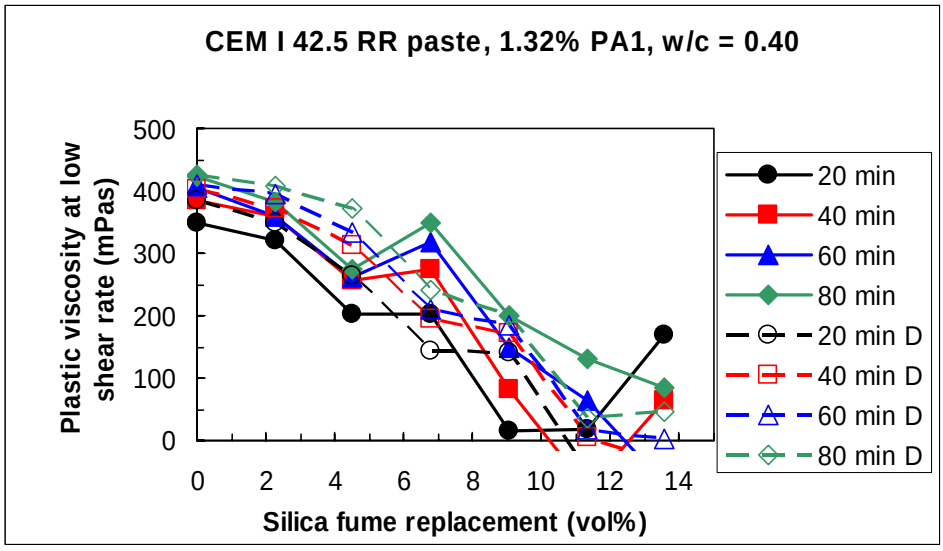

Fig. A.1.2: Plastic viscosity, μ_{pl}, as a function of silica fume replacing cement and time (20 minutes between each interval) derived from low shear rate range. 1.32 % PA1 superplasticizer was added by mass of powder (D = delayed plasticizer addition)

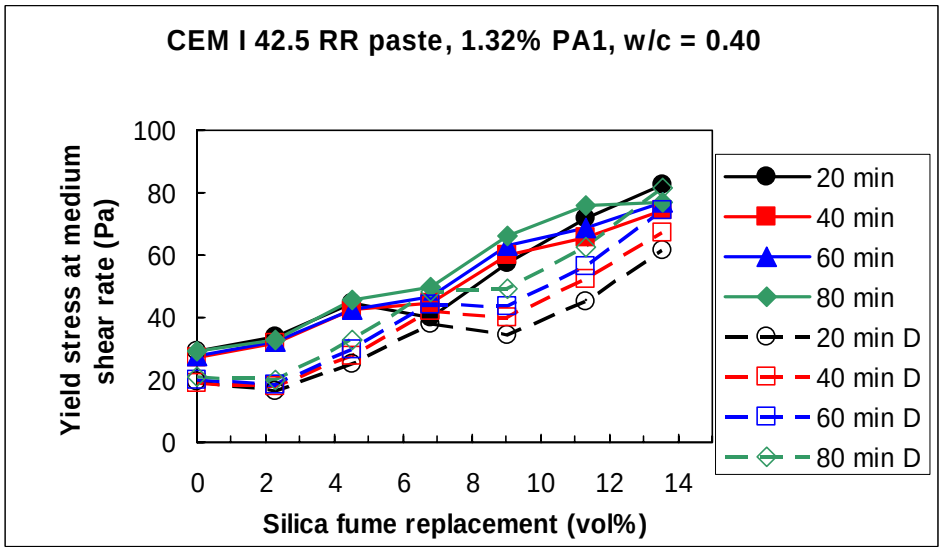

Fig. A.1.3: Yield stress, τ_{ym}, as a function of silica fume replacing cement and time (20 minutes between each interval) derived from medium shear rate range. 1.32 % PA1 superplasticizer was added by mass of powder (D = delayed plasticizer addition)

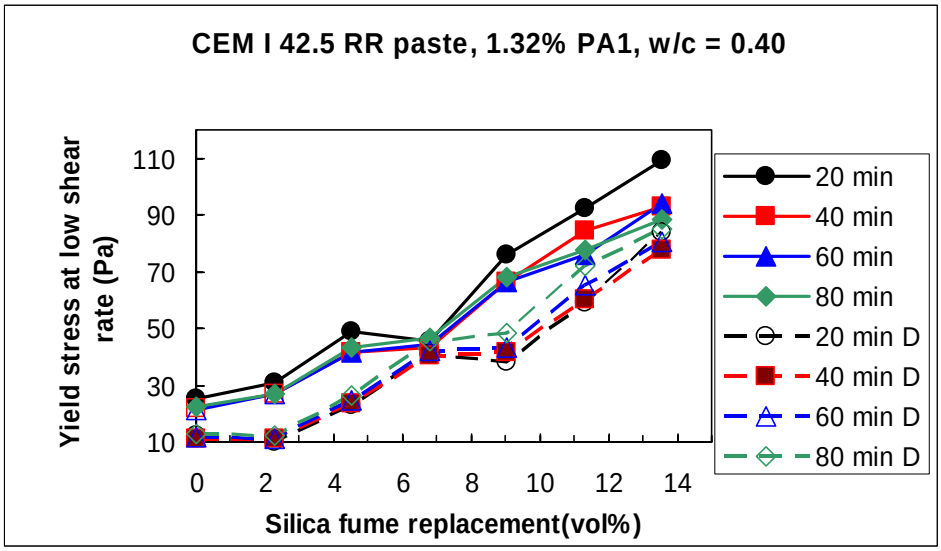

Fig. A.1.4: Yield stress, $\tau_{yl,}$ as a function of silica fume replacing cement and time (20 minutes between each interval) derived from low shear rate range. 1.32 % PA1 superplasticizer was added by mass of powder (D = delayed plasticizer addition)

As may be deduced from Fig. A.1.1, the plastic viscosity in the medium range is rather independent of silica fume dosage when PA1 is added to the mix water, while it is decreasing with increasing SF replacement when PA1 is added delayed. In the low shear rate range (see Fig. A.1.2), plastic viscosity is decreasing with increasing SF dosage no matter whether PA1 is delayed or not. For both the medium (Fig. A.1.3) and low (Fig. A.1.4) shear rates the yield stress is increasing with increasing SF replacement. Delayed PA1 addition does not affect the slope of this trend, but the yield stress level is a little lower for the delayed PA1 dosage. The time effect (20 minutes between intervals 1, 5, 9 and 13) is minor for the PA1 pastes but there is usually a trend of marginal increase in viscosity and yield stress with increasing time.

The plastic viscosity at medium and low shear rate range for cement paste with 1.32% delayed SNF addition is plotted as a function of SF replacement in Figs. 5 and 6, respectively. Similar plots for yield stress are depicted in Figs. A.1.7 and A.1.8. The general trend is increasing viscosity (opposite as for PA1 pastes) and yield stress with increasing SF replacement independently of shear rate range. The time effect is more predominant in the case of SNF than for pastes with PA1. This effect could be a result of stronger retardation of surface hydration by PA1 than with SNF (see Chapter 8.2.3), since the carboxylic groups of PA1 co-ordinates strongly with Ca-sites. Increased water binding (i.e. surface hydration) will lead to increased solid volume fraction in a two-fold manner (reduction of liquid water and increased volume of solids) and thereby higher viscosity.

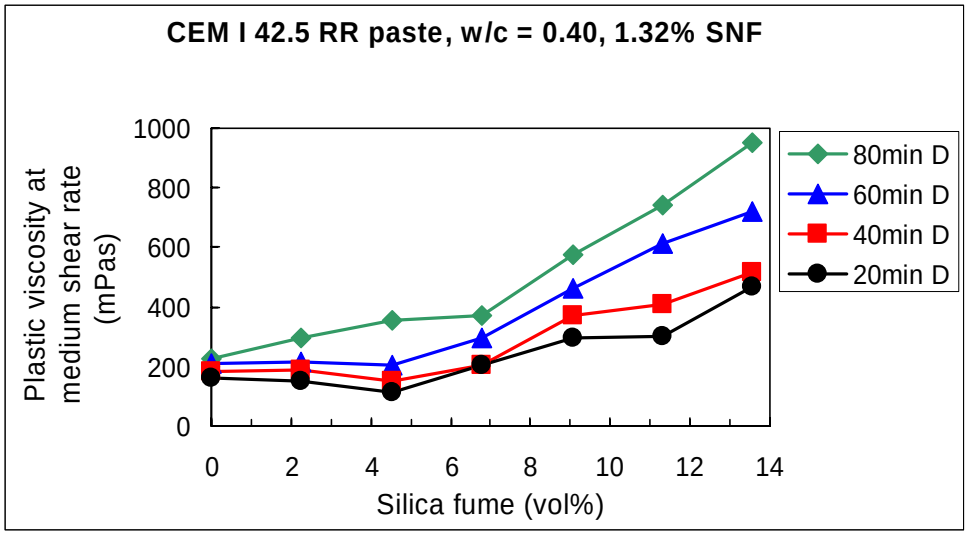

Fig. A.1.5: Plastic viscosity, μ_{pm}, as a function of silica fume replacing cement and time (20 minutes between each interval) derived from medium shear rate range. 1.32 % SNF superplasticizer was added by mass of powder (D = delayed plasticizer addition)

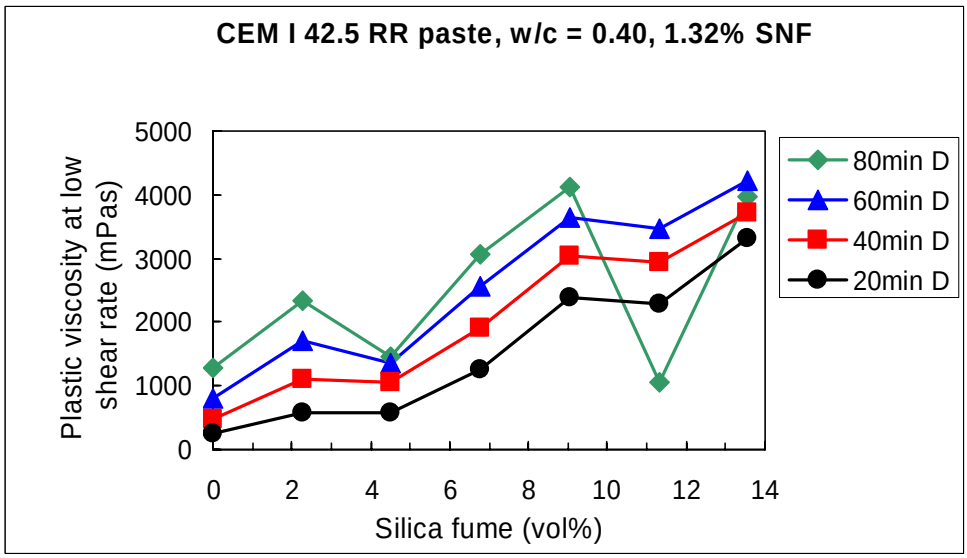

Fig. A.1.6: Plastic viscosity, μ_{pl}, as a function of silica fume replacing cement and time (20 minutes between each interval) derived from low shear rate range. 1.32 % SNF superplasticizer was added by mass of powder (D = delayed plasticizer addition)

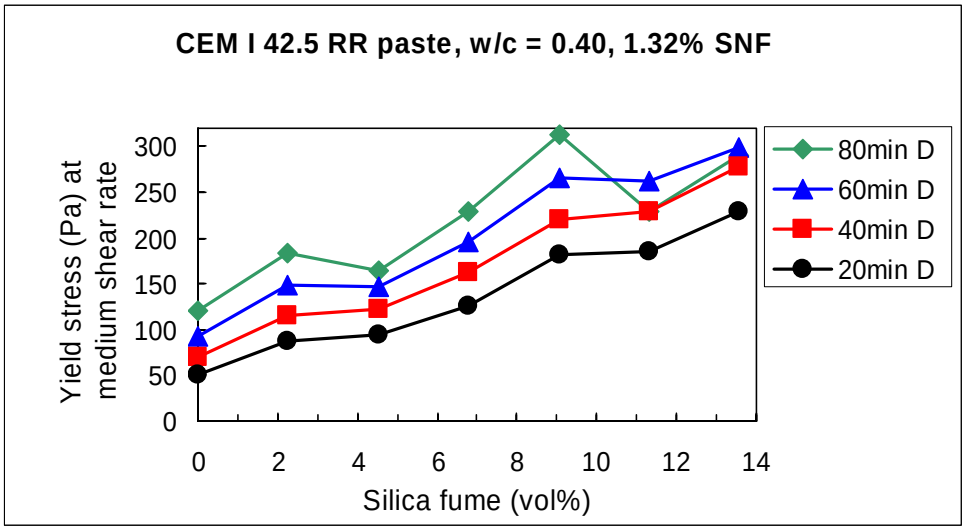

Fig. A.1.7: Yield stress, τ_{ym}, as a function of silica fume replacing cement and time (20 minutes between each interval) derived from medium shear rate range. 1.32 % SNF superplasticizer was added by mass of powder (D = delayed plasticizer addition)

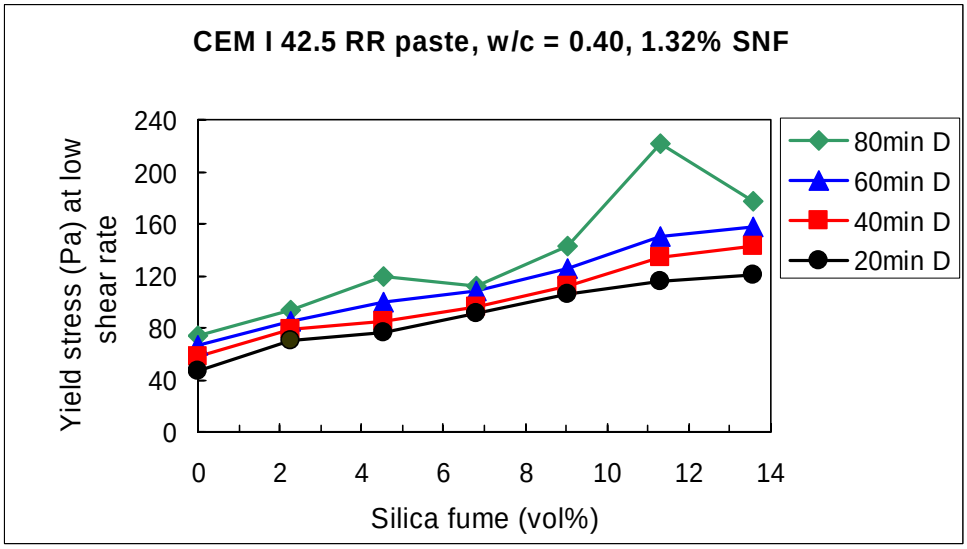

Fig. A.1.8: Yield stress, τ_{yl}, as a function of silica fume replacing cement and time (20 minutes between each interval) derived from low shear rate range. 1.32 % SNF superplasticizer was added by mass of powder (D = delayed plasticizer addition)

The decreasing viscosity with increasing SF can be understood with packing of SF particles (average 0.15 μm) in the gaps between cement grains (average 10 μm) and thereby squeezing water out between the cement grains. Another possible explanation is the ball-bearing effect of rather spherical small particles on the irregular cement grains. Wallevik (1990) reported for concrete plasticized with lignosulphonate that replacing cement with SF until a certain amount (2, 4 and 6 % SF for 200, 300 and 400 kg cement/m^3, respectively) significantly reduced (20, 30 and 50 %, respectively) the h-value (analogous to plastic viscosity), while the g-value (analogous to yield stress) was roughly constant. Further replacement of cement with SF up to 20 % gave a substantial increase (80, 140 and 180 % for 200, 300 and 400 kg cement/m^3, respectively) of the g-value, while the h-value increased more gradually.

However, one should bear in mind that results for concrete can not be directly transferred to paste even though the rheology of matrix dominates the rheology of concrete. For instance, since matrix of concrete contains a lot of filler and air that is not stable in paste.

The substantial increased yield stress with increasing SF replacement can be explained by the ionisation of SF surface and possible bridging with polyvalent cations like calcium;

$$2 \equiv Si\text{-}OH + Ca^{2+} + 2\ OH^- = \equiv Si\text{-}O^-\ {}^+Ca^+\ {}^-O\text{-}Si\equiv + 2H_2O \qquad (A.1.2)$$

Alternatively, Ca^{2+} can adsorb to the surface of SF and then the anionic polymers (PA1 and SNF) can adsorb on the positive charged sites thus created. Jolicoeur and Simard (1998) pointed out this effect after the observation of SNF being adsorbed to minor extent by SF slurry, but being equally adsorbed by cement paste and cementitious paste with SF replacing cement.

The results from the Bingham plots of cement pastes with SNF added to the mix water are not included in the plots of Figs. A.1.5-8 since the values were so much higher than for the pastes with delayed addition of SNF. Furthermore, the results were more uncertain as the mixes became very thick with increasing SF replacement (only up to 5 % SF could be tested). The obtained results are listed in Table A.1.1 instead. The values in Table 1 show clearly the high shear thinning effect of cementitious pastes with SNF as $\mu_{pm}/\mu_{pl} << 1$ (from 0.30 to 0.15). As a comparison, pastes with PA1 start out with a small shear thinning effect, $\mu_{pm}/\mu_{pl} \approx 0.85$, which transfers into shear thickening as the SF replacement dosage increases (ends up with $\mu_{pm}/\mu_{pl} \approx 5$).

Table A.1.1: Flow curve evaluation of cementitious paste with 1.32 % SNF (added with mix water)

SF (vol%) /Interval	Medium $\dot{\gamma}$ range			Low $\dot{\gamma}$ range		
	μ_{pm} (mPa·s)	τ_{ym} (Pa)	R^2	μ_{lm} (mPa·s)	τ_{yl} (Pa)	R^2
0.00 / 1	616	209.4	0.9969	3,086	90.2	0.9880
2.26 / 1	421	194.7	0.9948	2,805	91.3	0.9750
4.52 / 1	704	234.1	0.9914	3,337	103.4	0.9966
6.79 / 1	1,163	257.5	0.9906	3,810	121.6	0.9985
0.00 / 5	678	229.2	0.9893	3,157	100.6	0.9896
2.26 / 5	481	217.0	0.9978	3,069	101.0	0.9847
4.52 / 5	666	264.7	0.9897	3,613	113.6	0.9957
6.79 / 5	747	332.6	0.9785	4,145	141.3	0.9956
0.00 / 9	602	276.1	0.9921	3,521	114.3	0.9940
2.26 / 9	590	249.2	0.9995	3,337	111.7	0.9935
4.52 / 9	1,105	235.5	0.9087	3,228	132.9	0.9974
6.79 / 9	1,434	200.8	0.9705	2,847	161.9	0.9935
0.00 / 13	689	289.9	0.9429	3,847	123.2	0.9928
2.26 / 13	725	268.6	0.9931	3,730	118.9	0.9925
4.52 / 13	906	283.4	0.9877	3,559	147.8	0.9959
6.79 / 13	696	237.5	0.9975	2,311	153.2	0.9437

The observation that paste viscosity increases with SF replacement when SNF is used as a plasticizer, and is decreasing when PA1 is used as a plasticizer, may mean that one plasticizer does something to SF that the other one does not. The observation could be explained if PA1 prevents SF from forming agglomerates.

A.1.3 Results and discussion of series 2

A.1.3.1 Cement pastes

The plastic viscosity, μ_p, and yield stress, τ_y, were obtained from the Bingham equation (eq. 1) between shear stress, τ, and shear rate, $\dot{\gamma}$, from flow curves for both a medium shear rate range (linear fit of 6 points from 152 to 118 s^{-1} to give μ_{pm} and τ_{ym}) and a low shear rate range (linear fit of 6 points from 43 to 8 s^{-1} to give μ_{pl} and τ_{yl}). When the Bingham equation is used for both low and medium shear rate ranges, the viscosity dependence of shear rate (thickening or thinning) can simply be evaluated by the ratio μ_{pm}/μ_{pl}.

Table A.1.2: Gel strength after 10 min resting, $\tau_{10\ min}$ (interval no. 5) and flow curve evaluation of cementitious paste (w/c = 0.40) with 0.79 % PA2. Untreated and densified (d) silica fume, and momentary and delayed (D) addition of PA2, are compared for 0 and 13.6 vol% (9.9 mass%) replacement of cement with silica fume as a function of time (25 min between each interval)

SF (vol%) /Interval	$\tau_{10\ min}$ (Pa)	Bingham in medium $\dot{\gamma}$ range			Bingham in low $\dot{\gamma}$ range		
		μ_{pm} (mPa·s)	τ_{ym} (Pa)	R^2	μ_{lm} (mPa·s)	τ_{yl} (Pa)	R^2
0 / 1	46	216	22.0	0.9990	182	24.4	0.9991
0 / 1 D	21	218	12.5	0.9991	240	11.4	0.9998
13.6 / 1	103	133	23.4	0.9995	7	30.2	0.1722
13.6 / 1 D	46	120	18.7	0.9989	80	21.0	0.9933
13.6 d / 1	65	208	21.9	0.9983	118	27.3	0.9372
13.6 d / 1 D	74	205	22.9	0.9987	106	28.2	0.9063
0 / 7	39	192	27.6	0.9995	216	25.1	0.9996
0 / 7 D	21	216	18.2	0.9994	281	13.4	0.9999
13.6 / 7	87	127	26.5	0.9952	39	31.0	0.8780
13.6 / 7 D	44	112	23.9	0.9991	96	24.3	0.9954
13.6 d / 7	61	189	27.6	0.9990	155	28.7	0.9799
13.6 d / 7 D	69	192	27.6	0.9995	147	29.1	0.9714
0 / 13	44	218	30.9	0.9998	249	27.7	0.9997
0 / 13 D	26	259	20.6	0.9997	325	15.6	0.9999
13.6 / 13	87	127	29.7	0.9992	75	31.6	0.9607
13.6 / 13 D	46	122	27.7	0.9996	107	27.7	0.9963
13.6 d / 13	69	216	33.1	0.9994	187	33.8	0.9887
13.6 d / 13 D	74	221	32.2	0.9995	180	33.6	0.9782
0 / 19	49	275	34.6	0.9995	308	31.7	0.9998
0 / 19 D	37	337	21.5	0.9995	383	18.4	1.0000
13.6 / 19	109	139	33.9	0.9996	80	35.9	0.9652
13.6 / 19 D	55	137	31.4	0.9993	111	32.0	0.9966
13.6 d / 19	130	250	41.7	0.9993	217	42.8	0.9968
13.6 d / 19 D	123	255	40.1	0.9995	212	41.7	0.9956

The plastic viscosities as a function of silica fume replacement with 0.79 % PA2 at medium and low shear rate ranges are plotted in Figs. A.1.9 and 10, while the corresponding yield

stresses are plotted in Figs. A.1.11 and 12, respectively. The regression factors (R^2) for the linear analysis were usually >0.99. However, sometimes the flow curves in the lower shear rate range resulted in lower R^2 when they were curved or when they were rather flat (even if they were linear, due to uncertain slope).

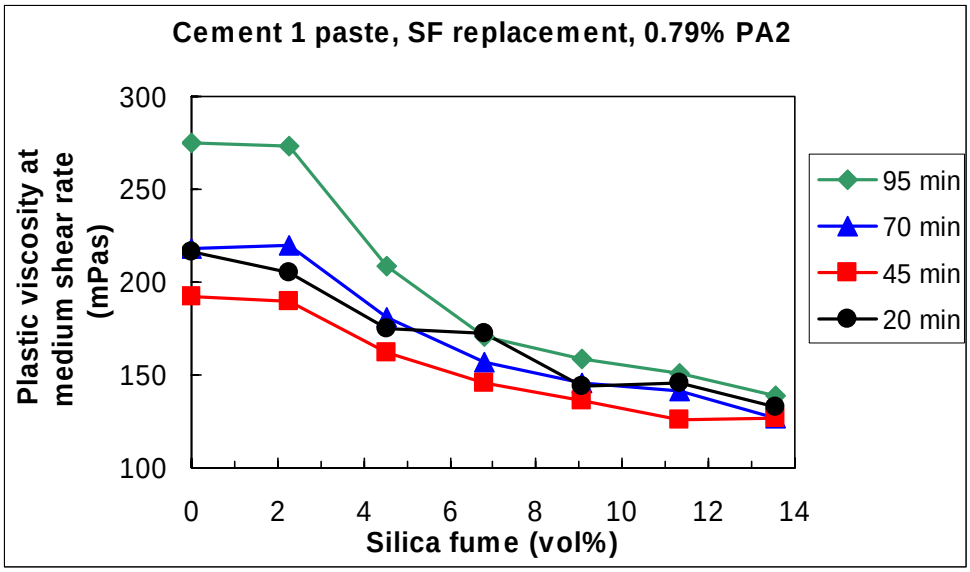

Fig. A.1.9: Plastic viscosity, μ_{pm}, as a function of silica fume replacing cement 1 and time (25 minutes between each interval) derived from medium shear rate range. 0.79% PA2 was added by mass of powder

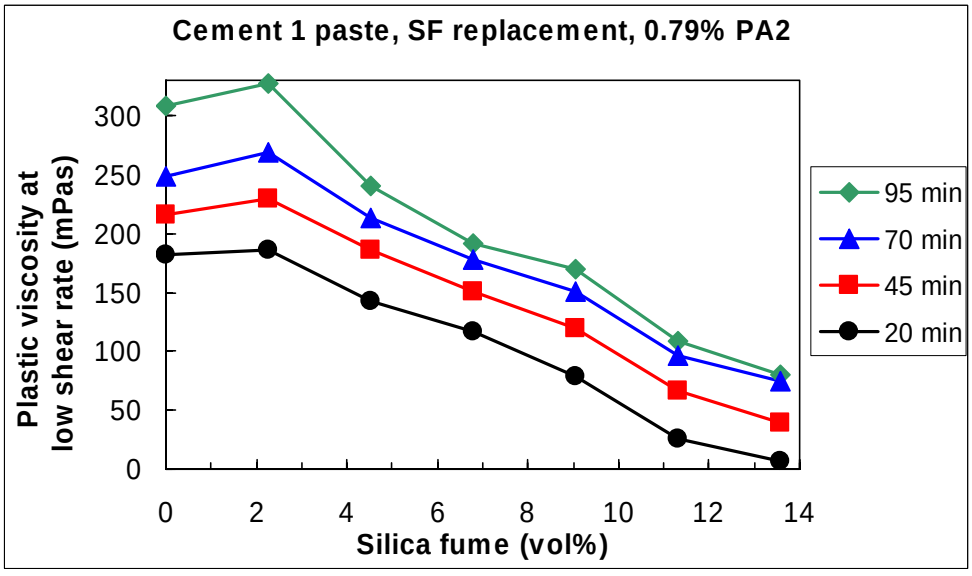

Fig. A.1.10: Plastic viscosity, μ_{pl}, as a function of silica fume replacing cement 1 and time (25 minutes between each interval) derived from low shear rate range. 0.79% PA2 was added by mass of powder

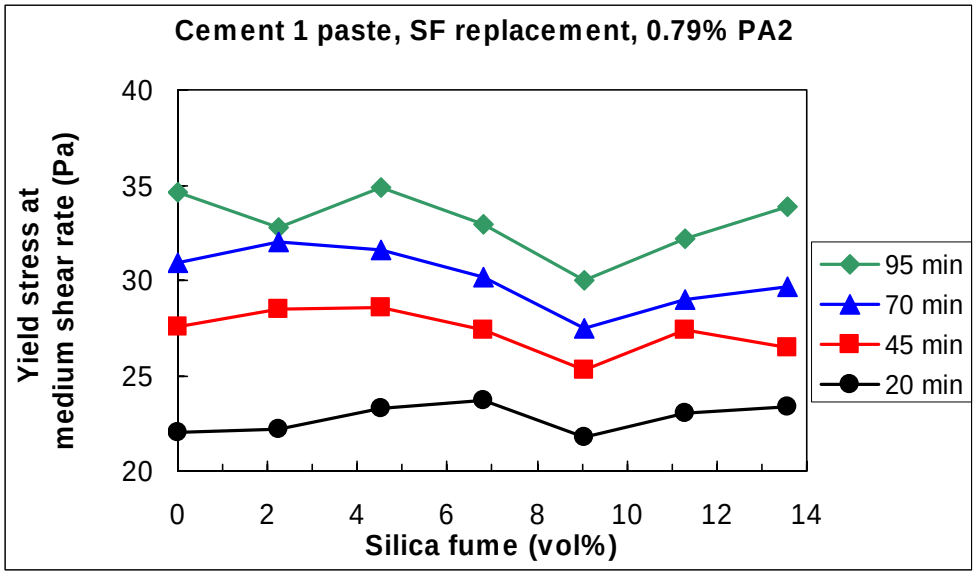

Fig. A.1.11: Yield stress, τ_{ym}, as a function of silica fume replacing cement 1 and time (25 minutes between each interval) derived from medium shear rate range. 0.79% PA2 was added by mass of powder

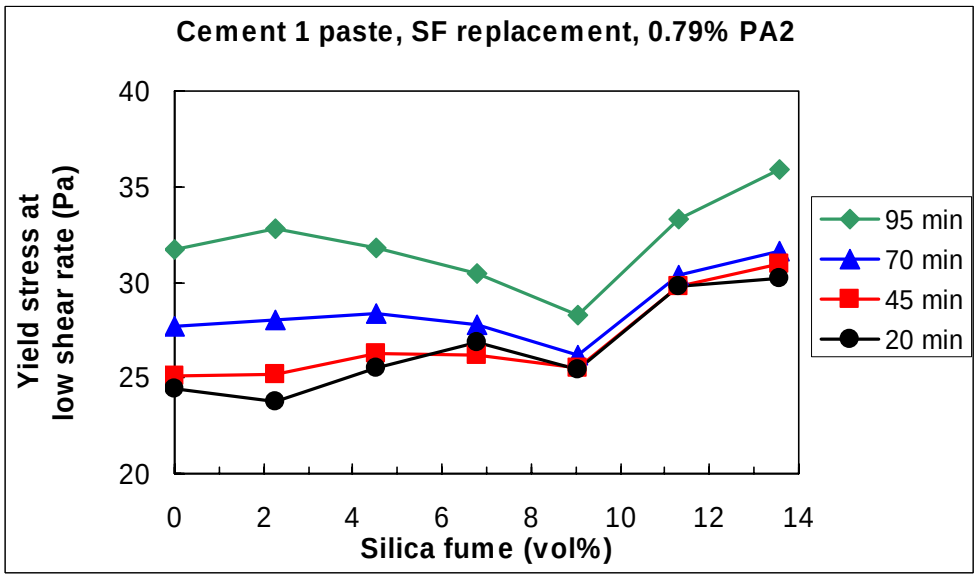

Fig. A.1.12: Yield stress, $\tau_{yl,}$ as a function of silica fume replacing cement 1 and time (25 minutes between each interval) derived from low shear rate range. 0.79% PA2 was added by mass of powder

As may be deduced from Fig. A.1.9, the plastic viscosity in the medium range is reduced with increasing silica fume (untreated unless else is specified) replacement when PA2 is added to the mix water. In the low shear rate range (see Fig. A.1.10), plastic viscosity is decreasing to an even lower level with increasing SF replacement. An exception is for the lowest SF replacement (2.26 vol%) that gives roughly the same viscosity as cement paste without SF. The time effect (25 minutes between intervals 1, 7, 13 and 19) is significant in the low shear rate range with increasing viscosity with time. In the high shear rate range a significant viscosity increase is only observed for the last interval and for the 3 mixes with the lowest SF replacement (0.00, 2.26 and 4.52 vol%). For both the medium (Fig. A.1.11) and low (Fig.

A.1.12) shear rates the yield stress is rather constant with increasing SF replacement noting the ordinate scale. The time effect of the yield stress is the other way around; largest at medium shear rate and only increased yield stress for the last interval at low shear rate range.

Increased viscosity with increasing time can be explained by surface hydration of the cement grains that leads to increased volume fraction of solids in a two-fold manner; removing liquid water and creating solid hydrates (as discussed in Chapter 2.4.4).

Figs. A.1.13 and A.1.14 illustrate the yield stress and plastic viscosity of industry cement pastes with 0.79% PA2 and limestone replacing cement in volume increments. The trends were the same independent of the shear rate ranges. The figures illustrate that both yield stress and plastic viscosity decrease with increasing limestone replacement.

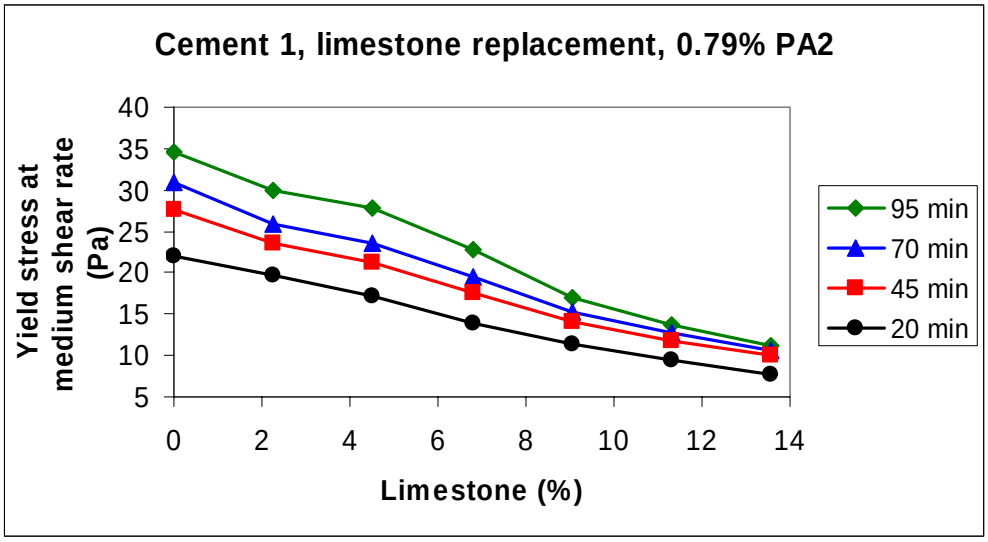

Fig. A.1.13: Yield stress, $\tau_{ym,}$ as a function of limestone replacing cement 1 and time (25 minutes between each interval) derived from low shear rate range. 0.79% PA2 was added by mass of powder

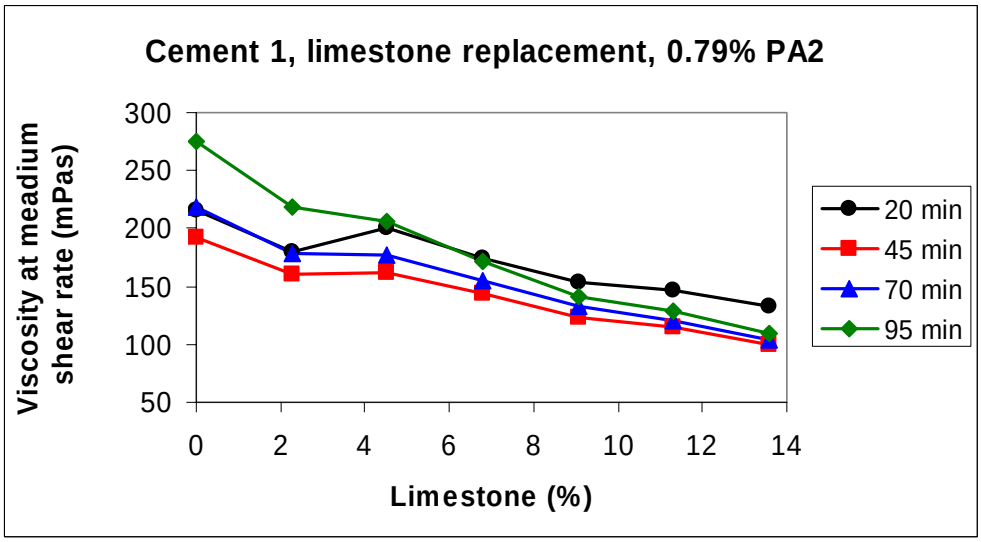

Fig. A.1.14: Plastic viscosity, $\mu_{pm,}$ as a function of silica fume replacing cement 1 and time (25 minutes between each interval) derived from low shear rate range. 0.79% PA2 was added by mass of powder

A.1.3.2 Limestone pastes

The parameters from Bingham fits at low and medium shear rate ranges are listed in Table A.1.3 for all limestone slurries with silica fume. Clearly for 10 vol% SF dosage (Fig. A.1.13) it is impossible to use a Bingham model in the low 52-8 s^{-1} due to the abnormal curvature. Some of the Bingham analyses in Table A.1.3 give negative yield stress, τ_y, which has no physical meaning but is rather a consequence of linear extrapolation as outlined by Justnes et al (2003).

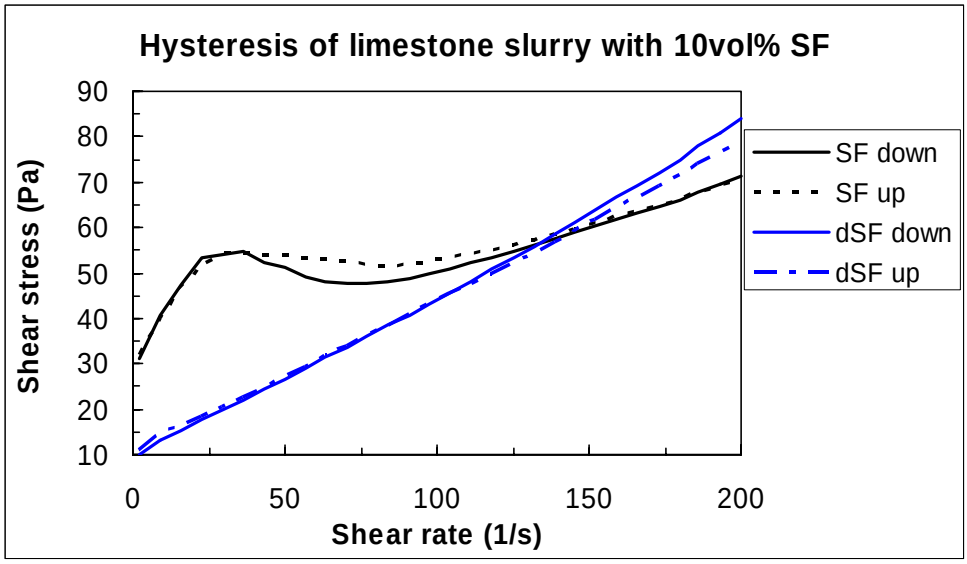

Fig. A.1.13: Effect of densified silica fume (dSF) versus untreated silica fume (SF) on up/down flow curves (interval 7) of limestone slurry (w/ls = 0.30) with 10 vol% SF replacement of limestone

Table A.1.3: Flow curve evaluation of limestone slurry (w/ls = 0.30) with 0.79 % PA. Untreated and densified (d) silica fume, and momentary and delayed (D) addition of PA, are compared for 0 to 10 vol% (8.4 mass%) replacement of limestone with silica fume as a function of time (25 min between each interval). Note that the mixes with 0.00 and 1.67 silica fume had segregation tendencies (not stable). - = extremely curved plot, not possible to make a linear Bingham fit

SF (vol%) /Interval	Bingham in medium $\dot{\gamma}$ range			Bingham in low $\dot{\gamma}$ range		
	μ_{pm} (mPa·s)	τ_{ym} (Pa)	R^2	μ_{lm} (mPa·s)	τ_{yl} (Pa)	R^2
0.00/1	636	-44.4	0.9850	171	-1.2	0.9854
1.67/1	295	-13.2	0.9956	147	-0.6	0.9964
3.33/1	320	-14.6	0.9948	171	-0.3	0.9884
5.00/1	269	-6.5	0.9984	187	0.6	0.9998
6.67/1	234	2.5	0.9950	196	5.9	0.9981
8.33/1	224	14.2	0.9993	50	24.8	0.9227
10.0/1	178	35.9	0.9935	-	-	-
10.0d/1	362	14.9	0.9988	178	27.0	0.9848
0.00/7	271	-10.3	0.9990	141	-0.9	0.9911
1.67/7	269	-8.7	0.9983	153	-0.6	0.9971
3.33/7	234	-6.8	0.9988	165	-0.3	0.9780
5.00/7	229	-3.3	0.9996	183	0.4	0.9999
6.67/7	242	2.3	0.9993	212	5.3	0.9987
8.33/7	231	12.0	0.9987	131	18.2	0.9974
10.0/7	203	29.4	0.9990	-	-	-
10.0d/7	387	5.0	0.9988	326	10.3	0.9998
0.00/13	315	-12.0	0.9989	158	-1.1	0.9888
1.67/13	303	-9.8	0.9989	176	-0.8	0.9962
3.33/13	234	-5.2	0.9989	173	-0.2	0.9970
5.00/13	233	-2.9	0.9991	193	0.2	0.9997
6.67/13	246	3.7	0.9971	233	4.9	0.9994
8.33/13	242	10.9	0.9995	175	15.4	0.9995
10.0/13	209	28.4	0.9992	-	-	-
10.0d/13	381	2.4	0.9989	350	5.8	0.9999
0.00/19	349	-12.8	0.9990	171	-1.2	0.9854
1.67/19	348	-11.2	0.9992	208	-1.1	0.9925
3.33/19	271	-6.3	0.9988	193	-0.3	0.9994
5.00/19	249	-3.2	0.9991	206	0.1	0.9996
6.67/19	272	3.0	0.9993	257	4.6	0.9994
8.33/19	253	10.5	0.9993	208	13.8	0.9995
10.0/19	219	27.0	0.9983	-	-	-
10.0d/19	391	4.3	0.9990	363	4.3	0.9998

Note that τ_y has higher negative values for the 2 first mixes (lowest SF) in Table A.1.3 since the flow curve may be steeper due to partial segregation (slightly unstable mixes). Apart from those, the plastic viscosity at medium shear rate range seems rather unaffected by silica fume replacement, while it is increasing with increasing SF replacement for the low shear rate

range. It is interesting to see that the yield stress derived from the low shear rate range is close to zero (Newtonian liquid) until about 6 vol% SF replacement were it increases. This is good agreement with directly observed gel strength. Densified SF (10 vol%) gives higher plastic viscosity and lower yield stress than for 10 vol% untreated SF. The higher plastic viscosity can be understood by larger grain shaped agglomerates that can hold some water internally and have smaller outer surface.

A.1.4 Conclusions

The following conclusions can be drawn from studying the rheology of cementitious paste where CEM 42.5 RR is increasingly replaced by silica fume (SF) and two superplasticizers have been used as dispersants added delayed or with mix water (series 1):

1. Analyzing the flow curves with the linear Bingham approach for a medium and low shear rate range, shows increasing yield stresses with increasing SF replacement in all cases.
2. The plastic viscosity has a decreasing tendency with increasing SF replacement when PA1 is used, in particular at low shear rates. The plastic viscosity increases, on the other hand, when SNF is used as a plasticizer. SNF leads to a shear thinning behaviour of the paste. PA1 leads only to marginal shear thinning without SF and for lowest SF dosage, which transfers into a substantial shear thickening behaviour at the highest SF replacement (10 vol%).

The following conclusions can be drawn from studying the rheology of cementitious paste where Cement 1 (described by Table 3.1-3.3 in Chapter 3) is increasingly replaced by silica fume (SF) or limestone dispersed with a polyether grafted polyacrylate combined with a viscosifier (PA2) added delayed or with mix water (series 2):

1. There are no large shear thinning/thickening effects in general for the cementitious pastes. The largest shear thinning was for cement paste without silica fume and delayed addition of PA2, while the largest shear thickening was for cementitious paste with 10 % SF. The plastic viscosity has a decreasing tendency with increasing SF replacement, while yield stress was rather constant, at low and medium shear rate ranges. This can be due to particle packing between cement grains displacing water or by ball-bearing effect of silica spheres.
2. Both yield stress and plastic viscosity decreased with increasing limestone replacement.
3. A tendency of increasing plastic viscosity with increasing time (measured in 25 min intervals) was explained by surface hydration increasing the fraction of solids in the slurry both by removing liquid and by creating solid hydrates.

A.2 Correlating cement characteristics with flow resistance

White cement with the following composition has been used in some of the rheological studies:

Table A.2.1: Composition of White cement determined by Rietveld analysis

Type	**CEM I 52.5 N, white**
Alite	69.2
Belite	23.0
Ferrite	0.3
Cubic Aluminate	2.3
Orthorhomic Aluminate	0.0
Lime	0.5
Periclase	0.2
Gypsum	0.0
Semihydrate	0.8
Anhydrite	2.1
Calcite	0.9
Portlandite	0.4
Quartz	0.0
Arcanite	0.3

A.2.1 Pastes prepared of Cements 1-5 (described in Table 3.1-3-3) with w/c = 0.40 and 0.53% SNF per cement weight.

A.2.1.1 Medium shear rate range (152-118 s^{-1}):

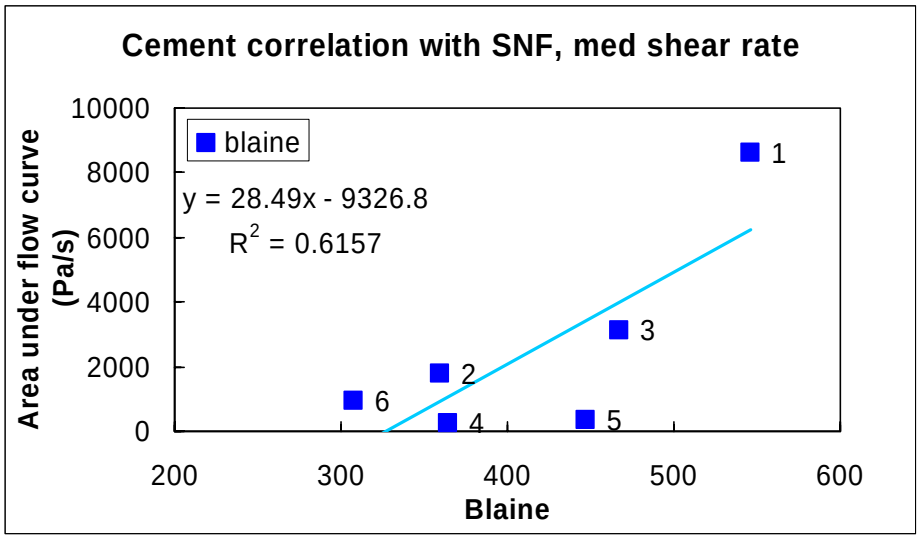

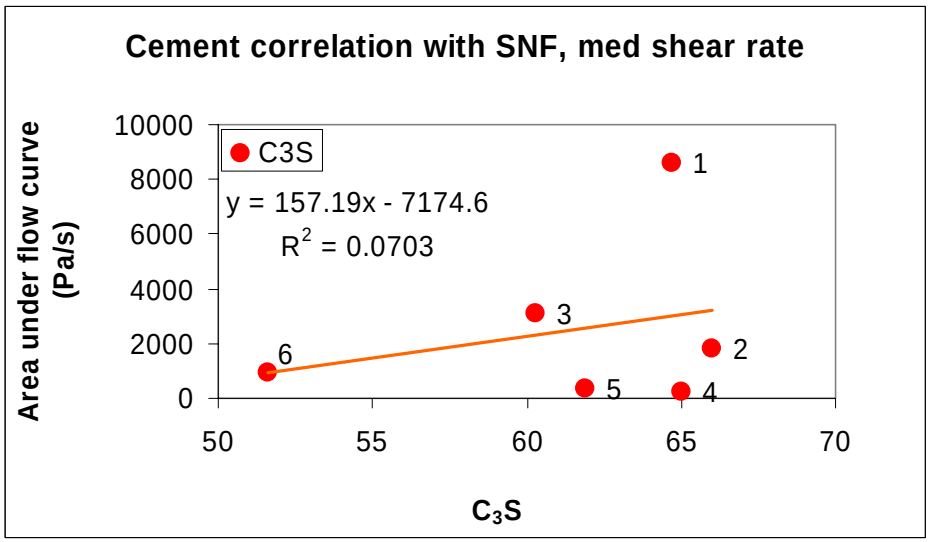

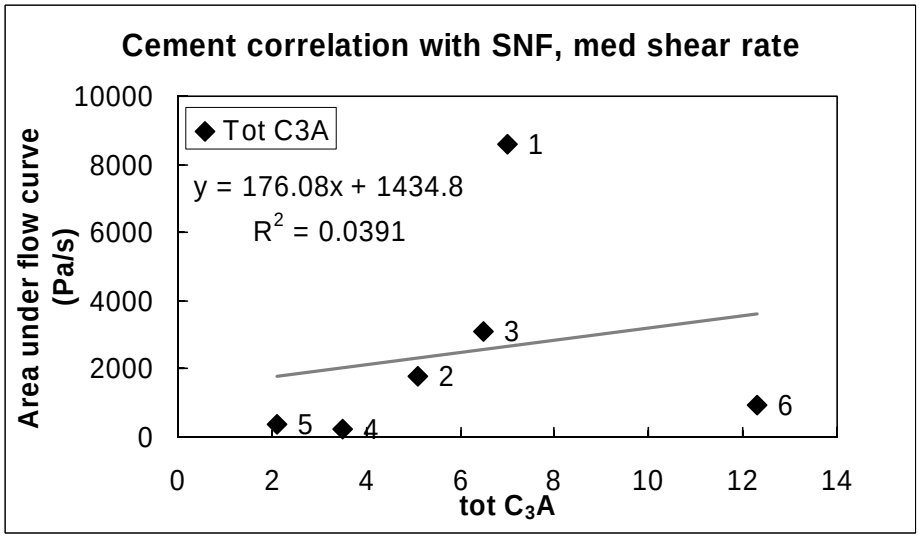

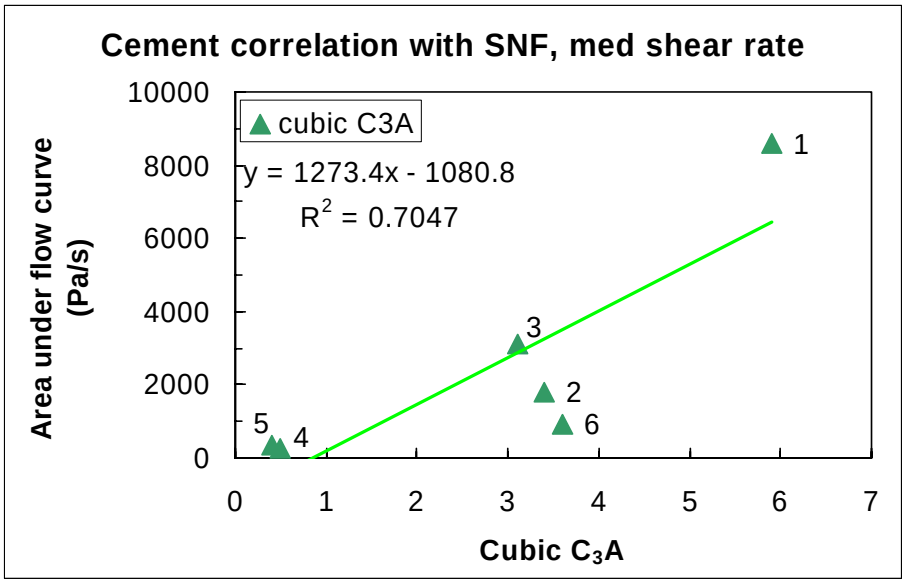
Cement correlation with SNF, med shear rate
cubic C3A
y = 1273.4x - 1080.8
R2 = 0.7047
Area under flow curve (Pa/s)
Cubic C3A
10000
8000
6000
4000
2000
0
0
1
2
3
4
5
6
7
1
2
3
4
5
6

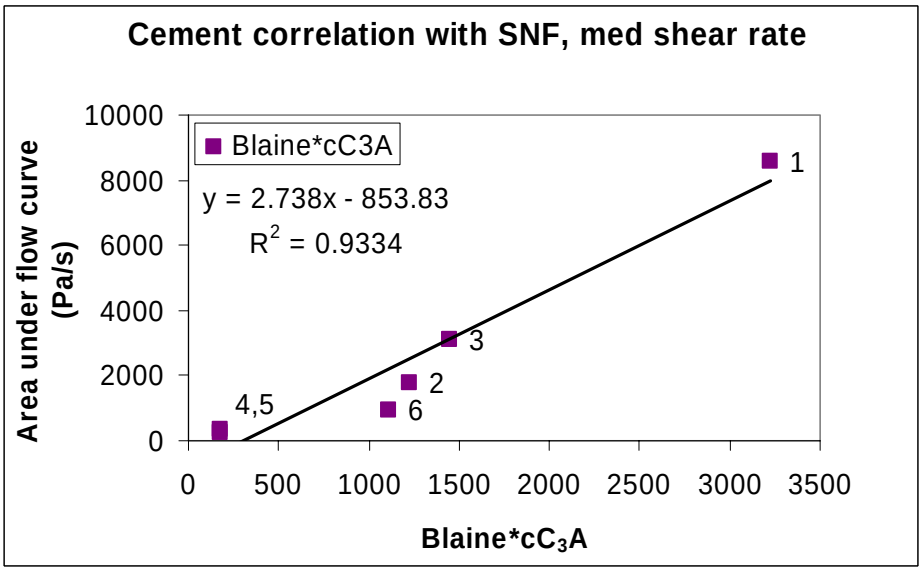
Cement correlation with SNF, med shear rate
Blaine*cC3A
y = 2.738x - 853.83
R2 = 0.9334
Area under flow curve (Pa/s)
Blaine*cC3A
10000
8000
6000
4000
2000
0
0
500
1000
1500
2000
2500
3000
3500
1
2
3
4,5
6

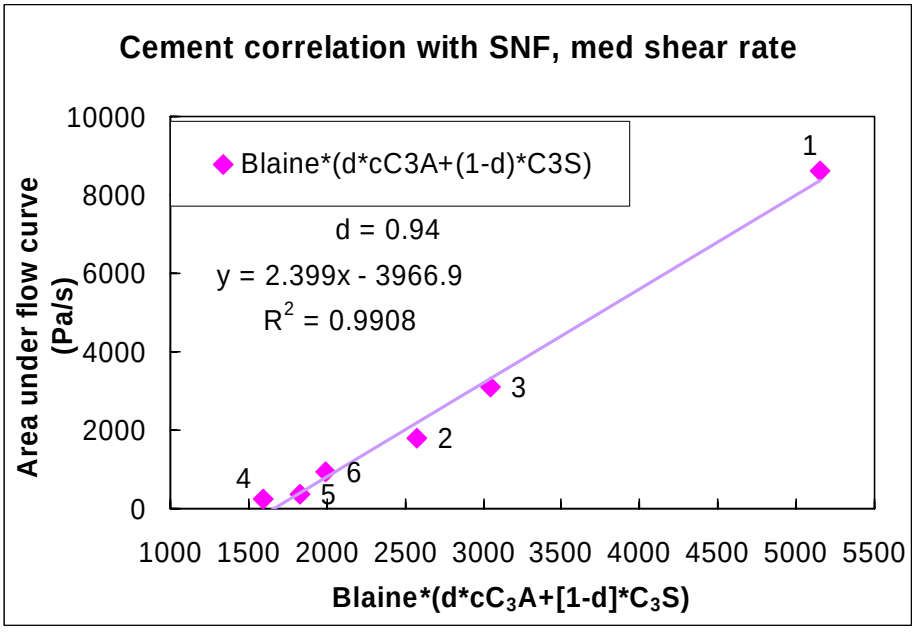
Cement correlation with SNF, med shear rate
Blaine*(d*cC3A+(1-d)*C3S)
d = 0.94
y = 2.399x - 3966.9
R2 = 0.9908
Area under flow curve (Pa/s)
Blaine*(d*cC3A+[1-d]*C3S)
10000
8000
6000
4000
2000
0
1000
1500
2000
2500
3000
3500
4000
4500
5000
5500
1
2
3
4
5
6

A.2.1.2 Low shear rate range (43-8.8 s^{-1}):

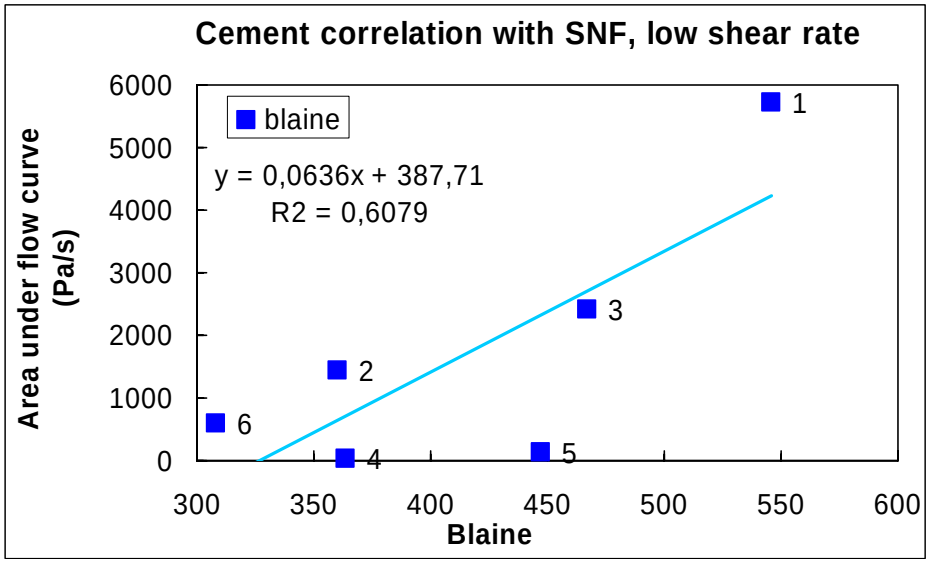

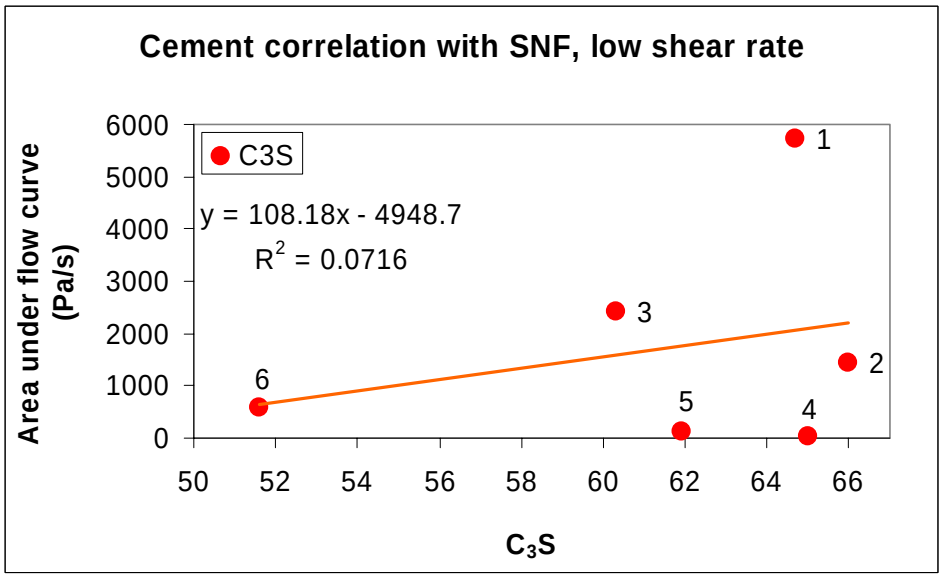

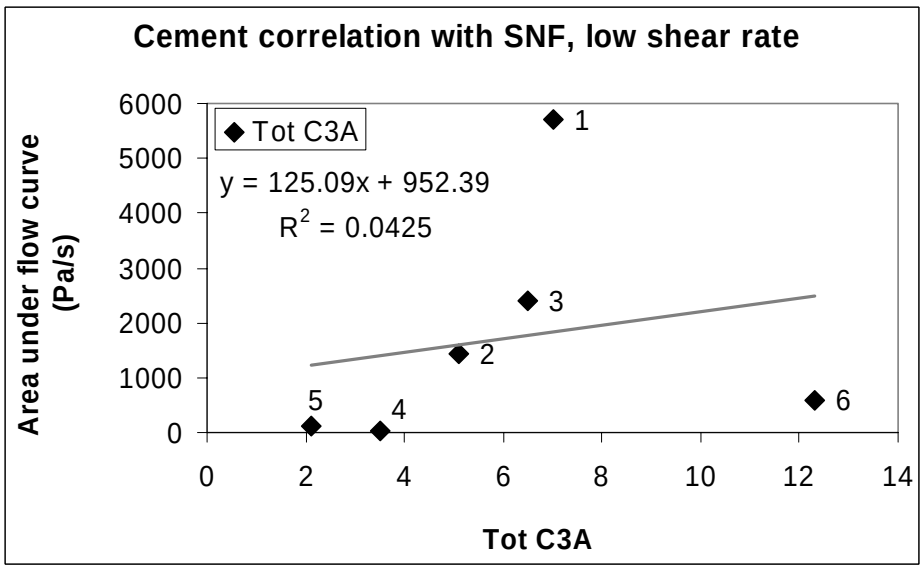

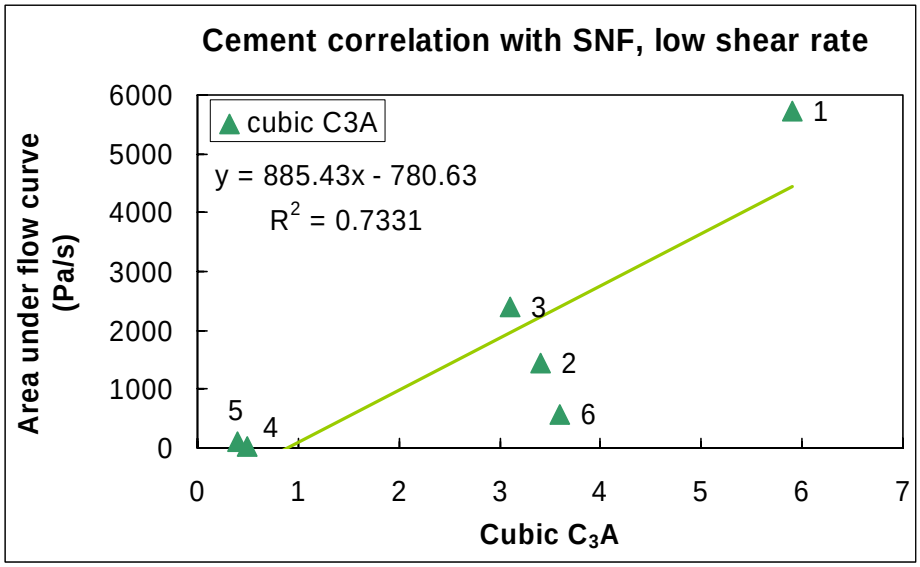
Cement correlation with SNF, low shear rate
Area under flow curve (Pa/s)
cubic C3A
y = 885.43x - 780.63
R2 = 0.7331
Cubic C3A
0
1000
2000
3000
4000
5000
6000
0
1
2
3
4
5
6
7
1
2
3
4
5
6

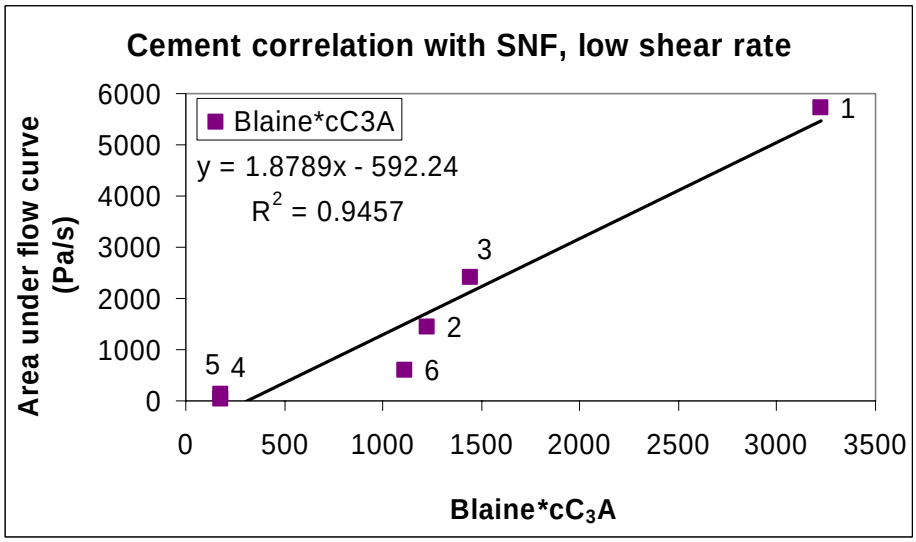
Cement correlation with SNF, low shear rate
Area under flow curve (Pa/s)
Blaine*cC3A
y = 1.8789x - 592.24
R2 = 0.9457
Blaine*cC3A
0
1000
2000
3000
4000
5000
6000
0
500
1000
1500
2000
2500
3000
3500
1
2
3
4
5
6

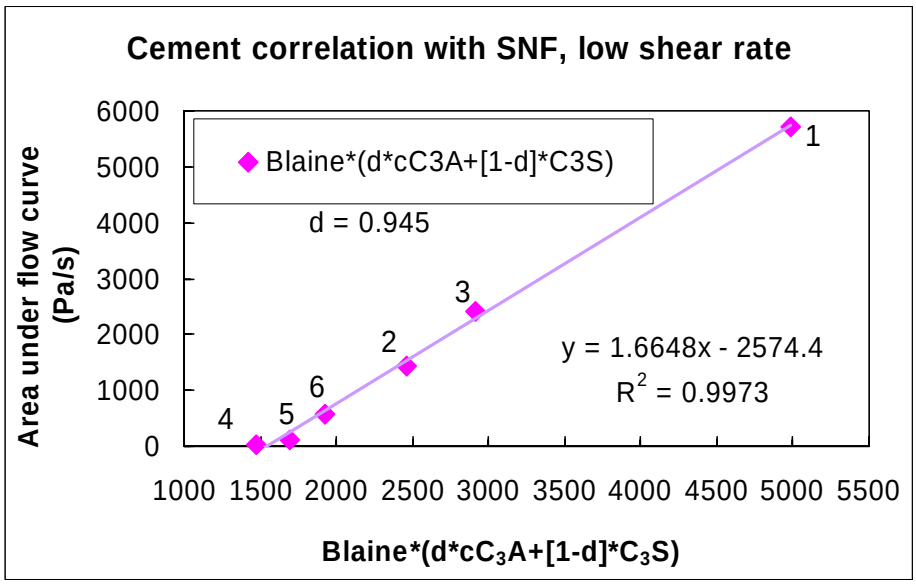
Cement correlation with SNF, low shear rate
Area under flow curve (Pa/s)
Blaine*(d*cC3A+[1-d]*C3S)
d = 0.945
y = 1.6648x - 2574.4
R2 = 0.9973
Blaine*(d*cC3A+[1-d]*C3S)
0
1000
2000
3000
4000
5000
6000
1000
1500
2000
2500
3000
3500
4000
4500
5000
5500
1
2
3
4
5
6

A.2.2 Correlations for the cements 1-4 (described by Table 3.1 - 3-3) + White Portland cement (described by Table A.2.1) with w/c = 0.32 and 0.61% SNF per cement weight

A.2.2.1 Medium shear rate range (152-118 s^{-1}):

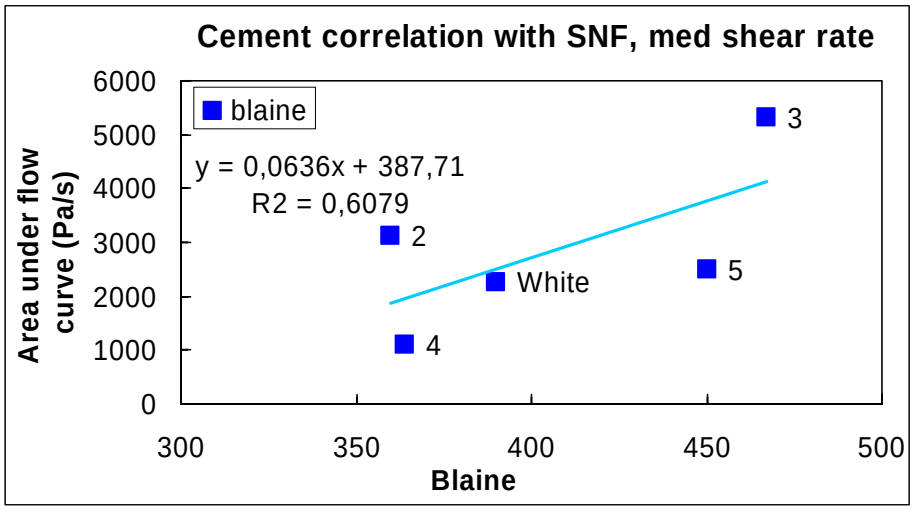

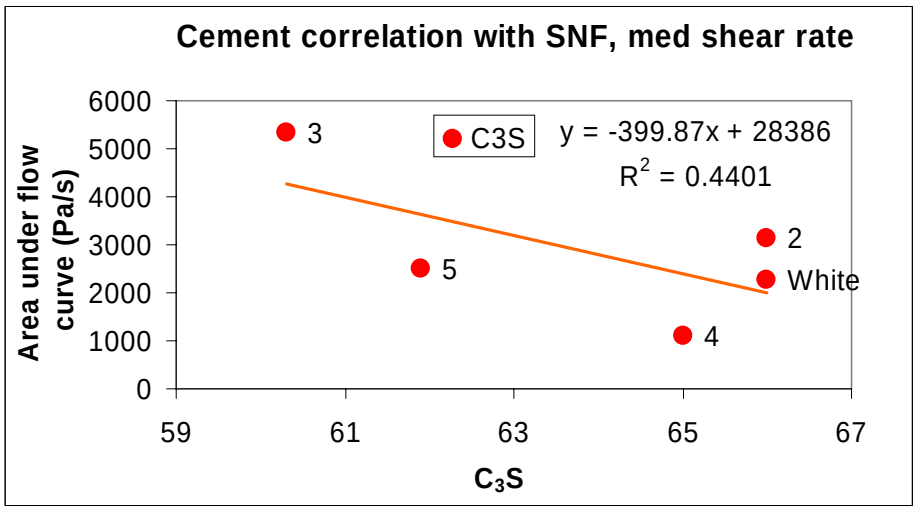

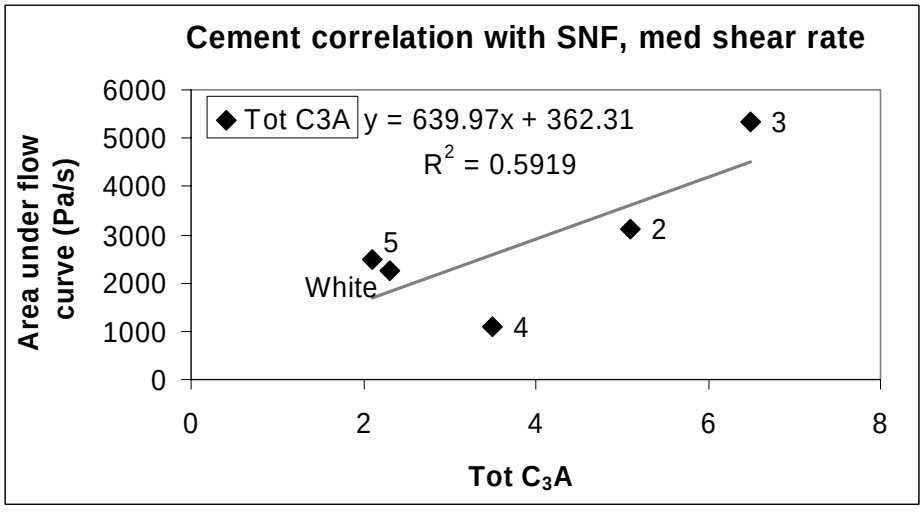

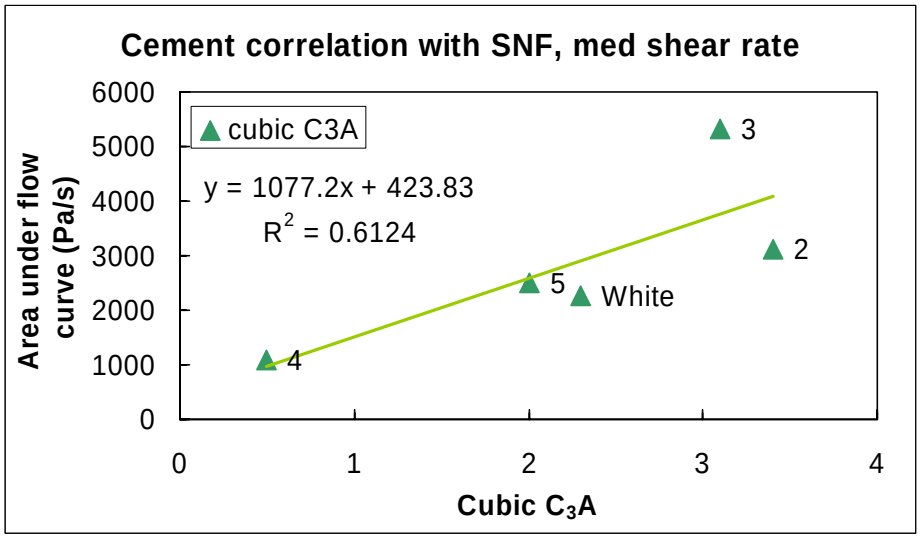
Cement correlation with SNF, med shear rate
cubic C3A
y = 1077.2x + 423.83
R2 = 0.6124
3
2
5
White
4
Area under flow curve (Pa/s)
Cubic C3A
0
1000
2000
3000
4000
5000
6000
0
1
2
3
4

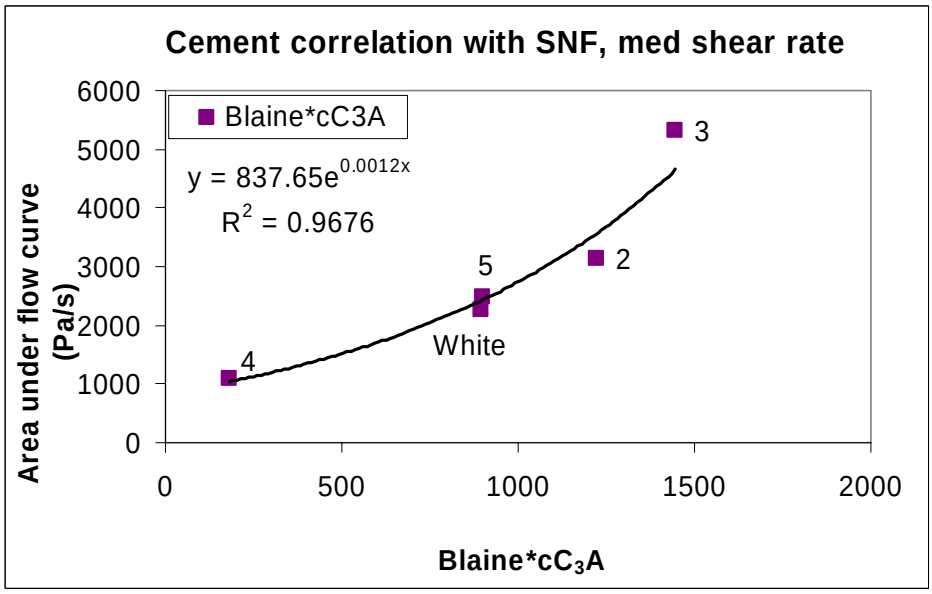
Cement correlation with SNF, med shear rate
Blaine*cC3A
y = 837.65e0.0012x
R2 = 0.9676
3
2
5
White
4
Area under flow curve (Pa/s)
Blaine*cC3A
0
1000
2000
3000
4000
5000
6000
0
500
1000
1500
2000

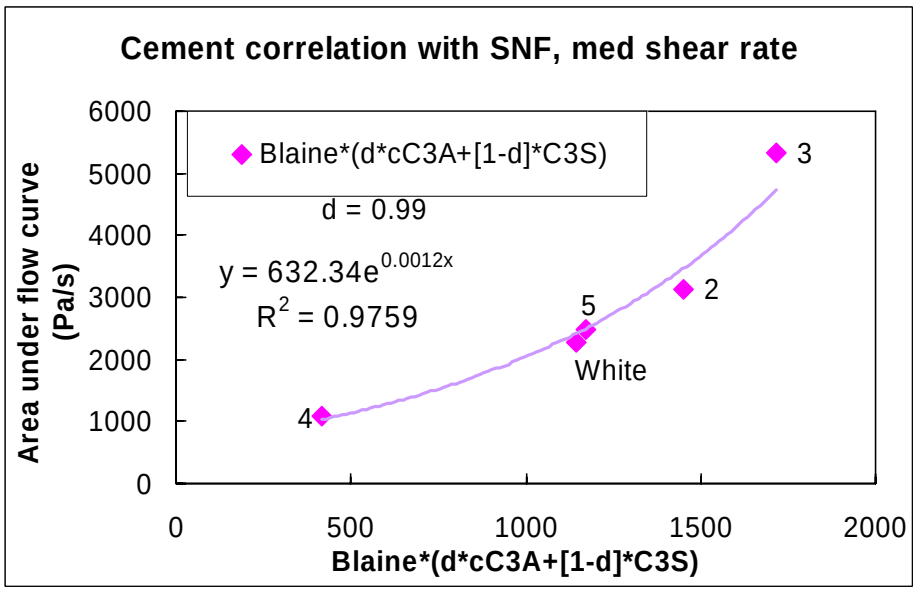
Cement correlation with SNF, med shear rate
Blaine*(d*cC3A+[1-d]*C3S)
d = 0.99
y = 632.34e0.0012x
R2 = 0.9759
3
2
5
White
4
Area under flow curve (Pa/s)
Blaine*(d*cC3A+[1-d]*C3S)
0
1000
2000
3000
4000
5000
6000
0
500
1000
1500
2000

A.2.2.2 Low shear rate range (43-8.8 s^{-1}):

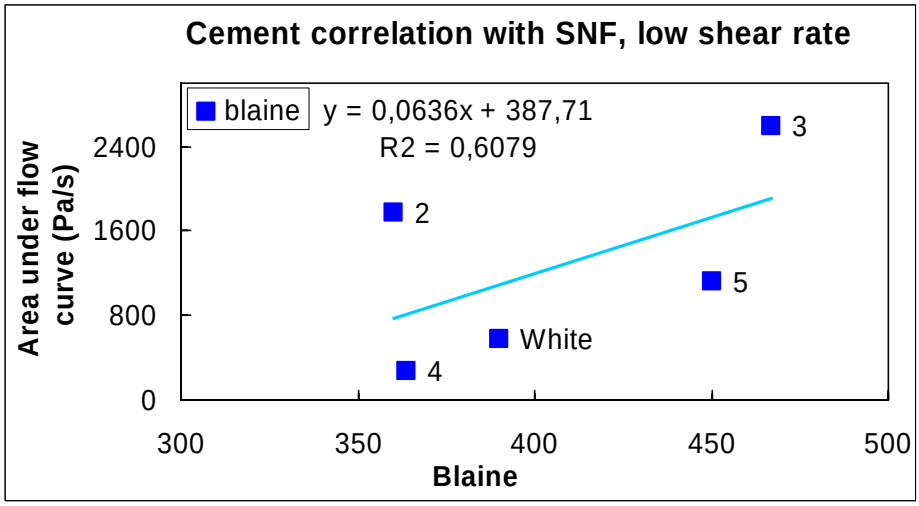

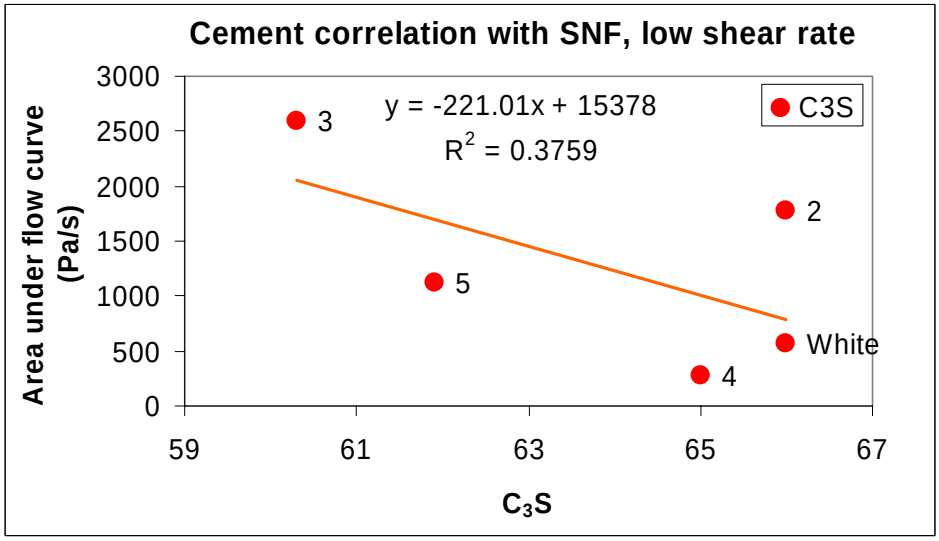

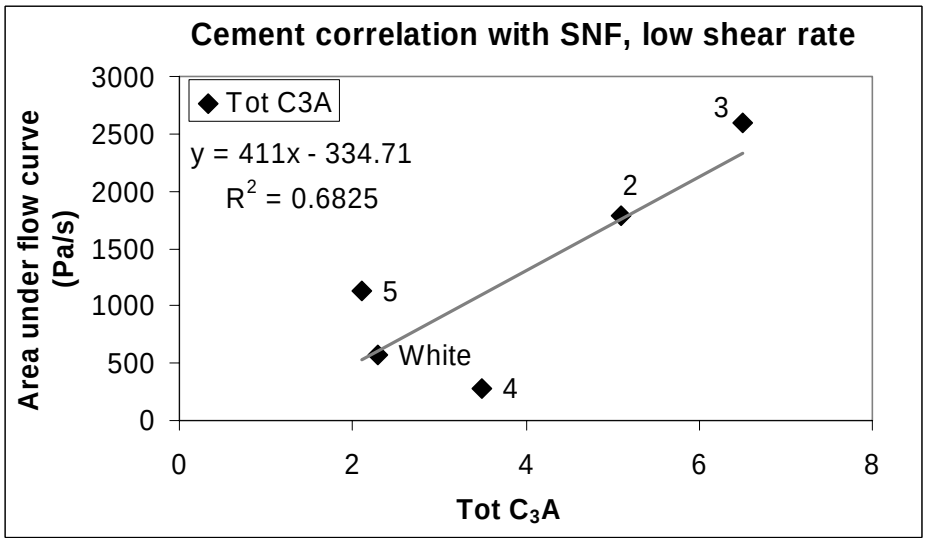

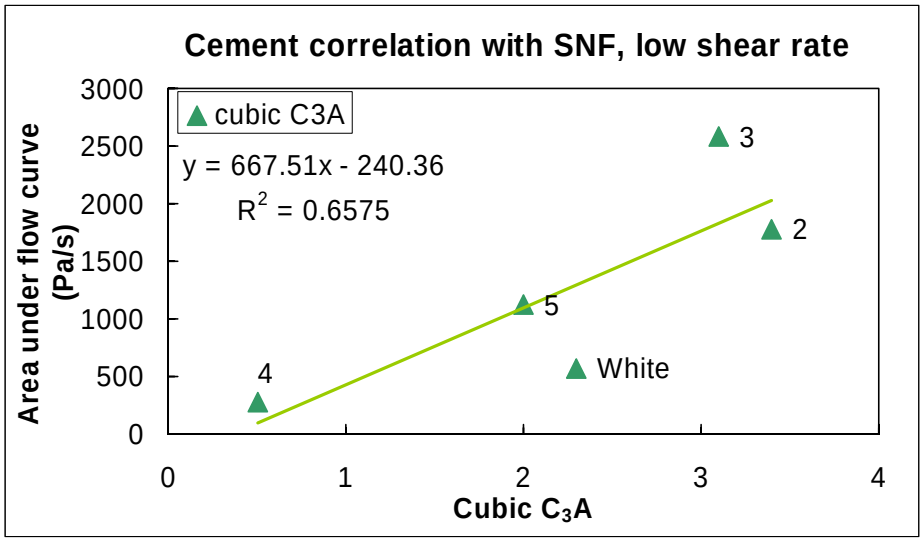
Cement correlation with SNF, low shear rate
cubic C3A
y = 667.51x - 240.36
R2 = 0.6575
3
2
5
4
White
Area under flow curve (Pa/s)
Cubic C3A
0
500
1000
1500
2000
2500
3000
0
1
2
3
4

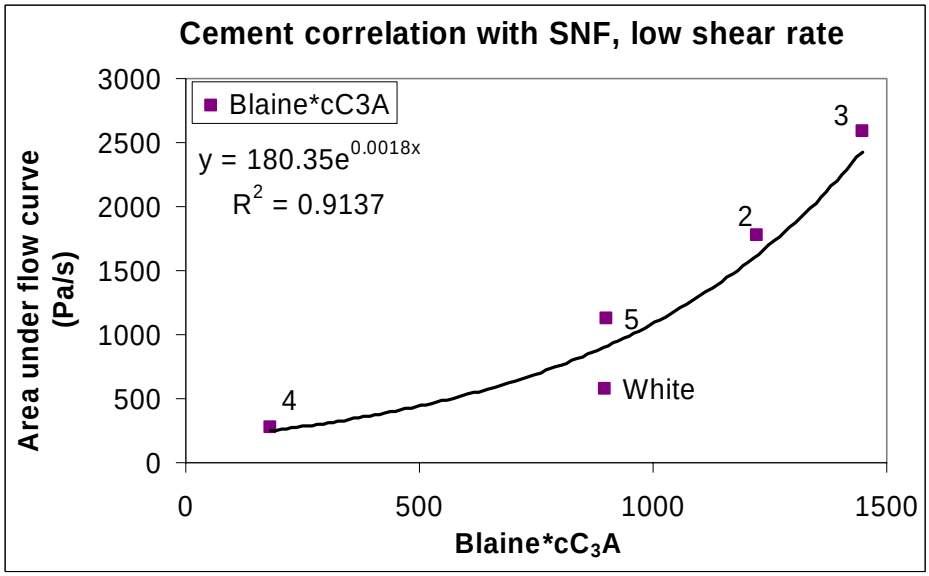
Cement correlation with SNF, low shear rate
Blaine*cC3A
y = 180.35e0.0018x
R2 = 0.9137
3
2
5
4
White
Area under flow curve (Pa/s)
Blaine*cC3A
0
500
1000
1500
2000
2500
3000
0
500
1000
1500

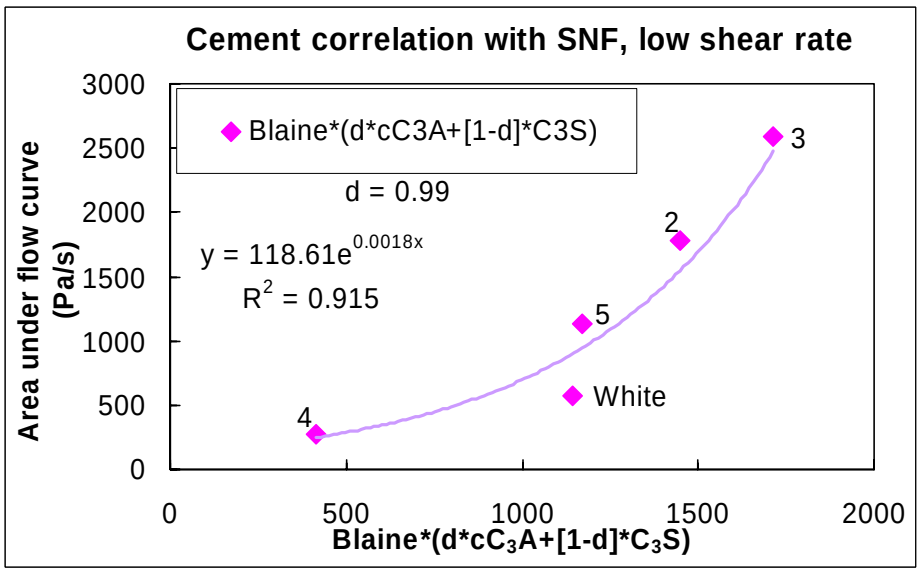
Cement correlation with SNF, low shear rate
Blaine*(d*cC3A+[1-d]*C3S)
d = 0.99
y = 118.61e0.0018x
R2 = 0.915
3
2
5
4
White
Area under flow curve (Pa/s)
Blaine*(d*cC3A+[1-d]*C3S)
0
500
1000
1500
2000
2500
3000
0
500
1000
1500
2000

A.2.3 Correlations for the cements 1-5 (described by Table 3.1 -3-3) with w/c = 0.40 and 0.53% LS per cement weight

A.2.3.1 Medium shear rate range (152-118 s^{-1}):

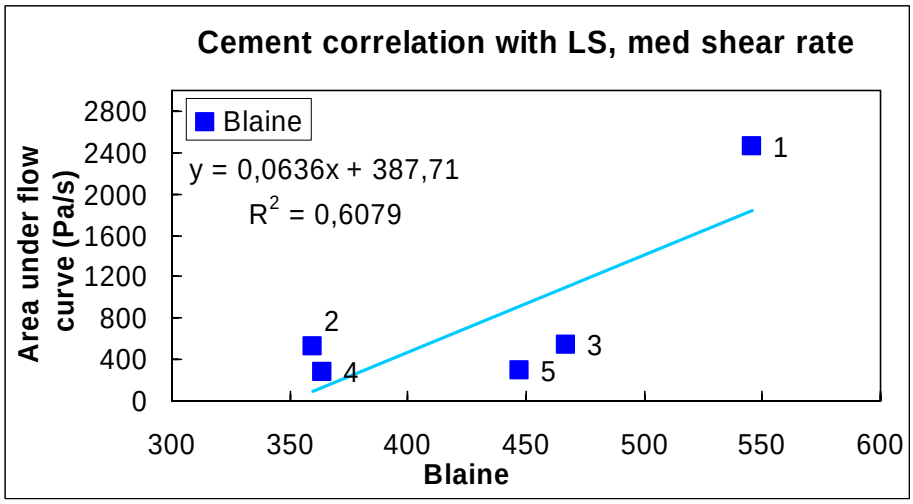

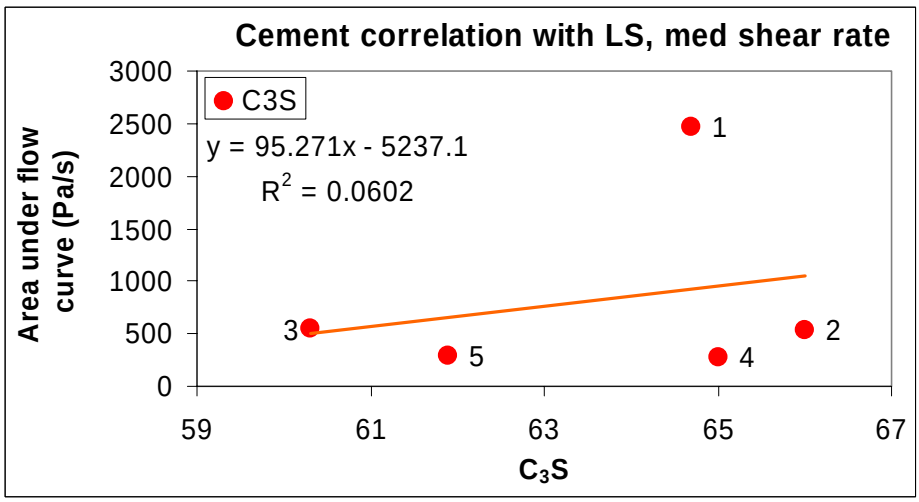

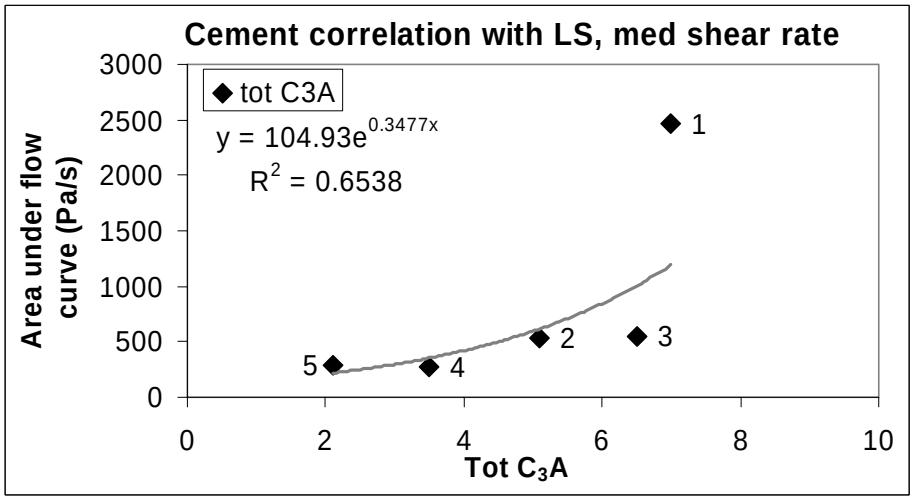

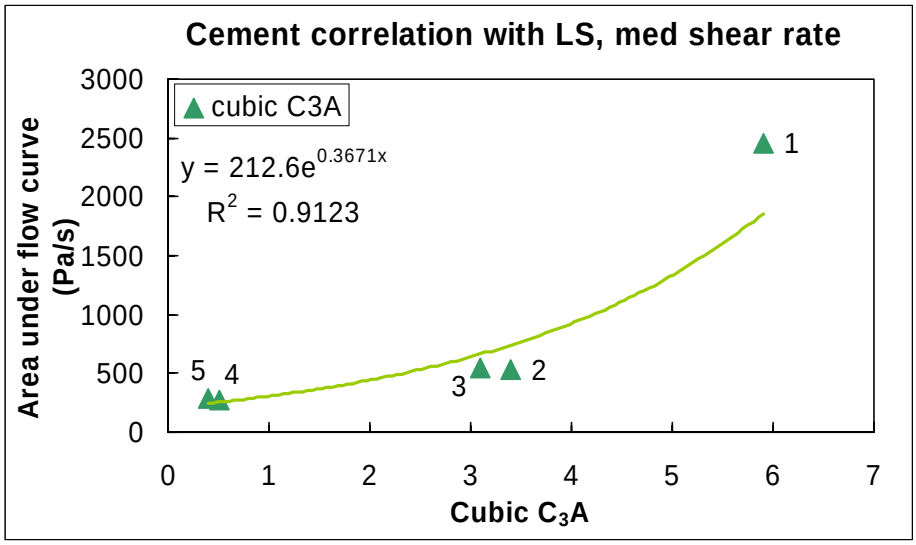
Cement correlation with LS, med shear rate
cubic C3A
y = 212.6e^0.3671x
R^2 = 0.9123
Area under flow curve (Pa/s)
Cubic C3A
1
2
3
4
5

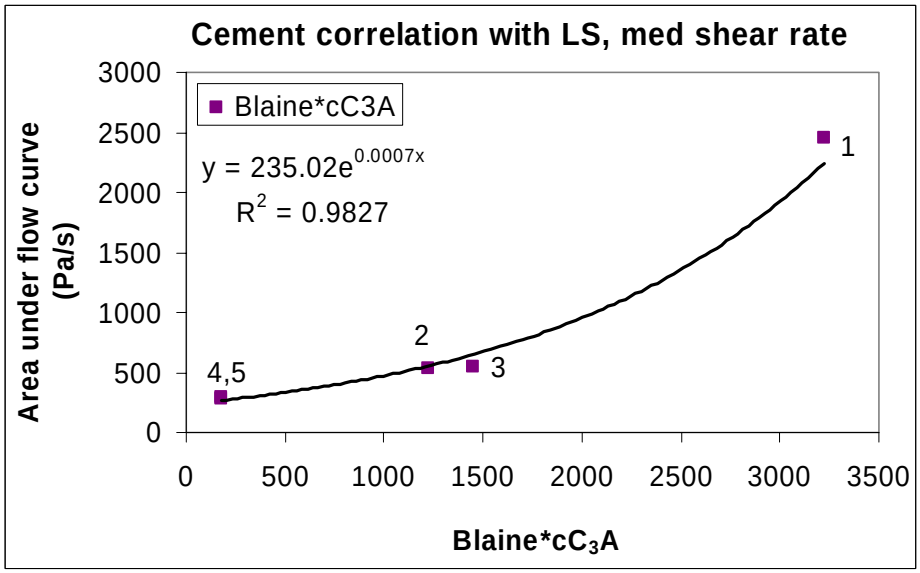
Cement correlation with LS, med shear rate
Blaine*cC3A
y = 235.02e^0.0007x
R^2 = 0.9827
Area under flow curve (Pa/s)
Blaine*cC3A
1
2
3
4,5

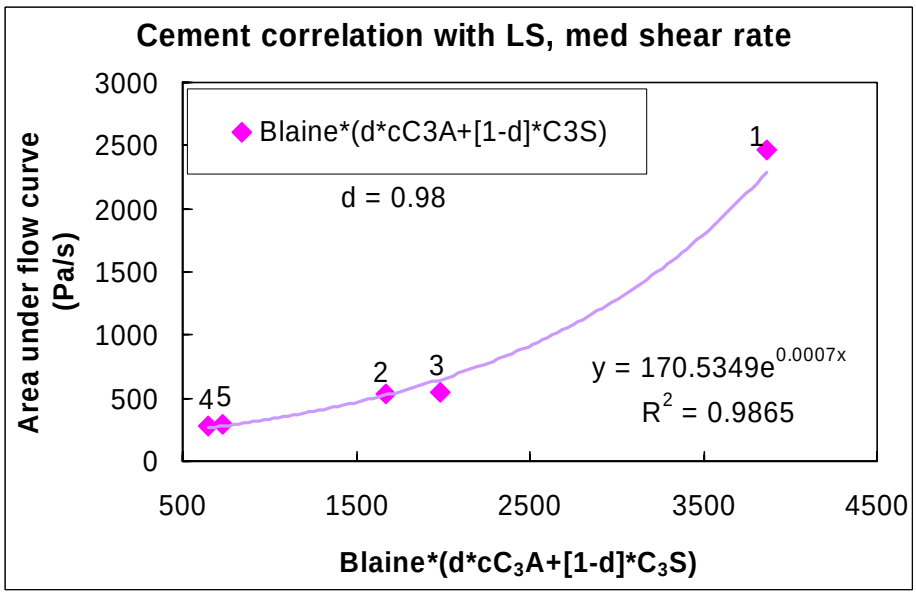
Cement correlation with LS, med shear rate
Blaine*(d*cC3A+[1-d]*C3S)
d = 0.98
y = 170.5349e^0.0007x
R^2 = 0.9865
Area under flow curve (Pa/s)
Blaine*(d*cC3A+[1-d]*C3S)
1
2
3
45

A.2.2.3 Low shear rate range (43-8.8 s^{-1}):

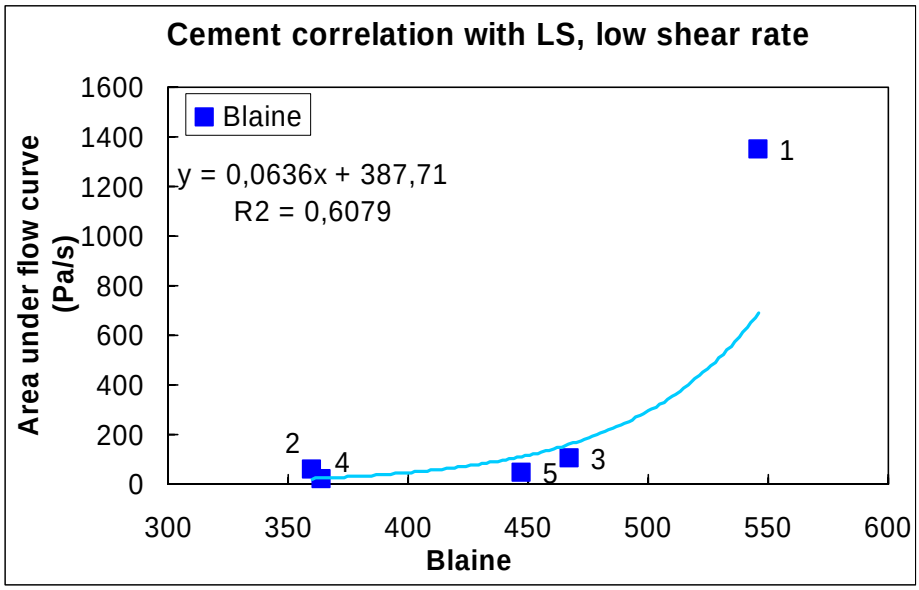

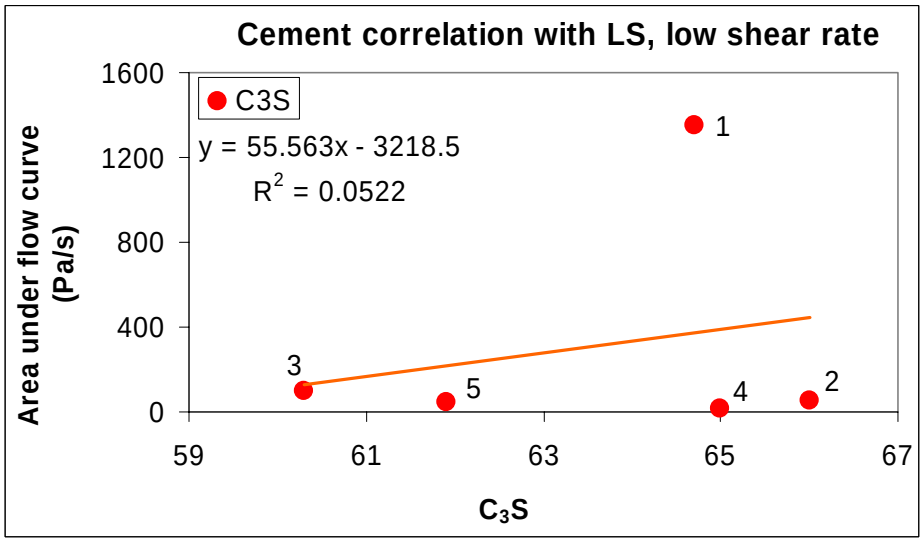

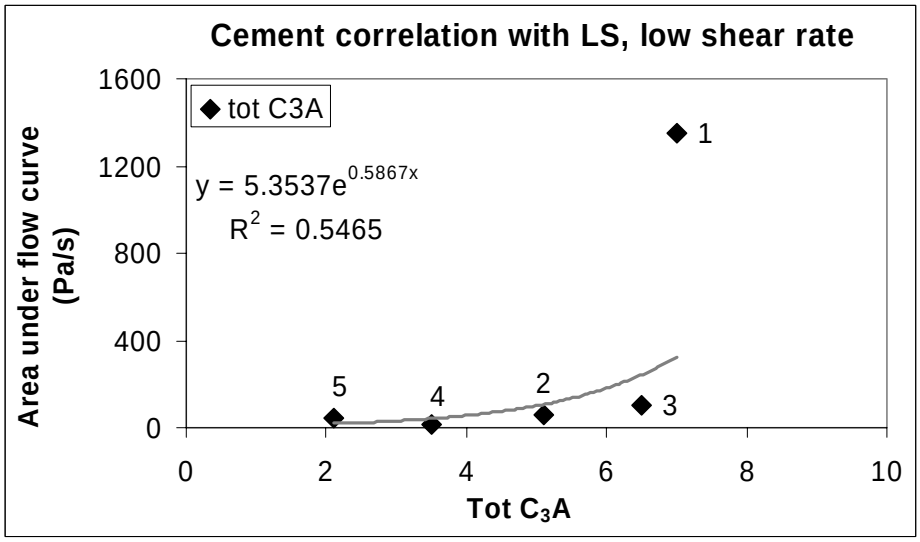

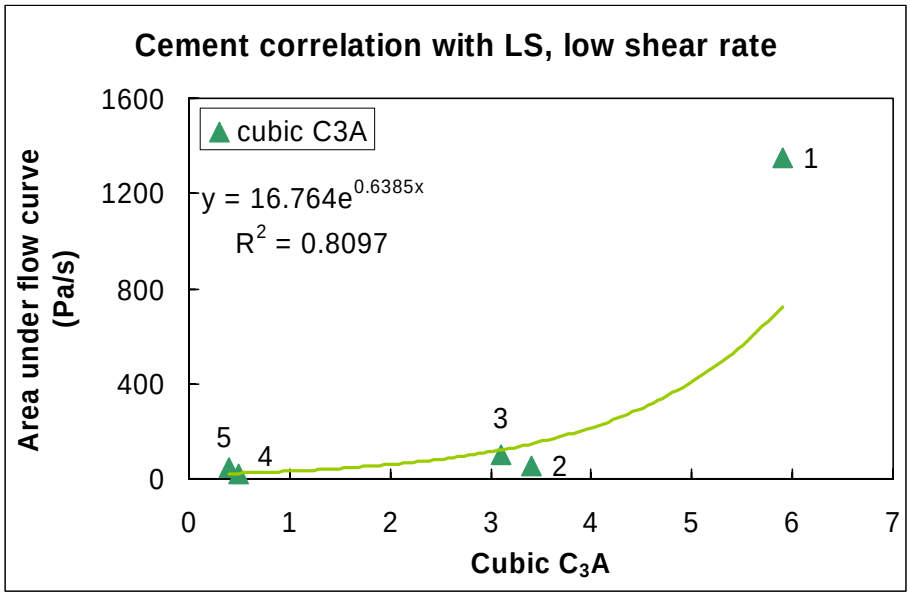
Cement correlation with LS, low shear rate
cubic C3A
y = 16.764e^0.6385x
R^2 = 0.8097
Area under flow curve (Pa/s)
Cubic C3A
1600
1200
800
400
0
0
1
2
3
4
5
6
7
1
2
3
4
5

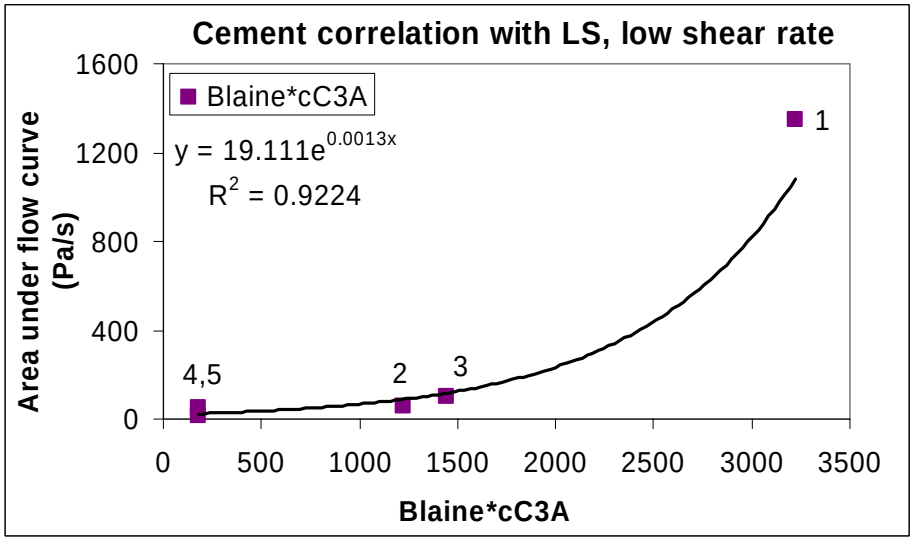
Cement correlation with LS, low shear rate
Blaine*cC3A
y = 19.111e^0.0013x
R^2 = 0.9224
Area under flow curve (Pa/s)
Blaine*cC3A
1600
1200
800
400
0
0
500
1000
1500
2000
2500
3000
3500
1
2
3
4,5

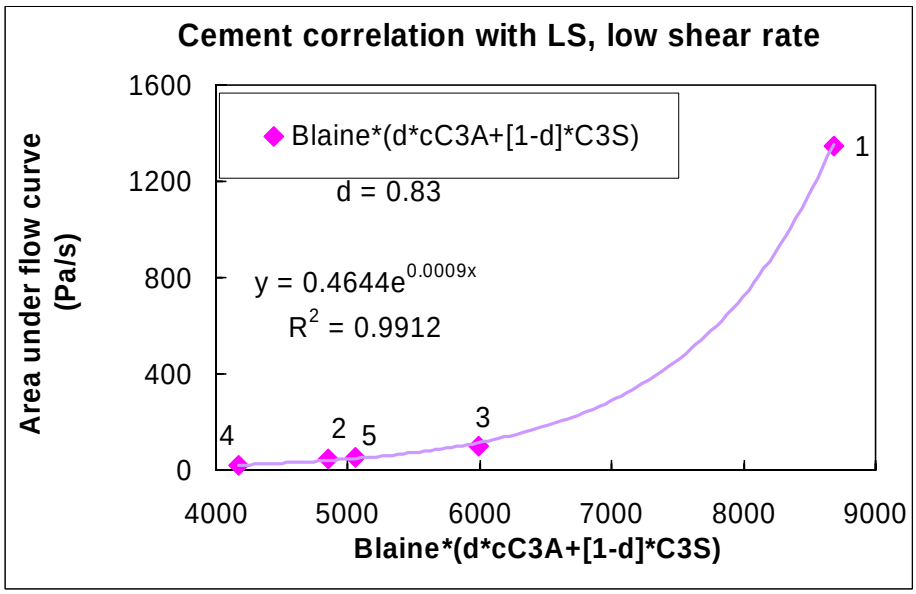
Cement correlation with LS, low shear rate
Blaine*(d*cC3A+[1-d]*C3S)
d = 0.83
y = 0.4644e^0.0009x
R^2 = 0.9912
Area under flow curve (Pa/s)
Blaine*(d*cC3A+[1-d]*C3S)
1600
1200
800
400
0
4000
5000
6000
7000
8000
9000
1
2
3
4
5

A.2.4 Correlations for the cements 1-6 (described by Table 3.1 – 3.3) with w/c = 0.37 and 1% LS per cement weight

A.2.4.1 Medium shear rate range (152-118 s^{-1}):

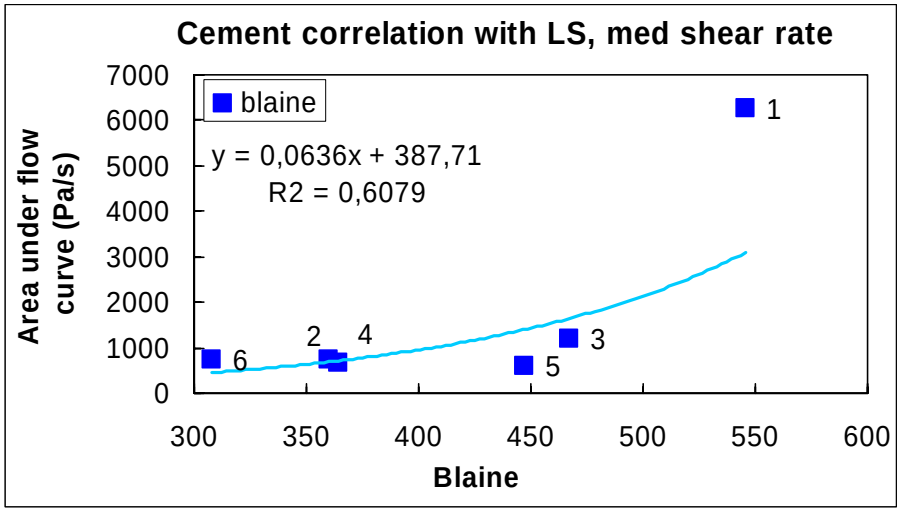

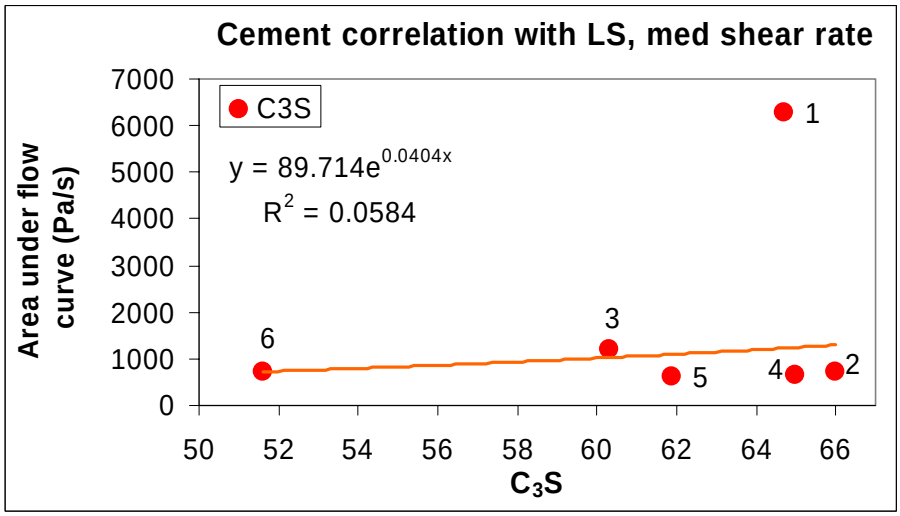

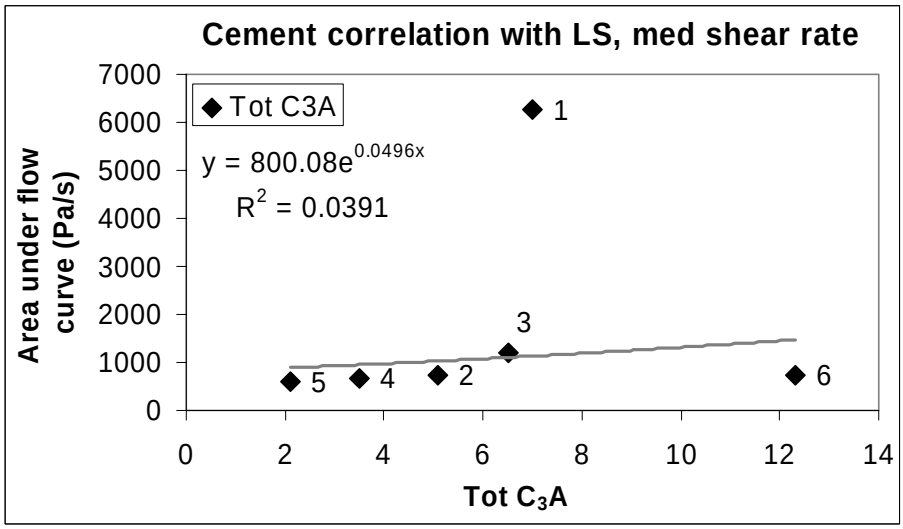

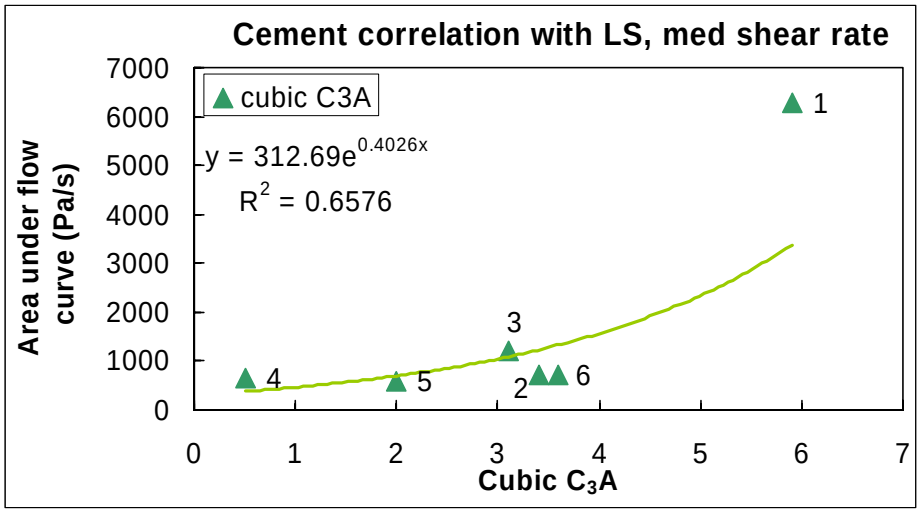
Cement correlation with LS, med shear rate
cubic C3A
y = 312.69e^0.4026x
R^2 = 0.6576
Area under flow curve (Pa/s)
Cubic C3A
7000
6000
5000
4000
3000
2000
1000
0
0
1
2
3
4
5
6
7
1
2
3
4
5
6

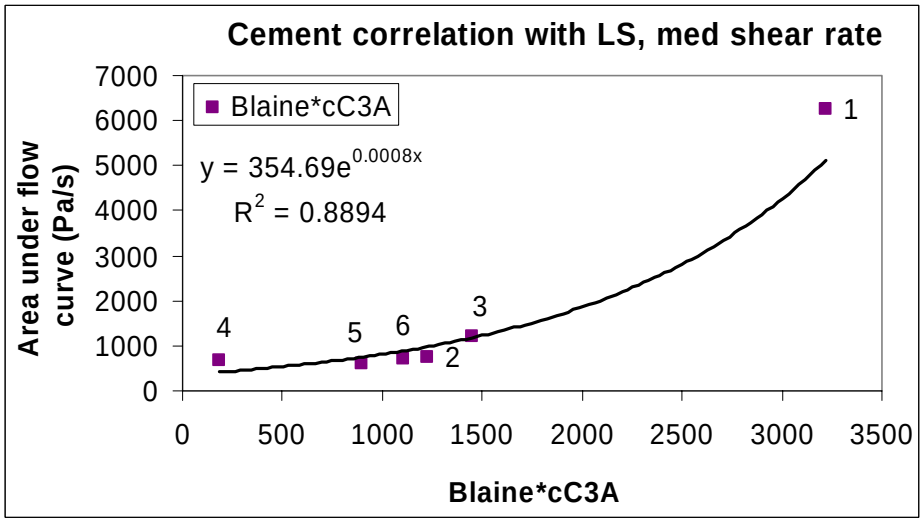
Cement correlation with LS, med shear rate
Blaine*cC3A
y = 354.69e^0.0008x
R^2 = 0.8894
Area under flow curve (Pa/s)
Blaine*cC3A
7000
6000
5000
4000
3000
2000
1000
0
0
500
1000
1500
2000
2500
3000
3500
1
2
3
4
5
6

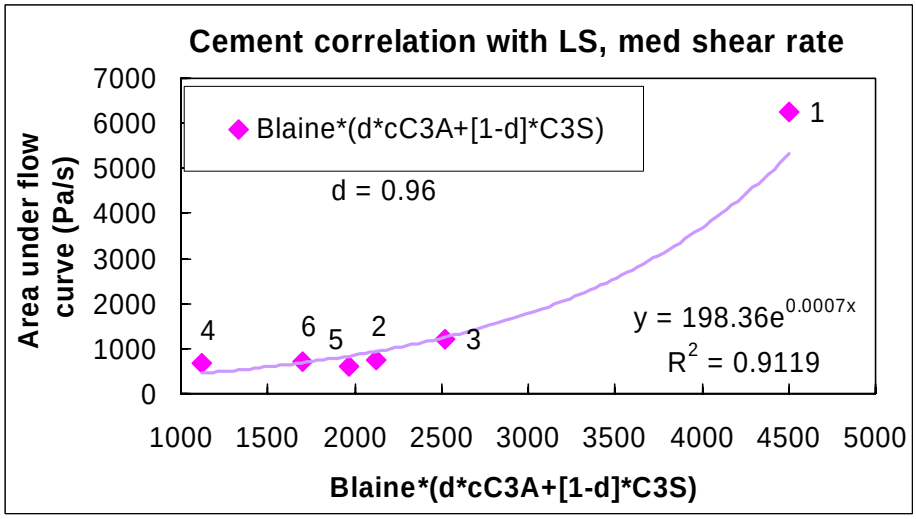
Cement correlation with LS, med shear rate
Blaine*(d*cC3A+[1-d]*C3S)
d = 0.96
y = 198.36e^0.0007x
R^2 = 0.9119
Area under flow curve (Pa/s)
Blaine*(d*cC3A+[1-d]*C3S)
7000
6000
5000
4000
3000
2000
1000
0
1000
1500
2000
2500
3000
3500
4000
4500
5000
1
2
3
4
5
6

A.2.4.2 Low shear rate range (43-8.8 s^{-1}):

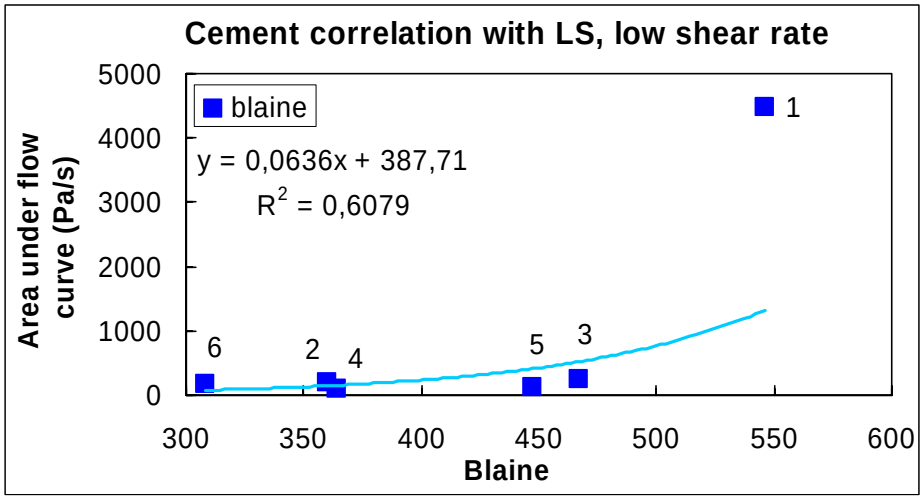

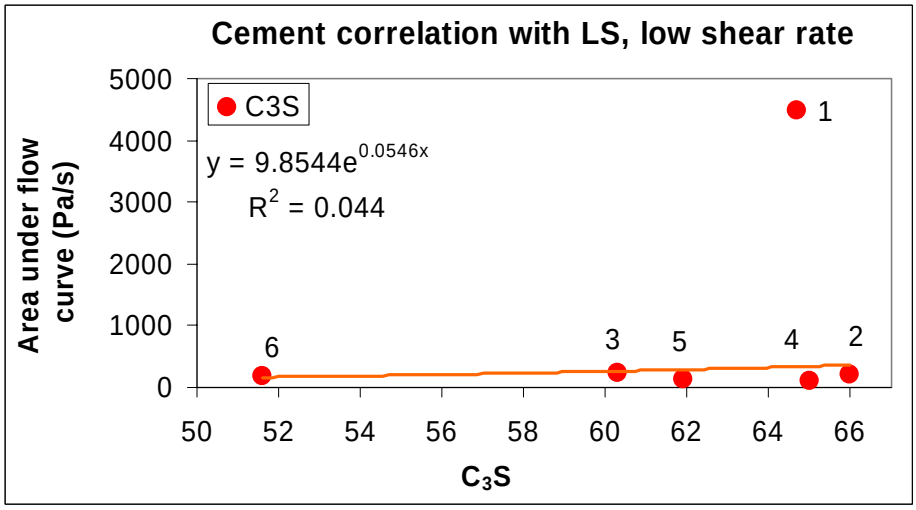

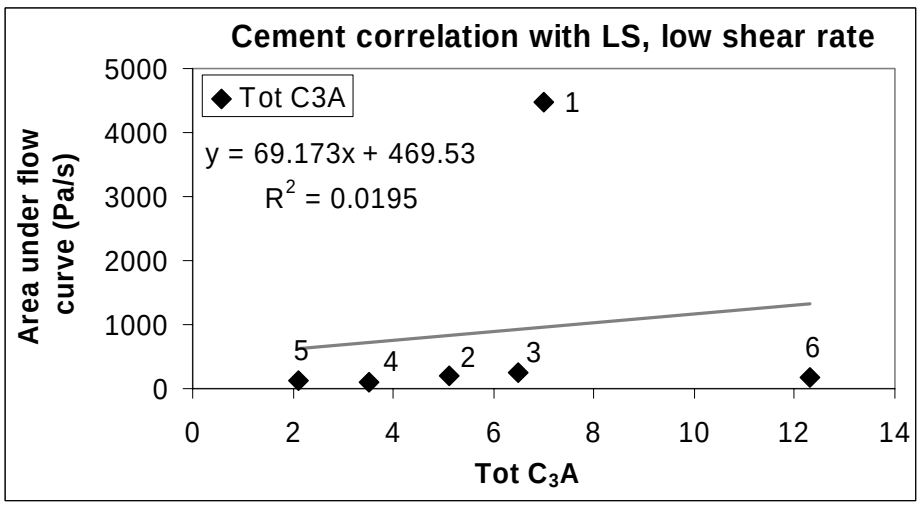

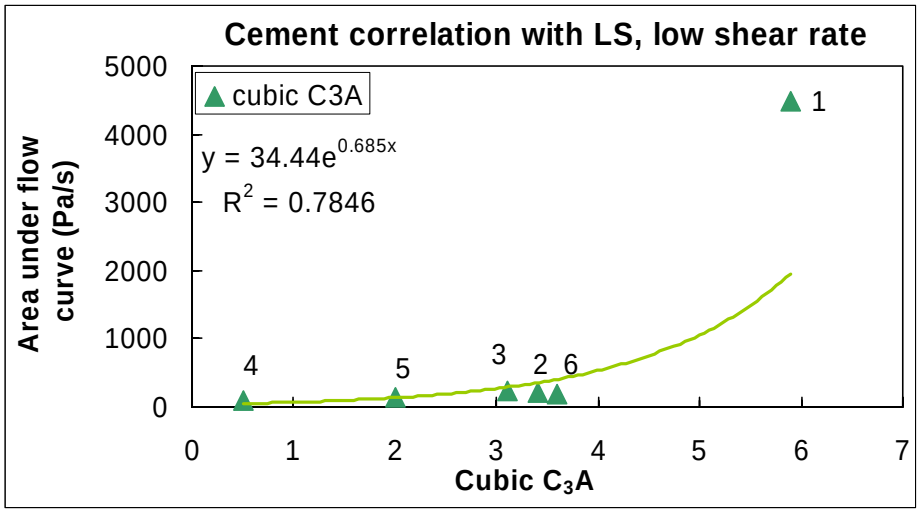
Cement correlation with LS, low shear rate
cubic C3A
y = 34.44e^0.685x
R^2 = 0.7846
Area under flow curve (Pa/s)
Cubic C3A
1
2
3
4
5
6

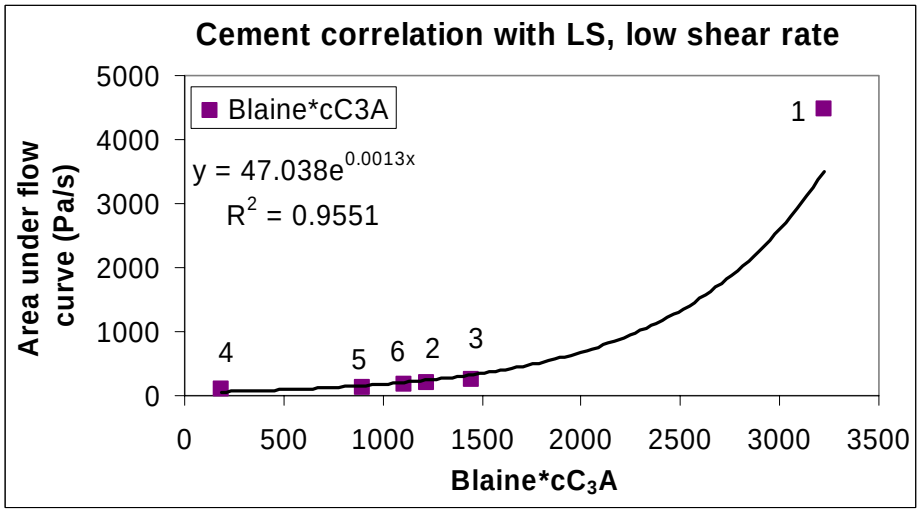
Cement correlation with LS, low shear rate
Blaine*cC3A
y = 47.038e^0.0013x
R^2 = 0.9551
Area under flow curve (Pa/s)
Blaine*cC3A
1
2
3
4
5
6

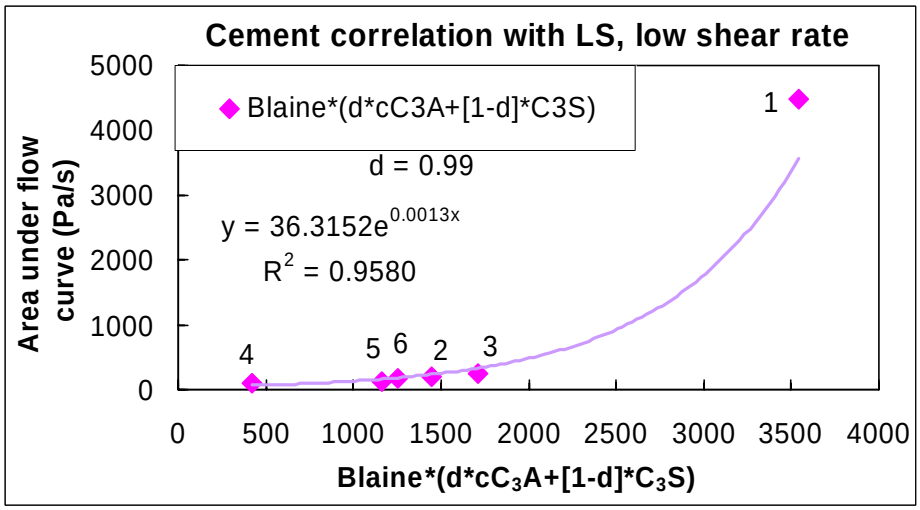
Cement correlation with LS, low shear rate
Blaine*(d*cC3A+[1-d]*C3S)
d = 0.99
y = 36.3152e^0.0013x
R^2 = 0.9580
Area under flow curve (Pa/s)
Blaine*(d*cC3A+[1-d]*C3S)
1
2
3
4
5
6

A.2.5 Correlations for the cements 1-5 (described by Table 3.1-3-3) with w/c = 0.40 and 0.53% PA2 per cement weight.

A.2.5.1 Medium shear rate range (152-118 s^{-1}):

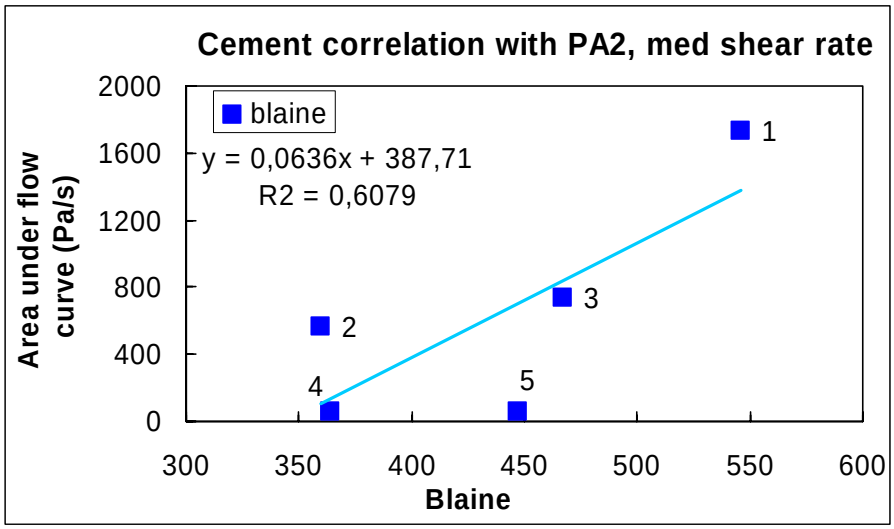

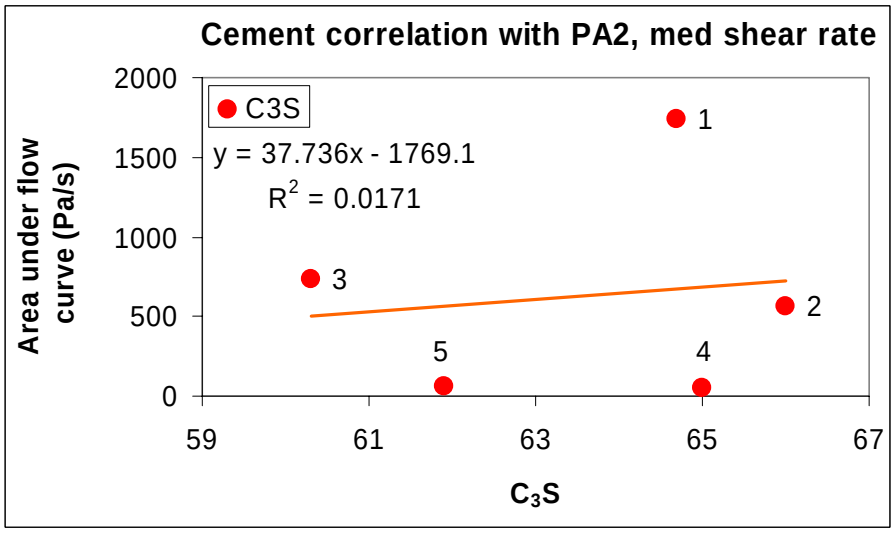

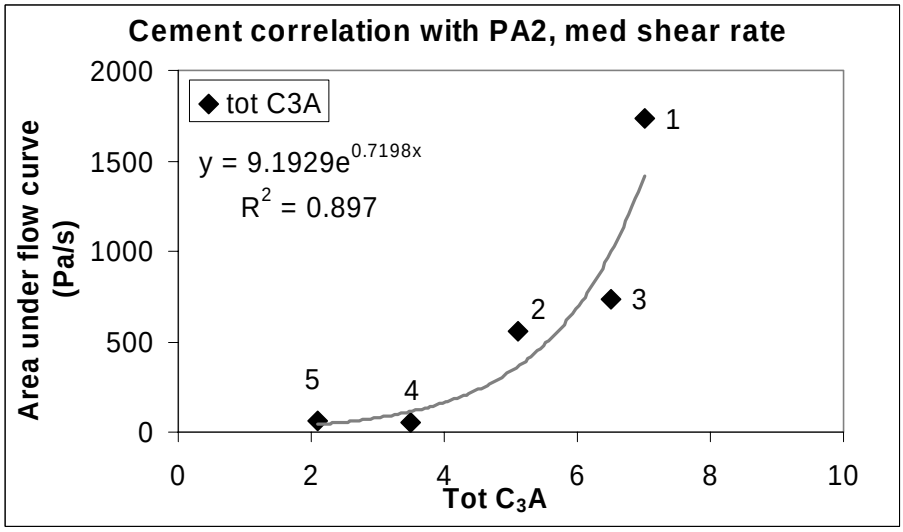

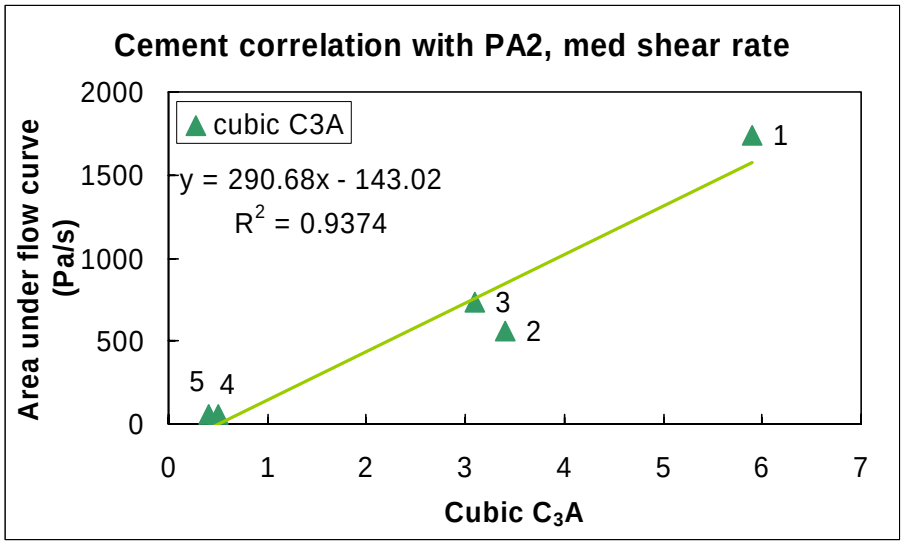
Cement correlation with PA2, med shear rate
Area under flow curve (Pa/s)
2000
1500
1000
500
0
cubic C3A
y = 290.68x - 143.02
R2 = 0.9374
1
3
2
5
4
0
1
2
3
4
5
6
7
Cubic C3A

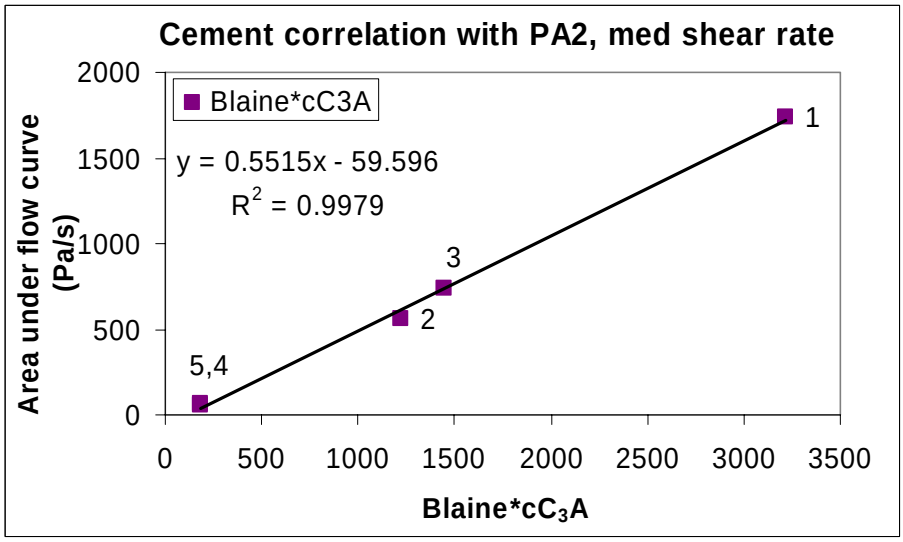
Cement correlation with PA2, med shear rate
Area under flow curve (Pa/s)
2000
1500
1000
500
0
Blaine*cC3A
y = 0.5515x - 59.596
R2 = 0.9979
1
3
2
5,4
0
500
1000
1500
2000
2500
3000
3500
Blaine*cC3A

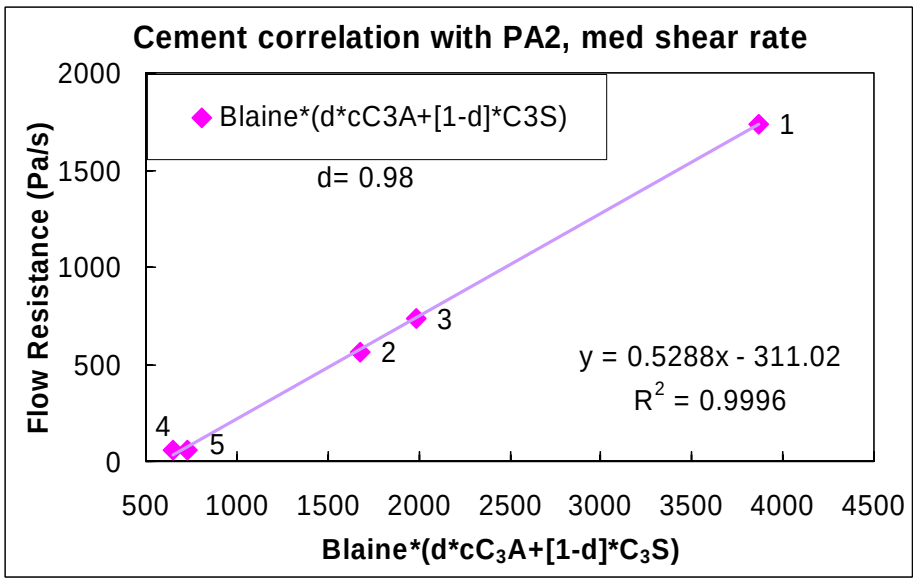
Cement correlation with PA2, med shear rate
Flow Resistance (Pa/s)
2000
1500
1000
500
0
Blaine*(d*cC3A+[1-d]*C3S)
d= 0.98
1
3
2
y = 0.5288x - 311.02
R2 = 0.9996
4
5
500
1000
1500
2000
2500
3000
3500
4000
4500
Blaine*(d*cC3A+[1-d]*C3S)

A.2.5.2 Low shear rate range (43-8.8 s^{-1}):

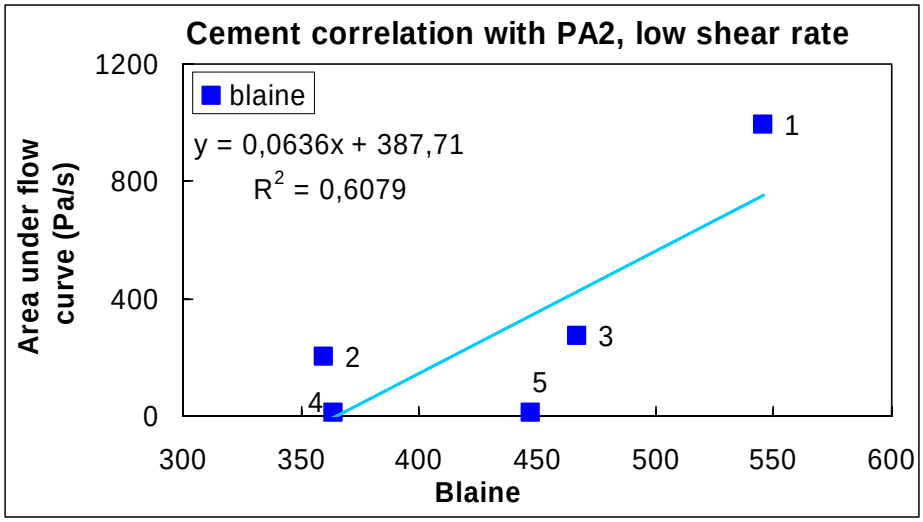

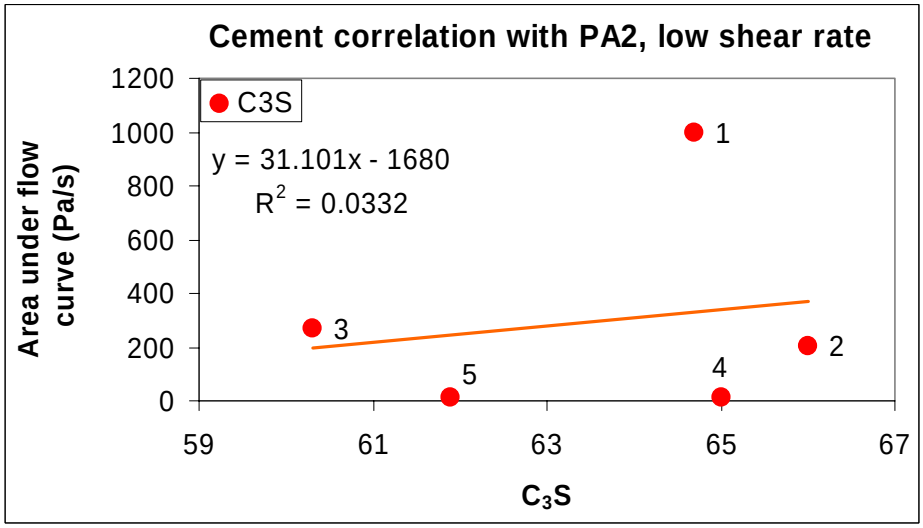

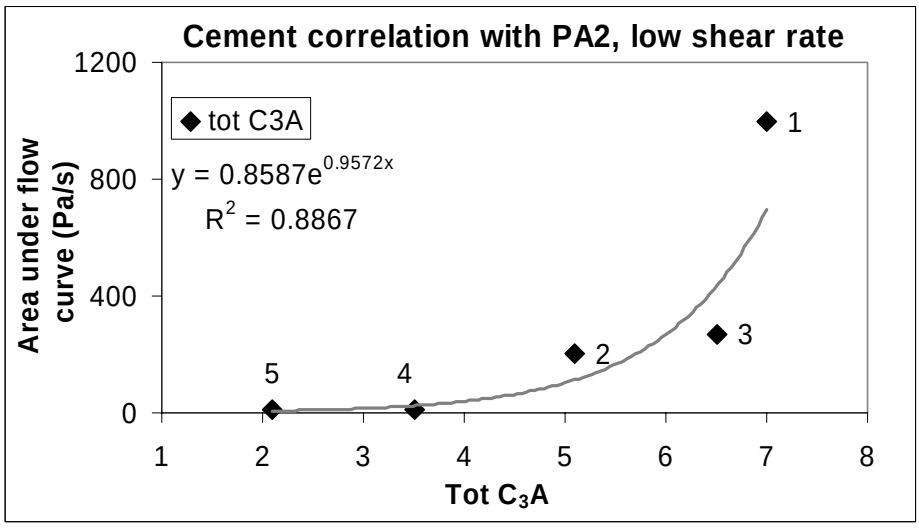

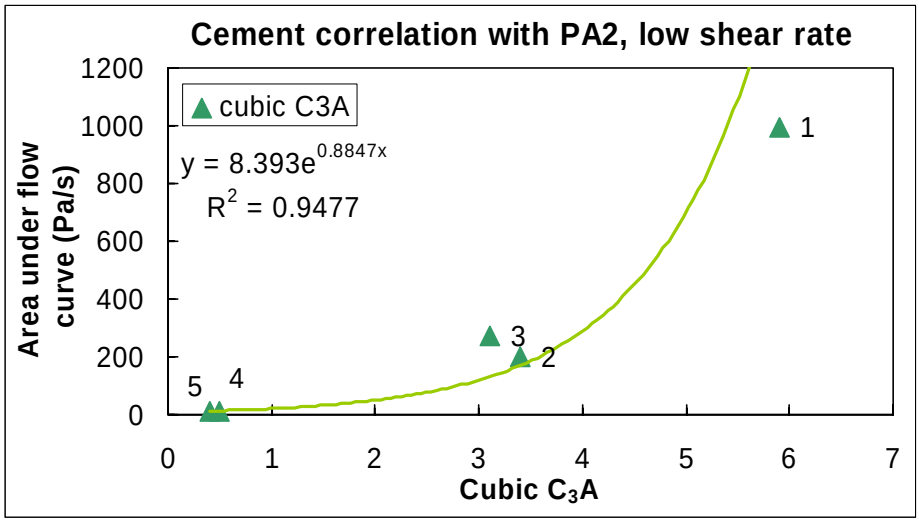
Cement correlation with PA2, low shear rate
cubic C3A
y = 8.393e^0.8847x
R^2 = 0.9477
Area under flow curve (Pa/s)
Cubic C3A
1
2
3
4
5

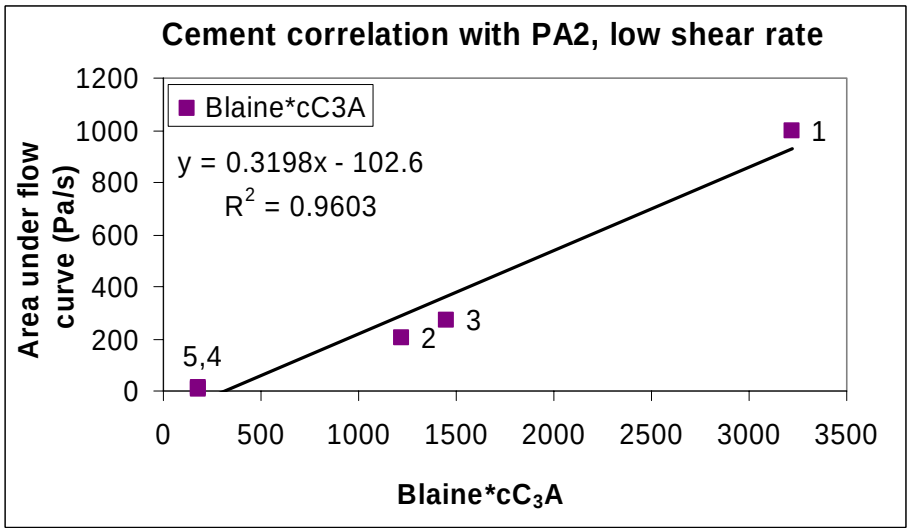
Cement correlation with PA2, low shear rate
Blaine*cC3A
y = 0.3198x - 102.6
R^2 = 0.9603
Area under flow curve (Pa/s)
Blaine*cC3A
1
2
3
5,4

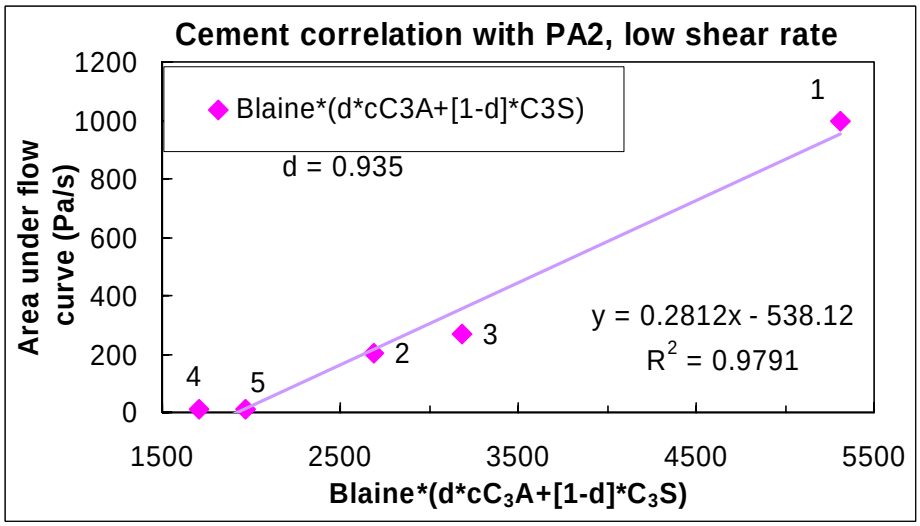
Cement correlation with PA2, low shear rate
Blaine*(d*cC3A+[1-d]*C3S)
d = 0.935
y = 0.2812x - 538.12
R^2 = 0.9791
Area under flow curve (Pa/s)
Blaine*(d*cC3A+[1-d]*C3S)
1
2
3
4
5

A.2.6 Correlations for the cements 1-5 (described by Table 3.1 - 3-3) with w/c = 0.40, 6.79 vol % SF and 0.53% PA per cement weight

A.2.6.1 Medium shear rate range (152-118 s^{-1}):

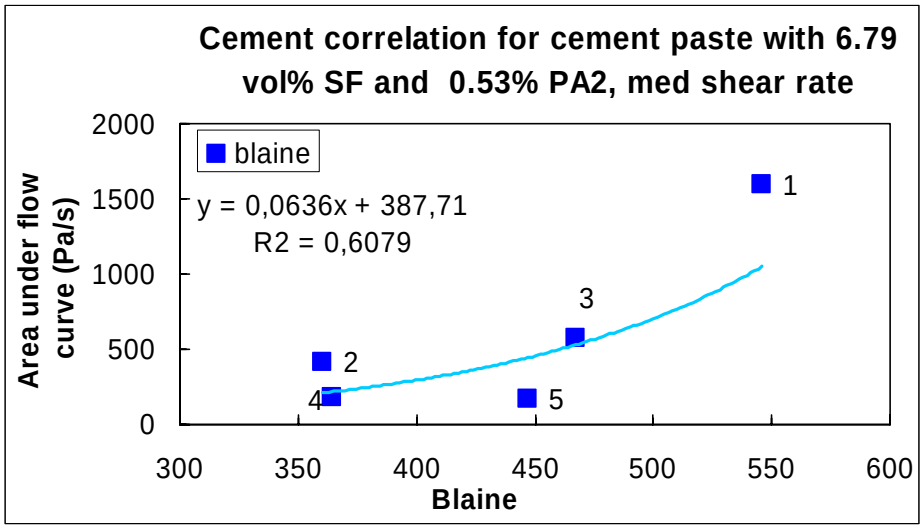

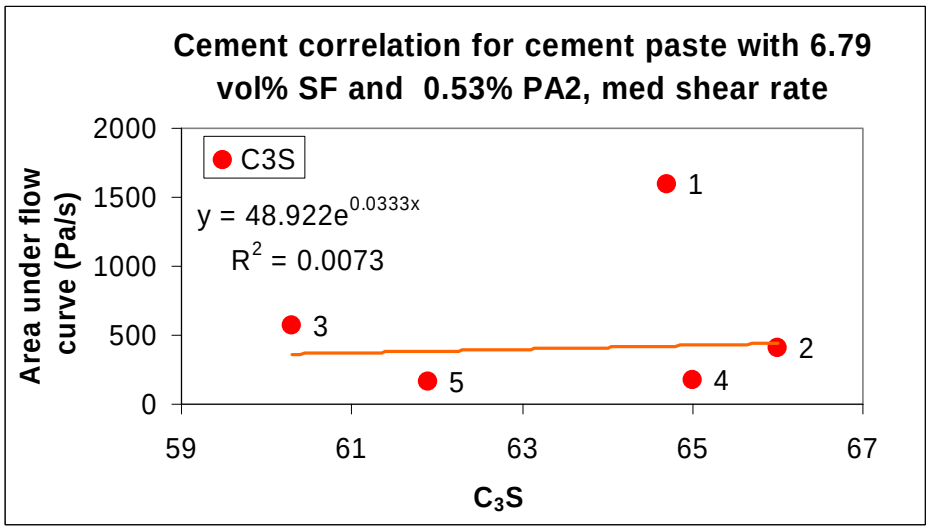

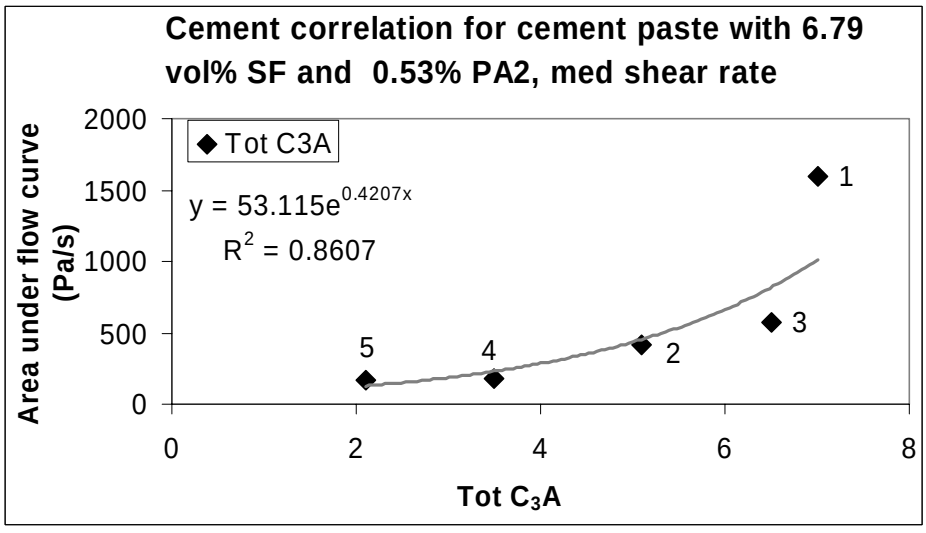

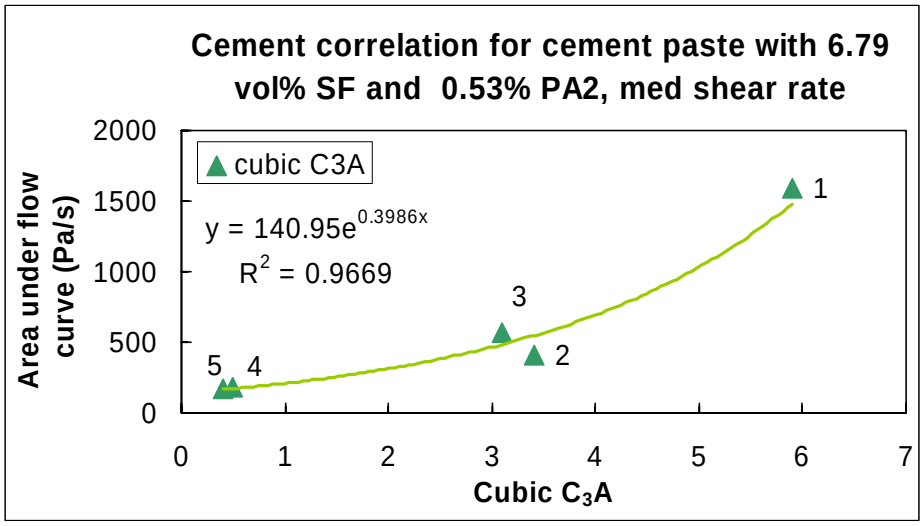
Cement correlation for cement paste with 6.79 vol% SF and 0.53% PA2, med shear rate
Area under flow curve (Pa/s)
cubic C3A
y = 140.95e^0.3986x
R^2 = 0.9669
Cubic C3A
2000
1500
1000
500
0
0
1
2
3
4
5
6
7
1
2
3
4
5

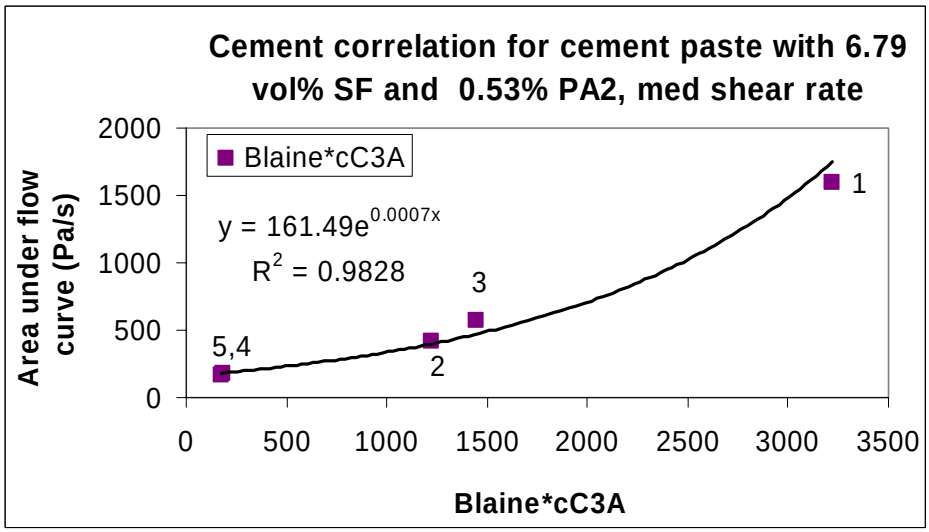
Cement correlation for cement paste with 6.79 vol% SF and 0.53% PA2, med shear rate
Area under flow curve (Pa/s)
Blaine*cC3A
y = 161.49e^0.0007x
R^2 = 0.9828
Blaine*cC3A
2000
1500
1000
500
0
0
500
1000
1500
2000
2500
3000
3500
1
2
3
5,4

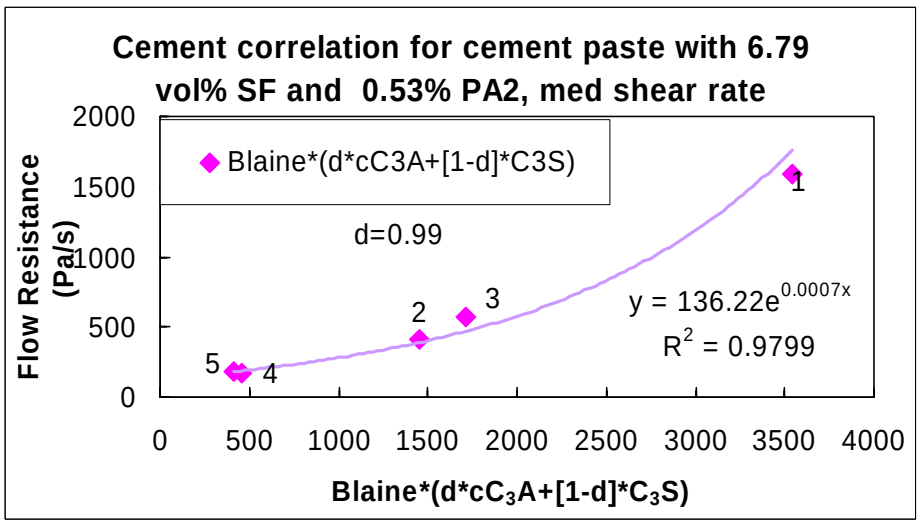
Cement correlation for cement paste with 6.79 vol% SF and 0.53% PA2, med shear rate
Flow Resistance (Pa/s)
Blaine*(d*cC3A+[1-d]*C3S)
d=0.99
y = 136.22e^0.0007x
R^2 = 0.9799
Blaine*(d*cC3A+[1-d]*C3S)
2000
1500
1000
500
0
0
500
1000
1500
2000
2500
3000
3500
4000
1
2
3
4
5

A.2.6.2 Low shear rate range (43-8.8 s^{-1}):

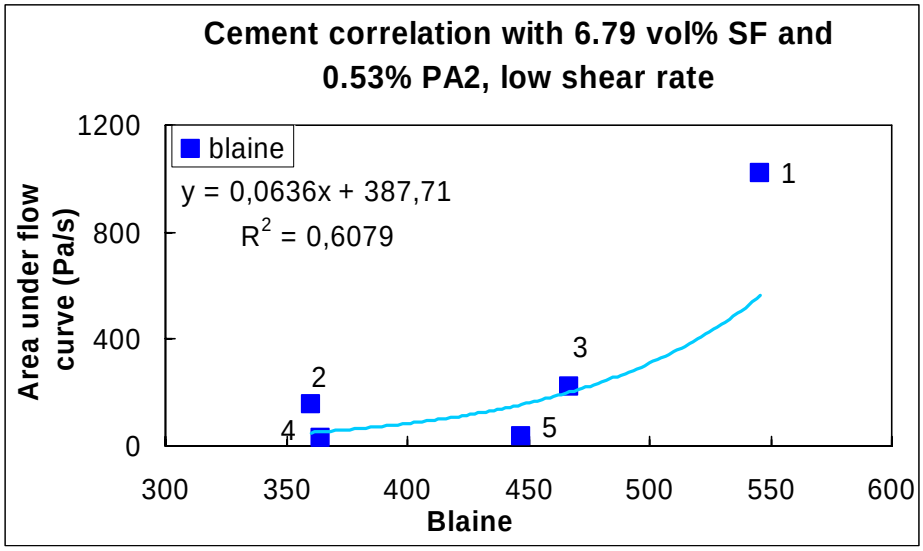

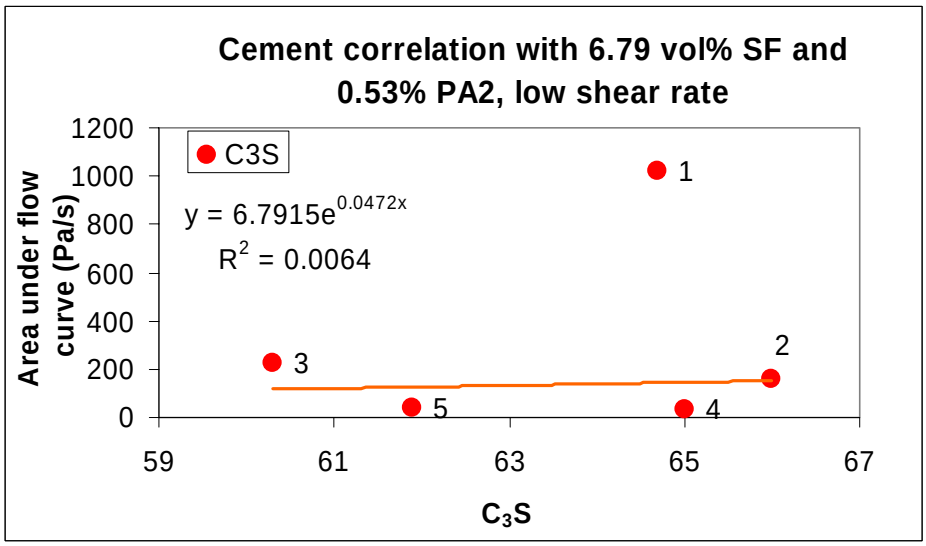

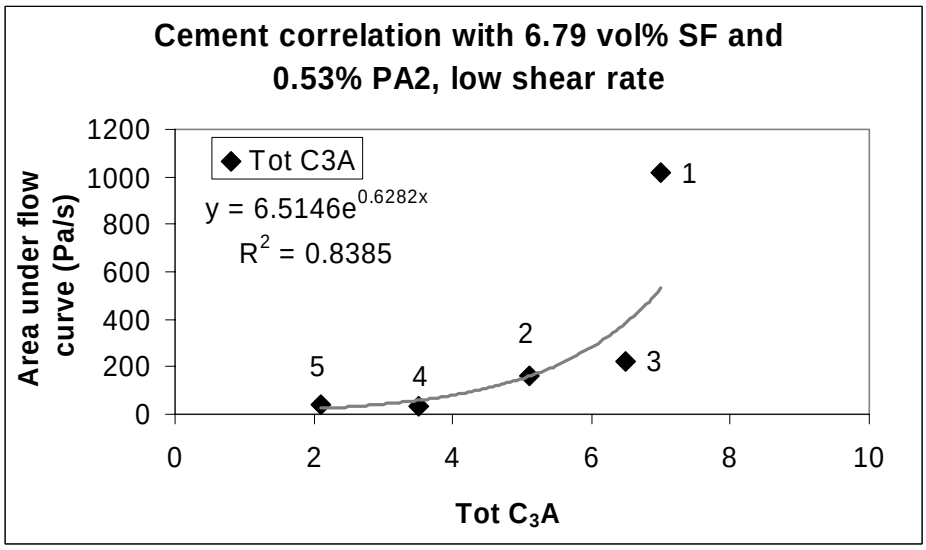

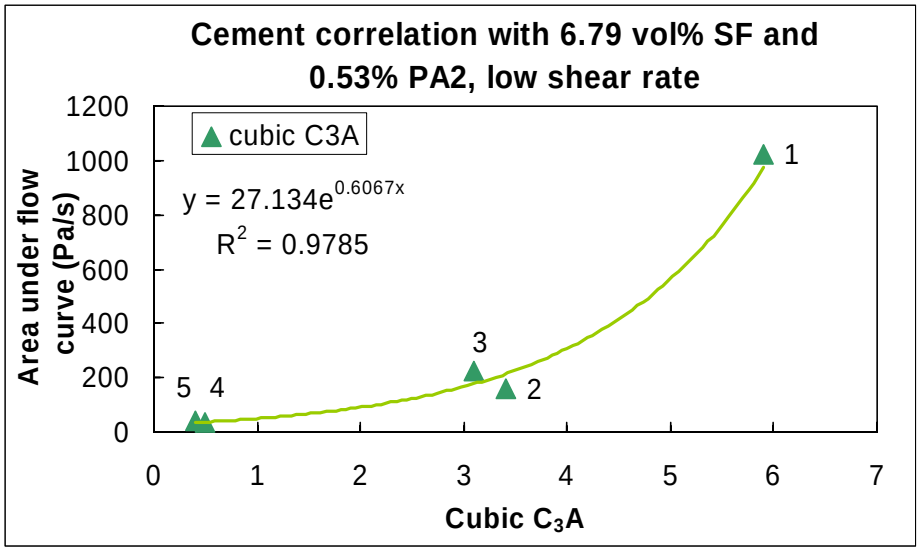
Cement correlation with 6.79 vol% SF and 0.53% PA2, low shear rate
cubic C3A
y = 27.134e^0.6067x
R^2 = 0.9785
Area under flow curve (Pa/s)
Cubic C3A
1200
1000
800
600
400
200
0
0
1
2
3
4
5
6
7
1
2
3
4
5

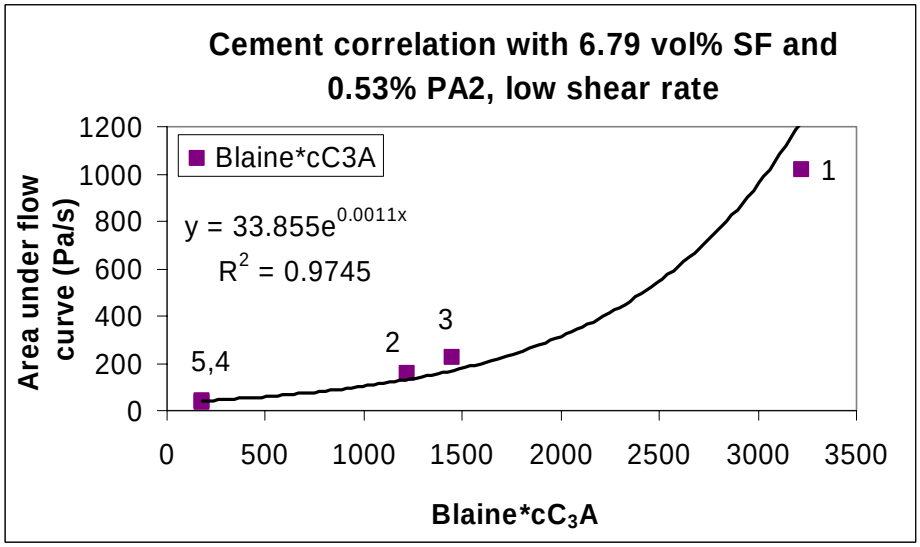
Cement correlation with 6.79 vol% SF and 0.53% PA2, low shear rate
Blaine*cC3A
y = 33.855e^0.0011x
R^2 = 0.9745
Area under flow curve (Pa/s)
Blaine*cC3A
1200
1000
800
600
400
200
0
0
500
1000
1500
2000
2500
3000
3500
1
2
3
5,4

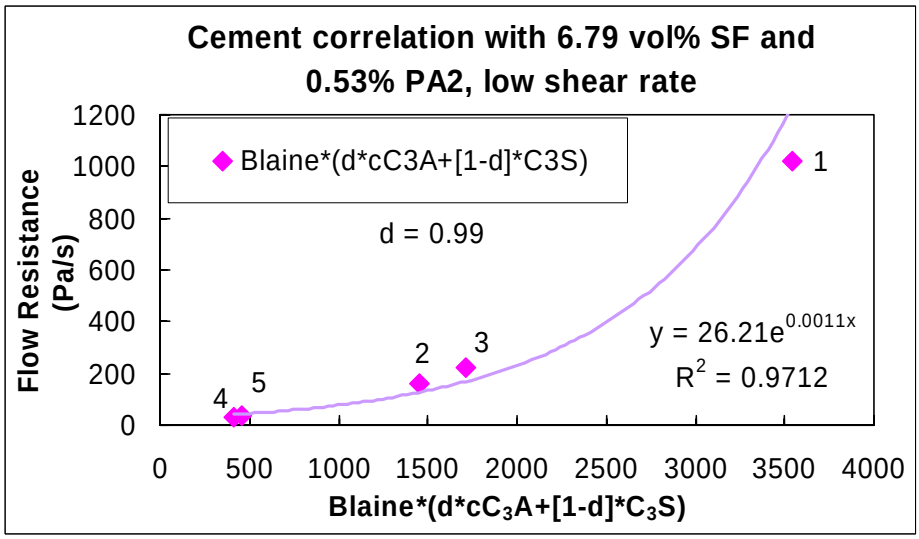
Cement correlation with 6.79 vol% SF and 0.53% PA2, low shear rate
Blaine*(d*cC3A+[1-d]*C3S)
d = 0.99
y = 26.21e^0.0011x
R^2 = 0.9712
Flow Resistance (Pa/s)
Blaine*(d*cC3A+[1-d]*C3S)
1200
1000
800
600
400
200
0
0
500
1000
1500
2000
2500
3000
3500
4000
1
2
3
4
5

A.2.7 Correlations for the cements 1-6 (described by Table 3.1 – 3.3) with w/c = 0.32 and 0.61% PA per cement weight

A.2.7.1 Medium shear rate range (152-118 s^{-1}):

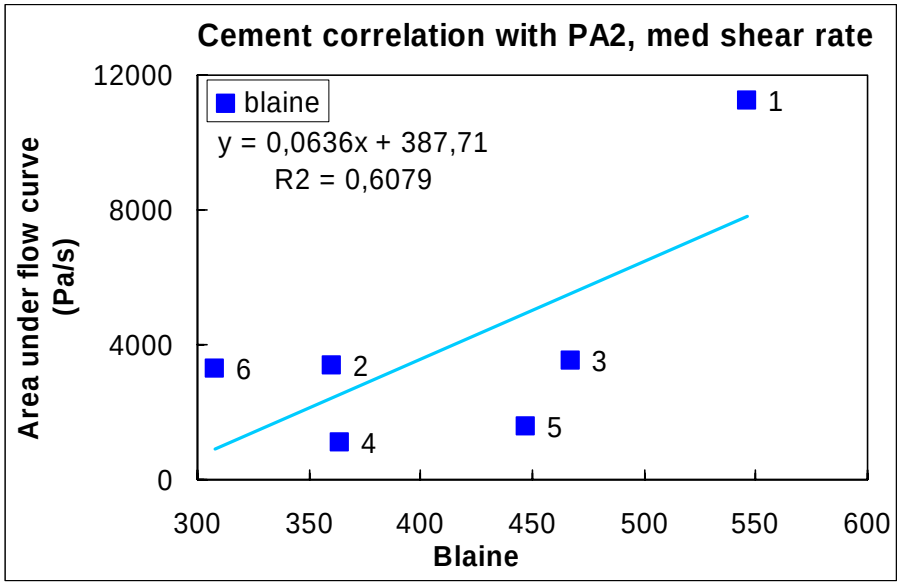

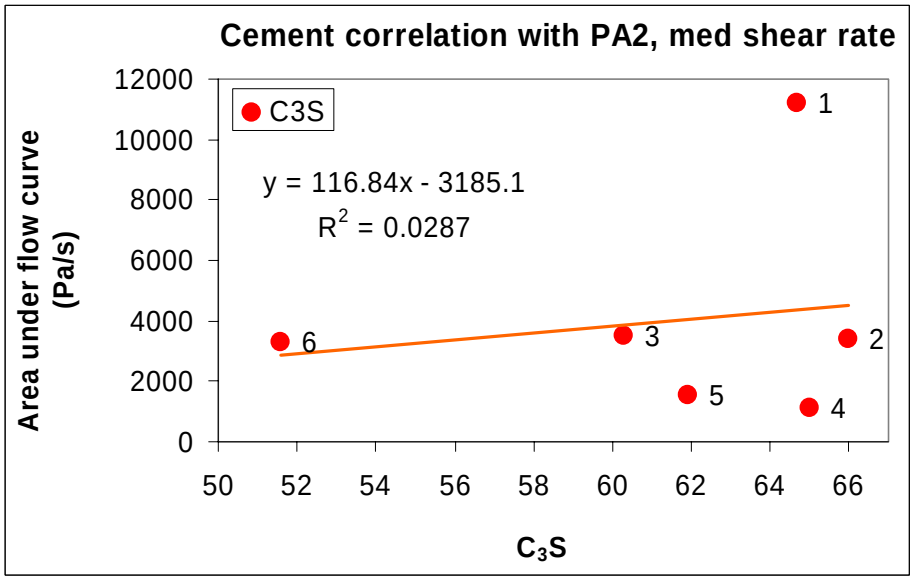

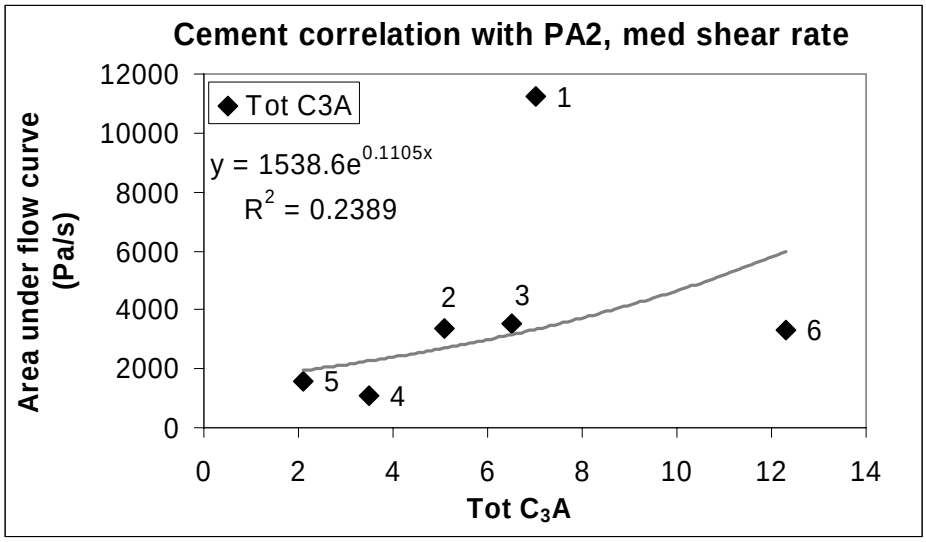
Cement correlation with PA2, med shear rate
Tot C3A
y = 1538.6e^0.1105x
R^2 = 0.2389
Area under flow curve (Pa/s)
Tot C3A
12000
10000
8000
6000
4000
2000
0
0
2
4
6
8
10
12
14
1
2
3
4
5
6

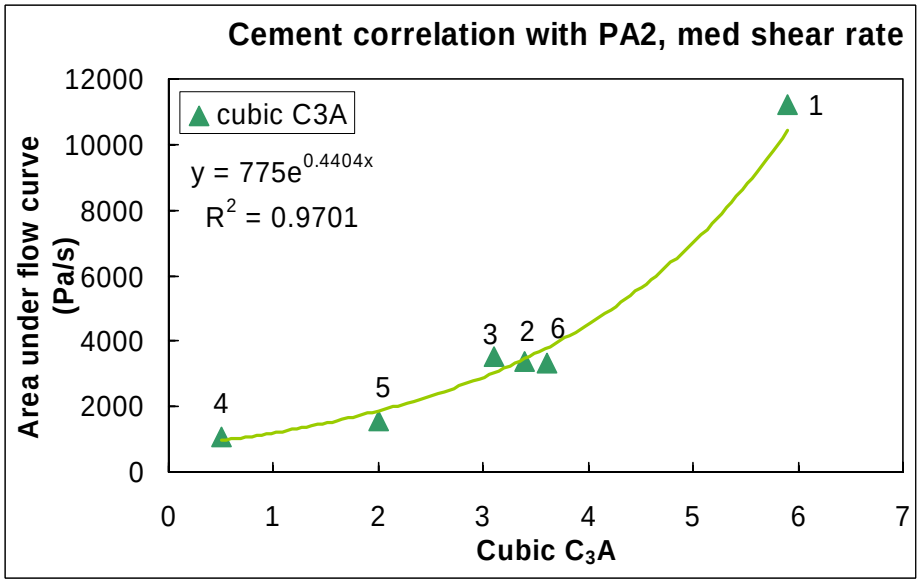
Cement correlation with PA2, med shear rate
cubic C3A
y = 775e^0.4404x
R^2 = 0.9701
Area under flow curve (Pa/s)
Cubic C3A
12000
10000
8000
6000
4000
2000
0
0
1
2
3
4
5
6
7
1
2
3
4
5
6

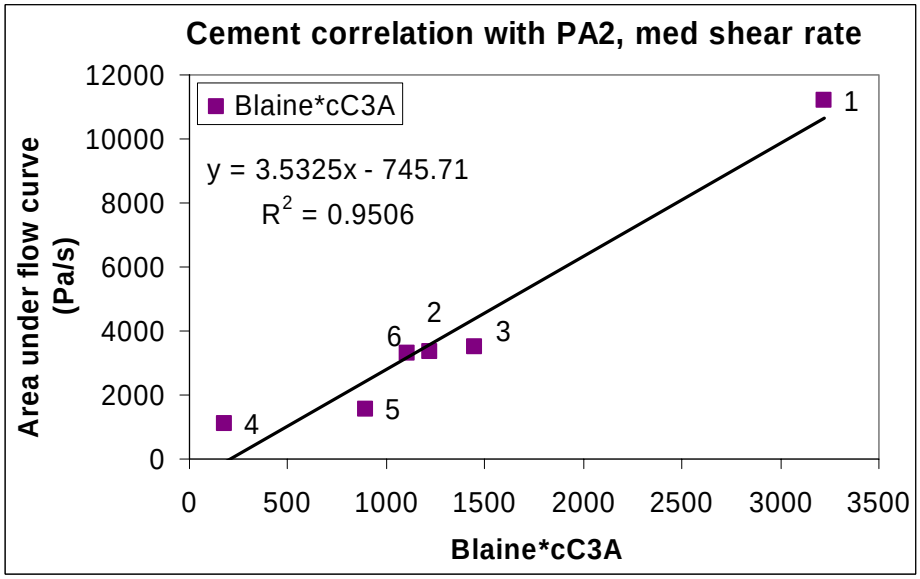
Cement correlation with PA2, med shear rate
Blaine*cC3A
y = 3.5325x - 745.71
R^2 = 0.9506
Area under flow curve (Pa/s)
Blaine*cC3A
12000
10000
8000
6000
4000
2000
0
0
500
1000
1500
2000
2500
3000
3500
1
2
3
4
5
6

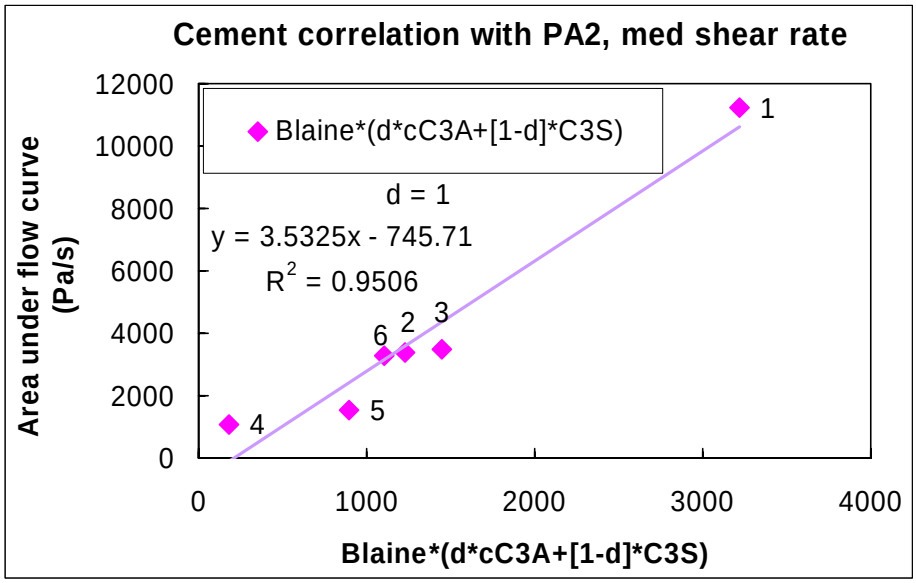
Cement correlation with PA2, med shear rate
Area under flow curve (Pa/s)
Blaine*(d*cC3A+[1-d]*C3S)
d = 1
y = 3.5325x - 745.71
R2 = 0.9506
1
2
3
4
5
6
0
2000
4000
6000
8000
10000
12000
0
1000
2000
3000
4000
Blaine*(d*cC3A+[1-d]*C3S)

A.2.7.2 Low shear rate range (43-8.8 s^{-1}):

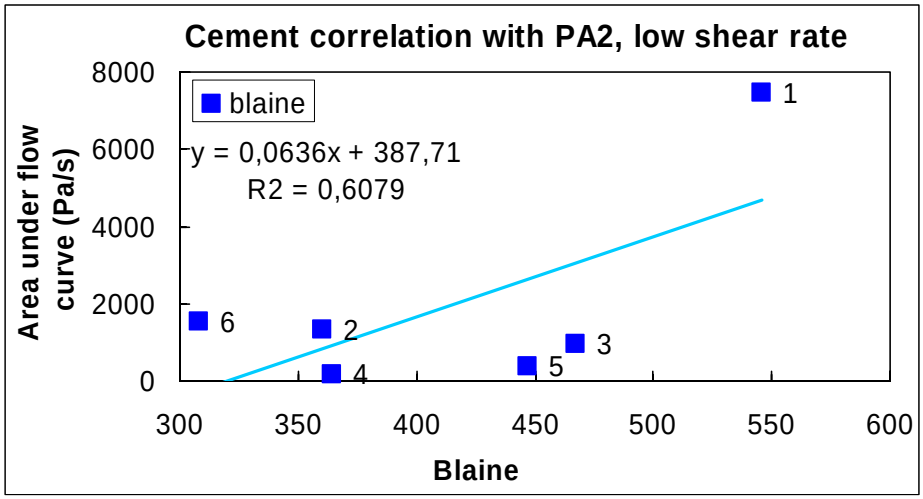

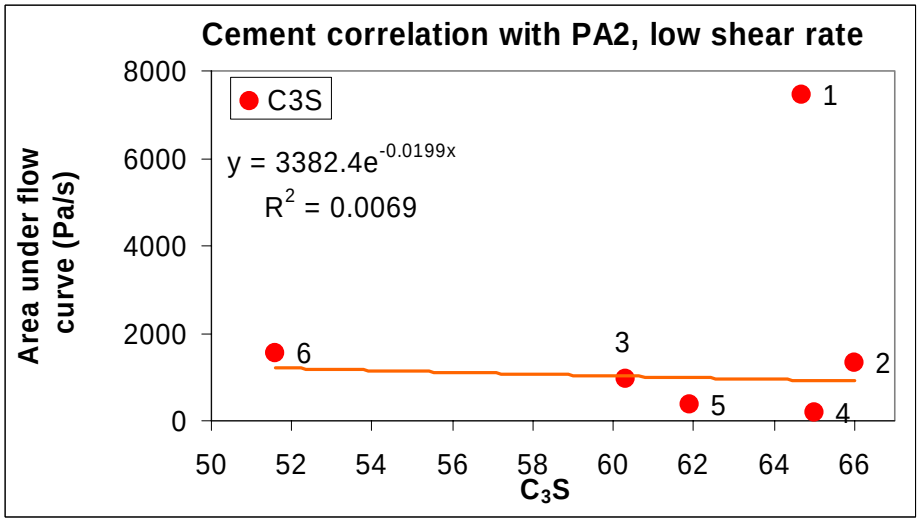

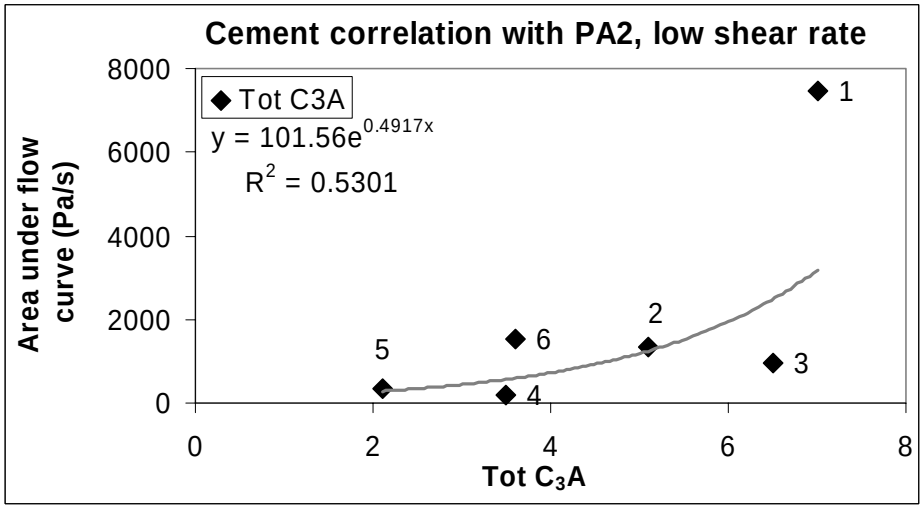

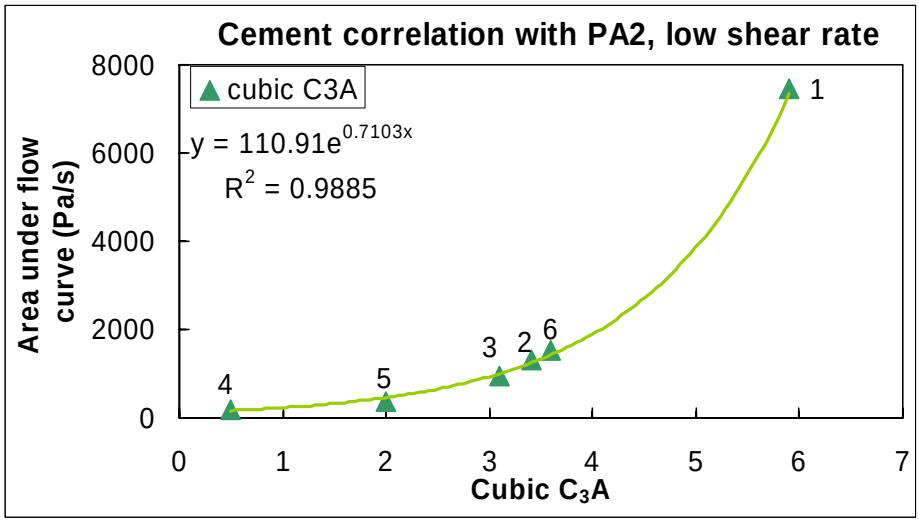
Cement correlation with PA2, low shear rate
cubic C3A
y = 110.91e^0.7103x
R^2 = 0.9885
Area under flow curve (Pa/s)
Cubic C3A
8000
6000
4000
2000
0
0
1
2
3
4
5
6
7
1
2
3
4
5
6

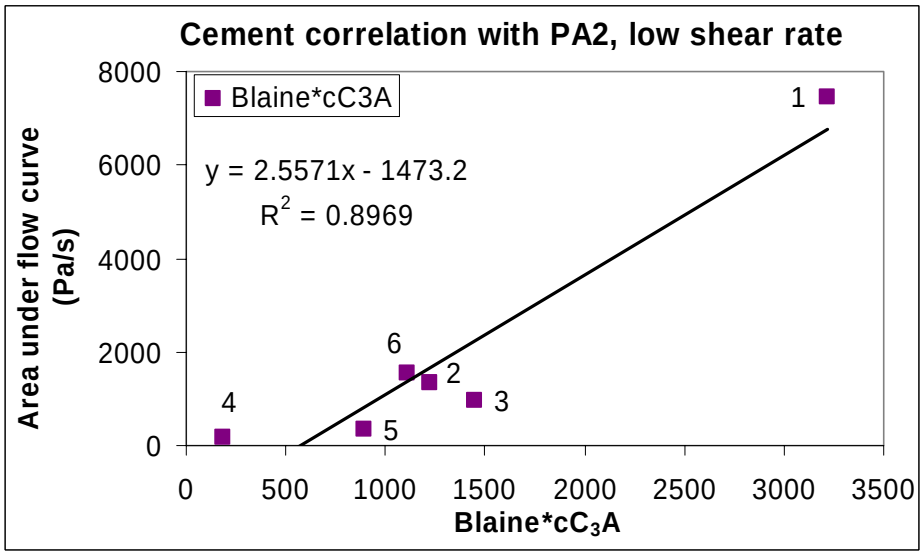
Cement correlation with PA2, low shear rate
Blaine*cC3A
y = 2.5571x - 1473.2
R^2 = 0.8969
Area under flow curve (Pa/s)
Blaine*cC3A
8000
6000
4000
2000
0
0
500
1000
1500
2000
2500
3000
3500
1
2
3
4
5
6

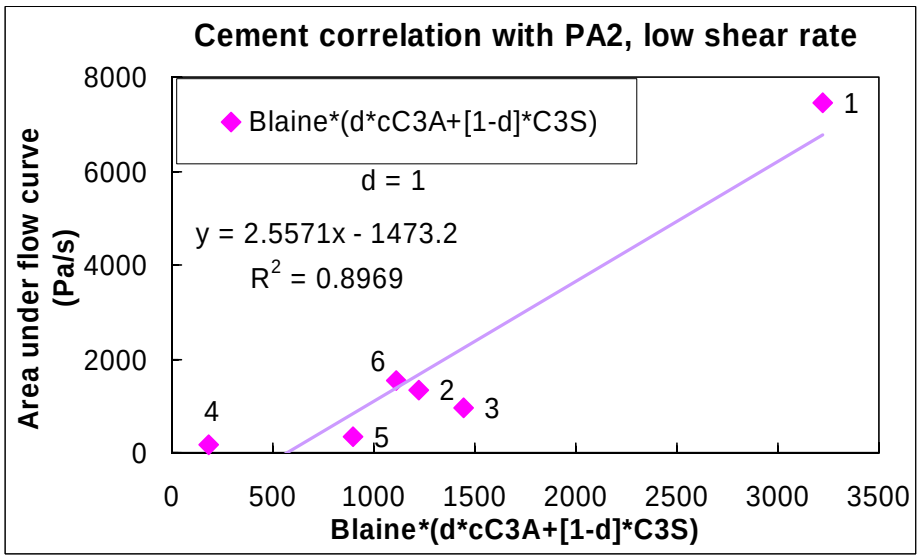
Cement correlation with PA2, low shear rate
Blaine*(d*cC3A+[1-d]*C3S)
d = 1
y = 2.5571x - 1473.2
R^2 = 0.8969
Area under flow curve (Pa/s)
Blaine*(d*cC3A+[1-d]*C3S)
8000
6000
4000
2000
0
0
500
1000
1500
2000
2500
3000
3500
1
2
3
4
5
6

A.2.8 Bingham data for cement type correlations

w/c = 0.40 0.53% SNF		Low shear rate			Medium shear rate		
Cement	**Time (Min)**	μ_{p_l} **(Pa·s)**	τ_{yl} **(Pa)**	$\mathbf{R^2}$	μ_{pm} **(Pa·s)**	τ_{ym} **(Pa)**	$\mathbf{R^2}$
1 CEM I 42.5 RR	20	2.637	97.68	0.9784	0.350	205.50	0.9963
	45	3.115	101.31	0.9933	0.333	245.46	0.9959
	70	3.429	112.01	0.9970	0.476	280.49	0.9995
	95	3.683	157.83	0.9990	1.044	344.52	0.9910
2 CEM I 42.5 R	20	0.089	39.96	0.9979	0.111	37.90	0.9981
	45	0.117	46.39	0.9901	0.113	46.10	0.9987
	70	0.178	53.93	0.9560	0.135	55.03	0.9990
	95	0.260	61.08	0.9115	0.159	64.50	0.9989
3 CEM II A-V 42.5 R	20	0.211	65.96	0.9578	0.177	67.16	0.9995
	45	0.693	66.20	0.8317	0.203	84.95	0.9888
	70	0.968	73.09	0.8697	0.241	101.31	0.9927
	95	1.258	80.93	0.9086	0.295	118.10	0.9995
4 CEM I 52.5 R-LA	20	0.027	-0.04	0.9845	0.065	-1.49	0.9983
	45	0.035	-0.04	0.9875	0.047	0.99	0.9913
	70	0.042	0.07	0.9950	0.048	1.14	0.9975
	95	0.051	0.21	0.9979	0.051	1.38	0.9981
5 CEM I 42.5 R-LA	20	0.073	1.56	0.9978	0.063	2.24	0.9969
	45	0.073	2.20	0.9959	0.065	2.30	0.9991
	70	0.079	3.09	0.9952	0.068	3.50	0.9990
	95	0.084	4.26	0.9947	0.072	4.88	0.9975
6 CEM I 42.5 N	20	0.093	14.55	0.9812	0.044	14.78	0.8601
	45	0.100	20.52	0.9732	0.108	18.65	0.9562
	70	0.108	27.10	0.9927	0.102	26.66	0.9324
	95	0.131	33.42	0.9648	0.076	37.24	0.9869

w/c=0.40 0.53% LS		Low shear rate			Medium shear rate		
Cement	**Time (min)**	μ_{pl} **(Pa·s)**	τ_{yl} **(Pa)**	$\mathbf{R^2}$	μ_{pm} **(Pa·s)**	τ_{ym} **(Pa)**	$\mathbf{R^2}$
1 CEM I 42.5 RR	20	0.216	33.94	0.9813	0.345	25.82	0.9984
	45	0.269	24.24	0.9983	0.277	24.41	0.9994
	70	0.304	21.19	0.9994	0.289	22.61	0.9996
	95	0.332	20.11	0.9999	0.310	21.55	0.9995
2 CEM I 42.5 R	20	0.089	-0.65	0.9875	0.157	-5.60	0.9982
	45	0.073	-0.47	0.9892	0.077	0.25	0.9994
	70	0.076	-0.46	0.9918	0.078	0.76	0.9967
	95	0.061	-0.47	0.9596	0.072	1.58	0.9968
3 CEM II A-V 42.5 R	20	0.120	-0.16	0.9997	0.101	2.25	0.9991
	45	0.123	-0.23	0.9995	0.115	0.55	1.0000
	70	0.127	-0.23	0.9996	0.121	0.32	0.9983
	95	0.130	-0.24	0.9995	0.125	0.43	0.9989
4 CEM I 52.5 R-LA	20	0.032	-0.30	0.9434	0.082	-2.90	0.9989
	45	0.018	-0.08	0.9631	0.051	-0.90	0.9993
	70	0.014	-0.06	0.9806	0.056	-1.10	0.9941
	95	0.015	-0.05	0.9850	0.062	-1.37	0.9945
5 CEM I 42.5 R-LA	20	0.060	-0.18	0.9978	0.050	1.87	0.9529
	45	0.052	-0.20	0.9943	0.048	1.15	0.9996
	70	0.055	-0.03	0.9891	0.043	2.17	0.9985
	95	0.054	-0.26	0.9910	0.048	1.57	0.9996

w/c=0.40 0.53% PA		Low shear rate			Medium shear rate		
Cement	**Time (min)**	μ_{pl} **(Pa·s)**	τ_{yl} **(Pa)**	$\mathbf{R^2}$	μ_{pm} **(Pa·s)**	τ_{ym} **(Pa)**	$\mathbf{R^2}$
1 CEM I 42.5 RR	20	0.182	24.43	0.9991	0.216	21.99	0.9990
	45	0.216	25.07	0.9996	0.192	27.61	0.9995
	70	0.249	27.66	0.9997	0.218	30.94	0.9998
	95	0.308	31.75	0.9998	0.275	34.57	0.9995
2 CEM I 42.5 R	20	0.109	3.07	0.9986	0.098	3.31	0.9994
	45	0.105	2.31	0.9987	0.085	3.75	1.0000
	70	0.109	2.20	0.9987	0.089	3.63	0.9995
	95	0.113	2.26	0.9988	0.092	3.77	0.9991
3 CEM II A-V 42.5 R	20	0.112	5.03	0.9998	0.144	2.24	0.9988
	45	0.098	3.76	0.9998	0.109	2.75	0.9988
	70	0.098	3.37	0.9998	0.111	2.05	0.9995
	95	0.098	3.25	0.9999	0.109	2.26	0.9986
4 CEM I 52.5 R-LA	20	0.010	0.00	0.9892	0.000	1.65	0.0724
	45	0.012	-0.02	0.9965	0.041	-1.10	0.9720
	70	0.014	-0.03	0.9963	0.041	-1.02	0.9817
	95	0.017	-0.03	0.9979	0.040	-0.77	0.9839
5 CEM I 42.5 R-LA	20	0.013	-0.02	0.9995	0.008	0.67	0.9412
	45	0.018	-0.03	0.9975	0.023	0.44	0.9986
	70	0.021	-0.04	0.9969	0.026	0.38	0.9997
	95	0.023	-0.01	0.9988	0.028	0.31	0.9997

w/c=0.32 0.61% SNF		Low shear rate			Medium shear rate		
Cement	**Time (min)**	μ_{pl} **(Pa·s)**	τ_{yl} **(Pa)**	R^2	μ_{pm} **(Pa·s)**	τ_{ym} **(Pa)**	R^2
2 CEM I 42.5 R	20	0.428	41.04	0.9494	0.320	48.65	0.9906
	45	0.460	51.73	0.9771	0.343	56.24	0.9766
	70	0.504	62.21	0.8269	0.376	62.74	0.9976
	95	0.620	70.12	0.9229	0.353	77.58	0.9700
3 CEM II A-V 42.5 R	20	0.712	57.16	0.9864	0.591	76.81	0.9961
	45	0.850	74.72	0.9308	0.649	77.89	0.9977
	70	1.164	89.25	0.9197	0.569	112.25	0.9966
	95	1.511	102.02	0.9239	0.544	139.62	0.9869
4 CEM I 52.5 R-LA	20	0.200	3.04	0.9145	0.260	-3.11	0.9899
	45	0.218	1.38	0.9160	0.174	5.67	0.9530
	70	0.154	5.13	0.7217	0.217	1.62	0.9729
	95	0.241	1.87	0.8859	0.245	0.29	0.9992
CEM I 52.5 N, White	20	0.379	6.84	0.9965	0.525	-4.14	0.9966
	45	0.350	7.87	0.9968	0.415	2.29	0.9963
	70	0.387	11.45	0.9992	0.470	1.58	0.9936
	95	0.453	18.13	0.9997	0.415	21.03	0.9959
5 CEM I 42.5 R-LA	20	0.312	24.90	0.9985	0.409	18.03	0.9930
	45	0.275	47.89	0.9966	0.396	41.68	0.9967
	70	0.290	74.03	0.9988	0.422	67.32	0.9967
	95	0.735	91.11	0.9363	0.464	100.59	0.9980
6 CEM I 42.5 N	20	0.840	88.42	0.8833	0.372	102.44	0.9958
	45	1.079	95.14	0.9253	0.389	117.47	0.9939
	70	1.260	105.52	0.9386	0.376	136.96	0.9904
	95	1.675	122.28	0.9711	0.350	180.50	0.9963

w/c=0.37 1% LS		Low shear rate			Medium shear rate		
Cement	**Time (min)**	μ_{pl} **(Pa·s)**	τ_{yl} **(Pa)**	$\mathbf{R^2}$	μ_{pm} **(Pa·s)**	τ_{ym} **(Pa)**	$\mathbf{R^2}$
1 CEM I 42.5 RR	20	1.583	90.63	0.9169	0.590	104.98	0.9780
	45	1.814	87.03	0.9333	0.494	103.13	0.9932
	70	0.839	105.60	0.5950	0.443	102.65	0.9995
	95	0.575	115.20	0.4715	0.473	103.80	0.9671
2 CEM I 42.5 R	20	0.138	2.63	0.6768	0.154	0.80	0.9944
	45	0.158	0.74	0.7851	0.117	4.05	0.8251
	70	0.132	1.51	0.9690	0.162	-2.39	0.8991
	95	0.151	0.13	0.9490	0.135	-0.15	0.9308
3 CEM II A-V 42.5 R	20	0.270	0.02	0.9990	0.204	7.51	0.9560
	45	0.254	0.20	0.9998	0.232	2.02	0.9026
	70	0.268	0.01	0.9992	0.212	5.33	0.9981
	95	0.268	-0.14	0.9994	0.256	-0.79	0.9775
4 CEM I 52.5 R-LA	20	0.118	-0.15	0.9649	0.106	5.26	0.9559
	45	0.138	-0.11	0.9921	0.149	0.02	0.9676
	70	0.132	-0.43	0.9802	0.118	2.60	0.9568
	95	0.124	-0.27	0.9843	0.090	6.26	0.8409
5 CEM I 42.5 R-LA	20	0.143	0.21	0.9965	0.107	3.31	0.9854
	45	0.128	0.19	0.9988	0.115	-0.13	0.9739
	70	0.128	0.29	0.9984	0.087	3.59	0.8156
	95	0.125	0.40	0.9991	0.086	3.35	0.9446
6 CEM I 42.5 N	20	0.177	0.84	0.9987	0.127	4.31	0.9123
	45	0.149	1.02	0.9989	0.105	4.57	0.8674
	70	0.146	1.07	0.9980	0.113	2.80	0.9036
	95	0.141	1.27	0.9965	0.136	-0.55	0.9258

w/c=0.32 0.61% PA		Low shear rate			Medium shear rate		
Cement	**Time (min)**	μ_{pl} **(Pa·s)**	τ_{yl} **(Pa)**	$\mathbf{R^2}$	μ_{pm} **(Pa·s)**	τ_{ym} **(Pa)**	$\mathbf{R^2}$
1 CEM I 42.5 RR	20	0.460	208.29	0.9860	1.421	138.48	0.9980
	45	0.439	156.14	0.9516	1.074	115.29	0.9947
	70	0.435	139.08	0.9698	0.932	110.26	0.9968
	95	0.468	133.22	0.9772	0.843	112.02	0.9981
2 CEM I 42.5 R	20	0.538	24.82	0.9998	0.568	22.62	0.9947
	45	0.519	17.42	0.9997	0.509	16.30	0.9972
	70	0.501	14.40	0.9994	0.464	15.06	0.9956
	95	0.480	12.84	0.9986	0.432	14.16	0.9989
3 CEM II A-V 42.5 R	20	0.594	12.56	0.9999	0.846	-11.02	0.9958
	45	0.549	11.26	1.0000	0.669	1.13	0.9995
	70	0.507	10.24	0.9999	0.636	-1.02	0.9981
	95	0.471	8.94	0.9997	0.597	-2.66	0.9972
CEM I 52.5 N, White	20	0.247	11.20	0.6523	0.514	-12.22	0.9957
	45	0.303	4.71	0.7885	0.531	-16.76	0.9747
	70	0.244	7.31	0.8607	0.511	-15.20	0.9962
	95	0.278	5.10	0.7482	0.565	-19.19	0.9882
4 CEM I 52.5 R-LA	20	0.192	0.39	0.9997	0.318	-10.49	0.9961
	45	0.192	0.20	0.9994	0.292	-8.88	0.9885
	70	0.195	-0.08	0.9986	0.291	-7.82	0.9893
	95	0.201	-0.29	0.9946	0.336	-13.26	0.9928
5 CEM I 42.5 R-LA	20	0.268	3.55	0.9953	0.416	-10.24	0.9642
	45	0.247	3.11	0.9998	0.458	-17.03	0.9973
	70	0.247	2.50	0.9998	0.459	-17.06	0.9958
	95	0.237	2.26	0.9985	0.477	-20.89	0.9964
6 CEM I 42.5 N	20	0.446	33.35	0.9999	0.555	22.50	0.9971
	45	0.357	17.23	0.9990	0.352	16.69	0.9995
	70	0.327	12.24	0.9986	0.312	11.28	0.9859
	95	0.311	9.79	0.9992	0.254	13.51	0.9832

A.2.9 Influence of Blaine on rheological properties

Characteristics of the 4 cements made of the same clinker, but ground to different fineness (Blaine).

Bingham parameters and gel strengths for the described cement pastes with w/c = 0.40 and 0.35% SNF per cement weight.

		Low shear rate range			**Medium shear rate range**			**Gel strenght**	
Blaine	**Time (min)**	μ_{pl} **(Pa·s)**	τ_{yl} **(Pa)**	$\mathbf{R^2}$	μ_{pm} **(Pa·s)**	τ_{ym} **(Pa)**	$\mathbf{R^2}$	$\tau_{10\text{sec}}$ **(Pa)**	$\tau_{10\text{min}}$ **(Pa)**
495	20	0.743	49	0.8904	0.170	71	0.9974	43	63
	45	1.127	54	0.9236	0.228	88	0.9932	63	107
	70	1.614	60	0.9710	0.323	110	0.9959	>90	>110
	95	1.846	78	0.9889	0.430	149	0.9884	>90	>110
444	20	0.225	34	0.9016	0.095	39	0.9986	22	37
	45	0.341	39	0.8842	0.107	48	0.9980	29	62
	70	0.588	45	0.8947	0.157	61	0.9982	42	43
	95	0.881	53	0.8896	0.228	75	0.9932	61	>80
392	20	0.109	20	0.9858	0.072	21	0.9975	16	27
	45	0.129	23	0.9754	0.068	26	0.9978	18	27
	70	0.167	26	0.9616	0.077	31	0.9994	20	41
	95	0.273	32	0.9441	0.103	39	0.9995	27	62
356	20	0.087	13	0.9924	0.059	15	0.9995	10	14
	45	0.093	15	0.9938	0.057	17	0.9966	12	17
	70	0.098	17	0.9933	0.059	19	0.9995	16	21
	95	0.114	20	0.9908	0.065	23	0.9989	18	27

A.3 Heat of hydration

A.3.1 Initial peak of hydration

Calorimetric measurements performed on cement pastes of Cements 1-6 as described by Table 3.1 - 3.3 in Chapter 3 with 0.32% Polyacrylate (PA2), SNF and lignosulfonate (LS). The w/c ratio was equal to 0.40 for all mixtures. All measurements consist of two parallels in order to monitor the reproducibility.

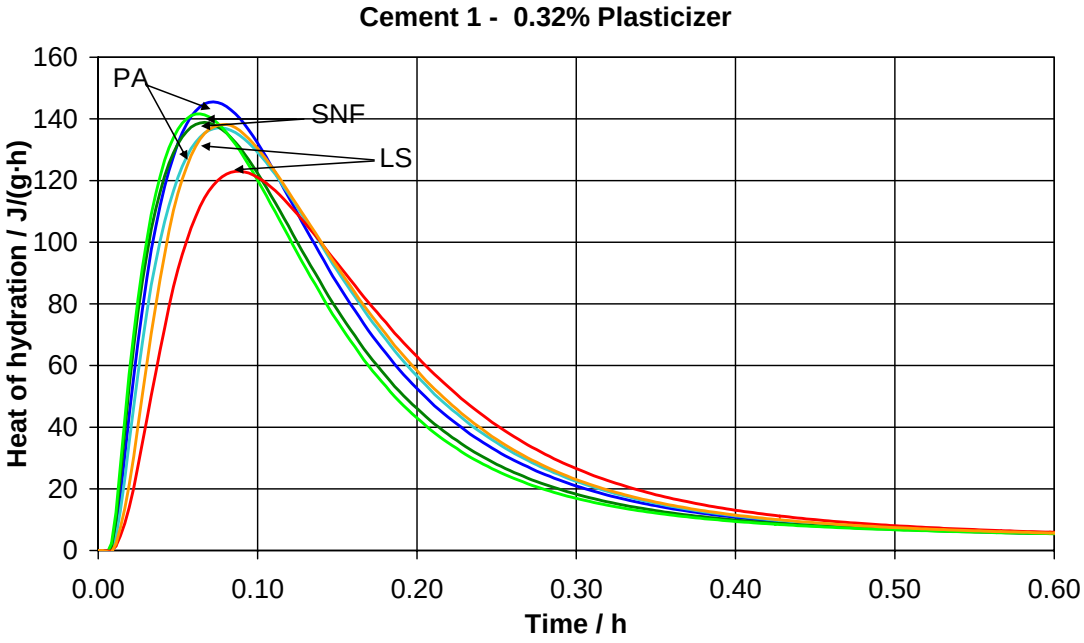

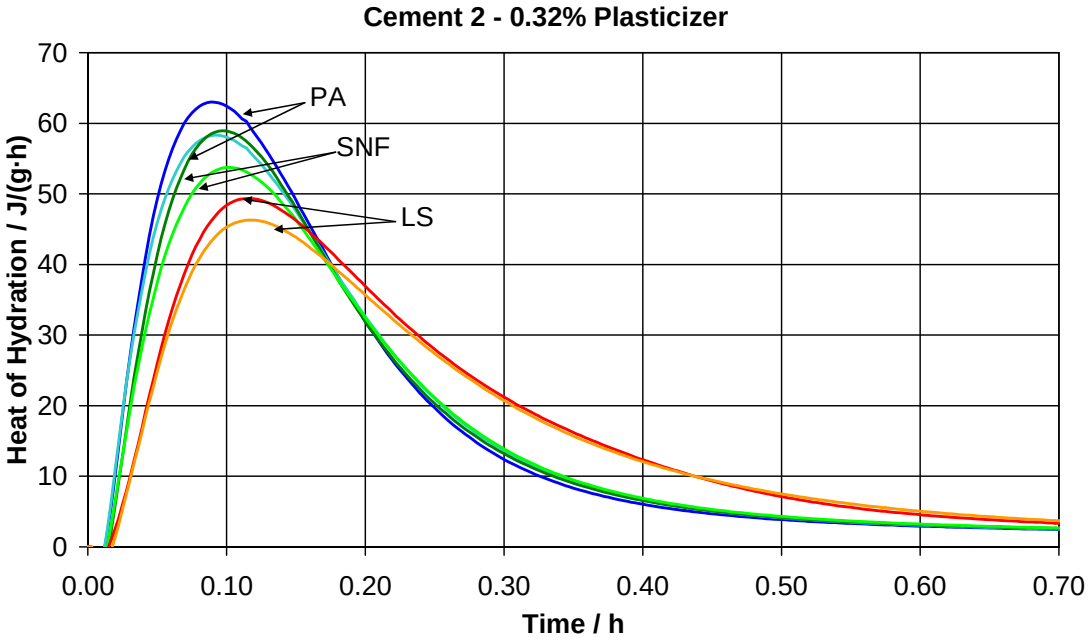

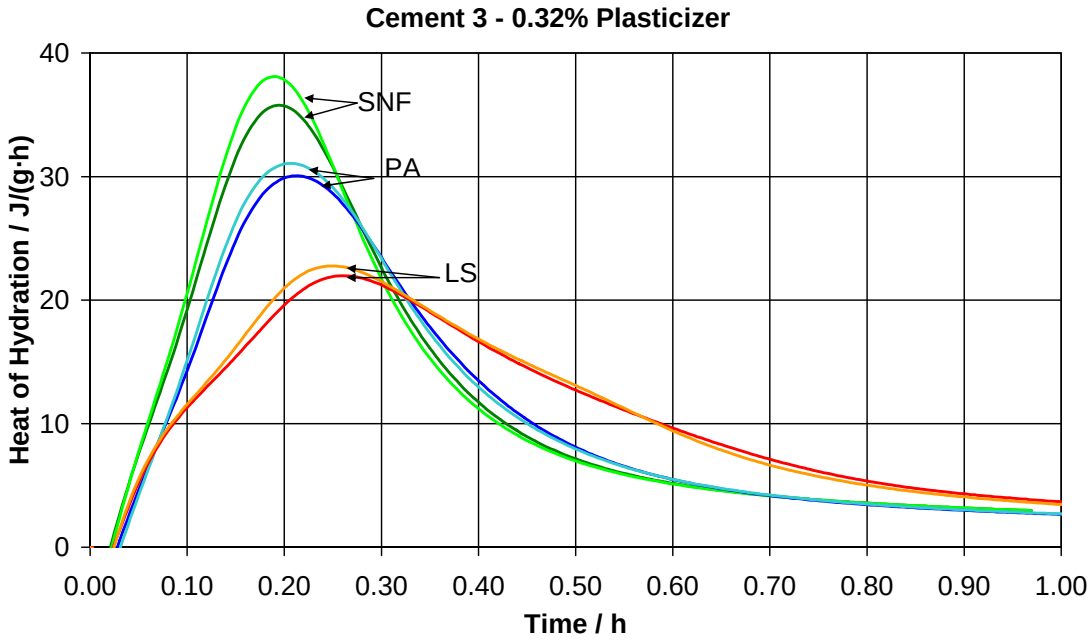
Cement 3 - 0.32% Plasticizer
Heat of Hydration / J/(g·h)
Time / h
SNF
PA
LS
0
10
20
30
40
0.00
0.10
0.20
0.30
0.40
0.50
0.60
0.70
0.80
0.90
1.00

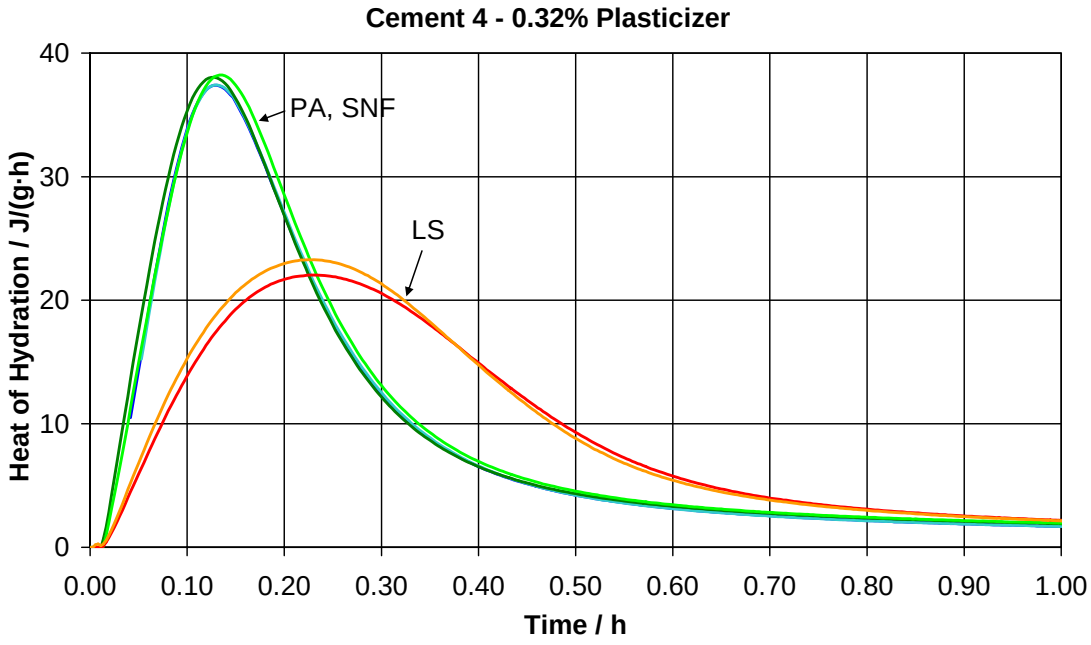
Cement 4 - 0.32% Plasticizer
Heat of Hydration / J/(g·h)
Time / h
PA, SNF
LS
0
10
20
30
40
0.00
0.10
0.20
0.30
0.40
0.50
0.60
0.70
0.80
0.90
1.00

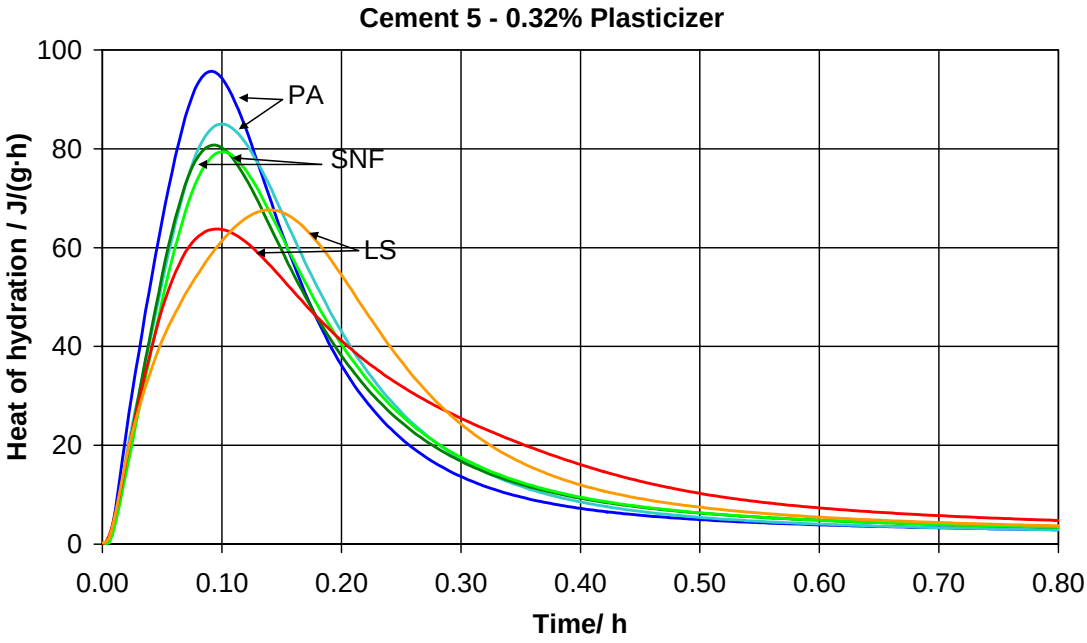
Cement 5 - 0.32% Plasticizer
Heat of hydration / J/(g·h)
Time/ h
PA
SNF
LS
0
20
40
60
80
100
0.00
0.10
0.20
0.30
0.40
0.50
0.60
0.70
0.80

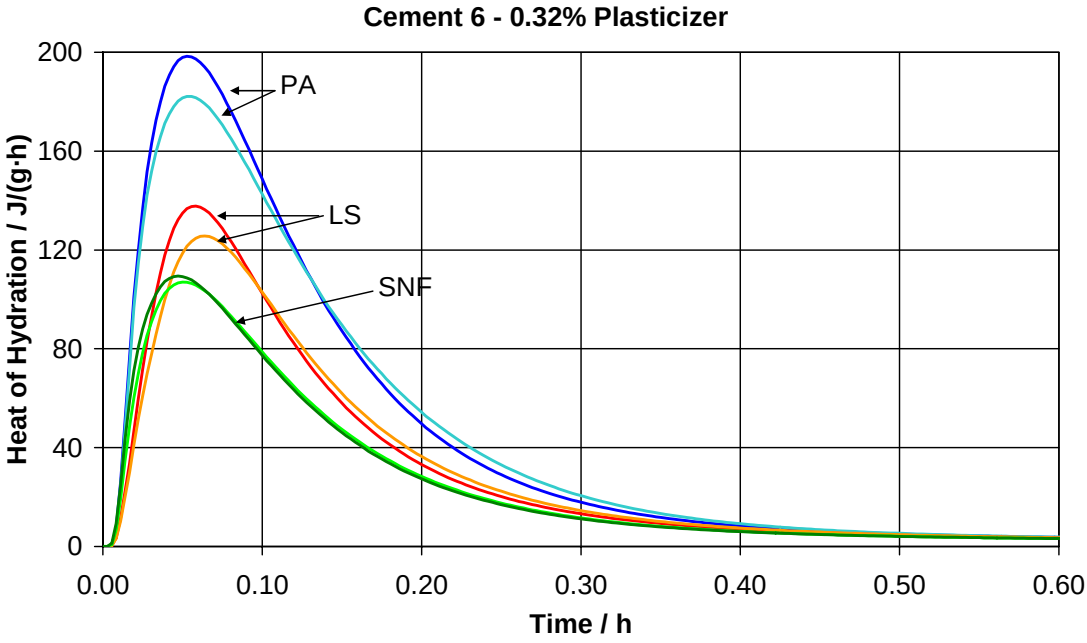
Cement 6 - 0.32% Plasticizer
Heat of Hydration / J/(g·h)
Time / h
PA
LS
SNF
0
40
80
120
160
200
0.00
0.10
0.20
0.30
0.40
0.50
0.60

A.3.2 Main heat of hydration

Calorimetric measurements performed on the Cements 1-4 and 6 (as described in Tables 3.1–3.3 in Chapter 3) with and without the superplasticizers Polyacrylate (PA2), SNF and lignosulfonate (LS). The w/c ratio was equal to 0.40 for all mixtures. All measurements consist of two parallels in order to monitor the reproducibility.

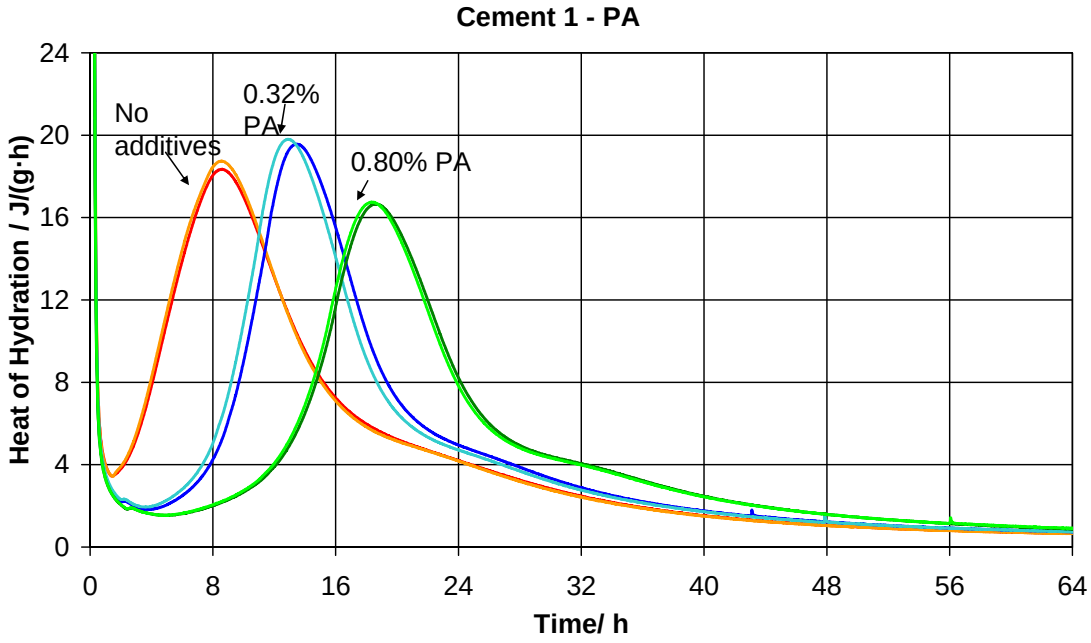

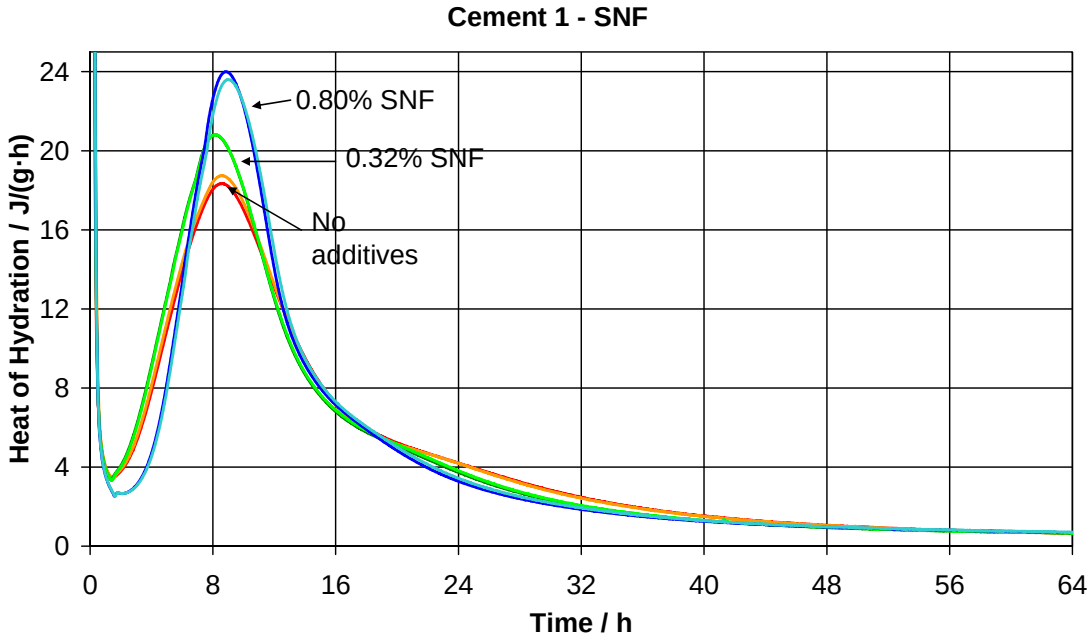

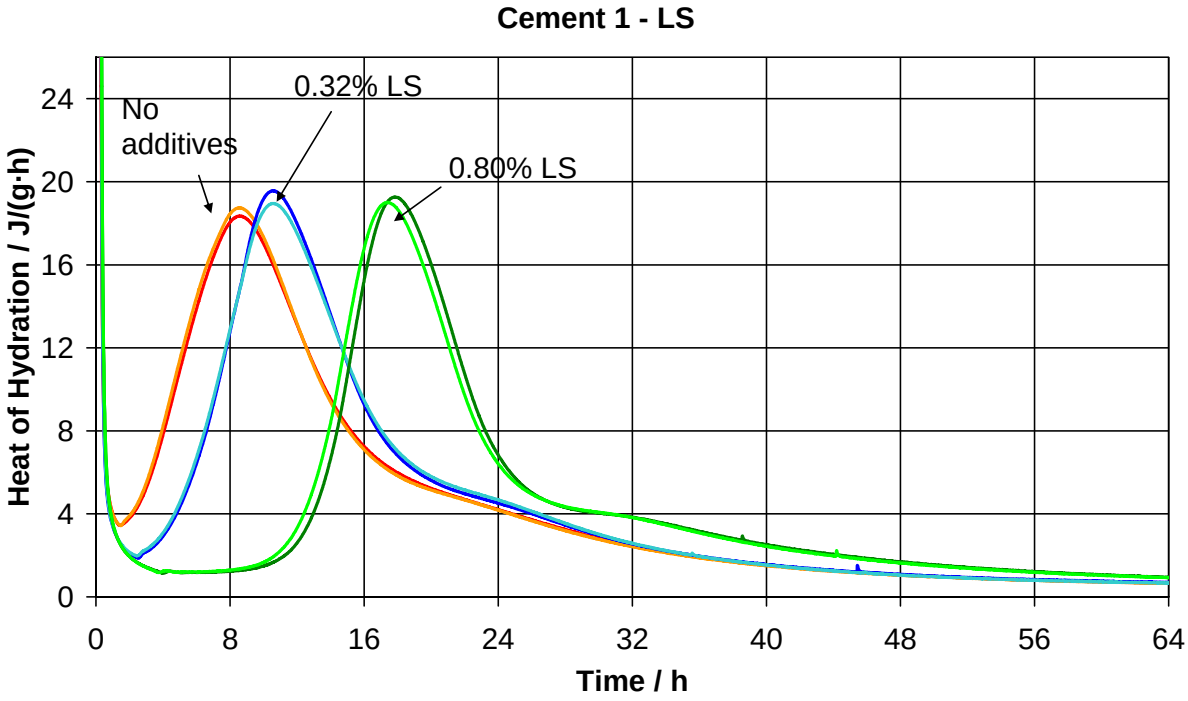
Cement 1 - LS
No additives
0.32% LS
0.80% LS
Heat of Hydration / J/(g·h)
Time / h
0
4
8
12
16
20
24
0
8
16
24
32
40
48
56
64

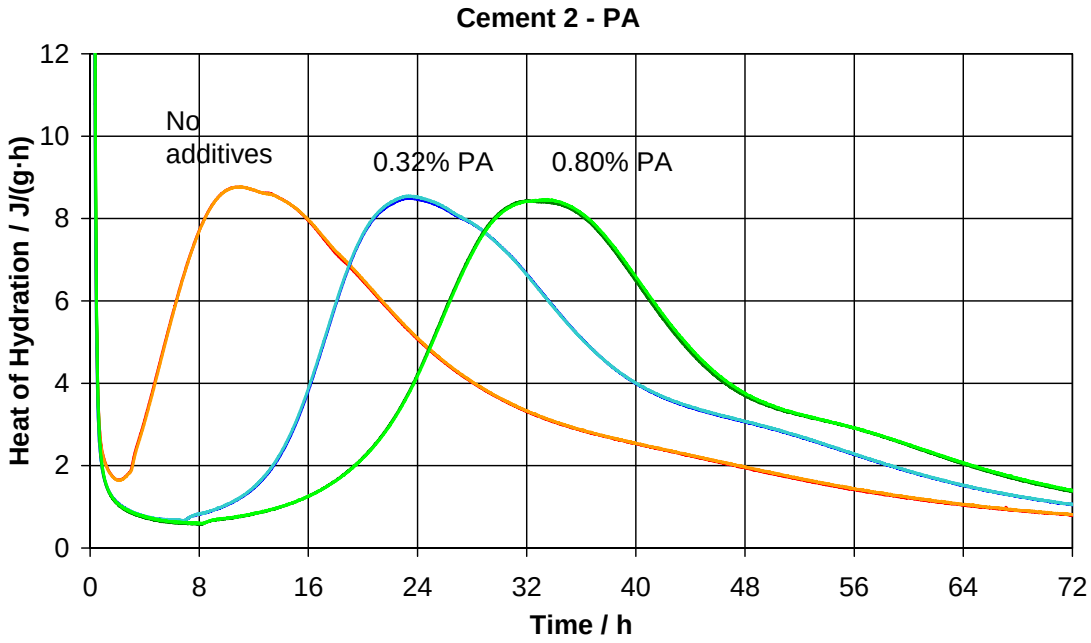
Cement 2 - PA
Heat of Hydration / J/(g·h)
Time / h
No additives
0.32% PA
0.80% PA
0
2
4
6
8
10
12
0
8
16
24
32
40
48
56
64
72

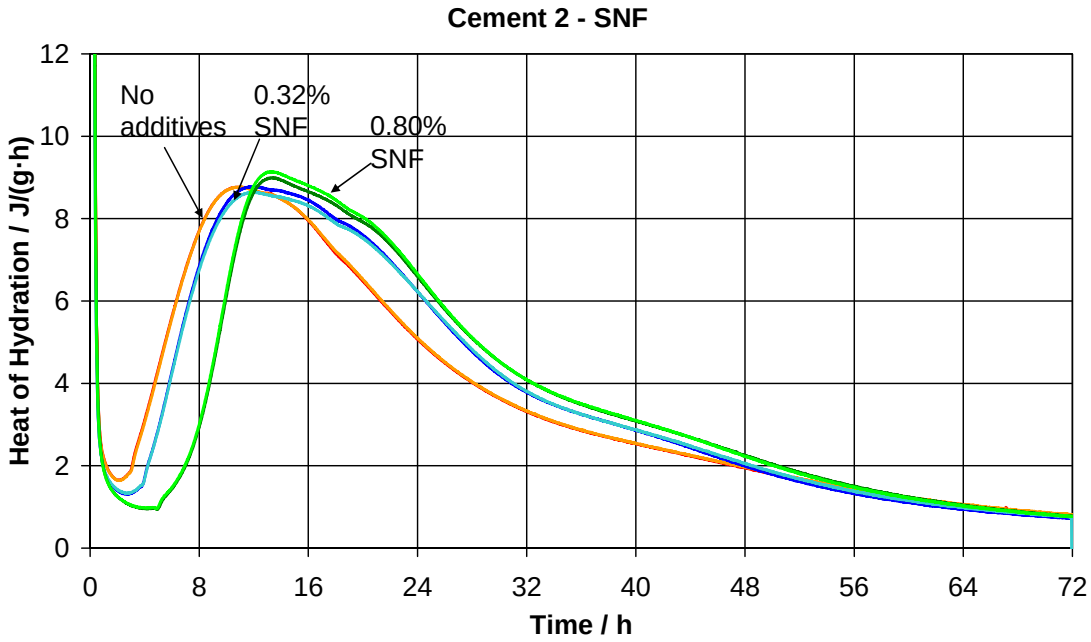
Cement 2 - SNF
Heat of Hydration / J/(g·h)
Time / h
No additives
0.32% SNF
0.80% SNF
0
2
4
6
8
10
12
0
8
16
24
32
40
48
56
64
72

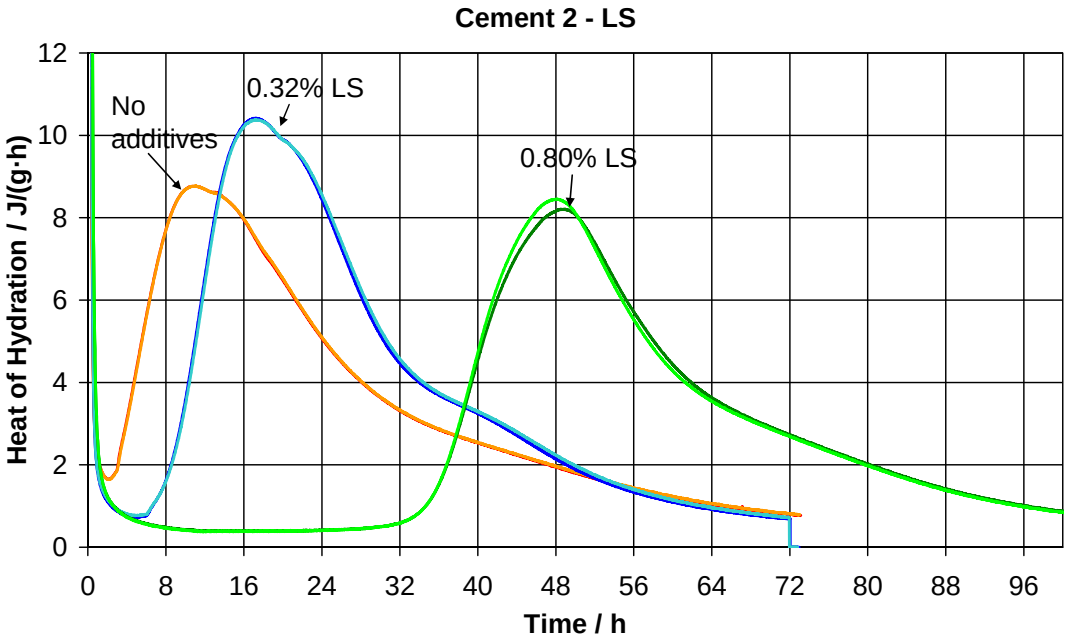
Cement 2 - LS
Heat of Hydration / J/(g·h)
Time / h
No additives
0.32% LS
0.80% LS
0
2
4
6
8
10
12
0
8
16
24
32
40
48
56
64
72
80
88
96

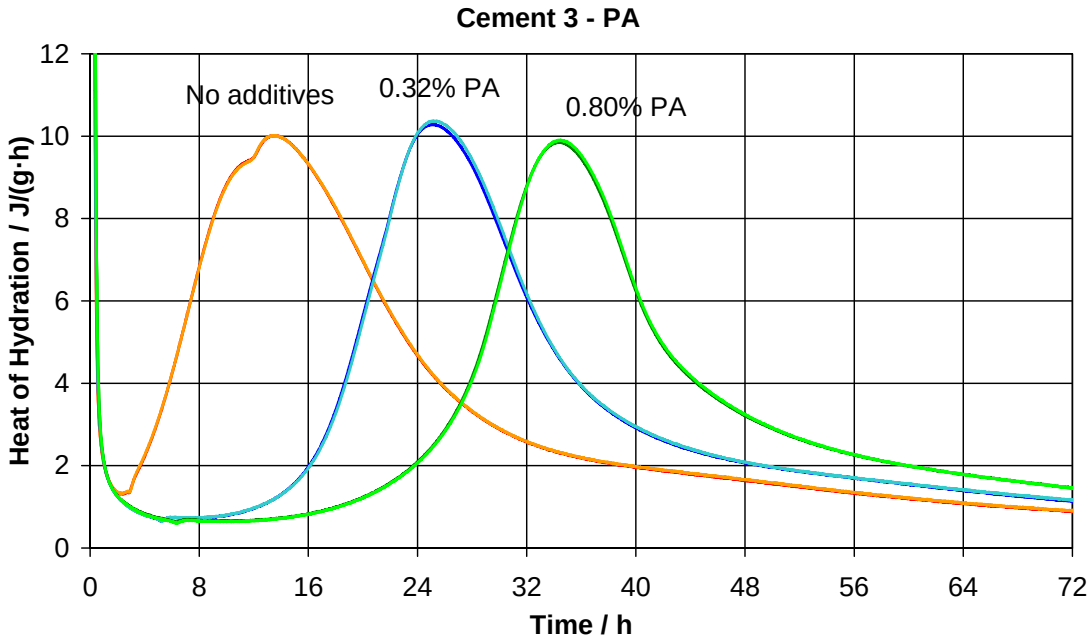
Cement 3 - PA
No additives
0.32% PA
0.80% PA
Heat of Hydration / J/(g·h)
Time / h
0
2
4
6
8
10
12
0
8
16
24
32
40
48
56
64
72

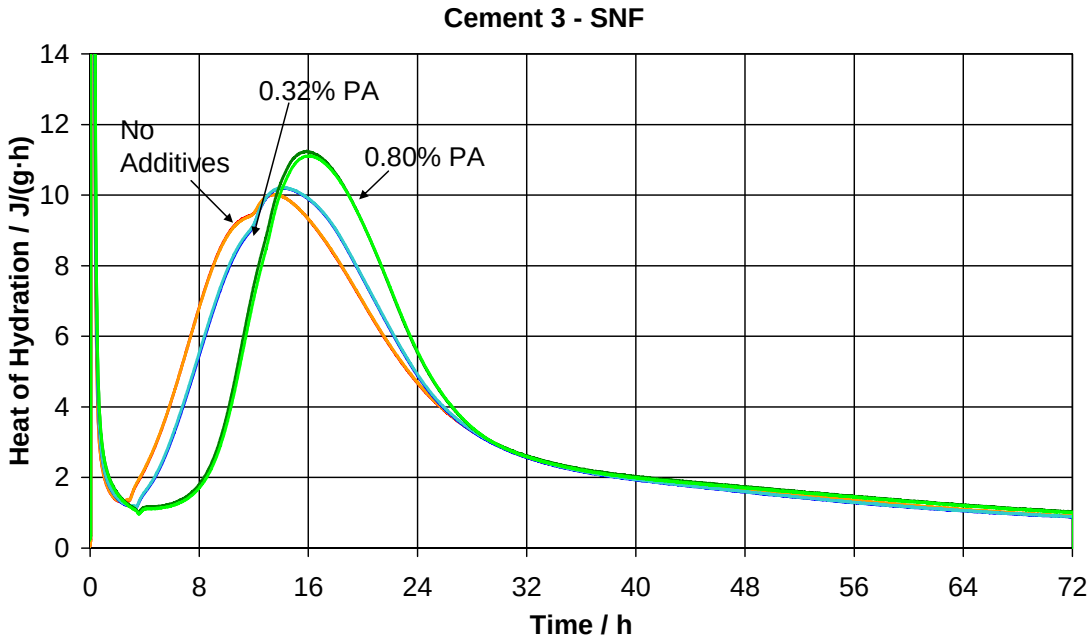
Cement 3 - SNF
0.32% PA
No
Additives
0.80% PA
Heat of Hydration / J/(g·h)
Time / h
0
2
4
6
8
10
12
14
0
8
16
24
32
40
48
56
64
72

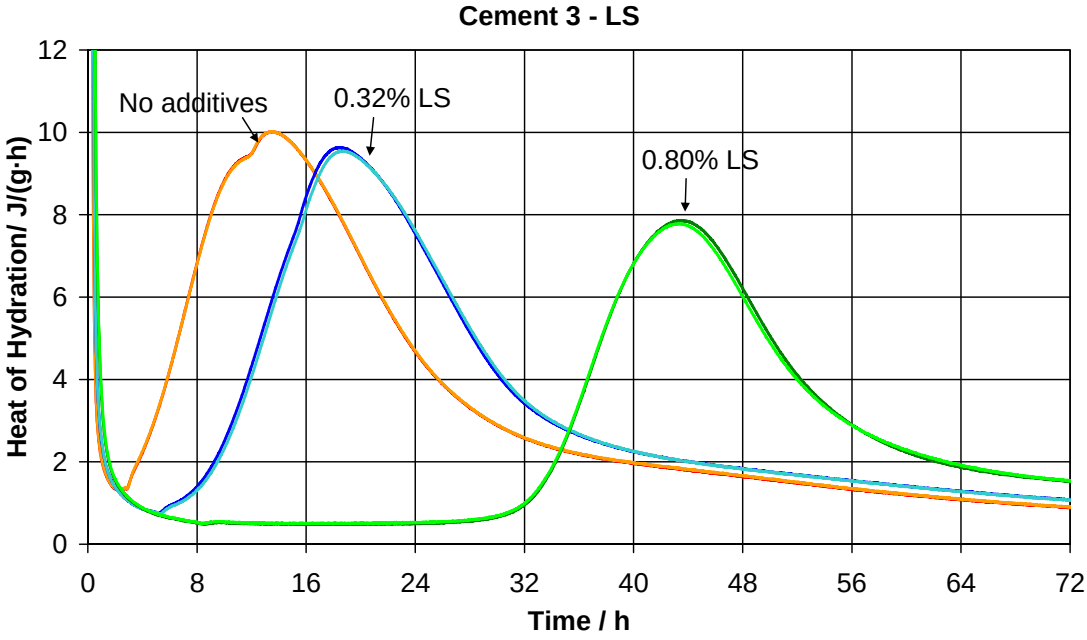
Cement 3 - LS
No additives
0.32% LS
0.80% LS
Heat of Hydration/ J/(g·h)
Time / h
0
2
4
6
8
10
12
0
8
16
24
32
40
48
56
64
72

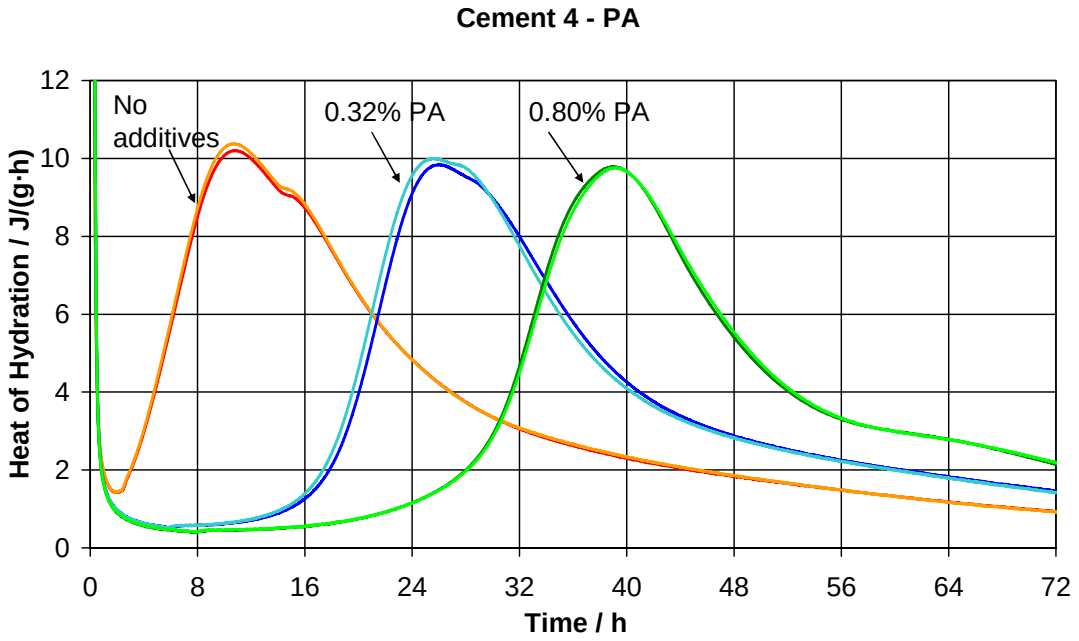
Cement 4 - PA
No additives
0.32% PA
0.80% PA
Heat of Hydration / J/(g·h)
Time / h
0
2
4
6
8
10
12
0
8
16
24
32
40
48
56
64
72

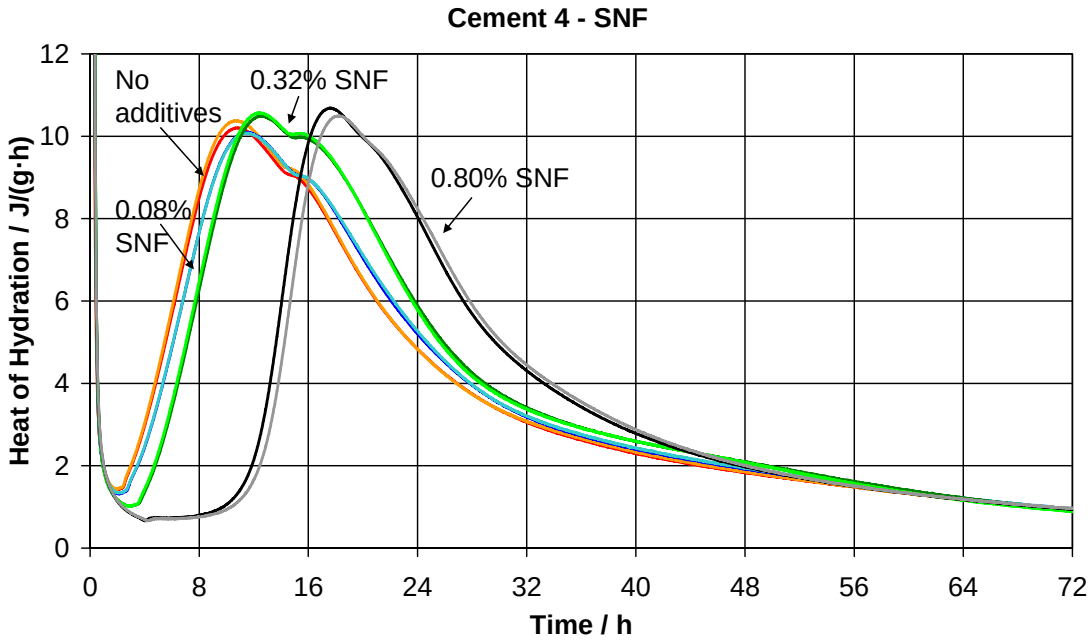
Cement 4 - SNF
No additives
0.32% SNF
0.80% SNF
0.08% SNF
Heat of Hydration / J/(g·h)
Time / h
0
2
4
6
8
10
12
0
8
16
24
32
40
48
56
64
72

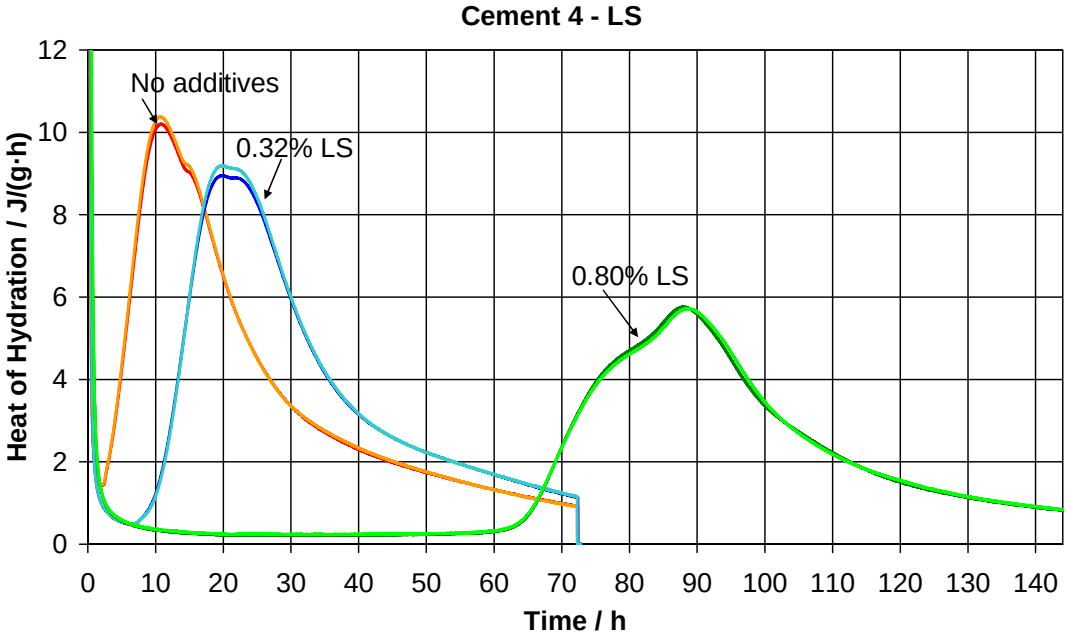
Cement 4 - LS
No additives
0.32% LS
0.80% LS
Heat of Hydration / J/(g·h)
Time / h
0
2
4
6
8
10
12
0
10
20
30
40
50
60
70
80
90
100
110
120
130
140

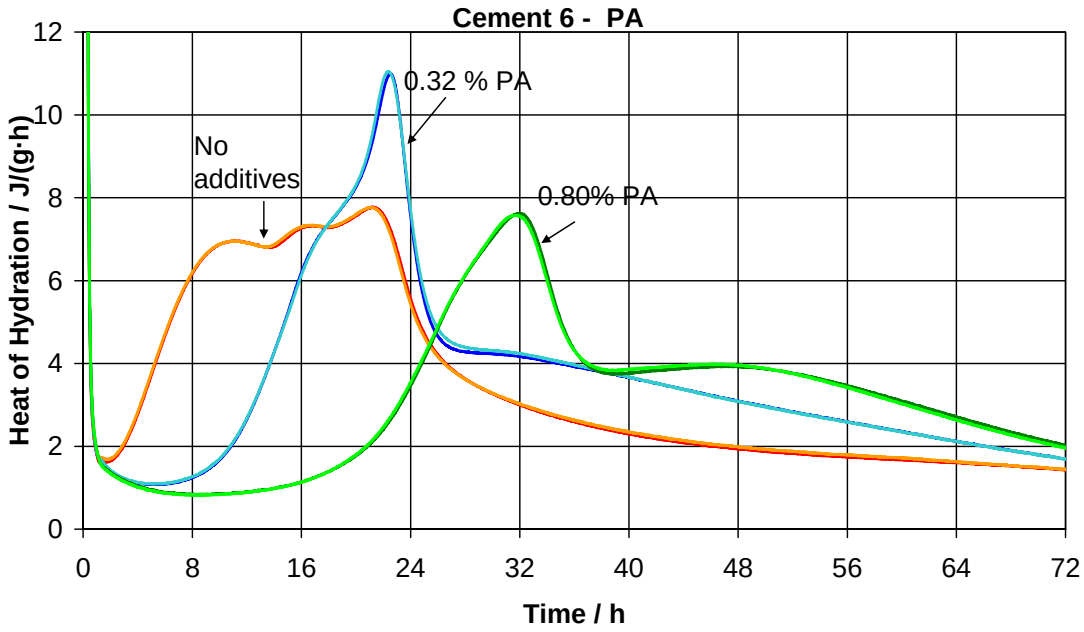
Cement 6 - PA
Heat of Hydration / J/(g·h)
Time / h
0.32 % PA
No additives
0.80% PA
0
2
4
6
8
10
12
0
8
16
24
32
40
48
56
64
72

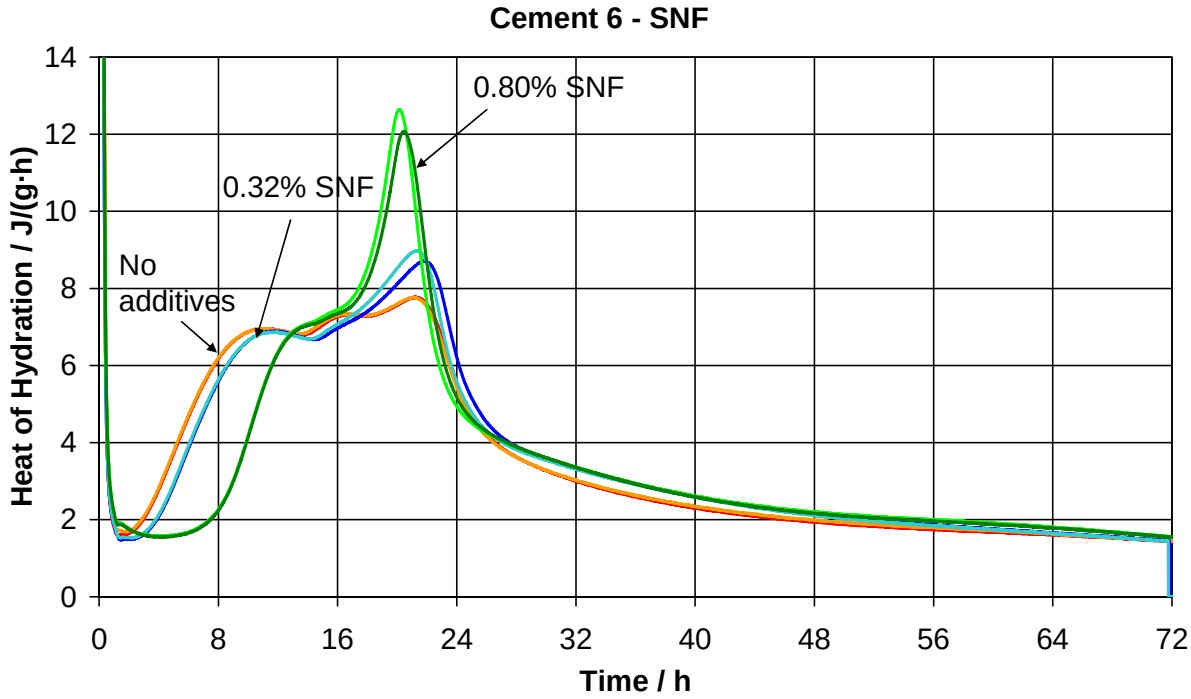
Cement 6 - SNF
Heat of Hydration / J/(g·h)
Time / h
0.80% SNF
0.32% SNF
No additives
0
2
4
6
8
10
12
14
0
8
16
24
32
40
48
56
64
72

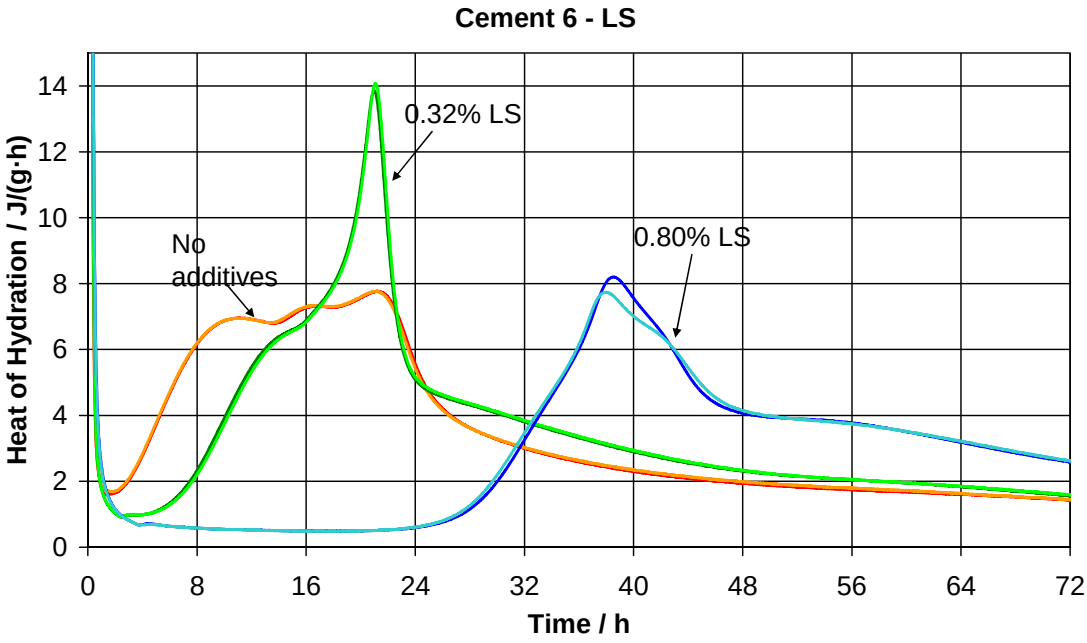
Cement 6 - LS
Heat of Hydration / J/(g·h)
Time / h
0.32% LS
0.80% LS
No additives
0
2
4
6
8
10
12
14
0
8
16
24
32
40
48
56
64
72

A.4 Calibration curves for UV-absorption measurements – SNF and lignosulphonate

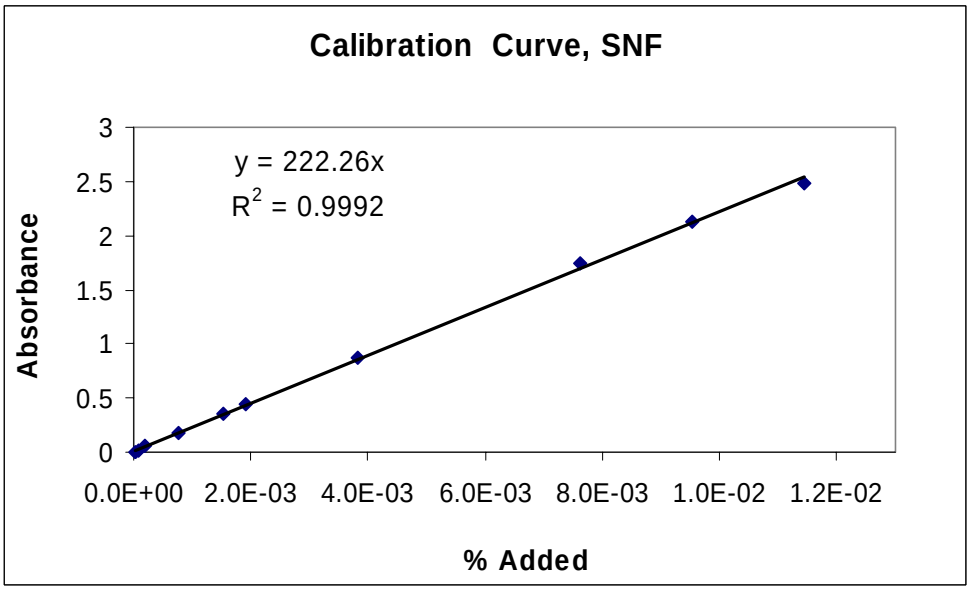

Fig. A.4-1: Calibration curve for absorbance of SNF.

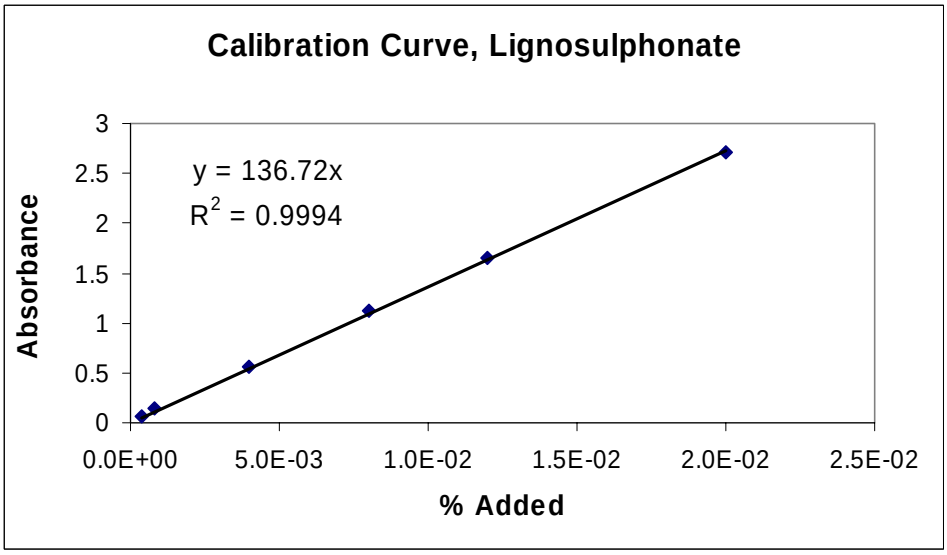

Fig. A.4-2: Calibration curve for absorbance of lignosulphonate.

A.5 ADSORPTION –FLOW RESISTANCE CURVES BY THE UV METHOD

Measurements by UV spectroscopy of consumed amount of SNF and LS superplasticizers on Cements 1-5. The superplasticizers were added with the water or delayed 5 minutes (D). The water cement ratio was 0.40 for all mixtures.

FR (low) = flow resistance at low shear rate range.

A.5.1 Pastes with SNF

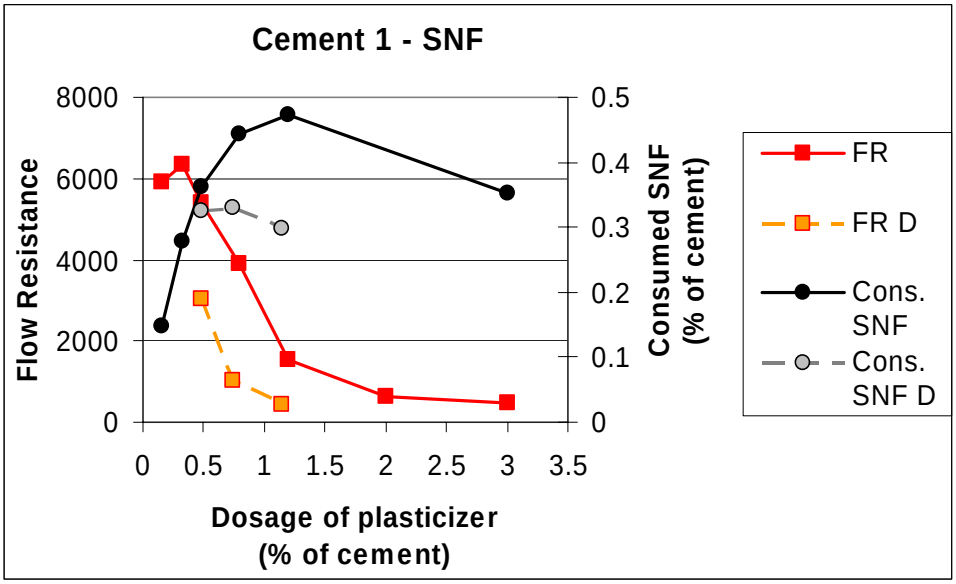

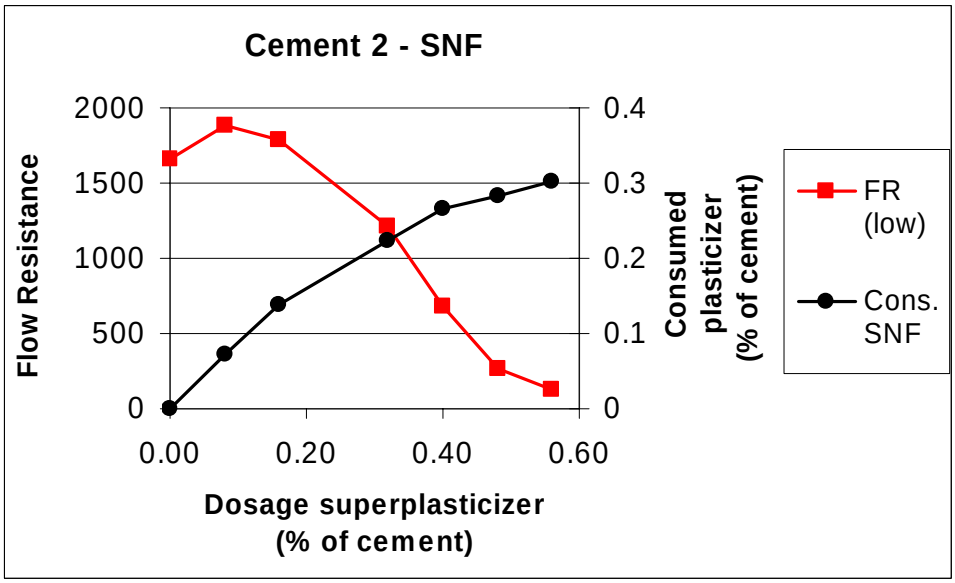

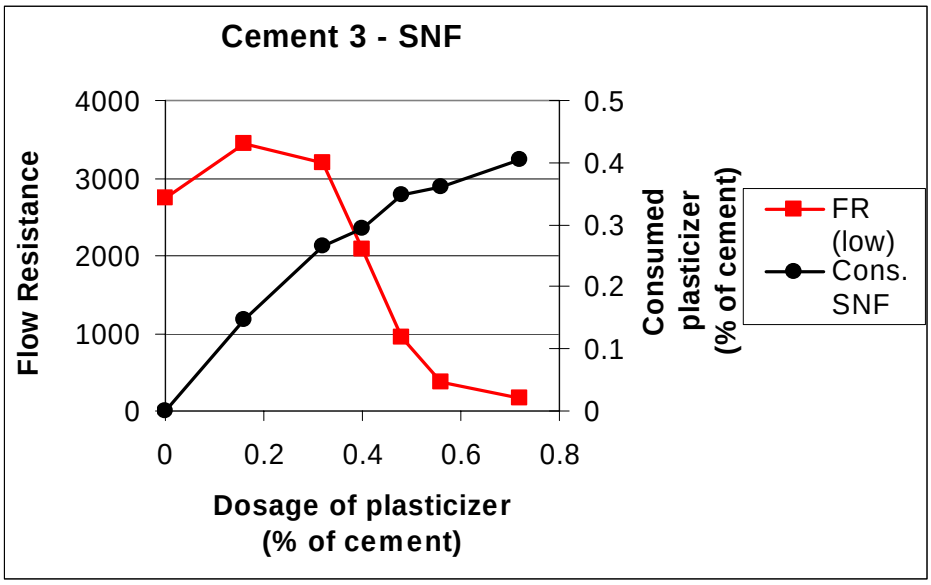
Cement 3 - SNF
Flow Resistance
4000
3000
2000
1000
0
0.5
0.4
0.3
0.2
0.1
0
0
0.2
0.4
0.6
0.8
Consumed plasticizer (% of cement)
Dosage of plasticizer (% of cement)
FR (low)
Cons. SNF

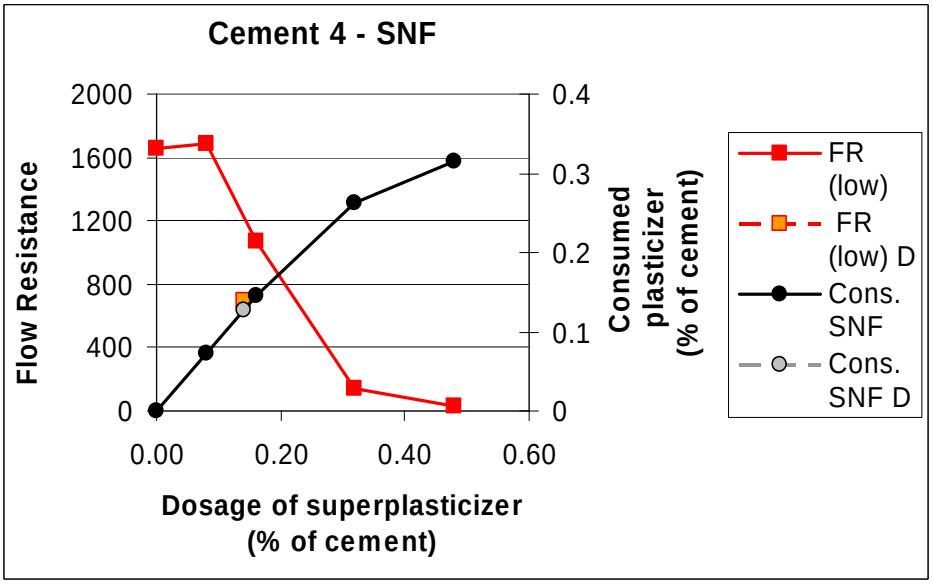
Cement 4 - SNF
Flow Resistance
2000
1600
1200
800
400
0
0.4
0.3
0.2
0.1
0
0.00
0.20
0.40
0.60
Consumed plasticizer (% of cement)
Dosage of superplasticizer (% of cement)
FR (low)
FR (low) D
Cons. SNF
Cons. SNF D

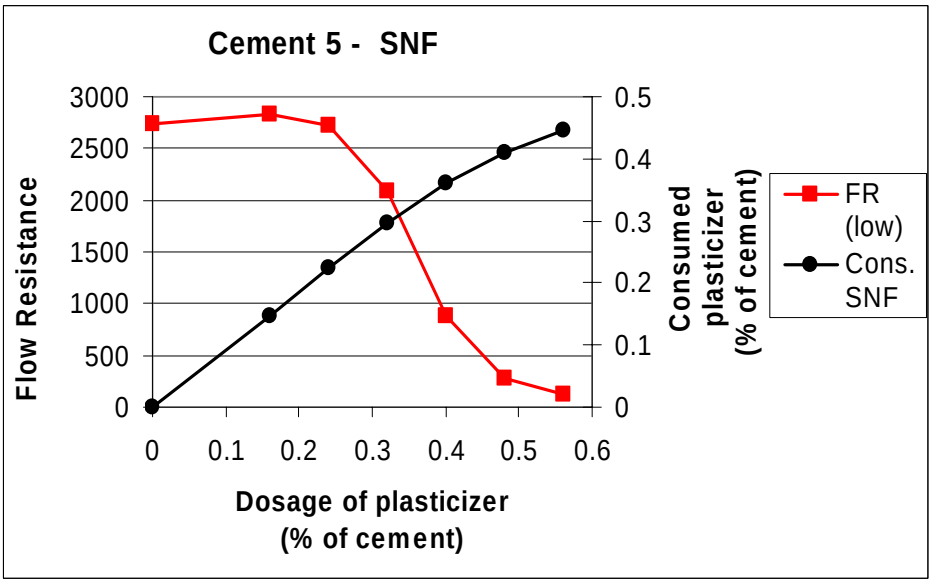
Cement 5 - SNF
Flow Resistance
3000
2500
2000
1500
1000
500
0
0.5
0.4
0.3
0.2
0.1
0
0
0.1
0.2
0.3
0.4
0.5
0.6
Consumed plasticizer (% of cement)
Dosage of plasticizer (% of cement)
FR (low)
Cons. SNF

A.5.2 Pastes with lignosulphonate

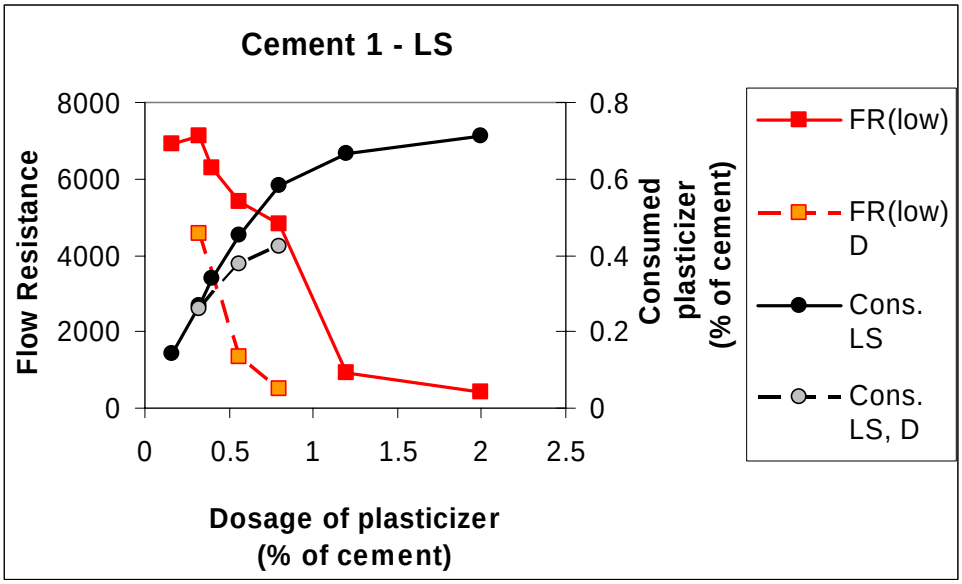

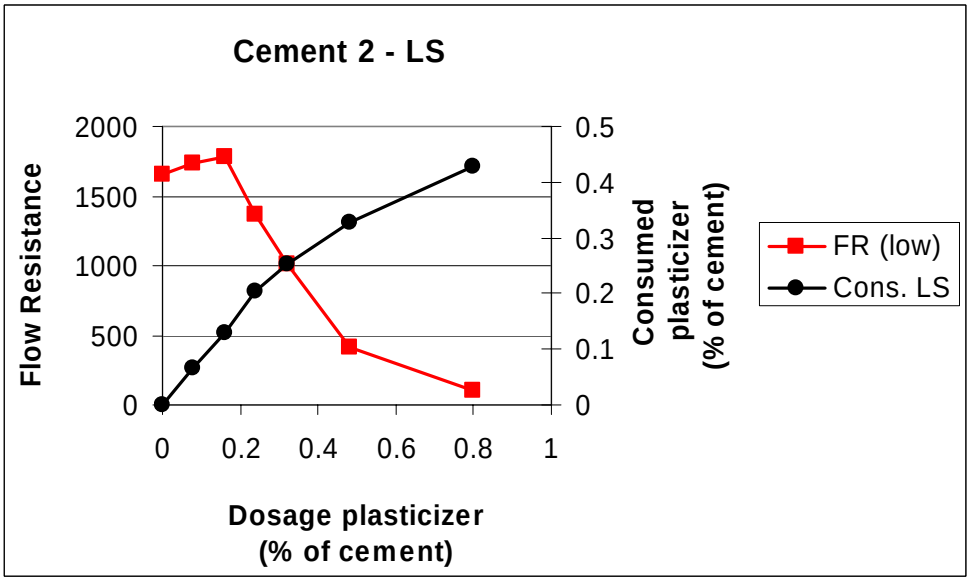

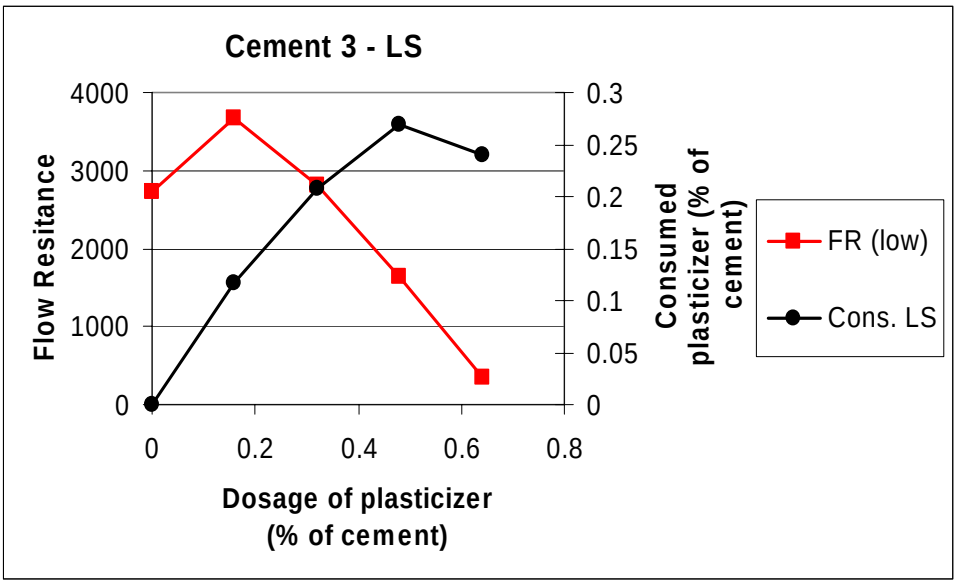
Cement 3 - LS
Flow Resitance
Consumed plasticizer (% of cement)
Dosage of plasticizer (% of cement)
FR (low)
Cons. LS

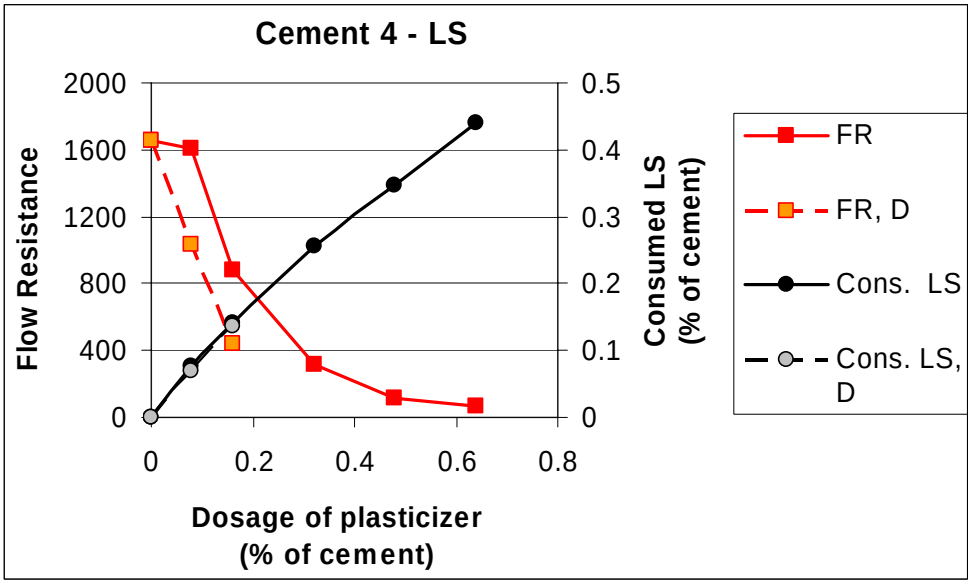
Cement 4 - LS
Flow Resistance
Consumed LS (% of cement)
Dosage of plasticizer (% of cement)
FR
FR, D
Cons. LS
Cons. LS, D

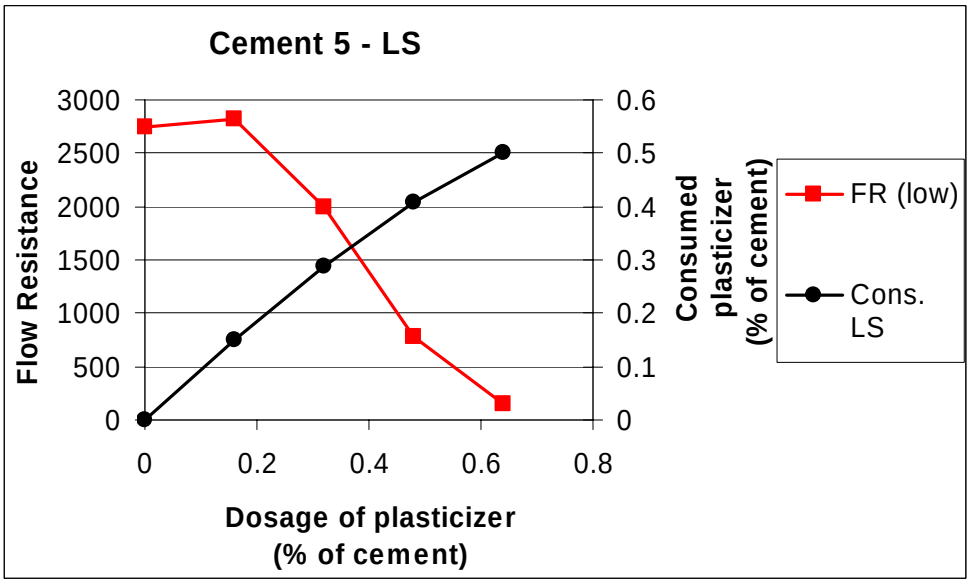
Cement 5 - LS
Flow Resistance
Consumed plasticizer (% of cement)
Dosage of plasticizer (% of cement)
FR (low)
Cons. LS

A.6 Flow Resistance – plasticizer consumption measured by TOC

Measurements of consumed amount of PA, SNF and LS superplasticizers on Cements 1-6 as described by Tables 3.1 – 3.3. The water cement ratio was ranged from 0.30 to 0.40 in order to achieve stable slurries.

FR (low) = flow resistance at low shear rate range.

A.6.1 Pastes with lignosulphonate

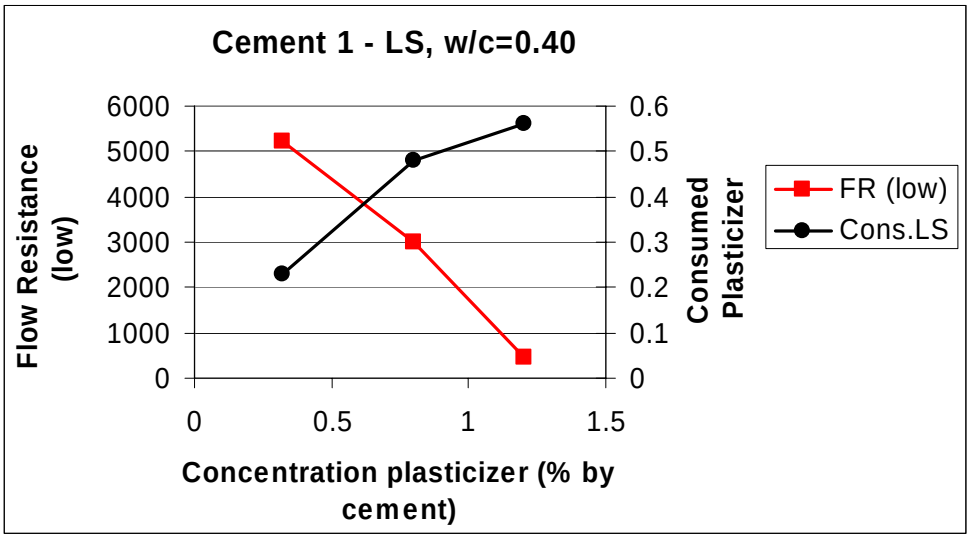

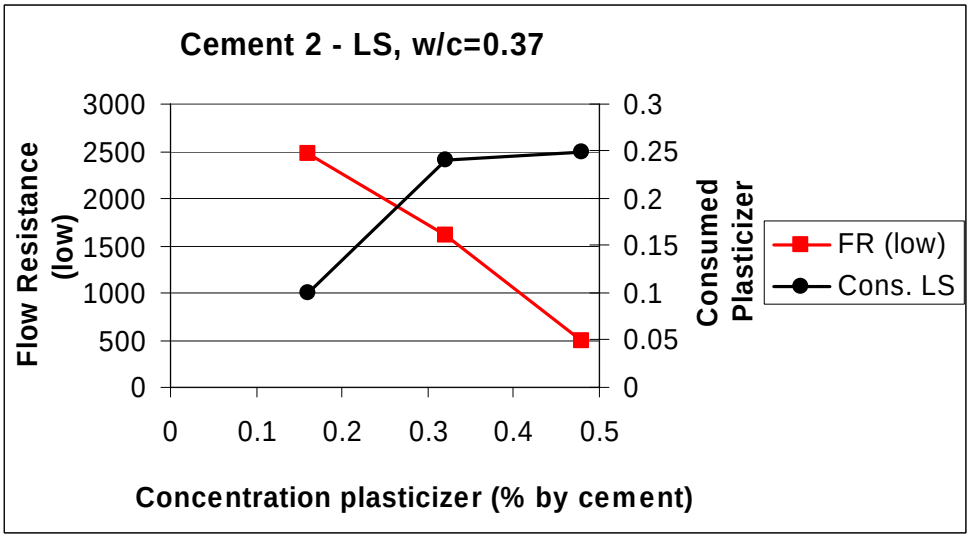

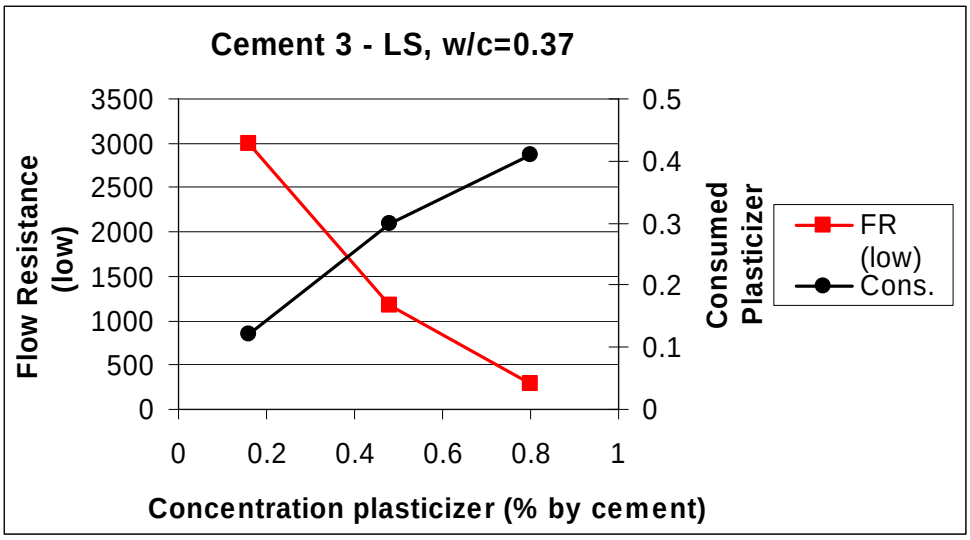
Cement 3 - LS, w/c=0.37
Flow Resistance (low)
Consumed Plasticizer
FR (low)
Cons.
Concentration plasticizer (% by cement)

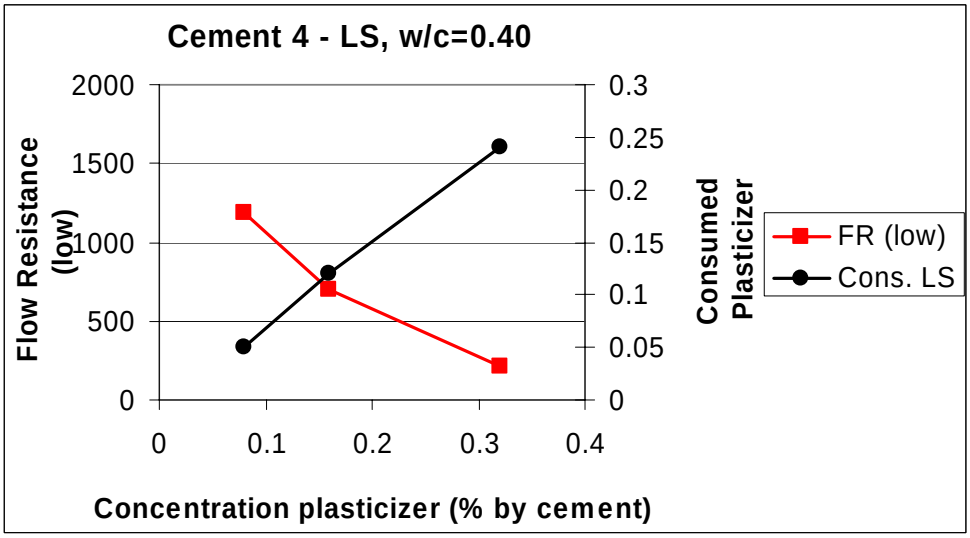
Cement 4 - LS, w/c=0.40
Flow Resistance (low)
Consumed Plasticizer
FR (low)
Cons. LS
Concentration plasticizer (% by cement)

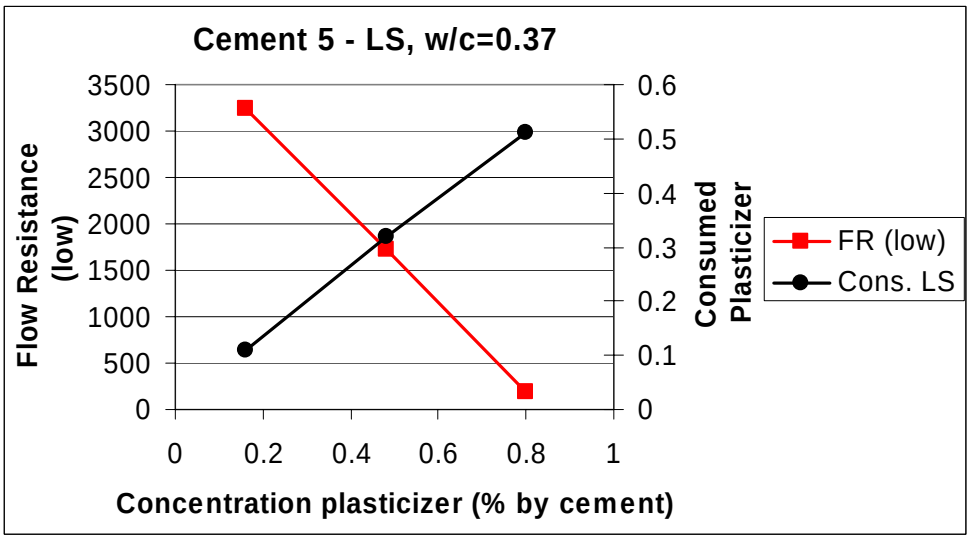
Cement 5 - LS, w/c=0.37
Flow Resistance (low)
Consumed Plasticizer
FR (low)
Cons. LS
Concentration plasticizer (% by cement)

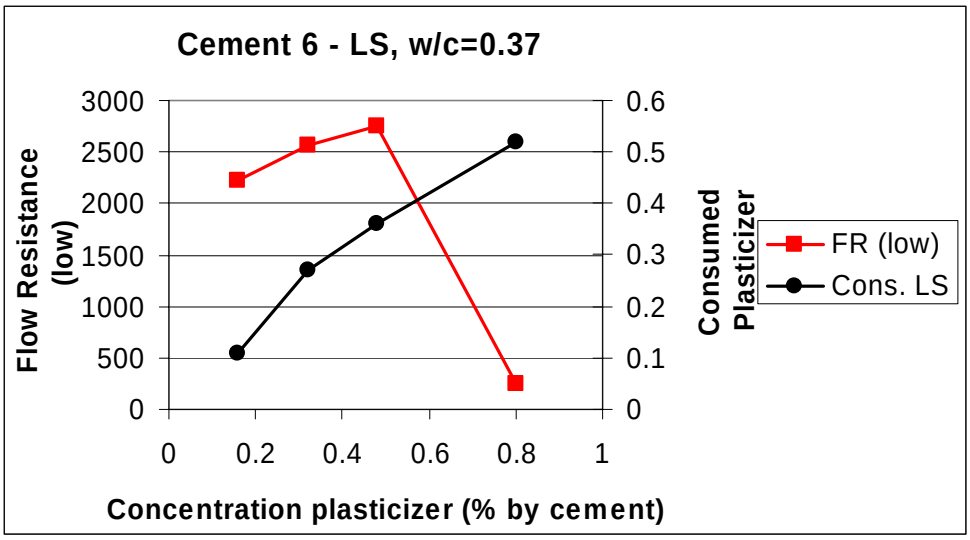
Cement 6 - LS, w/c=0.37
Flow Resistance (low)
3000
2500
2000
1500
1000
500
0
0.6
0.5
0.4
0.3
0.2
0.1
0
Consumed Plasticizer
0
0.2
0.4
0.6
0.8
1
Concentration plasticizer (% by cement)
FR (low)
Cons. LS

A.6.2 Pastes with SNF

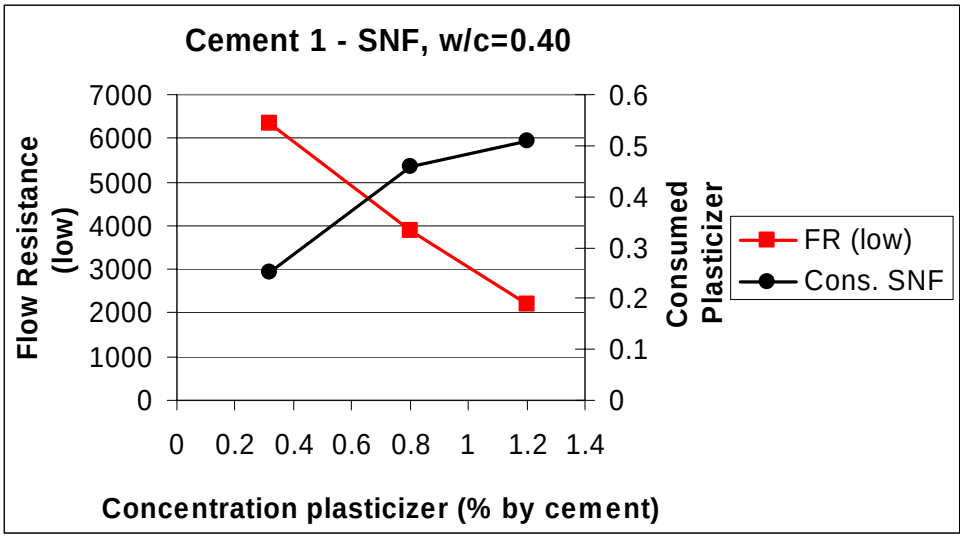

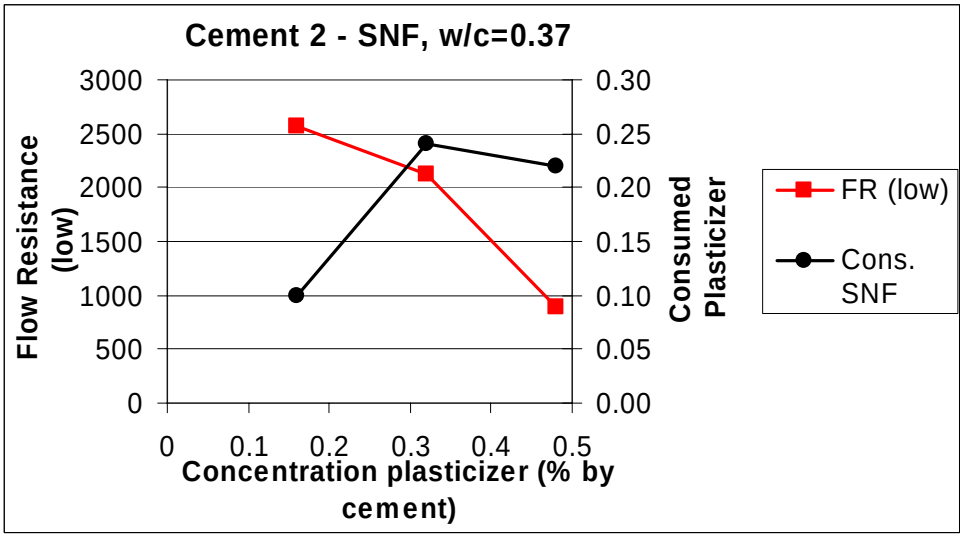

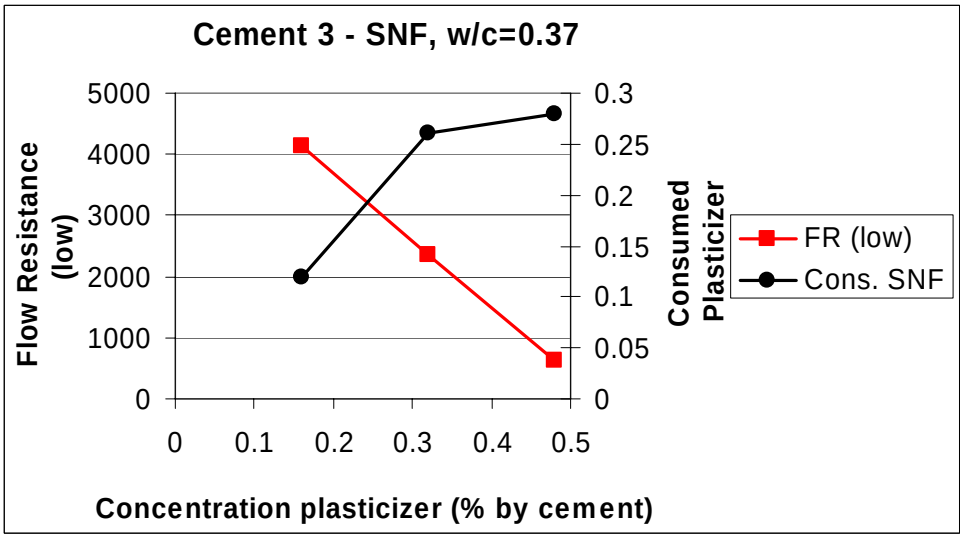

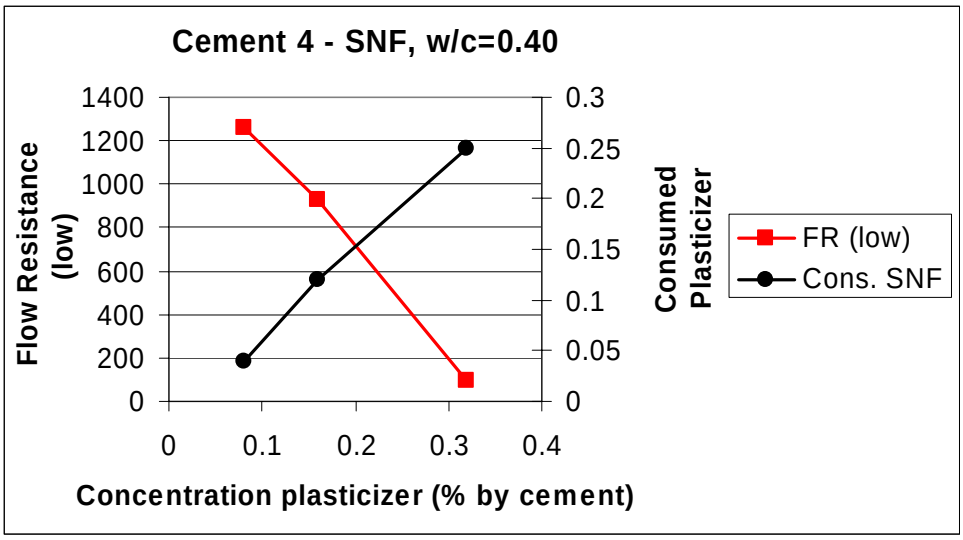
Cement 4 - SNF, w/c=0.40
Flow Resistance (low)
Consumed Plasticizer
FR (low)
Cons. SNF
Concentration plasticizer (% by cement)

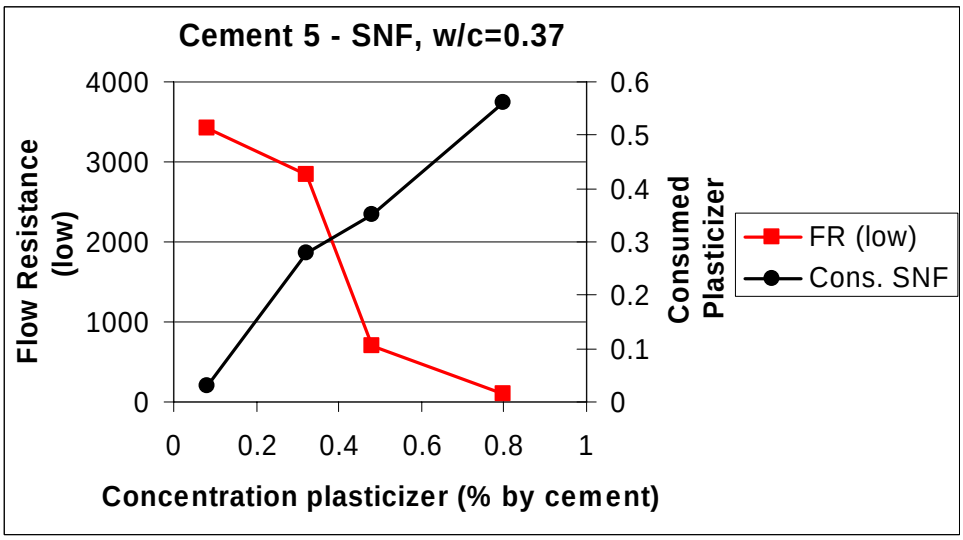
Cement 5 - SNF, w/c=0.37
Flow Resistance (low)
Consumed Plasticizer
FR (low)
Cons. SNF
Concentration plasticizer (% by cement)

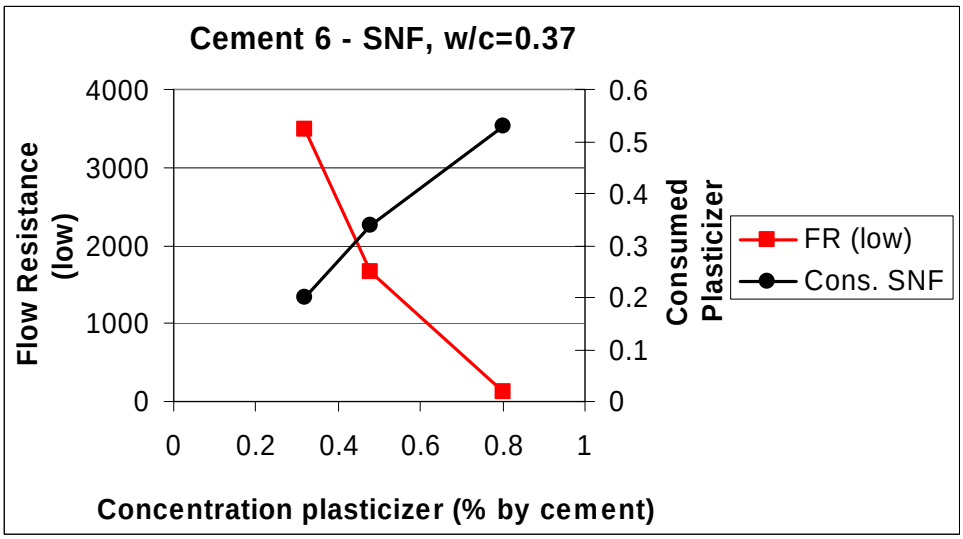
Cement 6 - SNF, w/c=0.37
Flow Resistance (low)
Consumed Plasticizer
FR (low)
Cons. SNF
Concentration plasticizer (% by cement)

A.6.3 Pastes with Polyacrylate (PA2)

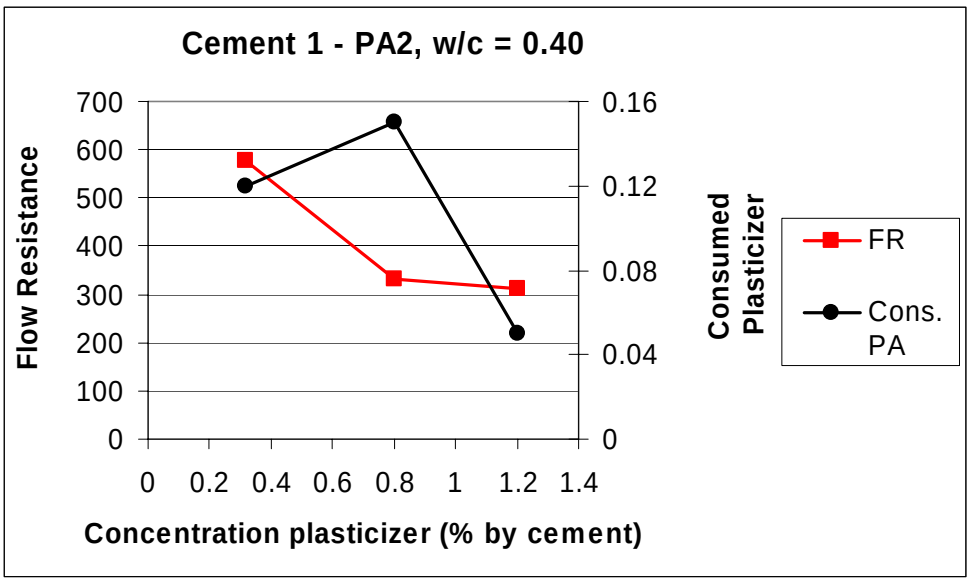

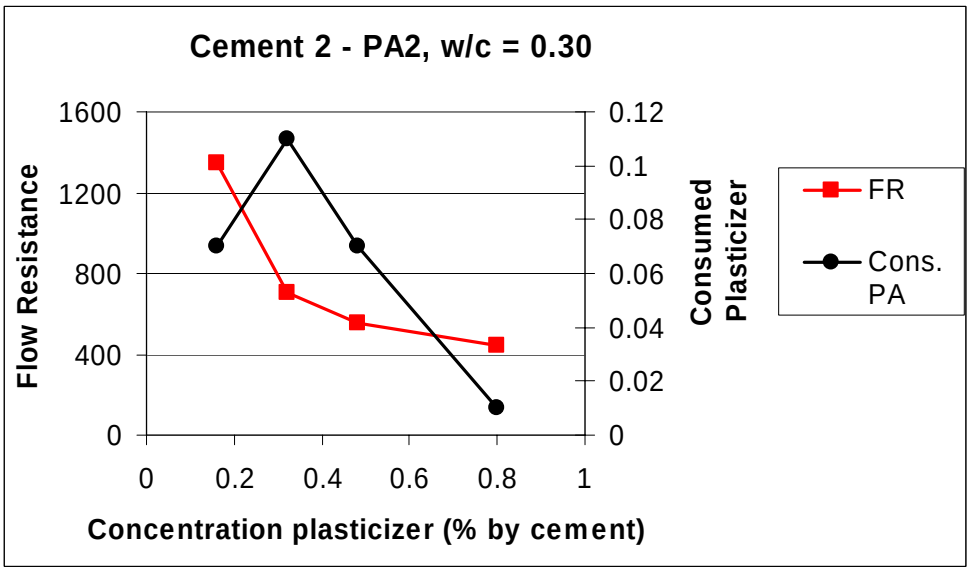

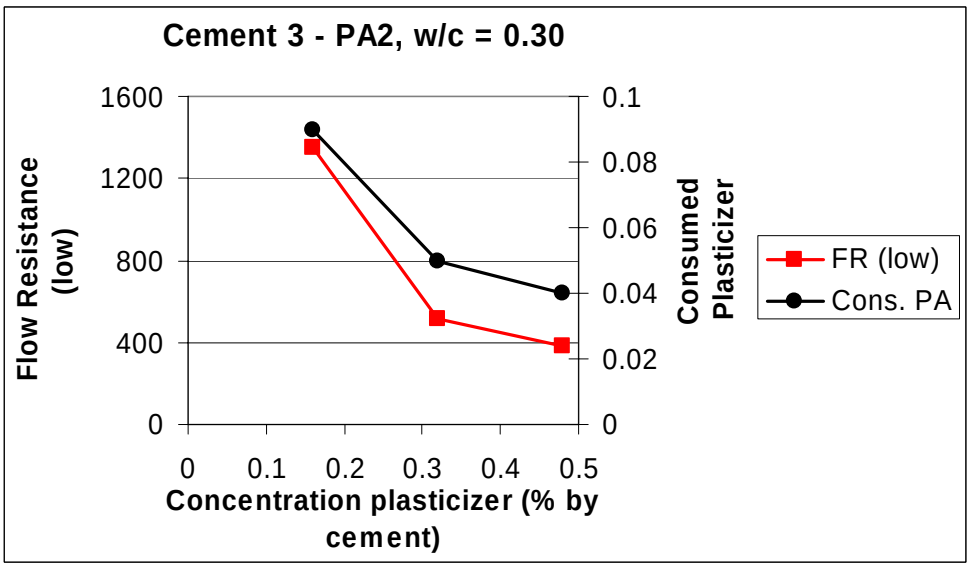

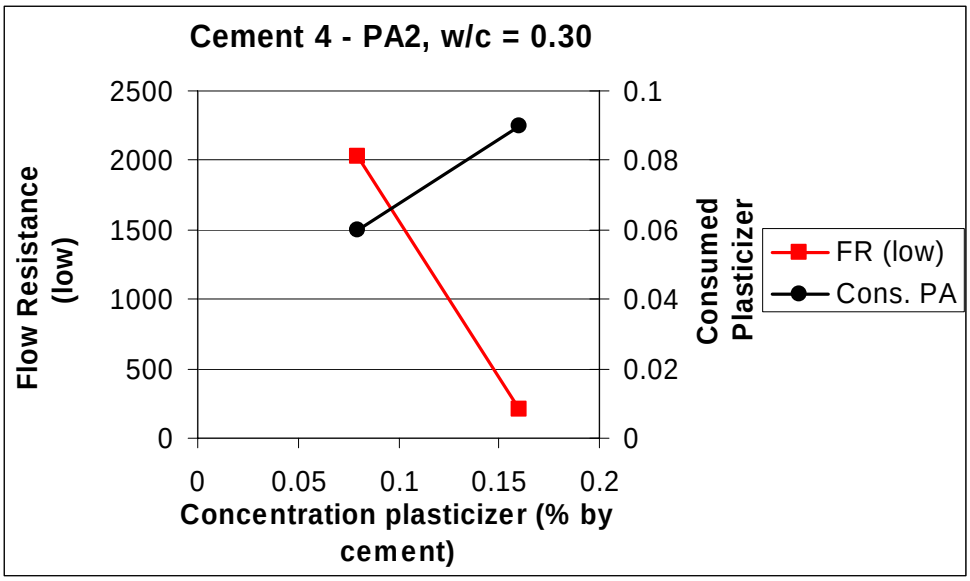
Cement 4 - PA2, w/c = 0.30
Flow Resistance (low)
2500
2000
1500
1000
500
0
0.1
0.08
0.06
0.04
0.02
0
Consumed Plasticizer
0
0.05
0.1
0.15
0.2
Concentration plasticizer (% by cement)
FR (low)
Cons. PA

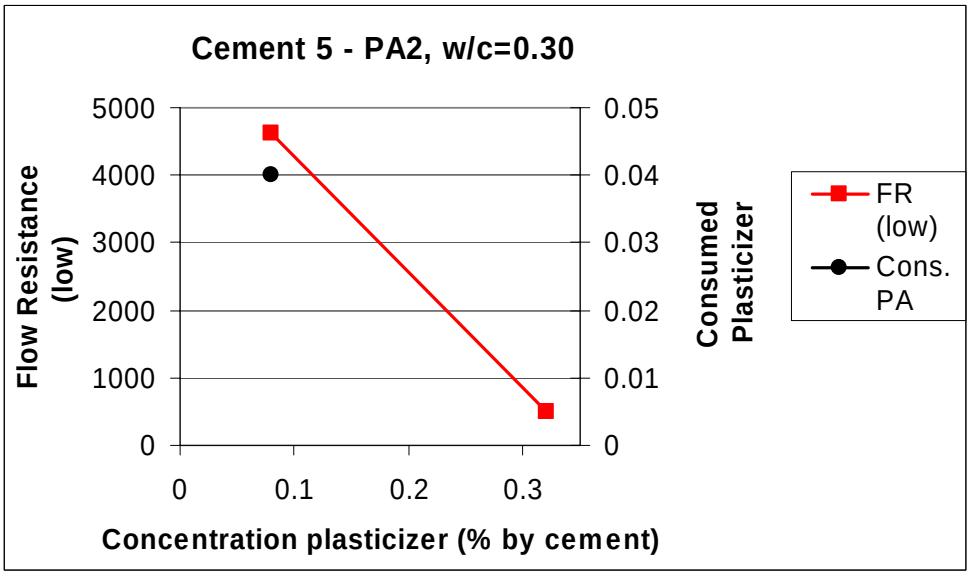
Cement 5 - PA2, w/c=0.30
Flow Resistance (low)
5000
4000
3000
2000
1000
0
0.05
0.04
0.03
0.02
0.01
0
Consumed Plasticizer
0
0.1
0.2
0.3
Concentration plasticizer (% by cement)
FR (low)
Cons. PA

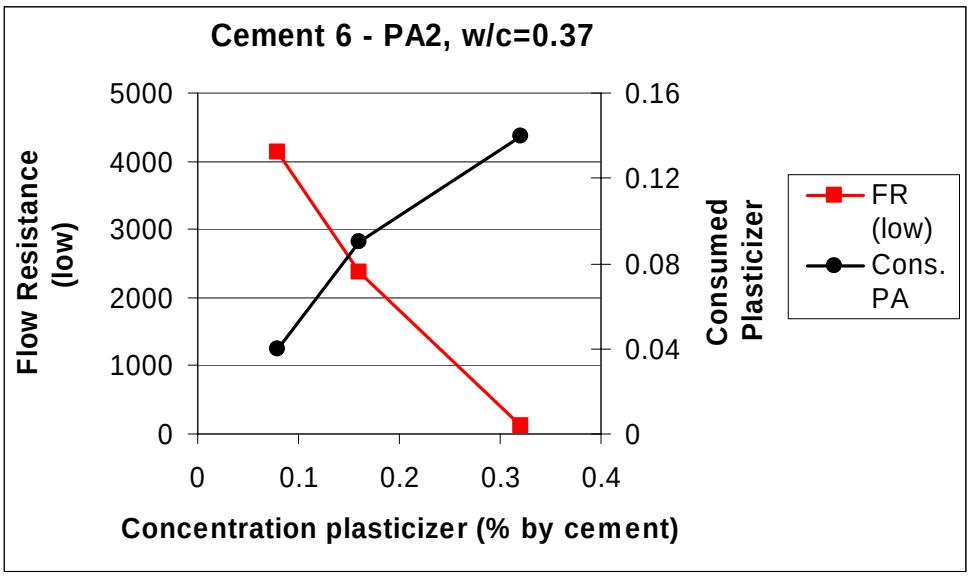
Cement 6 - PA2, w/c=0.37
Flow Resistance (low)
5000
4000
3000
2000
1000
0
0.16
0.12
0.08
0.04
0
Consumed Plasticizer
0
0.1
0.2
0.3
0.4
Concentration plasticizer (% by cement)
FR (low)
Cons. PA

A.7 Correlation of saturation dosage of SNF with various cement characteristics

The correlations are performed on Cements 1-5 as described in Table 3.1-3.3. The water-cement ratio was 0.40 for all mixtures.

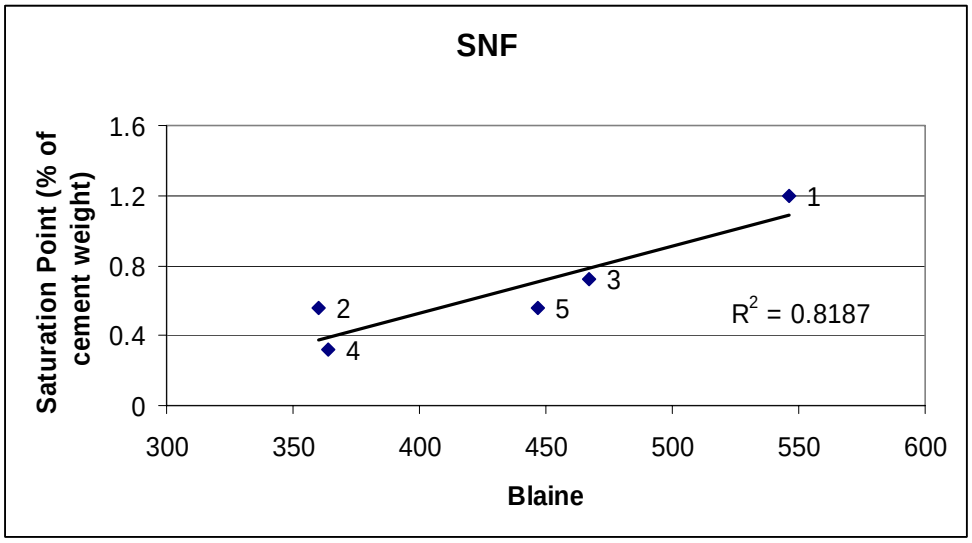

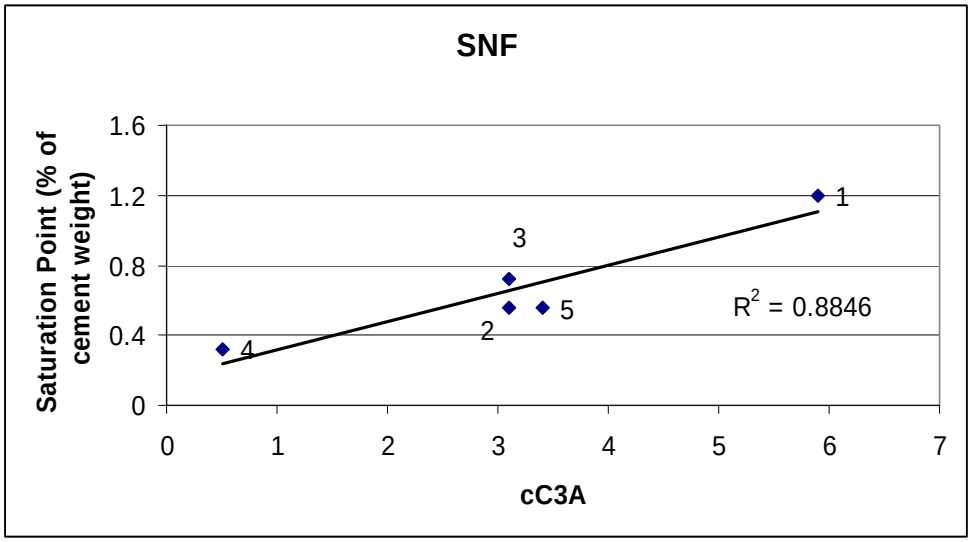

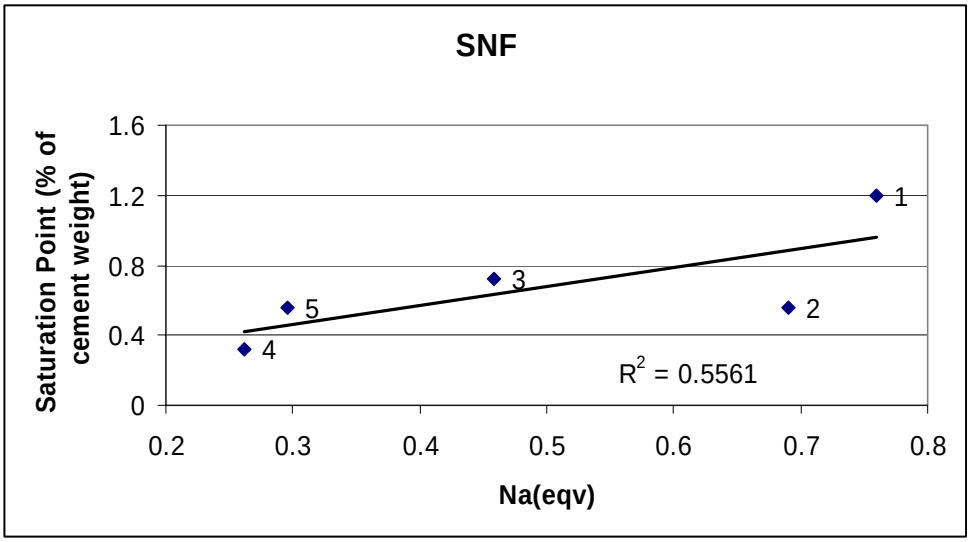
SNF
Saturation Point (% of cement weight)
1.6
1.2
0.8
0.4
0
0.2
0.3
0.4
0.5
0.6
0.7
0.8
Na(eqv)
1
2
3
4
5
R2 = 0.5561

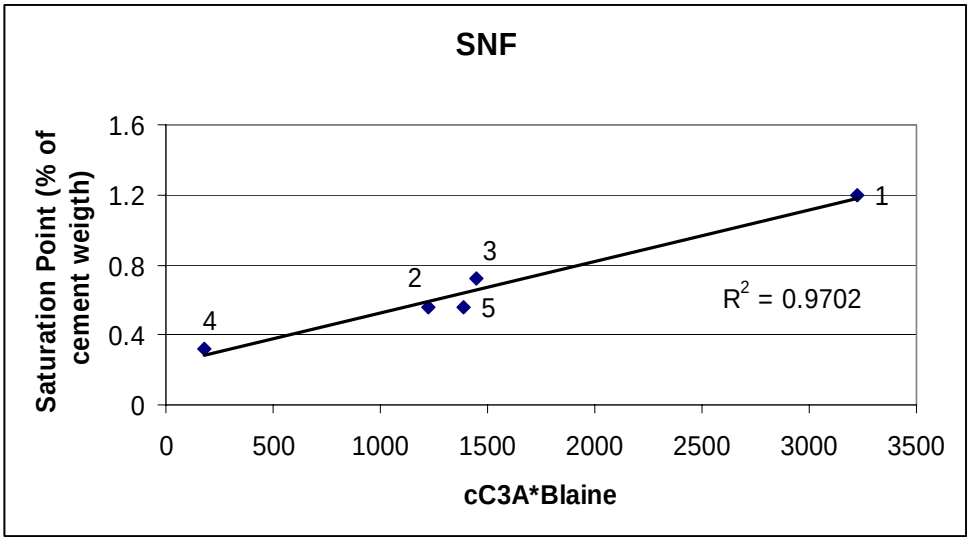
SNF
Saturation Point (% of cement weigth)
1.6
1.2
0.8
0.4
0
0
500
1000
1500
2000
2500
3000
3500
cC3A*Blaine
1
2
3
4
5
R2 = 0.9702

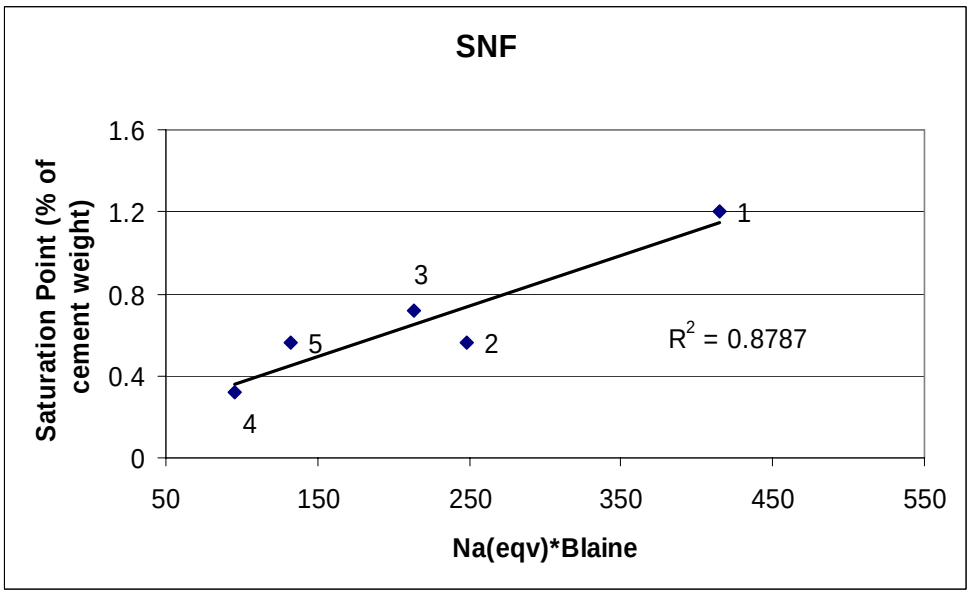
SNF
Saturation Point (% of cement weight)
1.6
1.2
0.8
0.4
0
50
150
250
350
450
550
Na(eqv)*Blaine
1
2
3
4
5
R2 = 0.8787

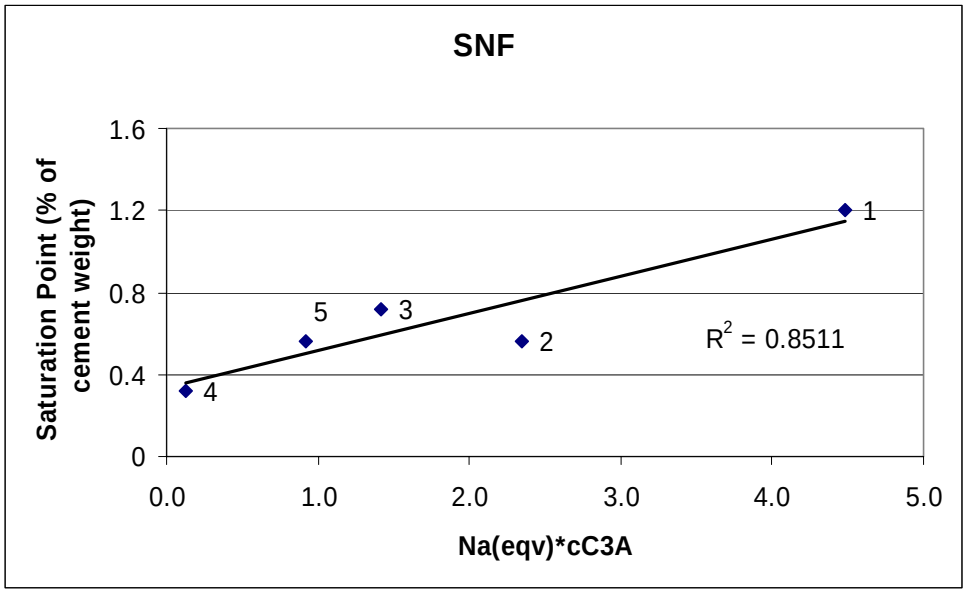
SNF
Saturation Point (% of cement weight)
1.6
1.2
0.8
0.4
0
0.0
1.0
2.0
3.0
4.0
5.0
Na(eqv)*cC3A
1
2
3
4
5
R2 = 0.8511

A.8 Tabulated data from TOC – measurements

Polyacrylate						
Cement number and type	**Time (min)**	**w/c**	**SP dosage (% of cement weight)**	**Consumed (% pr cement)**	**Consumed (mg/m^2)**	**FlowRes (low)**
1 CEM I 42.5 RR	20	0.40	0.32	0.12	2.12	578
	45			0.12	2.12	488
	70			0.12	2.12	461
	95			0.12	2.12	437
1 CEM I 42.5 RR	20	0.40	0.8	0.15	2.78	331
	45			0.15	2.78	328
	70			0.15	2.78	321
	95			0.13	2.45	319
1 CEM I 42.5 RR	20	0.40	1.2	0.05	0.96	310
	45			0.05	0.96	346
	70			0.05	0.96	356
	95			0.05	0.96	349
4 CEM I 52.5 R-LA	20	0.40	0.08	0.03	0.81	137
	45			0.03	0.84	151
	70			0.03	0.84	169
	95			0.03	0.86	184
4 CEM I 52.5 R-LA	20	0.30	0.08	0.06	1.62	2024
	45			0.06	1.62	2376
	70			0.06	1.60	2576
	95			0.06	1.60	2809
4 CEM I 52.5 R-LA	20	0.30	0.16	0.09	2.51	205
	45			0.08	2.41	215
	70			0.09	2.45	222
	95			0.09	2.47	226
6 CEM I 42.5 N	20	0.37	0.08	0.04	1.39	4126
	45			0.04	1.30	3692
	70			0.04	1.30	3621
	95			0.04	1.34	3802
6 CEM I 42.5 N	20	0.37	0.16	0.09	3.05	2367
	45			0.09	3.02	1652
	70			0.09	3.00	1405
	95			0.09	2.98	1319
6 CEM I 42.5 N	20	0.37	0.32	0.14	4.59	440
	45			0.15	4.82	360
	70			0.15	4.82	353
	95			0.15	4.82	373

Polyacrylate						
Cement number and type	**Time (min)**	**w/c**	**SP dosage (% of cement weight)**	**Consumed (% pr cement)**	**Consumed (mg/m^2)**	**FlowRes (low)**
5: CEM I 42.5 R-LA	20	0.30	0.08	0.04	0.84	4618
	45			0.05	1.15	4417
5 CEM I 42.5 R-LA	20	0.37	0.16	0.09	1.93	121
	45			0.09	1.93	132
	70			0.09	1.96	135
	95			0.09	1.94	142
5 CEM I 42.5 R-LA	20	0.30	0.16	0.09	1.90	502
	45			0.09	1.96	525
	70			0.09	1.96	527
	95			0.09	1.96	560
2 CEM I 42.5 R	20	0.30	0.16	0.07	1.81	1734
	45			0.06	1.61	1556
	70			0.07	1.81	1501
	95			0.07	1.81	1483
2 CEM I 42.5 R	20	0.30	0.32	0.11	2.98	709
	45			0.09	2.39	662
	70			0.09	2.39	644
	95			0.09	2.39	634
2 CEM I 42.5 R	20	0.30	0.48	-0.14	-4.03	553
	45			0.07	1.81	528
	70			0.04	1.03	521
	95			0.04	1.11	513
2 CEM I 42.5 R	20	0.30	0.8	0.01	0.25	440
	45			0.01	0.25	429
	70			0.01	0.25	425
	95			0.01	0.25	417
3 CEM II A-V 42.5 R-LA	20	0.30	0.16	0.09	1.86	1352
	45			0.09	1.86	1457
	70			0.09	1.89	1468
	95			0.09	1.91	1448
3 CEM II A-V 42.5 R-LA	20	0.30	0.32	0.05	0.97	516
	45			0.12	2.46	519
	70			0.12	2.61	503
	95			0.13	2.76	493
3 CEM II A-V 42.5 R-LA	20	0.30	0.48	0.04	0.82	383
	45			0.07	1.56	395
	70			0.07	1.41	392
	95			0.07	1.41	380

SNF						
Cement number and type	**Time (min)**	**w/c**	**SP dosage (% of cement weight)**	**Consumed (% pr cement)**	**Consumed (mg/m^2)**	**FlowRes (low)**
1 CEM I 42.5 RR	20	0.40	0.32	0.25	4.58	6357
	45			0.25	4.57	7613
	70			0.25	4.60	8817
	95			0.25	4.66	7064
1 CEM I 42.5 RR	20	0.40	0.8	0.46	8.34	3898
	45			0.48	8.84	4198
	70			0.50	9.16	4835
	95			0.53	9.66	6448
1 CEM I 42.5 RR	20	0.40	1.2	0.51	9.33	2208
	45			0.53	9.66	2273
	70			0.53	9.66	2435
	95			0.58	10.65	2632
4 CEM I 52.5 R-LA	20	0.40	0.08	0.04	1.26	1261
	45			0.04	1.26	1466
	70			0.05	1.29	1606
	95			0.05	1.29	1686
4 CEM I 52.5 R-LA	20	0.40	0.16	0.12	3.38	926
	45			0.12	3.38	1160
	70			0.12	3.38	1285
	95			0.12	3.38	1381
4 CEM I 52.5 R-LA	20	0.40	0.32	0.25	7.22	98
	45			0.26	7.40	145
	70			0.26	7.53	227
	95			0.27	7.61	346
6 CEM I 42.5 N	20	0.40	0.08	0.04	1.31	1792
	45			0.04	1.29	1802
	70			0.04	1.29	1795
	95			0.04	1.29	1810
6 CEM I 42.5 N	20	0.40	0.16	0.11	3.65	1786
	45			0.11	3.65	1903
	70			0.11	3.65	1897
	95			0.11	3.68	1884
6 CEM I 42.5 N	20	0.40	0.32	0.26	8.47	1839
	45			0.26	8.47	2080
	70			0.26	8.47	2201
	95			0.26	8.47	2415

SNF						
Cement number and type	**Time (min)**	**w/c**	**SP dosage (% of cement weight)**	**Consumed (% pr cement)**	**Consumed (mg/m^2)**	**FlowRes (low)**
6 CEM I 42.5 N	20	0.37	0.32	0.20	6.46	3483
	45			0.20	6.46	3707
	70			0.21	6.75	3890
	95			0.21	6.75	3999
6 CEM I 42.5 N	20	0.37	0.48	0.34	11.13	1668
	45			0.34	11.13	2079
	70			0.35	11.43	2358
	95			0.35	11.43	2739
6 CEM I 42.5 N	20	0.37	0.8	0.53	17.27	132
	45			0.52	16.98	147
	70			0.52	16.98	167
	95			0.52	16.98	200
5 CEM I 42.5 R-LA	20	0.37	0.08	0.03	0.62	3411
	45			0.02	0.46	3684
	70			0.02	0.52	4073
	95			0.03	0.58	4335
5 CEM I 42.5 R-LA	20	0.37	0.32	0.28	6.28	2846
	45			0.28	6.30	3402
	70			0.28	6.32	3732
	95			0.29	6.34	4219
5 CEM I 42.5 R-LA	20	0.37	0.48	0.35	7.86	707
	45			0.36	8.06	1368
	70			0.36	8.06	1999
	95			0.36	8.06	2624
5 CEM I 42.5 R-LA	20	0.37	0.8	0.56	12.46	98
	45			0.53	11.86	95
	70			0.54	12.06	106
	95			0.57	12.66	112

SNF						
Cement number and type	**Time (min)**	**w/c**	**SP dosage (% of cement weight)**	**Consumed (% pr cement)**	**Consumed (mg/m^2)**	**FlowRes (low)**
2 CEM I 42.5 R	20	0.37	0.16	0.10	2.70	2577
	45			0.09	2.58	2512
	70			0.10	2.75	2640
	95			0.10	2.78	2762
2 CEM I 42.5 R	20	0.37	0.32	0.24	6.55	2130
	45			0.24	6.55	2304
	70			0.24	6.80	2473
	95			0.25	6.93	2553
2 CEM I 42.5 R	20	0.37	0.48	0.22	6.05	894
	45			0.24	6.55	1178
	70			0.25	7.05	1441
	95			0.25	7.05	1709
3 CEM II A-V 42.5 R-LA	20	0.37	0.16	0.12	2.53	4139
	45			0.12	2.57	3762
	70			0.12	2.57	4070
	95			0.12	2.59	4517
3 CEM II A-V 42.5 R-LA	20	0.37	0.32	0.26	5.46	2354
	45			0.26	5.62	2920
	70			0.27	5.77	3210
	95			0.27	5.77	3563
3 CEM II A-V 42.5 R-LA	20	0.37	0.48	0.28	6.04	624
	45			0.26	5.46	1204
	70			0.28	6.04	1562
	95			0.29	6.23	1869

Lignosulphonate						
Cement number and type	**Time (min)**	**w/c**	**SP dosage (% of cement weight)**	**Consumed (% pr cement)**	**Adsorbed (mg/m^2)**	**FlowRes (low)**
1 CEM I 42.5 RR	20	0.4	0.32	0.23	4.16	5227
	45			0.23	4.16	5498
	70			0.23	4.18	5453
	95			0.23	4.25	5634
1 CEM I 42.5 RR	20	0.4	0.80	0.48	8.73	2995
	45			0.50	9.22	2569
	70			0.52	9.55	2421
	95			0.52	9.55	2377
1 CEM I 42.5 RR	20	0.4	1.20	0.56	10.21	464
	45			0.54	9.88	383
	70			0.53	9.72	376
	95			0.56	10.21	367
4 CEM I 52.5 R-LA	20	0.4	0.08	0.05	1.36	1189
	45			0.05	1.38	1393
	70			0.05	1.38	1479
	95			0.05	1.41	1577
4 CEM I 52.5 R-LA	20	0.4	0.16	0.12	3.37	703
	45			0.12	3.42	780
	70			0.05	1.51	846
	95			0.12	3.39	910
4 CEM I 52.5 R-LA	20	0.4	0.32	0.24	6.82	213
	45			0.24	6.82	227
	70			0.21	6.15	272
	95			0.24	7.00	315
6 CEM I 42.5 N	20	0.37	0.16	0.11	3.55	2223
	45			0.11	3.57	2063
	70			0.11	3.55	1997
	95			0.11	3.55	1989
6 CEM I 42.5 N	20	0.37	0.32	0.27	8.64	2570
	45			0.27	8.64	2466
	70			0.27	8.67	2410
	95			0.27	8.69	2410
6 CEM I 42.5 N	20	0.37	0.48	0.36	11.62	2752
	45			0.35	11.36	2629
	70			0.36	11.62	2493
	95			0.36	11.62	2502
6 CEM I 42.5 N	20	0.37	0.80	0.52	16.80	255
	45			0.54	17.57	245
	70			0.54	17.57	248
	95			0.56	18.09	254

Lignosulphonate						
Cement number and type	**Time (min)**	**w/c**	**SP dosage (% of cement weight)**	**Consumed (% pr cement)**	**Adsorbed (mg/m^2)**	**FlowRes (low)**
5 CEM I 42.5 R-LA	20	0.37	0.16	0.11	2.54	3249
	45			0.11	2.43	3500
	70			0.11	2.54	3591
	95			0.11	2.55	3887
5 CEM I 42.5 R-LA	20	0.37	0.48	0.32	7.09	1719
	45			0.33	7.44	2123
	70			0.34	7.62	2426
	95			0.34	7.62	2639
5 CEM I 42.5 R-LA	20	0.37	0.80	0.51	11.35	191
	45			0.52	11.53	183
	70			0.53	11.71	180
	95			0.54	12.06	188
2 CEM I 42.5 R	20	0.37	0.16	0.10	2.79	2468
	45			0.10	2.79	2602
	70			0.10	2.81	2688
	95			0.10	2.84	2746
2 CEM I 42.5 R	20	0.37	0.32	0.24	6.61	1604
	45			0.24	6.61	1638
	70			0.24	6.61	1712
	95			0.24	6.61	1774
2 CEM I 42.5 R	20	0.37	0.48	0.25	7.06	488
	45			0.26	7.28	416
	70			0.27	7.50	411
	95			0.28	7.73	420
3 CEM II A-V 42.5 R-LA	20	0.37	0.16	0.12	2.59	2991
	45			0.12	2.59	3174
	70			0.12	2.62	3364
	95			0.12	2.64	3535
3 CEM II A-V 42.5 R-LA	20	0.37	0.48	0.30	6.32	1173
	45			0.30	6.32	932
	70			0.30	6.32	980
	95			0.30	6.49	1037
3 CEM II A-V 42.5 R-LA	20	0.37	0.80	0.41	8.72	288
	45			0.41	8.72	311
	70			0.42	8.89	316
	95			0.42	9.06	323

A.9 Flow Loss

Table A.9-1: Flow Loss for cements without superplasticizer. 0.16% SNF and LS has been added to Cement 1 due to its very high consistency. FR (low) = Flow resistance in the low shear rate range (43-8.8 s^{-1})

Pure cements			
Cement number and type	**Time (min)**	**FR (low)**	**Flow Loss (%)**
1 CEM I 42.5 RR (0.16% LS)	20	6913	
	45	8284	20
	70	6135	-11
	95	5351	-23
1 CEM I 42.5 RR (0.16% SNF)	20	5897	
	45	7066	20
	70	8209	39
	95	6683	13
2 CEM I 42.5 R	20	1655	
	45	1882	14
	70	1994	20
	95	1995	21
3 CEM II A-V 42.5 R	20	2732	
	45	3231	18
	70	3342	22
	95	3393	24
4 CEM I 52.5 R-LA	20	1653	
	45	1975	19
	70	2092	27
	95	2156	30
5 CEM I 42.5 R-LA	20	2740	
	45	3128	14
	70	3408	24
	95	4144	51
6 CEM I 42.5 N	20	4126	
	45	3692	-11
	70	3621	-12
	95	3802	-8

Table A.9-2: Flow loss measurements for pastes with SNF.
Water cement ratio was equal to 0.40 for all slurries.
FR (low) = Flow resistance in the low shear rate range (43-8.8 s^{-1})

SNF				
Cement number and type	**Dose SNF (%)**	**Time (min)**	**FR (low)**	**Flow Loss (%)**
1 CEM I 42.5 RR	0.16	20	5897	
		45	7066	20
		70	8209	39
		95	6683	13
1 CEM I 42.5 RR	0.32	20	6357	
		45	7613	20
		70	8817	39
		95	7064	11
1 CEM I 42.5 RR	0.40	20	6186	
		45	6890	11
		70	7778	26
		95	7542	22
1 CEM I 42.5 RR	0.48	20	5410	
		45	5930	10
		70	5363	-1
		95	3773	-30
1 CEM I 42.5 RR	0.80	20	3898	
		45	4198	8
		70	4835	24
		95	6448	65
1 CEM I 42.5 RR	1.20	20	1523	
		45	1878	23
		70	2016	32
		95	2563	68
1 CEM I 42.5 RR	2.00	20	640	
		45	841	31
		70	970	52
		95	1309	105
1 CEM I 42.5 RR	3.00	20	492	
		45	610	24
		70	747	52
		95	1048	113
2 CEM I 42.5 R	0.00	20	1655	
		45	1882	14
		70	1994	20
		95	1995	21

SNF				
Cement number and type	**Dose SNF (%)**	**Time (min)**	**FR (low)**	**Flow Loss (%)**
2 CEM I 42.5 R	0.08	20	1888	
		45	2119	12
		70	2189	16
		95	2238	19
2 CEM I 42.5 R	0.16	20	1787	
		45	2012	13
		70	2165	21
		95	2232	25
2 CEM I 42.5 R	0.32	20	1214	
		45	1619	33
		70	2003	65
		95	2316	91
2 CEM I 42.5 R	0.40	20	681	
		45	897	32
		70	1169	72
		95	1430	110
2 CEM I 42.5 R	0.48	20	261	
		45	428	64
		70	661	154
		95	924	255
2 CEM I 42.5 R	0.56	20	127	
		45	180	42
		70	287	127
		95	418	230
3 CEM II A-V 42.5 R	0.00	20	2732	
		45	3231	18
		70	3342	22
		95	3393	24
3 CEM II A-V 42.5 R	0.16	20	3436	
		45	3708	8
		70	4214	23
		95	4643	35
3 CEM II A-V 42.5 R	0.32	20	3200	
		45	3710	16
		70	4054	27
		95	4259	33
3 CEM II A-V 42.5 R	0.40	20	2080	
		45	2583	24
		70	3052	47
		95	3481	67

SNF				
Cement number and type	**Dose SNF (%)**	**Time (min)**	**FR (low)**	**Flow Loss (%)**
3 CEM II A-V 42.5 R	0.48	20	947	
		45	1550	64
		70	2049	116
		95	2539	168
3 CEM II A-V 42.5 R	0.56	20	377	
		45	580	54
		70	871	131
		95	1183	214
3 CEM II A-V 42.5 R	0.72	20	172	
		45	203	18
		70	260	51
		95	329	92
4 CEM I 52.5 R-LA	0.00	20	1653	
		45	1975	19
		70	2092	27
		95	2156	30
4 CEM I 52.5 R-LA	0.08	20	1686	
		45	2038	21
		70	2104	25
		95	2157	28
4 CEM I 52.5 R-LA	0.16	20	1072	
		45	1412	32
		70	1667	56
		95	1832	71
4 CEM I 52.5 R-LA	0.32	20	143	
		45	223	56
		70	375	163
		95	594	317
4 CEM I 52.5 R-LA	0.48	20	31	
		45	20	-35
		70	23	-26
		95	24	-24

SNF				
Cement number and type	**Dose SNF (%)**	**Time (min)**	**FR (low)**	**Flow Loss (%)**
5 CEM I 42.5 R-LA	0.00	20	2740	
		45	3128	14
		70	3408	24
		95	4144	51
5 CEM I 42.5 R-LA	0.16	20	2835	
		45	3387	19
		70	3542	25
		95	3599	27
5 CEM I 42.5 R-LA	0.24	20	2718	
		45	3216	18
		70	3381	24
		95	3831	41
5 CEM I 42.5 R-LA	0.32	20	2082	
		45	2688	29
		70	3202	54
		95	3657	76
5 CEM I 42.5 R-LA	0.40	20	874	
		45	1678	92
		70	2301	163
		95	2995	242
5 CEM I 42.5 R-LA	0.48	20	276	
		45	483	75
		70	844	205
		95	1394	404
5 CEM I 42.5 R-LA	0.56	20	116	
		45	153	32
		70	207	78
		95	279	141
6 CEM I 42.5 N	0.32	20	3483	
		45	3707	6
		70	3890	12
		95	3999	15
6 CEM I 42.5 N	0.48	20	1668	
		45	2079	25
		70	2358	41
		95	2739	64
6 CEM I 42.5 N	0.80	20	132	
		45	147	11
		70	167	27
		95	200	52

Table A.9-3: Flow loss measurements for pastes with LS.
Water cement ratio was equal to 0.40 for all slurries.
FR (low) = Flow resistance in the low shear rate range (43-8.8 s^{-1})

LS				
Cement number and type	**Dose LS (%)**	**Time (min)**	**FR (low)**	**Flow Loss (%)**
1 CEM I 42.5 RR	0.16	20	6913	
		45	8284	20
		70	6135	-11
		95	5351	-23
1 CEM I 42.5 RR	0.32	20	7114	
		45	7784	9
		70	3225	-55
		95	3657	-49
1 CEM I 42.5 RR	0.40	20	6277	
		45	7007	12
		70	6051	-4
		95	4965	-21
1 CEM I 42.5 RR	0.56	20	5409	
		45	5692	5
		70	5898	9
		95	6275	16
1 CEM I 42.5 RR	0.80	20	4833	
		45	4156	-14
		70	4337	-10
		95	4594	-5
1 CEM I 42.5 RR	1.06	20	1406	
		45	1112	-21
		70	1073	-24
		95	1074	-24
1 CEM I 42.5 RR	1.20	20	904	
		45	848	-6
		70	882	-2
		95	963	7
1 CEM I 42.5 RR	1.60	20	337	
		45	326	-3
		70	345	2
		95	356	6

LS				
Cement number and type	**Dose LS (%)**	**Time (min)**	**FR (low)**	**Flow Loss (%)**
1 CEM I 42.5 RR	2.00	20	419	
		45	379	-10
		70	385	-8
		95	400	-5
1 CEM I 42.5 RR	2.60	20	437	
		45	441	1
		70	468	7
		95	508	16
2 CEM I 42.5 R	0.00	20	1655	
		45	1882	14
		70	1994	20
		95	1995	21
2 CEM I 42.5 R	0.08	20	1733	
		45	1950	13
		70	2005	16
		95	2042	18
2 CEM I 42.5 R	0.16	20	1779	
		45	1910	7
		70	2054	15
		95	2124	19
2 CEM I 42.5 R	0.24	20	1371	
		45	1493	9
		70	1629	19
		95	1745	27
2 CEM I 42.5 R	0.32	20	1009	
		45	1083	7
		70	1183	17
		95	1265	25
2 CEM I 42.5 R	0.48	20	414	
		45	354	-14
		70	373	-10
		95	394	-5
2 CEM I 42.5 R	0.80	20	104	
		45	117	12
		70	120	16
		95	123	18

LS				
Cement number and type	**Dose LS (%)**	**Time (min)**	**FR (low)**	**Flow Loss (%)**
3 CEM II A-V 42.5 R	0.00	20	2732	
		45	3231	18
		70	3342	22
		95	3393	24
3 CEM II A-V 42.5 R	0.16	20	3681	
		45	3716	1
		70	3901	6
		95	4106	12
3 CEM II A-V 42.5 R	0.32	20	2801	
		45	2873	3
		70	2962	6
		95	3132	12
3 CEM II A-V 42.5 R	0.48	20	1645	
		45	1442	-12
		70	1480	-10
		95	1534	-7
3 CEM II A-V 42.5 R	0.64	20	352	
		45	311	-12
		70	344	-2
		95	366	4
4 CEM I 52.5 R-LA	0.00	20	1653	
		45	1975	19
		70	2092	27
		95	2156	30
4 CEM I 52.5 R-LA	0.08	20	1606	
		45	1816	13
		70	1940	21
		95	2000	24
4 CEM I 52.5 R-LA	0.16	20	880	
		45	1045	19
		70	1227	39
		95	1351	54
4 CEM I 52.5 R-LA	0.32	20	320	
		45	394	23
		70	480	50
		95	537	68

LS				
Cement number and type	**Dose LS (%)**	**Time (min)**	**FR (low)**	**Flow Loss (%)**
4 CEM I 52.5 R-LA	0.48	20	115	
		45	71	-39
		70	75	-35
		95	89	-23
4 CEM I 52.5 R-LA	0.64	20	64	
		45	57	-12
		70	52	-19
		95	49	-23
5 CEM I 42.5 R-LA	0.00	20	2740	
		45	3128	14
		70	3408	24
		95	4144	51
5 CEM I 42.5 R-LA	0.16	20	2823	
		45	3208	14
		70	3377	20
		95	3421	21
5 CEM I 42.5 R-LA	0.32	20	2002	
		45	2145	7
		70	2336	17
		95	2474	24
5 CEM I 42.5 R-LA	0.48	20	783	
		45	1141	46
		70	1398	79
		95	1618	107
5 CEM I 42.5 R-LA	0.64	20	156	
		45	158	2
		70	178	14
		95	213	37

LS				
Cement number and type	**Dose LS (%)**	**Time (min)**	**FR (low)**	**Flow Loss (%)**
6 CEM I 42.5 N	0.16	20	2223	
		45	2063	-7
		70	1997	-10
		95	1989	-11
6 CEM I 42.5 N	0.32	20	2570	
		45	2466	-4
		70	2410	-6
		95	2410	-6
6 CEM I 42.5 N	0.48	20	2752	
		45	2629	-4
		70	2493	-9
		95	2502	-9
6 CEM I 42.5 N	0.80	20	255	
		45	245	-4
		70	248	-3
		95	254	0

Table A.9-4: Flow loss measurements for pastes with PA2.
Water cement ratio was in the range of 0.30-0.40.
FR (low) = Flow resistance in the low shear rate range (43-8.8 s^{-1})

PA2				
Cement number and type (w/c)	**Dose PA (%)**	**Time (min)**	**FR (low)**	**Flow Loss (%)**
1 CEM I 42.5 RR (0.40)	0.32	20	578	
		45	488	-16
		70	461	-20
		95	437	-24
1 CEM I 42.5 RR (0.40)	0.80	20	331	
		45	328	-1
		70	321	-3
		95	319	-4
1 CEM I 42.5 RR (0.40)	1.20	20	310	
		45	347	12
		70	356	15
		95	349	13
2 CEM I 42.5 R (0.30)	0.16	20	1737	
		45	1556	-10
		70	1502	-14
		95	1483	-15
2 CEM I 42.5 R (0.30)	0.32	20	709	
		45	662	-7
		70	644	-9
		95	634	-11
2 CEM I 42.5 R (0.30)	0.48	20	554	
		45	528	-5
		70	521	-6
		95	513	-7
2 CEM I 42.5 R (0.30)	0.80	20	440	
		45	429	-3
		70	425	-3
		95	417	-5

PA				
Cement (w/c)	**Dose PA (%)**	**Time (min)**	**FR (low)**	**Flow Loss (%)**
3 CEM II A-V 42.5 R (0.30)	0.16	20	1352	
		45	1457	8
		70	1468	9
		95	1448	7
3 CEM II A-V 42.5 R (0.30)	0.32	20	516	
		45	520	1
		70	503	-3
		95	493	-4
3 CEM II A-V 42.5 R (0.30)	0.48	20	383	
		45	395	3
		70	392	2
		95	380	-1
4 CEM I 52.5 R-LA (0.30)	0.08	20	2024	
		45	2376	17
		70	2577	27
		95	2809	39
4 CEM I 52.5 R-LA (0.30)	0.16	20	205	
		45	215	5
		70	222	8
		95	226	10
5 CEM I 42.5 R-LA (0.30)	0.08	20	4619	
		45	4419	-4
		70	3923	-15
		95	2493	-46
5 CEM I 42.5 R-LA (0.30)	0.16	20	502	
		45	525	5
		70	527	5
		95	560	12
6 CEM I 42.5 N (0.37)	0.08	20	4127	
		45	3693	-11
		70	3622	-12
		95	3803	-8
6 CEM I 42.5 N (0.37)	0.16	20	2368	
		45	1653	-30
		70	1405	-41
		95	1319	-44
6 CEM I 42.5 N (0.37)	0.32	20	440	
		45	361	-18
		70	353	-20
		95	373	-15

A.10 Bingham analysis of flow curves for cement pastes with LS and SNF prepared for UV-absorption measurements

Table A.10-1: Bingham data for cement pastes made with w/c = 0.40 and SNF as superplasticizer. The plasticizer added with the mixing water (*0 min*) or delayed (*5 minutes* after water addition). *Mix no.1* contains 0% SF, while *Mix.4* contains 6.8 vol% SF

SNF					LOW SHEAR RATE RANGE			MEDIUM SHEAR RATE RANGE					
Cement number and type	**Mix no**	**Time added (min)**	**Dose (% of cement weight)**	**Time (min)**	μ_{pl} (Pa·s)	τ_{yl} (Pa)	R^2	μ_{pm} (Pa·s)	τ_{ym} (Pa)	R^2	μ_{pm}/μ_{pl}	τ_{10sec} **(Pa)**	τ_{10min} **(Pa)**
1 CEM I 42.5 RR	1	0	**0.16**	20	3.26	87.79	0.9993	1.15	231.55	0.9906	0.35	185	164
				45	3.62	112.65	0.9987	1.42	271.63	0.9973	0.39	220	>300
				70	3.90	138.84	0.9984	1.94	262.00	0.9913	0.50	>250	>300
				95	4.09	88.64	0.9899	1.88	253.49	0.8321	0.46	>250	>300
1 CEM I 42.5 RR	1	0	**0.32**	20	3.32	99.49	0.9978	0.74	272.75	0.9978	0.22	175	171
				45	3.63	128.21	0.9985	1.34	280.12	0.9952	0.37	225	>350
				70	4.13	152.25	0.9989	0.96	405.67	0.9560	0.23	>300	>350
				95	3.65	113.26	0.9957	2.71	188.31	0.9696	0.74	>300	>350
1 CEM I 42.5 RR	1	0	**0.48**	20	3.07	78.34	0.9972	0.85	213.23	0.9980	0.28	112	125
				45	3.84	74.23	0.9987	0.71	268.98	0.9781	0.18	119	125
				70	2.43	93.78	0.9976	0.94	235.91	0.9899	0.39	119	110
				95	2.04	57.67	0.9995	1.00	132.70	0.9990	0.49	82	101
1 CEM I 42.5 RR	1	5	**0.48**	20	1.12	59.18	0.9483	0.40	89.28	0.9967	0.36	48	>80
				45	1.66	66.90	0.9704	0.44	122.65	0.9995	0.27	>60	>80
				70	2.12	75.32	0.9847	0.50	157.04	0.9981	0.23	>60	>80
				95	2.39	88.98	0.9893	0.59	190.98	0.9995	0.25	>60	>80

SNF					LOW SHEAR RATE RANGE			MEDIUM SHEAR RATE RANGE					
Cement number and type	**Mix no**	**Time added (min)**	**Dose (% of cement weight)**	**Time (min)**	μ_{pl} (Pa·s)	τ_{yl} (Pa)	R^2	μ_{pm} (Pa·s)	τ_{ym} (Pa)	R^2	μ_{pm}/μ_{pl}	τ_{10sec} **(Pa)**	τ_{10min} **(Pa)**
1 CEM I 42.5 RR	1	0	**0.80**	20	0.64	96.17	0.6919	0.17	107.88	0.9777	0.26	54	82
				45	0.77	101.43	0.7503	0.13	121.61	0.9593	0.16	64	109
				70	1.04	112.85	0.7694	0.11	144.71	0.9696	0.11	89	229
				95	2.23	128.97	0.9163	0.18	205.39	0.9782	0.08	148	>350
1 CEM I 42.5 RR	1	5	**0.80**	20	0.30	21.90	0.9997	0.31	21.24	0.9991	1.03	20	25
				45	0.35	30.25	0.9986	0.37	28.41	0.9995	1.07	22	27
				70	0.39	37.28	0.9949	0.42	35.06	0.9991	1.07	24	-
				95	-		-						-
1 CEM I 42.5 RR	1	0	**1.00**	20	3.22	96.77	0.9930	0.55	249.33	0.9980	0.17	132	116
				45	3.60	107.73	0.9968	0.72	283.01	0.9951	0.20	168	156
				70	3.74	130.28	0.9985	0.91	324.63	0.9985	0.24	>250	>350
				95	4.37	106.42	0.9909	1.77	237.43	0.9933	0.40	>250	>350
1 CEM I 42.5 RR	1	5	**1.00**	20	2.28	80.06	0.9806	0.48	167.18	0.9972	0.21	80	126
				45	2.87	92.62	0.9953	0.42	233.31	0.9967	0.15	98	116
				70	3.38	118.37	0.9954	0.53	301.50	0.9971	0.16	140	200
				95	3.56	146.49	0.9946	1.01	310.12	0.9991	0.28	234	>500
1 CEM I 42.5 RR	4	0	**1.00**	20	3.26	92.62	0.9941	0.41	241.80	0.9989	0.13	185	150
				45	3.58	108.11	0.9969	0.39	303.47	0.9939	0.11	227	292
				70	3.62	131.74	0.9962	0.65	318.04	0.9786	0.18	308	>600
				95	3.52	136.21	0.9982	1.59	236.36		0.45	359	>600

SNF					LOW SHEAR RATE RANGE			MEDIUM SHEAR RATE RANGE					
Cement number and type	**Mix no**	**Time added (min)**	**Dose (% of cement weight)**	**Time (min)**	μ_{pl} (Pa·s)	τ_{yl} (Pa)	R^2	μ_{pm} (Pa·s)	τ_{ym} (Pa)	R^2	μ_{pm} / μ_{pl}	τ_{10sec} **(Pa)**	τ_{10min} **(Pa)**
1 CEM I 42.5 RR	4	5	**1.00**	20	2.56	92.91	0.9633	0.26	199.73	0.9928	0.10	100	134
					3.35	94.61	0.9925	0.33	249.16	0.9965	0.10	123	156
					3.83	124.66	0.9983	0.35	334.11	0.9920	0.09	194	503
					4.27	161.23	0.9988	0.69	414.25	0.9867	0.16	378	>600
1 CEM I 42.5 RR	1	0	**1.20**	20	0.11	41.66	0.9930	0.16	39.10	0.9989	1.42	29	43
					0.12	51.84	0.9841	0.17	50.59	0.9993	1.43	36	56
					0.11	56.09	0.9630	0.20	53.12	0.9997	1.76	41	78
					0.04	73.85	0.9232	0.22	65.62	0.9995	5.00	52	110
1 CEM I 42.5 RR	1	5	**1.20**	20	0.27	5.73	0.9999	0.29	4.17	0.9992	1.06	10	13
					0.32	7.47	0.9999	0.31	7.24	0.9991	0.99	12	16
					0.35	9.11	0.9999	0.35	8.59	0.9992	1.01	12	19
					0.37	11.27	0.9999	0.38	10.42	0.9993	1.02	14	27
1 CEM I 42.5 RR	1	0	**2.00**	20	0.20	13.43	0.9989	0.18	14.76	0.9995	0.87	26	35
					0.23	18.54	0.9994	0.18	22.66	0.9995	0.76	29	40
					0.25	21.95	0.9999	0.21	25.27	0.9995	0.83	32	73
					0.24	32.00	0.9974	0.25	32.00	0.9996	1.04	41	78
1 CEM I 42.5 RR	1	0	**3.00**	20	0.26	7.71	0.9987	0.22	9.39	0.9994	0.85	32	40
				45	0.28	10.50	0.9985	0.22	14.14	0.9998	0.77	32	46
				70	0.31	13.81	0.9992	0.24	18.37	0.9996	0.77	36	90
				95	0.34	21.92	1.0000	0.29	25.27	0.9996	0.85	52	96

SNF					LOW SHEAR RATE RANGE			MEDIUM SHEAR RATE RANGE					
Cement number and type	**Mix no**	**Time added (min)**	**Dose (% of cement weight)**	**Time (min)**	μ_{pl} (Pa·s)	τ_{yl} (Pa)	R^2	μ_{pm} (Pa·s)	τ_{ym} (Pa)	R^2	μ_{pm}/μ_{pl}	τ_{10sec} **(Pa)**	τ_{10min} **(Pa)**
2 CEM I 42.5 R	1	0	**0.08**	20	0.97	29.86	0.9883	0.23	66.49	0.9962	0.24	38	77
				45	1.09	33.76	0.9986	0.30	73.10	0.9995	0.27	41	26
				70	1.06	36.39	0.9989	0.26	81.73	0.9928	0.24	41	48
				95	1.11	36.74	0.9999	0.26	86.03	0.9896	0.24	44	60
2 CEM I 42.5 R	1	0	**0.16**	20	0.74	32.92	0.9802	0.21	60.28	0.9997	0.29	37	29
				45	0.97	33.32	0.9889	0.22	69.32	0.9955	0.23	43	44
				70	1.06	35.73	0.9979	0.24	76.79	0.9849	0.22	50	59
				95	1.10	36.71	0.9994	0.24	82.31	0.9924	0.22	53	61
2 CEM I 42.5 R	1	0	**0.32**	20	0.25	28.83	0.9750	0.14	33.94	0.9988	0.57	22	41
				45	0.41	36.63	0.9605	0.19	46.42	0.9996	0.46	29	60
				70	0.58	43.32	0.9597	0.24	56.93	0.9983	0.42	39	82
				95	0.72	48.71	0.9512	0.28	68.07	0.9810	0.39	43	89
2 CEM I 42.5 R	1	0	**0.40**	20	0.17	15.56	0.9876	0.12	17.37	0.9989	0.72	10	16
				45	0.20	21.12	0.9844	0.14	23.33	0.9993	0.70	18	27
				70	0.26	27.26	0.9747	0.16	31.50	0.9989	0.60	20	33
				95	0.34	33.00	0.9773	0.19	39.29	0.9989	0.55	23	41
2 CEM I 42.5 R	1	0	**0.48**	20	0.14	3.86	0.9954	0.11	4.93	0.9985	0.80	4	7
				45	0.16	8.47	0.9951	0.11	10.50	0.9991	0.74	7	13
				70	0.18	14.72	0.9926	0.14	16.40	0.9996	0.77	14	21
				95	0.20	21.70	0.9921	0.16	23.73	0.9996	0.77	19	33

SNF					LOW SHEAR RATE RANGE			MEDIUM SHEAR RATE RANGE					
Cement number and type	**Mix no**	**Time added (min)**	**Dose (% of cement weight)**	**Time (min)**	μ_{pl} (Pa·s)	τ_{yl} (Pa)	R^2	μ_{pm} (Pa·s)	τ_{ym} (Pa)	R^2	μ_{pm}/μ_{pl}	τ_{10sec} **(Pa)**	τ_{10min} **(Pa)**
2 CEM I 42.5 R	1	0	**0.56**	20	0.12	0.64	0.9999	0.10	1.98	0.9983	0.85	2	2
				45	0.13	1.98	0.9977	0.09	4.32	0.9994	0.72	3	4
				70	0.15	4.56	0.9939	0.10	7.25	0.9990	0.68	5	7
				95	0.16	8.17	0.9927	0.12	10.33	0.9988	0.75	9	12
3 CEM II A-V 42.5 R	1	0	**0.00**	20	1.33	45.74	0.9995	0.51	132.09	0.9873	0.38	57	71
				45	1.38	58.69	0.9965	0.66	129.55	0.9767	0.48	68	74
				70	1.40	61.34	0.9946	0.78	121.94	0.9939	0.56	72	74
				95	1.42	62.34	0.9966	0.86	113.96	0.9990	0.61	75	74
3 CEM II A-V 42.5 R	1	0	**0.16**	20	1.40	64.05	0.9937	0.65	143.50	0.9989	0.46	102	100
				45	1.47	70.33	0.9973	0.97	117.94	0.9995	0.66	113	149
				70	1.58	81.60	0.9769	1.15	112.55	1.0000	0.72	118	205
				95	1.72	90.23	0.9661	1.25	120.43	0.9985	0.73	135	237
3 CEM II A-V 42.5 R	1	0	**0.32**	20	1.34	58.23	0.9719	0.44	102.65	0.9995	0.33	74	90
				45	1.61	66.37	0.9867	0.46	132.59	0.9980	0.29	85	104
				70	1.69	74.39	0.9840	0.48	155.01	0.9978	0.29	93	87
				95	1.80	77.36	0.9840	0.52	164.29	0.9987	0.29	103	87
3 CEM II A-V 42.5 R	1	0	**0.40**	20	0.56	45.94	0.9520	0.27	58.12	0.9993	0.48	35	44
				45	0.83	53.59	0.9455	0.32	76.43	0.9928	0.38	42	54
				70	1.10	60.07	0.9455	0.38	92.74	0.9976	0.34	50	69
				95	1.35	65.94	0.9546	0.44	106.65	0.9995	0.33	65	88

SNF					LOW SHEAR RATE RANGE			MEDIUM SHEAR RATE RANGE					
Cement number and type	**Mix no**	**Time added (min)**	**Dose (% of cement weight)**	**Time (min)**	μ_{pl} (Pa·s)	τ_{yl} (Pa)	R^2	μ_{pm} (Pa·s)	τ_{ym} (Pa)	R^2	μ_{pm}/μ_{pl}	τ_{10sec} **(Pa)**	τ_{10min} **(Pa)**
3 CEM II A-V 42.5 R	1	0	**0.48**	20	0.24	21.53	0.9946	0.20	23.25	0.9995	0.83	22	32
				45	0.35	36.20	0.9792	0.24	40.98	0.9995	0.68	27	37
				70	0.51	46.40	0.9515	0.29	55.63	0.9993	0.56	33	44
				95	0.72	55.07	0.9341	0.33	71.16	0.9965	0.46	41	62
3 CEM II A-V 42.5 R	1	0	**0.56**	20	0.18	6.24	0.9987	0.18	6.06	0.9995	0.96	10	10
				45	0.22	11.27	0.9972	0.19	12.68	0.9993	0.86	15	14
				70	0.25	19.00	0.9979	0.21	20.91	0.9994	0.84	20	21
				95	0.29	27.13	0.9958	0.23	29.89	0.9998	0.81	22	28
3 CEM II A-V 42.5 R	1	0	**0.72**	20	0.15	1.05	0.9999	0.16	0.20	0.9995	1.06	5	4
				45	0.17	1.43	1.0000	0.18	1.29	0.9984	1.01	7	9
				70	0.21	2.26	0.9998	0.21	1.44	0.9993	1.03	9	7
				95	0.23	3.52	0.9998	0.24	2.56	0.9990	1.02	10	8
4 CEM I 52.5 R-LA	1	0	**0.00**	20	0.84	26.12	0.9750	0.18	59.61	0.9991	0.22	41	26
				45	1.09	29.40	0.9951	0.19	73.45	0.9902	0.17	41	34
				70	1.15	31.23	0.9982	0.18	80.39	0.9782	0.16	47	44
				95	1.16	33.00	0.9994	0.19	84.91	0.9876	0.16	52	86
4 CEM I 52.5 R-LA	1	0	**0.08**	20	0.86	26.68	0.9840	0.22	60.83	0.9991	0.26	47	31
				45	1.10	30.90	0.9968	0.21	82.25	0.9834	0.19	52	44
				70	1.13	32.23	0.9983	0.24	87.40	0.9884	0.21	59	62
				95	1.16	32.91	0.9992	0.26	91.03	0.9896	0.22	66	73

SNF					LOW SHEAR RATE RANGE			MEDIUM SHEAR RATE RANGE					
Cement number and type	**Mix no**	**Time added (min)**	**Dose (% of cement weight)**	**Time (min)**	μ_{pl} (Pa·s)	τ_{yl} (Pa)	R^2	μ_{pm} (Pa·s)	τ_{ym} (Pa)	R^2	μ_{pm}/μ_{pl}	τ_{10sec} **(Pa)**	τ_{10min} **(Pa)**
4 CEM I 52.5 R-LA	1	0	**0.16**	20	0.44	19.69	0.9712	0.16	35.49	0.9997	0.35	26	57
				45	0.63	24.69	0.9713	0.19	48.19	0.9992	0.30	37	17
				70	0.79	28.04	0.9831	0.22	57.82	0.9995	0.28	41	20
				95	0.90	30.12	0.9935	0.24	63.78	0.9989	0.26	47	33
4 CEM I 52.5 R-LA	1	5	**0.16**	20	0.32	12.15	0.9841	0.11	25.22	0.9995	0.36	16	27
				45	0.57	18.29	0.9762	0.17	41.51	0.9997	0.29	24	43
				70	0.73	23.20	0.9807	0.21	50.60	0.9987	0.28	32	54
				95	0.87	25.96	0.9906	0.25	59.23	0.9991	0.28	37	24
4 CEM I 52.5 R-LA	1	0	**0.32**	20	0.11	1.35	0.9990	0.07	4.24	0.9987	0.66	3	4
				45	0.12	3.27	0.9922	0.08	5.86	0.9973	0.62	5	10
				70	0.14	7.37	0.9856	0.08	10.39	0.9983	0.61	10	17
				95	0.15	13.34	0.9934	0.09	16.84	0.9995	0.60	16	26
4 CEM I 52.5 R-LA	1	0	**0.48**	20	0.05	-0.28	0.9712	0.11	-3.64	0.9974	2.25	<0.5	<1
				45	0.03	-0.15	0.9705	0.06	0.69	0.9965	1.92	<0.5	<1
				70	0.03	-0.16	0.9780	0.06	1.04	0.9907	1.70	<0.5	<1
				95	0.03	-0.12	0.9865	0.06	1.06	0.9955	1.73	<0.5	<1
5 CEM I 42.5 R-LA	1	0	**0.00**	20	1.37	44.67	0.9997	0.28	114.07	0.9810	0.20	55	59
				45	1.35	56.60	0.9980	0.22	153.89	0.9865	0.17	65	128
				70	1.46	61.95	0.9980	0.57	141.08	0.9934	0.39	79	149
				95	1.35	86.18	0.9879	0.70	139.47	0.9824	0.51	108	>200

SNF					LOW SHEAR RATE RANGE			MEDIUM SHEAR RATE RANGE					
Cement number and type	**Mix no**	**Time added (min)**	**Dose (% of cement weight)**	**Time (min)**	μ_{pl} (Pa·s)	τ_{yl} (Pa)	R^2	μ_{pm} (Pa·s)	τ_{ym} (Pa)	R^2	μ_{pm}/μ_{pl}	τ_{10sec} **(Pa)**	τ_{10min} **(Pa)**
5 CEM I 42.5 R-LA	1	0	**0.16**	20	1.42	46.31	0.9987	0.19	139.30	0.9385	0.13	80	64
				45	1.48	60.69	0.9985	0.27	158.63	0.9686	0.18	90	52
				70	1.59	62.29	0.9974	0.38	163.17	0.9832	0.24	108	>170
				95	1.73	59.91	0.9917	0.79	127.75	0.9989	0.46	129	>170
5 CEM I 42.5 R-LA	1	0	**0.32**	20	0.76	40.86	0.9782	0.27	67.12	0.9909	0.35	43	11
				45	1.12	49.22	0.9761	0.26	90.73	0.9928	0.23	63	30
				70	1.48	55.13	0.9989	0.30	116.10	0.9995	0.20	>80	>100
				95	1.57	66.11	0.9948	0.44	137.65	0.9995	0.28	>80	>100
5 CEM I 42.5 R-LA	1	0	**0.40**	20	0.21	20.04	0.9876	0.09	27.20	0.9990	0.41	23	44
				45	0.48	36.47	0.9651	0.14	54.37	0.9990	0.30	35	9
				70	0.78	46.73	0.9573	0.23	74.19	0.9932	0.29	52	19
				95	1.17	56.57	0.9615	0.30	100.10	0.9995	0.25	78	>100
5 CEM I 42.5 R-LA	1	0	**0.48**	20	0.11	5.13	0.9940	0.10	5.65	0.9981	0.86	8	16
				45	0.13	10.66	0.9965	0.10	11.98	0.9995	0.77	14	21
				70	0.19	19.72	0.9945	0.11	24.08	0.9987	0.58	18	37
				95	0.33	32.15	0.9766	0.13	43.22	0.9998	0.41	23	37
5 CEM I 42.5 R-LA	1	0	**0.56**	20	0.09	1.13	0.9998	0.09	0.98	0.9993	1.00	4	4
				45	0.09	2.12	0.9980	0.09	1.73	0.9995	0.98	5	6
				70	0.10	3.49	0.9962	0.09	3.51	0.9977	0.93	7	8
				95	0.11	5.32	0.9955	0.10	5.74	0.9985	0.89	9	13

SNF					LOW SHEAR RATE RANGE			MEDIUM SHEAR RATE RANGE					
Cement number and type	**Mix no**	**Time added (min)**	**Dose (% of cement weight)**	**Time (min)**	μ_{pl} (Pa·s)	τ_{yl} (Pa)	R^2	μ_{pm} (Pa·s)	τ_{ym} (Pa)	R^2	μ_{pm}/μ_{pl}	τ_{10sec} **(Pa)**	τ_{10min} **(Pa)**
5 CEM I 42.5 R-LA	1	0	**1.00**	20	0.10	19.49	0.9933	0.07	20.48	0.9995	0.76	34	65
				45	0.20	36.57	0.9314	0.08	42.30	0.9990	0.41	41	70
				70	0.41	44.37	0.9023	0.13	57.10	0.9995	0.31	46	70
				95	0.67	50.98	0.8941	0.17	72.20	0.9991	0.25	53	82
5 CEM I 42.5 R-LA	1	5	**1.00**	20	0.06	-0.05	0.9938	0.06	1.03	0.9991	1.02	<0.8	<1
				45	0.06	0.35	0.9994	0.06	0.94	0.9989	1.01	<0.8	<1
				70	0.07	0.83	0.9997	0.07	1.54	0.9983	0.93	4	1
				95	0.08	1.47	0.9987	0.07	2.15	0.9974	0.90	4	2
5 CEM I 42.5 R-LA	4	0	**1.00**	20	0.14	42.34	0.7518	0.07	44.54	0.9985	0.50	47	86
				45	0.39	51.97	0.7681	0.10	63.05	0.9985	0.25	52	52
				70	0.68	56.61	0.8121	0.13	76.69	0.9995	0.20	63	118
				95	1.00	60.82	0.8456	0.19	88.91	0.9876	0.19	78	>130
5 CEM I 42.5 R-LA	4	5	**1.00**	20	0.09	12.62	0.9936	0.07	13.38	0.9995	0.84	17	33
				45	0.12	24.57	0.9898	0.08	27.11	0.9991	0.66	25	40
				70	0.20	35.58	0.9436	0.10	40.92	0.9989	0.48	29	48
				95	0.34	44.15	0.8861	0.12	54.04	0.9995	0.35	68	67

Table A.10-2: Bingham data for cement pastes made with w/c = 0.40 and LS as superplasticizer. The plasticizer added with the mixing water (*0 min*) or delayed (*5 minutes* after water addition). *Mix no.1* contains 0% SF, while *Mix.4* contains 6.8 vol% SF

LS					LOW SHEAR RATE RANGE			MEDIUM SHEAR RATE RANGE					
Cement number and type	**Mix no**	**Time added (min)**	**Dose (% of cement weight)**	**Time (min)**	μ_{pl} (Pa·s)	τ_{yl} (Pa)	R^2	μ_{pm} (Pa·s)	τ_{ym} (Pa)	R^2	μ_{pm}/μ_{pl}	τ_{10sec} **(Pa)**	τ_{10min} **(Pa)**
1 CEM I 42.5 RR	1	0	**0.16**	20	4.13	94.82	0.9977	1.39	296.25	0.9997	0.34	178	109
				45	3.51	151.47	0.9838	2.18	252.78	0.9988	0.62	199	152
				70	4.97	52.29	0.9883	1.70	323.30	0.8956	0.34	235	306
				95	2.84	82.26	0.9930	3.64	-134.40	0.8477	1.28	>300	172
1 CEM I 42.5 RR	1	0	**0.24**	20	3.11	82.22	0.9989	1.11	221.02	0.9919	0.36	132	118
				45	3.20	84.76	0.9938	0.98	257.75	0.9960	0.31	146	122
				70	4.39	38.75	0.9855	1.51	236.25	0.9981	0.34	171	>250
				95	2.45	88.06	0.9876			0.7978	0.00	92	246
1 CEM I 42.5 RR	1	0	**0.32**	20	3.68	112.48	0.9974	1.35	294.97	0.9989	0.37	180	149
				45	3.55	134.78	0.9863	1.56	262.68	0.5468	0.44	180	170
				70	1.95	44.32	0.9991	1.05	91.97	0.9964	0.54	69	84
				95	1.73	62.04	0.9973	0.78	147.50	0.9951	0.45	133	170
1 CEM I 42.5 RR	1	5	**0.32**	20	2.32	72.71	0.9944	0.65	159.59	0.9988	0.28	94	105
				45	2.51	81.87	0.9958	0.48	207.01	0.9978	0.19	97	121
				70	2.66	80.02	0.9942	0.50	217.96	0.9982	0.19	111	118
				95	2.97	88.32	0.9935	0.60	241.72	0.9985	0.20	119	97
1 CEM I 42.5 RR	1	0	**0.40**	20	3.62	89.60	0.9984	0.86	269.36	0.9974	0.24	133	136
				45	3.88	104.55	0.9948	0.90	302.72	0.9793	0.23	151	212
				70	2.34	116.16	0.9970	1.63	170.64	0.9240	0.70	126	131
				95	2.37	83.29	0.9889	0.60	182.32	0.9971	0.25	133	156

LS					LOW SHEAR RATE RANGE			MEDIUM SHEAR RATE RANGE					
Cement number and type	**Mix no**	**Time added (min)**	**Dose (% of cement weight)**	**Time (min)**	μ_{pl} (Pa·s)	τ_{yl} (Pa)	R^2	μ_{pm} (Pa·s)	τ_{ym} (Pa)	R^2	μ_{pm}/μ_{pl}	τ_{10sec} **(Pa)**	τ_{10min} **(Pa)**
1 CEM I 42.5 RR	1	0	**0.48**	20	3.07	78.34	0.9972	0.85	213.23	0.9980	0.28	112	125
				45	3.84	74.23	0.9987	0.71	268.98	0.9781	0.18	119	125
				70	2.43	93.78	0.9976	0.94	235.91	0.9899	0.39	119	110
				95	2.04	57.67	0.9995	1.00	132.70	0.9990	0.49	82	101
1 CEM I 42.5 RR	1	0	**0.56**	20	3.02	79.34	0.9958	0.74	192.75	0.9995	0.24	97	129
				45	3.10	85.45	0.9934	0.59	218.20	0.9995	0.19	102	109
				70	3.37	84.57	0.9962	0.61	235.53	0.9909	0.18	102	124
				95	3.38	94.93	0.9861	0.53	266.37	0.9773	0.16	121	145
1 CEM I 42.5 RR	1	5	**0.56**	20	0.46	27.66	0.9988	0.38	33.56	0.9995	0.83	29	37
				45	0.53	30.44	0.9993	0.41	39.74	0.9993	0.78	35	39
				70	0.58	34.56	0.9989	0.49	40.96	0.9964	0.84	38	44
				95	0.62	38.57	0.9927	0.51	46.56	0.9970	0.82	44	49
1 CEM I 42.5 RR	1	0	**0.80**	20	2.11	85.33	0.9562	0.65	131.89	0.9977	0.31	73	114
				45	1.22	88.60	0.8661	0.35	113.50	0.9663	0.29	66	109
				70	10.64	95.18	0.8619	0.35	112.50	0.9963	0.03	69	109
				95	1.06	105.45	0.8284	0.38	119.74	0.9976	0.35	82	105
1 CEM I 42.5 RR	1	5	**0.80**	20	0.48	1.96	0.9995	0.39	7.10	0.9996	0.82	19	12
				45	0.50	1.90	0.9994	0.37	10.53	0.9995	0.73	17	13
				70	0.54	2.10	0.9994	0.40	11.92	0.9996	0.73	19	13
				95	0.59	2.32	0.9995	0.43	12.42	0.9995	0.74	21	15

LS					LOW SHEAR RATE RANGE			MEDIUM SHEAR RATE RANGE					
Cement number and type	**Mix no**	**Time added (min)**	**Dose (% of cement weight)**	**Time (min)**	μ_{pl} (Pa·s)	τ_{yl} (Pa)	R^2	μ_{pm} (Pa·s)	τ_{ym} (Pa)	R^2	μ_{pm}/μ_{pl}	τ_{10sec} **(Pa)**	τ_{10min} **(Pa)**
1 CEM I 42.5 RR	1	0	**1.20**	20	0.37	16.89	1.0000	0.35	16.87	0.9992	0.94	38	62
				45	0.37	15.10	0.9998	0.30	19.46	0.9996	0.81	38	62
				70	0.41	15.28	0.9997	0.33	19.72	0.9993	0.82	43	59
				95	0.46	16.32	0.9996	0.38	20.84	0.9997	0.83	43	65
1 CEM I 42.5 RR	1	0	**1.60**	20	0.33	1.20	0.9993	0.30	2.28	0.9991	0.90	<5	42
				45	0.31	1.45	0.9990	0.26	4.15	0.9994	0.84	<5	40
				70	0.33	1.58	0.9990	0.27	4.63	0.9995	0.83	<5	38
				95	0.34	1.70	0.9991	0.28	4.35	0.9996	0.85	<5	36
1 CEM I 42.5 RR	1	0	**2.00**	20	0.39	2.18	0.9983	0.34	3.23	0.9991	0.88	<5	51
				45	0.35	2.02	0.9984	0.29	5.11	0.9996	0.83	<5	45
				70	0.36	2.02	0.9985	0.30	5.00	0.9996	0.84	<5	40
				95	0.37	2.09	0.9986	0.31	4.78	0.9995	0.85	<5	38

LS					LOW SHEAR RATE RANGE			MEDIUM SHEAR RATE RANGE					
Cement number and type	**Mix no**	**Time added (min)**	**Dose (% of cement weight)**	**Time (min)**	μ_{pl} (Pa·s)	τ_{yl} (Pa)	R^2	μ_{pm} (Pa·s)	τ_{ym} (Pa)	R^2	μ_{pm}/μ_{pl}	τ_{10sec} **(Pa)**	τ_{10min} **(Pa)**
2 CEM I 42.5 R	1	0	**0.00**	20	0.82	26.91	0.9748	0.17	60.64	0.9997	0.21	32	61
				45	0.96	29.91	0.9928	0.20	69.91	0.9989	0.21	35	65
				70	1.00	32.39	0.9974	0.19	76.30	0.9900	0.19	35	49
				95	0.97	33.05	0.9987	0.19	77.00	0.9907	0.20	35	33
2 CEM I 42.5 R	1	0	**0.08**	20	0.83	28.81	0.9825	0.24	58.67	0.9996	0.29	35	69
				45	0.99	31.19	0.9897	0.23	69.34	0.9941	0.23	39	37
				70	1.00	32.46	0.9961	0.25	69.26	0.9915	0.25	44	37
				95	1.02	33.16	0.9975	0.26	69.73	0.9928	0.25	44	46
2 CEM I 42.5 R	1	0	**0.16**	20	0.66	34.70	0.9802	0.22	56.59	0.9994	0.33	37	67
				45	0.83	34.01	0.9826	0.24	63.28	0.9997	0.29	42	56
				70	0.96	35.14	0.9962	0.30	68.10	0.9995	0.31	47	56
				95	0.99	36.36	0.9956	0.24	75.70	0.9890	0.24	52	67
2 CEM I 42.5 R	1	0	**0.24**	20	0.44	28.60	0.9888	0.21	39.68	0.9990	0.49	25	44
				45	0.48	31.13	0.9877	0.22	44.76	0.9994	0.46	31	47
				70	0.56	33.11	0.9913	0.25	49.35	0.9998	0.44	34	49
				95	0.61	35.22	0.9922	0.27	52.59	0.9995	0.44	38	52
2 CEM I 42.5 R	1	0	**0.32**	20	0.36	20.14	0.9887	0.24	24.49	0.9981	0.67	20	32
				45	0.36	22.19	0.9931	0.21	30.70	0.9996	0.59	25	36
				70	0.38	24.65	0.9969	0.23	33.49	0.9998	0.61	25	40
				95	0.41	26.30	0.9973	0.25	35.74	0.9999	0.61	25	40

LS					LOW SHEAR RATE RANGE			MEDIUM SHEAR RATE RANGE					
Cement number and type	**Mix no**	**Time added (min)**	**Dose (% of cement weight)**	**Time (min)**	μ_{pl} (Pa·s)	τ_{yl} (Pa)	R^2	μ_{pm} (Pa·s)	τ_{ym} (Pa)	R^2	μ_{pm} / μ_{pl}	τ_{10sec} **(Pa)**	τ_{10min} **(Pa)**
2 CEM I 42.5 R	1	0	**0.48**	20	0.26	5.27	0.9992	0.22	7.79	0.9994	0.83	7	12
				45	0.24	4.07	0.9993	0.19	8.14	0.9994	0.77	7	11
				70	0.25	4.49	0.9991	0.19	8.48	0.9994	0.77	9	13
				95	0.25	5.11	0.9991	0.19	9.11	0.9996	0.78	9	16
2 CEM I 42.5 R	1	0	**0.80**	20	0.12	-0.12	0.9950	0.12	0.32	0.9983	0.99	0	2
				45	0.15	-0.32	0.9917	0.13	1.96	0.9992	0.91	<0.1	1
				70	0.15	-0.35	0.9931	0.14	1.83	0.9996	0.92	<0.1	1
				95	0.16	-0.40	0.9951	0.14	1.55	0.9995	0.92	<0.1	1
3 CEM II A-V 42.5 R	1	0	**0**	20	1.33	45.74	0.9995	0.51	132.09	0.9873	0.38	132	57
				45	1.38	58.69	0.9965	0.66	129.55	0.9767	0.48	130	68
				70	1.40	61.34	0.9946	0.78	121.94	0.9939	0.56	122	72
				95	1.42	62.34	0.9966	0.86	113.96	0.999	0.61	114	75
3 CEM II A-V 42.5 R	1	0	**0.16**	20	1.37	71.61	0.9730	0.72	134.41	0.9987	0.52	92	97
				45	1.51	69.37	0.9992	0.72	144.63	0.9962	0.47	100	135
				70	1.64	71.16	0.9943	0.78	145.85	0.9932	0.48	114	88
				95	1.62	77.51	0.9792	0.80	156.57	0.9934	0.49	109	85
3 CEM II A-V 42.5 R	1	0	**0.32**	20	1.24	48.47	0.9878	0.51	86.86	0.9943	0.42	65	<35
				45	1.24	51.54	0.9903	0.43	98.75	0.9941	0.35	71	69
				70	1.25	53.92	0.9861	0.44	103.65	0.9995	0.35	68	69
				95	1.33	56.67	0.9837	0.44	111.65	0.9995	0.33	74	88

LS					LOW SHEAR RATE RANGE			MEDIUM SHEAR RATE RANGE					
Cement number and type	**Mix no**	**Time added (min)**	**Dose (% of cement weight)**	**Time (min)**	μ_{pl} (Pa·s)	τ_{yl} (Pa)	R^2	μ_{pm} (Pa·s)	τ_{ym} (Pa)	R^2	μ_{pm}/μ_{pl}	τ_{10sec} **(Pa)**	τ_{10min} **(Pa)**
3 CEM II A-V 42.5 R	1	0	**0.48**	20	0.58	32.93	0.9931	0.45	35.87	0.9971	0.78	<2.16	49
				45	0.47	30.07	0.9957	0.35	36.09	0.9992	0.75	<2.37	43
				70	0.45	31.49	0.9952	0.35	36.85	0.9995	0.77	<2.21	41
				95	0.46	32.93	0.9925	0.34	39.00	0.9995	0.75	<1.81	39
3 CEM II A-V 42.5 R	1	0	**0.64**	20	0.32	1.94	1.0000	0.30	1.86	0.9990	0.94	7	5
				45	0.32	0.94	0.9999	0.29	2.46	0.9994	0.93	7	5
				70	0.34	1.27	0.9999	0.31	3.15	0.9995	0.91	7	5
				95	0.35	1.64	1.0000	0.32	3.67	0.9994	0.92	-	-
4 CEM I 52.5 R-LA	1	0	0	20	0.84	26.12	0.9750	0.18	59.61	0.9991	0.22	41	26
				45	1.09	29.40	0.9951	0.19	73.45	0.9902	0.17	41	34
				70	1.15	31.23	0.9982	0.18	80.39	0.9782	0.16	47	44
				95	1.16	33.00	0.9994	0.19	84.91	0.9876	0.16	52	86
4 CEM I 52.5 R-LA	1	0	**0.08**	20	0.76	27.04	0.9781	0.18	58.15	0.9996	0.24	43	20
				45	1.00	26.96	0.9961	0.24	65.31	0.9955	0.24	43	34
				70	1.06	29.18	0.9968	0.22	74.76	0.9772	0.21	50	43
				95	1.07	30.82	0.9992	0.21	81.25	0.9834	0.19	54	48
4 CEM I 52.5 R-LA	1	5	**0.08**	20	0.48	17.61	0.9771	0.14	38.37	0.9990	0.30	25	41
					0.69	21.92	0.9799	0.19	49.28	0.9995	0.27	34	49
					0.83	24.02	0.9859	0.23	56.34	0.9990	0.28	38	26
					0.97	24.67	0.9942	0.25	62.62	0.9998	0.25	42	41

LS					LOW SHEAR RATE RANGE			MEDIUM SHEAR RATE RANGE					
Cement number and type	**Mix no**	**Time added (min)**	**Dose (% of cement weight)**	**Time (min)**	μ_{pl} (Pa·s)	τ_{yl} (Pa)	R^2	μ_{pm} (Pa·s)	τ_{ym} (Pa)	R^2	μ_{pm}/μ_{pl}	τ_{10sec} **(Pa)**	τ_{10min} **(Pa)**
4 CEM I 52.5 R-LA	1	0	**0.16**	20	0.38	15.87	0.9847	0.17	28.41	0.9992	0.46	22	41
					0.47	18.19	0.9740	0.17	35.64	0.9996	0.37	24	38
					0.55	21.34	0.9783	0.21	40.16	0.9996	0.39	30	54
					0.64	22.76	0.9810	0.24	43.63	0.9998	0.37	33	54
4 CEM I 52.5 R-LA	1	0	**0.32**	20	0.18	4.51	0.9889	0.12	7.51	0.9989	0.67	5	12
					0.20	6.23	0.9834	0.11	11.76	1.0000	0.57	8	15
					0.21	8.54	0.9825	0.13	13.60	0.9995	0.60	10	20
					0.23	9.80	0.9871	0.14	15.28	0.9984	0.60	13	25
4 CEM I 52.5 R-LA	1	0	**0.48**	20	0.12	0.25	0.9979	0.11	0.81	0.9984	0.92	<0.5	3
					0.09	-0.12	0.9842	0.09	1.37	0.9993	1.10	<0.5	2
					0.09	-0.08	0.9888	0.08	2.83	0.9987	0.95	<0.5	2
					0.10	0.06	0.9921	0.09	2.80	0.9990	0.88	<0.5	2
4 CEM I 52.5 R-LA	1	0	**0.64**	20	0.06	0.37	0.9851	0.07	0.42	0.9997	1.23	<0.5	<0.5
					0.07	-0.10	0.9694	0.08	1.46	0.9987	1.20	<0.5	<0.5
					0.06	-0.09	0.9630	0.09	0.73	0.9995	1.39	<0.5	<0.5
					0.06	-0.06	0.9585	0.08	1.61	0.9991	1.40	<0.5	<0.5
4 CEM I 52.5 R-LA	1	5	**0.16**	20	0.26	6.05	0.9852	0.13	13.66	0.9985	0.50	8	8
				45	0.34	9.70	0.9783	0.13	22.76	0.9992	0.39	14	13
				70	0.40	12.93	0.9749	0.16	27.80	0.9996	0.41	19	23
				95	0.47	14.87	0.9772	0.20	30.88	0.9994	0.42	>20	>30

LS					LOW SHEAR RATE RANGE			MEDIUM SHEAR RATE RANGE					
Cement number and type	**Mix no**	**Time added (min)**	**Dose (% of cement weight)**	**Time (min)**	μ_{pl} (Pa·s)	τ_{yl} (Pa)	R^2	μ_{pm} (Pa·s)	τ_{ym} (Pa)	R^2	μ_{pm}/μ_{pl}	τ_{10sec} **(Pa)**	τ_{10min} **(Pa)**
5 CEM I 42.5 R-LA	1	0	**0.00**	20	1.37	44.67	0.9997	0.28	114.07	0.9810	0.20	55.30	58.50
				45	1.35	56.60	0.9980	0.22	153.89	0.9865	0.17	64.55	127.50
				70	1.46	61.95	0.9980	0.57	141.08	0.9934	0.39	79.15	149.00
				95	1.35	86.18	0.9879	0.70	139.47	0.9824	0.51	107.50	>200
5 CEM I 42.5 R-LA	1	0	**0.16**	20	1.33	48.08	0.9996	0.28	119.37	0.9756	0.21	68.45	48.25
				45	1.43	56.69	0.9983	0.27	138.16	0.9895	0.19	78.85	<40
				70	1.49	60.06	0.9998	0.25	161.83	0.9668	0.16	86.65	<40
				95	1.51	60.80	0.9985	0.32	167.65	0.9662	0.21	99.70	51.70
5 CEM I 42.5 R-LA	1	0	**0.32**	20	0.78	38.06	0.9801	0.35	58.89	0.9940	0.45	48.80	24.25
				45	0.87	39.98	0.9863	0.30	71.10	0.9995	0.34	54.80	48.10
				70	0.98	42.65	0.9887	0.35	72.41	0.9961	0.36	61.45	44.15
				95	1.10	43.77	0.9939	0.36	79.01	0.9951	0.33	65.10	40.55
5 CEM I 42.5 R-LA	1	0	**0.48**	20	0.27	15.97	0.9959	0.18	20.43	0.9992	0.69	19.65	26.75
				45	0.37	23.69	0.9950	0.22	32.02	0.9995	0.60	24.30	31.60
				70	0.46	28.78	0.9938	0.27	40.12	0.9995	0.58	30.10	37.35
				95	0.54	33.06	0.9831	0.31	46.78	0.9995	0.58	37.20	40.60
5 CEM I 42.5 R-LA	1	0	**0.64**	20	0.17	0.16	0.9998	0.15	0.54	0.9990	0.91	2.58	3.40
				45	0.16	0.50	0.9999	0.13	2.69	0.9995	0.83	3.90	3.40
				70	0.16	0.96	1.0000	0.15	2.09	0.9993	0.92	5.14	4.71
				95	0.18	1.46	1.0000	0.16	3.32	0.9999	0.86	5.90	4.22

A.11 Bingham analysis flow curves for cement pastes with SNF, LS and PA2 prepared for TOC-measurements

Table A.11.1: Bingham data at low and medium shear rate range for cement pastes made with PA as superplasticizer

PA2				Low shear rate range			Medium shear rate range					
Cement number and type	**w/c**	**Dose (% of cement weight)**	**Time (min)**	μ_{pl} **(Pa·s)**	τ_{yl} **(Pa)**	R^2	μ_{pm} **(Pa·s)**	τ_{ym} **(Pa)**	R^2	μ_{pm}/μ_{pl}	τ_{10sec} **(Pa)**	τ_{10min} **(Pa)**
1 CEM I 42.5 RR	0.40	0.32	20	0.29	9.45	0.9991	0.26	12.27	0.9324	0.91	25	31
			45	0.24	8.15	0.9965	0.20	10.36	0.9739	0.85	9	34
			70	0.22	7.67	0.9985	0.11	21.46	0.9590	0.48	9	28
			95	0.22	7.15	0.9994	0.17	10.66	0.9461	0.79	6	25
1 CEM I 42.5 RR	0.40	0.80	20	0.28	2.45	0.9957	0.28	1.14	0.9538	1.00	23	35
			45	0.28	2.39	0.9993	0.28	0.72	0.9903	0.99	18	27
			70	0.27	2.37	0.9993	0.27	0.07	0.8160	1.00	16	25
			95	0.28	2.17	0.9996	0.27	0.13	0.9811	0.98	13	20
1 CEM I 42.5 RR	0.40	1.20	20	0.29	1.62	0.9979	0.32	-4.21	0.9966	1.13	2	26
			45	0.33	1.62	0.9995	0.35	-3.75	0.9934	1.07	2	17
			70	0.33	1.71	0.9966	0.35	-2.12	0.9875	1.05	2	13
			95	0.33	1.64	0.9991	0.34	-1.24	0.9920	1.04	1	10

PA2				Low shear rate range			Medium shear rate range					
Cement number and type	**w/c**	**Dose (% of cement weight)**	**Time (min)**	μ_{pl} **(Pa·s)**	τ_{yl} **(Pa)**	R^2	μ_{pm} **(Pa·s)**	τ_{ym} **(Pa)**	R^2	μ_{pm} / μ_{pl}	$\tau_{10\,sec}$ **(Pa)**	$\tau_{10\,min}$ **(Pa)**
2 CEM I 42.5 R	0.30	0.16	20	0.75	31.25	0.9993	0.76	25.99	0.9978	1.02	32	24
			45	0.73	26.50	0.9996	0.69	26.56	0.9940	0.94	28	21
			70	0.73	25.03	0.9996	0.69	24.00	0.9902	0.95	27	20
			95	0.71	25.03	0.9996	0.68	23.22	0.9893	0.96	27	21
2 CEM I 42.5 R	0.30	0.32	20	0.52	7.29	0.9993	0.53	3.41	0.9757	1.02	17	18
			45	0.51	6.02	0.9992	0.50	2.50	0.9850	0.98	14	15
			70	0.52	5.40	0.9991	0.52	0.79	0.9994	1.00	13	15
			95	0.52	4.98	0.9992	0.51	3.25	0.9947	0.98	11	13
2 CEM I 42.5 R	0.30	0.48	20	0.47	3.86	0.9976	0.59	-11.30	0.9893	1.24	13	20
			45	0.47	3.24	0.9985	0.49	-2.56	0.9962	1.05	8	16
			70	0.47	2.93	0.9986	0.51	-3.01	0.9957	1.07	5	13
			95	0.48	2.46	0.9995	0.53	-5.32	0.9962	1.10	4	11
2 CEM I 42.5 R	0.30	0.80	20	0.44	1.55	0.9998	0.58	-12.78	0.9981	1.32	1	7
			45	0.42	1.66	0.9996	0.50	-8.83	0.9945	1.20	<0.5	3
			70	0.42	1.56	0.9991	0.48	-6.22	0.9980	1.16	<0.5	1
			95	0.42	1.28	0.9988	0.50	-7.87	0.9961	1.19	<0.5	1
3 CEM II A-V 42.5 R	0.30	0.16	20	0.79	18.79	0.9730	1.16	-17.64	0.9982	1.47	16	26
			45	0.74	23.72	0.9506	1.09	-5.46	0.9988	1.48	19	23
			70	0.83	21.18	0.9905	1.05	1.27	0.9977	1.26	13	20
			95	0.75	23.19	0.9756	1.07	-2.92	0.9951	1.43	19	16

PA2				Low shear rate range			Medium shear rate range					
Cement number and type	**w/c**	**Dose (% of cement weight)**	**Time (min)**	μ_{pl} **(Pa·s)**	τ_{yl} **(Pa)**	R^2	μ_{pm} **(Pa·s)**	τ_{ym} **(Pa)**	R^2	μ_{pm} / μ_{pl}	$\tau_{10\,sec}$ **(Pa)**	$\tau_{10\,min}$ **(Pa)**
3 CEM II A-V 42.5 R	0.30	0.32	20	0.48	2.48	0.9983	0.70	-19.11	0.9962	1.45	6	10
			45	0.49	2.52	0.9995	0.72	-21.77	0.9957	1.48	6	8
			70	0.48	2.27	0.9998	0.70	-19.10	0.9836	1.45	6	8
			95	0.47	2.33	0.9994	0.70	-20.56	0.9926	1.51	6	7
3 CEM II A-V 42.5 R	0.30	0.48	20	0.40	0.83	0.9993	0.67	-26.88	0.9959	1.69	<0.5	3
			45	0.40	1.11	0.9995	0.60	-19.16	0.9915	1.50	<0.5	3
			70	0.40	1.01	0.9992	0.62	-20.15	0.9903	1.52	<0.5	3
			95	0.40	0.82	0.9998	0.57	-14.04	0.9892	1.42	<0.5	3
4 CEM I 52.5 R-LA	0.40	0.08	20	0.13	0.67	0.9966	0.12	1.40	0.9834	0.93	1	2
			45	0.13	1.09	0.9788	0.12	1.43	0.9424	0.96	1	2
			70	0.14	1.42	0.9982	0.13	1.58	0.9877	0.97	1	1
			95	0.15	1.56	0.9971	0.14	1.67	0.9891	0.96	1	1
4 CEM I 52.5 R-LA	0.30	0.08	20	0.61	43.53	0.9969	0.76	30.77	0.9914	1.26	50	64
			45	0.73	50.41	0.9916	0.86	36.35	0.9980	1.18	50	53
			70	0.82	53.80	0.9890	0.87	43.26	0.9973	1.05	55	53
			95	0.88	59.10	0.9766	0.86	51.44	0.9971	0.98	61	>100
4 CEM I 52.5 R-LA	0.30	0.16	20	0.20	0.81	0.9956	0.40	-15.37	0.9994	1.97	3	6
			45	0.21	0.82	0.9994	0.36	-9.97	0.9851	1.68	3	6
			70	0.23	0.65	0.9983	0.37	-10.73	0.9948	1.64	3	6
			95	0.23	0.65	0.9985	0.38	-10.19	0.9881	1.65	3	5

PA2				Low shear rate range			Medium shear rate range					
Cement number and type	**w/c**	**Dose (% of cement weight)**	**Time (min)**	μ_{pl} **(Pa·s)**	τ_{yl} **(Pa)**	R^2	μ_{pm} **(Pa·s)**	τ_{ym} **(Pa)**	R^2	μ_{pm}/μ_{pl}	$\tau_{10\,sec}$ **(Pa)**	$\tau_{10\,min}$ **(Pa)**
4 CEM I 52.5 R-LA	0.30	0.32	20	unstable								
5 CEM I 42.5 R-LA	0.37	0.16	20	0.11	0.79	0.9970	0.15	-1.62	0.9677	1.37	2	2
			45	0.11	0.93	0.9931	0.22	-8.36	0.9752	1.98	2	1
			70	0.11	1.00	0.9937	0.27	-12.62	0.9924	2.35	2	1
			95	0.13	0.75	0.9901	0.30	-15.26	0.9861	2.28	2	1
5 CEM I 42.5 R-LA	0.30	0.08	20	1.75	88.99	0.9717	1.76	39.42	0.9904	1.00	182	112
			45	1.42	92.07	0.9896	1.16	90.36	0.9945	0.82	162	237
			70	1.83	66.60	0.9805	0.95	115.90	0.9974	0.52	150	177
			95	1.31	38.66	0.9821	0.82	63.97	0.9232	0.62	131	129
5 CEM I 42.5 R-LA	0.30	0.16	20	0.29	7.14	0.9987	0.65	-25.09	0.9944	2.21	>25	>30
			45	0.30	7.69	0.9990	0.67	-26.49	0.9899	2.27	9	7
			70	0.31	7.42	0.9982	0.66	-23.48	0.9969	2.12	10	7
			95	0.33	7.85	0.9988	0.78	-32.16	0.9954	2.36	10	7
5 CEM I 42.5 R-LA	0.30	0.32	20	unstable								

PA2				Low shear rate range			Medium shear rate range					
Cement number and type	**w/c**	**Dose (% of cement weight)**	**Time (min)**	μ_{pl} **(Pa·s)**	τ_{yl} **(Pa)**	R^2	μ_{pm} **(Pa·s)**	τ_{ym} **(Pa)**	R^2	μ_{pm} / μ_{pl}	$\tau_{10\,sec}$ **(Pa)**	$\tau_{10\,min}$ **(Pa)**
6 CEM I 42.5 N	0.37	0.08	20	1.08	92.07	0.9544	0.51	116.33	0.9875	0.47	94	76
			45	0.85	85.52	0.9227	0.33	106.94	0.9915	0.39	94	76
			70	0.82	83.90	0.8986	0.26	108.73	0.9928	0.31	100	153
			95	0.88	87.83	0.8919	0.24	117.70	0.9890	0.27	114	125
6 CEM I 42.5 N	0.37	0.16	20	0.17	65.15	0.9954	0.34	51.74	0.9824	1.97	<35	87
			45	0.14	44.79	0.9976	0.19	41.17	0.9985	1.39	<35	45
			70	0.12	37.92	0.9972	0.17	35.35	0.9544	1.36	<35	42
			95	0.13	35.35	0.9938	0.15	33.97	0.9892	1.21	<35	47
6 CEM I 42.5 N	0.37	0.32	20	0.17	8.44	0.9981	0.16	9.52	0.9532	0.91	21	35
			45	0.14	6.84	0.9885	0.17	3.32	0.9675	1.17	19	30
			70	0.17	6.04	0.9959	0.15	5.48	0.9899	0.91	17	28
			95	0.17	6.47	0.9898	0.18	2.49	0.8950	1.09	19	27
6 CEM I 42.5 N	0.37	0.48	20	unstable								

Table A.11.2: Bingham data for cement pastes made with SNF as superplasticizer

SNF				Low shear rate range			Medium shear rate range					
Cement number and type	**w/c**	**Dose (% of cement weight)**	**Time (min)**	μ_{pl} **(Pa·s)**	τ_{yl} **(Pa)**	$\mathbf{R^2}$	μ_{pm} **(Pa·s)**	τ_{ym} **(Pa)**	$\mathbf{R^2}$	μ_{pm} / μ_{pl}	$\tau_{10\,sec}$ **(Pa)**	$\tau_{10\,min}$ **(Pa)**
1 CEM I 42.5 RR	0.40	0.32	20	3.32	99.49	0.9978	0.74	272.75	0.9978	0.22	175	171
			45	3.63	128.21	0.9985	1.34	280.12	0.9952	0.37	225	>350
			70	4.13	152.25	0.9989	0.96	405.67	0.9560	0.23	>300	>350
			95	3.65	113.26	0.9957	2.71	188.31	0.9696	0.74	>300	>350
1 CEM I 42.5 RR	0.40	0.80	20	0.64	96.17	0.6919	0.17	107.88	0.9777	0.26	54	82
			45	0.77	101.43	0.7503	0.13	121.61	0.9593	0.16	64	109
			70	1.04	112.85	0.7694	0.11	144.71	0.9696	0.11	89	229
			95	2.23	128.97	0.9163	0.18	205.39	0.9782	0.08	148	>350
1 CEM I 42.5 RR	0.40	1.20	20	0.13	61.09	0.8976	0.21	56.49	0.9910	1.57	49	146
			45	0.08	64.44	0.9179	0.22	54.81	0.9619	2.80	49	164
			70	0.06	69.66	0.5922	0.15	67.01	0.9960	2.64	53	139
			95	0.09	74.51	0.4039	0.16	70.65	0.8707	1.85	62	111

SNF				Low shear rate range			Medium shear rate range					
Cement number and type	**w/c**	**Dose (% of cement weight)**	**Time (min)**	μ_{pl} **(Pa·s)**	τ_{yl} **(Pa)**	$\mathbf{R^2}$	μ_{pm} **(Pa·s)**	τ_{ym} **(Pa)**	$\mathbf{R^2}$	μ_{pm} / μ_{pl}	$\tau_{10\,sec}$ **(Pa)**	$\tau_{10\,min}$ **(Pa)**
2 CEM I 42.5 R	0.37	0.16	20	1.14	45.98	0.9998	0.43	95.62	0.9912	0.37	62	62
			45	1.12	44.22	0.9976	0.37	93.53	0.9949	0.33	62	59
			70	1.12	48.28	0.9995	0.34	99.67	0.9873	0.31	65	66
			95	1.21	49.23	0.9975	0.35	105.50	0.9963	0.29	69	75
2 CEM I 42.5 R	0.37	0.32	20	0.72	43.55	0.9914	0.31	63.57	0.9989	0.43	38	48
			45	0.81	46.22	0.9927	0.27	75.16	0.9895	0.34	44	49
			70	0.92	48.33	0.9919	0.31	79.61	0.9877	0.33	52	49
			95	1.02	47.97	0.9949	0.32	83.04	0.9955	0.31	60	66
2 CEM I 42.5 R	0.37	0.48	20	0.24	19.87	0.9848	0.18	21.36	0.9971	0.74	14	29
			45	0.29	26.75	0.9759	0.17	32.36	0.9448	0.58	25	35
			70	0.36	32.72	0.9780	0.17	42.55	0.9900	0.48	24	39
			95	0.40	39.54	0.9872	0.22	47.48	0.9945	0.54	31	43

SNF				Low shear rate range			Medium shear rate range					
Cement number and type	**w/c**	**Dose (% of cement weight)**	**Time (min)**	μ_{pl} **(Pa·s)**	τ_{yl} **(Pa)**	R^2	μ_{pm} **(Pa·s)**	τ_{ym} **(Pa)**	R^2	μ_{pm}/μ_{pl}	τ_{10sec} **(Pa)**	τ_{10min} **(Pa)**
3 CEM II A-V 42.5 R	0.37	0.16	20	1.44	83.68	0.9720	0.84	121.89	0.9642	0.58	123	66
			45	1.58	68.40	0.9818	0.90	126.55	0.9969	0.57	113	66
			70	1.73	73.93	0.9919	0.81	145.01	0.9908	0.47	118	71
			95	1.63	90.10	0.9971	0.71	157.37	0.9849	0.43	129	110
3 CEM II A-V 42.5 R	0.37	0.32	20	0.85	46.54	0.9526	0.55	53.92	0.9965	0.64	44	31
			45	1.25	52.67	0.9689	0.63	83.38	0.9971	0.50	48	>70
			70	1.42	56.88	0.9847	0.62	99.04	0.9839	0.44	>60	>70
			95	1.44	66.85	0.9854	0.62	118.44	0.9904	0.43	>60	>70
3 CEM II A-V 42.5 R	0.37	0.48	20	0.33	9.56	0.9992	0.32	8.65	0.9978	0.95	10	6
			45	0.44	23.65	0.9925	0.34	26.67	0.9952	0.76	17	10
			70	0.52	32.20	0.9899	0.36	38.07	0.9968	0.70	22	13
			95	0.57	39.79	0.9923	0.38	47.17	0.9949	0.67	25	25
4 CEM I 52.5 R-LA	0.40	0.08	20	0.65	19.75	0.9838	0.19	49.87	0.9352	0.29	34	25
			45	0.77	22.58	0.9837	0.21	52.76	0.9809	0.27	38	25
			70	0.85	24.75	0.9824	0.22	56.87	0.9948	0.26	38	25
			95	0.88	26.18	0.9781	0.22	60.03	0.9666	0.25	38	23
4 CEM I 52.5 R-LA	0.40	0.16	20	0.41	16.19	0.9811	0.21	26.70	0.9859	0.50	25	27
			45	0.36	19.10	0.9799	0.21	35.99	0.9303	0.58	30	23
			70	0.65	20.36	0.9798	0.21	43.57	0.9317	0.32	33	16
			95	0.70	21.96	0.9836	0.24	43.56	0.9952	0.34	36	23

SNF				Low shear rate range			Medium shear rate range					
Cement number and type	**w/c**	**Dose (% of cement weight)**	**Time (min)**	μ_{pl} **(Pa·s)**	τ_{yl} **(Pa)**	R^2	μ_{pm} **(Pa·s)**	τ_{ym} **(Pa)**	R^2	μ_{pm}/μ_{pl}	$\tau_{10\,sec}$ **(Pa)**	$\tau_{10\,min}$ **(Pa)**
4 CEM I 52.5 R-LA	0.40	0.32	20	0.11	-0.06	0.9957	0.10	2.32	0.9323	0.89	1	0
			45	0.14	0.61	0.9976	0.11	2.70	0.9919	0.79	1	1
			70	0.17	2.10	0.9974	0.11	6.51	0.9875	0.62	3	2
			95	0.20	4.80	0.9917	0.12	8.95	0.9734	0.59	5	3
5 CEM I 42.5 R-LA	0.37	0.08	20	1.65	56.65	0.9932	0.61	144.36	0.9950	0.37	103	54
			45	1.75	62.10	0.9942	0.52	165.90	0.9943	0.30	108	80
			70	1.72	74.06	0.9867	0.81	144.49	0.9938	0.47	130	138
			95	1.81	79.52	0.9855	1.09	131.15	0.9974	0.60	>160	>200
5 CEM I 42.5 R-LA	0.37	0.32	20	1.37	47.51	0.9911	0.52	86.29	0.9987	0.38	78	54
			45	1.59	58.11	0.9992	0.51	119.56	0.9970	0.32	94	77
			70	1.73	64.22	0.9978	0.46	142.37	0.9906	0.27	118	109
			95	1.80	76.76	0.9999	0.58	169.46	0.9929	0.32	>160	>200
5 CEM I 42.5 R-LA	0.37	0.48	20	0.20	15.57	0.9982	0.18	16.70	0.9319	0.90	22	37
			45	0.37	30.35	0.9892	0.20	38.45	0.9966	0.54	33	25
			70	0.57	43.66	0.9886	0.23	62.45	0.9927	0.41	41	34
			95	0.76	56.79	0.9830	0.28	84.20	0.9842	0.37	57	52
5 CEM I 42.5 R-LA	0.37	0.80	20	0.11	-0.06	0.9951	0.13	-0.43	0.9517	1.14	<0.1	1
			45	0.11	-0.19	0.9987	0.15	-0.63	0.9913	1.31	<0.1	2
			70	0.13	-0.32	0.9872	0.11	2.25	0.9469	0.81	1	3
			95	0.13	0.03	0.9947	0.13	-0.21	0.9959	1.06	2	3

SNF				Low shear rate range			Medium shear rate range					
Cement number and type	**w/c**	**Dose (% of cement weight)**	**Time (min)**	μ_{pl} **(Pa·s)**	τ_{yl} **(Pa)**	R^2	μ_{pm} **(Pa·s)**	τ_{ym} **(Pa)**	R^2	μ_{pm}/μ_{pl}	$\tau_{10\,sec}$ **(Pa)**	$\tau_{10\,min}$ **(Pa)**
6 CEM I 42.5 N	0.40	0.08	20	0.94	28.15	0.9849	0.30	62.18	0.9628	0.32	46	25
			45	0.98	27.04	0.9811	0.25	64.89	0.9800	0.26	38	28
			70	0.92	28.39	0.9781	0.23	64.56	0.9554	0.25	34	30
			95	0.91	28.73	0.9698	0.21	67.39	0.9692	0.23	38	32
6 CEM I 42.5 N	0.40	0.16	20	1.00	25.99	0.9918	0.24	70.18	0.9477	0.24	42	22
			45	1.07	27.69	0.9875	0.25	69.39	0.9815	0.24	40	22
			70	1.05	27.86	0.9842	0.25	66.36	0.9941	0.24	40	18
			95	1.01	28.63	0.9820	0.20	70.66	0.9726	0.20	42	27
6 CEM I 42.5 N	0.40	0.32	20	0.61	37.68	0.9859	0.21	57.41	0.9144	0.35	39	29
			45	0.78	40.26	0.9720	0.27	59.77	0.9063	0.35	43	33
			70	0.93	39.91	0.9763	0.22	72.54	0.9908	0.24	47	45
			95	1.14	40.66	0.9762	0.26	80.26	0.9959	0.23	57	65
6 CEM I 42.5 N	0.37	0.32	20	1.31	67.84	0.9992	0.47	120.89	0.9949	0.36	>80	>90
			45	1.37	73.10	0.9930	0.48	127.49	0.9950	0.35	>80	>90
			70	1.48	75.42	0.9985	0.43	139.14	0.9966	0.29	>80	>90
			95	1.48	79.13	0.9837	0.43	150.22	0.9879	0.29	>80	>90

SNF				Low shear rate range			Medium shear rate range					
Cement number and type	**w/c**	**Dose (% of cement weight)**	**Time (min)**	μ_{pl} **(Pa·s)**	τ_{yl} **(Pa)**	R^2	μ_{pm} **(Pa·s)**	τ_{ym} **(Pa)**	R^2	μ_{pm} / μ_{pl}	$\tau_{10\,sec}$ **(Pa)**	$\tau_{10\,min}$ **(Pa)**
6 CEM I 42.5 N	0.37	0.48	20	0.22	42.88	0.9546	0.17	44.91	0.9812	0.77	40	38
			45	0.33	52.00	0.8944	0.18	58.05	0.9852	0.54	44	50
			70	0.41	57.95	0.8802	0.16	70.21	0.9675	0.40	48	44
			95	0.56	64.96	0.8732	0.17	83.62	0.9077	0.31	>50	>60
6 CEM I 42.5 N	0.37	0.80	20	0.14	0.22	0.9984	0.12	2.36	0.9423	0.82	3	3
			45	0.15	0.36	0.9984	0.15	0.24	0.9879	0.96	3	3
			70	0.16	0.62	0.9992	0.13	4.64	0.8992	0.76	4	4
			95	0.17	1.31	0.9985	0.16	1.12	0.9570	0.94	6	5

Table A.11.3: Bingham data for cement pastes made with LS as superplasticizer

LS				Low shear rate range			Medium shear rate range					
Cement number and type	**w/c**	**Dose (% of cement weight)**	**Time (min)**	μ_{pl} **(Pa·s)**	τ_{yl} **(Pa)**	$\mathbf{R^2}$	μ_{pm} **(Pa·s)**	τ_{ym} **(Pa)**	$\mathbf{R^2}$	μ_{pm} / μ_{pl}	$\tau_{10\,sec}$ **(Pa)**	$\tau_{10\,min}$ **(Pa)**
1 CEM I 42.5 RR	0.40	0.32	20	2.97	75.21	0.9946	0.79	196.01	0.9936	0.26	105	79
			45	3.00	82.66	0.9952	0.54	226.32	0.9954	0.18	105	76
			70	3.19	76.44	0.9978	0.54	236.41	0.9985	0.17	111	79
			95	3.36	77.09	0.9950	0.65	236.03	0.9956	0.19	118	93
1 CEM I 42.5 RR	0.40	0.80	20	0.96	61.91	0.9145	0.60	66.10	0.9921	0.63	61	227
			45	0.58	59.50	0.8950	0.35	67.80	0.9938	0.61	61	187
			70	0.44	58.95	0.9029	0.33	62.94	0.9915	0.74	61	152
			95	0.37	59.59	0.8707	0.31	60.85	0.9861	0.83	61	130
1 CEM I 42.5 RR	0.40	1.20	20	0.45	1.84	0.9995	0.46	-3.06	0.9821	1.01	<5	20
			45	0.37	1.70	0.9987	0.30	6.56	0.9921	0.81	<5	17
			70	0.36	1.61	0.9988	0.29	6.88	0.9708	0.80	<5	16
			95	0.35	1.55	0.9996	0.30	5.19	0.9672	0.84	<5	16

LS				Low shear rate range			Medium shear rate range					
Cement number and type	**w/c**	**Dose (% of cement weight)**	**Time (min)**	μ_{pl} **(Pa·s)**	τ_{yl} **(Pa)**	$\mathbf{R^2}$	μ_{pm} **(Pa·s)**	τ_{ym} **(Pa)**	$\mathbf{R^2}$	μ_{pm} / μ_{pl}	$\tau_{10\,\mathrm{sec}}$ **(Pa)**	$\tau_{10\,\mathrm{min}}$ **(Pa)**
2 CEM I 42.5 R	0.37	0.16	20	1.07	44.40	0.9976	0.42	82.32	0.9967	0.40	57	39
			45	1.13	46.58	0.9964	0.39	85.77	0.9911	0.35	61	46
			70	1.13	49.21	0.9959	0.36	95.02	0.9919	0.31	61	46
			95	1.21	48.86	0.9974	0.35	97.89	0.9940	0.29	66	52
2 CEM I 42.5 R	0.37	0.32	20	0.60	31.19	0.9951	0.32	43.40	0.9835	0.53	28	36
			45	0.63	31.57	0.9960	0.28	46.82	0.9882	0.45	35	38
			70	0.61	34.04	0.9924	0.25	52.76	0.9810	0.40	35	40
			95	0.60	36.17	0.9876	0.25	52.09	0.9914	0.42	38	40
2 CEM I 42.5 R	0.37	0.48	20	0.29	6.87	0.9978	0.28	5.95	0.9829	0.97	6	12
			45	0.26	5.48	0.9973	0.18	10.63	0.8625	0.71	7	11
			70	0.24	5.84	0.9973	0.19	9.86	0.9645	0.80	7	12
			95	0.23	6.31	0.9918	0.22	4.17	0.8826	0.98	8	13

LS				Low shear rate range			Medium shear rate range					
Cement number and type	**w/c**	**Dose (% of cement weight)**	**Time (min)**	μ_{pl} **(Pa·s)**	τ_{yl} **(Pa)**	R^2	μ_{pm} **(Pa·s)**	τ_{ym} **(Pa)**	R^2	μ_{pm}/μ_{pl}	$\tau_{10\,sec}$ **(Pa)**	$\tau_{10\,min}$ **(Pa)**
3 CEM II A-V 42.5 R	0.37	0.16	20	1.35	52.26	0.9966	0.74	92.14	0.9953	0.54	78	50
			45	1.42	55.70	0.9992	0.63	115.86	0.9928	0.44	86	57
			70	1.51	59.10	0.9957	0.54	131.01	0.9909	0.36	86	60
			95	1.57	62.53	0.9950	0.53	138.81	0.9952	0.34	95	62
3 CEM II A-V 42.5 R	0.37	0.48	20	0.65	17.40	0.9982	0.58	18.68	0.9946	0.89	22	16
			45	0.62	11.13	0.9998	0.55	15.86	0.9975	0.88	18	11
			70	0.61	12.94	0.9996	0.53	18.17	0.9990	0.87	19	11
			95	0.60	14.64	0.9989	0.51	20.21	0.9995	0.84	19	11
3 CEM II A-V 42.5 R	0.37	0.80	20	0.35	-0.61	0.9984	0.31	3.24	0.9958	0.90	<0.5	5
			45	0.37	-0.42	0.9991	0.36	-1.14	0.9324	0.98	<0.5	2
			70	0.37	-0.41	0.9991	0.32	4.06	0.9918	0.87	<0.5	1
			95	0.38	-0.35	0.9998	0.36	0.05	0.9703	0.94	<0.5	1
4 CEM I 52.5 R-LA	0.40	0.08	20	0.57	19.77	0.9747	0.20	43.60	0.9658	0.35	33	23
			45	0.70	22.17	0.9766	0.24	46.30	0.9980	0.35	36	22
			70	0.75	23.50	0.9838	0.25	48.90	0.9928	0.33	40	25
			95	0.76	26.09	0.9704	0.25	52.36	0.9171	0.32	40	25
4 CEM I 52.5 R-LA	0.40	0.16	20	0.34	11.71	0.9915	0.22	16.27	0.9793	0.65	16	27
			45	0.38	12.76	0.9863	0.18	24.45	0.9358	0.48	17	21
			70	0.43	13.85	0.9857	0.19	28.13	0.9692	0.44	21	20
			95	0.44	15.10	0.9850	0.21	29.20	0.9952	0.47	23	20

LS				Low shear rate range			Medium shear rate range					
Cement number and type	**w/c**	**Dose (% of cement weight)**	**Time (min)**	μ_{pl} **(Pa·s)**	τ_{yl} **(Pa)**	R^2	μ_{pm} **(Pa·s)**	τ_{ym} **(Pa)**	R^2	μ_{pm} / μ_{pl}	$\tau_{10\,sec}$ **(Pa)**	$\tau_{10\,min}$ **(Pa)**
4 CEM I 52.5 R-LA	0.40	0.32	20	0.23	0.24	0.9958	0.22	0.28	0.9904	0.94	2	3
			45	0.22	0.98	0.9998	0.19	3.97	0.9894	0.85	2	3
			70	0.24	1.74	0.9949	0.18	6.66	0.9236	0.77	3	3
			95	0.27	2.17	0.9980	0.22	5.39	0.9631	0.80	3	3
5 CEM I 42.5 R-LA	0.37	0.16	20	1.49	56.18	0.9775	0.66	111.94	0.9959	0.44	90	68
			45	1.71	58.21	0.9991	0.34	157.28	0.9828	0.20	90	73
			70	1.70	60.69	0.9910	0.30	166.93	0.9284	0.17	100	112
			95	1.66	70.25	0.9767	0.47	162.63	0.9722	0.29	123	142
5 CEM I 42.5 R-LA	0.37	0.48	20	0.57	35.31	0.9873	0.34	45.17	0.9935	0.59	49	145
			45	0.64	45.28	0.9896	0.27	68.16	0.9895	0.43	56	111
			70	0.77	50.54	0.9713	0.30	78.10	0.9995	0.38	63	89
			95	0.86	54.61	0.9725	0.35	79.41	0.9961	0.41	66	71
5 CEM I 42.5 R-LA	0.37	0.80	20	0.22	-0.20	0.9974	0.23	-1.38	0.9878	1.03	1	5
			45	0.20	0.23	0.9971	0.16	2.80	0.9995	0.82	2	6
			70	0.19	0.35	0.9973	0.12	7.28	0.9054	0.65	3	6
			95	0.19	0.54	0.9951	0.16	1.88	0.9138	0.83	5	7
6 CEM I 42.5 N	0.37	0.16	20	1.15	35.27	0.9987	0.71	59.37	0.9754	0.62	56	27
			45	1.07	32.57	0.9935	0.48	69.48	0.9733	0.45	52	29
			70	1.09	30.07	0.9971	0.41	72.33	0.9893	0.38	52	32
			95	1.09	29.62	0.9926	0.37	74.83	0.9876	0.34	52	37

LS				Low shear rate range			Medium shear rate range					
Cement number and type	**w/c**	**Dose (% of cement weight)**	**Time (min)**	μ_{pl} **(Pa·s)**	τ_{yl} **(Pa)**	$\mathbf{R^2}$	μ_{pm} **(Pa·s)**	τ_{ym} **(Pa)**	$\mathbf{R^2}$	μ_{pm} / μ_{pl}	$\tau_{10\,sec}$ **(Pa)**	$\tau_{10\,min}$ **(Pa)**
6 CEM I 42.5 N	0.37	0.32	20	1.01	49.03	0.9990	0.61	74.14	0.9989	0.61	68	47
			45	0.97	46.75	0.9940	0.47	80.50	0.9967	0.48	68	44
			70	0.95	45.69	0.9980	0.40	80.28	0.9967	0.42	68	66
			95	0.96	45.47	0.9992	0.32	89.95	0.9924	0.33	68	57
6 CEM I 42.5 N	0.37	0.48	20	0.67	63.35	0.9992	0.32	88.17	0.8540	0.48	64	88
			45	0.64	60.15	0.9965	0.32	78.73	0.9794	0.50	68	63
			70	0.64	56.44	0.9983	0.29	76.19	0.9772	0.45	68	73
			95	0.64	56.83	0.9958	0.27	74.94	0.9620	0.42	73	80
6 CEM I 42.5 N	0.37	0.80	20	0.22	1.79	0.9937	0.18	3.32	0.9720	0.81	10	14
			45	0.21	1.75	0.9992	0.17	2.85	0.9944	0.83	11	13
			70	0.20	2.00	0.9991	0.17	2.58	0.9847	0.86	11	13
			95	0.20	2.24	0.9988	0.17	3.06	0.9934	0.85	12	13

A.12 Effect of temperature on the rheology of cement pastes and plasticizer adsorption

A.12.1 Flow Curves

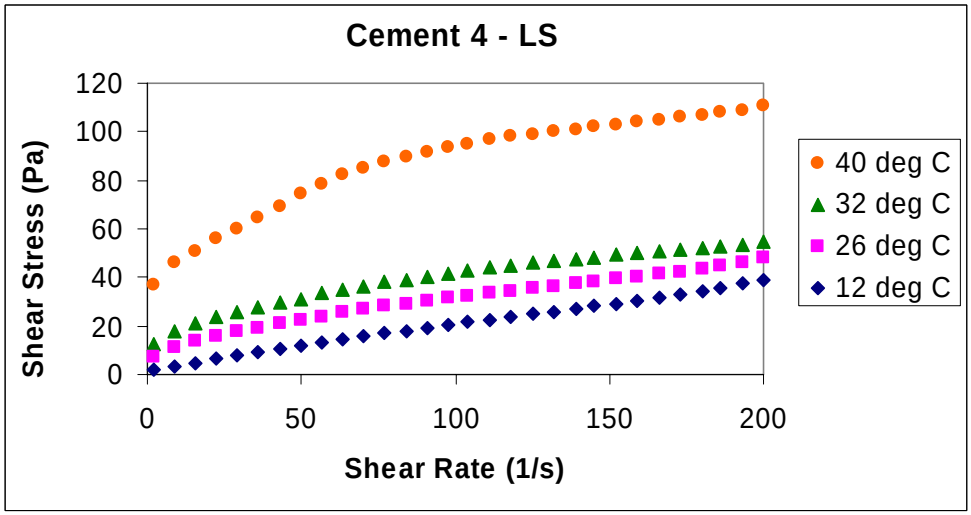

Fig. A.12.1: Effect of temperature on shear stress measurements on Cement 4 pastes with 0.25% LS.

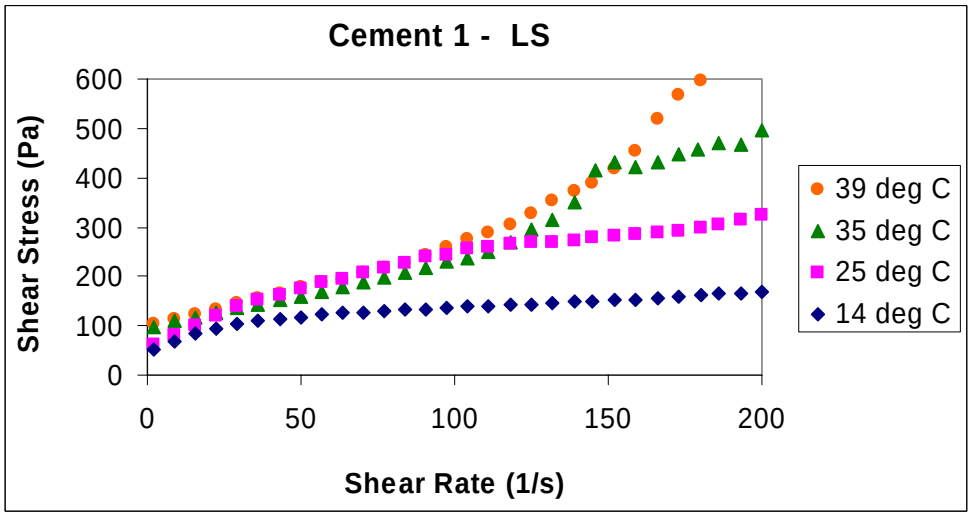

Fig. A.12.2: Effect of temperature on shear stress measurements on Cement 1 pastes with 0.65% LS.

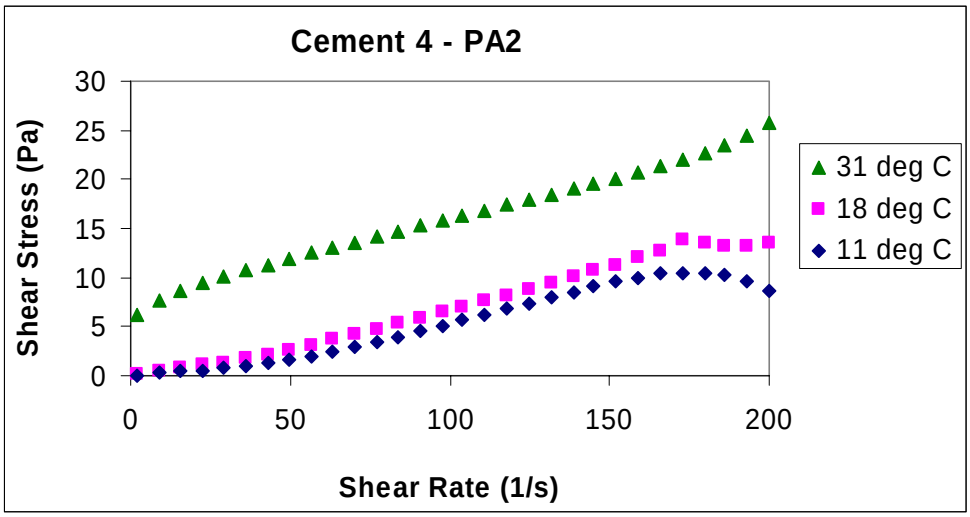

Fig. A.12.3: Effect of temperature on shear stress measurements on Cement 4 pastes with 0.10% PA2.

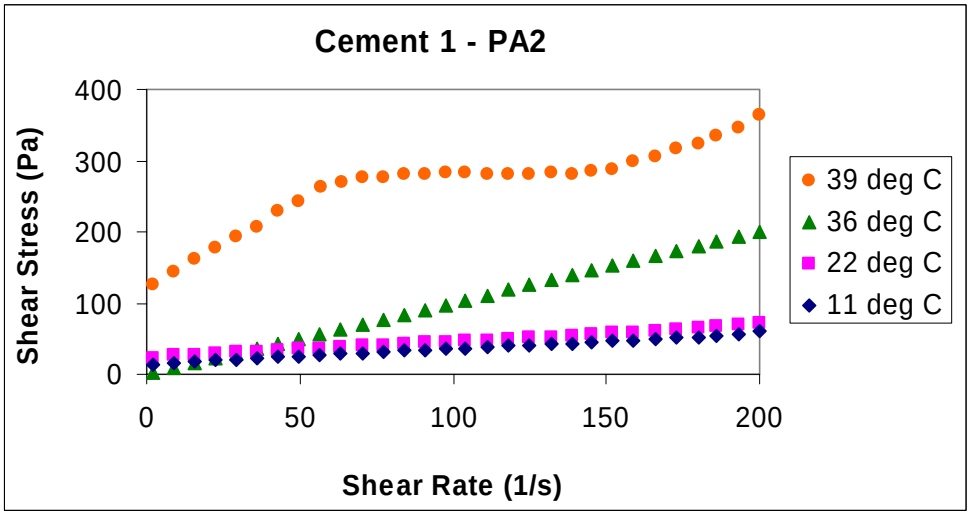

Fig. A.12.4: Effect of temperature on shear stress measurements on Cement 1 pastes with 0.20% PA2.

A.12.2 Flow resistance measurements at medium shear rate range (152-118 s^{-1})

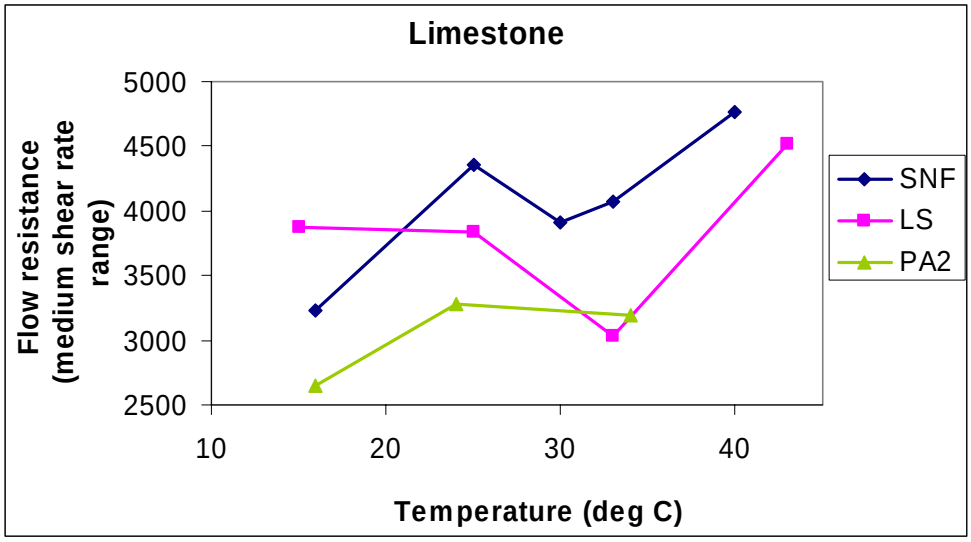

Fig. A.12.5: Flow Resistance in the medium shear rate (152-118 s^{-1}) for limestone pastes with SNF, LS and PA2 as superplasticizers at various temperatures.

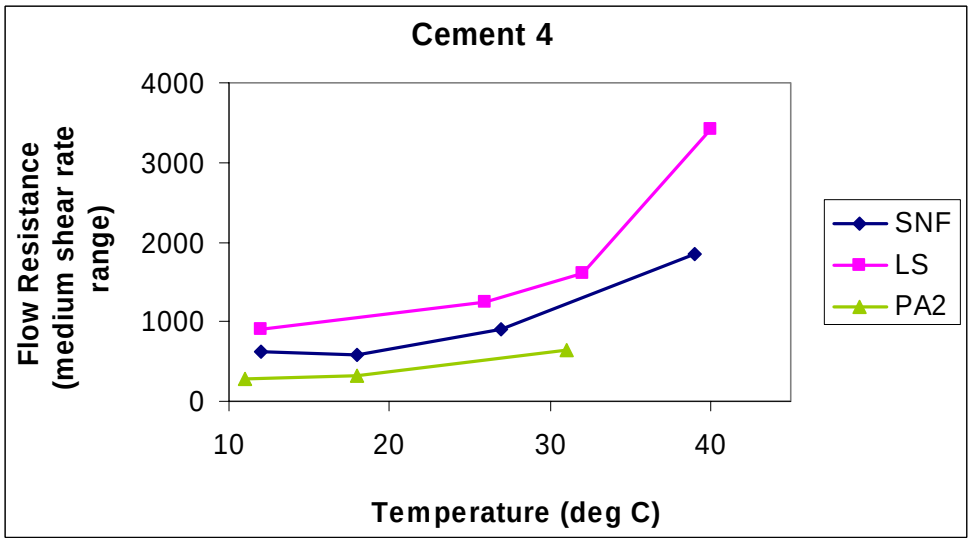

Fig. A.12.6: Flow Resistances in the medium shear rate range (152-118 s^{-1}) for Cement 4 pastes with SNF, LS and PA2 as superplasticizers at various temperatures.

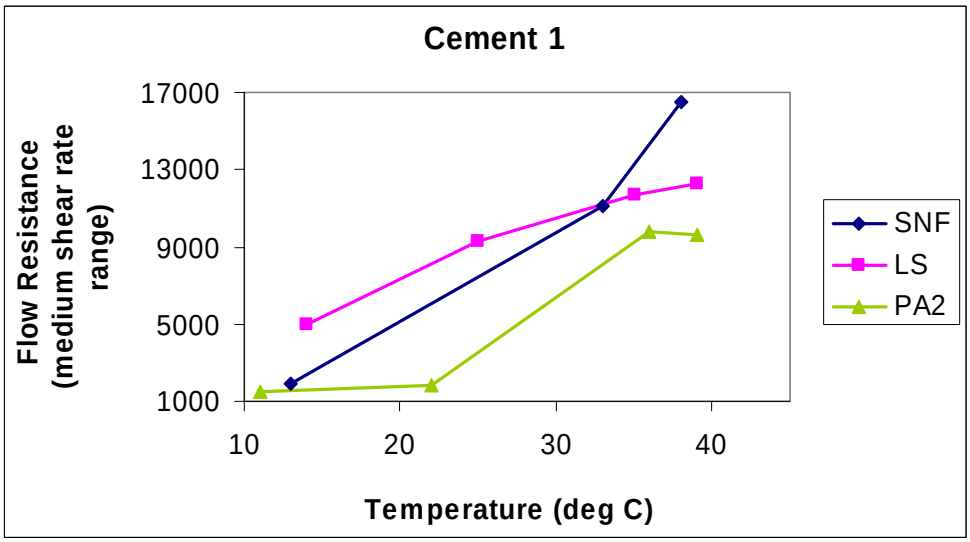

Fig. A.12.7: Flow Resistances in the medium shear rate range (152-118 s^{-1}) for Cement 1 pastes with SNF, LS and PA2 as superplasticizers at various temperatures.

A.12.3 Reproducibility of TOC Measurements

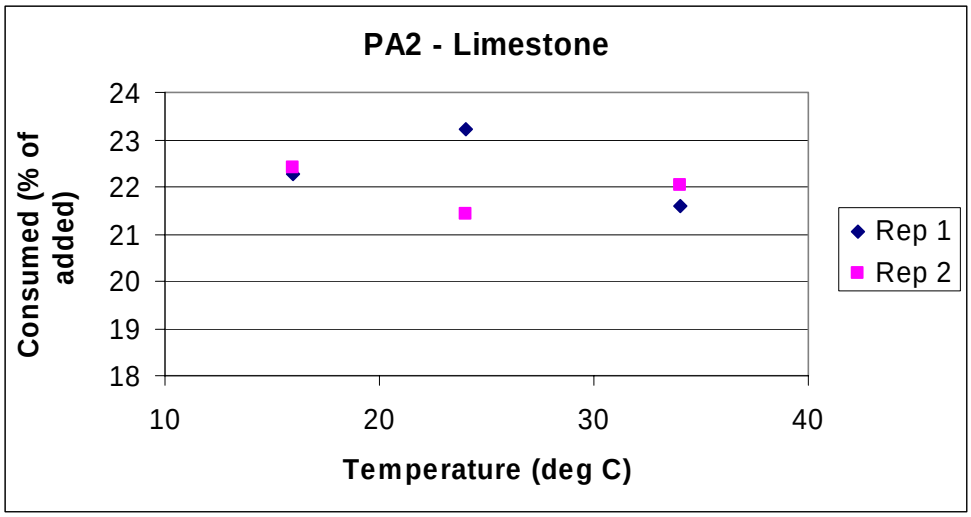

Fig. A.12.8: Reproducibility of TOC-measurements for adsorption of PA2 on limestone.

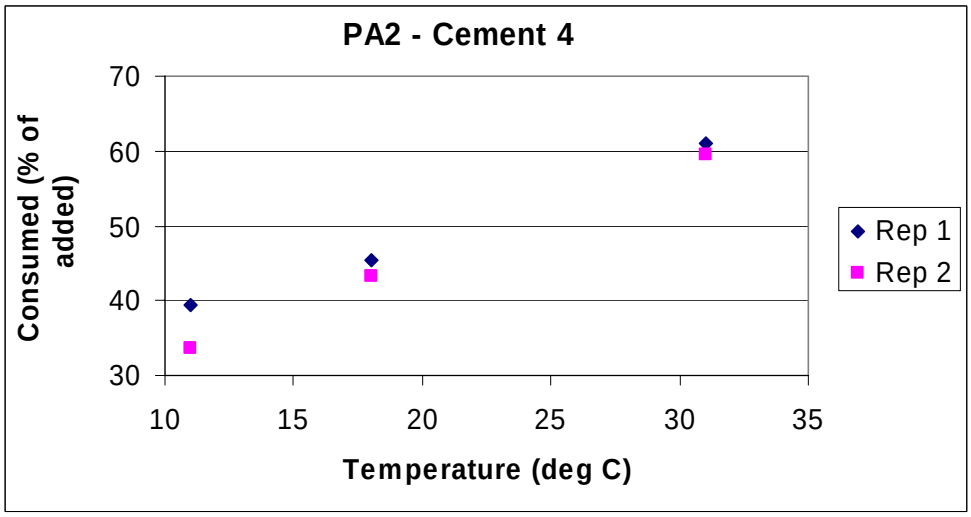

Fig. A.12.9: Reproducibility of TOC-measurements for adsorption of PA2 on Cement 4.

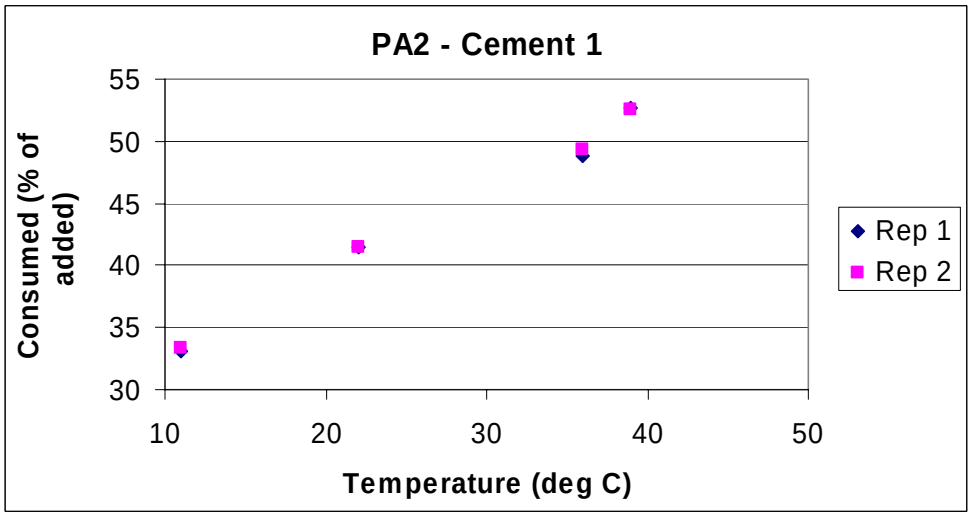

Fig. A.12.10: Reproducibility of TOC-measurements for adsorption of PA2 on Cement 1.

A.12.4 Flow resistance (FR) at medium and low shear rate range and gel strengths from the rheological measurements on limestone and cement pastes with SNF, LS and PA as superplasticizers (SP).

Adsorbent	SP	Dosage (%)	T (^{o}C)	Consumed SP (% of added)	$\tau_{10\,sec}$ [Pa]	$\tau_{10\,min}$ [Pa]	FR_{Medium} [Pa/s]	FR_{Low} [Pa/s]
Limestone	SNF	0.32	16	19.2	<0.5	<0.5	3227	376
			25	28.6	5	8	4355	732
			30	24.3	6	32	3912	694
			33	25.0	20	>70	4075	967
			40	13.8	>50	>50	4768	1788
Limestone	LS	0.32	15	34.1	<0.5	<0.5	3877	460
			25	34.7	<0.5	<0.5	3836	490
			33	32.2	<0.5	<0.5	3027	361
			43	25.9	-----	>60	4523	1128
Limestone	PA2	0.10	16	22.4	2.	4	2647	297
			24	21.4	5	37	3282	472
			34	22.0	14	>70	3187	643
Cement 4	SNF	0.25	12	84.5	4	13	631	166
			18	86.8	4	15	590	164
			27	91.2	21	64	905	479
			39	90.1	66	>170	1848	1239
Cement 4	LS	0.25	12	79.3	10	>80	899	242
			26	86.3	16	50	1253	569
			32	86.4	34	>80	1602	833
			40	87.2	193	>250	3417	1977
Cement 4	PA2	0.10	11	39.5	<0.3	<0.3	279	23
			18	45.5	<0.5	0.6	331	44
			31	61.1	27	>50	637	330
Cement 1	SNF	0.65	13	72.0	<40	>250	1883	1233
			22	72.0	124	162	------	3823
			33	69.3	>250	>300	11093	7416
			38	67.9	-----	-----	16516	8008
Cement 1	LS	0.65	14	73.5	>180	>200	4996	3314
			25	78.8	140	>170	9272	4324
			35	79.4	>300	>350	11689	4501
			39	79.5	>250	>300	12247	4764
Cement 1	PA2	0.20	11	33.2	39	41	1456	688
			22	41.5	26	52	1822	1022
			36	48.8	>250	>300	9818	6647
			39	52.7	>250	>300	9636	6326

A.12.5: Bingham data for the rheological measurements on limestone and cement pastes with SNF, LS and PA as superplasticizers (SP).

				Medium shear rate range (152-118s^{-1})			Low shear rate range (43-8.8s^{-1})		
Powder	**SP**	**Dosage Plast (%)**	**T (^{o}C)**	μ_{pm} **[Pa·s]**	τ_{ym} **[Pa]**	**R^2**	μ_{pl} **[Pa·s]**	τ_{yl} **[Pa]**	**R^2**
Limestone	SNF	0.32	16	1.005	-40.7	0.9971	0.537	-2.8	0.9942
			20	0.732	-18.0	0.9786	0.471	-2.3	0.9943
			23	0.528	-11.9	0.9991	0.376	-0.7	0.9980
			25	1.240	-39.4	0.9899	0.845	-0.4	0.9985
			30	1.042	-25.3	0.9837	0.780	0.2	0.9982
			33	0.875	2.0	0.9741	0.949	3.8	0.9993
			40	0.476	75.9	0.9516	1.216	20.6	0.9729
Limestone	LS	0.32	15	1.057	28.6	0.9993	0.690	-4.2	0.9934
			25	0.951	-15.5	0.9984	0.761	-5.2	0.9938
			33	0.798	-18.6	0.9984	0.561	-3.8	0.9918
			43	0.570	56.3	0.9598	1.466	-4.2	0.9993
Limestone	PA2	0.10	16	0.801	-30.2	0.9987	0.403	-1.6	0.9906
			24	0.894	-24.1	0.9985	0.552	-0.4	0.9952
			34	0.650	6.0	0.9995	0.649	2.1	0.9982
Cement 4	SNF	0.25	12	0.109	3.9	0.9986	0.154	0.9	0.9999
			18	0.111	2.4	0.9981	0.138	1.2	0.9990
			27	0.076	16.4	0.9992	0.194	8.9	0.9817
			33	0.078	9.4	0.9988	0.174	4.0	0.9907
			39	0.101	40.7	0.9983	0.329	27.6	0.9828
Cement 4	LS	0.25	12	0.165	4.3	0.9991	0.210	1.6	0.9980
			26	0.142	17.7	0.9995	0.276	9.4	0.9852
			32	0.128	29.8	0.9994	0.337	15.6	0.9899
			40	0.146	80.7	0.9991	0.680	40.3	0.9992
Cement 4	PA2	0.10	11	0.083	-2.9	0.9995	0.029	-0.1	0.9782
			18	0.091	-2.6	0.9995	0.047	0.1	0.9882
			31	0.081	7.9	0.9983	0.106	6.9	0.9871

				Medium shear rate range (152-118s^{-1})			Low shear rate range (43-8.8s^{-1})		
Powder	**SP**	**Dosage Plast (%)**	**T (^{o}C)**	μ_{pm} **[Pa·s]**	τ_{ym} **[Pa]**	**R^2**	μ_{pl} **[Pa·s]**	τ_{yl} **[Pa]**	**R^2**
Cement 1	SNF	0.65	13	0.186	30.2	0.9996	0.145	32.4	0.9957
			22	-	-	-	1.349	76.0	0.9559
			33	0.203	2989.0	0.9888	2.596	149.4	0.9968
			38	-	-	0.4464	3.420	147.0	0.9713
			39	1.249	354.5	0.9819	3.292	190.1	0.9916
Cement 1	LS	0.65	14	0.295	107.1	0.9995	1.337	61.5	0.9570
			25	0.492	206.3	0.9782	2.434	62.8	0.9903
			35	5.052	-337.9	0.9653	1.222	100.0	0.9972
			39	3.334	-89.7	0.9956	1.578	98.6	0.9995
Cement 1	PA2	0.20	11	0.205	15.2	0.9990	0.240	13.9	0.9990
			22	0.229	22.3	0.9989	0.210	24.5	0.9990
			36	0.721	191.3	0.9976	3.334	107.4	0.9942
			39	0.150	263.4	0.5411	2.466	121.4	0.9958